RAS AND OTHER GTPASES IN CANCER: FROM BASIC TO APPLIED RESEARCH

EDITED BY: Veronica Aran, Piero Crespo, Kwang-jin Cho and Jin Rui Liang
PUBLISHED IN: Frontiers in Molecular Biosciences and
Frontiers in Cell and Developmental Biology

frontiers Research Topics

ISSN 1664-8714
ISBN 978-2-88974-081-9
DOI 10.3389/978-2-88974-081-9

About Frontiers

Frontiers is more than just an open-access publisher of scholarly articles: it is a pioneering approach to the world of academia, radically improving the way scholarly research is managed. The grand vision of Frontiers is a world where all people have an equal opportunity to seek, share and generate knowledge. Frontiers provides immediate and permanent online open access to all its publications, but this alone is not enough to realize our grand goals.

Frontiers Journal Series

The Frontiers Journal Series is a multi-tier and interdisciplinary set of open-access, online journals, promising a paradigm shift from the current review, selection and dissemination processes in academic publishing. All Frontiers journals are driven by researchers for researchers; therefore, they constitute a service to the scholarly community. At the same time, the Frontiers Journal Series operates on a revolutionary invention, the tiered publishing system, initially addressing specific communities of scholars, and gradually climbing up to broader public understanding, thus serving the interests of the lay society, too.

Dedication to Quality

Each Frontiers article is a landmark of the highest quality, thanks to genuinely collaborative interactions between authors and review editors, who include some of the world's best academicians. Research must be certified by peers before entering a stream of knowledge that may eventually reach the public - and shape society; therefore, Frontiers only applies the most rigorous and unbiased reviews.
Frontiers revolutionizes research publishing by freely delivering the most outstanding research, evaluated with no bias from both the academic and social point of view. By applying the most advanced information technologies, Frontiers is catapulting scholarly publishing into a new generation.

What are Frontiers Research Topics?

Frontiers Research Topics are very popular trademarks of the Frontiers Journals Series: they are collections of at least ten articles, all centered on a particular subject. With their unique mix of varied contributions from Original Research to Review Articles, Frontiers Research Topics unify the most influential researchers, the latest key findings and historical advances in a hot research area! Find out more on how to host your own Frontiers Research Topic or contribute to one as an author by contacting the Frontiers Editorial Office: frontiersin.org/about/contact

RAS AND OTHER GTPASES IN CANCER: FROM BASIC TO APPLIED RESEARCH

Topic Editors:
Veronica Aran, Instituto Estadual do Cérebro Paulo Niemeyer (IECPN), Brazil
Piero Crespo, Institute of Biomedicine and Biotechnology of Cantabria, Spanish National Research Council (CSIC), Spain
Kwang-jin Cho, Wright State University, United States
Jin Rui Liang, ETH Zürich, Switzerland

Citation: Aran, V., Crespo, P., Cho, K.-J., Liang, J. R., eds. (2022). Ras and Other GTPases in Cancer: From Basic to Applied Research. Lausanne: Frontiers Media SA. doi: 10.3389/978-2-88974-081-9

Table of Contents

frontiers in Molecular Biosciences

EDITORIAL
published: 29 November 2021
doi: 10.3389/fmolb.2021.804818

Editorial: Ras and Other GTPases in Cancer: From Basic to Applied Research

Kwang-jin Cho[1], *Jin Rui Liang*[2], *Piero Crespo*[3] *and Veronica Aran*[4]*

[1]Department of Biochemistry and Molecular Biology, Boonshoft School of Medicine, Wright State University, Dayton, OH, United States, [2]Department of Biology, ETH Zürich, Zürich, Switzerland, [3]Instituto de Biomedicina y Biotecnología de Cantabria (IBBTEC), Consejo Superior de Investigaciones Científicas (CSIC)-Universidad de Cantabria, Santander, Spain, [4]Instituto Estadual do Cérebro Paulo Niemeyer, Rio de Janeiro, Brazil

Keywords: small GTPases, Ras, Rho, Rap, RAS mutations, SmgGDS, cmp4, cancer therapy

Editorial on the Research Topic

Ras and Other GTPases in Cancer: From Basic to Applied Research

OPEN ACCESS

Edited by:
William C. Cho,
QEH, Hong Kong SAR, China

Reviewed by:
Nava Segev,
University of Illinois at Chicago, United States
Guangpu Li,
University of Oklahoma Health Sciences Center, United States
Francisco Yanguas,
University of Oslo, Norway

****Correspondence:***
Veronica Aran
varanponte@gmail.com

Specialty section:
This article was submitted to Molecular Diagnostics and Therapeutics, a section of the journal Frontiers in Molecular Biosciences

Received: *29 October 2021*
Accepted: *09 November 2021*
Published: *29 November 2021*

Citation:
Cho K-j, Liang JR, Crespo P and Aran V (2021) Editorial: Ras and Other GTPases in Cancer: From Basic to Applied Research. Front. Mol. Biosci. 8:804818. doi: 10.3389/fmolb.2021.804818

In the current Research Topic (RT), we provide insights on the small GTPase biology, from protein synthesis to disease, by presenting a Research Topic of original and review articles describing distinct GTPases, with special attention to RAS proteins. The RAS superfamily comprises a large family of small GTPases, where the members of the RAS, RHO, and RAB families are the most well-characterized. These small proteins cycle between a GDP-bound inactive and a GTP-bound active state, thus mediating several cellular processes such as intracellular trafficking, cytoskeletal organization, cell migration, proliferation, differentiation, and gene expression (Bos 2018; Gray et al., 2020).

RAS is considered a central protooncogene in cancer. There are different RAS proteins (K-RAS, N-RAS, and H-RAS) and gain-of-function missense mutations in RAS genes are frequently found in a variety of tumors (Hobbs et al., 2016). Although there are different RAS isoforms, most research to date have concentrated their efforts in studying K-RAS, since it is the most mutated isoform in cancer. In addition, the K-RAS gene undergoes alternative splicing generating the splicing variants K-RAS4A and K-RAS4B. In this RT, Aran discusses the roles of both splicing variants in cancer and since K-RAS4A, the under-studied splicing variant, shares the same oncogenic point mutations with K-RAS4B and has strong transforming capability, the author emphasizes the importance of investigating K-RAS4A in RAS-driven cancer and developing anti-RAS therapies.

RAS undergoes several posttranslational modifications (PTMs) that facilitate its attachment to membranes, where it drives its signal transduction. The cysteine in the C-terminal CAAX motif (where A is aliphatic and X is any amino acid) is first prenylated, allowing the cytosolic RAS proteins to bind the ER, where the -AAX residues are cleaved and the now C-terminal prenylated cysteine is methylated. H-, N- and K-RAS4A are also palmitoylated. Busquets-Hernandez and Triola contribute a review on the role of lipid modifications, specifically palmitoylation, on the regulation of RAS activity; how palmitoylation orchestrates RAS distribution over different subcellular compartments and its compartmentalization within membrane subdomains, and how it impacts on RAS functions. The authors also discuss the potential of these to be translated into therapeutics.

Brandt et al. provide a review on the role of Small GTP-binding protein GDP dissociation stimulator (SmgGDS) as major regulators of the prenylation, post-prenylation processing, and trafficking of RAS and RHO small GTPase family members. The authors further provide new strategies for therapeutic targeting of SmgGDS in cancer, involving splice-switching oligonucleotides and peptide inhibitors. Moreover, the signal transduction and subcellular localization of RAS proteins can be further regulated

by reversible PTMs at their G4 and G5 motifs, including S-oxygenation, S-nitrosylation, monoubiquitylation, acetylation, and methylation. Osaka et al. provide a review discussing the mechanisms of these PTMs and propose that targeting these PTM mechanisms can be a good starting point for developing a new therapeutic approach for RAS-driven cancers.

Recently, direct K-RASG12C mutant inhibitors showed promising outcomes in clinical trials (Canon et al., 2019; Hallin et al., 2020), but since this mutant is found only in a small portion of K-RAS-driven cancers, pan-K-RAS therapies are still needed. Since most functional RAS proteins localize to the plasma membrane (PM), targeting the RAS-PM interaction represents a potential alternative strategy to disrupt RAS signaling activity. Zhou et al., in their review, summarizes the latest mechanistic insights on how different RAS isoforms undergo spatial segregation with different PM lipid species and how this could impact on the recruitment of their respective effectors and activation of different downstream signaling pathways. The authors further discuss the possibility of targeting RAS nanoclusters as a potential therapeutic approach to treat RAS pathologies. Moreover, Henkels et al. described how pharmacological agents disrupting K-RAS-PM interaction could be beneficial to block oncogenic K-RAS activity, thus representing clinical utility. K-RAS membrane organization is dependent on Calmodulin (CaM) and has significant impact on cancer stem cell tumorigenesis. Here, Okutachi et al. describes a novel CaM inhibitor, Calmirasone1, which has higher on-target inhibition on K-RAS compared to its off-target substrates including H-RAS and B-RAF. This discovery has exciting future applications for the interrogation of the cancer biology of CaM-associated K-RAS activities.

Tisi et al. describe a novel RAS inhibitor, cmp4, which exerts antiproliferative effects on cancer cells resistant to EGFR-aimed therapy. Cmp4 binds an extended Switch II pocket on H-RAS and K-RAS and induces a conformational change that abrogates guanine nucleotide exchange and impedes RAS effector binding. In this respect, cmp4 could provide a template for future drugs exploiting this promising mechanism of action.

Bartolacci et al. reviewed the recent advances concerning the relationship between RAS and lipid metabolism in cancer, describing how lipids and oxidative stress can either promote or sensitize to ferroptosis (i.e., an iron-dependent programmed cell death defined by the existence of oxidative stress and lipid peroxidation) RAS-driven cancers, which is still a controversial subject. The authors argue that RAS mutations have tissue-specific effects on metabolism, probably due to the intrinsic metabolic wiring present in distinct tumor types, and that the combination between ferroptosis inducers with existing chemotherapeutic agents, could be of potential clinical benefit.

Finally, RAS related proteins (RAP) are members of the RAS superfamily, sharing 50–60% sequence homology with RAS, and being involved in cell adhesion, migration, and polarity (Bokoch 1993). There are five different RAP family members, which are shown to be involved in the tumorigenesis of multiple cancer types (Bokoch 1993; Simanshu et al., 2017). Kumari et al. utilize authoritative multi-omics databases to investigate the association of RAP gene family expression with molecular and clinicopathological features in hepatocellular carcinoma (HCC). Their study reveals significant associations of one of the RAP family members, RAP2A expression with several HCC pathways, including cell cycle-related pathways and metabolic pathways, suggesting RAP2A as a therapeutic target and prognostic biomarker in HCC.

Overall, this RT discusses the role of small GTPases in carcinogenesis and up-to-date strategies to block their oncogenic activities in cancer. We hope that the selected articles will inspire and motivate basic and clinical research scientists to further investigate several unanswered questions concerning the GTPases world. Despite being small proteins in size, their biological importance is substantial.

AUTHOR CONTRIBUTIONS

All Editorial authors contributed to the writing of this article, provided critical feedback, and approved its final version.

ACKNOWLEDGMENTS

We thank all the authors and reviewers for their contribution and for making this Research Topic possible and relevant for the scientific community.

REFERENCES

Bokoch, G. M. (1993). Biology of the Rap Proteins, Members of the Ras Superfamily of GTP-Binding Proteins. *Biochem. J.* 289 (Pt 1) (Pt 1), 17–24. doi:10.1042/bj2890017

Bos, J. L. (2018). From Ras to Rap and Back, a Journey of 35 Years. *Cold Spring Harb Perspect. Med.* 8. doi:10.1101/cshperspect.a031468

Canon, J., Rex, K., Saiki, A. Y., Mohr, C., Cooke, K., Bagal, D., et al. (2019). The Clinical KRAS(G12C) Inhibitor AMG 510 Drives Anti-tumour Immunity. *Nature* 575, 217–223. doi:10.1038/s41586-019-1694-1

Gray, J. L., Delft, F., and Brennan, P. E. (2020). Targeting the Small GTPase Superfamily through Their Regulatory Proteins. *Angew. Chem. Int. Ed.* 59, 6342–6366. doi:10.1002/anie.201900585

Hallin, J., Engstrom, L. D., Hargis, L., Calinisan, A., Aranda, R., Briere, D. M., et al. (2020). The KRASG12C Inhibitor MRTX849 Provides Insight toward Therapeutic Susceptibility of KRAS-Mutant Cancers in Mouse Models and Patients. *Cancer Discov.* 10, 54–71. doi:10.1158/2159-8290.cd-19-1167

Hobbs, G. A., Der, C. J., and Rossman, K. L. (2016). RAS Isoforms and Mutations in Cancer at a Glance. *J. Cel Sci* 129, 1287–1292. doi:10.1242/jcs.182873

Simanshu, D. K., Nissley, D. V., and McCormick, F. (2017). RAS Proteins and Their Regulators in Human Disease. *Cell* 170, 17–33. doi:10.1016/j.cell.2017.06.009

Conflict of Interest: The authors declare that the research was conducted in the absence of any commercial or financial relationships that could be construed as a potential conflict of interest.

frontiers in Molecular Biosciences

ORIGINAL RESEARCH
published: 17 February 2021
doi: 10.3389/fmolb.2021.625979

The Multi-Level Mechanism of Action of a Pan-Ras Inhibitor Explains its Antiproliferative Activity on Cetuximab-Resistant Cancer Cells

*Renata Tisi[1†], Michela Spinelli[1,2†], Alessandro Palmioli[1], Cristina Airoldi[1,2], Paolo Cazzaniga[2,3], Daniela Besozzi[2,3], Marco S. Nobile[3,4], Elisa Mazzoleni[1], Simone Arnhold[1], Luca De Gioia[1,2], Rita Grandori[1], Francesco Peri[1], Marco Vanoni[1,2] and Elena Sacco[1,2]**

[1]*Department of Biotechnology and Biosciences, University of Milan-Bicocca, Milan, Italy,* [2]*SYSBIO-ISBE-IT–Candidate National Node of Italy for ISBE, Research Infrastructure for Systems Biology Europe, Milan, Italy,* [3]*Bicocca Bioinformatics, Biostatistics and Bioimaging Centre - B4, Milano, Italy,* [4]*Department of Industrial Engineering and Innovation Sciences, Eindhoven University of Technology, Eindhoven, Netherlands*

OPEN ACCESS

Edited by:
Piero Crespo,
Consejo Superior De Investigaciones Científicas, Spain

Reviewed by:
Sayan Chakraborty,
*Institute of Molecular and Cell Biology (A*STAR), Singapore*
Amancio Carnero,
Sevilla University, Spain

***Correspondence:**
Elena Sacco
elena.sacco@unimib.it

†These authors have contributed equally to this work

Specialty section:
This article was submitted to Molecular Diagnostics and Therapeutics, a section of the journal Frontiers in Molecular Biosciences

Received: *04 November 2020*
Accepted: *11 January 2021*
Published: *17 February 2021*

Citation:
Tisi R, Spinelli M, Palmioli A, Airoldi C, Cazzaniga P, Besozzi D, Nobile MS, Mazzoleni E, Arnhold S, De Gioia L, Grandori R, Peri F, Vanoni M and Sacco E (2021) The Multi-Level Mechanism of Action of a Pan-Ras Inhibitor Explains its Antiproliferative Activity on Cetuximab-Resistant Cancer Cells. Front. Mol. Biosci. 8:625979. doi: 10.3389/fmolb.2021.625979

Ras oncoproteins play a crucial role in the onset, maintenance, and progression of the most common and deadly human cancers. Despite extensive research efforts, only a few mutant-specific Ras inhibitors have been reported. We show that cmp4–previously identified as a water-soluble Ras inhibitor– targets multiple steps in the activation and downstream signaling of different Ras mutants and isoforms. Binding of this pan-Ras inhibitor to an extended Switch II pocket on HRas and KRas proteins induces a conformational change that down-regulates intrinsic and GEF-mediated nucleotide dissociation and exchange and effector binding. A mathematical model of the Ras activation cycle predicts that the inhibitor severely reduces the proliferation of different Ras-driven cancer cells, effectively cooperating with Cetuximab to reduce proliferation even of Cetuximab-resistant cancer cell lines. Experimental data confirm the model prediction, indicating that the pan-Ras inhibitor is an appropriate candidate for medicinal chemistry efforts tailored at improving its currently unsatisfactory affinity.

Keywords: RasG13D, RasG12V, anti-cancer agent, exchange factor, intrinsic nucleotide dissociation and exchange, Raf1 binding, mathematical modeling & simulation, cetuximab

1 INTRODUCTION

Ras proteins are small guanine nucleotide-binding (G) proteins with low intrinsic GTPase activity, cycling between a GDP-bound inactive state and a GTP-bound active state. They act as molecular switches in signaling pathways regulating many cellular processes, including cell proliferation, growth, survival, adhesion, migration, energy, and redox homeostasis (Simanshu et al., 2017). Ras activity is regulated in response to specific extracellular stimuli, by the competitive action between Guanine nucleotide Exchange Factors (GEFs) promoting the nucleotide dissociation and GDP/GTP exchange, and GTPase Activating Proteins (GAPs), which provide an essential catalytic group for GTP hydrolysis (Scheffzek et al., 1997; Boriack-Sjodin et al., 1998; Bos et al., 2007). In human cells, three *RAS* genes encode four homologous but functionally distinct isoforms (HRas, NRas, and KRas4A and K-Ras4B) (Omerovic et al., 2007; Lu et al., 2016a). Gain-of-function missense mutations, mainly located at codons 12, 13, and 61, constitutively activate Ras proteins and can

be detected in approximately one-third of all human cancers. Oncogenic Ras mutants contribute to tumor onset, maintenance, progression, and influence the efficacy of both cytotoxic and targeted therapies (Li et al., 2018). For this reason, many efforts, mostly promoted by the RAS initiative (https://www.cancer.gov/research/key-initiatives/ras), have been devoted to investigating the mechanistic role of *RAS* oncogenes in cancer and to explore different strategies for attenuating the aberrant Ras oncoproteins signaling, as widely reviewed (Sacco et al., 2012c; Welsch et al., 2017; Gorfe and Cho, 2021; Ni et al., 2019; Spencer-Smith and O'Bryan, 2019; Khan et al., 2020; Tisi et al., 2020).

Notably, each oncogenic mutation occurring in *RAS* genes induces conformational changes in the encoded protein that alter the residence time of the protein in the GTP-bound active state (Hunter et al., 2015) and make the oncoprotein surface more or less prone to the functional binding not only with modulators and effectors but also with specific pharmacophore groups or classes of molecule drugs. The Ras^{G12V} mutant presents a weak intrinsic and GAP-mediated GTP hydrolysis, and it is particularly aggressive and refractory to exchange inhibitors (Hunter et al., 2015). We first proved that the Ras^{G13D} mutant shows self-sufficiency in nucleotide dissociation (Palmioli et al., 2009b). Structural and functional studies (Smith et al., 2013; Hunter et al., 2015; Lu et al., 2016b; Johnson et al., 2019; Rabara et al., 2019) indicate that this mutant remains sensitive to the catalytic activity of GEFs and of at least one GAP, Nf1. Active and selective inhibitors for these oncogenic mutants are not yet available. On the contrary, compounds that covalently bind the highly reactive cysteine in the $KRas^{G12C}$ mutant selectively inhibit its function (Ostrem et al., 2013; Lito et al., 2016; Patricelli et al., 2016; Hansen et al., 2018a; Janes et al., 2018). After optimization for clinical use, they show a promising anti-tumor effect in $KRAS^{G12C}$-positive patients (Canon et al., 2019; Hallin et al., 2020).

We previously demonstrated that a class of small water-soluble molecules (cmp2-4), specifically binds the Switch II (β-3/α-2) region of wild type HRas-GDP. These compounds inhibit GEF-catalyzed nucleotide exchange, attenuate Ras signaling, and reduce Ras-dependent cell proliferation in mouse fibroblasts (Palmioli et al., 2009a; Sacco et al., 2011). Here we demonstrate that cmp4 binds an extended Switch II pocket on HRas and KRas proteins harboring different mutations. cmp4 decreases the intrinsic and GEF-mediated nucleotide dissociation and exchange on wild type and G13D mutated Ras proteins, interferes with Ras binding to GEFs (RasGRF1 and Sos1) and the Raf1 effector, and reduces mitogen-activated protein kinases signaling and cell viability of $KRas^{G13D}$ cancer cells. A mathematical model of Ras signaling (Stites et al., 2007; McFall et al., 2019), appropriately modified according to recent data (Johnson et al., 2017; Johnson et al., 2019), predicts the ability of cmp4 to inhibit the proliferation of different Ras-driven cancer cells. In keeping with the model prediction, experimental data on human cancer cell lines expressing different Ras oncoproteins confirm that cmp4 is a pan-Ras inhibitor able to cooperate with Cetuximab to inhibit proliferation of Cetuximab-resistant cell lines. Although cmp4 currently has an unsatisfactory affinity for Ras, targeted medicinal chemistry efforts could turn it into a valuable and needed clinical drug.

2 MATERIALS AND METHODS

2.1 Compounds and Recombinant

cmp4 was synthesized as described (Palmioli et al., 2009a). Recombinant N-terminal His-tagged wild type and G13D mutated H-Ras proteins (residues 1-166 of the mature protein) and Sos1 catalytic domain (aa553-1024 of the mature protein) were expressed in M15 [pREP4] *E. coli* strain harboring a pQETM-derived plasmid (Qiagen) and purified by affinity chromatography using a Ni^{2+}-NTA column (Qiagen), as described (Palmioli et al., 2009b; Palmioli et al., 2017; Sacco et al., 2012a). The N-terminal GST-tagged RasGRF1 catalytic domain (residues 976–1262 of the mature protein), was expressed in BL21 [pLysE] *E.coli* strain harbouring a pGEX2T-derived plasmid and purified by glutathione–sepharose chromatography (Amersham Bioscience) as described (Palmioli et al., 2017).

2.2 Mass Spectrometry Experiments

Mass-spectrometry measurements were performed on a hybrid quadrupole-Time-of-Flight (Q-TOF) instrument (QSTAR ELITE, Applied Biosystems, Foster City, CA, United States), equipped with a nano-ESI sample source. Metal-coated borosilicate capillaries (Proxeon, Odense, DK), with medium-length emitter tip of 1-mm internal diameter, were used to infuse the sample. The instrument was calibrated using the renine-inhibitor (1757.9 Da) (Applied Biosystems, Foster City, CA, United States) and its fragment (109.07 Da) as standards. Spectra were acquired in the 1500–3000 m/z range, with accumulation time of 1 s, ion-spray voltage of 1200–1500 V, declustering potential of 80 V, and instrument interface of 50°C. Spectra were averaged over a time period of at least 3 min. Data analysis was performed by the program Analyst QS 2.0 (Applied Biosystems, Foster City, CA, United States). The samples were prepared in 5 mM ammonium acetate pH 6.5.

2.3 NMR analysis

For the experiments with the free ligand, cmp4 was dissolved in a $[D_{11}]$-Tris buffer at pH = 7.3, 5 mM $MgCl_2$. COSY and HSQC experiments were performed by using the standard sequences. For the binding experiments, wild type or G13D mutated HRas was dissolved in 500 μL of the same $[D_{11}]$-Tris buffer, containing an amount of GDP equimolar to the protein, and transferred into a 5 mm NMR tube; 50 μL of the ligand solution dissolved in the same buffer were added slowly. Final protein concentration was 50 μM, final ligand concentration was 1 mM.

STD experiments were performed without saturation of the residual HDO signal and with spin-lock to avoid the presence of protein resonances in the spectra. A train of Gaussian-shaped pulses of 50 ms each was employed, with a total saturation time of the protein envelope of 2 s. An off-resonance frequency of δ = 40 ppm and on-resonance frequency δ = −1.5 ppm (protein aliphatic signals region) were applied. Spectra were acquired

with a Varian Mercury 400 MHz instrument and processed using the program Mestre-Nova 9.

2.4 Flexible Docking Algorithm

Docking analyses were performed in Maestro 10.1 suite (Schrödinger) (https://www.schrodinger.com/citations#Maestro). All docking calculations were performed using the Glide software (Glide, version 6.7, Schrödinger, LLC, New York, NY, 2015). The receptor-based molecular docking was carried forward after preparing ligands and proteins as suggested by the developer's protocols. For HRas and KRas, the pockets corresponding to the residues identified by experimental data on HRas were used as the input for grid receptor definition in induced-fit docking (IFD) workflow with flexible ligand option. The protocol generates alternative cmp4 poses not considering clashes with amino acids side-chains, then optimize the structures obtained by allowing the protein to undergo sidechain or backbone movements during the process (Schrödinger Suite 2015-2 Induced Fit Docking protocol; Glide version 6.7, Schrödinger, LLC, New York, NY, 2015; Prime version 4.0, Schrödinger, LLC, New York, NY, 2015). The IFD extended sampling protocol was employed, generating up to 20 poses per ligand on each iteration. The OPLS 2005 force field (Jorgensen et al., 1996) was used for the minimisation stage, in which residues within 10 Å of each ligand pose were optimised. All other parameters were set to their default values. GLIDE molecular docking output GScore (empirical scoring function) is reported, which is calculated by calculating ligand–protein interaction energies, root mean square deviation (RMSD), hydrogen bonds, hydrophobic interactions, internal energy, π–π stacking interactions, and desolvation. GLIDE Emodel was used to choose the best pose for the ligand in each structure, while IFD Score is based on the Prime calculation of energy content of the structure, and also considers the strain in the receptor and ligands.

2.5 Dissociation and Exchange Reactions

Intrinsic and GEF-mediated dissociation and exchange of mant-guanine nucleotides (mant-GXP, GXP being GDP or GTP; Molecular Probes; Invitrogen) assays were performed essentially as described in (Lenzen et al., 1995; Sacco et al., 2012b). Briefly, for dissociation reactions HRas protein was pre-loaded with mant-GXP by incubating for 30 min 250 μM HRas with 750 μM mant-GXP in 40 mM Hepes pH 7.5, 1 mM $MgCl_2$, 2.5 mM DTE, 20 mM EDTA. Then 30 mM $MgCl_2$ was added and the solution was incubated for further 30 min. Free nucleotides were removed by gel filtration using PD10 desalting columns (Amersham Bioscience) equilibrated with Lenzen buffer (40 mM Hepes, pH 7.5, 5 mM DTE, 10 mM $MgCl_2$), and HRas-mant-GXP complex was concentered using centricon 10 KDa (Merck Millipore). The exchange reactions on Ras protein were performed by adding directly in an UV-cuvette 0.25 μM HRas-GXP, and an opportune concentration of cmp4 in Lenzen buffer. After 300 seconds of incubation, a 5-fold excess of mant-GXP (1.25 μM) and a specific concentration of the exchange factor (0 or 0.0625 μM as indicated) were added. The fluorescence measurements were carried out at 25°C using a LS45 fluorescence spectrometer (Perkin-Elmer) with an excitation wavelength of 366 nm and emission wavelength of 442 nm. The reactions were monitored for at least 1500 s. The dissociation reactions were performed in a UV-cuvette by adding to 0.25 μM HRas-mant-GXP, preincubated for 300 s with the opportune concentration of cmp4, 200 μM GXP and a specific concentration of the exchange factor (0, 0.0125, 0.025, 0.0416, 0.125 −0.25 μM), as indicated. Exchange data were fitted to a nonlinear "growth-sigmoidal Hill" curve (n = 1), while dissociation data were fitted to an "Exponential decay" curve, using the OriginPro 8.0 software (OriginLab Corporation, MA United States). The initial exchange or dissociation rate for each reaction (initial slope) was determined by computing the first derivative at time zero of the corresponding fitted curves. In the graphs, the maximum value of relative fluorescence (100 on Y-axis) represents the fully loaded Ras status obtained as a start point in dissociation reaction and plateau of an exchange curve obtained in the absence of cmp4.

To measure the affinity for entering nucleotide, a plate-based GDP/GTP titration assay was adapted from the method previously described (Ostrem et al., 2013): 1 μM HRas-mant-GDP complex was added to 96-well black plates in 40 mM Hepes, pH 7.5, 5 mM DTE, 1 mM $MgCl_2$. The fluorescence was measured on a Variant Cary Eclipse fluorescence spectrometer (Agilent), with 360 nm excitation and 440 nm emission, before and after 2 h incubation at 25°C with a 5 mM EDTA solution with different concentrations of GDP or GTP, as indicated.

Results for each nucleotide were fitted to a sigmoidal curve using the OriginPro 8.0 software.

2.6 Surface Plasmon Resonance Analysis and G-LISA

Surface Plasmon Resonance experiments were carried out by using a BIAcoreX system (BIAcore, GEHealthcare). His-tagged HRas-GDP was immobilized onto a NTA-sensor chip surface (carboxymethylated dextran matrix pre-immobilized with NTA; BIAcore, GEHealthcare), obtaining a surface density of about 4500 resonance units. No nickel solution was injected over the reference cell. The binding with GST-fused RasGRF1 was monitored in real time in the presence of increasing concentrations of cmp4 (0-500 μM). All experiments were performed in HBS-P+ buffer (BIAcore, GE Healthcare) at a flow rate of 10 μL/min. Surface regeneration was accomplished by injecting EDTA (350 mM) in the flowing buffer (30 s contact) two or three times. The evaluation of binding kinetics was performed by using the Biaevaluation software, v. 3.0 (BIAore) and by considering a 1:1 Langmuir interaction. Notably, the value of k_{off} measured in the SPR experiments cannot correspond to the physiological dissociation constants because the absence of free nucleotide in the experiments substantially affects this parameter.

Ras G-LISA Activation assay kit (Cytoskeleton, Inc. BK131) was used to measure the levels of HRas-GTP bound to the Ras binding domain of Raf1 (RBD-Raf1) in the presence of increasing concentrations of cmp4 (range 0.08-500 μM). HRas-GTP 0.4 nM was preincubated in batch with cmp4 for 5 min at RT and then transferred in 96-well coated with RBD-Raf1. After incubation at

4°C for 30 min, the plate was washed three times with washing buffer before the addition of antigen-presenting buffer. The captured HRas-GTP was incubated with the anti-Ras antibody followed by HRP-conjugated secondary antibody. Ras activity was quantified by measuring absorbance at 490 nm.

2.7 Cell Lines and Proliferation Assay

Human breast cancer cell line MDA-MB-231, obtained from the American Type Culture Collection, was routinely grown at 37°C in a humidified atmosphere of 5% CO_2 in Dulbecco's modified Eagle's medium (D-MEM) (Sigma D6429) supplemented with 10% Newborn Calf Serum (NCS), 2 mM glutamine, 100 units/ml penicillin and 100 mg/ml streptomycin. Human colon adenocarcinoma cell line SW48 ($KRAS^{WT/WT}$) and the isogenic SW48 expressing heterozygous $KRas^{G13D}$ ($KRAS^{WT/G13D}$) or $KRas^{G12V}$ ($KRAS^{WT/G12V}$) were obtained from Horizon Discovery Ltd. Cells were cultured in humidified atmosphere of 5% CO_2 at 37°C in RPMI 1640 (Sigma R0883) supplemented with 10% Fetal Bovine Serum, 2 mM glutamine, 100 units/ml penicillin and 100 mg/ml streptomycin. Cells were passaged using trypsin–EDTA.

For growth kinetics and RealTime-Glo™ MT Cell Viability Assay (Promega, #G9713) cells were plated into respectively 6-well or 96-well flat-bottomed culture plates at the density of 3000 cells/cm^2. At 18h after seeding, predetermined concentrations of cmp4 (or water) were added to the cell culture. After 24, 48, and 72 h from treatment, cells were harvested and counted by Coulter Counter to obtain growth curves or treated with 500 X NanoLuciferase and 500 X MT cell viability substrate. The luminescence at different time points after treatment was recorded by using a Victor Multilabel Plate Reader (Perkin Elmer). The viability of cells treated with increasing concentrations of cmp4 was tested relative to the viability of the same cells treated with vehicle (water). Viability results were analyzed by using OriginPro 8.0 software and a nonlinear growth/sigmoidal Hill curve ($n = 1$) to calculate the relative IC50 values.

2.8 MAPK Activity

Breast cancer MDA-MB231 were plated (6000 cells/cm^2) in 60-mm tissue culture dishes. After 18 h different concentrations of cmp4 (or vehicle) were added to the cell culture. After 48 h from treatment, both plate-adherent and in suspension cells were harvested in lysis buffer from PathSscan Sandwich ELISA kit (Cell Signaling). The detection of endogenous levels of Phospho-p44/42 MAPK was performed according to manufacturer's instructions, and the results were normalized on total protein content measured by Bradford analysis.

2.9 Mathematical Model

The computational analysis was performed starting from the mechanistic model presented in McFall et al. (2019), where a system of Ordinary Differential Equations (ODEs) is introduced to describe the Ras signaling network. The system of ODEs corresponds to the reactions reported in **Supplementary Table S1**, where reactions R_1-R_8 follow the mass-action kinetics, while reactions R_9, R_{10}, R_{11} follow the Michaelis-Menten kinetics; reaction R_9 describes the GAP activity, while reactions R_{10} and R_{11} describe the GEF activity. The 11 reactions can be used to simulate both the wild type and mutant proteins by assuming different values of the kinetic parameters. In particular, the kinetic parameters of Ras^{G13D} and Ras^{G12V} mutants were obtained by scaling the wild type parameters (4th column) according to the corresponding alpha factors reported in the 5th and 6th columns of **Supplementary Table S2**. The scaling factors of Ras^{G13D}, related to reaction R_9, were modified according to the results presented in (Johnson et al., 2019).

Specifically, the computational investigation presented in this work was performed with COPASI (Hoops et al., 2006) (version 4.27), exploiting the LSODA numerical integrator (Petzold, 1983). LSODA is an efficient simulation algorithm capable of dealing with stiff systems by automatically switching between explicit (the Adams' method) and implicit integration methods (backward differentiation formulae). The accuracy in the description of the solution of the system of ODEs is controlled by the relative tolerance, that is the maximum error allowed in the solution, and absolute tolerance, which is the maximum error allowed in case the solution approaches zero. In the simulations performed here, we considered the following setting: relative tolerance 1e-6, absolute tolerance 1e-12, maximum number of steps executed to generate the solution, at each iteration, 1e5. COPASI was also exploited to perform a parameter sweep analysis (PSA) to investigate the effect of the parameter variations on the emergent dynamics and on the steady-state values of pivotal components of the model. The simulations concerning the PSA have been run by generating a set of different initial conditions for the model, considering a fixed range of variation of the parameter under investigation, and then executing the corresponding simulations with LSODA. In particular, the PSA was performed by varying a single kinetic parameter, considering a logarithmic sampling of values within the specified range. The responsiveness of the Ras^{G13D} mutant variant to GEF activity was analyzed by performing a PSA where the V_{max} of GEF-mediated exchange reactions (R_{10} and R_{11}) was multiplied for a parameter gamma, which varied in the range 0-1, where the top value represents the maximal activation of the GEF and the lower value represents the loss of GEF function. The basal level of unstimulated GEF activity is set as corresponding to a gamma value of 0.1.

The effect of different concentrations of Cetuximab and cmp4 was simulated by perturbing the reference parameterization (4th column of **Supplementary Table S2**) of the model as reported in **Supplementary Table S1**. In detail, the maximal action that could be obtained by an inhibitor acting by rescuing EGFR hyperactivation was simulated by dividing $K_{M,10}$ and $K_{M,11}$ by 10. The effectiveness of Cetuximab-like inhibitors was analyzed by a PSA performed by multiplying the V_{max} of GEF-mediated exchange reactions (R_{10} and R_{11}) for a parameter gamma. This parameter was varied in the range 0-1, where the absence of EGFR stimulation is represented by a 0.1 value. cmp4 (at 100 μM) expected effect was simulated by multiplying $K_{M,10}$ and $K_{M,11}$ by 0.5, $k_{2\text{-}5}$ by 0.5, and k_6 by 0.23 (yielding a half amount of Ras-GTP-Eff complex formation).

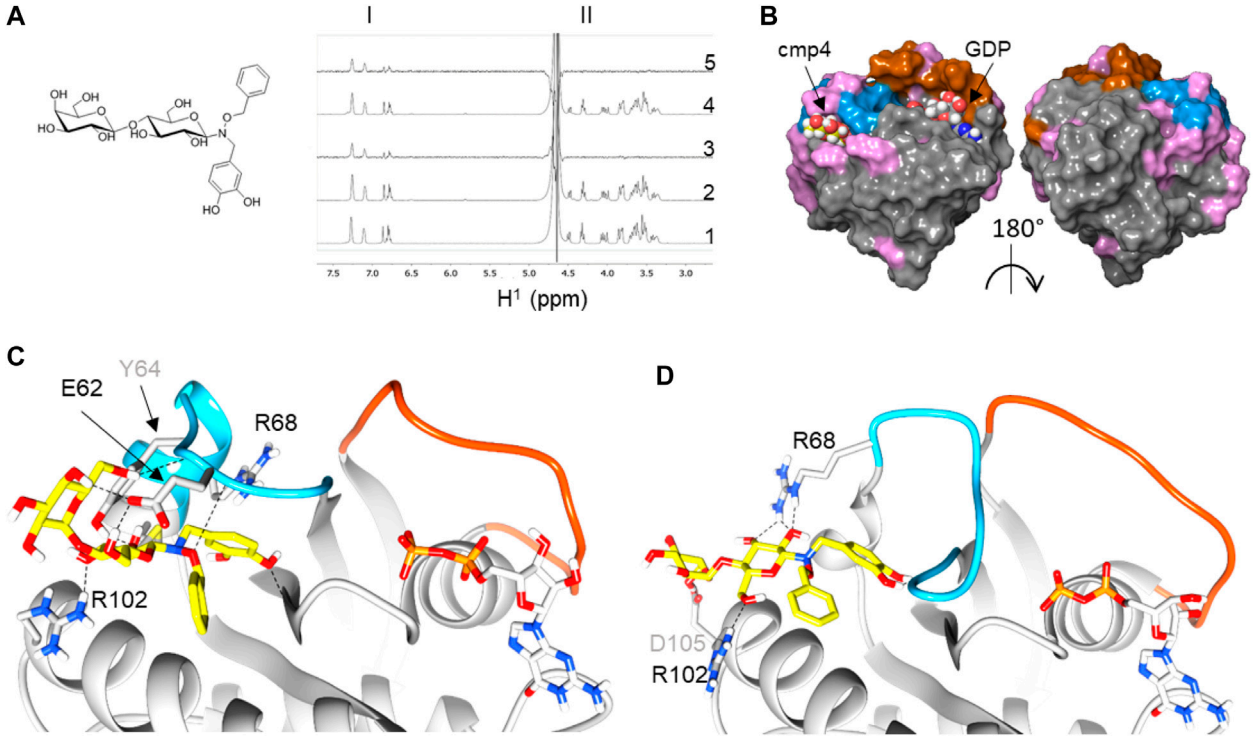

FIGURE 1 | Reconstruction of a binding pose for cmp4 on wild-type and G13D mutated HRas-GDP complexes. **(A)** Chemical structure of cmp4; **(B)** NMR analysis traces report including aromatic resonance (region I), sugar resonance, and aliphatic CH_2 (region II): 1)^{1}H NMR spectrum of 1 mM cmp4; 2) ^{1}H NMR spectrum of a sample containing 1 mM cmp4 and 50 μM HRas-GDP wt; 3) STD-NMR spectrum of a sample containing 1 mM cmp4 and 50 μM HRas-GDP wt; 4) ^{1}H NMR spectrum of a sample containing 1 mM cmp4 and 50 μM HRas^{G13D}-GDP; 5) STD-NMR spectrum of a sample containing 1 mM cmp4 and 50 μM HRas^{G13D}-GDP. **(C)** Docking pose of cmp4 on PDB structure of HRas-GDP (PDB ID: 4q21). The image shows switch I (red), switch II (blue) and displays in pink the residues of Ras that undergo significant chemical shift perturbations after binding with cmp4 (Sacco et al., 2011); **(D,E)** Molecular detail of the selected pose of cmp4 on: **(D)** HRas-GDP (PDB ID: 4q21); **(E)** HRas^{G13D}GDP (PDB ID:6dzh). Ras residues that are directly involved in binding with cmp4 are indicated. The backbone in the Switch I region is colored in red while the backbone in the Switch II region is colored in blue. The GDP nucleotide (grey) and cmp4 (yellow) are drawn in sticks. Heteroatoms are in red (oxygen) and blue (nitrogen).

3 RESULTS

3.1 cmp4 Binds to both GDP-Bound Wild Type and G13D Mutated HRas Proteins

By NMR analysis, we previously showed that cmp4 (**Figure 1A**) binds HRas-GDP (Sacco et al., 2011) and –mainly through its aromatic moiety–in a binding pocket located between the α2-(Switch II) and α3-helices (**Figure 1B**). Flexible docking indicates that cmp4 binds to an extended Switch II pocket (here referred to as SII-EP) of HRas and KRas (**Figures 1C,D**; **Supplementarys S1A,B** and **Table S3**). This pocket partially overlaps with the Switch II groove (SII-G) identified on KRas by structural analysis in Gentile et al. (2017) (**Supplementary Figures S2A,D,G**). Results of an STD-NMR analysis of HRas-GDP with cmp4 (**Figure 1B**) and additional data collected on similar compounds (Palmioli et al., 2009b; Palmioli et al., 2009a; Palmioli et al., 2017; Colombo et al., 2010; Sacco et al., 2011) support the pivotal role of the benzyl group and the pyrocatechol group for Ras binding. We used these results to filter the top 10 poses in this and other docking experiments.

cmp4 is a much bulkier molecule than the compound reported in Gentile et al. (2017) and occupies a larger pocket than the one there described (**Supplementary Figures S2B,E,H**), protruding towards the Gly^{12} P-loop. The cmp4 pyrocatechol group, as obtained in all of the docking best scoring poses, is much farther from this loop than the G12C binding compounds first described to target an allosteric switch II pocket (Ostrem et al., 2013; Patricelli et al., 2016) (**Supplementary Figures S2C,F,I**). Notably, catechol interacts with residues not only in α2-(switch II) (Glu^{62}, Tyr^{64}, Arg^{68}) and α3-helices (Tyr^{96}, Arg^{102}) but also with the backbone of Gly^{10} in the P-loop (see the ligand interactions plot in **Supplementary Figure S1A**).

STD analysis on HRas^{G13D} mutant protein saturated with cmp4 shows that cmp4 also interacts with the mutant protein. Flexible docking indicates that cmp4 maintains a similar positioning within the binding pocket of HRas^{G13D}-GDP, or in KRas^{G13D}-GDP as well, despite the partial switch II unfolding observed in the oncoprotein (**Figures 1E,D**; **Supplementary Figures S1C,D**). The top docking scores were slightly lower than obtained on the wild type proteins (**Supplementary Table S3**).

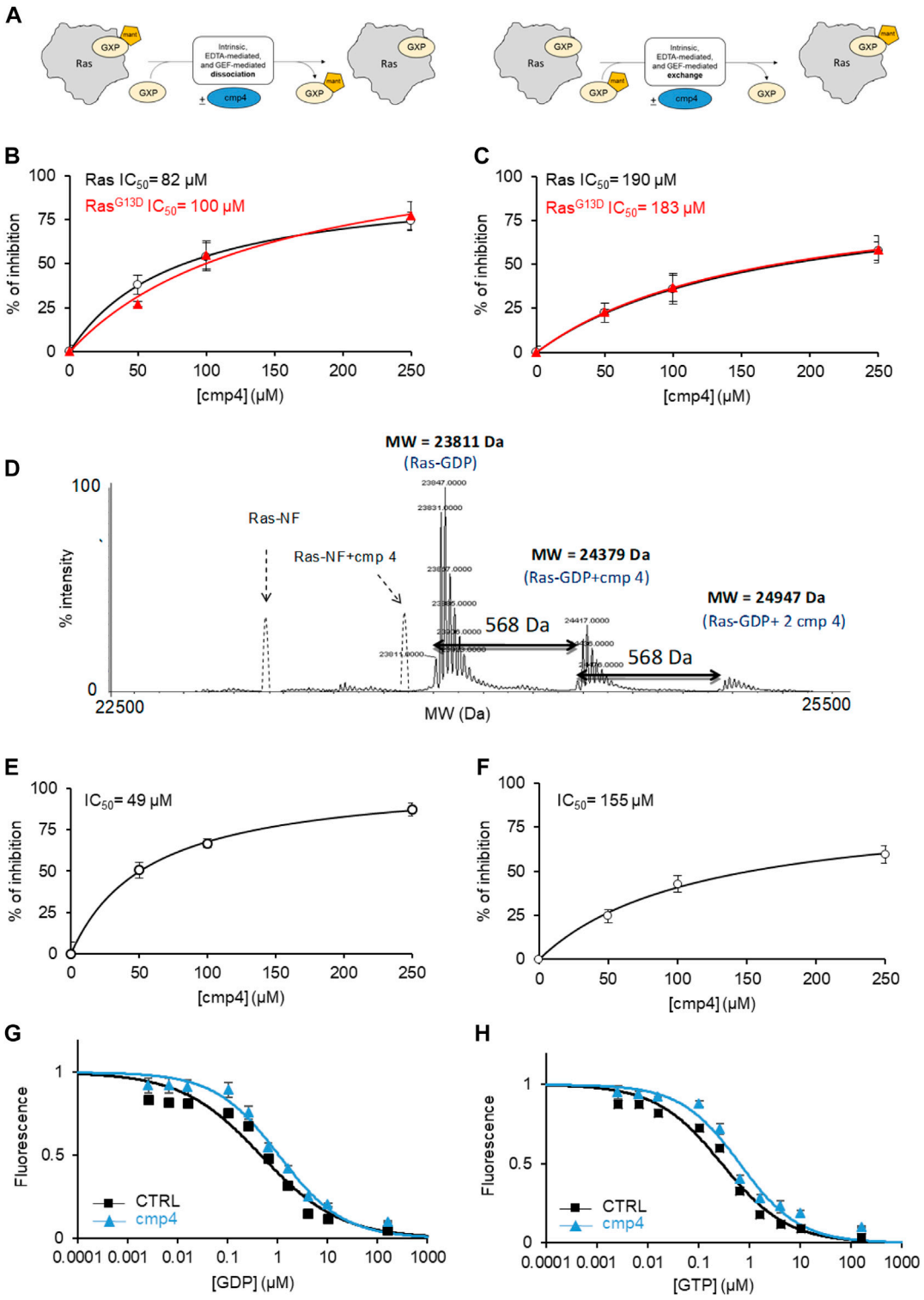

FIGURE 2 | cmp4 counteracts nucleotide dissociation from Ras complex. **(A)** Scheme depicting the different experiments for nucleotide dissociation or exchange, using nucleotides (GDP or GTP, namely GXP) conjugated with the fluorescent moiety MANT; **(B,C)** inhibitory efficacy of cmp4 on GEF-mediated nucleotide dissociation **(B,C)** exchange on HRas (black) and $HRas^{G13D}$ (red). **(D)** Mass spectrometry analysis of HRas-GDP in presence of cmp4. The dashed peaks correspond to the expected positions of the nucleotide free-Ras and Ras complexed with cmp4 without GDP. **(E,F)** Inhibitory efficacy of cmp4 on intrinsic nucleotide dissociation **(E)** and exchange **(F)** on $HRas^{G13D}$; the initial dissociation or exchange rate of each reaction was determined computing the first derivative at time 0 of the fitted curves reported in **Supplementary Figure S4**. **(G,H)** EDTA-mediated competition between mant-GDP loaded on H-Ras and free unlabelled GDP **(G)** or GTP **(H)**.

Since the pathological effect of Ras hyperactivity is due to the active, GTP-bound form, and the phenol-derived compounds occupying the Switch II groove (SII-G), identified by structural analysis in Gentile *et al.* (**Supplementary Figure S1A**), were reported to target Ras active form as well (Gentile et al., 2017), we also assessed whether the SII-EP pocket in GTP-bound HRas and $HRas^{G13D}$. is available to cmp4 interaction. Due to the different conformation of Switch II, this pocket seems to be less available in the GTP-bound complex (**Supplementary Figure S3**), leading to a maximal docking score decreased in comparison to that observed in the GDP-bound form (**Supplementary Table S3**), but still consistent with data previously reported for compounds binding to analogous pockets (Ostrem et al., 2013; Lito et al., 2016; Patricelli et al., 2016).

3.2 cmp4 Inhibits the Intrinsic and GEF Mediated-Nucleotide Dissociation and Exchange on Wild Type and G13D Mutated HRas in a Dose-Dependent Manner

mant-GDP is a nucleotide analog whose fluorescence increases upon Ras binding. The decrease in fluorescence following incubation of the Ras-mant-GDP complex with an excess of unlabeled GTP allows us to follow nucleotide exit (**Figure 2A**, left) The increase in fluorescence obtained after incubation of a Ras-GDP complex with an excess of mant-GDP directly monitors nucleotide entry (**Figure 2A**, right). In the normal Ras activation cycle, the entry of a new nucleotide immediately follows the nucleotide exit.

We previously demonstrated that cmp4 interferes with the function of the exchange factor RasGRF1 on HRas (Sacco et al., 2011). Here we show that cmp4 inhibits the GEF-catalyzed nucleotide dissociation and exchange reaction on wild type and G13D mutated HRas with similar efficiency (**Figures 2B,C**; **Supplementary Table S4**). **Supplementary Figures S4A–D** show the actual dissociation and exchange curves. We used the initial rates of each reaction (mean of at least three independent experiments) for calculating the IC50 reported in **Figures 2B,C** and **Supplementary Table S4**. The inhibitory effect of cmp4 on both dissociation and exchange reactions is independent of the GEF hSos1 vs. RasGRF1, (Sacco et al., 2011) and of the entering nucleotide, GDP or GTP (**Supplementary Figure S5**).

The docking results presented in **Figure 1** suggest that cmp4 may form a stable Ras-nucleotide-cmp4 ternary complex, without promoting dissociation of the Ras-bound nucleotide, similar to peptide Ras inhibitors developed in our laboratory (Sacco et al., 2012b). The deconvoluted mass spectrum of 10 μM HRas-GDP in the presence of a 10-fold excess of cmp4 (**Figure 2D**) shows no signal corresponding to the nucleotide-free Ras/cmp4 complex. Except for a minor fraction of Ras-GDP binding a second inhibitor molecule at a low affinity, non-specific site, the HRas-GDP-cmp4 ternary complex is the most abundant species.

It was therefore of interest to monitor whether cmp4 can inhibit intrinsic (i.e., non GEF-catalyzed) nucleotide dissociation and exchange. We first tested the effect of cmp4 on $HRas^{G13D}$, whose intrinsic nucleotide exchange rate is much higher than that of wild-type HRas (Palmioli et al., 2009b; Smith et al., 2013; Hunter et al., 2015; Johnson et al., 2019). **Supplementary Figures S4E–H** reports the actual dissociation and exchange curves. The inhibitor efficiently reduces the abnormally fast intrinsic nucleotide dissociation and exchange reactions on $HRas^{G13D}$ in a dose-dependent manner (**Figures 2E,F**). The inhibitory effect is also appreciable on the intrinsic activities of wild type HRas, which are very slow *per se* (see the inserts in **Supplementary Figures S4E,G**).

Titration with unlabeled GDP and GTP of a HRas-mant-GDP complex in the presence of EDTA allows monitoring whether a drug alters the affinity for the entering nucleotide. **Figures 2G,H** indicate that cmp4 alters the entry of both nucleotides without discriminating between GDP and GTP, unlike the SII-P binding molecules described by Ostrem et al. (2013).

These results suggest that cmp4 binding to the Switch II extended pocket (SII-EP) counteracts nucleotide release, even in conditions favoring nucleotide release, as observed in $HRas^{G13D}$ (Johnson et al., 2019), and/or in the presence of EDTA or a GEF catalytic domain.

3.3 cmp4 Reduces the Affinity of HRas-GDP for RasGRF1 and Raf1 Ras Binding Domain in a Dose-Dependent Manner

The inhibitory efficiency of cmp4 on the nucleotide dissociation rate on both wild type and G13D mutated HRas decreases with increasing RasGRF1 concentration (**Figure 3A**), suggesting that the GEF could force the nucleotide dissociation even on cmp4-bound Ras, counteracting the inhibitor action. In order to bind the GEF catalytic domain with the highest affinity, HRas has to undergo a conformational change that allows nucleotide release (Boriack-Sjodin et al., 1998), as evidenced by the superposition of HRas structures respectively in GDP-bound and nucleotide-free $Sos1_{cat}$-bound form (**Figure 3B**). Notably, the same kind of interaction is also envisioned for the catalytic domain of RasGRF1, due to homology with Sos1 (Freedman et al., 2006).

SPR binding experiments analyzed the interaction between Ras and GEF in the presence of increasing concentrations of cmp4 (**Figure 3C**). cmp4 affects GEF (RasGRF1) binding to Ras-GDP in a dose-dependent manner, with an estimated EC_{50} of 170 μM. In particular, cmp4 dose-dependently reduces the association rate, and so the k_{on} of the interaction (**Figure 3C**, inset), suggesting that the compound reduces the formation of the Ras/GEF complex, a key intermediate in Ras activation cycle. This finding agrees with the observation that cmp4 stabilizes the nucleotide-bound HRas conformation by bridging Switch I and Switch II (**Figure 1D**). This stabilized connection between Switch I and II would make Ras more refractory to the formation of the high-affinity complex with the GEF and to its catalytic action (Boriack-Sjodin et al., 1998).

The aberrant mitogenic signaling in Ras-driven cancer cells largely depends on the increased recruitment of the downstream effectors Raf1, from the constitutively active Ras oncoproteins (Metcalfe et al., 1993; Warne et al., 1993). Accordingly, molecules disrupting Ras/Raf1 association block KRas downstream signaling and impair Ras-mediated tumorigenic proliferation

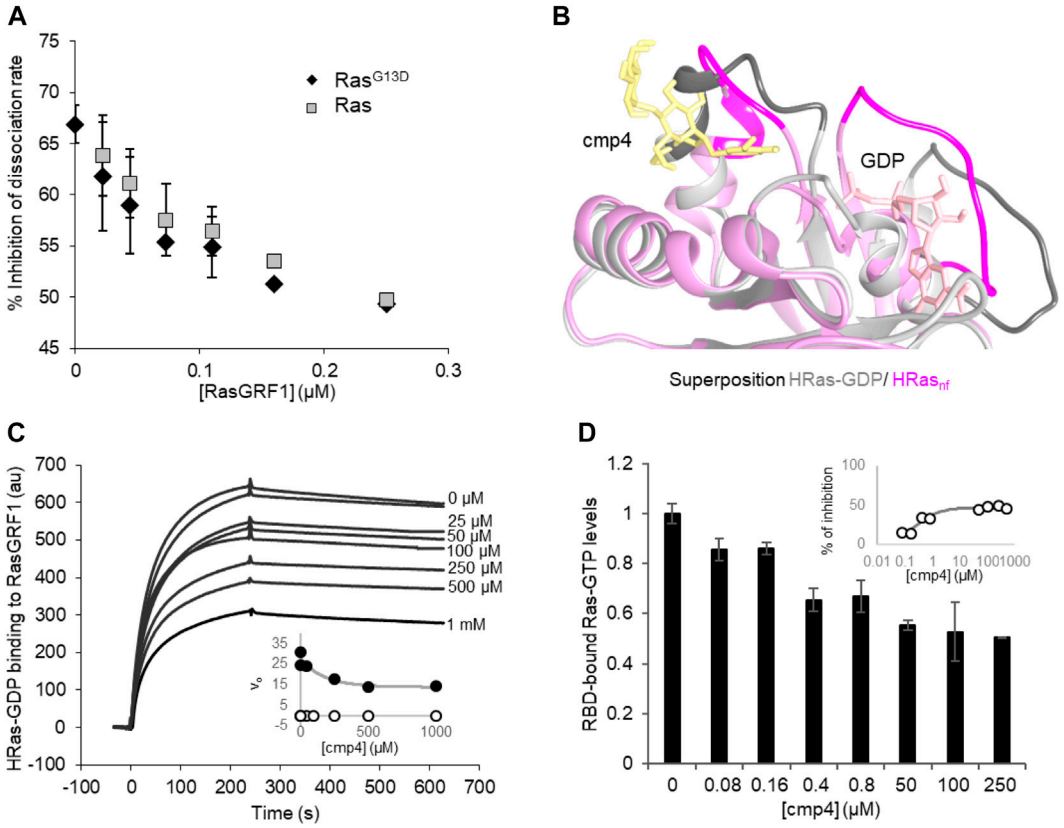

FIGURE 3 | cmp4 affects HRas binding to GEF (RasGRF1) and effector (Raf1-RBD) in a dose-dependent manner. **(A)** Inhibition of nucleotide dissociation rate on both HRas and $HRas^{G13D}$ (1 μM) in the presence of 100 μM cmp4 and increasing concentrations of RasGRF1 (range 0.01–0.25 μM). **(B)** Best fitting pose of cmp4 on HRas-GDP (pink) was superimposed to the structure of nucleotide-free Ras ($HRas_{nf}$, in grey) from the crystal structure of the hSos1 catalytic domain associated with HRas (PDB ID: 1bkd). Switch I and II regions are stained darker. GDP is in pink, cmp4 in yellow; **(C)** Biacore-based direct measurement of 0.5 μM GEF (GST-RasGRF1) binding to His-HRas-GTP in the presence of increasing concentrations of cmp4 (25–1000 μM). In the insert kinetics analysis of RasGRF1 binding to HRas-GDP in the presence of different concentrations of cmp4, relative to SPR curves. All points for initial association rate (v_{on}, closed symbols, v_{off}, open symbols) were fitted respectively to a nonlinear 'growth-sigmoidal Hill' curve (n = 1), which is reported in the graph as a thin line; **(D)** Levels of HRas-GTP bound to a Ras binding domain (RBD) of Raf1 in the presence of increasing concentrations of cmp4 (range 0–500 μM), detected with the G-LISA® kit (Cytoskeleton, Inc. BK131). Data were normalized to Ras-GTP levels measured in the absence of cmp4 (control). All data are significant at 99%, as calculated by Student's t-test in comparison to control. In the inset, the percentage of inhibition of Ras-GTP bound to RBD as a function of cmp4 concentration, relative to the G-LISA experiment. All points were fitted respectively to a nonlinear 'growth-sigmoidal Hill' curve (n = 1).

(Waldmann et al., 2004; Athuluri-Divakar et al., 2016; Trinh et al., 2016; Liu et al., 2017; McGee et al., 2018; Wiechmann et al., 2019). To assess the ability of cmp4 to affect Ras-GTP/Raf1 binding, we performed an ELISA assay with increasing concentrations of cmp4 (from 0 to 500 μM). **Figure 3D** shows that cmp4 reduces in a dose-response manner the amount of Ras-GTP complex bound to the effector Ras binding domain of Raf1 (RBD-Raf1) with an EC_{50} value of about 0.45 μM (IC_{50} about 250 μM, **Figure 3D**, insert).

3.4 cmp4 Reduces Cell Proliferation and MAPK Activation in $KRas^{G13D}$ Expressing Cancer Cells

KRas–the predominantly Ras isoform mutated in cancer–presents a different amino acid in front of the binding pocket (glutamine instead of histidine in position 95) and a more disordered Switch II region even in the active conformation (Johnson et al., 2019) when compared to HRas. Docking poses and their scores (**Supplementarys Figures S1B,D**; **Table S3**) suggest that the pocket in KRas and $KRas^{G13D}$ is equally available for cmp4 binding, consistently with the inhibitory effect exerted by cmp4 on KRas-transformed mouse fibroblasts (Sacco et al., 2011).

Here we evaluated the effect of cmp4 on MDA-MB-231, human breast cancer cells expressing $KRas^{G13D}$. cmp4 reduces the proliferation of MDA-MB-231 cells in a dose-dependent manner (**Figure 4A**, IC_{50} of about 125 μM at 72 h), causing a significant cell detachment (see microscopy images in **Figure 4B**). MTT assays (**Figure 4C**) show that cmp4 significantly affects the viability of MDA-MB-231 cells already after 24 h-treatment. The reduced proliferative potential of cells treated with cmp4 correlates with a dose-dependent decrease of the level of activated/phosphorylated mitogen-activated protein kinases

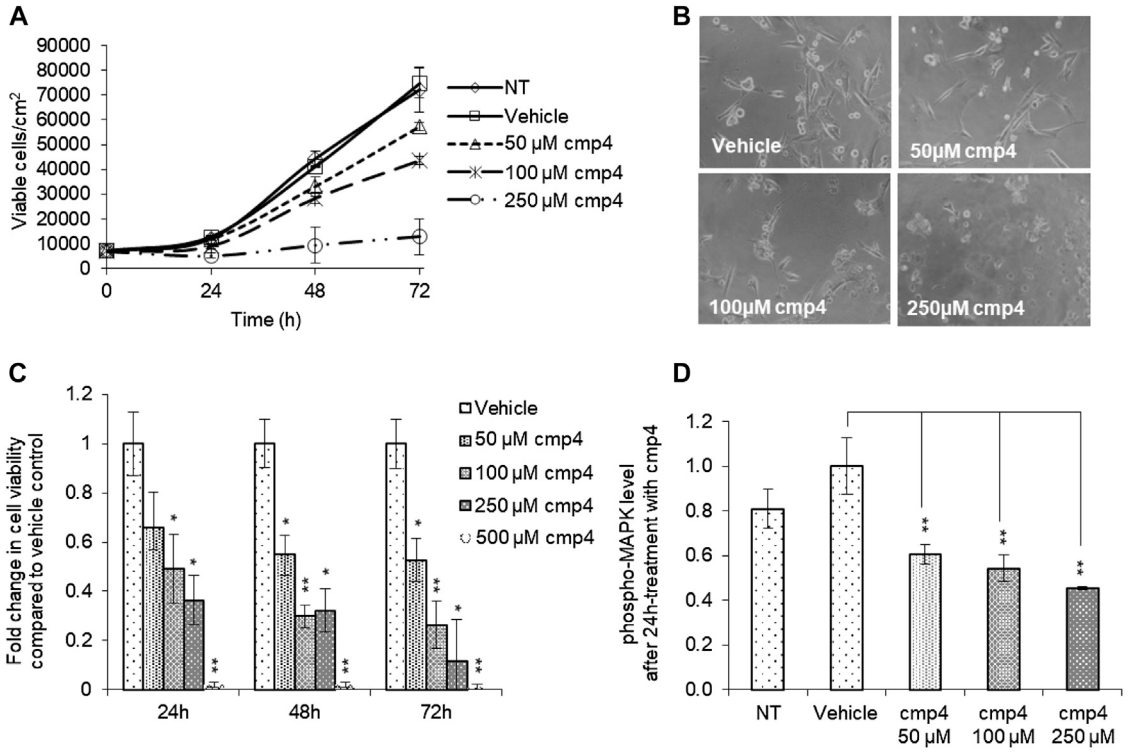

FIGURE 4 | Effect of cmp4 on cell viability and Ras signaling of human breast cancer MDA-MB-231 cell line expressing $KRas^{G13D}$. **(A)** Growth curves of MDA-MB-231 treated with increasing concentration of cmp4 or vehicle (deionized water) supplemented in the growth medium. After 24, 48, and 72 h of treatment cells were trypsinized and counted with a Burker chamber. **(B)** Microscopy analysis of MDA-MB-231 treated for 48 h with different concentrations of cmp4. **(C)** Cell viability of MDA-MB-231 cells treated with increasing concentration of cmp4, or vehicle (deionized water) for 24, 48, and 72 h as measured by MTT assay; data were normalized on cells treated with vehicle imposed as equal to 1. **(D)** Phosphorylated MAPK level in cell lysates from MDA-MB-231 cells no treated or 24 h-treated with cmp4 or vehicle. Data were normalized on the phospho-MAPK level in MDA-MB-231 treated with vehicle imposed as equal to 1. Data shown are mean and standard deviation of two independent experiments, each performed in triplicate. Single and double asterisk above histograms indicates a statistical significance of 95% and 99% respectively, calculated by Student's t-test in comparison to cells treated with vehicle.

(MAPKs), as revealed by an ELISA assay performed on cell lysates collected after 24-h treatment with cmp4 (**Figure 4D**). Since high doses of cmp4 were administered to the cells, due to its low Ras affinity, we cannot exclude that the inhibition of proliferation is ascribable to off-target effects. However, the correlation between MAPK and cellular proliferation is consistent with a predominant specific effect on Ras activity.

3.5 Validation of the Mechanism of Action of cmp4 in Isogenic Cell Lines Expressing Different KRas Oncoproteins

Different Ras mutants produce a spectrum of distinct phenotypic effects and may display a significant difference in their ability to respond to therapies targeting the Ras pathway (Johnson et al., 2019). A recent computational model of the Ras activation cycle allows to explain and reproduce some of these different phenotypic traits, such as the peculiar sensitivity of *KRAS* mutants to Cetuximab, a drug targeting EGFR hyperactivation (McFall et al., 2019). Since results presented above and literature data (Sacco et al., 2011) indicate that cmp4 may interfere with multiple steps of the Ras activation cycle, we decided to use this model together with experiments on isogenic cell lines expressing different Ras mutant proteins to validate the mechanism of action of cmp4.

The model of the Ras activation cycle (**Figure 5A**) consists of 11 reactions (**Supplementary Table S1**). The first 8 reactions follow the mass-action kinetics, with a single kinetic parameter, while reactions R_9, R_{10}, R_{11} follow the Michaelis-Menten kinetics and require two different parameters. Parameter values can be changed to tailor the model to different cell systems. **Supplementary Table S2** reports parameters used in this paper, that have been partially modified compared to McFall et al. (2019), by taking into account recent literature (Johnson et al., 2019; Rabara et al., 2019) and our own data. GEF activation induced by the interaction of a Growth Factor with its cognate receptor (reaction not included in the model) is simulated by an abrupt increase (up to 10-fold) of the V_{max} of the GEF-catalyzed reactions, i.e., $V_{max,10}$ and $V_{max,11}$ (grey arrow pointing to GEF in **Figure 5A**). **Figure 5B** (left panel) reports the results of a simulation of virtual cells in the absence of growth factor stimulation. Starting from nucleotide-free Ras, a rapid

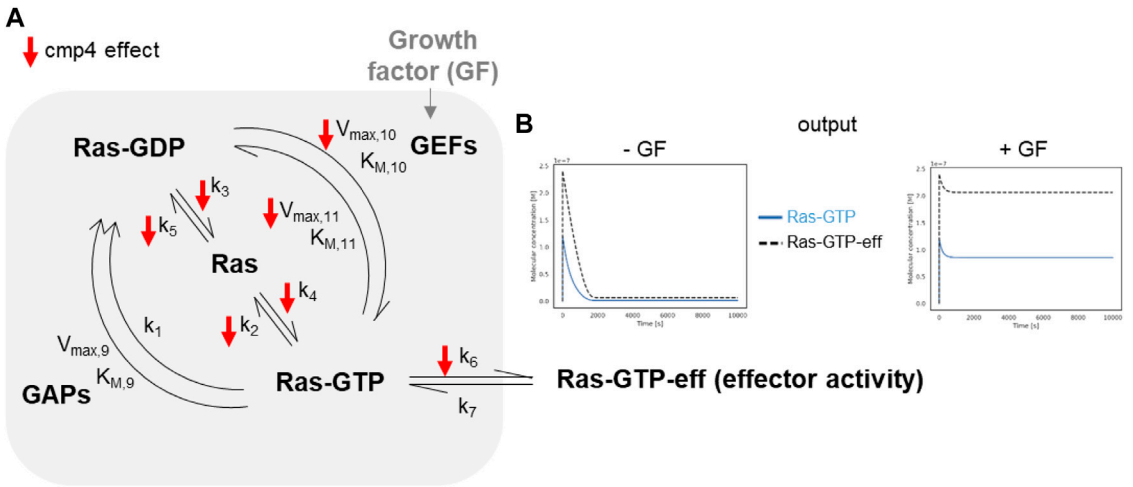

FIGURE 5 | *In silico* modeling of Ras signalling network. **(A)** Scheme depicting the species and the reactions constituting the mathematical model. The parameters affected by cmp4 are indicated by red arrows. **(B)** Example of the output obtained simulating growth factor unstimulated **(left)** and stimulated **(right)** conditions of a wild type system. The level of effector activity, that is the level of the complex Ras-GTP-eff, is evaluated as the steady-state value reached during the dynamic simulation.

association of Ras with the available nucleotides is observed (guided by the fast reactions R_4 and R_5), then the level of Ras-GTP (grey line) and of the Ras-GTP-effector complex (dotted line) reach a steady state over the course of the simulation, characterized by a low level for both the species. When $V_{max,10}$ and $V_{max,11}$ are increased (simulating growth factor stimulation, **Figure 5B** right panel), both Ras-GTP and the Ras-GTP-Effector complex reach a steady-state level that is higher than the basal level observed in the absence of growth factor. In the following, we will use the steady-state level of the Ras-GTP-Effector complex to estimate the proliferation state of the simulated cell lines and to compare simulated and experimental data.

The small red arrows in **Figure 5A** indicate the steps within the Ras activation cycle affected by cmp4. They include the reactions describing the intrinsic association to, and dissociation from, the nucleotide (R_2-R_5), reactions describing association to the effector (R_6), and GEF-mediated reactions allowing nucleotide exchange (R_{10} and R_{11}). To study the effect of cmp4 on the Ras activation cycle we instantiated three different models representing a cell line endowed with a constitutively active EGFR mutant ($EGFR^{G719S}$). This mutant receptor constitutively recruits GEFs to the plasma membrane causing an aberrant Ras activation. We simulated this mutation by imposing the maximal value for $V_{max,10}$ and $V_{max,11}$. The wild type cell line carries two wild type *KRAS* alleles, while two mutant cell lines express $KRas^{G13D}$ and $KRas^{G12V}$ in heterozygosis. Simulation of these virtual cell lines shows that the $KRAS^{WT/G12V}$ heterozygous mutant is the most aggressive based on the level of total KRas-effector complex, followed by the wild type and by the $KRAS^{WT/G13D}$ (**Figures 6A–C**). Although surprising at first sight, this result likely reflects the lower affinity of the $KRas^{G13D}$ mutant protein for Raf1 (Johnson et al., 2019).

As confirmed by our results (**Figure 7A**), the presence of the GAP-insensitive $KRas^{G12V}$ mutant confers resistance to the treatment with Cetuximab (Burgess et al., 2003; Seshacharyulu et al., 2012). Computational results predict that the theoretical maximal effect exerted by Cetuximab (i.e., a complete reversion of GEFs activation) leads to a reduction of virtual proliferation (i.e., a reduction in the level of the Ras-GTP-effector complex) of 95% in the SW48 $KRAS^{WT/WT}$ model, of 87% in the SW48 $KRAS^{WT/G13D}$ model and only of 20% in the SW48 $KRAS^{WT/G12V}$ model (**Figures 6D–F**). These simulation results are consistent with Ras^{G13D} being responsive to GEFs action (Palmioli et al., 2009b; Smith et al., 2013; Johnson et al., 2019) and **Supplementary Figure S4**, whereas $KRas^{G12V}$ is fully active even if GEFs are not activated (**Supplementary Figure S6**).

The potential inhibitory effect of cmp4 was tested on all the models, in the hypothesis that it could behave as a panRas inhibitor. The appropriate constants (**Figure 5A**) were modified with respect to the untreated case, by considering the biochemical effect induced by treatment with 100 μM cmp4 in the appropriate *in vitro* assay (see **Supplementary Table S1** for actual values used in simulation experiments). Both experimental cell viability assays and simulation results indicate that all three virtual cell lines are sensitive to cmp4 (**Figures 6G–I**, **7B**), the SW48 $KRAS^{WT/G12V}$ cell line being the less sensitive (**Supplementary Table S5**).

These results prompted us to test whether the combined use of both drugs could improve the pharmacological treatment of the G12V mutant. Simulation results indicate that the combined treatment is additive or nearly additive in the three cell line models SW48. The effect is striking in the $KRAS^{WT/WT}$ and $KRAS^{WT/G13D}$ models (**Figure 7C**, black and grey bars, respectively), but nevertheless noticeable also in the $KRAS^{WT/G12V}$ model, where complete inhibition of the EGFR

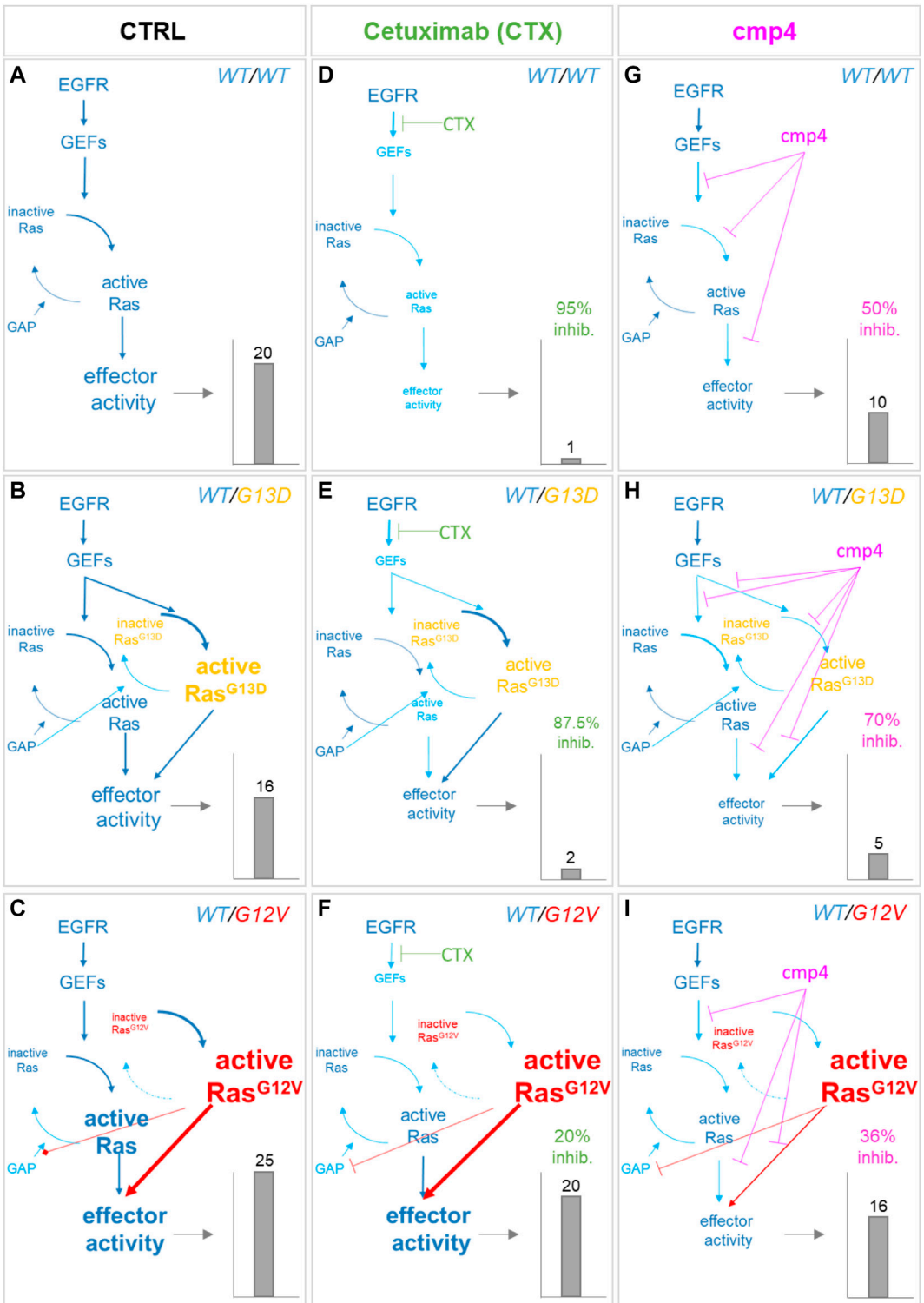

FIGURE 6 | Simulation of the effect of Cetuximab and cmp4 on Ras signaling in human colorectal cancer SW48 isogenic cellular models. **(A–I)** *In silico* modeling of Ras signaling network in SW48 isogenic cellular models, expressing a hyper-activated EGF receptor mutant in combination with different Ras variants: either wild type Ras (**A**,**D**,**G**; SW48 $KRAS^{WT/WT}$) or $KRas^{G13D}$ (**B**,**E**,**H**; SW48 $KRAS^{WT/G13D}$) or $KRas^{G12V}$ (**C**,**F**,**I**; SW48 $KRAS^{WT/G12V}$). The different cellular systems were simulated under untreated condition (**A–C**; CTRL), or treated with the following drugs: Cetuximab **(D–F)**, used at an ideal concentration completely blocking EGFR activity, which represent the maximal effect obtainable with the single mechanism of action based on GEF-mediated nucleotide exchange inhibition; cmp4 **(G–I)**, used at the concentration of 100 μM, which is around IC_{50} for this compound on multilevel mechanisms of action (**Supplementary Table S1**). For each panel, the dimension and

(*Continued*)

FIGURE 6 | colour of the characters are indicative of the level of the components or their activity in the simulation. The resulting effector activity is illustrated as a histogram on the right of each panel, and its fold change normalized on wild type unstimulated cells is reported on top. For panels **(D–I)**, the inhibition efficacy is calculated with respect to the untreated corresponding model.

cascade (i.e., leaving $V_{max,10}$ and $V_{max,11}$ at their basal level) has only a 10% effect on the level of the Ras-GTP-effector complex (**Figure 7C**, white bars). We fully confirmed these simulation results by measuring the inhibition in cell proliferation of the three cell lines treated with a combination of the two drugs (**Supplementary Figure S7**) and in particular with 0.5 nM Cetuximab (CTX), 100 μM, cmp4, or a combination of the two drugs (**Figure 7D**), validating the multi-level mechanism of action of cmp4 suggested by the molecular docking and biochemical assays described above.

4 DISCUSSION

Reported success in the direct targeting of Ras proteins, long postulated as undruggable, has paved the way to the possible pharmacological inhibition of Ras in anti-cancer therapy. Best results, so far, were obtained with mutation-specific inhibitors, such as irreversible inhibitors binding mutant Ras^{G12C} proteins (Ostrem et al., 2013; Lito et al., 2016; Patricelli et al., 2016; Hansen et al., 2018b; Janes et al., 2018). These molecules target the SII-P allosteric cavity in the GDP-bound form and prevent the GEF-mediated nucleotide exchange and, indirectly, effector engagement. Notably, the *in vivo* efficacy of these inhibitors depends on the fact that Ras^{G12C} does not permanently remain in a GTP-bound form, likely because of relevant retained intrinsic GTPase activity (Hunter et al., 2015). Ras oncoproteins with impairment of both intrinsic and GAP-mediated GTP hydrolysis, such as Ras^{G12R}, Ras^{G12V}, and Ras^{QL61} (Hunter et al., 2015), would be refractory to this inhibitory action mechanism. Other promising compounds targeting a cryptic

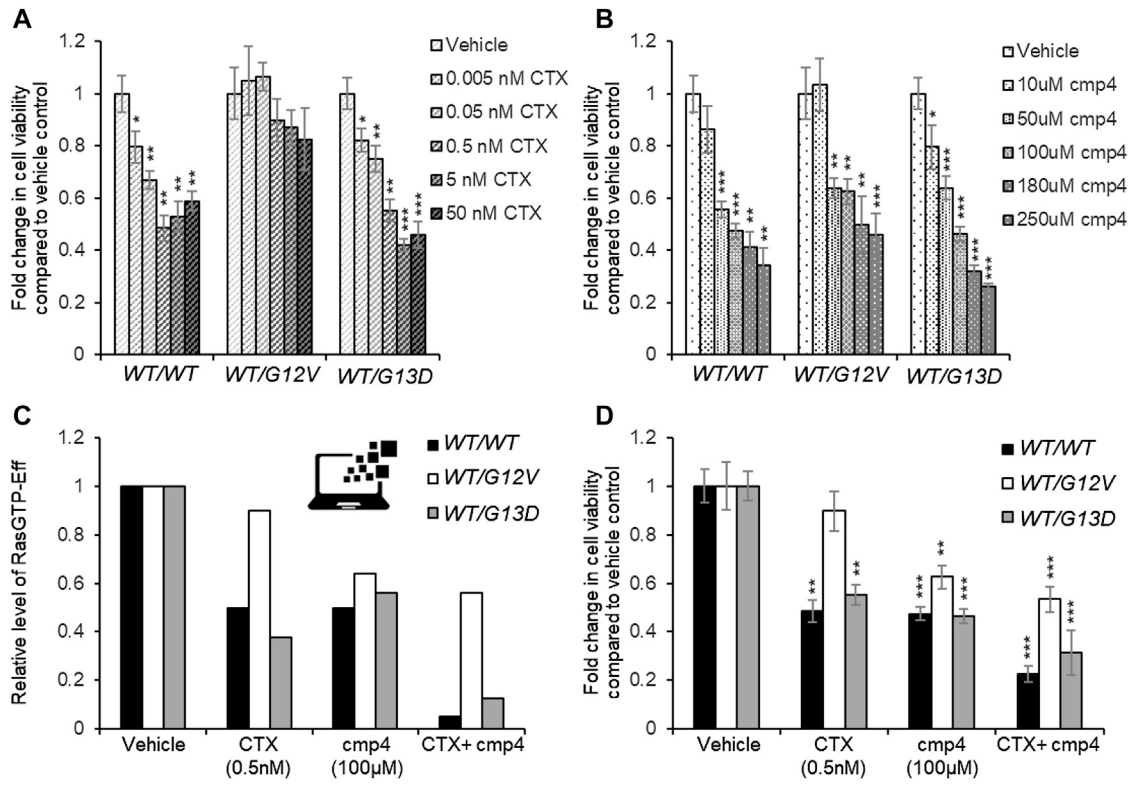

FIGURE 7 | Effect of 72 h-treatment with cmp4 and/or Cetuximab (CTX) on cell viability of human colorectal cancer SW48 isogenic cell lines. **(A–C)** Relative cell viability of SW48 $KRAS^{WT/WT}$, SW48 $KRAS^{WT/G12V}$, and SW48 $KRAS^{WT/G13D}$ cells treated for 72 h with different concentrations of CTX **(A)** or cmp4 **(B)**. **(C)** Results from the simulations of the SW48 $KRAS^{WT/WT}$, SW48 $KRAS^{WT/G12V}$ and SW48 $KRAS^{WT/G13D}$ mathematical models either untreated or treated with the following drugs: 0.5 nM CTX (corresponding to an inhibition of nearly 70% of GEF activity); 100 μM cmp4, which is around IC_{50} for this compound on multilevel mechanisms of action; a combination of both. **(D)** Relative cell viability of SW48 $KRAS^{WT/WT}$, SW48 $KRAS^{WT/G12V}$, and SW48 $KRAS^{WT/G13D}$ cells treated for 72 h either with 0.5 nM CTX, 100 μM cmp4, or a combination of both. Data were normalized on cells treated with vehicle taken equal to 1. Single, double, and triple asterisk above histograms in **(A,B,D)** indicates a statistical significance of 95%, 99%, and 99.9% respectively, calculated by Student's t-test in comparison to cells treated with vehicle.

phenol-capturing groove near SII-P in both GDP- and GTP-bound forms of non-G12C Ras mutants were identified (Gentile et al., 2017). They are reversible inhibitors preventing the GEF-mediated nucleotide exchange and PI3K engagement, but they do not affect the binding to Raf1. These inhibitors seem particularly interesting for targeting the HRas isoform, which is a more potent activator of PI3K than KRas isoform (Yun et al., 1998). Although new powerful approaches for inhibiting Ras signaling in cancer have been recently developed (Gilardi et al., 2020; Shin et al., 2020) the challenge for the identification of inhibitors effective on the non-G12C pathological Ras variants is still open.

Here we show that cmp4 is a water-soluble pan-Ras inhibitor with a complex, multi-level mechanism of action. cmp4 is the product of rational design from a lead compound in which a 3,4-dihydroxyphenyl group (catechol) and a benzyloxy group, are interconnected by a linear linker (Palmioli et al., 2009b). cmp4 targets the SII-G pocket, as the compounds identified by Gentile et al. (2017). Since cmp4 is bulkier, it occupies a more extended region protruding towards the G12(P-)loop, here named SII-EP (**Supplementary Figures S2E,H**). The catechol group of cmp4 can undergo several different interactions with residues not only in α2-(switch II) (such as Glu^{62}, Tyr^{64}, and Arg^{68}) and α3-helices (such as Tyr^{96} and Arg^{102}), but also with the backbone of Gly^{10} in the P-loop (see ligand interactions plot in **Supplementary Figure S1**). Natural compounds containing a pyrocatechol group also target this pocket: 5-O-caffeoylquinic acid (5-CQA) takes contact with HRas-GDP through its aromatic caffeic acid moiety but is less efficient in inhibiting RasGRF1 binding (Palmioli et al., 2017). Although the residues in Switch II are the most affected upon cmp4 binding according to NMR analysis, the residues revealing a change in their chemical environment are more widespread along Ras protein (Sacco et al., 2011) suggesting that the binding of the compound could induce a deeper conformational rearrangement that cannot be reproduced by any docking protocol, in agreement with the effects observed for other compounds binding to this area (Ostrem et al., 2013; Gentile et al., 2017).

Treatment with cmp4 prevents intrinsic and GEF-mediated nucleotide exchange, both in wild type and in the G13D-mutated Ras protein, which is self-sufficient in nucleotide dissociation although remaining sensitive to GEF catalytic activity. In addition, cmp4 reduces Ras/Raf1 binding. This effect suggests that cmp4 is able to accommodate in the Switch II pocket of GTP-bound Ras proteins, either interfering with the hydrogen bonds network involved in stabilizing the State 2 Switch I conformation, required for Raf1 binding (Buhrman et al., 2007), or at least destabilizing the ordered Switch II conformation (R state) which allows high-affinity binding to Raf1. A more disordered T State is indeed adopted whenever α3 helix is shifted towards Switch II (Johnson et al., 2019). The presence of cmp4 in the SII-EP site could counteract the shift to the R state, which is characterized by a narrower pocket (Buhrman et al., 2010).

Simulation of the multi-level action mechanism of cmp4 in a computational model describing the Ras activation cycle in conditions designed to represent cells with a constitutively active EGF Receptor, suggests that the compound can work on different Ras oncoproteins, including $KRas^{G13D}$ and $KRas^{G12V}$. cmp4 effectively cooperates with compounds blocking the Ras signaling cascade at the level of the EGF Receptor, such as Cetuximab. A near additive effect is observed even in the presence of the Ras^{G12V} mutant that makes virtual and real cells insensitive to the inhibition of GEF activity resulting from treatments with Cetuximab. *In vitro* growth inhibition induced by cmp4 and Cetuximab (administered individually or in combination) on isogenic SW48-derived cell lines expressing different Ras mutant proteins fully confirm the simulation results.

5 CONCLUSION

With its multi-level mechanism of action that is only minimally superimposed with that of Cetuximab, cmp4 is a good candidate for medicinal chemistry efforts tailored at improving its currently unsatisfactory affinity for Ras proteins.

As a pan-Ras inhibitor, cmp4 is able to inhibit not only Ras oncoproteins but also the wild type variant when activated in a stimulus-dependent way. This would allow cmp4-based drugs to be effectively used in combination therapies with Cetuximab to reduce the proliferation of tumor cells expressing the constitutively activated RTK receptor, but also suggests certain cytotoxicity on proliferating cells in general, given that proliferation in mammalian cells is essentially promoted by Ras signaling. A low affinity is desired when dealing with treatments affecting wild-type Ras, in order to avoid general toxicity to non-proliferating cells, although the affinity of cmp4 still needs some improvement for this aim. It is noteworthy that the development of drugs specific for a pathogenic Ras variant could be achieved by adding chemical groups that can efficiently interact with the variant molecular features, such as the glutamate residue present in G12D or G13D KRas mutants, gaining in specificity and affinity for the targeted oncoprotein and allowing the administration of lower doses, ineffective on wild-type Ras proteins.

DATA AVAILABILITY STATEMENT

The raw data supporting the conclusions of this article will be made available by the authors, without undue reservation.

AUTHOR CONTRIBUTIONS

RT, SA, and LG planned, performed, and discussed molecular docking experiments; MS, EM, and ES performed and discussed laboratory experiments (biochemistry and cell biology); PC, DB, MN, and RT planned, performed, and discussed simulation experiments, PC wrote the first draft of simulation methods and results; AP, CA, and FP planned, performed and

discussed organic chemistry and NMR experiments; RG planned, performed and discussed MS experiments; MV and ES conceived the experimental plan, discussed all results and figures. RT, MV, and ES wrote the paper.

FUNDING

This work was supported by funds from the Italian Ministry of University and Research (MIUR) through grants "Research facilitation fund (Fondo per le Agevolazioni alla Ricerca–FAR)" to ES and MV, and "Dipartimenti di Eccellenza 2017" to University of Milano Bicocca.

ACKNOWLEDGMENTS

The authors would like to thank Annalisa D'Urzo to have implemented a preliminary version of the Ras-cycle mathematical model.

SUPPLEMENTARY MATERIAL

The Supplementary Material for this article can be found online at: https://www.frontiersin.org/articles/10.3389/fmolb.2021.625979/full#supplementary-material.

REFERENCES

Athuluri-Divakar, S. K., Vasquez-Del Carpio, R., Dutta, K., Baker, S. J., Cosenza, S. C., Basu, I., et al. (2016). Divakar 2016 cell small molecule RAS-mimetic disrupts RAS association with effector proteins to block signaling. *Cell* 165, 643–655. doi:10.1016/j.cell.2016.03.045

Boriack-Sjodin, P. A., Margarit, S. M., Bar-Sagi, D., and Kuriyan, J. (1998). The structural basis of the activation of Ras by Sos. *Nature* 394, 337–343. doi:10.1038/28548

Bos, J. L., Rehmann, H., and Wittinghofer, A. (2007). GEFs and GAPs: critical elements in the control of small G proteins. *Cell* 129, 865–877. doi:10.1016/j.cell.2007.05.018

Buhrman, G., Holzapfel, G., Fetics, S., and Mattos, C. (2010). Allosteric modulation of Ras positions Q61 for a direct role in catalysis. *Proc. Natl. Acad. Sci. U.S.A* 107, 4931–4936. doi:10.1073/pnas.0912226107

Buhrman, G., Wink, G., and Mattos, C. (2007). Article transformation efficiency of RasQ61 mutants linked to structural features of the switch regions in the presence of Raf. *Structure*. 15, 1618–1629. doi:10.1016/j.str.2007.10.011

Burgess, A. W., Cho, H. S., Eigenbrot, C., Ferguson, K. M., Garrett, T. P. J., Leahy, D. J., et al. (2003). An open-and-shut case? recent insights into the activation of EGF/ErbB receptors. *Mol. Cell* 12, 541–552. doi:10.1016/S1097-2765(03)00350-2

Canon, J., Rex, K., Saiki, A. Y., Mohr, C., Cooke, K., Bagal, D., et al. (2019). The clinical KRAS(G12C) inhibitor AMG 510 drives anti-tumour immunity. *Nature* 575, 217–223. doi:10.1038/s41586-019-1694-1

Colombo, S., Palmioli, A., Airoldi, C., Tisi, R., Fantinato, S., Olivieri, S., et al. (2010). Structure-activity studies on arylamides and arysulfonamides Ras inhibitors. *Curr. Cancer Drug Targets* 10, 192–199. doi:10.2174/156800910791054185

Freedman, T. S., Sondermann, H., Friedland, G. D., Kortemme, T., Bar-Sagi, D., Marqusee, S., et al. (2006). A Ras-induced conformational switch in the Ras activator Son of sevenless. *Proc. Natl. Acad. Sci. U.S.A.* 103, 16692–16697. doi:10.1073/pnas.0608127103

Gentile, D. R., Rathinaswamy, M. K., Jenkins, M. L., Moss, S. M., Siempelkamp, B. D., Renslo, A. R., et al. (2017). Ras binder induces a modified switch-II pocket in GTP and GDP states. *Cell Chem. Biol.* 24, 1455–1466.e14. doi:10.1016/j.chembiol.2017.08.025

Gilardi, M., Wang, Z., Proietto, M., Chilla, A., Calleja-Valera, J., Goto, Y., et al. (2020). Tipifarnib as a precision therapy for HRAS-mutant head and neck squamous cell carcinomas. *Mol. Cancer Ther*. 19, 1784–1796. doi:10.1158/1535-7163.MCT-19-0958

Gorfe, A. A., and Cho, K. J. (2021). Approaches to inhibiting oncogenic K-Ras. *Small GTPases*, 1–10. doi:10.1080/21541248.2019.1655883

Hallin, J., Engstrom, L. D., Hargi, L., Calinisan, A., Aranda, R., Briere, D. M., et al. (2020). The KRASG12C inhibitor MRTX849 provides insight toward therapeutic susceptibility of KRAS-mutant cancers in mouse models and patients. *Cancer Discov.* 10, 54–71. doi:10.1158/2159-8290.CD-19-1167

Hansen, R., Peters, U., Babbar, A., Chen, Y., Feng, J., Janes, M. R., et al. (2018a). The reactivity-driven biochemical mechanism of covalent KRASG12C inhibitors. *Nat. Struct. Mol. Biol.* 25, 454–462. doi:10.1038/s41594-018-0061-5

Hansen, R., Peters, U., Babbar, A., Chen, Y., Feng, J., Janes, M. R., et al. (2018b). The reactivity-driven biochemical mechanism of covalent KRASG12C inhibitors. *Nat. Struct. Mol. Biol* 25, 454–462. doi:10.1038/s41594-018-0061-5

Hoops, S., Sahle, S., Gauges, R., Lee, C., Pahle, J., Simus, N., et al. (2006). COPASI–a complex pathway simulator. *Bioinformatics* 22, 3067–3074. doi:10.1093/bioinformatics/btl485

Hunter, J. C., Manandhar, A., Carrasco, M. A., Gurbani, D., Gondi, S., and Westover, K. D. (2015). Biochemical and structural analysis of common cancer-associated KRAS mutations. *Mol. Cancer Res.* 13, 1325–1335. doi:10.1158/1541-7786.MCR-15-0203

Janes, M. R., Zhang, J., Li, L. S., Hansen, R., Peters, U., Guo, X., et al. (2018). Targeting KRAS mutant cancers with a covalent G12C-specific inhibitor. *Cell* 172, 578–589.e17. doi:10.1016/j.cell.2018.01.006

Johnson, C. W., Reid, D., Parker, J. A., Salter, S., Knihtila, R., Kuzmic, P., et al. (2017). The small GTPases K-Ras, N-Ras, and H-Ras have distinct biochemical properties determined by allosteric effects. *J. Biol. Chem.* 292, 12981–12993. doi:10.1074/jbc.M117.778886

Johnson, C. W., Lin, Y.-J., Reid, D., Parker, J., Pavlopoulos, S., Dischinger, P., et al. (2019). Isoform-specific destabilization of the active site reveals a molecular mechanism of intrinsic activation of KRas G13D. *Cell Rep.* 28, 1538–1550.e7. doi:10.1016/j.celrep.2019.07.026

Jorgensen, W. L., Maxwell, D. S., and Tirado-rives, J. (1996). Development and testing of the OPLS all-atom force field on conformational energetics and properties of organic liquids. *J. Am. Chem. Soc.* 7863, 11225–11236. doi:10.1021/ja9621760

Khan, I., Rhett, J. M., and O'Bryan, J. P. (2020). Therapeutic targeting of RAS: new hope for drugging the "undruggable. *Biochim. Biophys. Acta Mol. Cell Res.* 1867, 118570. doi:10.1016/j.bbamcr.2019.118570

Lenzen, C., Cool, R., and Wittinghofer, A. (1995). Analysis of intrinsic and CDC25-stimulated guanine nucleotide exchange of p21ras-nucleotide complexes by fluorescence measurements. *Methods Enzym.* 255, 95–109. doi:10.1016/s0076-6879(95)55012-7

Li, S., Balmain, A., and Counter, C. M. (2018). A model for RAS mutation patterns in cancers: finding the sweet spot. *Nat. Rev. Cancer* 18, 767–777. doi:10.1038/s41568-018-0076-6

Lito, P., Solomon, M., Li, L., Hansen, R., and Rosen, N. (2016). Allele-specific inhibitors inactivate mutant KRAS G12C by a trapping mechanism. *Science* 351, 604–608. doi:10.1126/science.aad6204

Liu, L. J., Wang, W., Huang, S. Y., Hong, Y., Li, G., Lin, S., et al. (2017). Inhibition of the Ras/Raf interaction and repression of renal cancer xenografts in vivo by an enantiomeric iridium(III) metal-based compound. *Chem. Sci.* 8, 4756–4763. doi:10.1039/c7sc00311k

Lu, S., Jang, H., Muratcioglu, S., Gursoy, A., Keskin, O., Nussinov, R., et al. (2016a). Ras conformational ensembles, allostery, and signaling. *Chem. Rev.* 116, 6607–6665. doi:10.1021/acs.chemrev.5b00542

Lu, S., Jang, H., Nussinov, R., and Zhang, J. (2016b). The structural basis of oncogenic mutations G12, G13, and Q61 in small GTPase K-Ras4B. *Sci. Rep.* 6, 1–15. doi:10.1038/srep21949

McFall, T., Diedrich, J. K., Mengistu, M., Littlechild, S. L., Paskvan, K. V., Sisk-Hackworth, L., et al. (2019). A systems mechanism for KRAS mutant

allele–specific responses to targeted therapy. *Sci. Signal*. 12, eaaw8288. doi:10.1126/scisignal.aaw8288

McGee, J. H., Shim, S. Y., Lee, S. J., Swanson, P. K., Jiang, S. Y., Durney, M. A., et al. (2018). Exceptionally high-affinity Ras binders that remodel its effector domain. *J. Biol. Chem* 293, 3265–3280. doi:10.1074/jbc.M117.816348

Metcalfe, C., Biochem, J., Owens, G. K., Bjorkerud, S., Lyons, R. M., Gentry, L. E., et al. (1993). Complexes of Ras. GTP with Raf-1 and mitogen-activated protein kinase kinase. *Science* 260, 1658–61. doi:10.1126/science.8503013

Ni, D., Li, X., He, X., Zhang, H., Zhang, J., and Lu, S. (2019). Drugging K-RasG12C through covalent inhibitors: mission possible? *Pharmacol. Ther*. 202, 1–17. doi:10.1016/j.pharmthera.2019.06.007

Omerovic, J., Laude, A. J., and Prior, I. A. (2007). Ras proteins: paradigms for compartmentalised and isoform-specific signalling. *Cell. Mol. Life Sci*. 64, 2575–2589. doi:10.1007/s00018-007-7133-8

Ostrem, J. M., Peters, U., Sos, M. L., Wells, J. A., and Shokat, K. M. (2013). K-Ras(G12C) inhibitors allosterically control GTP affinity and effector interactions. *Nature* 503, 548–551. doi:10.1038/nature12796

Palmioli, A., Ciaramelli, C., Tisi, R., Spinelli, M., De Sanctis, G., Sacco, E., et al. (2017). Natural compounds in cancer prevention: effects of coffee extracts and their main polyphenolic component, 5-O-Caffeoylquinic acid, on oncogenic ras proteins. *Chem. Asian J* 12, 2457–2466. doi:10.1002/asia.201700844

Palmioli, A., Sacco, E., Abraham, S., Thomas, C. J., Domizio, A. D, Gioia, L. De, et al. (2009a). First experimental identification of Ras-inhibitor binding interface using a water-soluble Ras ligand. *Bioorganic Med. Chem. Lett*. 19, 4217–4222. doi:10.1016/j.bmcl.2009.05.107

Palmioli, A., Sacco, E., Airoldi, C., Di Nicolantonio, F., D'Urzo, A., Shirasawa, S., et al. (2009b). Selective cytotoxicity of a bicyclic Ras inhibitor in cancer cells expressing K-RasG13D. *Biochem. Biophys. Res. Commun*. 386, 593–597. doi:10.1016/j.bbrc.2009.06.069

Patricelli, M. P., Janes, M. R., Li, L. S., Hansen, R., Peters, U., Kessler, L. V., et al. (2016). Selective inhibition of oncogenic KRAS output with small molecules targeting the inactive state. *Cancer Discov*. 6, 316–329. doi:10.1158/2159-8290.CD-15-1105

Petzold, L. (1983). Automatic selection of methods for solving stiff and nonstiff systems of ordinary differential equations. *SIAM J. Sci. Stat. Comput*. 4, 136–148. doi:10.1137/0904010

Rabara, D., Tran, T. H., Dharmaiah, S., Stephens, R. M., McCormick, F., Simanshu, D. K., et al. (2019). KRAS G13D sensitivity to neurofibromin-mediated GTP hydrolysis. *Proc. Natl. Acad. Sci. U.S.A*. 116, 22122–22131. doi:10.1073/pnas.1908353116

Sacco, E., Abraham, S. J., Palmioli, A., Damore, G., Bargna, A., Mazzoleni, E., et al. (2011). Binding properties and biological characterization of new sugar-derived Ras ligands. *Medchemcomm* 2, 396–401. doi:10.1039/c0md00264j

Sacco, E., Farina, M., Greco, C., Lamperti, S., Busti, S., DeGioia, L., et al. (2012a). Regulation of hSos1 activity is a system-level property generated by its multi-domain structure. *Biotechnol. Adv*. 30, 154–168. doi:10.1016/j.biotechadv.2011.07.017

Sacco, E., Metalli, D., Spinelli, M., Manzoni, R., Samalikova, M., Grandori, R., et al. (2012b). Novel RasGRF1-derived Tat-fused peptides inhibiting Ras-dependent proliferation and migration in mouse and human cancer cells. *Biotechnol. Adv*. 30, 233–243. doi:10.1016/j.biotechadv.2011.05.011

Sacco, E., Spinelli, M., and Vanoni, M. (2012c). Approaches to Ras signaling modulation and treatment of Ras-dependent disorders: a patent review (2007 present). *Expert Opin. Ther. Pat*. 22, 1263), 1287. doi:10.1517/13543776.2012.728586

Scheffzek, K., Ahmadian, M. R., Kabsch, W., Wiesmüller, L., Lautwein, A., Schmitz, F., et al. (1997). The Ras-RasGAP complex: Structural basis for GTPase activation and its loss in oncogenic ras mutants. *Science* 277, 333–338. doi:10.1126/science.277.5324.333

Seshacharyulu, P., Ponnusamy, M. P., Haridas, D., Jain, M., Ganti, A. K., and Batra, S. K. (2012). Targeting the EGFR signaling pathway in cancer therapy. *Expert Opin. Ther. Targets* 16, 15–31. doi:10.1517/14728222.2011.648617

Shin, S. M., Kim, J. S., Park, S. W., Jun, S. Y., Kweon, H. J., Choi, D. K., et al. (2020). Direct targeting of oncogenic RAS mutants with a tumor-specific cytosol-penetrating antibody inhibits RAS mutant–driven tumor growth. *Sci. Adv* 6, eaay2174. doi:10.1126/sciadv.aay2174

Simanshu, D. K., Nissley, D. V., and McCormick, F. (2017). RAS proteins and their regulators in human disease. *Cell* 170, 17–33. doi:10.1016/j.cell.2017.06.009

Smith, M. J., Neel, B. G., and Ikura, M. (2013). NMR-based functional profiling of RASopathies and oncogenic RAS mutations. *Proc. Natl. Acad. Sci. U.S.A*. 110, 4574–4579. doi:10.1073/pnas.1218173110

Spencer-Smith, R., and O'Bryan, J. P. (2019). Direct inhibition of RAS: quest for the holy grail?. *Semin. Cancer Biol*. 54, 138–148. doi:10.1016/j.semcancer.2017.12.005

Stites, E. C., Trampont, P. C., Ma, Z., and Ravichandran, K. S. (2007). Network analysis of oncogenic Ras activation in cancer. *Science* 318, 463–467. doi:10.1126/science.1144642

Tisi, R., Gaponenko, V., Vanoni, M., and Sacco, E. (2020). Natural products attenuating biosynthesis, processing, and activity of ras oncoproteins: state of the art and future perspectives. *Biomolecules* 10, 1535. doi:10.3390/biom10111535

Trinh, T. B., Upadhyaya, P., Qian, Z., and Pei, D. (2016). Discovery of a direct ras inhibitor by screening a combinatorial library of cell-permeable bicyclic peptides. *ACS Comb. Sci*. 18, 75–85. doi:10.1021/acscombsci.5b00164

Waldmann, H., Karaguni, I. M., Carpintero, M., Gourzoulidou, E., Herrmann, C., Brockmann, C., et al. (2004). Sulindac-derived ras pathway inhibitors target the ras-raf interaction and downstream effectors in the ras pathway. *Angew. Chemie Int. Ed*. 43, 454–458. doi:10.1002/anie.200353089

Warne, P. H., Viciana, P. R., and Downward, J. (1993). The amino-terminal region of Raf-1 in vitro. *Nature* 364, 352–355

Welsch, M. E., Kaplan, A., Chambers, J. M., Stokes, M. E., Bos, P. H., Zask, A., et al. (2017). Multivalent small-molecule pan-RAS inhibitors. *Cell* 168, 878–889.e29. doi:10.1016/j.cell.2017.02.006

Wiechmann, S., Maisonneuve, P., Grebbin, B. M., Hoffmeister, M., Kaulich, M., Clevers, H., et al. (2019). Competitive inhibitors of Ras effector binding. bioRxiv:548750.

Yun, C., Yan, I., and Greene, L. A. (1998). Prevention of PC12 cell death by N-acetylcysteine requires activation of the Ras pathway. *J Neurosci*. 18, 4042–4049. doi:10.1523/JNEUROSCI.18-11-04042.1998

Conflict of Interest: The authors declare that the research was conducted in the absence of any commercial or financial relationships that could be construed as a potential conflict of interest.

frontiers in Molecular Biosciences

MINI REVIEW
published: 17 March 2021
doi: 10.3389/fmolb.2021.659861

Palmitoylation as a Key Regulator of Ras Localization and Function

*Carla Busquets-Hernández and Gemma Triola**

Department of Biological Chemistry, Laboratory of Chemical Biology, Institute of Advanced Chemistry of Catalonia (IQAC-CSIC), Barcelona, Spain

Ras proteins require membrane association for proper function. This process is tightly regulated by reversible palmitoylation that controls not only the distribution over different subcellular compartments but also Ras compartmentalization within membrane subdomains. As a result, there is a growing interest in protein palmitoylation and the enzymes that control this process. In this minireview, we discuss how palmitoylation affects the localization and function of Ras proteins. A better understanding of the regulatory mechanism controlling protein lipidation is expected to provide new insights into the functional role of these modifications and may ultimately lead to the development of novel therapeutic approaches.

Keywords: Ras, palmitoylation, acylation, lipid posttranslational modifications, cancer, membrane subdomains, thioesterases

OPEN ACCESS

Edited by:
Piero Crespo, Instituto de Biomedicina y Biotecnología de Cantabria, Consejo Superior de Investigaciones Científicas, Spain

Reviewed by:
David Santamaria, Spanish National Cancer Research Center (CNIO), Spain
Lorena Agudo Ibáñez, Centro de Investigación Biomédica en Red del Cáncer (CIBERONC), Spain

***Correspondence:**
Gemma Triola
gemma.triola@iqac.csic.es

Specialty section:
This article was submitted to Molecular Diagnostics and Therapeutics, a section of the journal Frontiers in Molecular Biosciences

Received: *28 January 2021*
Accepted: *22 February 2021*
Published: *17 March 2021*

Citation:
Busquets-Hernández C and Triola G (2021) Palmitoylation as a Key Regulator of Ras Localization and Function. Front. Mol. Biosci. 8:659861. doi: 10.3389/fmolb.2021.659861

INTRODUCTION

The Ras superfamily of small GTPases comprises more than 150 monomeric G proteins. Their ability to act as molecular switches upon stimulation by upstream signals, alternating between the GTP-bound active state and the inactive GDP-bound form, allows Ras proteins to play a role in a diverse array of biological processes such as cell proliferation, signaling, differentiation and survival (Simanshu et al., 2017). Some of the most prominent members of the Ras superfamily are the four Ras isoforms which are encoded by three different genes: H-Ras, N-Ras and K-Ras that generates two splice variants, K-Ras4A and K-Ras4B. The four isoforms share a highly conserved G domain but mainly differ in the hypervariable region (HVR) which comprises the last 24 amino acids and several posttranslational modifications. Hence, all proteins undergo a three-step maturation pathway at the C-terminus known as CaaX box processing (Lowy and Willumsen, 1989; Ahearn et al., 2012) which includes farnesylation of the cysteine, proteolytic cleavage of the last three amino acids (aaX) (Boyartchuk et al., 1997) and carboxyl methylation (Clarke et al., 1988; Dai et al., 1998). Since the prenyl moiety is essential but not sufficient to mediate the stable membrane association required for proper signaling, all isoforms display additional membrane targeting motifs (Hancock et al., 1990). N-Ras and H-Ras are both palmitoylated at either one or two cysteine residues, respectively. K-Ras4B contains a polybasic stretch of eight lysines and K-Ras4A presents a palmitoylated cysteine and two polybasic regions (**Figure 1A**). As a result of these differences, the four isoforms show distinct subcellular localization and distribution in membrane microdomains, and generate distinct signaling outputs (Rocks et al., 2005). However, other factors can also influence Ras signaling. Thus, apart from the HVR, the G-domain and its modifications (ubiquitination, sumoylation, acetylation, glucosylation and nitrosylation) may also contribute to a particular membrane orientation and isoform specific signaling (Kapoor et al., 2012; Ahearn et al., 2018). In addition, some functional redundancy has been suggested for the different isoforms,

as although only K-Ras is essential for normal mouse embryogenesis, its function can be replaced by H-Ras, however, associated to significant cardiotoxicity (Potenza et al., 2005).

Ras proteins are among the most frequently altered oncogenes in human cancers (Hobbs et al., 2016) and overall, approximately 20% of cancer patients harbor Ras mutations (Prior et al., 2020). Point mutations occur in hotspots codons (mainly 12, 13, and 61) and lead to constitutively active proteins resulting in uncontrolled proliferation. However, the prevalence of each isoform in human cancers is not uniform. K-Ras is by far the most frequently mutated isoform (76%), whereas N-Ras contributes to the 17% of human cancers and H-Ras to the remaining 7%. Furthermore, each isoform is related to different types of cancer. While K-Ras is usually associated to lung, colorectal and pancreatic cancers, N-Ras is more predominant in skin melanomas and H-Ras in bladder carcinomas (Prior et al., 2012).

All the above mentioned factors reveal the increasing complexity of Ras biology. From one side, Ras signaling capacity and functional heterogeneity depends on specific isoforms and mutations. However, the extent to which the lipidation state determines the resident time, the specific subcellular localization or the partition into different membrane subdomains, and by doing so, it enables accessibility to a preferential set of effector proteins, is poorly understood. In this minireview we will discuss how changes in the acylation pattern influence the spatial and functional heterogeneity of Ras proteins.

SUBCELLULAR LOCALIZATION AND FUNCTION

H-Ras and N-Ras

The localization of palmitoylated isoforms is determined by the reversible nature of this modification. Although S-acyl groups of some proteins do not turn over or they do it at a very low rate, some other proteins, such as the Ras isoforms, show a very rapid cycling. Thus, after palmitoylation at the Golgi by palmitoyl acyl transferases (PATs) (Stix et al., 2020), N/H-Ras are transferred to the plasma membrane (PM) via the secretory pathway. In their way to the PM, fully palmitoylated and active H-/N-Ras can also localize at recycling endosomes (Misaki et al., 2010). Next, depalmitoylation is mediated by thioesterases (Won et al., 2018) and occurs everywhere in the cell. Depalmitoylated Ras then traffics back to the Golgi where it can be reacylated (Rocks et al., 2005, 2010; **Figure 1B**). Due to the presence of two fatty acid moieties, depalmitoylation of H-Ras takes longer causing enrichment at the PM, whereas N-Ras, bearing only one palmitate, is predominantly localized at the Golgi. Moreover, the combined action of PATs and thioesterases results in an acylation/deacylation cycle that has a shorter half-life than that of the protein (∼6 min for N-Ras and around 20 min for H-Ras vs. ∼24 h protein half-life) (Magee et al., 1987) and introduces an additional level of regulation in the spatial and temporal modulation of Ras signaling (Rocks et al., 2005, 2010). Interestingly, marked differences can exist in the turnover rates of oncogenic and wild type Ras, despite sharing similar subcellular localizations (Baker et al., 2003).

H-Ras

H-Ras gets palmitoylated by DHHC9/Golga7, a member of the Asp-His-His-Cys (DHHC) family of PATs that comprises 23 different proteins. Additional involvement of DHHC18 has also been suggested (Swarthout et al., 2005; Yokoi et al., 2016). Thioester cleavage was initially proven by APT1 (Duncan and Gilman, 1998), APT2 (Tomatis et al., 2010) and the lysosomal PPT1 (Camp and Hofmann, 1993; Verkruyse and Hofmann, 1996). The interaction of H-Ras with both APT1/2, mainly occurring at the PM, was also confirmed by FRET studies (Pedro et al., 2017). More recently, the involvement of other thioesterases has also been suggested since the disruption of APT1 gene in yeast did not completely abolished H-Ras deacylation (Duncan and Gilman, 2002). ABHD17, a member of the mammalian α,β hydrolase-domain (ABHD) family of serine hydrolases (SH) has been shown to deacylate an overexpressed H-Ras in HEK293T cells, but this effect could not be observed in neurons (Yokoi et al., 2016). As the SH family consists of over 100 members and most of them have not known substrate yet, it can not be discarded that additional thioesterases acting on H-Ras may be identified in the future.

Apart from the enzymes involved in de/acylation, FKBP12 may add an additional layer of regulation by controlling the time of residence of H-Ras at the PM. FKBP12 promotes the *cis/trans* isomerization of the peptidyl-prolyl bond at position 178–179, which facilitates depalmitoylation probably by rendering the thioester bond accessible to membrane associated thioesterases. Interaction of FKBP12 with N-Ras has also been detected, but not with K-Ras (Ahearn et al., 2011).

Some studies have suggested that the individual palmitoyl residues may have different roles. Thus, whereas a C184S mutant was present at both the PM and the Golgi, a C181S mutant was mostly localized at Golgi (Roy et al., 2005a). Moreover, the deacylation rate of the C184S mutant significantly increased upon overexpression of APT2, whereas the rate of the C181S mutant did not change (Pedro et al., 2017). Studies with monopalmitoylated mutants may shed light on the role and substrate specificity of these positions. However, results should be interpreted with caution since singly palmitoylated H-Ras species do not seem to be present in cells (Yokoi et al., 2016).

Because of the continuous cycle of de/acylation, H-Ras populations are present at and signal from both the PM and the Golgi apparatus under steady-state conditions. However, functional Ras can also signal from additional subcellular compartments, such as the Endoplasmic Reticulum (ER) (Chiu et al., 2002; Fehrenbacher et al., 2009) and the differential subcellular localizations contribute to its wide signaling repertoire. Thus, organelle-specific interaction with effectors may be behind the variety of biological responses observed, such as proliferation (Chiu et al., 2002; Arozarena et al., 2004) or apoptosis (Herrero et al., 2016; Casar et al., 2018). Studies with engineered proteins have provided insight into H-Ras biology and its relationship with effector proteins. Hence, an active H-Ras directed to Golgi or ER led to the correlation of signaling outputs with defined subcellular protein pools (Matallanas et al., 2006; Agudo-Ibáñez et al., 2007) and enabled the identification of organelle-specific protein-protein

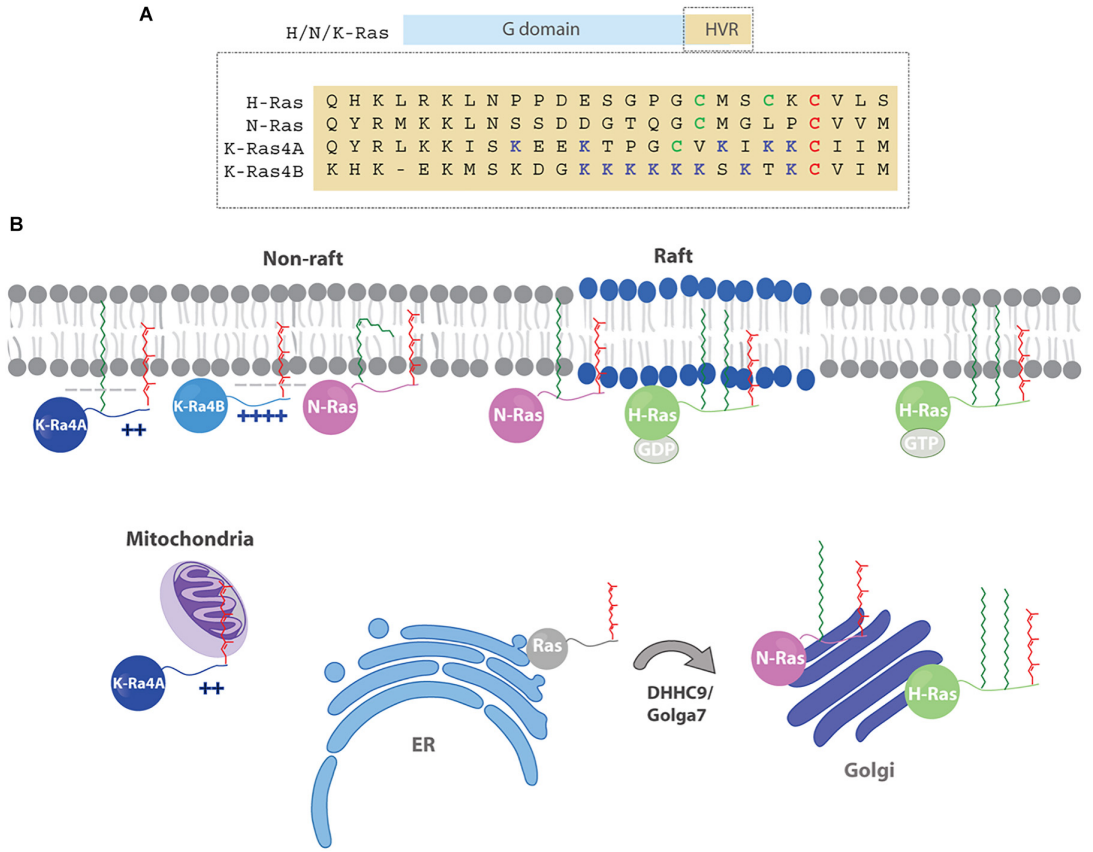

FIGURE 1 | (A) The Ras isoforms contain a highly homologous G domain (90%) and a C-terminal hypervariable region (HVR) that comprises the last 24 amino acids. The HVR exhibit a low degree of homology between isoforms (~ 10%) and present different post-translational lipid modifications. Red cysteines (C) are farnesylated, green cysteines (C) are palmitoylated, blue lysines (K) are polybasic residues. **(B)** Ras membrane distribution is dynamic and depends on membrane targeting motifs (polybasic sequences and lipids) and changes in palmitoylation state that combined, modulate Ras trafficking and localization to specific membranes (PM, endomembranes, subdomains). Hence, farnesylated H/N-Ras get palmitoylated at the Golgi apparatus by DHHC9/Golga7 and then are transferred to the PM via the secretory pathway. After depalmitoylation, H/N-Ras traffic back to the Golgi to be reacylated. Due to the presence of two palmitoyl moieties H-Ras gets enriched in the PM, whereas N-Ras is predominantly localized at the Golgi. Once in the membrane, H-Ras segregates in different microdomains (rafts, non-rafts) in a GDP/GTP dependent manner. Palmitoylated N-Ras associates preferentially with raft/non-raft boundary regions, although a N-Ras protein modified with an unsaturated palmitoleic shows preferential accumulation in fluid domains. The localization of K-Ras4A on the PM relies on the presence of polybasic regions and a palmitoylated cystine, whereas K-Ras4B is palmitoylation independent. After depalmitoylation, K-Ras4A travels to the mitochondria and binds HK1.

interactions (Santra et al., 2019). Specific interactions were also unveiled employing an engineered exchange factor able to activate different subcellular pools of endogenous H-Ras (Herrero et al., 2020). In addition, activation at distinct subcellular sites also provides a temporal control of signaling, that is transient and rapid at the PM but slower and sustained at Golgi.

N-Ras

The singly palmitoylated **N-Ras** is predominantly localized at the Golgi apparatus under steady-state conditions. Palmitoylation of N-Ras is also mediated by DHHC9/Golga7 and, similarly to H-Ras, N-Ras can be depalmitoylated by the broad substrate-tolerant APT1 and APT2 (Rocks et al., 2010; Görmer et al., 2012; Vartak et al., 2014). Depalmitoylated N-Ras is then transported to the Golgi by the chaperone PDE6δ (phosphodiesterase of retinal rod subunit δ) which binds the prenyl group and enhances the cytoplasmic diffusion of the protein. PDE6δ can also transport K-Ras4B (Chen et al., 2010) and facilitates its delivery to membranes (Weise et al., 2012), but has much less effect on H-Ras. The reason behind this selectivity may be the degree of palmitoylation that negatively affects binding with PDE6δ, as only 25% of H-Ras is depalmitoylated at steady-state compared to the 50% of N-Ras (Chandra et al., 2012; Zimmermann et al., 2013). Depletion of PDE6δ or small-molecule based inhibition of Ras-PDE6δ interaction results in Ras mislocalization and consequently, in attenuated signaling (Chandra et al., 2012; Zimmermann et al., 2013).

Because lipidation impairment causes Ras mislocalization, significant efforts have been made to identify thioesterase inhibitors that might be not only interesting for fundamental research but also offer potential applications in drug discovery (**Table 1**). As a result, small-molecule inhibitors of thioesterases have emerged as key players in the study of de/acylation processes. The first potent APT1/2 inhibitors were the β-lactones

TABLE 1 | Enzymes and proteins that have been implicated in Ras metabolism and trafficking.

		Ras isoforms				
	Proteins	**H-Ras**	**N-Ras**	**K-Ras4A**	**K-Ras4B**	**Inhibitors**
PATs	DHHC9/Golga7	■	■			
	DHHC18	■				
Thioesterases	APT1	■	■	■		■
	APT2	■	■			■
	ABHD10			■		
	ABHD17	■	■			■
Deacylase	SIRT2			■		JH-T4
Isomerases	FKBP12	■	■			
Chaperones	PDE6δ	■	■		■	Deltarasin
	VPS35		■			

Known inhibitors targeting these proteins are depicted on the right columns. Selectivity profile of thioesterase inhibitors: red, Palm M; dark blue, ML348, light blue, ML349; purple, ABD957.

Palmostatin B and M that led to impaired localization and signaling of N-Ras and H-Ras (Dekker et al., 2010; Hedberg et al., 2011; Rusch et al., 2011). However, the role of APT1/2 was later questioned, since their overexpression showed little effect on N-Ras localization (Agudo-Ibáñez et al., 2015) and selective inhibitors of APT1 or APT2 could not preserve the palmitoylation state of N-Ras (Adibekian et al., 2010a,b). Currently, there are accumulating evidences indicating that other thioesterases might contribute to the regulation of N-Ras palmitate turnover. Relevant candidates are the three isoforms ABHD17A/B/C, localized to PM and Rab6- and Rab11-positive endosomes and also targeted by Palmostatin M (Lin and Conibear, 2015). Thus, overexpression of ABHD17 redistributed N-Ras from the PM to intracellular membranes and a selective inhibitor of ABHD17, ABD957, has shown to inhibit the growth of cells that depend on N-Ras as an oncogenic driver (Remsberg et al., 2020). However, since ABD957 only partially impairs N-Ras depalmitoylation, additional, yet unknown, thioesterases may not be discarded (Lin and Conibear, 2015). Apart from the *cis/trans* isomerase FKBP12 mentioned above, an additional chaperone protein, VPS35, has also been involved in the regulation of N-Ras subcellular trafficking (Zhou et al., 2016).

K-Ras

The K-Ras gene has two splice variants, K-Ras4A and K-Ras4B, both of them encoding oncogenic proteins when K-Ras is activated by mutation. It has been long considered that K-Ras4A was the minor splice variant and that its contribution to oncogenesis or tumor maintenance was negligible. However, RT-qPCR-based measurements revealed that K-Ras4A accounted for 10–50% of total K-Ras in cell lines derived from colon carcinoma and melanoma, and the relative abundance of K-Ras4A was even higher in primary human tumors (Tsai et al., 2015). All together, these recent advances have renewed the interest in the K-Ras4A isoform as a potential therapeutic target.

The two K-Ras splice variants have distinct mechanism of subcellular trafficking. Both variants require an essential farnesyl moiety, but localization and trafficking of K-Ras4B relies on the presence of polybasic residues that anchor the protein to the inner leaflet of the PM, whereas the membrane-targeting signals in K-Ras4A are two polybasic regions and an additional palmitoyl group, that independently contribute to the PM localization and signal output. Hence, only mutation of either region combined with loss of palmitoylation caused a significant reduction in ERK phosphorylation (Tsai et al., 2015) or abolished the ability to induce leukemia in mice (Zhao et al., 2015). Interestingly, in contrast to K-Ras4B and N-Ras, PDE6δ does not seem to function as a cytosolic chaperone for K-Ras4A (Tsai et al., 2015). K-Ras has also been implicated in the biogenesis of exosomes, tiny extracellular vesicles involved in cell-cell communication that have been also considered potential Ras signaling pathways (Sexton et al., 2019).

Recently, super-resolution immunofluorescence microscopy studies confirmed that the non-palmitoylated form of K-Ras4A also localizes on the outer mitochondrial membrane, where it specifically interacts with Hexokinase 1 (HK1), an enzyme that initiates glucose metabolism. Upon binding, K-Ras4A blocks the allosteric inhibition of HK1 resulting in an enhanced glucose consumption, which might contribute to the metabolic reprogramming of tumor cells aimed to sustain rapid tumor growth (Amendola et al., 2019). The interaction occurs only with the GTP-bound form and it requires the presence of the prenyl moiety but it is negatively regulated by palmitoylation. It is currently unknown which are the enzymes responsible for K-Ras4A de/acylation. However, it has been suggested that palmitoylation may be in charge of a PM-resident enzyme, whereas mitochondrial depalmitoylation could be performed by APT1 or ABHD10 (Cao et al., 2019). In addition, a third lipid modification could act as an additional regulatory mechanism for K-Ras4A. Hence, Lin et al. have shown that K-Ras4A can also be reversibly acylated with palmitic acid at lysine residues located at the HVR (K182/184/185). Lysine acylation occurs on fully lipidated proteins and lipid removal, that promotes its transforming activity, is mediated by Sirtuin 2 (Jing et al., 2017) and inhibited by JH-T4 (Spiegelman et al., 2019) (**Table 1**). Lysine acylation has been also detected on H-Ras (K170) and N-Ras, but these proteins are not substrates of Sirtuin 2. Further work is required to elucidate the role lysine acylation on H-/N-Ras and to identify the enzymes that control this process.

MEMBRANE MICRODOMAIN LOCALIZATION OF RAS PROTEINS

Lipidation not only regulates the subcellular localization of Ras proteins, but also its lateral segregation and distribution between membrane microdomains, which is crucial for efficient signal transmission. Thus, the lateral heterogenous composition of cellular membranes results in the transient formation of distinct subcompartments: packed domains enriched with cholesterol and sphingolipids referred to as lipid ordered (l_o) domains o rafts, and more fluid domains termed liquid disordered (l_d) domains or non-rafts. In this second part, we will give a brief overview on

Ras segregation in membrane subdomains (for a more detailed description see Erwin et al., 2017 and references herein).

Initial studies by Hancock et al. showed that **H-Ras** segregation within membrane microdomains was GDP/GTP-dependent. H-Ras resides in lipid rafts in its inactive form, but the active GTP-bound form as well as the active mutant HRasV12 migrate to l_d membranes (Prior et al., 2001; Rotblat et al., 2004), where they can activate proliferation and differentiation (Herrero et al., 2016; **Figure 1B**). However, GDP/GTP-dependent H-Ras partitioning may also be cell-specific (Agudo-Ibáñez et al., 2015). These different lateral segregations might regulate the biological output of H-Ras by a yet unknown mechanism. Thus, Ras signaling from rafts results in phosphorylation of epidermal growth factor receptor and cytosolic phospholipase A_2, whereas signaling from fluid domains causes activation of kinase suppressor of Ras 1 (Casar et al., 2009). Moreover, H/N-Ras signals from lipid rafts or ER yield big tumors but with a reduced propensity to disseminate, whereas signaling from Golgi and disordered regions displayed higher migration rates (Agudo-Ibáñez et al., 2015; García-Ibáñez et al., 2020).

The effect of lipidation in membrane partitioning and clustering behavior of **N-Ras** has also been widely characterized. Initial studies in homogeneous membranes showed the formation of dimers (Güldenhaupt et al., 2012), that could be an initial step to the formation of small nanoclusters (Erwin et al., 2016). More complex systems gave, however, controversial results. Thus, the first insight into N-Ras microlocalization suggested that N-Ras was mainly found in rafts (Matallanas et al., 2003) at least in its GTP-form (Prior et al., 2001; Roy et al., 2005b).

A major advancement in the field came with the development of semisynthetic methods to obtain fully lipidated Ras proteins in quantities enabling biophysical studies (Triola et al., 2012). Hence, atomic force microscopy studies performed in heterogeneous model membranes revealed that N-Ras partitioning occurs preferentially into l_d domains followed by time-dependent clustering in domain (l_o/l_d) boundaries regions (Weise et al., 2009, 2010). No significant GDP/GTP-dependent partitioning was observed, although the inactive form showed stronger membrane association (Gohlke et al., 2010). Moreover, upon membrane binding, N-Ras showed free rotation of the G-domain, what may facilitate its interaction with effectors (Werkmuller et al., 2013). Accumulation in l_o/l_d phase boundaries could also be observed in viral membrane extracts (Vogel et al., 2009) or using a FRET-based study (Shishina et al., 2018).

Recent breakthroughs have developed more sensitives techniques that revealed that N-Ras S-acylation is not restricted to the saturated palmitate but also includes the unsaturated palmitoleate. Characterization of palmitoleated N-Ras distribution in model membranes indicated a different behavior compared to the saturated N-Ras, showing a rapid membrane insertion and preferentially clustering in the l_d domains. Interestingly, these results suggest that S-acylation with different fatty acids may be an additional regulation point in N-Ras signaling (Schulte-Zweckel et al., 2019). The existence of thioesterases or PATs specifically committed to palmitoleated N-Ras remains elusive (Schulte-Zweckel et al., 2019). However, the fact that the 23 DHHCs have shown marked differences in fatty acid selectivity might suggest some substrate specificity (Greaves et al., 2017).

Currently, there is no information about the lateral segregation behavior of K-Ras4A. On the contrary, the splice variant K-Ras4B is better characterized. Thus, the polybasic **K-Ras 4B** preferentially distributes in l_d domains and spontaneous assembles to form new domains containing proteins and lipids (Weise et al., 2011). The presence of the prenyl group combined with the precise amino acid sequence of the polybasic region define the lipid composition of these nanoclusters (Zhou et al., 2017). The enrichments was independent of GDP/GTP loading but the active form showed bigger clusters (Kapoor et al., 2012). K-Ras4B distribution on the l_d domain was also observed in GUVs made from the envelope membrane of viral lipids (Weise et al., 2011) and protein-containing GPMVs (Erwin et al., 2016). Transport to the membrane is mediated by PDE6δ, whereas phosphorylation at Ser181 facilitates the PM dissociation (Zhang et al., 2017). Extraction from negatively charged membranes can also be performed in a GDP/GTP-independent manner by Calmodulin (Sperlich et al., 2016).

CONCLUSIONS AND PERSPECTIVES

It is becoming clear that the differential spatiotemporal distribution on organelles and subdomains has a key role in regulating the functional versatility of Ras proteins. As reversible lipidation is critical for maintaining the correct localization of H-/N- and probably KRas4A, a better understanding of the mechanism and dynamics by which S-acylation is controlled will provide new insights into the functional role of these modifications. Major outstanding questions still remain unanswered, such as how is the dynamic of lipid turnover regulated, how the presence of saturated or unsaturated fatty acids may influence protein function, which are all the enzymes involved in de/acylation and their selectivity profile or whether changes in the S-acylation (turnover rate, fatty acid identity) are linked with specific disease states. Furthermore, an increase in our knowledge of the mechanism and outcomes of protein S-acylation could lead to the identification of novel therapeutic opportunities.

AUTHOR CONTRIBUTIONS

CB-H wrote the manuscript. GT wrote and revised the manuscript. Both authors contributed to the article and approved the submitted version.

FUNDING

Financial support from the Caixa Foundation under the agreement LCF/PR/HR20/52400006 and the Ministerio de Ciencia e Innocación (RTI2018-096323-b-100) are gratefully acknowledged.

ACKNOWLEDGMENTS

We acknowledge support of the publication fee by the CSIC Open Access Publication Support Initiative through its Unit of Information Resources for Research (URICI). We apologize to all the colleagues whose relevant work could not be cited due to space restrictions.

REFERENCES

Adibekian, A., Martin, B. R., Chang, J. W., Hsu, K. L., Tsuboi, K., Bachovchin, D. A., et al. (2010a). *"Characterization of a Selective, Reversible Inhibitor of Lysophospholipase 1 (LYPLA1)," in Probe Reports from the NIH Molecular Libraries Program*. Bethesda, MD: National Center for Biotechnology Information.

Adibekian, A., Martin, B. R., Chang, J. W., Hsu, K. L., Tsuboi, K., Bachovchin, D. A., et al. (2010b). *"Characterization of a Selective, Reversible Inhibitor of Lysophospholipase 2 (LYPLA2)," in Probe Reports from the NIH Molecular Libraries Program*. Bethesda, MD: National Center for Biotechnology Information.

Agudo-Ibáñez, L., Herrero, A., Barbacid, M., and Crespo, P. (2015). H-Ras distribution and signaling in plasma membrane microdomains are regulated by acylation and deacylation events. *Mol. Cell. Biol.* 35, 1898–1914. doi: 10.1128/mcb.01398-14

Agudo-Ibáñez, L., Núñez, F., Calvo, F., Berenjeno, I. M., Bustelo, X. R., and Crespo, P. (2007). Transcriptomal profiling of site-specific Ras signals. *Cell. Signal.* 19, 2264–2276. doi: 10.1016/j.cellsig.2007.06.025

Ahearn, I., Zhou, M., and Philips, M. R. (2018). Posttranslational modifications of RAS proteins. *Cold Spring Harb. Perspect. Med.* 8:a031484. doi: 10.1101/cshperspect.a031484

Ahearn, I. M., Haigis, K., Bar-Sagi, D., and Philips, M. R. (2012). Regulating the regulator: post-translational modification of RAS. *Nat. Rev. Mol. Cell Biol.* 13, 39–51. doi: 10.1038/nrm3255

Ahearn, I. M., Tsai, F. D., Court, H., Zhou, M., Jennings, B. C., Ahmed, M., et al. (2011). FKBP12 binds to acylated h-ras and promotes depalmitoylation. *Mol. Cell.* 41, 173–185. doi: 10.1016/j.molcel.2011.01.001

Amendola, C. R., Mahaffey, J. P., Parker, S. J., Ahearn, I. M., Chen, W. C., Zhou, M., et al. (2019). KRAS4A directly regulates hexokinase 1. *Nature* 576, 482–486. doi: 10.1038/s41586-019-1832-9

Arozarena, I., Matallanas, D., Berciano, M. T., Sanz-Moreno, V., Calvo, F., Muñoz, M. T., et al. (2004). Activation of H-Ras in the endoplasmic reticulum by the rasGRF family guanine nucleotide exchange factors. *Mol. Cell. Biol.* 24, 1516–1530. doi: 10.1128/mcb.24.4.1516-1530.2004

Baker, T. L., Zheng, H., Walker, J., Coloff, J. L., and Buss, J. E. (2003). Distinct rates of palmitate turnover on membrane-bound cellular and oncogenic H-Ras. *J. Biol. Chem.* 278, 19292–19300. doi: 10.1074/jbc.M206956200

Boyartchuk, V. L., Ashby, M. N., and Rine, J. (1997). Modulation of ras and a-factor function by carboxyl-terminal proteolysis. *Science* 275, 1796–1800.

Camp, L. A., and Hofmann, S. L. (1993). Purication and properties of a palmitoyl-protein thioesterase that cleaves palmitate from H-Ras. *J. Biol. Chem.* 268, 22566–22574.

Cao, Y., Qiu, T., Kathayat, R. S., Azizi, S. A., Thorne, A. K., Ahn, D., et al. (2019). ABHD10 is an S-depalmitoylase affecting redox homeostasis through peroxiredoxin-5. *Nat. Chem. Biol.* 15, 1232–1240. doi: 10.1038/s41589-019-0399-y

Casar, B., Arozarena, I., Sanz-Moreno, V., Pinto, A., Agudo-Ibáñez, L., Marais, R., et al. (2009). Ras subcellular localization defines extracellular signal-regulated kinase 1 and 2 substrate specificity through distinct utilization of scaffold proteins. *Mol. Cell. Biol.* 29, 1338–1353. doi: 10.1128/mcb.01359-08

Casar, B., Badrock, A. P., Jiménez, I., Arozarena, I., Colón-Bolea, P., Lorenzo-Martín, L. F., et al. (2018). RAS at the Golgi antagonizes malignant transformation through PTPRκ-mediated inhibition of ERK activation. *Nat. Commun.* 9:3595. doi: 10.1038/s41467-018-05941-8

Chandra, A., Grecco, H. E., Pisupati, V., Perera, D., Cassidy, L., Skoulidis, F., et al. (2012). The GDI-like solubilizing factor PDEδ sustains the spatial organization and signalling of Ras family proteins. *Nat. Cell Biol.* 14, 148–158. doi: 10.1038/ncb2394

Chen, Y.-X., Koch, S., Uhlenbrock, K., Weise, K., Das, D., Gremer, L., et al. (2010). Synthesis of the Rheb and K-Ras4B GTPases. *Angew. Chemie Int. Ed Engl.* 49, 6090–6095. doi: 10.1002/anie.201001884

Chiu, V. K., Bivona, T., Hach, A., Sajous, J. B., Silletti, J., Wiener, H., et al. (2002). Ras signalling on the endoplasmic reticulum and the Golgi. *Nat. Cell. Biol.* 4, 343–350. doi: 10.1038/ncb783

Clarke, S., Vogel, J. P., Deschenes, R. J., and Stock, J. (1988). Posttranslational modification of the ha-ras oncogene protein: evidence for a third class of protein carboxyl methyltransferases. *Proc. Natl. Acad. Sci. U. S. A.* 85, 4643–4647.

Dai, Q., Choy, E., Chiu, V., Romano, J., Slivka, S. R., Steitz, S. A., et al. (1998). Mammalian prenylcysteine carboxyl methyltransferase is in the endoplasmic reticulum. *J. Biol. Chem.* 273, 15030–15034.

Dekker, F. J., Rocks, O., Vartak, N., Menninger, S., Hedberg, C., Balamurugan, R., et al. (2010). Small-molecule inhibition of APT 1 affects Ras localization and signaling. *Nat. Chem. Biol.* 6, 449–456.

Duncan, J. A., and Gilman, A. G. (1998). A cytoplasmic acyl-protein thioesterase that removes palmitate from G protein α subunits and p21RAS. *J. Biol. Chem.* 273, 15830–15837. doi: 10.1074/jbc.273.25.15830

Duncan, J. A., and Gilman, A. G. (2002). Characterization of Saccharomyces cerevisiae acyl-protein thioesterase 1, the enzyme responsible for G protein alpha subunit deacylation in vivo. *J. Biol. Chem.* 277, 31740–31752. doi: 10.1074/jbc.M202505200

Erwin, N., Patra, S., Dwivedi, M., Weise, K., and Winter, R. (2017). Influence of isoform-specific Ras lipidation motifs on protein partitioning and dynamics in model membrane systems of various complexity. *Biol. Chem.* 398, 547–563. doi: 10.1515/hsz-2016-0289

Erwin, N., Sperlich, B., Garivet, G., Waldmann, H., Weise, K., and Winter, R. (2016). Lipoprotein insertion into membranes of various complexity: Lipid sorting, interfacial adsorption and protein clustering. *Phys. Chem. Chem. Phys.* 18, 8954–8962. doi: 10.1039/c6cp00563b

Fehrenbacher, N., Bar-Sagi, D., and Philips, M. (2009). Ras/MAPK signaling from endomembranes. *Mol. Oncol.* 3, 297–307. doi: 10.1016/j.molonc.2009.06.004

García-Ibáñez, Y., Riesco-Eizaguirre, G., Santisteban, P., Casar, B., and Crespo, P. (2020). RAS subcellular localization inversely regulates thyroid tumor growth and dissemination. *Cancers (Basel).* 12:2588. doi: 10.3390/cancers12092588

Gohlke, A., Triola, G., Waldmann, H., and Winter, R. (2010). Influence of the lipid anchor motif of N-Ras on the interaction with lipid membranes: a surface plasmon resonance study. *Biophys. J.* 98, 2226–2235. doi: 10.1016/j.bpj.2010.02.005

Görmer, K., Bürger, M., Kruijtzer, J. A. W., Vetter, I., Vartak, N., Brunsveld, L., et al. (2012). Chemical-biological exploration of the limits of the ras de- and repalmitoylating machinery. *Chem. BioChem.* 13, 1017–1023. doi: 10.1002/cbic.201200078

Greaves, J., Munro, K. R., Davidson, S. C., Riviere, M., Wojno, J., Smith, T. K., et al. (2017). Molecular basis of fatty acid selectivity in the zDHHC family of S-acyltransferases revealed by click chemistry. *Proc. Natl. Acad. Sci.* 114:201612254. doi: 10.1073/pnas.1612254114

Güldenhaupt, J., Rudack, T., Bachler, P., Mann, D., Triola, G., Waldmann, H., et al. (2012). N-Ras forms dimers at POPC membranes. *Biophys. J.* 103, 1585–1593. doi: 10.1016/j.bpj.2012.08.043

Hancock, J. P., Paterson, H., and Marshall, C. J. (1990). A polybasic domain or palmitoylation is required in addition to the CAAX motif to localize p21ras to the plasma membrane. *Cell* 63, 133–139.

Hedberg, C., Dekker, F. J., Rusch, M., Renner, S., Wetzel, S., Vartak, N., et al. (2011). Development of highly potent inhibitors of the ras-targeting human acyl protein thioesterases based on substrate similarity design. *Angew. Chem. Int. Ed Engl.* 50, 9832–9837. doi: 10.1002/anie.201102965

Herrero, A., Casar, B., Colón-Bolea, P., Agudo-Ibáñez, L., and Crespo, P. (2016). Defined spatiotemporal features of RAS-ERK signals dictate cell fate in MCF-7 mammary epithelial cells. *Mol. Biol. Cell.* 27, 1958–1968. doi: 10.1091/mbc.E15-02-0118

Herrero, A., Reis-Cardoso, M., Jiménez-Gómez, I., Doherty, C., Agudo-Ibañez, L., Pinto, A., et al. (2020). Characterisation of HRas local signal transduction networks using engineered site-specific exchange factors. *Small GTPases* 11, 371–383. doi: 10.1080/21541248.2017.1406434

Hobbs, G. A., Der, C. J., and Rossman, K. L. (2016). RAS isoforms and mutations in cancer at a glance. *J. Cell Sci.* 129, 1287–1292. doi: 10.1242/jcs.182873

Jing, H., Zhang, X., Wisner, S. A., Chen, X., Spiegelman, N. A., Linder, M. E., et al. (2017). SIRT2 and lysine fatty acylation regulate the transforming activity of K-Ras4a. *Elife* 6:e32436. doi: 10.7554/eLife.32436

Kapoor, S., Weise, K., Erlkamp, M., Triola, G., Waldmann, H., and Winter, R. (2012). The role of G-domain orientation and nucleotide state on the Ras isoform-specific membrane interaction. *Eur. Biophys. J.* 41, 801–813. doi: 10.1007/s00249-012-0841-5

Lin, D. T., and Conibear, E. (2015). ABHD17 proteins are novel protein depalmitoylases that regulate N-Ras palmitate turnover and subcellular localization. *Elife* 4:e11306. doi: 10.7554/eLife.11306

Lowy, D. R., and Willumsen, B. M. (1989). New clue to ras lipid glue. *Nature* 341, 384–385.

Magee, A. I., Gutierrez, L., Mckay, I. A., Marshall, C. J., and Hall, A. (1987). Dynamic fatty acylation of P21n-Ras. *Embo J.* 6, 3353–3357.

Matallanas, D., Arozarena, I., Berciano, M. T., Aaronson, D. S., Pellicer, A., Lafarga, M., et al. (2003). Differences on the inhibitory specificities of H-Ras, K-Ras, and N-Ras (N17) dominant negative mutants are related to their membrane microlocalization. *J. Biol. Chem.* 278, 4572–4581. doi: 10.1074/jbc.M209807200

Matallanas, D., Sanz-Moreno, V., Arozarena, I., Calvo, F., Agudo-Ibáñez, L., Santos, E., et al. (2006). Distinct utilization of effectors and biological outcomes resulting from site-specific ras activation: ras functions in lipid rafts and golgi complex are dispensable for proliferation and transformation. *Mol. Cell. Biol.* 26, 100–116. doi: 10.1128/mcb.26.1.100-116.2006

Misaki, R., Morimatsu, M., Uemura, T., Waguri, S., Miyoshi, E., Taniguchi, N., et al. (2010). Palmitoylated ras proteins traffic through recycling endosomes to the plasma membrane during exocytosis. *J. Cell Biol.* 191, 23–29. doi: 10.1083/jcb.200911143

Pedro, M. P., Vilcaes, A. A., Gomez, G. A., and Daniotti, J. L. (2017). Individual S-acylated cysteines differentially contribute to H-Ras endomembrane traffcking and acylation/deacylation cycles. *Mol. Biol. Cell.* 28, 962–974. doi: 10.1091/mbc.E16-08-0603

Potenza, N., Vecchione, C., Notte, A., De Rienzo, A., Rosica, A., Bauer, L., et al. (2005). Replacement of K-Ras with H-Ras supports normal embryonic development despite inducing cardiovascular pathology in adult mice. *EMBO Rep.* 6, 432–437. doi: 10.1038/sj.embor.7400397

Prior, I. A., Harding, A., Yan, J., Sluimer, J., Parton, R. G., and Hancock, J. F. (2001). GTP-dependent segregation of H-ras from lipid rafts is required for biological activity. *Nat. Cell Biol.* 3, 368–375. doi: 10.1038/35070050

Prior, I. A., Hood, F. E., and Hartley, J. L. (2020). The frequency of ras mutations in cancer. *Cancer Res.* 80, 2969–2974. doi: 10.1158/0008-5472.CAN-19-3682

Prior, I. A., Lewis, P. D., and Mattos, C. (2012). A comprehensive survey of ras mutations in cancer. *Cancer Res.* 72, 2457–2467. doi: 10.1158/0008-5472.CAN-11-2612

Remsberg, J. R., Suciu, R. M., Zambetti, N. A., Hanigan, T. W., Firestone, A. J., Inguva, A., et al. (2020). ABHD17 enzymes regulate dynamic plasma membrane palmitoylation and N-Ras-dependent cancer growth. *bioRxiv* 2020:108316. doi: 10.1101/2020.05.21.108316

Rocks, O., Gerauer, M., Vartak, N., Koch, S., Huang, Z. P., Pechlivanis, M., et al. (2010). The palmitoylation machinery is a spatially organizing system for peripheral membrane proteins. *Cell* 141, 458–471.

Rocks, O., Peyker, A., Kahms, M., Verveer, P. J., Koerner, C., Lumbierres, M., et al. (2005). An acylation cycle regulates localization and activity of palmitoylated Ras isoforms. *Science* 307, 1746–1752.

Rotblat, B., Prior, I. A., Muncke, C., Parton, R. G., Kloog, Y., Henis, Y. I., et al. (2004). Three separable domains regulate GTP-dependent association of H-ras with the plasma membrane. *Mol. Cell. Biol.* 24, 6799–6810. doi: 10.1128/MCB.24.15.6799-6810.2004

Roy, S., Plowman, S., Rotblat, B., Prior, I. A., Muncke, C., Grainger, S., et al. (2005a). Individual palmitoyl residues serve distinct roles in H-Ras trafficking, microlocalization, and signaling. *Mol. Cell. Biol.* 25, 6722–6733. doi: 10.1128/mcb.25.15.6722-6733.2005

Roy, S., Plowman, S., Rotblat, B., Prior, I. A., Muncke, C., Grainger, S., et al. (2005b). Individual palmitoyl residues serve distinct roles in H-Ras trafficking, microlocalization, and signaling. *Mol. Cell. Biol.* 25, 6722–6733.

Rusch, M., Zimmermann, T. J., Bürger, M., Dekker, F. J., Görmer, K., Triola, G., et al. (2011). Identification of acyl protein thioesterases 1 and 2 as the cellular targets of the ras-signaling modulators palmostatin B and M. *Angew. Chemie Int. Ed Engl.* 50, 9838–9842. doi: 10.1002/anie.201102967

Santra, T., Herrero, A., Rodriguez, J., von Kriegsheim, A., Iglesias-Martinez, L. F., Schwarzl, T., et al. (2019). An integrated global analysis of compartmentalized hras signaling. *Cell. Rep.* 26, 3100–3115. doi: 10.1016/j.celrep.2019.02.038

Schulte-Zweckel, J., Dwivedi, M., Brockmeyer, A., Janning, P., Winter, R., and Triola, G. (2019). A hydroxylamine probe for profiling S-acylated fatty acids on proteins †. *Chem. Commun* 55:11183. doi: 10.1039/c9cc05989j

Sexton, R. E., Mpilla, G., Kim, S., Philip, P. A., and Azmi, A. S. (2019). Ras and exosome signaling. *Semin. Cancer Biol.* 54, 131–137. doi: 10.1016/j.semcancer.2019.02.004

Shishina, A. K., Kovrigina, E. A., Galiakhmetov, A. R., Rathore, R., and Kovrigin, E. L. (2018). Study of förster resonance energy transfer to lipid domain markers ascertains partitioning of semisynthetic lipidated N-Ras in lipid raft nanodomains. *Biochemistry* 57, 872–881. doi: 10.1021/acs.biochem.7b01181

Simanshu, D. K., Nissley, D. V., and McCormick, F. (2017). RAS proteins and their regulators in human disease. *Cell* 170, 17–33. doi: 10.1016/j.cell.2017.06.009

Sperlich, B., Kapoor, S., Waldmann, H., Winter, R., and Weise, K. (2016). Regulation of K-Ras4B membrane binding by calmodulin. *Biophys. J.* 111, 113–122. doi: 10.1016/j.bpj.2016.05.042

Spiegelman, N. A., Hong, J. Y., Hu, J., Jing, H., Wang, M., Price, I. R., et al. (2019). A small-molecule SIRT2 inhibitor that promotes K-Ras4a lysine fatty-acylation. *Chem. MedChem.* 14, 744–748. doi: 10.1002/cmdc.201800715

Stix, R., Lee, C. J., Faraldo-Gómez, J. D., and Banerjee, A. (2020). Structure and mechanism of DHHC protein acyltransferases. *J. Mol. Biol.* 432, 4983–4998. doi: 10.1016/j.jmb.2020.05.023

Swarthout, J. T., Lobo, S., Farh, L., Croke, M. R., Greentree, W. K., Deschenes, R. J., et al. (2005). DHHC9 and GCP16 constitute a human protein fatty acyltransferase with specificity for H- and N-Ras. *J. Biol. Chem.* 280, 31141–31148. doi: 10.1074/jbc.M504113200

Tomatis, V. M., Trenchi, A., Gomez, G. A., and Daniotti, J. L. (2010). Acyl-protein thioesterase 2 catalizes the deacylation of peripheral membrane-associated GAP-43. *PLoS One* 5:e15045. doi: 10.1371/journal.pone.0015045

Triola, G., Waldmann, H., and Hedberg, C. (2012). Chemical biology of lipidated proteins. *ACS Chem. Biol.* 7, 87–99. doi: 10.1021/cb200460u

Tsai, F. D., Lopes, M. S., Zhou, M., Court, H., Ponce, O., Fiordalisi, J. J., et al. (2015). K-Ras4A splice variant is widely expressed in cancer and uses a hybrid membrane-targeting motif. *Proc. Natl. Acad. Sci. U S A.* 112, 779–784. doi: 10.1073/pnas.1412811112

Vartak, N., Papke, B., Grecco, H. E., Rossmannek, L., Waldmann, H., Hedberg, C., et al. (2014). The autodepalmitoylating activity of APT maintains the spatial organization of palmitoylated membrane proteins. *Biophys. J.* 106, 93–105. doi: 10.1016/j.bpj.2013.11.024

Verkruyse, L. A., and Hofmann, S. L. (1996). Lysosomal targeting of palmitoyl-protein thioesterase. *J. Biol. Chem.* 271, 15831–15836.

Vogel, A., Reuther, G., Weise, K., Triola, G., Nikolaus, J., Tan, K.-T., et al. (2009). The lipid modifications of ras that sense membrane environments and induce local enrichment. *Angew. Chemie Int. Ed Engl.* 48, 8784–8787. doi: 10.1002/anie.200903396

Weise, K., Kapoor, S., Denter, C., Nikolaus, J., Opitz, N., Koch, S., et al. (2011). Membrane-mediated induction and sorting of K-Ras microdomain signaling platforms. *J. Am. Chem. Soc.* 133, 880–887. doi: 10.1021/ja107532q

Weise, K., Kapoor, S., Werkmüller, A., Möbitz, S., Zimmermann, G., Triola, G., et al. (2012). Dissociation of the K-Ras4B/PDEδ complex upon contact with lipid membranes: MEMBRANE delivery instead of extraction. *J. Am. Chem. Soc.* 134, 11503–11510. doi: 10.1021/ja305518h

Weise, K., Triola, G., Brunsveld, L., Waldmann, H., and Winter, R. (2009). Influence of the lipidation motif on the partitioning and association of N-ras in model membrane subdomains. *J. Am. Chem. Soc.* 131, 1557–1564. doi: 10.1021/ja808691r

Weise, K., Triola, G., Janosch, S., Waldmann, H., and Winter, R. (2010). Visualizing association of lipidated signaling proteins in heterogeneous membranes-partitioning into subdomains, lipid sorting, interfacial adsorption, and protein association. *Biochim. Biophys. Acta* 1798, 1409–1417. doi: 10.1016/j.bbamem.2009.12.006

Werkmuller, A., Triola, G., Waldmann, H., and Winter, R. (2013). Rotational and translational dynamics of ras proteins upon binding to model membrane systems. *Chemphyschem* 14, 3698–3705. doi: 10.1002/cphc.201300617

Won, S. J., Cheung See Kit, M., and Martin, B. R. (2018). Protein depalmitoylases. *Crit. Rev. Biochem. Mol. Biol.* 53, 83–98. doi: 10.1080/10409238.2017.1409191

Yokoi, N., Fukata, Y., Sekiya, A., Murakami, T., Kobayashi, K., and Fukata, M. (2016). Identification of PSD-95 Depalmitoylating Enzymes. *J. Neurosci.* 36, 6431–6444. doi: 10.1523/JNEUROSCI.0419-16.2016

Zhang, S. Y., Sperlich, B., Li, F. Y., Al-Ayoubi, S., Chen, H. X., Zhao, Y. F., et al. (2017). Phosphorylation weakens but does not inhibit membrane binding and clustering of K-Ras4B. *ACS Chem. Biol.* 12, 1703–1710. doi: 10.1021/acschembio.7b00165

Zhao, H., Liu, P., Zhang, R., Wu, M., Li, D., Zhao, X., et al. (2015). Roles of palmitoylation and the KIKK membrane-targeting motif in leukemogenesis by oncogenic KRAS4A. *J. Hematol. Oncol.* 8:132. doi: 10.1186/s13045-015-0226-1

Zhou, M., Wiener, H., Su, W., Zhou, Y., Liot, C., Ahearn, I., et al. (2016). VPS35 binds farnesylated N-Ras in the cytosol to regulate N-Ras trafficking. *J. Cell. Biol.* 214, 445–458. doi: 10.1083/jcb.201604061

Zhou, Y., Prakash, P., Liang, H., Cho, K. J., Gorfe, A. A., and Hancock, J. F. (2017). Lipid-sorting specificity encoded in K-Ras membrane anchor regulates signal output. *Cell* 168, 239–251. doi: 10.1016/j.cell.2016.11.059

Zimmermann, G., Papke, B., Ismail, S., Vartak, N., Chandra, A., Hoffmann, M., et al. (2013). Small molecule inhibition of the KRAS-PDEδ interaction impairs oncogenic KRAS signalling. *Nature* 497, 638–642. doi: 10.1038/nature12205

Conflict of Interest: The authors declare that the research was conducted in the absence of any commercial or financial relationships that could be construed as a potential conflict of interest.

frontiers in Molecular Biosciences

REVIEW
published: 16 June 2021
doi: 10.3389/fmolb.2021.685135

SmgGDS: An Emerging Master Regulator of Prenylation and Trafficking by Small GTPases in the Ras and Rho Families

*Anthony C. Brandt, Olivia J. Koehn and Carol L. Williams**

Department of Pharmacology and Toxicology, Medical College of Wisconsin, Milwaukee, WI, United States

Newly synthesized small GTPases in the Ras and Rho families are prenylated by cytosolic prenyltransferases and then escorted by chaperones to membranes, the nucleus, and other sites where the GTPases participate in a variety of signaling cascades. Understanding how prenylation and trafficking are regulated will help define new therapeutic strategies for cancer and other disorders involving abnormal signaling by these small GTPases. A growing body of evidence indicates that splice variants of SmgGDS (gene name RAP1GDS1) are major regulators of the prenylation, post-prenylation processing, and trafficking of Ras and Rho family members. SmgGDS-607 binds pre-prenylated small GTPases, while SmgGDS-558 binds prenylated small GTPases. This review discusses the history of SmgGDS research and explains our current understanding of how SmgGDS splice variants regulate the prenylation and trafficking of small GTPases. We discuss recent evidence that mutant forms of RabL3 and Rab22a control the release of small GTPases from SmgGDS, and review the inhibitory actions of DiRas1, which competitively blocks the binding of other small GTPases to SmgGDS. We conclude with a discussion of current strategies for therapeutic targeting of SmgGDS in cancer involving splice-switching oligonucleotides and peptide inhibitors.

Keywords: Rap1GDS1, SmgGDS, splicing, lipidation, prenylation, trafficking, GEF, GDF

OPEN ACCESS

Edited by:
Kwang-jin Cho,
Wright State University, United States

Reviewed by:
Dharini Van Der Hoeven,
University of Texas Health Science Center at Houston, United States
Junjie Hu,
Institute of Biophysics (CAS), China

****Correspondence:***
Carol L. Williams
williams@mcw.edu

Specialty section:
This article was submitted to Cellular Biochemistry, a section of the journal Frontiers in Molecular Biosciences

Received: *24 March 2021*
Accepted: *27 May 2021*
Published: *16 June 2021*

Citation:
Brandt AC, Koehn OJ and Williams CL (2021) SmgGDS: An Emerging Master Regulator of Prenylation and Trafficking by Small GTPases in the Ras and Rho Families. Front. Mol. Biosci. 8:685135. doi: 10.3389/fmolb.2021.685135

INTRODUCTION

The Ras superfamily consists of over 150 different small GTPases belonging to specific families. The most well characterized small GTPases in this superfamily are members of the Ras family (36 members), Rho family (20 members), and Rab family (over 60 members) (Vigil et al., 2010; Gray et al., 2020). These proteins participate in important cellular signaling pathways that regulate gene expression, cytoskeletal organization, intracellular trafficking of proteins and vesicles, and cell migration, proliferation, and differentiation (Seabra et al., 2002; Hutagalung and Novick, 2011; Haga and Ridley, 2016) These small GTPases are activated when they bind guanine nucleotide exchange factors (GEFs) that induce the small GTPases to release GDP and bind GTP. There are 27 different GEFs that activate Ras family members, and 80 GEFs that activate Rho family members, providing extensive spatiotemporal control of these small GTPases (Vigil et al., 2010; Gray et al., 2020). Inappropriate or prolonged activation of these GTPases leads to dysregulated signaling that contributes to cancer initiation, progression, and metastasis (Seabra et al., 2002; Vigil et al., 2010; Alan and Lundquist, 2013; Haga and Ridley, 2016; Porter et al., 2016).

The intracellular site where a small GTPase is located defines how the GTPase will be activated and which signaling pathway it will modulate. Cell membranes are a major site for activation and signaling by small GTPases. Ras and Rho family members anchored at the plasma membrane are activated by membrane-localized GEFs and participate in signaling cascades initiated by plasma membrane receptors (Vigil et al., 2010; Gray et al., 2020). Rab family members anchored at endosomal membranes are activated by endosome-localized GEFs and participate in vesicular transport (Seabra et al., 2002; Hutagalung and Novick, 2011). The ability of these GTPases to anchor at membranes and participate in these signaling events depends on the presence of a prenyl group that is irreversibly attached to the C-terminus of the GTPase soon after it is synthesized in the cell (Lane and Beese, 2006; Wright and Philips, 2006; Wang and Casey, 2016). The prenyl group serves as a membrane anchor that is inserted into the lipid bilayer. If prenylation does not occur, the ability of these GTPases to localize at cell membranes is severely impaired.

Small GTPases that are activated by GEFs associated with membranes must be prenylated to localize at the membrane and interact with their GEFs. K-Ras4B is an excellent example of a small GTPase that relies primarily on membrane localization for its activity (Cox et al., 2015; Kattan and Hancock, 2020; Uprety and Adjei, 2020). However, recent studies indicate that under certain conditions, K-Ras4B might participate in signaling complexes that are not associated with membranes (Tulpule et al., 2021). Some small GTPases are known to be activated at sites other than membranes. For example, the Ras family members Rap1A and Rap1B (Mitra et al., 2003; Goto et al., 2010; Ntantie et al., 2013; Griffin et al., 2018) and the Rho family members RhoA (Dubash et al., 2011; Staus et al., 2014; Gayle et al., 2015) and Rac1 (Lanning et al., 2003; Michaelson et al., 2008; Huff et al., 2013; Navarro-Lerida et al., 2015; Justilien et al., 2017; Casado-Medrano et al., 2020) can enter the nucleus where they can be activated by nuclear GEFs and participate in nuclear signaling pathways. These findings suggest that prenylation that promotes membrane anchoring is not always required for Ras and Rho family members to become activated. This suggestion is supported by reports that inhibiting the prenylation of Rap1A, Rap1B, RhoA, and Rac1 increases the GTP-bound forms of these GTPases (Dunford et al., 2006; Khan et al., 2011; Khan et al., 2013; Ntantie et al., 2013; Reddy et al., 2015; Akula et al., 2019), indicating that certain GEFs can activate these GTPases before they are prenylated.

There is growing evidence that some small GTPases participate in signaling events before they are prenylated (Khan et al., 2011; Khan et al., 2013; Reddy et al., 2015; Akula et al., 2019), leading to the realization that cells must possess ways to promote or suppress the prenylation of a newly synthesized small GTPase. The best characterized mechanism that controls the prenylation of Ras and Rho family members involves the interaction of these small GTPases with SmgGDS (pronounced "smidge-G-D-S", gene name RAP1GDS1). SmgGDS has emerged as a major regulator of both the prenylation and intracellular trafficking of many GTPases in the Ras and Rho families (Berg et al., 2010; Ntantie et al., 2013; Williams, 2013; Schuld N. J. et al., 2014; Jennings et al., 2018; Garcia-Torres and Fierke, 2019; Nissim et al., 2019; Brandt et al., 2020; Liao et al., 2020). This review describes how these events are regulated by the two splice variants of SmgGDS, named SmgGDS-607 and SmgGDS-558, and compares SmgGDS to the proteins that regulate the prenylation and trafficking of Rab family members. We discuss how different proteins modulate the interactions of SmgGDS with oncogenic small GTPases in the Ras and Rho families, and present strategies to target SmgGDS therapeutically in cancer.

TABLE 1 | C-Terminal Sequences of Human Ras and Rho Family Members that have a Polybasic Region (PBR).

GTPase	C-terminal sequence[a]	Accession No.[b]
Rho family members		
RhoA	fematRaalqaRRgKKKsgclvl	NP_001300870
RhoC	fematRaglqvRKnKRRRgcpil	NP_001036144
RhoD	evalssRgRnfwRRitqgfcvvt	NP_055393
RhoG	faeavRavlnptpiKRgRscill	NP_001656
RhoH	tavnqaRRRnRRRlfsineckif	NP_001265298
Rac1	deaiRavlcpppvKKRKRKclll	NP_008839
Rac1b	deaiRavlcpppvKKRKRKclll	NP_061485
Rac2	deaiRavlcpqptRqqKRacsll	NP_002863
Rac3	deaiRavlcpppvKKpgKKctvf	NP_005043
Cdc42 (isof. 1)	fdeailaaleppepKKsRRcvll	NP_001782
Cdc42 (isof. 2)	fdeailaaleppetqpKrKccif	NP_426359
Rnd1 (Rho6)	lpsRselisstfKKeKaKscsim	NP_055285
Rnd2 (RhoN)	sgrpdRgnegeihKdRaKscnlm	NP_005431
Rnd3 (RhoE)	sRpelsavatdlRKdKaKsctvm	NP_005159
Ras family members		
K-Ras4A	RlKKisKeeKtpgcvKiKKciim	NP_001356715
K-Ras4B	hKeKmsKdgKKKKKKsKtKcvim	NP_001356716
R-Ras2 (TC21)	ecppspeptRKeKdKKgchcvif	NP_036382
M-Ras (R-Ras3)	KKKKtKwrgdRatgthKlqcvil	NP_001239019
Rap1A	vRqinRKtpveKKKpKKKsclll	NP_001010935
Rap1B	vRqinRKtpvpgKaRKKsscqll	NP_001010942
RalA	KeKngKKKRKslaKRiReRccil	NP_005393
RalB	nKdKngKKssKnKKsfKeRccll	NP_001356329
Rheb	RiileaeKmdgaasqgKsscsvm	NP_005605
RhebL1	tKviqeiaRvensygqeRRchlm	NP_653194
DiRas1 (Rig)	nidgKRsgKqKrtdRvKgKctlm	NP_660156
DiRas2	qidgKKsKqqKRKeKlKgKcvim	NP_060064
DiRas3	qepeKKsqmpntteKlldKciim	NP_004666

[a]*Basic amino acids that make up the PBR are capitalized.*
[b]*The NCBI Protein database accession number is provided.*

PRENYLATION OF RAS, RHO, AND RAB FAMILY MEMBERS

Newly synthesized small GTPases in the Ras and Rho families are soluble, hydrophilic proteins residing in the cytosol. The majority of these small GTPase have a C-terminal CAAX motif consisting of a cysteine (C), two aliphatic amino acids (AA), and a terminal amino acid (X). When a newly synthesized small GTPase enters the prenylation pathway, the CAAX motif undergoes prenylation and post-prenylation processing, converting the small GTPase to a hydrophobic protein that can anchor at membranes (Lane and Beese, 2006; Wright and Philips, 2006; Wang and Casey, 2016).

Ras and Rho family members are prenylated by a cytosolic prenyltransferase (PTase), which irreversibly attaches a hydrophobic prenyl group to the cysteine in the CAAX motif. Small GTPases that have a CAAX motif ending in alanine, glycine, serine, methionine, or phenylalanine receive a 15-carbon farnesyl group from farnesyltransferase (FTase). In contrast, if the CAAX motif ends in leucine or phenylalanine, the GTPase receives a 20-carbon geranylgeranyl group from geranylgeranyltransferase-I (GGTase-I) (Lane and Beese, 2006). The prenylated GTPase then undergoes post-prenylation processing at the endoplasmic reticulum by interacting with RCE1, which proteolytically cleaves the AAX from the CAAX motif, followed by carboxylmethylation by ICMT (Wright and Philips, 2006; Wang and Casey, 2016).

When post-prenylation processing is completed, the prenylated, hydrophobic GTPase can take two different routes to the plasma membrane. Small GTPases that have an additional cysteine near the CAAX motif, such as H-Ras and N-Ras, move to the Golgi to become palmitoylated before localizing at the plasma membrane (Wright and Philips, 2006; Wang and Casey, 2016). In contrast, small GTPases that have a C-terminal polybasic region (PBR) move directly from the endoplasmic reticulum through the aqueous cytosol to the plasma membrane (Wright and Philips, 2006; Wang and Casey, 2016). These PBR-containing small GTPases include K-Ras4B and many other members of the Ras and Rho families [reviewed in Williams (2013)] (**Table 1**). A protein that serves as a chaperone must shield the prenyl group of the small GTPase in a hydrophobic pocket as the GTPase moves through the cytosol to the plasma membrane (Azoulay-Alfaguter et al., 2015). Prenylated Ras family members interact with several chaperones, including PDEδ (Bhagatji et al., 2010; Dharmaiah et al., 2016), PRA1 (Figueroa et al., 2001; Bhagatji et al., 2010), and VPS35 (Zhou et al., 2016), while prenylated Rho family members are chaperoned by three RhoGDI proteins (Garcia-Mata et al., 2011).

Rab family members are prenylated in a pathway differing from the one that prenylates Ras and Rho family members. Newly synthesized Rab family members associate with the Rab Escort Protein REP1 before prenylation. A trimeric complex consisting of REP1, the Rab protein, and the Rab geranylgeranyltransferase (RabGGTase) is needed for the RabGGTase to sequentially prenylate two cysteines in the C-terminus of the Rab protein. After prenylation, REP1 serves as a chaperone for the prenylated Rab small GTPase as it moves through the cytosol to membranes. The importance of REP1 in this pathway is indicated by its interactions with both the pre-prenylated and prenylated forms of the Rab protein, facilitating prenylation of the newly synthesized Rab protein and then escorting the prenylated Rab protein to membranes (Preising and Ayuso, 2004; Goody et al., 2005; Leung et al., 2006; Wu et al., 2007).

The participation of REP1 in the prenylation and trafficking of newly synthesized Rab family members suggests that proteins with functions similar to REP1 might participate in the prenylation and trafficking of newly synthesized Ras and Rho family members. Such proteins that might assist Ras and Rho family members during prenylation were not known prior to the discovery of the two major splice variants of SmgGDS (Berg et al., 2010). The discovery of these SmgGDS splice variants has led to an increasing understanding of how cells can suppress or promote the prenylation of Ras and Rho family members, and has stimulated a growing exploration of how Ras and Rho family members can actively signal both before and after they are prenylated.

DISCOVERY OF SMGGDS AND ITS MAJOR SPLICE VARIANTS SMGGDS-607 AND SMGGDS-558

In 1990, members of the Takai laboratory isolated a protein from bovine brain that interacted with Rap1A and Rap1B, and they named this protein "small G protein guanine dissociation stimulator" or SmgGDS (Yamamoto et al., 1990). A cDNA encoding a SmgGDS protein having 558 amino acids was generated (Kaibuchi et al., 1991), and this SmgGDS cDNA was utilized in many studies to define the functions of SmgGDS. These studies indicated that SmgGDS binds multiple members of the Ras and Rho families that have a C-terminal PBR, including K-Ras4B, Rap1A, Rap1B, RhoA, RhoC, Rac1, Rac2, and Cdc42 (Mizuno et al., 1991; Hiraoka et al., 1992; Kikuchi et al., 1992; Orita et al., 1993; Yaku et al., 1994; Xu et al., 1997). Co-expression of this 558 amino acid form of SmgGDS with different small GTPases enhanced several cellular responses, including transformation and tumorigenesis of NIH3T3 cells induced by K-Ras4B (Fujioka et al., 1992), lamellipodia formation promoted by Rap1B (Yoshida et al., 1992), and NOX activation and neurite formation induced by Rac1 (Ando et al., 1992; Kikuchi et al., 1992; Mizuno et al., 1992).

SmgGDS has been the subject of several controversies regarding its interactions with small GTPases. One of these controversies arose from inconsistent reports that a small GTPase must be prenylated before it can associate with SmgGDS. Some groups reported that SmgGDS interacts only with prenylated small GTPases (Mizuno et al., 1991; Shirataki et al., 1991; Fujioka et al., 1992; Orita et al., 1993; Nakanishi et al., 1994), whereas others reported that SmgGDS can associate with small GTPases before they are prenylated (Chuang et al., 1994; Hutchinson and Eccleston, 2000; Hutchinson et al., 2000). This discrepancy might have occurred because these groups used different cDNAs encoding SmgGDS in their studies. Groups reporting that SmgGDS binds only prenylated GTPases utilized the cDNA that was generated in the original studies of SmgGDS (Mizuno et al., 1991; Nakanishi et al., 1994). In contrast, groups reporting that prenylation was unnecessary utilized SmgGDS cDNA clones generated in other studies (Chuang et al., 1994; Hutchinson and Eccleston, 2000; Hutchinson et al., 2000). The use of these different cDNA clones was not considered to be an important variable at the time, but it might have explained the disparate results obtained in these studies, if the cDNAs being utilized by these different groups encoded different forms of SmgGDS.

An explanation for these conflicting reports that only prenylated GTPases bind SmgGDS was provided in 2010, when the Williams group reported the identification of two

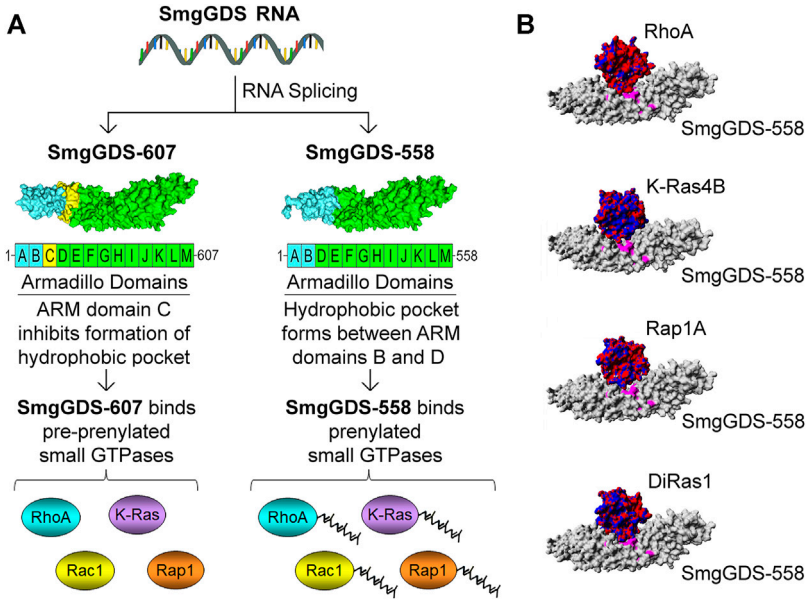

FIGURE 1 | Schematic illustration depicting how the SmgGDS splice variants, SmgGDS-607 and SmgGDS-558, interact with pre-prenylated and prenylated small GTPases, respectively. **(A)** SmgGDS-607 has 13 ARM domains named A–M. SmgGDS-607 binds pre-prenylated small GTPases because the presence of ARM domain C inhibits the formation of a hydrophobic pocket in SmgGDS-607. In contrast, SmgGDS-558 lacks ARM domain C, causing it to have only 12 ARM domains. SmgGDS-558 binds prenylated small GTPases because a hydrophobic pocket forms between ARM domains B and D, which accommodates the prenyl group of small GTPases. **(B)** Homology models indicate that SmgGDS-558 binds different Ras and Rho family members in a similar manner, suggesting that these small GTPases compete for binding to SmgGDS-558. SmgGDS-558 is depicted with a gray surface plot. The small GTPases are depicted with an electrostatic surface plot with negative charges indicated by red and positive charges indicated by blue [homology models adopted from Bergom et al. (2016)].

splice variants of SmgGDS that differ in their ability to bind prenylated GTPases (Berg et al., 2010). A long form of SmgGDS that has 607 amino acids was identified and named SmgGDS-607, and the shorter form of SmgGDS that has 558 amino acids was named SmgGDS-558 (Berg et al., 2010). The functions of these splice variants were defined by using two publicly available cDNA constructs encoding SmgGDS (Berg et al., 2010). One construct encoded SmgGDS-558 that was identified in the original studies of SmgGDS (Kaibuchi et al., 1991), and the other construct encoded SmgGDS containing 607 amino acids obtained from the National Institute of Technology and Evaluation (Chiba, Japan) (Berg et al., 2010). This cDNA construct encoding SmgGDS-607 had been used in previous studies, but it was not recognized that it encoded a form of SmgGDS differing from SmgGDS-558 (Shin et al., 2006). The two SmgGDS splice variants were found to have very different abilities to bind prenylated GTPases; SmgGDS-607 binds pre-prenylated GTPases before they enter the prenylation pathway, whereas SmgGDS-558 binds only prenylated small GTPases (Berg et al., 2010; Ntantie et al., 2013; Williams, 2013; Schuld N. J. et al., 2014). This discovery that two forms of SmgGDS interact differently with pre-prenylated vs. prenylated small GTPases resolved the earlier controversy that prenylation is required for a small GTPase to bind SmgGDS.

The structural features that cause SmgGDS-607 to bind pre-prenylated GTPases and SmgGDS-558 to bind prenylated GTPases are beginning to be understood. SmgGDS is composed of multiple armadillo (ARM) domains. An ARM domain consists of approximately 40 amino acids folded into alpha helices. ARM domains can be identified from the amino acid sequence of a protein using a paradigm provided by Andrade and colleagues (Andrade et al., 2001). Using this paradigm to identify ARM domains, it was determined that SmgGDS has 13 ARM domains, which were named A–M (Berg et al., 2010). In contrast, SmgGDS-558 was reported to have only 12 ARM domains due to the absence of ARM domain C (**Figure 1A**) (Berg et al., 2010). The designation of these ARM domains as A–M has become the established method to describe the arrangement of ARM domains in SmgGDS (Schuld, et al., 2014a; Schuld N. J. et al., 2014; Hauser et al., 2014; Gonyo et al., 2017; Shimizu et al., 2017; Shimizu et al., 2018). In 2018, the Shimizu group solved the crystal structure of SmgGDS-558 associated with prenylated RhoA (Shimizu et al., 2018). Analysis of this structure indicates that a hydrophobic pocket that can accommodate the prenyl group of RhoA forms between ARMs B and D in SmgGDS-558. In contrast, SmgGDS-607 cannot bind prenylated GTPases because the presence of ARM C precludes the formation of this hydrophobic pocket (Shimizu et al., 2018). (**Figure 1A**).

Another major controversy regarding SmgGDS arose from the proposal that SmgGDS is a GEF for many different Ras and Rho family members. Early studies suggested that SmgGDS might act as a GEF for multiple PBR-containing small GTPases, including Rap1A and Rap1B (Yamamoto et al., 1990; Kaibuchi et al., 1991; Mizuno et al., 1991; Hiroyoshi et al., 1991), K-Ras4B (Mizuno et al., 1991; Orita et al., 1993; Nakanishi et al., 1994; Yaku et al.,

1994), RhoA (Mizuno et al., 1991; Kikuchi et al., 1992; Yaku et al., 1994; Hutchinson et al., 2000; Hutchinson and Eccleston, 2000), Rac1 (Ando et al., 1992; Chuang et al., 1994), Rac2 (Fujioka et al., 1992; Xu et al., 1997), and Cdc42 (Yaku et al., 1994). These small GTPases bind to SmgGDS in a similar manner (**Figure 1B**) involving two main interactions. The PBR of the small GTPase has electrostatic interactions with an electronegative patch in SmgGDS, and the main body of the GTPase interacts with a binding groove in SmgGDS (Hamel et al., 2011). It was difficult to understand how SmgGDS could act as a GEF for so many Ras and Rho family members, because SmgGDS lacks the domains that are commonly associated with proteins that have GEF activity, including the CDC25 domain that activates Ras family members, and the DH domain that activates Rho family members. Several confounding issues hampered these earlier studies of the GEF activity of SmgGDS, including the use of crude protein preparations and long incubation times during the analysis of GDP/GTP exchange, and the fact that sophisticated methods of analyzing GEF activity were not yet widely available.

The Sondek group finally clarified the GEF activity of SmgGDS in 2011 (Hamel et al., 2011). Using real-time MANT-GDP exchange assays, these researchers demonstrated that both SmgGDS-558 and SmgGDS-607 are true GEFs for RhoA and RhoC, but they are unable to promote GDP/GTP exchange by K-Ras4B, Rap1A, Rap1B, RhoB, Rac1, Rac2, and Cdc42 (Hamel et al., 2011). Crystallographic analysis in 2018 indicated that SmgGDS promotes GDP/GTP exchange by RhoA through a unique mechanism that is not utilized by other GEFs (Shimizu et al., 2018). This analysis indicates that the switch I and switch II regions of RhoA undergo a conformational change when RhoA binds SmgGDS, which opens up the nucleotide-binding site in RhoA (Shimizu et al., 2018). This mechanism allows SmgGDS-607 and SmgGDS-558 to act as GEFs for pre-prenylated and prenylated RhoA, respectively. The incorrect statement that SmgGDS is a GEF for many small GTPases in the Ras and Rho families continues to appear in the literature and in online sources. This misleading statement should be amended to reflect our current knowledge that SmgGDS is a GEF for RhoA and RhoC, but not for other small GTPases (Hamel et al., 2011; Shimizu et al., 2018).

Even though SmgGDS has limited intrinsic GEF activity, SmgGDS still might promote the activity of many different small GTPases by serving as a scaffold that facilitates the interactions of GEFs with small GTPases bound to SmgGDS (Berg et al., 2010). The formation of a transient trimeric complex consisting of SmgGDS, a small GTPase, and the specific GEF that activates the small GTPase provides a specific mechanism for SmgGDS to increase the activities of different Ras and Rho family members. In support of this mechanism, it was reported that SmgGDS (now known to be SmgGDS-607) forms a complex with Rac1 and βPIX, which is a GEF for Rac1 (Shin et al., 2006). The association of a GEF with SmgGDS-607 provides a way to activate small GTPases before they are prenylated, since SmgGDS-607 only binds GTPases before they enter the prenylation pathway. In contrast, the association of a GEF with SmgGDS-558 will activate prenylated GTPases, since SmgGDS-558 binds small GTPases only after they have been prenylated.

COMPLEMENTARY ROLES OF SMGGDS-607 AND SMGGDS-558 IN THE PRENYLATION AND TRAFFICKING OF RAS AND RHO FAMILY MEMBERS

Multiple studies indicate that SmgGDS-607 and SmgGDS-558 work together to regulate the prenylation and trafficking of small GTPases in the Ras and Rho families (**Figure 2**) (Berg et al., 2010; Williams 2013; Schuld N. J. et al., 2014; Brandt et al., 2020). SmgGDS-607 binds newly synthesized small GTPases that possess a PBR and regulates their entry into the prenylation pathway (**Figure 2A**). It was originally proposed that SmgGDS-607 acts as a gatekeeper for small GTPases entering the prenylation pathway (Berg et al., 2010). Just as a gatekeeper has the power to open a gate but also to lock it shut, it was suggested that SmgGDS-607 can help small GTPases gain access to the prenylation pathway but also restrain small GTPases from inappropriately entering the prenylation pathway (Berg et al., 2010). This proposed role of SmgGDS-607 as a gatekeeper for the prenylation pathway is supported by reports that SmgGDS-607 can both facilitate (Berg et al., 2010; Ntantie et al., 2013; Garcia-Torres and Fierke, 2019; Nissim et al., 2019; Brandt et al., 2020) and suppress (Berg et al., 2010; Jennings et al., 2018; Garcia-Torres and Fierke, 2019) the prenylation of small GTPases that bind SmgGDS-607.

SmgGDS-607 recognizes the last amino acid in the CAAX motif of the GTPase, preferring to interact with small GTPases that have a CAAX motif ending in leucine rather than methionine (Schuld N. J. et al., 2014). This finding suggests that SmgGDS-607 preferentially binds small GTPases that are destined to become geranylgeranylated by GGTase-I, since GGTase-I prenylates small GTPases with a CAAX motif ending in leucine. Despite this preference for GTPases that will be geranylgeranylated, SmgGDS-607 also binds small GTPases that have a CAAX motif ending in methionine (Schuld N. J. et al., 2014; Garcia-Torres and Fierke, 2019; Nissim et al., 2019), which will be farnesylated by FTase, indicating that SmgGDS-607 probably regulates the prenylation of both geranylgeranylated and farnesylated small GTPases. The ability of SmgGDS-607 to deliver pre-prenylated Ras and Rho family members to PTases indicates that SmgGDS-607 has functional similarities to REP1, which delivers pre-prenylated Rab family members to RabGGTase (Preising and Ayuso, 2004; Goody et al., 2005; Wu et al., 2007).

SmgGDS-558 differs significantly from SmgGDS-607 because SmgGDS-558 binds only prenylated small GTPases (Berg et al., 2010; Williams 2013; Schuld N. J. et al., 2014). SmgGDS-558 may intercept PBR-containing small GTPases after they have been prenylated by the PTase and help them traffic to the ER for post-prenylation processing (**Figure 2B**). For this interaction to occur, SmgGDS-558 must bind prenylated small GTPases before the C-terminal AAX sequence is cleaved during post-prenylation processing. The ability of SmgGDS-558 to bind prenylated GTPases that retain the AAX sequence is supported by the finding that SmgGDS-558 binds small GTPases that were produced in reticulocyte lysates containing PTases but lacking

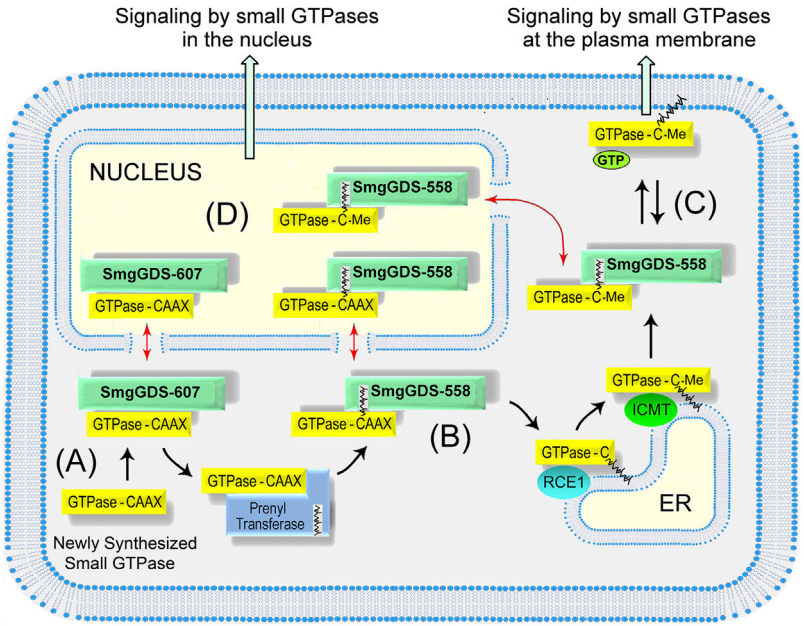

FIGURE 2 | Model depicting how SmgGDS splice variants regulate the prenylation and trafficking of small GTPases. **(A)** SmgGDS-607 binds a newly synthesized small GTPase and retains it until the correct signal causes SmgGDS-607 to release the pre-prenylated GTPase to the PTase. **(B)** SmgGDS-558 escorts newly prenylated small GTPases to the ER for post-prenylation processing. **(C)** SmgGDS-558 escorts prenylated and fully processed small GTPases from the ER to the plasma membrane. **(D)** Both SmgGDS splice variants might assist in nucleocytoplasmic shuttling of small GTPases (red arrows).

the membrane-associated enzyme needed for post-prenylation processing (Lanning et al., 2004; Bergom et al., 2016). Additionally, the Shimizu group solved the crystal structure of SmgGDS-558 bound to prenylated RhoA that still retained the AAX sequence because it had not undergone post-prenylation processing (Shimizu et al., 2018). SmgGDS-558 may help newly prenylated GTPases arrive at the ER membrane or facilitate their interactions with RCE1 and ICMT, which remove the AAX sequence and carboxylmethylate the prenylated GTPase at the ER membrane (**Figure 2B**). These proposed interactions of SmgGDS-558 with newly prenylated GTPases in the Ras and Rho families are functionally similar to the interactions of REP1 with newly prenylated GTPases in the Rab family (Preising and Ayuso, 2004; Goody et al., 2005; Leung et al., 2006; Wu et al., 2007).

It is likely that SmgGDS-558 also acts as a chaperone that helps prenylated small GTPases move to the plasma membrane or other regions of the cell after post-prenylation processing has been completed at the ER (**Figure 2C**) SmgGDS-558 has a hydrophobic pocket that can shield the prenyl group of small GTPases (Shimizu et al., 2018) moving through the aqueous cytosol. Chaperones that shield the prenyl groups of different Ras and Rho family members include PDEδ (Bhagatji et al., 2010; Dharmaiah et al., 2016), PRA1 (Figueroa et al., 2001; Bhagatji et al., 2010), VPS35 (Zhou et al., 2016), and RhoGDI (Garcia-Mata et al., 2011). The chaperone for prenylated Rab proteins is RabGDI (Preising and Ayuso, 2004; Goody et al., 2005; Leung et al., 2006; Wu et al., 2007). Each of these chaperones may have specialized functions. For example, PDEδ helps farnesylated Ras family members such as K-Ras4B move between the plasma membrane and endomembranes (Bhagatji et al., 2010; Dharmaiah et al., 2016), whereas RhoGDI helps geranylgeranylated Rho family members such as RhoA and Rac1 move mainly between the plasma membrane and the cytoplasm (Garcia-Mata et al., 2011). SmgGDS-558 may share multiple functions with these chaperones, since SmgGDS-558 binds multiple Ras and Rho family members that are farnesylated or geranylgeranylated.

In addition to escorting prenylated small GTPases to the plasma membrane, it is likely that SmgGDS-558 also escorts prenylated GTPases into the nucleus (**Figure 2D**). Nucleocytoplasmic shuttling by SmgGDS-558 was discovered in 2003, when it was found to have a N-terminal nuclear export sequence and to accumulate with Rac1 in the nucleus (Lanning et al., 2003). The PBR of Rac1 was discovered to function as a nuclear localization sequence, and exchanging the PBR of Rac1 with the PBR of RhoA, which lacks an NLS, inhibits the nuclear accumulation of Rac1 (Lanning et al., 2003; Lanning et al., 2004). Subsequent studies confirmed the nuclear accumulation of prenylated Rac1 (Michaelson et al., 2008). Several functions of nuclear Rac1 have been described, including controlling nuclear shape (Navarro-Lerida et al., 2015), stimulating rRNA synthesis (Justilien et al., 2017), promoting the cell cycle (Michaelson et al., 2008), inducing neoplastic transformation (Huff et al., 2013), and enhancing malignancy (Huff et al., 2013; Navarro-Lerida et al., 2015; Justilien et al., 2017). Rac1 is activated in the nucleus by the GEF ECT2 (Huff et al., 2013; Justilien et al., 2017), and it is inactivated by a nuclear variant of β1-chimaerin (Casado-Medrano et al., 2020). The binding of prenylated Rac1 to

SmgGDS-558 provides a way for prenylated Rac1 to enter the nucleus and participate in these signaling pathways.

While SmgGDS-558 serves as a nuclear chaperone for prenylated small GTPases, SmgGDS-607 might serve as a nuclear chaperone for pre-prenylated GTPases (**Figure 2D**). Pre-prenylated small GTPases can exhibit significant nuclear accumulation (Roberts et al., 2008; Lee et al., 2012; Ntantie et al., 2013; Navarro-Lerida et al., 2015; Wilson et al., 2015). Many small GTPases accumulate in the nucleus when they are maintained in the pre-prenylated state due to pharmacological inhibition of PTases or mutation of the cysteine in the CAAX motif (Lee et al., 2012; Navarro-Lerida et al., 2015; Wilson et al., 2015). The lack of a prenyl group will keep GTPases from anchoring at membranes, which might cause pre-prenylated GTPases to diffuse passively into the nucleus due to their small size (~21 kDa). The binding of a small GTPase to SmgGDS-607 provides a specific mechanism to control the nuclear entry of small GTPases before they are prenylated. SmgGDS-607 might serve as a chaperone that keeps pre-prenylated GTPases from inappropriately entering the nucleus, or alternatively SmgGDS-607 may actively promote the nuclear entry of some GTPases before they are prenylated. In addition to controlling entry into the nucleus, SmgGDS-558 and SmgGDS-607 might also utilize their N-terminal nuclear export sequence (Lanning et al., 2003) to escort small GTPases out of the nucleus and return them to the cytoplasm when nuclear signaling is completed (**Figure 2D**).

SIGNALING EVENTS AND PROTEIN PARTNERS OF SMGGDS CONTROL THE PRENYLATION AND TRAFFICKING OF RAS AND RHO FAMILY MEMBERS

Events that alter the interactions of SmgGDS with Ras and Rho family members are being recognized as important regulatory mechanisms that control the prenylation and trafficking of these small GTPases. When SmgGDS-607 binds a newly synthesized small GTPase, SmgGDS-607 may retain the small GTPase until the correct signal releases the small GTPase into the prenylation pathway (Berg et al., 2010; Schuld N. J. et al., 2014; Jennings et al., 2018; Garcia-Torres and Fierke, 2019). The signals that release a GTPase from SmgGDS-607 will determine when the GTPase will be prenylated, since the CAAX motif of the GTPase is inaccessible to the PTase as long as the GTPase is bound to SmgGDS-607 (Schuld N. J. et al., 2014). The major signal that releases a GTPase from SmgGDS-607 is thought to be GDP/GTP exchange (Berg et al., 2010), which could be stimulated by a GEF that interacts with the GTPase bound to SmgGDS-607 or by SmgGDS-607 acting as a direct GEF for RhoA or RhoC (Berg et al., 2010; Hamel et al., 2011; Jennings et al., 2018). The report that SmgGDS (now known to be SmgGD-607) forms a complex with Rac1 and the GEF βPIX (Shin et al., 2006) indicates that SmgGDS-607 can facilitate GDP/GTP exchange by bringing small GTPases into contact with their specific GEFs. It was found that GDP/GTP exchange accelerates the prenylation of Rap1 in cells (Berg et al., 2010) but the identities of the GEFs that initiate the prenylation of Rap1 or other GTPases have not yet been determined.

There are over 100 GEFs located in the cytoplasm, nucleus, and at the plasma membrane that can activate members of the Ras and Rho families (Vigil et al., 2010; Gray et al., 2020), and a small GTPase that is bound to SmgGDS-607 may interact with its GEFs in these different regions of the cell. Since SmgGDS is a nucleocytoplasmic shuttling protein that associates with small GTPases in both the cytoplasm and the nucleus (Lanning et al., 2003; Lanning et al., 2004; Gonyo et al., 2017), a pre-prenylated small GTPase that is bound to SmgGDS-607 is likely to encounter both cytoplasmic and nuclear GEFs. If a pre-prenylated GTPase that is bound to SmgGDS-607 encounters its GEF in the cytoplasm, the released GTPase can interact with the cytoplasmic PTase and become prenylated (**Figure 3A**). In contrast, if a pre-prenylated GTPase that is bound to SmgGDS-607 encounters its GEF in the nucleus, the GTPase may be released from SmgGDS-607 in the nucleus, where it may remain in a pre-prenylated state due to the absence of PTases in the nucleus (**Figure 3D**). More studies are needed to define how prenylation is controlled by GEFs that interact with GTPases bound to SmgGDS-607 in different regions of the cell.

Similar to the mechanisms that regulate SmgGDS-607, specific signaling events may control the ability of SmgGDS-558 to deliver and release prenylated small GTPases at specific sites in the cell. Certain signals may direct SmgGDS-558 to the ER membrane, the plasma membrane, or to the nucleus when a prenylated GTPase is bound to SmgGDS-558. The prenylated GTPase may be released from SmgGDS-558 at these sites when it encounters its GEF and undergoes GDP/GTP. By releasing a GTPase from SmgGDS-558, these GEFs will control when the small GTPase will undergo post-prenylation processing (**Figure 3B**) and where it will localize in the cell (**Figures 3C,E,F**). The specific GEFs that release prenylated GTPases from SmgGDS-558 have not yet been identified, but likely candidates include ECT2, Net1, and RapGEF5 which are GEFs that promote GDP/GTP exchange by different Ras and Rho family members in the nucleus and the cytoplasm (Dubash et al., 2011; Huff et al., 2013; Justilien et al., 2017; Griffin et al., 2018). Prenylated GTPases might be released from SmgGDS-558 at the plasma membrane when they encounter membrane-localized GEFs (**Figure 3C**), which will promote membrane association of the GTPases and their participation in signaling cascades at the plasma membrane.

In addition to GEFs, proteins called GDI displacement factors (GDFs) might also release prenylated GTPases from SmgGDS-558 (**Figure 3**). There are several known GDFs that release prenylated GTPases from chaperones such as RabGDI (Dirac-Svejstrup et al., 1997; Collins, 2003; Sivars et al., 2003; Ismail, 2017) and PDEδ (Ismail et al., 2011; Williams, 2011; Dharmaiah et al., 2016; Fansa and Wittinghofer, 2016; Ismail, 2017; Kuchler et al., 2018). Two well characterized GDFs that release farnesylated Ras family members from PDEδ are Arl2 and Arl3, which are members of the Arf family of small GTPases. Arl2 or Arl3 binds PDEδ when a farnesylated Ras family member is also bound to PDEδ, forming a trimeric complex. When the GTP-bound form of Arl2 or Arl3 binds PDEδ, the hydrophobic pocket of PDEδ becomes so narrow that the farnesylated Ras

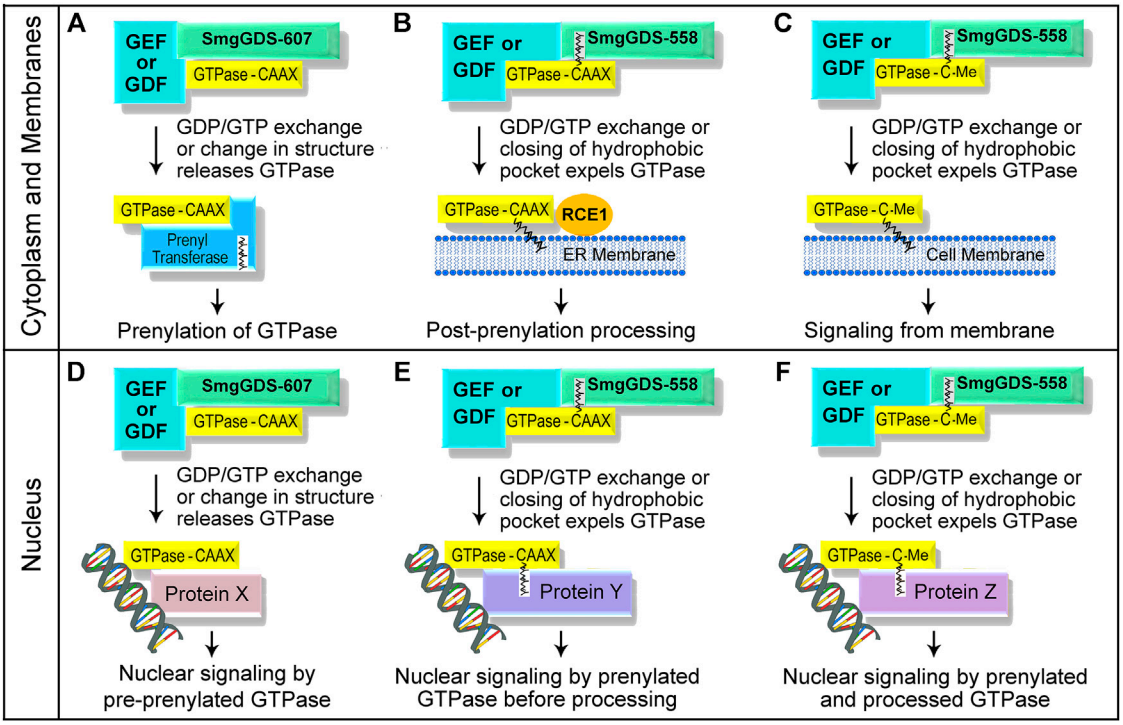

FIGURE 3 | Schematic illustration depicting how unidentified GEFs and GDFs might release small GTPases from SmgGDS splice variants in the cytoplasm and at membranes **(A–C)**, and in the nucleus **(D–F)**. The interactions of these proteins with SmgGDS will control when the small GTPases will be prenylated or undergo post-prenylation processing, and determine where the small GTPases will localize in the cell.

family member is expelled from PDEδ (Ismail et al., 2011; Williams 2011). The farnesylated GTPase that is expelled from PDEδ associates with membranes, where it participates in membrane-localized signaling cascades (Ismail et al., 2011; Williams, 2011; Fansa and Wittinghofer, 2016; Ismail, 2017; Kuchler et al., 2018). It is probable that specific GDFs induce SmgGDS-558 to release prenylated GTPases at membranes (**Figures 3B,C**) or in the nucleus (**Figures 3E,F**). GDF-like proteins may also induce SmgGDS-607 to release pre-prenylated GTPases to PTases (**Figure 3A**) or to nuclear proteins (**Figure 3D**).

Recent studies have identified two abnormal Rab proteins that might serve as GDFs for SmgGDS. These proteins consist of the N-terminal portions of RabL3 (Nissim et al., 2019) or Rab22a (Liao et al., 2020), and exhibit enhanced binding to SmgGDS-607 and SmgGDS-558 in pancreatic cancer (Nissim et al., 2019) and osteosarcoma (Liao et al., 2020), respectively, and are also detected in breast cancer (Nissim et al., 2019; Liao et al., 2020). These abnormal Rab proteins bind to SmgGDS when a member of the Ras or Rho family is also bound to SmgGDS, forming a trimeric complex (Nissim et al., 2019; Liao et al., 2020). The abnormal RabL3 protein that occurs in familial pancreatic cancer is a truncated protein consisting of the first 1–36 amino acids of RabL3, designated RabL3$^{1-36}$ (Nissim et al., 2019). This truncated RabL3$^{1-36}$ protein binds to SmgGDS-607 when K-Ras4B is bound, which increases the prenylation and membrane trafficking of K-Ras4B (Nissim et al., 2019). These findings suggest that RabL3$^{1-36}$ acts as a GDF that binds SmgGDS-607 when pre-prenylated K-Ras4B is also bound, promoting the release of K-Ras4B to the prenyltransferase and accelerating K-Ras4B prenylation, similar to the mechanism depicted in **Figure 3A**. The RabL3$^{1-36}$ protein might also serve as a GDF for SmgGDS-558, similar to the mechanism depicted in **Figure 3C**, because RabL3$^{1-36}$ forms a trimeric complex with SmgGDS-558 and K-Ras4B and accelerates the accumulation of newly synthesized K-Ras4B at membranes (Nissim et al., 2019).

In contrast to the RabL3$^{1-36}$ protein that arises by truncation (Nissim et al., 2019), the abnormal Rab22a proteins that occur in osteosarcoma are fusion proteins consisting of the first 1–38 amino acids of Rab22a followed by various sequences encoded by different regions of chromosome 20 (Liao et al., 2020). The Rab22a$^{1-38}$ portion of these fusion proteins binds to SmgGDS-607 when RhoA is bound (Liao et al., 2020). The formation of this trimeric complex accelerates the release of RhoA from SmgGDS-607, increases GTP-binding by RhoA, and enhances membrane localization of RhoA (Liao et al., 2020). Since only the pre-prenylated form of RhoA binds to SmgGDS-607 (Berg et al., 2010), it is likely that Rab22a$^{1-38}$ promotes the prenylation of RhoA by releasing pre-prenylated RhoA from SmgGDS-607 to the prenyltransferase (**Figure 3A**). However, the effect of Rab22a$^{1-38}$ on the prenylation of RhoA has not yet been determined. Intriguingly, both RabL3$^{1-36}$ and Rab22a$^{1-38}$ interact with several Ras and Rho family members in addition to K-Ras4B and RhoA (Nissim et al., 2019; Liao et al., 2020). It

was also reported that RabL3$^{1-36}$ and Rab22a$^{1-38}$ interact with both SmgGDS-607 and SmgGDS-558 (Nissim et al., 2019; Liao et al., 2020). These features suggest that RabL3$^{1-36}$ and Rab22a$^{1-38}$ may have broad roles as GDFs for multiple Ras and Rho family members that associate with SmgGDS-607 and SmgGDS-558.

In contrast to these mutant Rab proteins, which promote cancer by forming trimeric complexes with SmgGDS and an oncogenic small GTPase (Nissim et al., 2019; Liao et al., 2020), the GTPase DiRas1 (also known as Rig) seems to inhibit cancer by blocking the binding of small GTPases to SmgGDS. DiRas1 is a Ras family member that acts as a tumor suppressor in many types of cancer (reviewed in Li et al., 2019). DiRas1 binds to SmgGDS (Bergom et al., 2016; Gonyo et al., 2017; Garcia-Torres and Fierke, 2019) (**Figure 1B**) and inhibits the binding of other small GTPases, including RhoA, K-Ras4B, and Rap1A (Bergom et al., 2016). *In silico* docking indicates that DiRas1 directly competes with other small GTPases for binding to SmgGDS (Bergom et al., 2016), and DiRas1 binds with much stronger affinity than other Ras and Rho family members to SmgGDS-558 (Bergom et al., 2016) and to SmgGDS-607 (Garcia-Torres and Fierke, 2019). In cancer cells, ectopic expression of DiRas1 inhibits basal and RhoA-mediated NF-kB activity (Bergom et al., 2016) and provokes responses that can be attributed to reduced signaling by Ras and Rho family members [reviewed in Li et al. (2019)]. Ectopic expression of DiRas1 also alters nucleocytoplasmic shuttling of SmgGDS-558 and diminishes its interaction with UBF in the nucleus (Gonyo et al., 2017). These findings support the model that DiRas1 acts as a tumor suppressor by inhibiting the binding of other small GTPases to SmgGDS-607 and SmgGDS-558. DiRas1 is expressed in normal cells, and the binding of DiRas1 to SmgGDS in these cells may suppress SmgGDS interactions with Ras and Rho family members and keep the activity of these GTPases in check. In contrast, the loss of DiRas1 expression in malignant cells removes this brake, allowing SmgGDS to interact with Ras and Rho family members and promote their oncogenic activities (Bergom et al., 2016).

Taken together, these findings indicate that different GEFs, GDFs, and other proteins such as DiRas1 may regulate the interactions of SmgGDS-607 and SmgGDS-558 with pre-prenylated and prenylated GTPases, respectively, in different regions of the cell (**Figure 3**). These interactions will have profound effects on the prenylation, trafficking, and signaling by Ras and Rho family members (**Figure 3**). Future studies are needed to characterize the functions of the abnormal Rab proteins that might act as GDFs for SmgGDS (Nissim et al., 2019; Liao et al., 2020), and to characterize GEFs and other proteins that control the interactions of small GTPases with SmgGDS.

Post-translational modification of either SmgGDS or its small GTPase partner is another event that may alter the interactions between these proteins and affect the prenylation and trafficking of the small GTPase. Post-translational modifications of SmgGDS have not been well characterized. However, signaling cascades that promote the phosphorylation of serines in the PBR of small GTPases have been found to alter the prenylation of small GTPases (Ntantie et al., 2013; Williams, 2013; Wilson et al., 2015; Wilson et al., 2016). The binding of small GTPases to SmgGDS-607 depends on the electrostatic charge of the PBR (Hamel et al., 2011), and diminishing this charge by phosphorylation may diminish interactions with SmgGDS-607. The small GTPases K-Ras4B, Rap1A, Rap1B, and RhoA have serines in their PBRs that can be phosphorylated (reviewed in Williams, 2013), but Rap1B is the GTPase that seems to be most sensitive to phosphorylation-dependent regulation of prenylation (Ntantie et al., 2013; Williams, 2013; Wilson et al., 2015; Wilson et al., 2016).

Activation of A2B adenosine receptors or β-adrenergic receptors causes protein kinase A to phosphorylate two serines in the PBR of Rap1B before it is prenylated (Ntantie et al., 2013; Wilson et al., 2015; Wilson et al., 2016). This phosphorylation diminishes interactions of newly synthesized Rap1B with SmgGDS-607, suppressing Rap1B prenylation and causing pre-prenylated Rap1B to accumulate in the cytoplasm and nucleus (Ntantie et al., 2013; Wilson et al., 2015). The absence of prenylated Rap1B at the plasma membrane diminishes Rap1B-mediated cell–cell adhesion (Ntantie et al., 2013; Wilson et al., 2015), and the nuclear accumulation of pre-prenylated Rap1B may promote events that are known to be regulated by nuclear Rap1B, including signaling by β-catenin (Goto et al., 2010; Griffin et al., 2018). Together, these events induce cell scattering and promote the metastatic phenotype (Ntantie et al., 2013; Wilson et al., 2015). The finding that Rap1B prenylation is reduced in rat mammary tumors provides additional evidence that this pathway has a role in cancer (Ntantie et al., 2013). These findings indicate that chronic exposure of cancer cells to adenosine and norepinephrine in the tumor microenvironment may enhance metastasis by chronically suppressing Rap1B prenylation (Ntantie et al., 2013; Williams, 2013; Wilson et al., 2015; Wilson et al., 2016). There are undoubtedly many more undiscovered signaling cascades that control prenylation by regulating the interactions of small GTPases with SmgGDS-607.

THERAPEUTIC TARGETING OF SMGGDS IN CANCER

SmgGDS has a well-established role in cancer progression. SmgGDS expression is increased in breast, lung, and prostate cancer (Tew et al., 2008; Zhi et al., 2009; Hauser et al., 2014), and elevated SmgGDS expression is associated with poor prognosis in breast cancer (Hauser et al., 2014). SmgGDS promotes cell proliferation, migration, and NF-kB activity in breast, lung, prostate, and pancreatic cancer lines (Tew et al., 2008; Zhi et al., 2009; Berg et al., 2010; Schuld N. J. et al., 2014; Hauser et al., 2014; Gonyo et al., 2017; Brandt et al., 2020) and promotes tumorigenesis of human breast cancer and lung cancer xenografts in mouse models (Schuld N. et al., 2014; Hauser et al., 2014). Early studies of SmgGDS in cancer did not differentiate between SmgGDS-607 and SmgGDS-558 (Tew et al., 2008; Zhi et al., 2009), making it difficult to discern the roles of each splice variant. However, more recent studies have determined that the generation of SmgGDS-607 and SmgGDS-558 is uniquely regulated in cancer cells (Brandt et al., 2020), and both splice

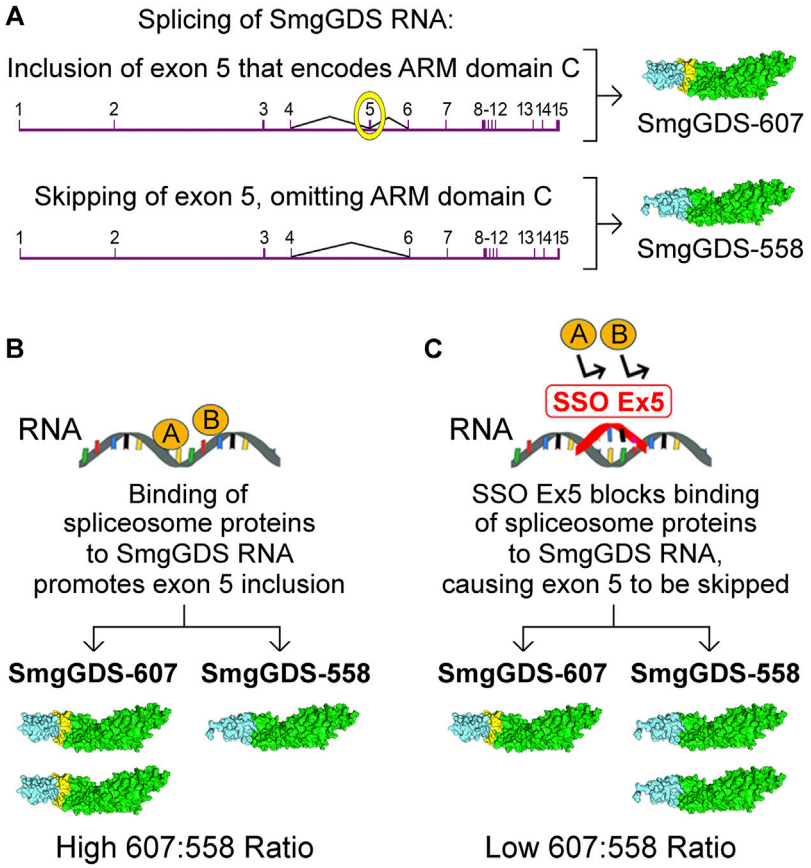

FIGURE 4 | Schematic illustration depicting the regulation of SmgGDS expression by the splice-switching oligonucleotide, SSO Ex5. **(A)** SmgGDS RNA contains 15 exons, and exon 5 encodes ARM domain C. Inclusion of exon 5 in mature SmgGDS mRNA generates SmgGDS-607, whereas omission of exon 5 in mature SmgGDS mRNA generates SmgGDS-558. **(B)** In cancer cells, the binding of unspecified spliceosome proteins to SmgGDS RNA promotes exon 5 inclusion and generates more SmgGDS-607 than SmgGDS-558. **(C)** Binding of SSO Ex5 to SmgGDS RNA promotes exon 5 skipping, generating more SmgGDS-558 than SmgGDS-607. Additional manuscript sections.

variants contribute to malignancy (Berg et al., 2010; Schuld N. et al., 2014; Hauser et al., 2014; Gonyo et al., 2017; Brandt et al., 2020).

An oncogenic splicing program that generates much more SmgGDS-607 than SmgGDS-558 occurs in breast and lung cancer (Brandt et al., 2020). A high ratio of SmgGDS-607: SmgGDS-558 (referred to as the 607:558 ratio) occurs in cells that are rapidly proliferating and migrating, and tissues that contain more proliferative and migratory cells have a higher 607:558 ratio (Brandt et al., 2020). For example, the 607:558 ratio is approximately 2:1 in the mouse spleen, which has a high proportion of cells that proliferate and migrate. In contrast, the 607:558 ratio is approximately 1:3 in the mouse brain, which contains mainly terminally differentiated, non-migratory cells. Most notably, the 607:558 ratio is highest in cancer cell lines, reaching a value of approximately 8:1 (Brandt et al., 2020). Additional evidence that a high 607:558 ratio is associated with malignancy is provided by the finding that the 607:558 ratio increases as mammary tumors develop in rat and mouse models, and a high 607:558 ratio in patients' breast tumors is associated with reduced survival (Brandt et al., 2020).

The very high 607:558 ratio in cancer cells may be related to the increased expression and diversity of Ras and Rho family members needed to maintain the malignant phenotype. The rapid proliferation and migration of cancer cells depends on signaling cascades regulated by many different Ras and Rho family members, resulting in increased expression of small GTPases in the Ras and Rho families in malignant cells (Gómez del Pulgar et al., 2005; Konstantinopoulos et al., 2007; Alan and Lundquist, 2013; Haga and Ridley, 2016; Porter et al., 2016; Wong et al., 2018). Cancer cells may require an elevated amount of SmgGDS-607 to bind the excessive number of newly synthesized small GTPases and facilitate their entry into the prenylation pathway. There is less of a need for SmgGDS-558 than for SmgGDS-607, because SmgGDS-558 intercepts only the proportion of small GTPases that have been released by SmgGDS-607 and have become prenylated. Despite requiring less SmgGDS-558 than SmgGDS-607, cancer cells still need a threshold level of SmgGDS-558, as indicated by reports that the RNAi-mediated depletion of SmgGDS-558 significantly diminishes malignancy (Berg et al., 2010; Schuld N. et al., 2014; Hauser et al., 2014).

The high 607:558 ratio in cancer cells offers a unique therapeutic opportunity to diminish malignancy. Splice-switching oligonucleotides (SSOs) that restore normal splicing are providing new therapies for cancer and other diseases (Havens and Hastings, 2016; El Marabti and Younis, 2018; Bonnal et al., 2020). The value of disrupting SmgGDS RNA splicing as a therapeutic option is demonstrated by the development of SSO Ex5, which is an SSO that lowers the high 607:558 ratio in cancer cells (Brandt et al., 2020). SSO Ex5 was developed by targeting the splicing events that generate SmgGDS-607 and SmgGDS-558 (**Figure 4**). SmgGDS-607 is generated when mature SmgGDS mRNA contains exon 5, which is the exon that encodes ARM C that is present only in SmgGDS-607 (**Figure 4A**). In contrast, SmgGDS-558 is generated when exon 5 is skipped during splicing of SmgGDS pre-mRNA (**Figure 4A**). The binding of currently undefined spliceosome proteins to SmgGDS pre-mRNA causes inclusion of exon 5, resulting in greater expression of SmgGDS-607 than SmgGDS-558 and a high 607:558 ratio (**Figure 4B**). When SSO Ex5 binds to SmgGDS pre-mRNA, SSO Ex5 blocks these spliceosome proteins and forces skipping of exon 5, which decreases SmgGDS-607 expression and increases SmgGDS-558 expression, lowering the 607:558 ratio (**Figure 4C**) (Brandt et al., 2020).

SSO Ex5 suppresses the prenylation of multiple Ras and Rho family members in cancer cells, consistent with SSO Ex5 reducing SmgGDS-607 expression (Brandt et al., 2020). This extensive loss of prenylation is accompanied by a broad range of effects, including changes in RNA expression indicating loss of signaling by Rac, RhoA, PI3K/AKT, and ERK/MAPK. Treatment of cancer cells with SSO Ex5 induces endoplasmic reticulum stress and the unfolded protein response, and ultimately causes apoptosis (Brandt et al., 2020). In addition to decreased SmgGDS-607 expression, it is likely that increased SmgGDS-558 expression also contributes to the effects of SSO Ex5. The excessive increase in the amount of SmgGDS-558 caused by SSO Ex5 might solubilize prenylated GTPases from membranes, due to cytosolic SmgGDS-558 capturing prenylated GTPases as they dissociate from membranes. Additionally, cells treated with SSO Ex5 may have more complexes of free SmgGDS-558 that can capture prenylated GTPases from membranes, because reduced prenylation will decrease the number of newly prenylated GTPases that normally bind to SmgGDS-558. Previous studies indicate that ectopic expression of SmgGDS-558 can solubilize prenylated GTPases from membranes (Kawamura et al., 1991; Kawamura et al., 1993; Nakanishi et al., 1994), and overexpression of SmgGDS-558 was found to promote apoptosis of cancer cells (Brandt et al., 2020). These results indicate that SSO Ex5 most likely inhibits malignancy by the combined effects of decreased SmgGDS-607 expression and increased SmgGDS-558 expression. The potential therapeutic value of SSOs that disrupt SmgGDS expression is indicated by the finding that intraperitoneal injection of SSO Ex5 diminishes mammary tumorigenesis in the aggressive MMTV-PyMT mouse model, without causing detectable deleterious side-effects in the mice (Brandt et al., 2020).

In addition to SSOs, other strategies to inhibit SmgGDS functions in cancer are beginning to be developed. Chemical inhibitors of SmgGDS have not been reported, but a peptide inhibitor that targets SmgGDS-607 has recently been described (Liao et al., 2020). The Kang laboratory generated a cell-penetrating synthetic peptide corresponding to the first 1–10 amino acids in Rab22a, based on their discovery that fusion proteins containing $Rab22a^{1-38}$ bind SmgGDS-607 in osteosarcoma (Liao et al., 2020). They found that this peptide binds to SmgGDS-607, blocks interactions of SmgGDS with $Rab22a^{1-38}$, decreases RhoA activity, and reduces cell migration and invasion. Furthermore, this peptide inhibitor diminishes lung metastases of osteosarcoma in a mouse model, and increases survival time of the mice bearing the tumors (Liao et al., 2020). These findings provide further evidence for the important role of SmgGDS in malignancy, and highlight the value of developing agents to target SmgGDS-607 and SmgGDS-558 in cancer. SmgGDS has recently been recognized to play a role in other disorders such as neurological deficits (Asiri et al., 2020), abnormal vascular branching (Wang et al., 2017), and development of aortic aneurysms (Nogi et al., 2018; Renard, 2018), indicating that the therapeutic targeting of SmgGDS should extend beyond our current efforts focused on cancer.

FUTURE DIRECTIONS

The importance of SmgGDS throughout the animal kingdom is indicated by phylogenetic analyses suggesting that it was present in the last common eukaryotic ancestor that existed over 500 million years ago (Gul et al., 2017). The expression of SmgGDS was maintained during metazoan development, and its functions have become more diverse and complex as animals evolved. The discovery of two complementary but distinctly different splice variants of SmgGDS that regulate the prenylation and trafficking of Ras and Rho family members has defined SmgGDS as a master regulator of these small GTPases. Despite our growing understanding of how SmgGDS interacts with these small GTPases, many questions remain. Some of these questions and critical focal points for future studies are included in the following list:

- *How do cells regulate the expression and activity of SmgGDS-607 and SmgGDS-558?*

The balanced expression of SmgGDS-607 and SmgGDS-558 in cells is regulated through specific splicing programs and spliceosome factors that have yet to be characterized. Additionally, cells control the activities of these splice variants through the actions of DiRas (Bergom et al., 2016), which is expressed in normal cells [reviewed by Li et al. (2019)], and by the actions of mutant forms of both RabL3 and Rab22, which are expressed in cancer cells (Nissim et al., 2019; Liao et al., 2020). There are undoubtedly more regulatory mechanisms that control the expression, stability, and activity of these SmgGDS splice variants in different physiological and pathophysiological conditions.

- *How do post-translational modifications of the SmgGDS splice variants affect their abilities to regulate small GTPases?*

Online databases such as PhosphoSitePlus® indicate that SmgGDS has multiple residues that are ubiquitinated, acetylated, or phosphorylated. Our understanding of how SmgGDS-607 and SmgGDS-558 might be post-translationally modified and how these modifications might affect SmgGDS functions is still very rudimentary.

- *Which small GTPases interact with SmgGDS, and what are the functional consequences of these interactions?*

SmgGDS preferentially binds small GTPases that contain a PBR, including RhoA, RhoC, Rac1, Cdc42, K-Ras4A, Rap1A, Rap1B, and DiRas1, as discussed above. SmgGDS probably binds many more PBR-containing small GTPases (**Table 1**), and these interactions may have multiple effects. In most cases, the binding of a small GTPase to SmgGDS regulates the prenylation and trafficking of the bound GTPase (**Figure 2**). However, some small GTPases control the activity of SmgGDS. For example, DiRas1 inhibits SmgGDS functions (Bergom et al., 2016), whereas RabL3$^{1-36}$ (Nissim et al., 2019), Rab22a$^{1-38}$ (Liao et al., 2020) and potentially wildtype Rab proteins might act as GDFs that control the ability of SmgGDS to release small GTPases in different locations in the cell. More studies are needed to clarify these interactions.

- *Which signaling pathways control the prenylation and trafficking of small GTPases by altering their interactions with SmgGDS?*

Activation of A2B adenosine receptors and β-adrenergic receptors promotes phosphorylation of serines in the PBR of pre-prenylated Rap1B. This phosphorylation of the PBR disrupts the interactions of pre-prenylated Rap1B with SmgGDS-607, suppressing the prenylation of Rap1B and causing it to accumulate in the nucleus instead of localizing at the cell membrane (Ntantie et al., 2013; Wilson et al., 2015; Wilson et al., 2016). Other small GTPases also have serines in their PBR that can be phosphorylated [reviewed in Williams (2013)], and it is possible that their prenylation and trafficking are regulated by signaling pathways that promote or suppress phosphorylation of their PBR.

- *What are the identities of the GEFs that regulate the prenylation and trafficking of small GTPases, and how do they interact with SmgGDS?*

Most studies of GEFs for Ras and Rho family members have focused on GEFs that activate prenylated small GTPases at membranes (Vigil et al., 2010; Gray et al., 2020). Very little is known about GEFs that interact with pre-prenylated small GTPases, or GEFs that interact with small GTPases as they complete the prenylation pathway and move to specific intracellular sites. The finding that the prenylation of some small GTPases is inhibited by the dominant negative mutation that suppresses GDP/GTP exchange (Berg et al., 2010) indicates that specific GEFs promote GDP/GTP exchange by pre-prenylated GTPases and facilitate their prenylation. The identification of these GEFs will provide important insights into the mechanisms that control the prenylation and trafficking of small GTPases.

- *How does SmgGDS participate in different diseases, and what are the best approaches to target SmgGDS therapeutically?*

It is well known that SmgGDS promotes cancer, and it is beginning to be recognized that SmgGDS also contributes to other pathologies, including neurological deficits (Asiri et al., 2020), and vascular abnormalities (Wang et al., 2017; Nogi et al., 2018; Renard, 2018). More studies are needed to define the roles of SmgGDS in these disorders and in other pathological conditions that involve abnormal activity of small GTPases. The therapeutic potential of SmgGDS SSOs (Brandt et al., 2020) and peptide inhibitors (Liao et al., 2020) is evident from recent pre-clinical cancer studies. However, with the crystal structure of SmgGDS now solved (Shimizu et al., 2018), developing small chemical inhibitors to disrupt interactions between SmgGDS and specific GTPase partners is a promising strategy to diminish the activity of oncogenic small GTPases in cancer, and potentially to regulate the activities of small GTPases that interact with SmgGDS in other disorders.

AUTHOR CONTRIBUTIONS

CW provided the original outline of the manuscript, and AB, OK, and CW contributed text, figures, and editorial changes.

FUNDING

Research from the Williams laboratory discussed in this article was supported by funding from the National Institutes of Health (R01 GM069700; R01 CA136799; R01 CA188871) and by the Joan K. Van Deuren Professor in Breast Cancer Research Award, the Kathleen M. Duffey Fogarty Eminent Scholar in Breast Cancer Research Award, and the Nancy Laning Sobczak Breast Cancer Research Award. Additional support was provided by the Wisconsin Breast Cancer Showhouse, the Rock River Cancer Research Foundation, and the Medical College of Wisconsin Cancer Center.

REFERENCES

Akula, M. K., Ibrahim, M. X., Ivarsson, E. G., Khan, O. M., Kumar, I. T., Erlandsson, M., et al. (2019). Protein Prenylation Restrains Innate Immunity by Inhibiting Rac1 Effector Interactions. *Nat. Comun.* 10, 3975. doi:10.1038/s41467-019-11606-x

Alan, J. K., and Lundquist, E. A. (2013). Mutationally Activated Rho GTPases in Cancer. *Small GTPases* 4 (3), 159–163. doi:10.4161/sgtp.26530

Ando, S., Kaibuchi, K., Sasaki, T., Hiraoka, K., Nishiyama, T., Mizuno, T., et al. (1992). Post-translational Processing of Rac P21s Is Important Both for Their Interaction with the GDP/GTP Exchange Proteins and for Their Activation of NADPH Oxidase. *J. Biol. Chem.* 267 (36), 25709–25713. doi:10.1016/s0021-9258(18)35665-5

Andrade, M. A., Petosa, C., O'Donoghue, S. I., Müller, C. W., and Bork, P. (2001). Comparison of ARM and HEAT Protein Repeats. *J. Mol. Biol.* 309 (1), 1–18. doi:10.1006/jmbi.2001.4624

Asiri, A., Aloyouni, E., Umair, M., Alyafee, Y., Al Tuwaijri, A., Alhamoudi, K. M., et al. (2020). MutatedRAP1GDS1causes a New Syndrome of Dysmorphic Feature, Intellectual Disability & Speech Delay. *Ann. Clin. Transl. Neurol.* 7 (6), 956–964. doi:10.1002/acn3.51059

Azoulay-Alfaguter, I., Strazza, M., and Mor, A. (2015). Chaperone-mediated Specificity in Ras and Rap Signaling. *Crit. Rev. Biochem. Mol. Biol.* 50, 194–202. doi:10.3109/10409238.2014.989308

Berg, T. J., Gastonguay, A. J., Lorimer, E. L., Kuhnmuench, J. R., Li, R., Fields, A. P., et al. (2010). Splice Variants of SmgGDS Control Small GTPase Prenylation and Membrane Localization. *J. Biol. Chem.* 285 (46), 35255–35266. doi:10.1074/jbc.m110.129916

Bergom, C., Hauser, A. D., Rymaszewski, A., Gonyo, P., Prokop, J. W., Jennings, B. C., et al. (2016). The Tumor-Suppressive Small GTPase DiRas1 Binds the Noncanonical Guanine Nucleotide Exchange Factor SmgGDS and Antagonizes SmgGDS Interactions with Oncogenic Small GTPases. *J. Biol. Chem.* 291 (12), 6534–6545. doi:10.1074/jbc.m115.696831

Bhagatji, P., Leventis, R., Rich, R., Lin, C.-j., and Silvius, J. R. (2010). Multiple Cellular Proteins Modulate the Dynamics of K-Ras Association with the Plasma Membrane. *Biophysical J.* 99 (10), 3327–3335. doi:10.1016/j.bpj.2010.10.001

Bonnal, S. C., López-Oreja, I., and Valcárcel, J. (2020). Roles and Mechanisms of Alternative Splicing in Cancer - Implications for Care. *Nat. Rev. Clin. Oncol.* 17 (8), 457–474. doi:10.1038/s41571-020-0350-x

Brandt, A. C., McNally, L., Lorimer, E. L., Unger, B., Koehn, O. J., Suazo, K. F., et al. (2020). Splice Switching an Oncogenic Ratio of SmgGDS Isoforms as a Strategy to Diminish Malignancy. *Proc. Natl. Acad. Sci. U.S.A.* 117 (7), 3627–3636. doi:10.1073/pnas.1914153117

Casado-Medrano, V., Barrio-Real, L., Gutiérrez-Miranda, L., González-Sarmiento, R., Velasco, E. A., Kazanietz, M. G., et al. (2020). Identification of a Truncated β1-chimaerin Variant that Inactivates Nuclear Rac1. *J. Biol. Chem.* 295 (5), 1300–1314. doi:10.1074/jbc.ra119.008688

Chuang, T. H., Xu, X., Quilliam, L. A., and Bokoch, G. M. (1994). SmgGDS Stabilizes Nucleotide-Bound and -free Forms of the Rac1 GTP-Binding Protein and Stimulates GTP/GDP Exchange through a Substituted Enzyme Mechanism. *Biochem. J.* 303 (Pt 3), 761–767. doi:10.1042/bj3030761

Collins, R. N. (2003). "Getting it On"-GDI Displacement and Small GTPase Membrane Recruitment. *Mol. Cel* 12 (5), 1064–1066. doi:10.1016/s1097-2765(03)00445-3

Cox, A. D., Der, C. J., and Philips, M. R. (2015). Targeting RAS Membrane Association: Back to the Future for Anti-RAS Drug Discovery? *Clin. Cancer Res.* 21 (8), 1819–1827. doi:10.1158/1078-0432.ccr-14-3214

Dharmaiah, S., Bindu, L., Tran, T. H., Gillette, W. K., Frank, P. H., Ghirlando, R., et al. (2016). Structural Basis of Recognition of Farnesylated and Methylated KRAS4b by PDEδ. *Proc. Natl. Acad. Sci. U.S.A.* 113 (44), E6766–E6775. doi:10.1073/pnas.1615316113

Dirac-Svejstrup, A. B., Sumizawa, T., and Pfeffer, S. R. (1997). Identification of a GDI Displacement Factor that Releases Endosomal Rab GTPases from Rab-GDI. *EMBO J.* 16 (3), 465–472. doi:10.1093/emboj/16.3.465

Dubash, A. D., Guilluy, C., Srougi, M. C., Boulter, E., Burridge, K., and García-Mata, R. (2011). The Small GTPase RhoA Localizes to the Nucleus and Is Activated by Net1 and DNA Damage Signals. *PLoS One* 6 (2), e17380. doi:10.1371/journal.pone.0017380

Dunford, J. E., Rogers, M. J., Ebetino, F. H., Phipps, R. J., and Coxon, F. P. (2006). Inhibition of Protein Prenylation by Bisphosphonates Causes Sustained Activation of Rac, Cdc42, and Rho GTPases. *J. Bone Miner. Res.* 21 (5), 684–694. doi:10.1359/jbmr.060118

El Marabti, E., and Younis, I. (2018). The Cancer Spliceome: Reprograming of Alternative Splicing in Cancer. *Front. Mol. Biosci.* 5, 80. doi:10.3389/fmolb.2018.00080

Fansa, E. K., and Wittinghofer, A. (2016). Sorting of Lipidated Cargo by the Arl2/Arl3 System. *Small GTPases* 7 (4), 222–230. doi:10.1080/21541248.2016.1224454

Figueroa, C., Taylor, J., and Vojtek, A. B. (2001). Prenylated Rab Acceptor Protein Is a Receptor for Prenylated Small GTPases. *J. Biol. Chem.* 276 (30), 28219–28225. doi:10.1074/jbc.m101763200

Fujioka, H., Kaibuchi, K., Kishi, K., Yamamoto, T., Kawamura, M., Sakoda, T., et al. (1992). Transforming and C-Fos Promoter/enhancer-Stimulating Activities of a Stimulatory GDP/GTP Exchange Protein for Small GTP-Binding Proteins. *J. Biol. Chem.* 267 (2), 926–930. doi:10.1016/s0021-9258(18)48373-1

Garcia-Mata, R., Boulter, E., and Burridge, K. (2011). The 'invisible Hand': Regulation of RHO GTPases by RHOGDIs. *Nat. Rev. Mol. Cel Biol.* 12 (8), 493–504. doi:10.1038/nrm3153

García-Torres, D., and Fierke, C. A. (2019). The Chaperone SmgGDS-607 Has a Dual Role, Both Activating and Inhibiting Farnesylation of Small GTPases. *J. Biol. Chem.* 294 (31), 11793–11804. doi:10.1074/jbc.ra119.007438

Gayle, S., Pan, Y., Landrette, S., and Xu, T. (2015). piggyBac Insertional Mutagenesis Screen Identifies a Role for Nuclear RHOA in Human ES Cell Differentiation. *Stem Cel Rep.* 4 (5), 926–938. doi:10.1016/j.stemcr.2015.03.001

Gómez del Pulgar, T., Benitah, S. A., Valerón, P. F., Espina, C., and Lacal, J. C. (2005). Rho GTPase Expression in Tumourigenesis: Evidence for a Significant Link. *Bioessays* 27 (6), 602–613. doi:10.1002/bies.20238

Gonyo, P., Bergom, C., Brandt, A. C., Tsaih, S.-W., Sun, Y., Bigley, T. M., et al. (2017). SmgGDS Is a Transient Nucleolar Protein that Protects Cells from Nucleolar Stress and Promotes the Cell Cycle by Regulating DREAM Complex Gene Expression. *Oncogene* 36 (50), 6873–6883. doi:10.1038/onc.2017.280

Goody, R. S., Rak, A., and Alexandrov, K. (2005). The Structural and Mechanistic Basis for Recycling of Rab Proteins between Membrane Compartments. *Cmls, Cel. Mol. Life Sci.* 62 (15), 1657–1670. doi:10.1007/s00018-005-4486-8

Goto, M., Mitra, R. S., Liu, M., Lee, J., Henson, B. S., Carey, T., et al. (2010). Rap1 Stabilizes -Catenin and Enhances -catenin-dependent Transcription and Invasion in Squamous Cell Carcinoma of the Head and Neck. *Clin. Cancer Res.* 16 (1), 65–76. doi:10.1158/1078-0432.ccr-09-1122

Gray, J. L., Delft, F., and Brennan, P. E. (2020). Targeting the Small GTPase Superfamily through Their Regulatory Proteins. *Angew. Chem. Int. Ed.* 59 (16), 6342–6366. doi:10.1002/anie.201900585

Griffin, J. N., Del Viso, F., Duncan, A. R., Robson, A., Hwang, W., Kulkarni, S., et al. (2018). RAPGEF5 Regulates Nuclear Translocation of β-Catenin. *Developmental Cel.* 44 (2), 248–260. doi:10.1016/j.devcel.2017.12.001

Gul, I. S., Hulpiau, P., Saeys, Y., and van Roy, F. (2017). Metazoan Evolution of the Armadillo Repeat Superfamily. *Cell. Mol. Life Sci.* 74 (3), 525–541. doi:10.1007/s00018-016-2319-6

Haga, R. B., and Ridley, A. J. (2016). Rho GTPases: Regulation and Roles in Cancer Cell Biology. *Small GTPases* 7 (4), 207–221. doi:10.1080/21541248.2016.1232583

Hamel, B., Monaghan-Benson, E., Rojas, R. J., Temple, B. R. S., Marston, D. J., Burridge, K., et al. (2011). SmgGDS Is a Guanine Nucleotide Exchange Factor that Specifically Activates RhoA and RhoC. *J. Biol. Chem.* 286 (14), 12141–12148. doi:10.1074/jbc.m110.191122

Hauser, A. D., Bergom, C., Schuld, N. J., Chen, X., Lorimer, E. L., Huang, J., et al. (2014). The SmgGDS Splice Variant SmgGDS-558 Is a Key Promoter of Tumor Growth and RhoA Signaling in Breast Cancer. *Mol. Cancer Res.* 12 (1), 130–142. doi:10.1158/1541-7786.mcr-13-0362

Havens, M. A., and Hastings, M. L. (2016). Splice-switching Antisense Oligonucleotides as Therapeutic Drugs. *Nucleic Acids Res.* 44 (14), 6549–6563. doi:10.1093/nar/gkw533

Hiraoka, K., Kaibuchi, K., Ando, S., Musha, T., Takaishi, K., Mizuno, T., et al. (1992). Both stimulatory and Inhibitory GDPGTP Exchange Proteins, Smg GDS and Rho GDI, Are Active on Multiple Small GTP-Binding Proteins. *Biochem. Biophysical Res. Commun.* 182 (2), 921–930. doi:10.1016/0006-291x(92)91820-g

Hiroyoshi, M., Kaibuchi, K., Kawamura, S., Hata, Y., and Takai, Y. (1991). Role of the C-Terminal Region of Smg P21, a Ras P21-like Small GTP-Binding Protein, in Membrane and Smg P21 GDP/GTP Exchange Protein Interactions. *J. Biol. Chem.* 266 (5), 2962–2969. doi:10.1016/s0021-9258(18)49941-3

Huff, L. P., Decristo, M. J., Trembath, D., Kuan, P. F., Yim, M., Liu, J., et al. (2013). The Role of Ect2 Nuclear RhoGEF Activity in Ovarian Cancer Cell Transformation. *Genes Cancer* 4 (11-12), 460–475. doi:10.1177/1947601913514851

Hutagalung, A. H., and Novick, P. J. (2011). Role of Rab GTPases in Membrane Traffic and Cell Physiology. *Physiol. Rev.* 91 (1), 119–149. doi:10.1152/physrev.00059.2009

Hutchinson, J. P., and Eccleston, J. F. (2000). Mechanism of Nucleotide Release from Rho by the GDP Dissociation Stimulator Protein. *Biochemistry* 39 (37), 11348–11359. doi:10.1021/bi0007573

Hutchinson, J. P., Rittinger, K., and Eccleston, J. F. (2000). Purification and Characterization of Guanine Nucleotide Dissociation Stimulator Protein. *Methods Enzymol.* 325, 71–82. doi:10.1016/s0076-6879(00)25432-3

Ismail, S. (2017). A GDI/GDF-like System for Sorting and Shuttling Ciliary Proteins. *Small GTPases* 8 (4), 208–211. doi:10.1080/21541248.2016.1213782

Ismail, S. A., Chen, Y.-X., Rusinova, A., Chandra, A., Bierbaum, M., Gremer, L., et al. (2011). Arl2-GTP and Arl3-GTP Regulate a GDI-like Transport System for Farnesylated Cargo. *Nat. Chem. Biol.* 7 (12), 942–949. doi:10.1038/nchembio.686

Jennings, B. C., Lawton, A. J., Rizk, Z., and Fierke, C. A. (2018). SmgGDS-607 Regulation of RhoA GTPase Prenylation Is Nucleotide-dependent. *Biochemistry* 57 (29), 4289–4298. doi:10.1021/acs.biochem.8b00567

Justilien, V., Ali, S. A., Jamieson, L., Yin, N., Cox, A. D., Der, C. J., et al. (2017). Ect2-Dependent rRNA Synthesis Is Required for KRAS-TRP53 -Driven Lung Adenocarcinoma. *Cancer Cell* 31 (2), 256–269. doi:10.1016/j.ccell.2016.12.010

Kaibuchi, K., Mizuno, T., Fujioka, H., Yamamoto, T., Kishi, K., Fukumoto, Y., et al. (1991). Molecular Cloning of the cDNA for Stimulatory GDP/GTP Exchange Protein for Smg P21s (Ras P21-like Small GTP-Binding Proteins) and Characterization of Stimulatory GDP/GTP Exchange Protein. *Mol. Cel. Biol.* 11 (5), 2873–2880. doi:10.1128/mcb.11.5.2873

Kattan, W. E., and Hancock, J. F. (2020). RAS Function in Cancer Cells: Translating Membrane Biology and Biochemistry into New Therapeutics. *Biochem. J.* 477 (15), 2893–2919. doi:10.1042/bcj20190839

Kawamura, M., Kaibuchi, K., Kishi, K., and Takai, Y. (1993). Translocation of Ki-Ras P21 between Membrane and Cytoplasm by Smg GDS. *Biochem. Biophysical Res. Commun.* 190 (3), 832–841. doi:10.1006/bbrc.1993.1124

Kawamura, S., Kaibuchi, K., Hiroyoshi, M., Hata, Y., and Takai, Y. (1991). Stoichiometric Interaction of Smg P21 with its GDPGTP Exchange Protein and its Novel Action to Regulate the Translocation of Smg P21 between Membrane and Cytoplasm. *Biochem. Biophysical Res. Commun.* 174 (3), 1095–1102. doi:10.1016/0006-291x(91)91533-i

Khan, O. M., Akula, M. K., Skålen, K., Karlsson, C., Ståhlman, M., Young, S. G., et al. (2013). Targeting GGTase-I Activates RHOA, Increases Macrophage Reverse Cholesterol Transport, and Reduces Atherosclerosis in Mice. *Circulation* 127 (7), 782–790. doi:10.1161/circulationaha.112.000588

Khan, O. M., Ibrahim, M. X., Jonsson, I.-M., Karlsson, C., Liu, M., Sjogren, A.-K. M., et al. (2011). Geranylgeranyltransferase Type I (GGTase-I) Deficiency Hyperactivates Macrophages and Induces Erosive Arthritis in Mice. *J. Clin. Invest.* 121 (2), 628–639. doi:10.1172/jci43758

Kikuchi, A., Kuroda, S., Sasaki, T., Kotani, K., Hirata, K., Katayama, M., et al. (1992). Functional Interactions of Stimulatory and Inhibitory GDP/GTP Exchange Proteins and Their Common Substrate Small GTP-Binding Protein. *J. Biol. Chem.* 267 (21), 14611–14615. doi:10.1016/s0021-9258(18)42085-6

Konstantinopoulos, P. A., Karamouzis, M. V., and Papavassiliou, A. G. (2007). Post-translational Modifications and Regulation of the RAS Superfamily of GTPases as Anticancer Targets. *Nat. Rev. Drug Discov.* 6 (7), 541–555. doi:10.1038/nrd2221

Küchler, P., Zimmermann, G., Winzker, M., Janning, P., Waldmann, H., and Ziegler, S. (2018). Identification of Novel PDEδ Interacting Proteins. *Bioorg. Med. Chem.* 26 (8), 1426–1434. doi:10.1016/j.bmc.2017.08.033

Lane, K. T., and Beese, L. S. (2006). Thematic Review Series: Lipid Posttranslational Modifications. Structural Biology of Protein Farnesyltransferase and Geranylgeranyltransferase Type I. *J. Lipid Res.* 47 (4), 681–699. doi:10.1194/jlr.r600002-jlr200

Lanning, C. C., Daddona, J. L., Ruiz-Velasco, R., Shafer, S. H., and Williams, C. L. (2004). The Rac1 C-Terminal Polybasic Region Regulates the Nuclear Localization and Protein Degradation of Rac1. *J. Biol. Chem.* 279 (42), 44197–44210. doi:10.1074/jbc.m404977200

Lanning, C. C., Ruiz-Velasco, R., and Williams, C. L. (2003). Novel Mechanism of the Co-regulation of Nuclear Transport of SmgGDS and Rac1. *J. Biol. Chem.* 278 (14), 12495–12506. doi:10.1074/jbc.m211286200

Lee, K., Chen, Q. K., Lui, C., Cichon, M. A., Radisky, D. C., and Nelson, C. M. (2012). Matrix Compliance Regulates Rac1b Localization, NADPH Oxidase Assembly, and Epithelial-Mesenchymal Transition. *MBoC* 23 (20), 4097–4108. doi:10.1091/mbc.e12-02-0166

Leung, K. F., Baron, R., and Seabra, M. C. (2006). Thematic Review Series: Lipid Posttranslational Modifications. Geranylgeranylation of Rab GTPases. *J. Lipid Res.* 47 (3), 467–475. doi:10.1194/jlr.r500017-jlr200

Li, X., Liu, S., Fang, X., He, C., and Hu, X. (2019). The Mechanisms of DIRAS Family Members in Role of Tumor Suppressor. *J. Cel. Physiol.* 234 (5), 5564–5577. doi:10.1002/jcp.27376

Liao, D., Zhong, L., Yin, J., Zeng, C., Wang, X., Huang, X., et al. (2020). Chromosomal Translocation-Derived Aberrant Rab22a Drives Metastasis of Osteosarcoma. *Nat. Cel. Biol.* 22 (7), 868–881. doi:10.1038/s41556-020-0522-z

Michaelson, D., Abidi, W., Guardavaccaro, D., Zhou, M., Ahearn, I., Pagano, M., et al. (2008). Rac1 Accumulates in the Nucleus during the G2 Phase of the Cell Cycle and Promotes Cell Division. *J. Cel Biol.* 181 (3), 485–496. doi:10.1083/jcb.200801047

Mitra, R. S., Zhang, Z., Henson, B. S., Kurnit, D. M., Carey, T. E., and D'Silva, N. J. (2003). Rap1A and rap1B Ras-Family Proteins Are Prominently Expressed in the Nucleus of Squamous Carcinomas: Nuclear Translocation of GTP-Bound Active Form. *Oncogene* 22 (40), 6243–6256. doi:10.1038/sj.onc.1206534

Mizuno, T., Kaibuchi, K., Ando, S., Musha, T., Hiraoka, K., Takaishi, K., et al. (1992). Regulation of the Superoxide-Generating NADPH Oxidase by a Small GTP-Binding Protein and its Stimulatory and Inhibitory GDP/GTP Exchange Proteins. *J. Biol. Chem.* 267 (15), 10215–10218. doi:10.1016/s0021-9258(19)50005-9

Mizuno, T., Kaibuchi, K., Yamamoto, T., Kawamura, M., Sakoda, T., Fujioka, H., et al. (1991). A Stimulatory GDP/GTP Exchange Protein for Smg P21 Is Active on the post-translationally Processed Form of C-Ki-Ras P21 and rhoA P21. *Proc. Natl. Acad. Sci.* 88 (15), 6442–6446. doi:10.1073/pnas.88.15.6442

Nakanishi, H., Kaibuchi, K., Orita, S., Ueno, N., and Takai, Y. (1994). Different Functions of Smg GDP Dissociation Stimulator and Mammalian Counterpart of Yeast Cdc25. *J. Biol. Chem.* 269 (21), 15085–15091. doi:10.1016/s0021-9258(17)36577-8

Navarro-Lérida, I., Pellinen, T., Sanchez, S. A., Guadamillas, M. C., Wang, Y., Mirtti, T., et al. (2015). Rac1 Nucleocytoplasmic Shuttling Drives Nuclear Shape Changes and Tumor Invasion. *Developmental Cel* 32 (3), 318–334. doi:10.1016/j.devcel.2014.12.019

Nissim, S., Leshchiner, I., Mancias, J. D., Greenblatt, M. B., Maertens, O., Cassa, C. A., et al. (2019). Mutations in RABL3 Alter KRAS Prenylation and Are Associated with Hereditary Pancreatic Cancer. *Nat. Genet.* 51 (9), 1308–1314. doi:10.1038/s41588-019-0475-y

Nogi, M., Satoh, K., Sunamura, S., Kikuchi, N., Satoh, T., Kurosawa, R., et al. (2018). Small GTP-Binding Protein GDP Dissociation Stimulator Prevents Thoracic Aortic Aneurysm Formation and Rupture by Phenotypic Preservation of Aortic Smooth Muscle Cells. *Circulation* 138 (21), 2413–2433. doi:10.1161/circulationaha.118.035648

Ntantie, E., Gonyo, P., Lorimer, E. L., Hauser, A. D., Schuld, N., McAllister, D., et al. (2013). An Adenosine-Mediated Signaling Pathway Suppresses Prenylation of the GTPase Rap1B and Promotes Cell Scattering. *Sci. Signal.* 6, 277. doi:10.1126/scisignal.2003374

Orita, S., Kaibuchi, K., Kuroda, S., Shimizu, K., Nakanishi, H., and Takai, Y. (1993). Comparison of Kinetic Properties between Two Mammalian Ras P21 GDP/GTP Exchange Proteins, Ras Guanine Nucleotide-Releasing Factor and Smg GDP Dissociation Stimulation. *J. Biol. Chem.* 268 (34), 25542–25546. doi:10.1016/s0021-9258(19)74425-1

Porter, A. P., Papaioannou, A., and Malliri, A. (2016). Deregulation of Rho GTPases in Cancer. *Small GTPases* 7 (3), 123–138. doi:10.1080/21541248.2016.1173767

Preising, M., and Ayuso, C. (2004). Rab Escort Protein 1 (REP1) in Intracellular Traffic: a Functional and Pathophysiological Overview. *Ophthalmic Genet.* 25 (2), 101–110. doi:10.1080/13816810490514333

Reddy, J. M., Samuel, F. G., McConnell, J. A., Reddy, C. P., Beck, B. W., and Hynds, D. L. (2015). Non-prenylatable, Cytosolic Rac1 Alters Neurite Outgrowth while Retaining the Ability to Be Activated. *Cell Signal.* 27 (3), 630–637. doi:10.1016/j.cellsig.2014.11.033

Renard, M. (2018). SmgGDS, a New Piece in the Thoracic Aortic Aneurysm and Dissection Puzzle. *J. Thorac. Dis.* 10 (Suppl. 33), S4133–S4136. doi:10.21037/jtd.2018.10.68

Roberts, P. J., Mitin, N., Keller, P. J., Chenette, E. J., Madigan, J. P., Currin, R. O., et al. (2008). Rho Family GTPase Modification and Dependence on CAAX Motif-Signaled Posttranslational Modification. *J. Biol. Chem.* 283 (37), 25150–25163. doi:10.1074/jbc.m800882200

Schuld, N., Hauser, A., Gastonguay, A., Wilson, J., Lorimer, E., and Williams, C. (2014a). SmgGDS-558 Regulates the Cell Cycle in Pancreatic, Non-small Cell Lung, and Breast Cancers. *Cell Cycle* 13 (6), 941–952. doi:10.4161/cc.27804

Schuld, N. J., Vervacke, J. S., Lorimer, E. L., Simon, N. C., Hauser, A. D., Barbieri, J. T., et al. (2014b). The Chaperone Protein SmgGDS Interacts with Small GTPases Entering the Prenylation Pathway by Recognizing the Last Amino Acid in the CAAX Motif. *J. Biol. Chem.* 289 (10), 6862–6876. doi:10.1074/jbc.m113.527192

Seabra, M. C., Mules, E. H., and Hume, A. N. (2002). Rab GTPases, Intracellular Traffic and Disease. *Trends Mol. Med.* 8 (1), 23–30. doi:10.1016/s1471-4914(01)02227-4

Shimizu, H., Toma-Fukai, S., Kontani, K., Katada, T., and Shimizu, T. (2018). GEF Mechanism Revealed by the Structure of SmgGDS-558 and Farnesylated RhoA Complex and its Implication for a Chaperone Mechanism. *Proc. Natl. Acad. Sci. U.S.A.* 115 (38), 9563–9568. doi:10.1073/pnas.1804740115

Shimizu, H., Toma-Fukai, S., Saijo, S., Shimizu, N., Kontani, K., Katada, T., et al. (2017). Structure-based Analysis of the Guanine Nucleotide Exchange Factor SmgGDS Reveals Armadillo-Repeat Motifs and Key Regions for Activity and GTPase Binding. *J. Biol. Chem.* 292 (32), 13441–13448. doi:10.1074/jbc.m117.792556

Shin, E.-Y., Lee, C.-S., Cho, T. G., Kim, Y. G., Song, S., Juhnn, Y.-S., et al. (2006). βPak-Interacting Exchange Factor-Mediated Rac1 Activation Requires smgGDS Guanine Nucleotide Exchange Factor in Basic Fibroblast Growth Factor-Induced Neurite Outgrowth. *J. Biol. Chem.* 281 (47), 35954–35964. doi:10.1074/jbc.m602399200

Shirataki, H., Kaibuchi, K., Hiroyoshi, M., Isomura, M., Araki, S., Sasaki, T., et al. (199120672–20677). Inhibition of the Action of the Stimulatory GDP/GTP Exchange Protein for Smg P21 by the Geranylgeranylated Synthetic Peptides Designed from its C-Terminal Region. *J. Biol. Chem.* 266 (31). doi:10.1016/s0021-9258(18)54761-x

Sivars, U., Aivazian, D., and Pfeffer, S. R. (2003). Yip3 Catalyses the Dissociation of Endosomal Rab-GDI Complexes. *Nature* 425, 6960856–6960859. doi:10.1038/nature02057

Staus, D. P., Weise-Cross, L., Mangum, K. D., Medlin, M. D., Mangiante, L., Taylor, J. M., et al. (2014). Nuclear RhoA Signaling Regulates MRTF-dependent SMC-specific Transcription. *Am. J. Physiology-Heart Circulatory Physiol.* 307 (3), H379–H390. doi:10.1152/ajpheart.01002.2013

Tew, G. W., Lorimer, E. L., Berg, T. J., Zhi, H., Li, R., and Williams, C. L. (2008). SmgGDS Regulates Cell Proliferation, Migration, and NF-Kb Transcriptional Activity in Non-small Cell Lung Carcinoma. *J. Biol. Chem.* 283 (2), 963–976. doi:10.1074/jbc.m707526200

Tulpule, A., Guan, J., Neel, D. S., Allegakoen, H. R., Lin, Y. P., Brown, D., et al. (2021). Kinase-mediated RAS Signaling via Membraneless Cytoplasmic Protein Granules. *Cell* 184 (10), 2649–2664. doi:10.1016/j.cell.2021.03.031

Uprety, D., and Adjei, A. A. (2020). KRAS: From Undruggable to a Druggable Cancer Target. *Cancer Treat. Rev.* 89, 102070. doi:10.1016/j.ctrv.2020.102070

Vigil, D., Cherfils, J., Rossman, K. L., and Der, C. J. (2010). Ras Superfamily GEFs and GAPs: Validated and Tractable Targets for Cancer Therapy?. *Nat. Rev. Cancer* 10 (12), 842–857. doi:10.1038/nrc2960

Wang, M., and Casey, P. J. (2016). Protein Prenylation: Unique Fats Make Their Mark on Biology. *Nat. Rev. Mol. Cel Biol.* 17 (2), 110–122. doi:10.1038/nrm.2015.11

Wang, S., Yin, Z., Zhao, B., Qi, Y., Liu, J., Rahimi, S. A., et al. (2017). Microgravity Simulation Activates Cdc42 via Rap1GDS1 to Promote Vascular branch Morphogenesis during Vasculogenesis. *Stem Cel Res.* 25, 157–165. doi:10.1016/j.scr.2017.11.002

Williams, C. (2013). A New Signaling Paradigm to Control the Prenylation and Trafficking of Small GTPases. *Cell Cycle* 12 (18), 2933–2934. doi:10.4161/cc.26230

Williams, R. L. (2011). Arls Squeeze the Fat Out. *Nat. Chem. Biol.* 7 (12), 863–864. doi:10.1038/nchembio.713

Wilson, J. M., Lorimer, E., Tyburski, M. D., and Williams, C. L. (2015). β-Adrenergic Receptors Suppress Rap1B Prenylation and Promote the Metastatic Phenotype in Breast Cancer Cells. *Cancer Biol. Ther.* 16 (9), 1364–1374. doi:10.1080/15384047.2015.1070988

Wilson, J. M., Prokop, J. W., Lorimer, E., Ntantie, E., and Williams, C. L. (2016). Differences in the Phosphorylation-dependent Regulation of Prenylation of Rap1A and Rap1B. *J. Mol. Biol.* 428 (24 Pt B), 4929–4945. doi:10.1016/j.jmb.2016.10.016

Wong, G. S., Zhou, J., Liu, J. B., Wu, Z., Xu, X., Li, T., et al. (2018). Targeting Wild-type KRAS-Amplified Gastroesophageal Cancer through Combined MEK and SHP2 Inhibition. *Nat. Med.* 24 (7), 968–977. doi:10.1038/s41591-018-0022-x

Wright, L. P., and Philips, M. R. (2006). Thematic Review Series: Lipid Posttranslational Modifications CAAX Modification and Membrane Targeting of Ras. *J. Lipid Res.* 47 (5), 883–891. doi:10.1194/jlr.r600004-jlr200

Wu, Y.-W., Tan, K.-T., Waldmann, H., Goody, R. S., and Alexandrov, K. (2007). Interaction Analysis of Prenylated Rab GTPase with Rab Escort Protein and GDP Dissociation Inhibitor Explains the Need for Both Regulators. *Proc. Natl. Acad. Sci.* 104 (30), 12294–12299. doi:10.1073/pnas.0701817104

Xu, X., Wang, Y., Barry, D. C., Chanock, S. J., and Bokoch, G. M. (1997). Guanine Nucleotide Binding Properties of Rac2 Mutant Proteins and Analysis of the Responsiveness to Guanine Nucleotide Dissociation Stimulator,. *Biochemistry* 36 (3), 626–632. doi:10.1021/bi962059h

Yaku, H., Sasaki, T., and Takai, Y. (1994). The Dbl Oncogene Product as a GDP/GTP Exchange Protein for the Rho Family: its Properties in Comparison with Those of Smg GDS. *Biochem. Biophysical Res. Commun.* 198 (2), 811–817. doi:10.1006/bbrc.1994.1116

Yamamoto, T., Kaibuchi, K., Mizuno, T., Hiroyoshi, M., Shirataki, H., and Takai, Y. (1990). Purification and Characterization from Bovine Brain Cytosol of Proteins that Regulate the GDP/GTP Exchange Reaction of Smg P21s, Ras P21-like GTP-Binding Proteins. *J. Biol. Chem.* 265 (27), 16626–16634. doi:10.1016/s0021-9258(17)46268-5

Yoshida, Y., Kawata, M., Miura, Y., Musha, T., Sasaki, T., Kikuchi, A., et al. (1992). Microinjection of smg/rap1/Krev-1 P21 into Swiss 3T3 Cells Induces DNA Synthesis and Morphological Changes. *Mol. Cel. Biol.* 12 (8), 3407–3414. doi:10.1128/mcb.12.8.3407

Zhi, H., Yang, X., Kuhnmuench, J., Berg, T., Thill, R., Yang, H., et al. (2009). SmgGDS Is Up-Regulated in Prostate Carcinoma and Promotes Tumour Phenotypes in Prostate Cancer Cells. *J. Pathol.* 217 (3), 389–397. doi:10.1002/path.2456

Zhou, M., Wiener, H., Su, W., Zhou, Y., Liot, C., Ahearn, I., et al. (2016). VPS35 Binds Farnesylated N-Ras in the Cytosol to Regulate N-Ras Trafficking. *J. Cel Biol.* 214 (4), 445–458. doi:10.1083/jcb.201604061

Conflict of Interest: The authors declare that the research was conducted in the absence of any commercial or financial relationships that could be construed as a potential conflict of interest.

frontiers in Molecular Biosciences

MINI REVIEW
published: 16 June 2021
doi: 10.3389/fmolb.2021.673096

Blocking K-Ras Interaction With the Plasma Membrane Is a Tractable Therapeutic Approach to Inhibit Oncogenic K-Ras Activity

*Karen M. Henkels, Kristen M. Rehl and Kwang-jin Cho**

Department of Biochemistry and Molecular Biology, School of Boonshoft School of Medicine, Wright State University, Dayton, OH, United States

Ras proteins are membrane-bound small GTPases that promote cell proliferation, differentiation, and apoptosis. Consistent with this key regulatory role, activating mutations of Ras are present in ~19% of new cancer cases in the United States per year. K-Ras is one of the three ubiquitously expressed isoforms in mammalian cells, and oncogenic mutations in this isoform account for ~75% of Ras-driven cancers. Therefore, pharmacological agents that block oncogenic K-Ras activity would have great clinical utility. Most efforts to block oncogenic Ras activity have focused on Ras downstream effectors, but these inhibitors only show limited clinical benefits in Ras-driven cancers due to the highly divergent signals arising from Ras activation. Currently, four major approaches are being extensively studied to target K-Ras–driven cancers. One strategy is to block K-Ras binding to the plasma membrane (PM) since K-Ras requires the PM binding for its signal transduction. Here, we summarize recently identified molecular mechanisms that regulate K-Ras–PM interaction. Perturbing these mechanisms using pharmacological agents blocks K-Ras–PM binding and inhibits K-Ras signaling and growth of K-Ras–driven cancer cells. Together, these studies propose that blocking K-Ras–PM binding is a tractable strategy for developing anti–K-Ras therapies.

Keywords: K-Ras, plasma membrane, mislocalization, cancer, recycing endosome, phosphatidylinositol, phosphatidylserine, sphingomyelin

OPEN ACCESS

Edited by:
Anton A. Buzdin, I. M. Sechenov First Moscow State Medical University, Russia

Reviewed by:
Sanjay Mishra, The Ohio State University, United States
Timofey Dmitrievich Lebedev, Engelhardt Institute of Molecular Biology (RAS), Russia

****Correspondence:***
Kwang-jin Cho
kwang-jin.cho@wright.edu

Specialty section:
This article was submitted to Molecular Diagnostics and Therapeutics, a section of the journal Frontiers in Molecular Biosciences

Received: *26 February 2021*
Accepted: *20 May 2021*
Published: *16 June 2021*

Citation:
Henkels KM, Rehl KM and Cho K-J (2021) Blocking K-Ras Interaction With the Plasma Membrane Is a Tractable Therapeutic Approach to Inhibit Oncogenic K-Ras Activity. Front. Mol. Biosci. 8:673096. doi: 10.3389/fmolb.2021.673096

INTRODUCTION

RAS genes were initially identified as the viral oncogenes of acute transforming retroviruses, and it was designated as a mammalian proto-oncogene when mutated *RAS* genes were discovered in human cancer cells (Barbacid, 1987). There are three main Ras isoforms—H-, N-, and K-Ras—in mammalian cells, and each is encoded by a different gene. *H-*, *N-*, and *K-RAS* are situated on chromosomes 11 (11p15.1-p15.5), 1 (1p22-p32), and 12 (12p12.1-pter), respectively (Barbacid, 1987). There are four exons that code for *H-* and *N-RAS*, while in *K-RAS*, there are two alternative fourth exons, exons 4A and 4B, that yield two splice variants, *K-Ras4A* and *K-Ras4B* (Barbacid, 1987). While H-, N-, and K-Ras4B are ubiquitously expressed in mammalian cells, K-Ras4A is precisely and spatiotemporally expressed in the murine lung, liver, and kidney (Pells et al., 1997). Knockout studies showed that neither *H-* nor *N-RAS* individually or in concert are required for normal murine embryogenesis (Esteban et al., 2001), whereas *K-RAS* is unequivocally crucial to embryonic development (Johnson et al., 1997; Koera et al., 1997). Intriguingly, K-Ras knockout mice

with spatiotemporally controlled expression of H-Ras by the *K-Ras* promoter have their embryonic lethality restored but develop dilated cardiomyopathy associated with arterial hypertension at an older age, reflecting the different molecular functions of Ras isoforms in the cell (Potenza et al., 2005).

While the three Ras isoforms are nearly identical, sharing ~90–100% homology in their N-terminal catalytic domain sequences, there is a considerable lack of homology in the C-terminal hypervariable region (HVR) of each isoform, which accounts for <15% homology being shared between any two isoforms (Hancock, 2003). These HVRs consist of two different signal sequences that allow Ras proteins to traffic to and interact with the inner leaflet of the plasma membrane (PM) (Hancock et al., 1989). The CAAX motif, the first signal sequence, is constituted by the last four amino acid residues in the HVR and is shared in common between the different Ras isoforms. For CAAX, C is cysteine, A is an aliphatic amino acid, and X is either serine or methionine (Hancock et al., 1989). Newly synthesized Ras GTPases are cytosolic and require a series of posttranslational modifications of the CAAX motif for interacting with endomembranes. First, the CAAX motif is farnesylated by a cytosolic farnesyltransferase (FTase) that covalently attaches a farnesyl group to the cysteine residue *via* a thioether bond. Farnesylated Ras interacts with the cytosolic leaflet of the endoplasmic reticulum (ER), where the AAX tripeptide is removed by the Ras and a-factor–converting enzyme (Rce1). The now C-terminal cysteine is methylated by isoprenylcysteine carboxyl methyltransferase (Icmt) (Hancock et al., 1989). The CAAX motif must be processed in this series of steps in order to maintain the correct forward trafficking of Ras isoforms, since knockout of either Rce1 or Icmt results in Ras mislocalization to the cytosol (Kim et al., 1999; Lau et al., 2014).

While the correctly modified CAAX motif can direct Ras to the ER and other endomembranes, the presence of the second C-terminal signal motif is required for maximal membrane affinity and PM localization (Hancock et al., 1990). The second signal sequence situated within the HVR varies between the different Ras isoforms such that both H-Ras, N-Ras, and K-Ras4A are palmitoylated (Cys181 and Cys184 for H-RasCys181 for N-Ras and Cys180 for K-Ras4A), while K-Ras4B has a stretch of six lysine residues, forming a polybasic domain (PBD) (Lys175-180) (Hancock et al., 1990). Palmitoylation of H- and N-Ras by the Ras palmitoyltransferase takes place in the ER and Golgi complex, where H- and N-Ras are transported *via* the classical secretory pathway to the PM (Apolloni et al., 2000). While palmitoylation of H- or N-Ras is a short-lived modification with rapid kinetics ($t_{1/2}$ of <20 min), the depalmitoylation/repalmitoylation machinery is important for delivering consistent H- and N-Ras distribution between the Golgi and the PM at a steady state (Rocks et al., 2005; Rocks et al., 2010). Palmitoylated Ras proteins diffuse from the PM to other endomembrane compartments to reach equilibrium, but depalmitoylation by poorly characterized thioesterases enhances the rate of diffusion, and thereby promotes their continuous redirection to the ER and Golgi for repalmitoylation and unidirectional trafficking back to the PM (Rocks et al., 2005; Rocks et al., 2010). The exact mechanism on how posttranslationally modified K-Ras4B (hereafter K-Ras) is transported from the ER to the PM is not fully characterized. Recent studies have demonstrated that the delta subunit of cGMP phosphodiesterase 6 (PDE6δ) functions, in part, as a K-Ras chaperone to maintain K-Ras–PM localization. PDE6δ binds the farnesyl moiety of cytosolic K-Ras, which is released in perinuclear membranes by the release factors Arl2 and 3, from where it is trapped on the recycling endosome (RE) by electrostatic interaction, and it returns to the PM *via* vesicular transport (Ismail et al., 2011; Chandra et al., 2012; Schmick et al., 2014). Once K-Ras is transported to the PM, it binds the PM through an electrostatic interaction of the strong positive charge of the C-terminal PBD with anionic phospholipid head groups in the inner PM leaflet (Yeung et al., 2008; Zhou et al., 2017).

K-RAS AND CANCER

Oncogenic mutations in Ras are found in about 18.7% of new cancer cases in the United States per year (1.3% for H-Ras, 3.1% for N-Ras, and 14.3% for K-Ras) (Prior et al., 2020). While the oncogenic mutant K-Ras is found in approximately 88% of pancreatic, 50% of colorectal, and 32% of lung cancers (Prior et al., 2020), no anti–K-Ras drugs are currently available in clinics. Human cancer cells harboring oncogenic mutant K-Ras reprogram their signaling network so that their survival and growth depend on oncogenic K-Ras signaling, a phenomenon called K-Ras addiction (Weinstein and Joe, 2008; Singh et al., 2009; Hayes et al., 2016). RNAi-mediated knockdown of oncogenic mutant K-Ras blocks cell survival and growth in a range of pancreatic and non-small-cell lung cancers (NSCLC), which provides the rationale that blocking oncogenic K-Ras activity is a valid approach to treat K-Ras-dependent cancers. Recently, two new K-Ras direct inhibitors have shown promising outcomes in clinical trials. AMG 510 and MRTX849 are small molecules that bind to the GDP-bound inactive K-RasG12C mutant and form a covalent bond to the mutant Cys, which locks K-Ras in the inactive conformation, resulting in blocked oncogenic signaling (Ostrem et al., 2013). These compounds exhibited pronounced anticancer effects in K-RasG12C tumor mice models and clinical trials with lung and colorectal cancer patients harboring the K-RasG12C mutant (Canon et al., 2019; Hallin et al., 2020). Despite the promising clinical outcome of these inhibitors, they are specific to the K-RasG12C mutant, which is found in ~3% of pancreatic, ~4% of colorectal, and ~13% of lung cancers that harbor any oncogenic mutations in K-Ras (Cox et al., 2014; Prior et al., 2020), suggesting that these inhibitors would be suitable only for a small portion of cancer patients with the oncogenic mutant K-Ras.

In addition to K-RasG12C–specific direct inhibitors, there are three other approaches that are currently being investigated for blocking all oncogenic mutant K-Ras activity. They are 1) blocking K-Ras interaction with the PM, 2) inhibiting K-Ras downstream effectors, and 3) dysregulating cell energy metabolism. This review will focus on mechanisms that

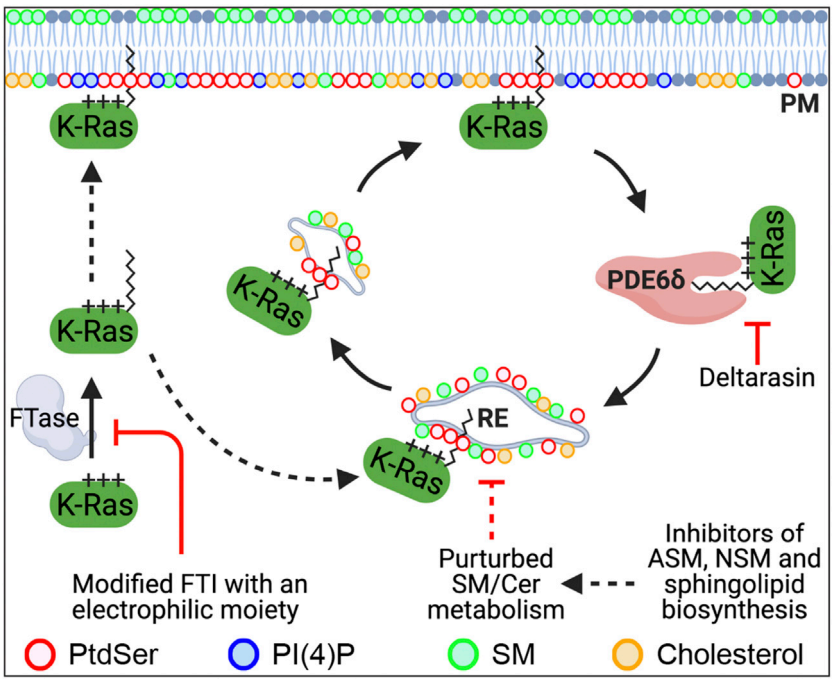

FIGURE 1 | Recently identified molecular mechanisms that regulate the PM localization of K-Ras. K-Ras farnesylated by FTase localizes to the PM. Once K-Ras dissociates from the PM, PDE6δ binds K-Ras *via* its farnesyl moiety and releases it in the perinuclear region. K-Ras is then translocated to the recycling endosome (RE) through electrostatic interaction, where it returns to the PM *via* RE-mediated vesicular transport. Blocking K-Ras prenylation or the K-Ras/PDE6δ interaction mislocalizes K-Ras from the PM. Perturbed SM/ceramide metabolism is proposed to dysregulate the RE *via* altering its lipid composition, resulting in depletion of PtdSer and K-Ras from the PM. FTase, farnesyltransferase; FTI, FTase inhibitor; PDE6δ, phosphodiesterase 6 δ; RE, recycling endosome; PtdSer, phosphatidylserine; SM, sphingomyelin; Cer, ceramide; PI4P, phosphatidylinositol 4-phosphate; ASM, acid sphingomyelinase; NSM, neural sphingomyelinase.

regulate the PM localization of K-Ras, which could be tractable targets for developing new anti–K-Ras therapeutics.

DISSOCIATING RAS FROM THE PLASMA MEMBRANE BLOCKS ITS SIGNAL TRANSDUCTION

Preventing Ras Prenylation Dissociates Ras From the PM and Inhibits Ras Signaling

Point mutations in the CAAX motif, which block posttranslational modification, prevent Ras–PM localization and completely inhibit all biological activities of oncogenic mutant Ras (Willumsen et al., 1984). Thus, farnesyltransferase inhibitors (FTIs) were designed to phenotypically mimic this mode of Ras inhibition. FTIs demonstrated marked antitumor activity in H-Ras–driven *in vivo* and *in vitro* models, which allowed phase I studies on FTIs in 1999, with some progressing to phase III clinical trials in 2002 (Baines et al., 2011). However, FTIs were ineffective with regard to pancreatic cancers in phase II and III clinical trials in which oncogenic mutant K-Ras was found in 88% of all pancreatic cancers (Cohen et al., 2003; Van Cutsem et al., 2004; Macdonald et al., 2005). It is because in FTI-treated cells, an alternative prenyltransferase, geranylgeranyltransferase (GGTase), efficiently attaches the more hydrophobic C20 geranylgeranyl moiety to K- and N-Ras, allowing K- and N-Ras to interact with the PM and conduct a signal transduction that is equipotent with the farnesylated forms (Baines et al., 2011). Concomitant inhibition of FTase with GGTase to completely block prenylation of K- and N-Ras has been tested, but this approach has suffered from dose-limiting toxicities (O'Bryan, 2019). Also, there are more than 100 proteins that are prenylated, and these combined inhibitors would induce prohibitive off-target effects, preventing their clinical effectiveness. A recent study has demonstrated a promising strategy to specifically inhibit K-Ras prenylation. A modified FTI with an electrophilic moiety specifically interacts with the CAAX motif of K-Ras but not H-Ras, resulting in the blockage of K-Ras farnesylation and geranylgeranylation, trapping K-Ras in the cytosol (Novotny et al., 2017). Further improvements of this approach could lead to a more potent inhibitor of K-Ras prenylation and activity (Novotny et al., 2017; O'Bryan, 2019).

Perturbing K-Ras/PDE6δ Interaction Blocks K-Ras–PM Binding and K-Ras Signaling

Recent studies have shown that blocking PDE6δ interaction with K-Ras is a tractable strategy to inhibit K-Ras–PM localization and oncogenic K-Ras signaling. PDE6δ binds the farnesyl moiety of K-Ras *via* its hydrophobic pocket and acts in part as a chaperone. The release factors Arl2 and 3 unload K-Ras

TABLE 1 | Summary of the compounds that inhibit K-Ras interaction with the PM.

Drug	Target mechanism	Cell lines tested	References
Deltarasin	Blocking interaction of PDE6 delta with farnesylated small GTPases	Panc-Tu-1, Capan-1, MIA-PaCa2, SW480, HCT-116, Hke3, A549, and H358	Zimmermann et al. (2013), Papke et al. (2016), Martin-Gago et al. (2017), Leung et al. (2018), Klein et al. (2019), O'Bryan (2019)
Staurosporine and its analogs	Perturbing endosomal recycling of PtdSer and depleting PtdSer PM content	MDCK and CHO	Cho et al. (2012b), Maekawa et al. (2016)
Fendiline and antidepressants	Functional inhibitor of ASM and depleting PtdSer PM content	MIA-PaCa2, MOH, HPAC, MPanc96, Hec-1a, Hec-1b, Hec50, NCI H23, SK-CO-1, SW948, SW1116, and Ca-Co2	van der Hoeven et al. (2013), Cho et al. (2016)
Avicin and its analogs	Inhibiting NSM and ASM	Jurkat, U2OS, NB4, AsPC-1, Panc10.05, MIA-PaCa2, HPAFII, Panc-1, H358, and H441	Wang et al. (2010), Garrido et al. (2020)
AMG510	Forms covalent bond with Cys in the K-RasG12C mutant, locking it in its inactive, GDP-bound form	H1792, H358, H23, Calu-1, MIA-PaCa2, NCI-H1373, NCIH 2030, NCI-H2122, SW1463, SW1573, SW837, and UM-UC-3	Ostrem et al. (2013), Canon et al. (2019)
MRTX849		H1792, H358, H23, Calu-1, MIA-PaCa2, H1373, H2122, SW1573, H2030, and KYSE-410	Ostrem et al. (2013), Hallin et al. (2020)
Modified farnesyltransferase inhibitors (FTIs)	Blocks the addition of a prenyl group to prevent Ras–membrane association	PSN-1 and SW-620	Novotny et al. (2017)

ASM, acid sphingomyelinase; NSM, neutral sphingomyelinase; FTIs, farnesyltransferase inhibitors; PtdSer, phosphatidylserine; PM, plasma membrane.

from PDE6δ in the perinuclear region, whence K-Ras binds to the recycling endosome (RE) for redelivery to the PM *via* vesicular transport (Chandra et al., 2012; Schmick et al., 2014). Deltarasin is a small molecule that binds to the hydrophobic pocket and inhibits PDE6δ/K-Ras interaction, resulting in K-Ras–PM mislocalization and abrogated signaling in K-Ras–driven cancer cells (**Figure 1** and **Table 1**) (Zimmermann et al., 2013). Second-generation PDE6δ inhibitors, which bind PDE6δ more tightly *via* extra hydrogen bonds, have demonstrated greater potency for blocking the growth of K-Ras–dependent but not K-Ras–independent pancreatic cancer cells (Papke et al., 2016; Martin-Gago et al., 2017). Moreover, deltarasin does not inhibit the growth of cells transformed with the oncogenic mutant B-Raf or the overexpressed epidermal growth factor receptor (EGFR) (Klein et al., 2019), suggesting that PDE6δ inhibitors are effective against K-Ras–dependent cancer cells. In addition, deltarasin functions independent of K-Ras, where it promotes autophagy by activating the AMPK/mTOR pathway, and concomitant inhibition of autophagy and PDE6δ potentiates deltarasin-mediated cell death by elevating reactive oxygen species (ROS) (Leung et al., 2018). These observations suggest that deltarasin elevates cellular ROS, which promotes autophagy (Zhang et al., 2016), and that deltarasin in combination with an autophagy inhibitor can be a plausible strategy for treating K-Ras–driven cancers (Leung et al., 2018).

However, PDE6δ interacts with other prenylated small GTPases including H-Ras, N-Ras, and Rap1 (Chandra et al., 2012; Dumbacher et al., 2018), suggesting that the effect of deltarasin may not be K-Ras–specific. Moreover, K-Ras knockout mice have embryonic lethality, whereas PDE6δ knockout mice develop normally (Johnson et al., 1997; Zhang et al., 2007), indicating that K-Ras is active in the absence of PDE6δ. In sum, PDE6δ interaction with K-Ras is a tractable target to inhibit oncogenic K-Ras activity, and further validation on the K-Ras specificity of PDE6δ would promote translation into the clinic.

REDUCING PHOSPHATIDYLSERINE CONTENT AT THE INNER PM LEAFLET REMOVES K-RAS FROM THE PM

Phosphatidylserine (PtdSer) is an anionic phospholipid synthesized from phosphatidylcholine (PtdCho) and phosphatidylethanolamine (PtdEth) by PtdSer synthase 1 and 2, respectively, in mammalian cells. While PtdSer is found in the ER and mitochondria, it is concentrated in the inner PM *via* mechanisms that are not fully elucidated (Leventis and Grinstein, 2010; Kay and Fairn, 2019). PM PtdSer plays key roles in physiological processes including the clearance of apoptotic cells, coagulation cascade, and recruitment and activation of signaling proteins (Leventis and Grinstein, 2010; Kay and Fairn, 2019). The anionic head group provides a negative electrostatic potential to the inner PM leaflet, which allows interaction with a stretch of positively charged amino acid residues, called PBD, of PM-localized proteins (Yeung et al., 2008). K-Ras binds PtdSer at the inner PM leaflet through the C-terminal PBD concomitantly with the farnesyl moiety, which provides specificity for PtdSer over other anionic phospholipids (Zhou et al., 2017). Recent studies have reported a number of mechanisms that can reduce PM PtdSer content, which in turn inhibits K-Ras–PM localization and oncogenic K-Ras signaling output.

Phosphatidylinositol 4-Phosphate Regulates the PM Distribution of PtdSer and K-Ras

Phosphatidylinositol (PI) is phosphorylated to PI 4-phosphate (PI4P) by four PI 4-kinases in mammalian cells: PI4K IIα and β (PI4K2A and 2B) and PI4K IIIα and β (PI4KA and PI4KB) (Balla, 2013). PI4KA and 2B localize primarily to the PM, whereas

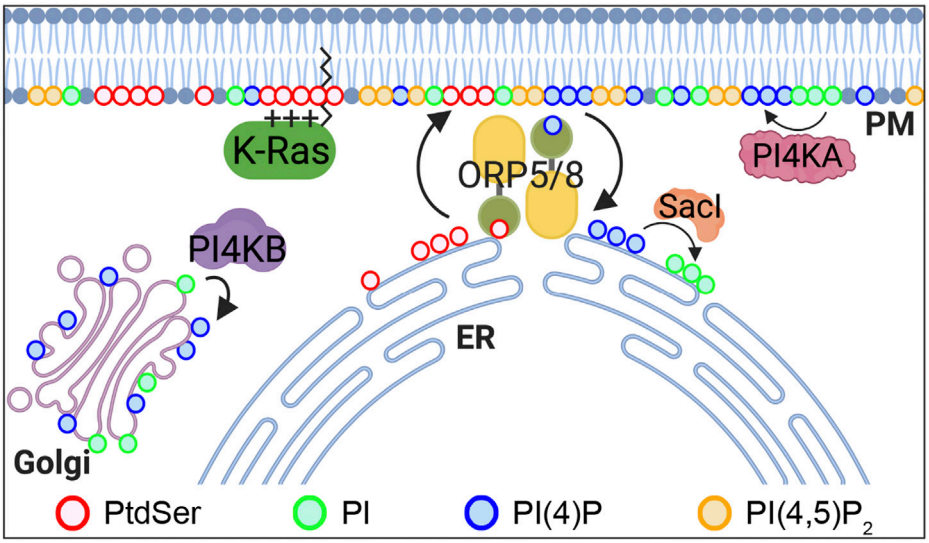

FIGURE 2 | PtdSer PM enrichment is regulated by ORP5 and 8. ORP5 and 8 are lipid transporters that exchange ER PtdSer with PM PI4P. The driving force of this process is a PI4P concentration gradient, whereby PI4P levels are high in the PM by PI4KA and are kept low at the ER by Sac1 phosphatase, which converts PI4P to PI. PI4P is also generated at the Golgi complex by PI4KB. ORP, oxysterol-binding protein–related protein; PtdSer, phosphatidylserine; PI, phosphatidylinositol; PI4P, PI 4-phosphate; PI(4,5)P2, PI(4,5)-bisphosphate; PI4KA, PI 4-kinase IIIα; PI4KB, PI 4-kinase IIIβ.

PI4K2A and PI4KB localize to the Golgi complex (Balla, 2013). In mammalian cells, oxysterol-binding protein–related proteins (ORPs) 5 and 8 exchange newly synthesized PtdSer from the ER for PI4P from the PM at ER–PM membrane contacting sites (MCSs) (**Figure 2**) (Chung et al., 2015; Moser von Filseck et al., 2015). This process is maintained by PM PI4P by PI4KA and the concomitant PI4P hydrolysis by Sac1 phosphatase in the ER to keep a PI4P concentration gradient across the PM and ER (Chung et al., 2015; Moser von Filseck et al., 2015). ORP5 and 8 recruitment to ER–PM MCSs further requires additional PM $PI(4,5)P_2$ (Ghai et al., 2017; Sohn et al., 2018). Several studies have reported that perturbing this exchange process reduces PM PtdSer content and inhibits K-Ras–PM binding and K-Ras signal output. $PI(4,5)P_2$ reduction by the rapamycin-recruitable 5-phosphatase domain of INPP5E to the PM blocks ORP5 and 8 recruitment to ER–PM MCSs, whereas increasing the PM $PI(4,5)P_2$ level by overexpressing PI4P 5-kinase (PIP5K) β reduces PM PI4P levels. In both cases, the exchange of ER PtdSer for PM PI4P is perturbed, resulting in PtdSer reduction in the inner PM leaflet (Ghai et al., 2017; Sohn et al., 2018). Also, the acute depletion of PM PI4P by rapamycin-recruitable Sac1 dissociates K-Ras, but not H-Ras, from the PM and inhibits K-Ras signaling (Gulyas et al., 2017). Ras proteins are spatially organized into nanoscale domains on the PM, called nanoclusters, which are critical for high-fidelity Ras signal output (Prior et al., 2003; Tian et al., 2007; Cho et al., 2012a; Cho and Hancock, 2013). PM PI4P depletion by either ORP5 or 8 knockdown or chemical inhibition redistributes PtdSer and K-Ras from the PM. It further disrupts K-Ras nanoclustering and abrogates K-Ras signal output and the growth of K-Ras–driven pancreatic cancer cells (Kattan et al., 2019). Consistently, ORP5 and 8 are highly expressed in certain types of cancer and involved in the prognosis of cancer patients. A high expression of ORP8 is observed in lung cancer tissues and hamster bile duct cancers in comparison to normal tissues (Fournier et al., 1999; Loilome et al., 2006). ORP5 overexpression enhances the invasion of pancreatic cancer cells, while ORP5 knockdown abrogates it *in vitro*. Moreover, the ORP5 mRNA level is significantly elevated in tumors harboring oncogenic mutant K-Ras compared with tumors with wild-type (WT) K-Ras in cohorts of pancreatic cancer, NSCLC, and 33 types of cancer in the TCGA (the Cancer Genome Atlas) database (Kattan et al., 2019). Further analysis of overall survival periods for patients in these three cohorts demonstrates that cancer patients with low ORP5 or 8 expression have better prognosis than patients with high ORP5 or 8 expression (Koga et al., 2008; Kattan et al., 2019).

In addition to PM PI4P, a recent study has demonstrated that Golgi PI4P is involved in the PM localization of PtdSer and K-Ras. Chemical inhibition of PI4KB, which depletes PI4P at the Golgi complex, but not the PM, translocates K-Ras and PtdSer from the PM to the mitochondria and endomembrane, respectively (Miller et al., 2019). Supplementation with exogenous PtdSer acutely returns K-Ras to the PM in Golgi PI4P–depleted cells, and mitochondrial PtdSer reduction by overexpressing PtdSer decarboxylase, which converts PtdSer to PtdEth at the mitochondria (Percy et al., 1983), redistributes K-Ras from the mitochondria to the endomembranes in Golgi PI4P–depleted cells (Miller et al., 2019). Furthermore, Golgi PI4P depletion inhibits Ras signaling in K-Ras–transformed but not H-Ras–transformed cells. Although the exact mechanism is yet to be elucidated, these data suggest that Golgi PI4P regulates the PM enrichment of PtdSer and thereby K-Ras–PM localization and K-Ras signaling (Miller et al., 2019). In sum, the PtdSer/PI4P

exchange mechanism at the ER–PM MCSs, which regulates the PM enrichment of PtdSer and thereby K-Ras–PM localization and signaling, is a viable target for developing anti–K-Ras therapies.

Perturbing Recycling Endosomal Activity Mislocalizes PtdSer and K-Ras From the PM

In addition to the non-vesicular transport of PtdSer by ORP5 and 8, PtdSer transports *via* the classical vesicular trafficking. Once PM PtdSer is endocytosed, it enters the sorting endosomes, where it either returns to the PM *via* the RE or is transported to lysosomes for its degradation by phospholipases (Leventis and Grinstein, 2010), suggesting that recycling endosomal activity is important for maintaining PM PtdSer content. Recent studies have reported that disruption of recycling endosomal activity depletes PtdSer and K-Ras from the PM. Acylpeptide hydrolase (APEH) removes the N-terminal acylated amino acids from acetylated proteins, and regulates the ubiquitin-mediated protein degradation (Shimizu et al., 2004). APEH knockdown or inhibition blocks endocytic recycling of the transferrin receptor (TfR) and EGFR and mislocalizes K-Ras and PtdSer from the PM (Tan et al., 2019). It also reduces nanoclustering of oncogenic K-Ras that remained at the PM and prevents oncogenic K-Ras signaling and growth of pancreatic cancer cells harboring oncogenic mutant K-Ras but not WT K-Ras. This study proposes that failure to maintain PtdSer and K-Ras at the PM in APEH-depleted cells is in part induced by aberrant RE function.

A protein kinase C (PKC) inhibitor, staurosporine, and its analogs accumulate PtdSer internalized from the PM in the RE, resulting in PM PtdSer depletion in a PKC-independent manner (Cho et al., 2012b). These compounds also induce K-Ras–PM dissociation and disrupt K-Ras PM nanoclustering (Cho et al., 2012b). Consistent with this, they abrogate K-Ras signaling and cell proliferation in K-Ras–transformed cells. Taken all together, perturbing recycling endosomal activity could prevent PM PtdSer replenishment through the RE, which results in K-Ras–PM dissociation and disrupted K-Ras nanoclustering and K-Ras signaling. The perturbed recycling endosomal activity could also block the PDE6δ/RE-mediated K-Ras–PM localization, further contributing to disrupted K-Ras–PM localization and signaling.

K-Ras and PtdSer PM Localization Is Regulated by Sphingomyelin/Ceramide Biosynthesis

Recent studies have demonstrated that perturbing the enzymes involved in sphingomyelin (SM) metabolism depletes the PM localization of PtdSer and K-Ras, and blocks oncogenic K-Ras signaling. Ceramide, which is synthesized in the ER, trafficks to the Golgi complex, where it is converted to SM. SM is further transported to the PM and lysosomes, where it is reverted to ceramide by sphingomyelinases (Gault et al., 2010). Several studies have reported that the inhibition of acid or neutral sphingomyelinase (ASM and NSM, respectively) dissociates PtdSer and K-Ras from the PM and inhibits oncogenic K-Ras signal transduction (**Figure 1**). A wide range of ASM inhibitors including tricyclic antidepressants elevates cellular SM contents and accumulates SM in vesicular structures. They also deplete PM PtdSer content and translocate K-Ras, but not H-Ras, from the PM to endomembranes (van der Hoeven et al., 2013; Cho et al., 2016; van der Hoeven et al., 2018). Also, K-Ras is dissociated from the PM in patient-derived Niemann–Pick type A and B cell lines, in which *SMPD1* gene–encoding ASM has inactivating and partial loss-of-function mutations, respectively (Cho et al., 2016; Schuchman and Desnick, 2017). These inhibitors further perturb oncogenic K-Ras PM nanoclustering and its signaling, and abrogate the growth of different types of human cancer cells expressing oncogenic mutant K-Ras but not WT K-Ras (Petersen et al., 2013; van der Hoeven et al., 2013; van der Hoeven et al., 2018). Supplementing ASM-inhibited cells with recombinant ASM returns PtdSer and K-Ras to the PM. Also, replenishing PM PtdSer content with exogenous PtdSer supplementation returns K-Ras to the PM and restores nanoclustering in ASM-inhibited cells, which indicates that K-Ras–PM dissociation occurs through PM PtdSer depletion (Cho et al., 2016). In addition, pharmacological inhibitors for enzymes in the SM/ceramide metabolic pathway redistribute PtdSer and K-Ras from the PM (van der Hoeven et al., 2018). They further perturb K-Ras nanoclustering and block the growth of pancreatic cancer cells harboring oncogenic mutant K-Ras (van der Hoeven et al., 2018). In a supplemental *C. elegans* study, RNAi-mediated knockdown of 14 genes encoding enzymes in the SM/ceramide biosynthesis pathway suppressed the LET-60G13D (a K-RasG13D ortholog in *C. elegans*)-induced multi-vulva phenotype (van der Hoeven et al., 2018).

Another approach to disrupt SM/ceramide metabolism is to alter the activity of NSM. Avicins, natural plant-derived triterpenoid saponins from *Acacia victoriae*, have proapoptotic, anti-inflammatory, and anticancer activities (Wang et al., 2010). A recent study demonstrated that avicin G, an isomer of avicin compounds, inhibits NSM and ASM, with a greater potency against NSM, and elevates cellular SM, ceramide, and PtdSer contents (Garrido et al., 2020). It also disrupts endosomal recycling of the EGFR and perturbs lysosomal activity by elevating the lysosomal pH (Garrido et al., 2020). Avicin G and other NSM inhibitors redistribute PtdSer from the PM, accumulate K-Ras in lysosomes, and increase the K-Ras protein level. Since K-Ras and PtdSer are proposed to be degraded in the lysosome (Lu et al., 2009; Leventis and Grinstein, 2010), the elevated K-Ras and PtdSer levels induced by avicin G, in part, account for the perturbed lysosomal activity (Garrido et al., 2020). It further perturbs K-Ras PM nanoclustering and blocks K-Ras signaling and the growth of K-Ras–addicted pancreatic and NSCLC cell lines (Garrido et al., 2020). Taken together, these studies propose that a correct SM/ceramide balance maintains the PM localization of PtdSer and K-Ras and that pharmacological agents that perturb the sphingolipid pathways could be a new strategy for developing anti–K-Ras therapies (van der Hoeven et al., 2018). One plausible mechanism of PM PtdSer depletion by altering the cellular SM contents is through perturbing recycling endosomal activity. The RE is enriched with cholesterol, SM, and PtdSer (Gagescu et al.,

2000; Uchida et al., 2011), and elevating cellular sphingolipid contents blocks endosomal recycling of the glucose transporter 1 and TfR (Finicle et al., 2018). Like avicin G, staurosporine and its analogs perturb the RE activity and elevate cellular SM content in a PKC-independent manner by reducing the protein level of ORMDL, which negatively regulates serine-palmitoyltransferase, the rate-limiting enzyme for sphingolipid biosynthesis (Maekawa et al., 2016). Taken all together, it is proposed that an increased cellular SM level changes SM content at the RE, which disrupts recycling endosomal activity. This, in turn, depletes PtdSer and mislocalizes K-Ras from the PM, as discussed above.

CONCLUSION

Despite the essential role of oncogenic mutant K-Ras in the growth and survival of pancreatic, lung, and colorectal cancers, there are no anti–K-Ras therapies available in the clinic. Several studies have reported that knockdown of endogenous oncogenic mutant K-Ras in a range of NCSLC and pancreatic cancer cell lines blocks their growth and survival, suggesting that blocking oncogenic K-Ras activity is a valid strategy for anti–K-Ras therapies. Ras drug discovery efforts have focused largely on inhibitors of Ras downstream effectors including B-Raf, C-Raf, PI3K, and MEK (Baines et al., 2011). One example is the multikinase inhibitor, Nexavar, used against renal cell and hepatocellular carcinoma (Llovet et al., 2008; Roberts, 2008), although it is unclear to what extent the efficacy of Nexavar towards these cancers is related to the inhibition of C-Raf, B-Raf, or VEGFR (Downward, 2003; Baines et al., 2011). B-Raf–specific inhibitors produce excellent, albeit often short-lived, responses in patients with B-Raf mutant melanoma (Flaherty et al., 2010). However, further studies have shown that B-Raf–specific inhibitors paradoxically activate the MAPK cascade in melanoma cells expressing oncogenic mutant N- or K-Ras *via* a mechanism that involves C-Raf hyperactivation (Heidorn et al., 2010; Cho et al., 2012a). These studies illustrate that blocking MAPK signaling with Raf kinase inhibitors is a limited approach to anti-Ras therapy.

Recently, two small molecules that directly bind and inhibit the K-RasG12C mutant have shown promising outcomes in clinical trials. While the K-RasG12C mutant is found in a small fraction of K-Ras–driven human cancers, these studies demonstrate that developing anti–K-Ras therapies is feasible. One approach to inhibit all oncogenic mutant K-Ras is to block its interaction with the PM since K-Ras must localize to the PM for its signal transduction. However, the exact molecular mechanisms of K-Ras transport to and maintenance at the PM are not fully elucidated. In this review, we discussed several recently identified mechanisms that regulate K-Ras–PM interaction and thereby the K-Ras signal cascade. Compounds that perturb these mechanisms dissociate K-Ras from the PM and block K-Ras signaling and K-Ras–dependent cancer cell growth. However, this approach has pitfalls including nonspecificity and cytotoxicity since it does not specifically target K-Ras. For example, PDE6δ can bind other farnesylated small GTPases *via* the same hydrophobic pocket as K-Ras. Thus, blocking this binding site by PDE6δ inhibitors can dysregulate the cellular localizations and activities of K-Ras and other small GTPases. Also, PtdSer at the inner PM leaflet recruits and promotes the activity of K-Ras and other proteins containing a polybasic domain (Leventis and Grinstein, 2010; Kay and Fairn, 2019). While PM PI4P regulates the PM enrichments of PtdSer, it can be further phosphorylated to different PIPs, which activate several essential signaling proteins (Balla, 2013). Therefore, while depleting PM PtdSer or perturbing the PI4P/PtdSer exchange mechanism prevents oncogenic mutant K-Ras activity, they can also perturb other essential signaling cascades. Nevertheless, many studies have reported that disrupting these molecular mechanisms blocks the growth of human cancer cells that are K-Ras–dependent but not K-Ras–independent *in vitro* and *in vivo*, suggesting that targeting these mechanisms is a valid approach for developing anti–K-Ras therapies.

Cancer chemotherapy is most effective when a combination of drugs targeting different molecular mechanisms are applied. There are four major approaches that are currently being perused for developing anti–K-Ras therapies, and any one approach alone may not be sufficient to completely block oncogenic K-Ras signaling due to high cytotoxicity and/or nonspecificity. A recent study has demonstrated that a K-RasG12C inhibitor potentiates the anticancer effect of the MEK, mTOR, and insulin-like growth factor 1 receptor (IFG1R) inhibitors in NSCLC cells. While combined mTOR, IGF1R, and MEK inhibition shows significant tumor regression in K-RasG12C–driven lung cancer mouse models, replacing the MEK inhibitor with a K-RasG12C inhibitor in combination demonstrates greater efficacy, specificity, and tolerability (Molina-Arcas et al., 2019). Moreover, the combination of the K-RasG12C inhibitor with anti–PD-1 immune checkpoint inhibition synergistically suppresses tumor growth in K-RasG12C–driven mouse models (Canon et al., 2019). Combination therapy of K-RasG12C inhibitors with anti–PD-1 or anti–PD-L1 in patients with solid tumors harboring the K-RasG12C mutant is currently in clinical trials (ClinicalTrials.gov identifier: NCT04185883, NCT03785249). Although combination therapy with K-RasG12C inhibitors and other anticancer approaches is promising, it is limited to K-RasG12C–specific cancers, which accounts for ~20% of K-Ras–driven cancers. Therefore, it would be worthwhile to examine the effects of combining pharmacological agents that can block all oncogenic mutant K-Ras by dissociating it from the PM with drugs developed for targeting the other approaches.

AUTHOR CONTRIBUTIONS

KH and KR wrote the draft, and KH, KR, and K-jC edited it.

FUNDING

This work was supported by grants from the National Cancer Institute (Grant no. R00CA188593 to K-jC).

REFERENCES

Apolloni, A., Prior, I. A., Lindsay, M., Parton, R. G., and Hancock, J. F. (2000). H-ras but Not K-Ras Traffics to the Plasma Membrane through the Exocytic Pathway. *Mol. Cel. Biol.* 20 (7), 2475–2487. doi:10.1128/mcb.20.7.2475-2487.2000

Baines, A. T., Xu, D., and Der, C. J. (2011). Inhibition of Ras for Cancer Treatment: the Search Continues. *Future Med. Chem.* 3 (14), 1787–1808. doi:10.4155/fmc.11.121

Balla, T. (2013). Phosphoinositides: Tiny Lipids with Giant Impact on Cell Regulation. *Physiol. Rev.* 93 (3), 1019–1137. doi:10.1152/physrev.00028.2012

Barbacid, M. (1987). Ras Genes. *Annu. Rev. Biochem.* 56, 779–827. doi:10.1146/annurev.bi.56.070187.004023

Canon, J., Rex, K., Saiki, A. Y., Mohr, C., Cooke, K., Bagal, D., et al. (2019). The Clinical KRAS(G12C) Inhibitor AMG 510 Drives Anti-tumour Immunity. *Nature*. 575 (7781), 217–223. doi:10.1038/s41586-019-1694-1

Chandra, A., Grecco, H. E., Pisupati, V., Perera, D., Cassidy, L., Skoulidis, F., et al. (2012). The GDI-like Solubilizing Factor PDEδ Sustains the Spatial Organization and Signalling of Ras Family Proteins. *Nat. Cel Biol.* 14 (2), 148–158. doi:10.1038/ncb2394

Cho, K. J., and Hancock, J. F. (2013). Ras Nanoclusters: a New Drug Target? *Small GTPases*. 4 (1), 57–60. doi:10.4161/sgtp.23145

Cho, K. J., Kasai, R. S., Park, J. H., Chigurupati, S., Heidorn, S. J., van der Hoeven, D., et al. (2012). Raf Inhibitors Target Ras Spatiotemporal Dynamics. *Curr. Biol.* 22 (11), 945–955. doi:10.1016/j.cub.2012.03.067

Cho, K. J., Park, J. H., Piggott, A. M., Salim, A. A., Gorfe, A. A., Parton, R. G., et al. (2012). Staurosporines Disrupt Phosphatidylserine Trafficking and Mislocalize Ras Proteins. *J. Biol. Chem.* 287 (52), 43573–43584. doi:10.1074/jbc.M112.424457

Cho, K. J., van der Hoeven, D., Zhou, Y., Maekawa, M., Ma, X., Chen, W., et al. (2016). Inhibition of Acid Sphingomyelinase Depletes Cellular Phosphatidylserine and Mislocalizes K-Ras from the Plasma Membrane. *Mol. Cel Biol.* 36 (2), 363–374. doi:10.1128/MCB.00719-15

Chung, J., Torta, F., Masai, K., Lucast, L., Czapla, H., Tanner, L. B., et al. (2015). INTRACELLULAR TRANSPORT. PI4P/phosphatidylserine Countertransport at ORP5- and ORP8-Mediated ER-Plasma Membrane Contacts. *Science*. 349 (6246), 428–432. doi:10.1126/science.aab1370

Cohen, S. J., Ho, L., Ranganathan, S., Abbruzzese, J. L., Alpaugh, R. K., Beard, M., et al. (2003). Phase II and Pharmacodynamic Study of the Farnesyltransferase Inhibitor R115777 as Initial Therapy in Patients with Metastatic Pancreatic Adenocarcinoma. *J. Clin. Oncol.* 21 (7), 1301–1306. doi:10.1200/JCO.2003.08.040

Cox, A. D., Fesik, S. W., Kimmelman, A. C., Luo, J., and Der, C. J. (2014). Drugging the Undruggable RAS: Mission Possible? *Nat. Rev. Drug Discov.* 13 (11), 828–851. doi:10.1038/nrd4389

Downward, J. (2003). Targeting RAS Signalling Pathways in Cancer Therapy. *Nat. Rev. Cancer* 3 (1), 11–22. doi:10.1038/nrc969

Dumbacher, M., Van Dooren, T., Princen, K., De Witte, K., Farinelli, M., Lievens, S., et al. (2018). Modifying Rap1-Signalling by Targeting Pde6delta Is Neuroprotective in Models of Alzheimer's Disease. *Mol. Neurodegener.* 13 (1), 50. doi:10.1186/s13024-018-0283-3

Esteban, L. M., Vicario-Abejón, C., Fernández-Salguero, P., Fernández-Medarde, A., Swaminathan, N., Yienger, K., et al. (2001). Targeted Genomic Disruption of H-Ras and N-Ras, Individually or in Combination, Reveals the Dispensability of Both Loci for Mouse Growth and Development. *Mol. Cel. Biol.* 21 (5), 1444–1452. doi:10.1128/mcb.21.5.1444-1452.2001

Finicle, B. T., Ramirez, M. U., Liu, G., Selwan, E. M., McCracken, A. N., Yu, J., et al. (2018). Sphingolipids Inhibit Endosomal Recycling of Nutrient Transporters by Inactivating ARF6. *J. Cel Sci.* 131 (12). doi:10.1242/jcs.213314

Flaherty, K. T., Puzanov, I., Kim, K. B., Ribas, A., McArthur, G. A., Sosman, J. A., et al. (2010). Inhibition of Mutated, Activated BRAF in Metastatic Melanoma. *N. Engl. J. Med.* 363 (9), 809–819. doi:10.1056/NEJMoa1002011

Fournier, M. V., Guimaraes da Costa, F., Paschoal, M. E., Ronco, L. V., Carvalho, M. G., and Pardee, A. B. (1999). Identification of a Gene Encoding a Human Oxysterol-Binding Protein-Homologue: a Potential General Molecular Marker for Blood Dissemination of Solid Tumors. *Cancer Res.* 59 (15), 3748–3753.

Gagescu, R., Demaurex, N., Parton, R. G., Hunziker, W., Huber, L. A., and Gruenberg, J. (2000). The Recycling Endosome of Madin-Darby Canine Kidney Cells Is a Mildly Acidic Compartment Rich in Raft Components. *Mol. Biol. Cel.* 11 (8), 2775–2791. doi:10.1091/mbc.11.8.2775

Garrido, C. M., Henkels, K. M., Rehl, K. M., Liang, H., Zhou, Y., Gutterman, J. U., et al. (2020). Avicin G Is a Potent Sphingomyelinase Inhibitor and Blocks Oncogenic K- and H-Ras Signaling. *Sci. Rep.* 10 (1), 9120. doi:10.1038/s41598-020-65882-5

Gault, C. R., Obeid, L. M., and Hannun, Y. A. (2010). An Overview of Sphingolipid Metabolism: from Synthesis to Breakdown. *Adv. Exp. Med. Biol.* 688, 1–23. doi:10.1007/978-1-4419-6741-1_1

Ghai, R., Du, X., Wang, H., Dong, J., Ferguson, C., Brown, A. J., et al. (2017). ORP5 and ORP8 Bind Phosphatidylinositol-4, 5-biphosphate (PtdIns(4,5)P 2) and Regulate its Level at the Plasma Membrane. *Nat. Commun.* 8 (1), 757. doi:10.1038/s41467-017-00861-5

Gulyas, G., Radvanszki, G., Matuska, R., Balla, A., Hunyady, L., Balla, T., et al. (2017). Plasma Membrane Phosphatidylinositol 4-phosphate and 4,5-bisphosphate Determine the Distribution and Function of K-Ras4B but Not H-Ras Proteins. *J. Biol. Chem.* 292 (46), 18862–18877. doi:10.1074/jbc.M117.806679

Hallin, J., Engstrom, L. D., Hargis, L., Calinisan, A., Aranda, R., Briere, D. M., et al. (2020). The KRAS(G12C) Inhibitor MRTX849 Provides Insight toward Therapeutic Susceptibility of KRAS-Mutant Cancers in Mouse Models and Patients. *Cancer Discov.* 10 (1), 54–71. doi:10.1158/2159-8290.CD-19-1167

Hancock, J. F., Magee, A. I., Childs, J. E., and Marshall, C. J. (1989). All Ras Proteins Are Polyisoprenylated but Only Some Are Palmitoylated. *Cell.* 57 (7), 1167–1177. doi:10.1016/0092-8674(89)90054-8

Hancock, J. F., Paterson, H., and Marshall, C. J. (1990). A Polybasic Domain or Palmitoylation Is Required in Addition to the CAAX Motif to Localize P21ras to the Plasma Membrane. *Cell.* 63 (1), 133–139. doi:10.1016/0092-8674(90)90294-o

Hancock, J. F. (2003). Ras Proteins: Different Signals from Different Locations. *Nat. Rev. Mol. Cel Biol.* 4 (5), 373–385. doi:10.1038/nrm1105

Hayes, T. K., Neel, N. F., Hu, C., Gautam, P., Chenard, M., Long, B., et al. (2016). Long-Term ERK Inhibition in KRAS-Mutant Pancreatic Cancer Is Associated with MYC Degradation and Senescence-like Growth Suppression. *Cancer Cell.* 29 (1), 75–89. doi:10.1016/j.ccell.2015.11.011

Heidorn, S. J., Milagre, C., Whittaker, S., Nourry, A., Niculescu-Duvas, I., Dhomen, N., et al. (2010). Kinase-dead BRAF and Oncogenic RAS Cooperate to Drive Tumor Progression through CRAF. *Cell.* 140 (2), 209–221. doi:10.1016/j.cell.2009.12.040

Ismail, S. A., Chen, Y.-X., Rusinova, A., Chandra, A., Bierbaum, M., Gremer, L., et al. (2011). Arl2-GTP and Arl3-GTP Regulate a GDI-like Transport System for Farnesylated Cargo. *Nat. Chem. Biol.* 7 (12), 942–949. doi:10.1038/nchembio.686

Johnson, L., Greenbaum, D., Cichowski, K., Mercer, K., Murphy, E., Schmitt, E., et al. (1997). K-ras Is an Essential Gene in the Mouse with Partial Functional Overlap with N-Ras. *Genes Development*. 11 (19), 2468–2481. doi:10.1101/gad.11.19.2468

Kattan, W. E., Chen, W., Ma, X., Lan, T. H., van der Hoeven, D., van der Hoeven, R., et al. (2019). Targeting Plasma Membrane Phosphatidylserine Content to Inhibit Oncogenic KRAS Function. *Life Sci. Alliance*. 2 (5), e201900431. doi:10.26508/lsa.201900431

Kay, J. G., and Fairn, G. D. (2019). Distribution, Dynamics and Functional Roles of Phosphatidylserine within the Cell. *Cell Commun Signal.* 17 (1), 126. doi:10.1186/s12964-019-0438-z

Kim, E., Ambroziak, P., Otto, J. C., Taylor, B., Ashby, M., Shannon, K., et al. (1999). Disruption of the Mouse Rce1 Gene Results in Defective Ras Processing and Mislocalization of Ras within Cells. *J. Biol. Chem.* 274 (13), 8383–8390. doi:10.1074/jbc.274.13.8383

Klein, C. H., Truxius, D. C., Vogel, H. A., Harizanova, J., Murarka, S., Martin-Gago, P., et al. (2019). PDEdelta Inhibition Impedes the Proliferation and Survival of Human Colorectal Cancer Cell Lines Harboring Oncogenic KRas. *Int. J. Cancer*. 144 (4), 767–776. doi:10.1002/ijc.31859

Koera, K., Nakamura, K., Nakao, K., Miyoshi, J., Toyoshima, K., Hatta, T., et al. (1997). K-ras Is Essential for the Development of the Mouse Embryo. *Oncogene*. 15 (10), 1151–1159. doi:10.1038/sj.onc.1201284

Koga, Y., Ishikawa, S., Nakamura, T., Masuda, T., Nagai, Y., Takamori, H., et al. (2008). Oxysterol Binding Protein-Related Protein-5 Is Related to Invasion and Poor Prognosis in Pancreatic Cancer. *Cancer Sci.* 99 (12), 2387–2394. doi:10.1111/j.1349-7006.2008.00987.x

Lau, H. Y., Ramanujulu, P. M., Guo, D., Yang, T., Wirawan, M., Casey, P. J., et al. (2014). An Improved Isoprenylcysteine Carboxylmethyltransferase Inhibitor Induces Cancer Cell Death and Attenuates Tumor Growth *In Vivo*. *Cancer Biol. Ther.* 15 (9), 1280–1291. doi:10.4161/cbt.29692

Leung, E. L. H., Luo, L. X., Liu, Z. Q., Wong, V. K. W., Lu, L. L., Xie, Y., et al. (2018). Inhibition of KRAS-dependent Lung Cancer Cell Growth by Deltarasin: Blockage of Autophagy Increases its Cytotoxicity. *Cell Death Dis.* 9 (2), 216. doi:10.1038/s41419-017-0065-9

Leventis, P. A., and Grinstein, S. (2010). The Distribution and Function of Phosphatidylserine in Cellular Membranes. *Annu. Rev. Biophys.* 39, 407–427. doi:10.1146/annurev.biophys.093008.131234

Llovet, J. M., Ricci, S., Mazzaferro, V., Hilgard, P., Gane, E., Blanc, J. F., et al. (2008). Sorafenib in Advanced Hepatocellular Carcinoma. *N. Engl. J. Med.* 359 (4), 378–390. doi:10.1056/NEJMoa0708857

Loilome, W., Yongvanit, P., Wongkham, C., Tepsiri, N., Sripa, B., Sithithaworn, P., et al. (2006). Altered Gene Expression in Opisthorchis Viverrini-Associated Cholangiocarcinoma in Hamster Model. *Mol. Carcinog.* 45 (5), 279–287. doi:10.1002/mc.20094

Lu, A., Tebar, F., Alvarez-Moya, B., Lopez-Alcala, C., Calvo, M., Enrich, C., et al. (2009). A clathrin-dependent pathway leads to KRas signaling on late endosomes en route to lysosomes. *J. Cel Biol.* 184 (6), 863–879. doi:10.1083/jcb.200807186

Macdonald, J. S., McCoy, S., Whitehead, R. P., Iqbal, S., Wade, J. L., 3rd, Giguere, J. K., et al. (2005). A Phase II Study of Farnesyl Transferase Inhibitor R115777 in Pancreatic Cancer: a Southwest Oncology Group (SWOG 9924) Study. *Invest. New Drugs.* 23 (5), 485–487. doi:10.1007/s10637-005-2908-y

Maekawa, M., Lee, M., Wei, K., Ridgway, N. D., and Fairn, G. D. (2016). Staurosporines Decrease ORMDL Proteins and Enhance Sphingomyelin Synthesis Resulting in Depletion of Plasmalemmal Phosphatidylserine. *Sci. Rep.* 6, 35762. doi:10.1038/srep35762

Martin-Gago, P., Fansa, E. K., Klein, C. H., Murarka, S., Janning, P., Schurmann, M., et al. (2017). A PDE6delta-KRas Inhibitor Chemotype with up to Seven H-Bonds and Picomolar Affinity that Prevents Efficient Inhibitor Release by Arl2. *Angew. Chem. Int. Ed. Engl.* 56 (9), 2423–2428. doi:10.1002/anie.201610957

Miller, T. E., Henkels, K. M., Huddleston, M., Salisbury, R., Hussain, S. M., Sasaki, A. T., et al. (2019). Depletion of Phosphatidylinositol 4-phosphate at the Golgi Translocates K-Ras to Mitochondria. *J. Cel Sci.* 132 (16). doi:10.1242/jcs.231886

Molina-Arcas, M., Moore, C., Rana, S., van Maldegem, F., Mugarza, E., Romero-Clavijo, P., et al. (2019). Development of Combination Therapies to Maximize the Impact of KRAS-G12c Inhibitors in Lung Cancer. *Sci. Transl Med.* 11 (510). doi:10.1126/scitranslmed.aaw7999

Moser von Filseck, J., Copic, A., Delfosse, V., Vanni, S., Jackson, C. L., Bourguet, W., et al. (2015). INTRACELLULAR TRANSPORT. Phosphatidylserine Transport by ORP/Osh Proteins Is Driven by Phosphatidylinositol 4-phosphate. *Science.* 349 (6246), 432–436. doi:10.1126/science.aab1346

Novotny, C. J., Hamilton, G. L., McCormick, F., and Shokat, K. M. (2017). Farnesyltransferase-Mediated Delivery of a Covalent Inhibitor Overcomes Alternative Prenylation to Mislocalize K-Ras. *ACS Chem. Biol.* 12 (7), 1956–1962. doi:10.1021/acschembio.7b00374

O'Bryan, J. P. (2019). Pharmacological Targeting of RAS: Recent success with Direct Inhibitors. *Pharmacol. Res.* 139, 503–511. doi:10.1016/j.phrs.2018.10.021

Ostrem, J. M., Peters, U., Sos, M. L., Wells, J. A., and Shokat, K. M. (2013). K-Ras(G12C) Inhibitors Allosterically Control GTP Affinity and Effector Interactions. *Nature.* 503 (7477), 548–551. doi:10.1038/nature12796

Papke, B., Murarka, S., Vogel, H. A., Martin-Gago, P., Kovacevic, M., Truxius, D. C., et al. (2016). Identification of Pyrazolopyridazinones as PDEdelta Inhibitors. *Nat. Commun.* 7, 11360. doi:10.1038/ncomms11360

Pells, S., Divjak, M., Romanowski, P., Impey, H., Hawkins, N. J., Clarke, A. R., et al. (1997). Developmentally-regulated Expression of Murine K-Ras Isoforms. *Oncogene.* 15 (15), 1781–1786. doi:10.1038/sj.onc.1201354

Percy, A. K., Moore, J. F., Carson, M. A., and Waechter, C. J. (1983). Characterization of Brain Phosphatidylserine Decarboxylase: Localization in the Mitochondrial Inner Membrane. *Arch. Biochem. Biophys.* 223 (2), 484–494. doi:10.1016/0003-9861(83)90613-6

Petersen, N. H., Olsen, O. D., Groth-Pedersen, L., Ellegaard, A. M., Bilgin, M., Redmer, S., et al. (2013). Transformation-associated Changes in Sphingolipid Metabolism Sensitize Cells to Lysosomal Cell Death Induced by Inhibitors of Acid Sphingomyelinase. *Cancer Cell.* 24 (3), 379–393. doi:10.1016/j.ccr.2013.08.003

Potenza, N., Vecchione, C., Notte, A., De Rienzo, A., Rosica, A., Bauer, L., et al. (2005). Replacement of K-Ras with H-Ras Supports normal Embryonic Development Despite Inducing Cardiovascular Pathology in Adult Mice. *EMBO Rep.* 6 (5), 432–437. doi:10.1038/sj.embor.7400397

Prior, I. A., Hood, F. E., and Hartley, J. L. (2020). The Frequency of Ras Mutations in Cancer. *Cancer Res.* 80, 2969–2974. doi:10.1158/0008-5472.CAN-19-3682

Prior, I. A., Muncke, C., Parton, R. G., and Hancock, J. F. (2003). Direct Visualization of Ras Proteins in Spatially Distinct Cell Surface Microdomains. *J. Cel Biol.* 160 (2), 165–170. doi:10.1083/jcb.200209091

Roberts, L. R. (2008). Sorafenib in Liver Cancer-Jjust the Beginning. *N. Engl. J. Med.* 359 (4), 420–422. doi:10.1056/NEJMe0802241

Rocks, O., Gerauer, M., Vartak, N., Koch, S., Huang, Z.-P., Pechlivanis, M., et al. (2010). The Palmitoylation Machinery Is a Spatially Organizing System for Peripheral Membrane Proteins. *Cell.* 141 (3), 458–471. doi:10.1016/j.cell.2010.04.007

Rocks, O., Peyker, A., Kahms, M., Verveer, P. J., Koerner, C., Lumbierres, M., et al. (2005). An Acylation Cycle Regulates Localization and Activity of Palmitoylated Ras Isoforms. *Science.* 307 (5716), 1746–1752. doi:10.1126/science.1105654

Schmick, M., Vartak, N., Papke, B., Kovacevic, M., Truxius, D. C., Rossmannek, L., et al. (2014). KRas Localizes to the Plasma Membrane by Spatial Cycles of Solubilization, Trapping and Vesicular Transport. *Cell.* 157 (2), 459–471. doi:10.1016/j.cell.2014.02.051

Schuchman, E. H., and Desnick, R. J. (2017). Types A and B Niemann-Pick Disease. *Mol. Genet. Metab.* 120 (1-2), 27–33. doi:10.1016/j.ymgme.2016.12.008

Shimizu, K., Kiuchi, Y., Ando, K., Hayakawa, M., and Kikugawa, K. (2004). Coordination of Oxidized Protein Hydrolase and the Proteasome in the Clearance of Cytotoxic Denatured Proteins. *Biochem. Biophys. Res. Commun.* 324 (1), 140–146. doi:10.1016/j.bbrc.2004.08.231

Singh, A., Greninger, P., Rhodes, D., Koopman, L., Violette, S., Bardeesy, N., et al. (2009). A Gene Expression Signature Associated with "K-Ras Addiction" Reveals Regulators of EMT and Tumor Cell Survival. *Cancer Cell.* 15 (6), 489–500. doi:10.1016/j.ccr.2009.03.022

Sohn, M., Korzeniowski, M., Zewe, J. P., Wills, R. C., Hammond, G. R. V., Humpolickova, J., et al. (2018). PI(4,5)P2 Controls Plasma Membrane PI4P and PS Levels *via* ORP5/8 Recruitment to ER-PM Contact Sites. *J. Cel Biol.* 217 (5), 1797–1813. doi:10.1083/jcb.201710095

Tan, L., Cho, K. J., Kattan, W. E., Garrido, C. M., Zhou, Y., Neupane, P., et al. (2019). Acylpeptide Hydrolase Is a Novel Regulator of KRAS Plasma Membrane Localization and Function. *J. Cel Sci.* 132 (15). doi:10.1242/jcs.232132

Tian, T., Harding, A., Inder, K., Plowman, S., Parton, R. G., and Hancock, J. F. (2007). Plasma Membrane Nanoswitches Generate High-Fidelity Ras Signal Transduction. *Nat. Cel Biol.* 9 (8), 905–914. doi:10.1038/ncb1615

Uchida, Y., Hasegawa, J., Chinnapen, D., Inoue, T., Okazaki, S., Kato, R., et al. (2011). Intracellular Phosphatidylserine Is Essential for Retrograde Membrane Traffic through Endosomes. *Proc. Natl. Acad. Sci. U S A.* 108 (38), 15846–15851. doi:10.1073/pnas.1109101108

Van Cutsem, E., van de Velde, H., Karasek, P., Oettle, H., Vervenne, W. L., Szawlowski, A., et al. (2004). Phase III Trial of Gemcitabine Plus Tipifarnib Compared with Gemcitabine Plus Placebo in Advanced Pancreatic Cancer. *J. Clin. Oncol.* 22 (8), 1430–1438. doi:10.1200/JCO.2004.10.112

van der Hoeven, D., Cho, K. J., Ma, X., Chigurupati, S., Parton, R. G., and Hancock, J. F. (2013). Fendiline Inhibits K-Ras Plasma Membrane Localization and Blocks K-Ras Signal Transmission. *Mol. Cel Biol.* 33 (2), 237–251. doi:10.1128/MCB.00884-12

van der Hoeven, D., Cho, K. J., Zhou, Y., Ma, X., Chen, W., Naji, A., et al. (2018). Sphingomyelin Metabolism Is a Regulator of K-Ras Function. *Mol. Cel Biol* 38 (3), e00373. doi:10.1128/MCB.00373-17

Wang, H., Haridas, V., Gutterman, J. U., and Xu, Z. X. (2010). Natural Triterpenoid Avicins Selectively Induce Tumor Cell Death. *Commun. Integr. Biol.* 3 (3), 205–208. doi:10.4161/cib.3.3.11492

Weinstein, I. B., and Joe, A. (2008). Oncogene Addiction. *Cancer Res.* 68 (9), 3077–3080. doi:10.1158/0008-5472.CAN-07-3293

Willumsen, B. M., Christensen, A., Hubbert, N. L., Papageorge, A. G., and Lowy, D. R. (1984). The P21 Ras C-Terminus Is Required for Transformation and Membrane Association. *Nature*. 310 (5978), 583–586. doi:10.1038/310583a0

Yeung, T., Gilbert, G. E., Shi, J., Silvius, J., Kapus, A., and Grinstein, S. (2008). Membrane Phosphatidylserine Regulates Surface Charge and Protein Localization. *Science*. 319 (5860), 210–213. doi:10.1126/science.1152066

Zhang, H., Li, S., Doan, T., Rieke, F., Detwiler, P. B., Frederick, J. M., et al. (2007). Deletion of PrBP/delta Impedes Transport of GRK1 and PDE6 Catalytic Subunits to Photoreceptor Outer Segments. *Proc. Natl. Acad. Sci. U S A.* 104 (21), 8857–8862. doi:10.1073/pnas.0701681104

Zhang, X., Yu, L., and Xu, H. (2016). Lysosome Calcium in ROS Regulation of Autophagy. *Autophagy*. 12 (10), 1954–1955. doi:10.1080/15548627.2016.1212787

Zhou, Y., Prakash, P., Liang, H., Cho, K.-J., Gorfe, A. A., and Hancock, J. F. (2017). Lipid-Sorting Specificity Encoded in K-Ras Membrane Anchor Regulates Signal Output. *Cell*. 168 (1-2), 239–251 e16. doi:10.1016/j.cell.2016.11.059

Zimmermann, G., Papke, B., Ismail, S., Vartak, N., Chandra, A., Hoffmann, M., et al. (2013). Small Molecule Inhibition of the KRAS-PDEdelta Interaction Impairs Oncogenic KRAS Signalling. *Nature*. 497 (7451), 638–642. doi:10.1038/nature12205

Conflict of Interest: The authors declare that the research was conducted in the absence of any commercial or financial relationships that could be construed as a potential conflict of interest.

frontiers in Molecular Biosciences

REVIEW
published: 17 June 2021
doi: 10.3389/fmolb.2021.686338

RAS Nanoclusters Selectively Sort Distinct Lipid Headgroups and Acyl Chains

Yong Zhou, Alemayehu A. Gorfe* and John F. Hancock**

Department of Integrative Biology and Pharmacology, University of Texas Health Science Center, Houston, TX, United States

RAS proteins are lipid-anchored small GTPases that switch between the GTP-bound active and GDP-bound inactive states. RAS isoforms, including HRAS, NRAS and splice variants KRAS4A and KRAS4B, are some of the most frequently mutated proteins in cancer. In particular, constitutively active mutants of KRAS comprise ~80% of all RAS oncogenic mutations and are found in 98% of pancreatic, 45% of colorectal and 31% of lung tumors. Plasma membrane (PM) is the primary location of RAS signaling in biology and pathology. Thus, a better understanding of how RAS proteins localize to and distribute on the PM is critical to better comprehend RAS biology and to develop new strategies to treat RAS pathology. In this review, we discuss recent findings on how RAS proteins sort lipids as they undergo macromolecular assembly on the PM. We also discuss how RAS/lipid nanoclusters serve as signaling platforms for the efficient recruitment of effectors and signal transduction, and how perturbing the PM biophysical properties affect the spatial distribution of RAS isoforms and their functions.

Keywords: RAS nanoclusters, phospholipids, electron microscopy, mitogen-activated protein kinases, depolarization, membrane curvature, cholesterol, polybasic domain

OPEN ACCESS

Edited by:
Jin Rui Liang,
ETH Zürich, Switzerland

Reviewed by:
James Michael,
Thomas Jefferson University, United States
Zhenlu Li,
Case Western Reserve University, United States

****Correspondence:***
Yong Zhou
yong.zhou@uth.tmc.edu
Alemayehu A. Gorfe
Alemayehu.G.Abebe@uth.tmc.edu
John F. Hancock
john.f.hancock@uth.tmc.edu

Specialty section:
This article was submitted to Molecular Diagnostics and Therapeutics, a section of the journal Frontiers in Molecular Biosciences

Received: *26 March 2021*
Accepted: *13 May 2021*
Published: *17 June 2021*

Citation:
Zhou Y, Gorfe AA and Hancock JF (2021) RAS Nanoclusters Selectively Sort Distinct Lipid Headgroups and Acyl Chains. Front. Mol. Biosci. 8:686338. doi: 10.3389/fmolb.2021.686338

INTRODUCTION

RAS isoforms, including HRAS, NRAS and KRAS4B are molecular switches that toggle between guanosine-5′-triphosphate (GTP)-bound active and guanosine diphosphate (GDP)-bound inactive states (Downward, 2003; Hancock, 2003; Cox et al., 2014; Cox et al., 2015; Prior et al., 2020). RAS proteins are key upstream regulators of the mitogen-activated protein kinases (MAPKs) signaling pathway, and participate in important cell functions including growth, division and proliferation (Cox et al., 2014; Cox et al., 2015; Prior et al., 2020). Mutations of RAS proteins are frequently found in many human diseases, and approximately 19% of all human cancers harbor RAS mutations (Cox et al., 2014; Cox et al., 2015; Prior et al., 2020). Mutations of KRAS4B are particularly prevalent in cancer, comprising ~80% of all RAS-related oncogenic mutations (Downward, 2003; Hancock, 2003; Cox et al., 2014; Cox et al., 2015; Prior et al., 2020). Mutations of KRAS4B are found in 98% of pancreatic, 45% of colorectal and 31% of lung tumors (Downward, 2003; Hancock, 2003; Cox et al., 2014; Cox et al., 2015; Prior et al., 2020). Despite >30 years of intense research, KRAS remains difficult to directly inhibit by small molecule ligands (Ledford, 2015). Targeting the interactions of RAS with the plasma membrane is an attractive alternative because: 1) normal and aberrant biological functions of RAS proteins, including the constitutively active oncogenic RAS mutants, are mostly restricted to the plasma membrane (PM); 2) the distinct C-terminal membrane-anchoring domains of RAS isoforms contribute to their isoform-specific biological activities; 3) RAS dimerization occurs only on the PM and contributes to the formation of RAS signaling

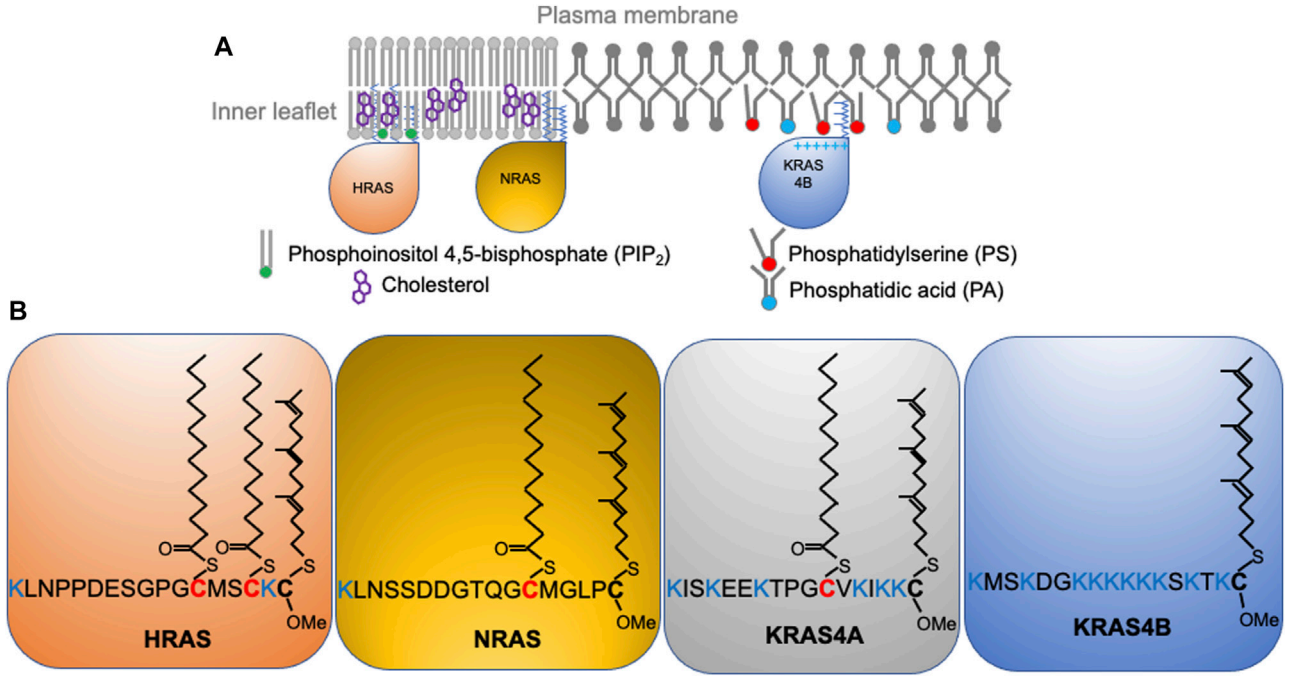

FIGURE 1 | RAS isoforms with distinct C-terminal membrane-anchoring domains interact with different lipids and form spatially non-overlapping domains on the plasma membrane. **(A)** RAS proteins, including HRAS, NRAS, and KRAS4B distribute to distinct locations on the inner leaflet of the plasma membrane. **(B)** RAS isoforms share near identical enzymatic G-domains (>95% homology) and variable C-terminal hypervariable regions (HVR). RAS isoforms undergo distinct posttranslational modifications to add acyl chains to their HVRs for selective lipid sorting and nanoclustering.

platforms on the PM. In this review, we will discuss the latest findings on how RAS isoforms undergo spatial distribution on the PM. We will specifically discuss the selective interactions of RAS proteins with distinct PM lipids, their lateral dynamics, and dimerization and oligomerization via specific interaction interfaces. We will also discuss our perspective on how RAS-RAS and RAS-lipid interactions might be targeted to inhibit aberrant RAS signaling.

Isoform-Specific Intracellular Transport of RAS

Wild type RAS predominantly signals from the inner surface of the PM (**Figure 1A**) where recruitment and activation of effector proteins occurs (Hancock, 2003; Cox et al., 2015; Zhou and Hancock, 2015; Zhou and Hancock, 2017). This is also the case for the constitutively active oncogenic mutants of RAS. Thus, proper PM localization and spatial distribution of both wild-type and mutant RAS proteins is essential to biology and pathology. All RAS isoforms share nearly identical G-domains (>95% sequence identity) and highly divergent C-terminal hypervariable regions (<20% homology) (**Figure 1B**). All RAS isoforms undergo multiple steps of posttranslational modifications that add structural features required for membrane interaction, and are transported to the PM via various intracellular trafficking routes. First, farnesyltransferases recognize the C-terminal CAAX motif to irreversibly add a poly-unsaturated and branched 15-carbon farnesyl chain to the cysteine residue at position 185 (Reiss et al., 1990). The prenyl anchor allows RAS to localize to the cytosolic side of the endoplasmic reticulum (ER) membrane, where RAS converting enzyme (Rce1) cleaves the AAX residues of CAAX (Boyartchuk et al., 1997; Kim et al., 1999). The farnesylated Cys is then methyl-esterified at the α-carboxyl group by isoprenylcysteine carboxyl methyltransferases (ICMT) (Hrycyna et al., 1991; Dai et al., 1998). All RAS isoforms undergo these modifications, but diverge in their further processing. NRAS is palmitoylated at Cys181 and HRAS is palmitoylated at Cys181 and Cys184 (**Figure 1B**) by palmitoyltransferases at the Golgi apparatus (Hancock et al., 1991; Hancock et al., 1989) before being transported to the PM via the classic vesicular trafficking pathways (Hancock et al., 1991; Hancock et al., 1989). Palmitoylation is reversible, and the thioester bond in RAS palmitoyl cysteines can be cleaved by the PM-resident thioesterases (Ahearn et al., 2011). Depalmitoylated NRAS and HRAS fall off the PM and return to the Golgi apparatus and, following repalmitoylation, recycle back to the PM (Hancock et al., 1991; Hancock et al., 1989). The reversible palmitoylation/depalmitoylation cycle therefore dynamically regulates the intracellular trafficking of NRAS and HRAS (Hancock et al., 1991; Hancock et al., 1989). Other chaperons, such as VPS26A, VPS29, and VPS35 also facilitate the transport of NRAS between intracellular compartments and the PM. By contrast, KRAS4B is not palmitoylated but instead contains a polybasic domain (PBD) composed of six lysine residues (Lys 175-180) immediately before the site of farnesylation (**Figure 1B**). Unlike NRAS and HRAS, KRAS4B does not go to the Golgi apparatus (Hancock et al., 1991).

Rather, the farnesylated KRAS4B molecules (**Figure 1B**) fall off the ER and undergo cytosolic diffusion facilitated by phosphodiesterase δ (PDEδ), which possesses a prenyl-binding pocket to sheath the farnesyl anchor of KRAS4B in the cytosol (Chandra et al., 2012; Schmick et al., 2015; Schmick et al., 2014). The fully processed KRAS4B, chaperoned by PDEδ, preferentially localizes to the recycling endosomes for delivery to the PM. It is still unclear how KRAS4B chooses the recycling endosomes, possibly facilitated by the electrostatic interactions between the KRAS4B PBD and anionic lipids enriched on the recycling endosomes (Chandra et al., 2012; Schmick et al., 2014; Schmick et al., 2015). Additionally, GPR31, a G protein-coupled receptor, also acts as a chaperon by associating with the farnesylated KRAS4B to aid in the transfer of KRAS4B to the PM (Fehrenbacher et al., 2017). Interestingly, intracellular transport of KRAS4B may not even need endomembrane organelles. A recent atomic force microscopy (AFM) study shows that KRAS4B can incorporate into membrane-less protein condensates formed by liquid-liquid phase separation (Li et al., 2021). The study revealed that the liquid droplets dissolve in the presence of a supported bilayer, with the released KRAS4B molecules attached to the bilayer and undergo nanoclustering (Li et al., 2021). Long thought a minor slice variant, KRAS4A is regaining attention in recent years with the discovery that it is widely expressed in many cancer cells (Tsai et al., 2015). KRAS4A is mainly localized to the PM but it also cycles among various endomembrane compartments. Its lipid anchor harbors two short segments of basic residues, a palmitoyl chain, and a farnesyl chain (**Figure 1B**), but unlike the similarly mono-palmitoylated NRAS, upon depalmitoylation KRAS4A localizes to the outer mitochondrial membrane (OMM) where it interacts with hexokinase 1 (Amendola et al., 2019). Taking together, the exiting data strongly suggest that the differences in the C-terminal membrane-anchoring domains of RAS isoforms contribute to their distinct intracellular trafficking properties.

Isoform-Specific Nanoclustering of RAS

Once localized to the PM, RAS proteins undergo lateral segregation in the x-y plane to form nanometer-sized domains or nanoclusters, which serve as isoform-specific signaling platforms. In addition to RAS, these nanoclusters contain other proteins and lipids that are important for effector recruitment and signal propagation. Prior et al. was the first to quantify how immunogold-labeled RAS isoforms laterally distribute on intact PM sheets using electron microscopy (EM)-univariate nanoclustering analysis (Prior et al., 2003). In this analysis, intact PM sheets of mammalian cells expressing green fluorescence protein (GFP)-tagged RAS are attached to poly-L-lysine- and pioloform-coated copper (for apical PM) or gold (for basolateral PM) EM grids (Prior et al., 2003). The fixed intact PM sheets are labeled with 4.5 nm gold nanoparticles conjugated to anti-GFP antibody. Transmission electron microscopy (TEM) is used to image these gold-labeled PM sheets at a magnification of 100,000X. **Figure 2A** shows a raw EM image of an intact PM sheet of 1 μm^2 area with gold-tagged GFP-KRAS4B. **Figure 2B** shows the same PM sheet, with the gold particles marked in different colors to illustrate the spatial distribution. ImageJ is used to assign the x, y coordinates for each gold particle. The Ripley's K-function is then used to calculate the spatial distribution of these gold particles and to quantify the extent of nanoclustering of the gold-labeled GFP-RAS on intact PM sheets (Ripley, 1977; Diggle, 1979; Diggle et al., 2000). As shown in **Figure 2C**, the extent of nanoclustering, $L(r)$-r, can be plotted as a function of radius r in nanometer. $L(r)$-r values above the 99% confidence interval (99% C.I.) indicate statistically significant nanoclustering. The peak $L(r)$-r value, termed as L_{max}, is generally used as a statistical summary for the nanoclustering event, which tightly correlates with the area-under-the-curve values of the K-function curve (Zhou et al., 2017). Number of neighboring gold particles within 15 nanometers of each gold is also calculated to estimate population distributions (**Figure 2D**). Other optical imaging techniques have been used to extensively validate the spatial distribution of RAS in intact and live cells. One of these is fluorescence lifetime imaging-fluorescence resonance energy transfer (FLIM-FRET), which has been used to measure the extent of co-localization of GFP- and RFP-tagged RAS in intact cells and tissues (Zhou et al., 2012; Zhou et al., 2014; Zhou et al., 2015; Zhou et al., 2017; Liang et al., 2019). The FRET efficiency between the GFP and RFP can be used to quantify close association (within 10 nm) among RAS molecules, and such measurements have been found to nicely correlate with the nanoclustering of RAS determined by the EM-spatial analysis. Raster image correlation spectroscopy (RICS), fluorescence correlation spectroscopy (FCS), fluorescence recovery after photobleaching (FRAP), total internal reflection fluorescence-single particle tracking (TIRF-SPT), and photoactivated localization microscopy (PALM), have also been used to measure the diffusion and population distribution of RAS monomers and nanoclusters in live cells (Murakoshi et al., 2004; Nan et al., 2015; Sarkar-Banerjee et al., 2017). Atomic force microscopy (AFM) has been used to image the lateral distribution purified full-length RAS proteins or the truncated minimal membrane anchoring domains on supported bilayers of co-existing lipid domains (Nicolini et al., 2006; Weise et al., 2011). *In silico* molecular dynamics (MD) simulations are also used to elucidate the physicochemical basis for the spatial segregation of RAS lipid anchors in one- or multi-component bilayers (Gorfe et al., 2004; Gorfe et al., 2007a; Gorfe et al., 2007b; Janosi and Gorfe, 2010; Janosi et al., 2012; Li et al., 2012). These quantitative super-resolution imaging and simulation studies consistently corroborate and demonstrate the spatiotemporal dynamics and isoform-specific organization of RAS proteins on membranes of different complexities.

As the sample Ripley's K-function curve in **Figure 2C** illustrates, peak clustering of GFP-RAS occurs at the radial length r of ~20 nm, suggesting that the most probable radius of GFP-RAS nanoclusters is approximately 20 nm (Prior et al., 2003; Plowman et al., 2005; Zhou et al., 2014; Zhou et al., 2015; Zhou et al., 2017; Liang and et al., 2019; Zhou et al., 2021). The K-function analysis further showed that RAS nanoclusters contain approximately 6–7 RAS molecules, and suggests that nearly half of GFP-RAS molecules exist as monomers, ~30% as dimers, >10% as trimers, and <10% of GFP-RAS form higher order multimers (Zhou et al., 2017). This population distribution

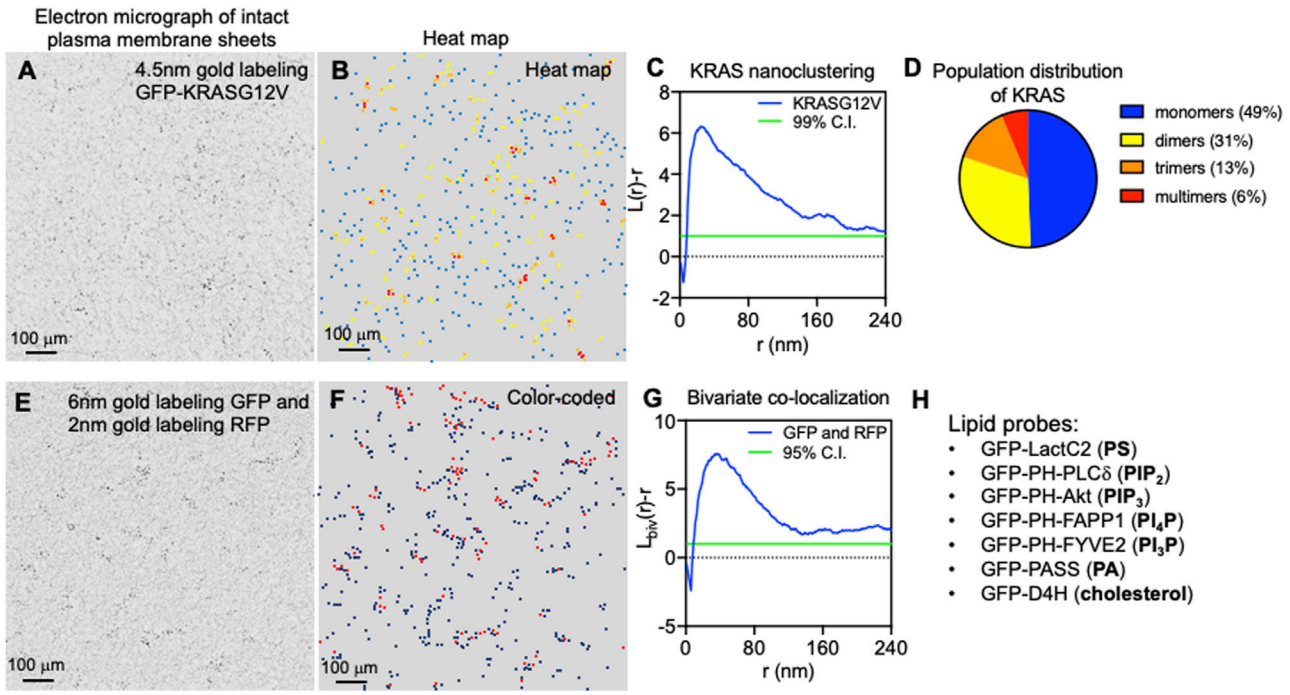

FIGURE 2 | Super-resolution electron microscopy quantitatively characterizes the spatial distribution of RAS on intact plasma membrane sheets. **(A)** A sample electron micrograph of an intact plasma membrane sheet with an area of 1 μm^2 is shown. Black dots indicate 4.5 nm gold nanoparticles conjugated to anti-GFP antibody that tag the GFP-tagged KRAS4B localized to the inner leaflet of the plasma membrane. **(B)** Gold nanoparticles are then color-coded to indicate spatial distribution in a heat map of the same electron micrograph as shown in *A*. **(C)** The Ripley's K-function calculates the spatial distribution of the gold particles shown in *A* and *B*. Extent of nanoclustering, $L(r)$-r, is plotted as a function of radius r in nanometer. $L(r)$-r values above the 99% confidence interval (99% C.I.) indicate statistically significant nanoclustering. The peak $L(r)$-r value, termed L_{max}, statistically summarizes the nanoclustering. **(D)** Further examination of the nanoclustering data in C allows calculation of the population distribution of cluster sizes. **(E)** A sample electron micrograph of an intact plasma membrane sheet with an area of 1 μm^2 is shown. Two populations of gold nanoparticles are observed: 6 nm gold particles conjugated to anti-GFP antibody and 2 nm gold coupled to anti-RFP antibody. These gold particles are color-coded and shown in **(F)**. **(G)** The Ripley's bivariate co-localization K-function calculates the co-clustering between the two populations of gold particles. Extent of co-clustering, $L_{biv}(r)$-r, is plotted as a function of radius r in nanometer. $L_{biv}(r)$-r values above the 95% confidence interval (95% C.I.) indicate statistically significant co-clustering. Integration of the $L_{biv}(r)$-r curve between r values of 10 and 110 nm yields a statistical summary, termed as L-bivariate integrated (LBI), to indicate co-clustering. **(H)** Lists a cohort of specific lipid-binding domains used to probe the spatial distribution of some major lipids in the inner leaflet of the plasma membrane.

is consistent across a range of methods and data sources, including EM-spatial analysis of intact PM sheets, RICS and PALM analyses of live cell PM, as well as predictions from MD simulations (Janosi et al., 2012; Nan et al., 2015; Sarkar-Banerjee et al., 2017). Experiments using SPT, which tracks GFP-tagged RAS on the PM of live mammalian cells, found that the lifetime of RAS nanoclusters is between 100 ms and 1 s, with nanoclusters of the GTP-bound active RAS having a longer lifetime near 1 s (Murakoshi et al., 2004).

The local environment within different RAS nanoclusters is distinct since the nanoclusters are spatially segregated in an isoform- and guanine nucleotide-specific manner. This has been quantified using a special form of EM-spatial analysis, which is a bivariate co-clustering analysis using cells co-expressing GFP- and red fluorescence protein (RFP)-tagged proteins. In these experiments, EM is performed on intact PM sheets of mammalian cells co-expressing two different RAS isoforms (or the same RAS isoform bound with either GTP or GDP) tagged with GFP and RFP and co-labeled with 6 nm gold nanoparticles conjugated to an anti-GFP antibody and 2 nm gold nanoparticles coupled to an anti-RFP antibody (Prior et al., 2003).

Figure 2E shows a raw EM image of an intact PM sheet of 1 μm^2 area containing 6 nm gold tagging GFP and 2 nm gold tagging RFP, with the larger 6 nm gold marked in black and the smaller 2 nm gold marked in red (**Figure 2F**). After digitization via ImageJ, spatial co-clustering between the 6-nm gold and 2-nm gold particles is calculated via the Ripley's bivariate co-clustering analysis. As illustrated in **Figure 2G**, extent of co-clustering, $L_{biv}(r)$-r, is plotted as a function of r in nanometer. $L_{biv}(r)$-r values above the 95% confidence interval (95% C.I.) indicate statistically significant co-clustering of the two populations of gold particles (Ripley, 1977; Diggle, 1979; Diggle et al., 2000). Such bivariate co-clustering analyses showed that co-clustering among HRAS, NRAS and KRAS4B is below the 95% C.I., suggesting minimal spatial overlap among the isoforms (Prior et al., 2003; Plowman et al., 2005). For each isoform, GTP- and GDP-bound RAS also show minimal co-clustering, indicating that the different nucleotide-bound forms of each RAS protein occupy distinct spaces on the PM inner leaflet (Prior et al., 2003). This spatial segregation is biologically important. For example, in a series of bivariate co-clustering analyses, acute depletion of cholesterol, via methyl β-cyclodextrin (MβCD), abolished the spatial

segregation between the active GTP-bound HRAS and the inactive GDP-bound HRAS on the PM, and resulted in an inhibition of HRAS signaling (Ariotti et al., 2014). Elimination of caveolae on the PM, via knocking down important caveolar structural component caveolin 1 (CAV1), also induced mixing of the active GTP-bound and the inactive GDP-bound HRAS on the PM, which compromised HRAS signaling (Ariotti et al., 2014). Taken together, RAS proteins form lateral nanoclusters on the PM in isoform- and guanine nucleotide-specific manners.

RAS Nanoclusters are Proteolipid Nano-Assemblies Acting as Signaling Scaffolds

RAS nanoclusters are the sites for effector recruitment and signaling (Hancock, 2003; Tian et al., 2007; Zhou and Hancock, 2015; Zhou and Hancock, 2017). They concentrate multiple RAS molecules within a small area of ~300 nm^2 on the PM (Prior et al., 2003; Plowman et al., 2005; Tian et al., 2007; Tian et al., 2010), increasing the probability of RAS-effector encounters. RAS nanoclusters are not exclusively "RAS oligomers" but rather molecular assemblies that contain other constituents needed for signaling propagation. The non-RAS constituents include lipids and other membrane-associated proteins, as well as the actin cytoskeleton structure. For example, EM-spatial analysis showed that nanoclustering of GFP-HRAS.GDP or GFP-KRAS4B.GTP was compromised upon Latrunculin A treatment to disrupt actin polymerization (Plowman et al., 2005; Zhou et al., 2014). Thus, actin is an important component in the nanoclustering of HRAS and KRAS4B on the PM. Expression of galectin-1 (Gal-1) enhanced the clustering of the constitutively active GFP-HRASG12V (Rotblat et al., 2004; Belanis et al., 2008), suggesting that Gal-1 is likely also a component of HRAS nanoclusters. This is supported by the observation that higher Gal-1 levels enhanced HRAS effector binding, MAPK signaling, and stemness of mutant HRAS-transformed mammalian cells (Blazevits et al., 2016; Posada et al., 2017). Furthermore, integration of molecular dynamics simulations, FLIM-FRET and EM-univariate nanoclustering analysis revealed that Gal-1 dimers formed complexes with the RAS-binding domain of RAS effectors, such as CRAF (Blazevits et al., 2016). This, in turn, stabilized nanoclusters of the GTP-bound active HRAS on the PM. Higher levels of galectin-3 (Gal-3), on the other hand, promoted the nanoclustering and effector binding of GFP-KRAS4BG12V (Elad-Sfadia et al., 2004; Shalom-Feuerstein et al., 2008), suggesting that Gal-3 is an integral component of the nanoclusters of active KRAS. Additional regulators of KRAS4B nanoclustering have been discovered through an extensive proteomic screen. These include nucleophosmin and nucleolin (Inder et al., 2009; Inder et al., 2010). Although primarily localized to the nucleus, a subset of nucleophosmin and nucleolin localize to the PM inner leaflet and become incorporated into KRAS4B nanoclusters, which results in further stabilization of KRAS4B nanoclusters and elevation of KRAS4B effector binding and MAPK signaling (Inder et al., 2009; Inder et al., 2010). FLIM-FRET and EM analysis showed that expression of the apoptosis-stimulating p53 protein (ASPP) family member, ASPP2, enhanced the nanoclustering and effector binding of HRASG12V, KRAS4BG12V and NRASG12V (Posada et al., 2016). Concordantly, expression of ASPP2 promoted MAPK signaling in mammalian cells transformed by HRASG12V, KRAS4BG12V or NRASG12V (Posada and et al., 2016). FLIM-FRET analysis and signaling assays revealed that ASPP2 competed with Gal-1 within the nanoclusters of HRASG12V and KRAS4BG12V (Posada et al., 2016). This competition resulted in an ASPP2-induced senescence of HRASG12V- and KRAS4BG12V-transformed mammalian cells, and abolished the HRAS- and KRAS4B-dependent formation of mammospheres of breast cancer cells (Posada and et al., 2016). Taken together, RAS nanoclusters on the PM are comprised of multiple protein and lipid constituents that, together, are important for effector recruitment and signal transduction.

RAS Nanoclusters Sort Lipids in a Headgroup- and Acyl Chain Structure-Specific Manner

Lipids are the major constituents of RAS nanoclusters on the PM. These lipids are not only important for the structural integrity and stability of RAS nanoclusters, but also directly participate in effector recruitment. This is because most effectors of RAS contain specific lipid-binding domains and require synergistic association with both GTP-bound active RAS and a specific set of lipids for an efficient PM targeting and activation (Ghosh et al., 1994; Ghosh et al., 1996; Li et al., 2018). Even constitutively active mutants of RAS require precise spatial organization and lipid sorting to efficiently recruit their effectors and propagate signals (Inder et al., 2008; Inder and Hancock, 2008). For example, a major KRAS4B effector, CRAF, contains binding domains for both phosphatidylserine (PS) and phosphatidic acid (PA) (Ghosh et al., 1994; Ghosh et al., 1996; Li et al., 2018). It has been shown that the presence of PS and PA in membranes promoted the binding and activation of CRAF in synthetic liposomes and cells (Ghosh et al., 1994; Ghosh et al., 1996). Moreover, phosphoinositol-3 kinase (PI3K), a major effector of HRAS, specifically recognizes phosphoinositol 4,5-bisphosphate (PIP_2) in the PM and converts it to phosphoinositol 3,4,5-trisphosphate (PIP_3) (Hemmings and Restuccia, 2012). Thus, a key biological function of RAS nanoclusters appears to involve concentrating distinct lipids appropriate for each type of RAS isoform to recruit its specific effectors. This partially explains how RAS isoforms that share the same set of effectors differ in their affinity for different effectors, including the fact that KRAS4B preferentially recruits RAF while HRAS favors PI3K (Stokoe et al., 1994).

The enrichment of specific lipids within different RAS nanoclusters has been investigated using EM-bivariate co-clustering analysis of GFP-tagged lipid-binding domains that bind specific lipids (some examples listed in **Figure 2H**) and RFP-tagged RAS proteins on intact PM sheets (Zhou et al., 2014; Zhou et al., 2015; Zhou et al., 2017; Liang et al., 2019; Zhou et al., 2021). These experiments were complemented by FLIM-FRET in

TABLE 1 | Nanoclusters of KRAS selectively enrich the mixed-chain PS species.

Lipid acute back	KRAS PM localization	KRAS nanoclustering	Lipids enriched in KRAS nanoclusters	KRAS recruitment of effector RAF
Brain PIP_2[a]	Unaffected	Unaffected	No	Unaffected
Brain PC[a]	Unaffected	Unaffected	Not tested	Not tested
Brain PE[a]	Unaffected	Unaffected	Not tested	Not tested
Brain PS[a,b,c]	Enhanced	Enhanced	Yes	Enhanced
DSPS (di 18:0 PS)[c,d,e]	Unaffected	Unaffected	No	Not tested
DOPS (di 18:1 PS)[c,d,e]	Enhanced	Unaffected	No	Unaffected
DLPS (di 18:2 PS)[c,e]	Enhanced	Unaffected	No	Unaffected
POPS (16:0 / 18:1 PS)[c,d,e]	Enhanced	Enhanced	Yes	Enhanced
SOPS (18:0 / 18:1 PS)[c,e]	Enhanced	Enhanced	Yes	Not tested

[a]*Cho et al., 2016* ***Mol Cell Biol.***
[b]*Zhou et al., 2014* ***Mol Cell Biol***
[c]*Zhou et al., 2017* ***Cell.***
[d]*Liang et al., 2019* ***Life Sci Alliance.***
[e]*Zhou et al., 2021* ***Proc Natl Acad Sci U S A.***

live cells expressing RFP-tagged RAS isoforms and spike-labeled TopFluor-tagged fluorescent lipids exogenously supplemented to these cells (Zhou et al., 2014; Zhou et al., 2015; Zhou et al., 2017; Liang et al., 2019; Zhou et al., 2021). The EM co-clustering analysis showed that RFP-KRAS4BG12V co-localized extensively with the PS probe GFP-LactC2 and the PA probe GFP-PASS, but not with the PIP_2 probe GFP-PH-PLCδ, the PIP_3 probe GFP-PH-Akt or the cholesterol probe GFP-D4H (Zhou et al., 2014; Zhou et al., 2015). On the other hand, RFP-tagged GDP-bound HRAS or its truncated minimal anchor (RFP-tH) were found to co-localize with probes of PIP_2 and cholesterol (Zhou et al., 2014; Zhou et al., 2015). The difference in cholesterol association between KRAS4B and HRAS is consistent with earlier studies where acute cholesterol depletion by treatment of cells with methyl β-cyclodextrin (MβCD) effectively disrupted the nanoclustering and signaling of GFP-HRAS.GDP and GFP-tH but not GFP-KRAS4BG12V or GFP-tK (Prior et al., 2003; Plowman et al., 2005). Concordantly, the purified full-length KRAS4B and tK partitioned into the cholesterol-poor liquid-disordered (L_d) domains of supported bilayers, as observed in atomic force microscopy (AFM) (Weise et al., 2011). MD simulations predicted that tH preferred to localize at the boundary between the cholesterol-enriched liquid-ordered (L_o) and L_d domains (Janosi et al., 2012; Li et al., 2012; Li and Gorfe, 2013), consistent with experimental findings that cholesterol depletion disrupted the nanoclustering of tH in the cell PM. That RFP-KRAS4BG12V does not co-localize with PIP_2 is surprising because the membrane-anchoring domain of KRAS4B is comprised of a hexa-lysine domain (**Figure 1B**) that is expected to interact with the PM primarily via electrostatics. Instead, the selective enrichment of the monovalent PS and PA over the multivalent PIP_2 suggests a significant non-electrostatic contribution.

Additional insights into the lipid composition of RAS nanoclusters came from experiments in cells involving depleting and then adding back of specific lipids. In this regard, PS is of particular interest because KRAS co-localized extensively with a PS-binding domain in EM-bivariate co-localization analysis, as well as FLIM-FRET (Zhou et al., 2014). PS is the most abundant anionic phospholipid in mammalian cells, and is asymmetrically enriched in the PM inner leaflet. Mammalian cells typically contain two PS synthases (PSS): PSS1 that catalyzes the conversion of phosphatidylcholine (PC) to PS and PSS2 that converts phosphatidylethanolamine (PE) to PS (Lee et al., 2012). To manipulate PS content, PSS1 in Chinese hamster ovarian (CHO) cells was knocked down to generate a mutant line, termed as PSA3 cells (Lee et al., 2012). When grown in dialyzed fetal bovine serum (DFBS), PSA3 cells generate 35% less total PS and markedly lower PS levels in the PM inner leaflet (Lee et al., 2012; Zhou et al., 2014; Zhou et al., 2015; Zhou et al., 2017; Liang et al., 2019; Zhou et al., 2021). In the DFBS-treated PSA3 cells, supplementation of ethanolamine (Etn), which is a ligand upstream of PSS2, stimulates PSS2 and dose-dependently (0–10 μM for 72 h) elevates PS in the PM (Lee et al., 2012; Zhou et al., 2014; Zhou et al., 2015; Zhou et al., 2017; Liang and et al., 2019; Zhou et al., 2021). Then, different extracts of mouse brain lipids were acutely added back (1-hour incubation) to the PS-depleted PSA3 cells (Zhou et al., 2014; Zhou et al., 2015; Zhou et al., 2017; Liang et al., 2019; Zhou et al., 2021). EM-univariate nanoclustering analysis of these cells showed that PS depletion effectively disrupted the nanoclustering and PM localization of GFP-KRAS4BG12V as well as the GFP-tK but had no effect on GFP-HRAS (Zhou et al., 2014; Zhou et al., 2015). Supplementation of Etn (0–10 μM for 72 h) dose-dependently elevated the nanoclustering and PM localization of GFP-KRAS4BG12V but not GFP-HRASG12V (Zhou et al., 2014). In the PS-depleted PSA3 cells, acute addback of mouse brain extract of PS, but not extracts of other lipids tested (PIP_2, PE, PC or cholesterol), recovered the nanoclustering and PM localization of GFP-KRAS4BG12V (Zhou et al., 2014; Cho et al., 2015). PS depletion disrupted the co-localization of GFP-KRAS4BG12V and RFP-tagged CRAF and thereby KRAS4B-dependent MAPK signaling, both of which were restored back to control levels upon the acute addback of PS but not any of the other lipids tested (Cho et al., 2015; Zhou et al., 2015; Zhou et al., 2017). **Table 1** summarizes how different lipid types with distinct headgroups impact the spatiotemporal organization and effector recruitment of KRAS. Taken together, RAS nanoclusters have distinct lipid

TABLE 2 | Nanoclusters of different RAS isoforms respond to membrane perturbations in distinct manners.

Membrane perturbations	KRAS4B.GDP (or tK)	KRAS4B.GTP	HRAS.GDP (or tH)	HRAS.GTP	NRAS.GDP (or tN)	NRAS.GTP
Cholesterol depletion[a,c,g]	Unaffected	Unaffected	Disrupted	Unaffected	Unaffected	Disrupted
Depolarization[d,g]	Enhanced	Enhanced	Unaffected	Unaffected	Not tested	Not tested
Curvature[f,g]						
Positive curvature	Disrupted	Disrupted	Enhanced	Enhanced	Not tested	Not tested
Negative curvature	Not tested	Unaffected	Disrupted	Not tested	Not tested	Not tested
Actin[b,f]	Not tested	Enhanced	Enhanced	Unaffected	Not tested	Not tested
Caveolae[h]	Disrupted	Disrupted	Enhanced	Enhanced	Not tested	Not tested

[a]*Prior et al., 2003* ***J Cell Biol.***
[b]*Plowman et al., 2005* ***Proc Natl Acad Sci U S A.***
[c]*Roy et al., 2005* ***Mol Cell Biol.***
[d]*Zhou et al., 2015* ***Science.***
[e]*Zhou et al., 2017* ***Cell.***
[f]*Liang et al., 2019* ***Life Sci Alliance.***
[g]*Zhou et al., 2021* ***Proc Natl Acad Sci U S A.***
[h]*Ariotti et al., 2014* ***J Cell Biol.***

contents that contribute to selective effector recruitment and signal propagation.

KRAS4B Nanoclusters Concentrate Phosphatidylserine Species With Specific Acyl Chain Structures

As already noted, KRAS4B is targeted to the PM primarily via its C-terminal lipid anchor harboring a hexa-lysine segment (Lys175-180, **Figure 2B**). Therefore, it has long been thought that charge-charge interactions dominate the association of the KRAS4B polybasic domain (PBD) with the PS- and PIP_2-enriched negatively charged PM inner leaflet. In this context, a surprising finding in the lipid mapping analysis described above was the suggestion that KRAS4B-PM interaction may involve more than just electrostatic complementarity, because KRAS4B nanoclusters were found to be selectively enriched with the monovalent PS but not the multivalent PIP_2 lipids. To further test this, different exogenous PS species were acutely added back to the PS depleted PSA3 cells and the nanoclustering of GFP-KRAS4BG12V was quantified using EM (Zhou et al., 2017; Liang et al., 2019; Zhou et al., 2021). These synthetic PS species have the same charged headgroup and thus can be assumed to have the same electrostatic interactions with the PBD of KRAS4B. Their distinct acyl chain length and unsaturation level, however, can be expected to result in different packing characteristics that would result in different structural properties of membranes. While all exogenously added PS species effectively transported to the PM (validated via measuring labeling density of the PS probe GFP-LactC2) (Zhou et al., 2017), only the PS species with unsaturated acyl chains effectively recovered the PM localization of GFP-KRAS4BG12V, while the fully saturated di18:0 PS (DSPS) did not (Zhou et al., 2017; Zhou et al., 2021). Intriguingly, only the mixed-chain PS species, 16:0/18:1 PS (POPS) and 18:0/18:1 PS (SOPS), effectively recovered the nanoclustering of GFP-KRAS4BG12V (Zhou et al., 2017; Zhou et al., 2021); the symmetric PS species, including DSPS, di18:1 PS (DOPS), di18:2 PS (DLPS), had no effect on the nanoclustering of GFP-KRAS4BG12V (Zhou et al., 2017; Zhou et al., 2021). Effects of different PS species with distinct acyl chain structures on the spatiotemporal organization of KRAS are summarized in **Table 1**. These data suggested that KRAS4B has the ability to recognize PS acyl chains and thus the structure of the bilayer core. Recruitment of effectors by KRAS4B was also found to be dependent on PS acyl chain structure. This has been shown by EM-bivariate co-clustering analysis of intact PM sheets as well as by FLIM-FRET analysis in intact cells, demonstrating that recruitment of RFP-CRAF by GFP-KRAS4BG12V was abolished by PS depletion and was selectively recovered by acute addback of only POPS, but not the other PS species that have been tested (Zhou et al., 2017). EM-bivariate co-clustering analysis further showed that only acute addback of the mixed-chain PS species (POPS and SOPS) induced co-clustering of GFP-LactC2 (a PS-specific binding domain) and RFP-KRAS4BG12V (Zhou et al., 2017). In sum, it is clear that KRAS nanoclusters are selectively enriched with mixed-chain PS species, and that KRAS4B possesses an exquisite capability to selectively target PS headgroups and sort PS species based on their acyl chain structure.

Nanoclusters Mediate Distinct Responses of RAS Isoforms to Perturbations of Plasma Membrane Biophysical Properties

The PM is not a homogeneous medium whose contents respond to perturbations in a similar manner. Rather, it is a highly heterogeneous and compartmentalized organelle (Simons and Ikonen, 1997; Simons and Toomre, 2000; Veatch and Keller, 2002; Baumgart et al., 2003; Veatch and Keller, 2003; Simons and Vaz, 2004; Veatch et al., 2007; Simons and Gerl, 2010) containing diverse nanometer-sized domains of different biophysical properties that respond to perturbations in distinct manners. Similarly, variations in the composition of nanoclusters of different Ras proteins suggest that RAS isoforms may responded to changing PM properties in distinct manners (summarized in **Table 2**). An important component of the PM is cholesterol, which plays key roles in the heterogeneity of the PM. In particular, cholesterol preferentially associates with saturated lipids and facilitates lipid phase separation into co-

existing cholesterol-enriched L_o and cholesterol-poor L_d domains (Simons and Ikonen, 1997; Simons and Toomre, 2000; Veatch and Keller, 2002; Baumgart et al., 2003; Veatch and Keller, 2003; Simons and Vaz, 2004; Veatch et al., 2007; Simons and Gerl, 2010). EM-spatial analysis revealed that acute cholesterol depletion by MβCD treatment significantly disrupted the nanoclustering of GFP-tagged inactive HRAS (GDP-bound) or the minimal membrane-anchoring of HRAS (tH) (Prior et al., 2003). On the other hand, cholesterol depletion by MβCD treatment had no effect on the nanoclustering of active GTP-bound HRAS, GTP- or GDP-bound KRAS4B, or the minimal membrane-anchoring domain of KRAS4B (tK) (Prior et al., 2003; Zhou et al., 2021). Thus, nanoclusters of inactive GFP-HRAS.GDP and active GFP-NRAS.GTP are cholesterol-dependent while nanoclusters of active GFP-HRAS.GTP, GFP-KRAS4B (both active GTP-bound and inactive GDP-bound) and GFP-NRAS.GDP are independent of cholesterol. This is consistent with results from atomic force microscopy (AFM) experiments, where KRAS4B was located in the cholesterol-poor L_d domains of supported bilayers while the palmitoylated NRAS anchor was located along the domain boundaries between the L_o and L_d domains (Weise et al., 2009; Weise et al., 2011). While domain preferences of tH have not been tested experimentally on supported bilayers, MD simulations predicted that it localized at L_o/L_d domain boundaries (Janosi et al., 2012; Li et al., 2012; Li and Gorfe, 2013). Cholesterol stabilizes domain boundaries and therefore tH nanoclusters. Thus, the spatial distribution of RAS proteins responds to cholesterol depletion in an isoform-specific manner.

Another important membrane property is curvature, which defines cell morphology and plays key roles in cell migration and intracellular trafficking (Baumgart et al., 2011; Bigay and Antonny, 2012; McMahon and Boucrot, 2015). Most membrane proteins that are known to sense or modulate membrane curvature, such as ion channels, receptors and Bin/Amphiphysin/Rvs (BAR) proteins, have a significant portion of their surface exposed to lipids. In contrast, a much smaller surface of monomeric RAS is directly exposed to lipids (**Figure 1A**), suggesting that membrane curvature sensing or modulation by Ras may involve cluster formation. Indeed, MD simulations of tH and full-length HRAS have shown a direct link between cluster formation, domain-segregation, and stabilization of membrane curvature (Janosi et al., 2012; Li et al., 2012; Prakash et al., 2012; Li and Gorfe, 2013; Li and Gorfe, 2013; Li and Gorfe, 2014; Li and Gorfe, 2014; Lin et al., 2015). Conversely, EM analysis has revealed that elevating PM curvature disrupted the nanoclustering and PM localization of GFP-KRAS4B but enhanced those of GFP-HRAS (consistent for both the full-length constitutively active mutants and the truncated membrane anchors) (Liang et al., 2019). This observation was made under multiple experimental conditions: 1) in intact PM sheets with curvature manipulated by the expression of different curvature-molding BAR domains; 2) in live cells grown over nanobars that induced quantifiable curvatures of the basolateral PM; 3) in isolated PM blebs with curvatures induced by exposure to hypo- and hypertonic buffers; and 4) in two-component synthetic liposomes of different sizes and curvatures (Liang and et al., 2019). In particular, depletion of endogenous PS in PSA3 cells grown in DFBS effectively abolished the ability of GFP-KRAS4B to respond to changing PM curvature (Liang and et al., 2019), suggesting that PS may mediate PM curvature sensing by KRAS4B. In the PS-depleted PSA3 cells, acute addback of only the mixed-chain POPS, but not the fully saturated DSPS and the mono-unsaturated DOPS, effectively restored the ability of GFP-KRAS4B to respond to changing PM curvature (Liang and et al., 2019). This was further supported by surface plasmon resonance (SPR) measurements using two-component synthetic liposomes, where binding of the purified full length KRAS4B to synthetic liposomes composed of the mixed-chain POPC/POPS (80/20) was enhanced as the vesicles became larger and less curved (Liang et al., 2019). On the other hand, KRAS4B binding was found to be independent of the size of vesicles composed of the mono-unsaturated DOPC/DOPS (80/20) lipids (Liang et al., 2019). A series of mouse embryonic fibroblast (MEF) mutant lines has been used to examine how RAS-dependent signaling responded to changing PM curvature. In these cell lines, all endogenous RAS isoforms have been knocked out and a specific KRAS mutant is expressed to generate RAS-less MEF lines (Drosten et al., 2010). Incubating RAS-less MEF expressing KRAS4BG12V in hypotonic buffers, which flattened the PM, significantly enhanced the KRAS4B-dependent MAPK signaling (Liang et al., 2019). On the other hand, in a RAS-less MEF line expressing a constitutively active RAS effector BRAFV600E mutant (with no RAS present), flattening of the PM via hypotonic buffers no longer affected MAPK signaling (Liang and et al., 2019). Taken together, the spatial distribution of RAS proteins responds to changing membrane curvature in an isoform-specific manner, with curvature sensing of KRAS4B being PS species-dependent.

Another important membrane property is electrostatics, more specifically transmembrane potential. It has long been known that transmembrane potential is associated with important intracellular signaling processes involved in cell growth and proliferation, and is correlated with cancer (Blackiston et al., 2009; Sundelacruz et al., 2009). Depolarization of the PM, as well as expression of depolarizing potassium channels, has been linked to elevated growth and proliferation and diminished apoptosis (Blackiston et al., 2009; Sundelacruz et al., 2009). However, the mechanism(s) behind this phenomenon has been poorly understood. A recent study using EM, FLIM-FRET, and FRAP showed that depolarizing the PM by increasing the extracellular potassium concentration or glutamate stimulation enhanced the nanoclustering of GFP-KRAS4BG12V and GFP-tK on the PM of non-polarized and polarized mammalian cells, as well as intact tissues of *Drosophila* brain (Zhou et al., 2015). PM depolarization also promoted nanoclustering PS and PIP_2 but not PA and PIP_3 lipids (Zhou et al., 2015). Nanoclustering and signaling of GFP-KRAS4BG12V did not respond to changing transmembrane potential in the PS-depleted PSA3 cells, but sensitivity was restored by Etn supplementation to increase endogenous PS levels (Zhou et al., 2015). In wild-type *Drosophila* embryos, depolarizing the PM similarly elevated signal output of the KRAS4B-dependent MAPK cascade whereas MAPK signaling was insensitive to PM depolarization in *Drosophila* embryos

expressing an inactive mutant of a PS flippase, ATP8B (Zhou et al., 2015). Since ATP8B actively maintains an asymmetric distribution of PS in the PM inner leaflet (Paulusma et al., 2008; Ha et al., 2014), deactivation of ATP8B effectively depletes PS in the inner leaflet. Taken together, these studies demonstrated that PS mediates the spatial redistribution and altered signaling of KRAS4B in response to changes in the PM membrane potential.

Mechanisms of Selective Lipid Sorting by RAS Proteins

RAS and other small GTPases use one or a few fatty acid chains with or without a PBD to target membranes. It is therefore intriguing that they would selectively sort lipid headgroup features and acyl chain structures, as do RAS proteins. It is becoming increasingly clear that this capability allows RAS proteins to respond to modulations of membrane biophysical properties in isoform- and guanine nucleotide-dependent manners. To systematically explore the molecular mechanisms underlying lipid sorting by RAS proteins, a series of studies have been conducted using EM-univariate and -bivariate analyses, FLIM-FRET, and MD simulations. Among the key observations of these studies was that the cholesterol dependence of the GDP-bound HRAS clustering is largely dictated by its palmitoyl chains at Cys181 and Cys184 (Roy et al., 2005). The nanoclustering of the constitutively active GFP-HRASG12V (with dual palmitoylation) did not respond to MβCD-induced cholesterol depletion (Roy et al., 2005), suggesting that GFP-HRASG12V does not co-localize with cholesterol. By contrast, MβCD-induced cholesterol depletion disrupted the nanoclustering of GFP-HRASG12V.C184S (HRAS mono-palmitoylated at Cys181) but not GFP-HRASG12V.C181S (mono-palmitoylated at Cys184) (Roy et al., 2005). This data suggests that the palmitoyl chain attached to Cys181 is key to driving the association of HRASG12V with cholesterol. This is, indeed, consistent with the finding that MβCD-induced cholesterol depletion effectively disrupted the nanoclustering GFP-NRASG12V, which is mono-palmitoylated on Cys181 (Prior et al., 2003), and predictions from free energy calculations that the second plamitoylation of HRAS was not required for high-affinity membrane binding but instead may modulate lateral dynamics (Gorfe and McCammon, 2008).

Although the C-terminal membrane-anchoring domain of HRAS plays important roles in membrane interactions, the catalytic G-domain may also contribute in some way. In earlier studies using MD simulations, it was found that the HRAS G-domain dynamically engaged the membrane in a nucleotide dependent manner (Abankwa et al., 2007; Abankwa et al., 2008; Abankwa et al., 2010). When GDP bound, the HRAS G-domain stayed away from the membrane while the HVR interacted with lipids and the palmitoyl chains fully inserted into the bilayer core. When GTP bound, the G-domain swinged up by almost 100 degrees to directly interacted with membrane lipids (Abankwa et al., 2007). As a result, a number of charged residues in switch I and II regions, including β2-β3 loop, helices α4 and α5, now extensively interacted with polar headgroups of lipids in the bilayer. This upward swing of the G-domain of HRAS caused its membrane-anchoring domain to move away from the membrane, which pulled the palmitoyl chains partially out of the bilayer (Abankwa et al., 2007). The resulting disorder in the palmitoyl chains was proposed to promote favorable interactions with the more disordered and thinner cholesterol-poor lipid domains (Gorfe et al., 2007a; Gorfe et al., 2007b; Abankwa et al., 2008; Abankwa et al., 2010). This was consistent with EM data showing that the nanoclustering of the constitutively active and GTP-bound GFP-HRASG12V was insensitive to cholesterol depletion by MβCD (Prior et al., 2003).

Inspired by a previous MD study that suggested the non-equivalency of the lysine residues of the PBD of the minimal membrane-anchoring domain (tK) of KRAS4B (Janosi and Gorfe, 2010), recent studies have focused on the nanoclustering of a cohort of PBD mutants in which each of the positively charged lysine residues was individually mutated to the neutral glutamine: GFP-KRAS4BG12V.K175Q, KRAS4BG12V.K176Q, KRAS4BG12V.K177Q, KRAS4BG12V.K178Q, KRAS4BG12V.K179Q, KRAS4BG12V.K180Q. Each of these mutants contains five lysine, and thus the six mutants have an identical total charge. It was found that KRASG12V.K177Q and KRASG12V.K178Q were remarkably weak in terms of both nanoclustering and PM binding compared with the other PBD mutants (Zhou et al., 2017). Further EM-bivariate co-clustering analysis revealed that these equally charged PBD mutants sorted distinct sets of lipids. In particular, nanoclusters of KRAS4BG12V.K177Q and KRAS4BG12V.K178Q were depleted of PS but enriched with PIP_2, while the other PBD mutants still maintained extensive PS content in their nanoclusters. On the other hand, nanoclusters of KRAS4BG12V.K175Q and KRAS4BG12V.K179Q contained higher levels of PIP_3. Nanoclusters of KRAS4BG12V.K178Q also contained significantly higher levels of PA. Another interesting PBD mutant involves the phosphorylation of Serine 181 via activation of protein kinase G (PKG) or the phosphomimetic mutant S181D of KRAS4B. EM-bivariate lipid mapping revealed that nanoclusters of the phosphorylated and S181D KRAS4B were depleted of PS but enriched with PIP_2 and PIP_3 (Zhou et al., 2017).

Further evidence for the notion of not-just-electrostatics came from the comparison of four additional KRAS PBD constructs (**Figure 3**): GFP-KRAS4BG12V (with the original hexa-lysine PBD), GFP-KRAS4BG12V.6R (the six contiguous lysines replaced with arginines), GFP-KRAS4BG12V.C20 (the 15-carbon farnesyl chain mutated to the 20-carbon geranylgeranyl chain), GFP-KRAS4BG12V.6R-C20 (a geranylgeranylated hexa-arginine PBD). These four constructs contain an equivalent number of charged residues. However, while the nanoclusters of the reference KRAS4BG12V were enriched with PS as expected, those of KRAS4BG12V.6R and KRAS4BG12V.C20 became more enriched with cholesterol and depleted of PA while KRAS4BG12V.6R-C20 remained similar to the reference (Zhou et al., 2021) (data summarized in a heat map shown in **Figure 4A**). In addition to lipid headgroups, these equivalently charged KRAS4B PBD mutants also sort distinct lipid acyl chains. In acute lipid addback assays using PSA3 cells, it was found that

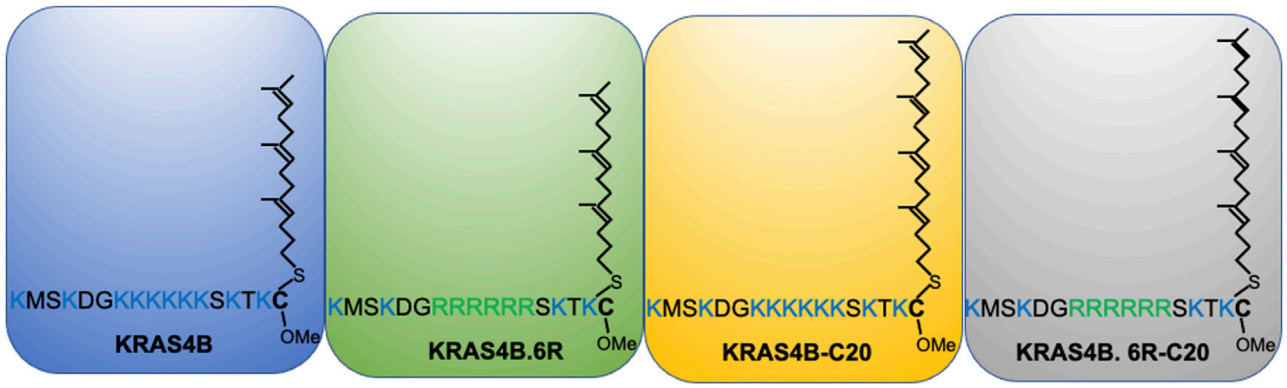

FIGURE 3 | KRAS4B PBD mutants that share an identical number of positively charged residues and thought to electrostatically interact with the plasma membrane in an equivalent manner.

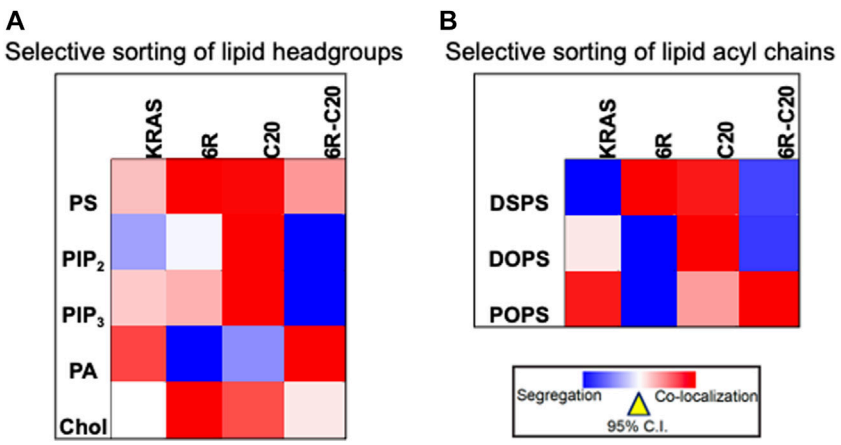

FIGURE 4 | Equivalently charged KRAS4B PBD constructs selectively sort distinct lipid headgroups and acyl chains. **(A)** A heat map of LBI values indicates distinct co-clustering between the GFP-tagged specific lipid-binding domains and the RFP-tagged KRAS4B PBD constructs. **(B)** A heat map of LBI values indicates co-clustering between the PS-specific domain, GFP-LactC2 and the RFP-tagged KRAS4B PBD constructs in PS-depleted PSA3 cells following acute addback of distinct synthetic PS species.

the reference GFP-KRAS4BG12V co-localized extensively with the mixed-chain POPS but not the symmetric DSPS and DOPS (Zhou et al., 2021) (data summarized in a heat map shown in **Figure 4B**). On the other hand, GFP-KRAS4BG12V.6R co-localized with only the fully saturated DSPS while GFP-KRAS4BG12V.C20 co-localized with the symmetric DSPS and DOPS (Zhou et al., 2021) (**Figure 4B**). GFP-KRAS4BG12V.6R-C20 associated more preferentially with POPS (Zhou et al., 2021) (**Figure 4B**), again similar with KRAS4B with the original PBD. As a result, these KRAS4B with equivalently charged PBDs responded to changing PM properties in distinct manners. As summarized in **Table 3**, EM-nanoclustering analysis showed that, while GFP-KRAS4BG12V with the original PBD was independent of cholesterol, nanoclusters of GFP-tagged KRAS4BG12V.6R, KRAS4BG12V.C20 and KRAS4BG12V.6R-C20 were disrupted upon acute cholesterol depletion. The nanoclustering of GFP-KRAS4BG12V.6R also lost its sensitivity to PM depolarization (**Table 3**). Also interestingly, the nanoclustering of GFP-KRAS4BG12V.6R and GFP-KRAS4BG12V.C20 was enhanced by elevating PM curvature, opposite of the curvature preferences of the equivalently charged counterparts GFP-KRAS4BG12V and GFP-KRAS4BG12V.6R-C20 (**Table 3**). A mechanistic insight into how this might work at the atomic level emerged from atomistic MD simulations that predicted that the PBDs, including the original farnesylated hexa-lysine tK and mutants such as tK-K177Q and tK-K178Q sampled a large conformational space but differed in the proportion of ordered (O), intermediate (I) and disordered (D) backbone conformations (Zhou et al., 2017; Zhou et al., 2021). Approximately 64% of the simulated tK anchor was in the D state, 35% in the I (29%) and about 6% in the O state (Zhou et al., 2017; Zhou et al., 2021). These conformations differed in their capacity to form salt bridges involving the lysine side chains with the PS headgroups, with D state being the most amenable (Zhou et al., 2017; Zhou et al., 2021). Mutations that enriched the D state would therefore interact

TABLE 3 | Nanoclusters of KRAS4B PBD constructs with identical numbers of charged residues respond to membrane perturbations in distinct manners.

Membrane perturbations	KRAS4B	KRAS4B.6R	KRAS4B-C20	KRAS4B.6R-C20
Cholesterol depletion[a,e]	Unaffected	Disrupted	Disrupted	Disrupted
Depolarization[c,e]	Enhanced	Unaffected	Enhanced	Enhanced
Curvature[d,e]				
Positive curvature	Disrupted	Enhanced	Enhanced	Disrupted
Negative curvature	Unaffected	Not tested	Not tested	Not tested
Actin[b,d]	Enhanced	Not tested	Not tested	Not tested
Caveolae[f]	Disrupted	Not tested	Not tested	Not tested

[a]*Prior et al., 2003* ***J Cell Biol.***
[b]*Plowman et al., 2005* ***Proc Natl Acad Sci U S A.***
[c]*Zhou et al., 2015* ***Science.***
[d]*Liang et al., 2019* ***Life Sci Alliance.***
[e]*Zhou et al., 2021* ***Proc Natl Acad Sci U S A.***
[f]*Ariotti et al., 2014* ***J Cell Biol.***

more favorably with PS lipids while those favoring the O state interacted less strongly. Consistent with this hypothesis and the experimental data described above, the less PS col-localizing tK-K177Q and tK-K178Q favored the O state (42 and 25% compared to 6% for tK) (Zhou et al., 2017). The geranylgeranylated tK, tK-C20, as well as the tK backbone phosphorylated at Serine 181, predominantly adopted the D states (Zhou et al., 2021). Taken together, the specific amino acid sequence and the prenyl anchor of KRAS4B together regulate the conformational plasticity of the prenylated PBD of KRAS4B and thereby determine its ability to selectively sort lipids.

In addition to the PBD, the G-domain of KRAS4B may also contribute to lipid sorting. This is because the G-domain has been shown to dynamically interact with membrane lipids in at least two dominant orientational states (OS): OS1 and OS2. Helices α3 or α5 and α4 contacted the bilayer in OS1, whereas β1, β2 and β3 and helix α2 directly contacted the bilayer in OS2 (Mazhab-Jafari et al., 2015; Prakash et al., 2016; Sarkar-Banerjee et al., 2017; Li et al., 2018; Prakash et al., 2019; Prakash and Gorfe, 2019; Neale and García, 2020). As a result, each OS presented distinct polar residues to interact with charged lipid headgroups in membranes. For example, Arg97, Lys101 and Arg135 in OS1 and Arg73 and Arg102 in OS2 might interact with PS headgroups in the bilayer, respectively (Prakash et al., 2016). Additionally, the orientational states of the G-domain also impact the dynamics of the backbone of the polybasic region within the C-terminal membrane anchoring domain since the Lys175-180 segment was more extended in OS2 than OS1 (Prakash et al., 2016; Prakash and Gorfe, 2019). Moreover, the dynamic oscillation between OS1 and OS2 may contribute to lipid sorting of KRAS4B in ways that are yet to be elucidated. Along this line, EM analysis showed that mutating Arg73 to the oppositely charged Glu disrupted the nanoclustering of GFP-KRAS4BG12V.R73E on intact PM sheets (Prakash et al., 2016). Taken together, the orientational dynamics of the G-domain may complement the intrinsically disordered lipid anchor in the selective sorting of lipids by KRAS4B.

RAS Dimerization Interfaces and Their Role in the Formation of High Order Oligomers

The PM provides a structural framework for both the signaling function and homodimerization of RAS proteins, and a growing body of evidence supports the notion that KRAS4B forms dimers and larger oligomers (or nanoclusters) in cells and synthetic membranes (Abankwa et al., 2007; Tian et al., 2007; Nan et al., 2015; Zhou and Hancock, 2015; Ambrogio et al., 2018). However, there are conflicting reports on whether oligomerization involves direct protein-protein interaction or is primarily mediated by lipids. Moreover, there are multiple predicted RAS dimerization interfaces [e.g., (Güldenhaupt et al., 2012; Muratcioglu et al., 2015; Sayyed-Ahmad et al., 2016)], which have been discussed in detail in several recent review articles included in refs (Abankwa and Gorfe, 2021; Van et al., 2021). There is debate regarding which of these interfaces is most relevant for function. We believe RAS utilizes various combinations of multiple interfaces to form oligomers of diverse sizes, topologies and internal structures. Such G-domain-mediated dimerization/oligomerization and lipid-mediated spatial segregation synergistically promote nanoclustering of RAS, which allows the formation of signaling platforms suitable for function in specific situations and pathways. With this in mind, here we will focus on two dimer models and how they might give rise to diverse high order oligomers.

Two partially overlapping protein-protein interaction interfaces (PPIs, termed i1 and i2) have been identified on the catalytic domain of KRAS4B by combining sequence analysis, protein-protein docking, and molecular simulations (Prakash et al., 2017). Potential of mean force (PMF) calculations suggested that both interfaces i1 and i2 were marginally stable in solution (calculated $K_d \approx 5$ and 100 mM) (Prakash and et al., 2017). This was consistent with a previous report on the absence of KRAS4B dimers in solution (Werkmüller et al., 2013). However, MD simulations of the i1 and i2 dimer models attached to a POPC/POPS bilayer led to improved interactions, especially at interface i1, and stabilization of the dimers (Prakash et al., 2017). Using BHK cells ectopically expressing selected i1 mutants followed by biochemical assays and EM analysis, it was found that neither charge-reversal mutations of interfacial ion pairs (K101E and E107K) nor a charge-swapping double mutant (K101E/E107K) affected membrane targeting (Prakash et al., 2017). However, the charge-reversal, but not the charge swapping, mutation significantly reduced clustering relative to the wild type

(Prakash et al., 2017). Introducing cysteines at the same positions (K101C/E107C) dramatically enhanced both membrane retention and clustering (Prakash et al., 2017), likely due to the formation of an intermolecular disulfide bond. Indeed, a corresponding QQ mutant that was unable to form a disulfide cross-link had no effect on membrane binding or clustering (Prakash et al., 2017). Moreover, by comparing dimer/monomer and oligomer/monomer ratios, it was found that the single-point charge reversal mutations reduced the dimer and higher oligomer fractions while the K101C/E107C mutation dramatically increased those fractions (Prakash et al., 2017). Further, immunoblotting the membrane fraction of wild type and K101C/E107C KRAS4B under a non-reducing condition indicated dimer and oligomer bands for both, with the latter being substantially more prominent (Prakash and., 2017). No oligomer bands were found in the cytosolic fraction (Prakash et al., 2017). A recent paramagnetic relaxation enhancement NMR spectroscopy revealed that GTP-bound active and GDP-bound inactive KRAS4B formed homodimers via an interface involving helices α4 and α5 (Lee et al., 2020). Specifically, electrostatic interactions between residue pairs of R135-E168, Q131-D154 and Q131-R161 contributed to the homodimerization of GTP-bound KRAS4B on bilayers, whereas dimers of GDP-bound KRAS4B was stabilized by E49-K172 and E162-K165 residue pairs. The α4/α5 interface of KRAS4B dimers has also been observed in size exclusion chromatography and small angle X-Ray Scattering (Packer et al., 2021). The presence of the RAS-binding domain of RAF further stabilized dimerization of KRAS4B on membrane. Combining FRET/electron paramagnetic resonance spectroscopy and MD simulations, a recent study also characterized helices α4 and α5 as an important dimer interface in NRAS (Rudack et al., 2021). Specifically, the most prevalent residue contact between the GDP-bound NRAS monomers was a salt bridge between D154 and R161 located on α5 (Rudack et al., 2021). Another prominent contact between the two NRAS monomers was between H131 of α4 helix and E49 of the β2-β3 loop (Rudack et al., 2021). These findings underscore the important role of helices α4 and α5 in stabilizing homodimers of RAS anchored to membranes. Taken together, these observations suggest that KRAS4B forms dimers and oligomers of diverse size and shape via interfaces i1 and i2 (Prakash and et al., 2017).

The above conclusion is further supported by a study that quantified the distribution of KRAS4B oligomers on the PM using a combination of single molecule experiments and molecular modeling (Sarkar-Banerjee et al., 2017). The study included fluorescence correlation spectroscopy (FCS) and FRAP in cells transiently expressing low levels of mGFP-tagged WT, K101E and K101C/E107C KRAS4B mutants (Sarkar-Banerjee et al., 2017). The FRAP analysis suggested K101E had a larger mobile fraction and a smaller percentage of cells with two distinct diffusivities. FCS showed that 50% (K101E), 58% (WT) and 89% (K101C/E107C) of the cells that had been analyzed yielded fluorescence autocorrelation profiles that were distinct from the monomeric controls POPS and GFP controls (Sarkar-Banerjee et al., 2017). The FCS data for the KRAS4B samples required a 3-component diffusion model for fitting, whereas all of the data for the controls could be fit to a bi-component diffusion model (Sarkar-Banerjee et al., 2017). The majority of cells expressing K101C/E107C gave rise to atypical fluorescence autocorrelation profiles compared with only about half of those expressing K101E (Sarkar-Banerjee et al., 2017). This suggested that the two mutants differ in their ability to form slowly diffusing species, which is consistent with the FRAP data. Further analysis with Raster image correlation spectroscopy (RICS) showed that K101E diffused at a rate similar to POPS while WT and especially K101C/E107C were significantly slower (Sarkar-Banerjee et al., 2017). Number and brightness (N&B) analysis of the RICS images further showed GFP-KRAS4BG12V existed as a combinations of monomers, dimers and larger oligomers (Sarkar-Banerjee et al., 2017). The monomer fraction of GFP-KRAS4BG12V was found to be 38%, which was comparable to the monomer fraction estimated by EM-nanoclustering analysis (~40%) (Plowman et al., 2005). In this analysis, GFP-KRAS4BG12V was found to exist mostly as a dimer (51%), with a minor percentage of trimer (10%). K101E was predominantly monomeric (73%) with a smaller (23%) fraction of dimers , whereas K101C/E107C was enriched in dimer (58%) and trimer (38%) but was depleted of monomers (Sarkar-Banerjee et al., 2017). Similar results were obtained when ion pairs E98-K165 and D105-K172 were predicted to stabilize larger oligomers including pentamers. For example, double charge-reversion (E98K/D105K) reduced clustering by about 40% without affecting membrane retention, whereas swapping charges had no effect (Sarkar-Banerjee et al., 2017). It has been proposed that KRAS4B self-assembly into oligomers of diverse sizes and shapes involved the use of varying pairwise interactions of i1 and i2 (Sarkar-Banerjee et al., 2017). The resulting structural models explained a number of previous observations (Plowman et al., 2005; Hancock, 2006; Kholodenko et al., 2010), including the average number of proteins per cluster and the average radius of RAS nanoclusters estimated by EM after accounting for the sizes of GFP, antibody, gold nanoparticle and nanocluster geometry (Plowman et al., 2005; Hancock, 2006; Zhou and Hancock, 2015).

Targeting RAS Nanoclusters for Treating RAS Pathology

As RAS nanoclusters are the main sites for the recruitment and activation of effectors, agents that perturb the RAS nanodomain structure or dynamics should have a therapeutic value against oncogenic RAS. Because PS is a major structural component of KRAS4B nanoclusters, perturbing the PS content of the nanoclusters is a particularly appealing therapeutic avenue. PS is actively transported intracellularly between the endoplasmic reticulum (ER), recycling endosomes, and the PM (Chandra et al., 2012; Schmick et al., 2014; Schmick et al., 2015). Perturbing PS transport can deplete the PS content of the PM and consequentially attenuate the oncogenic activities of mutant KRAS4B. Indeed, treatment of cells by fendiline, an acid sphingomyelinase (ASM) inhibitor (Gulbins et al., 2013), effectively depleted PS in the PM inner leaflet and thereby

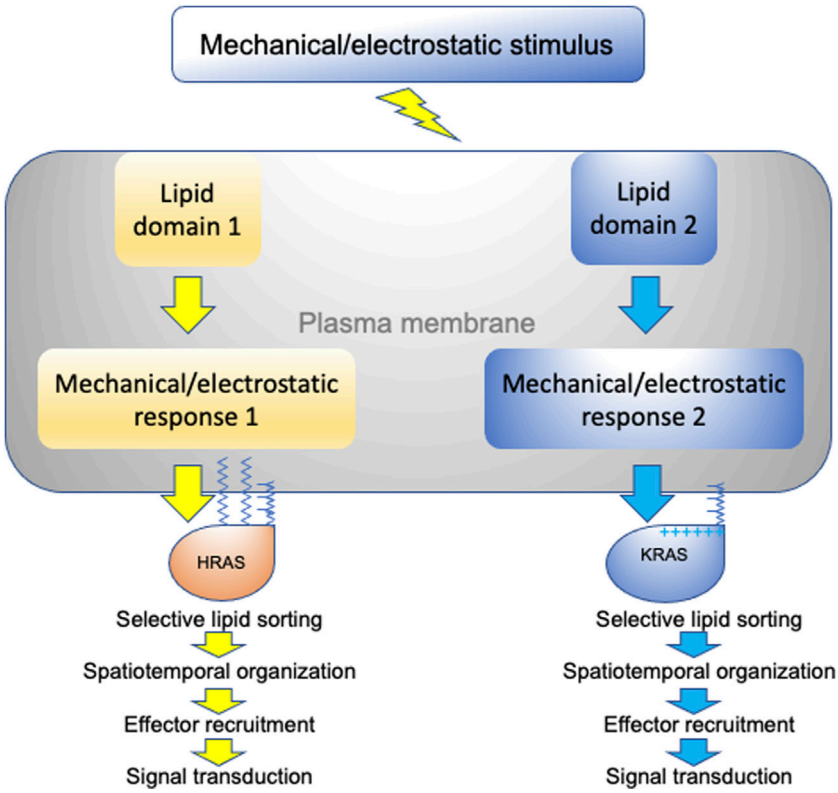

FIGURE 5 | A schematic description of RAS nanoclusters acting as transition hubs to couple extracellular stimuli with intracellular signaling networks. In a highly heterogeneous plasma membrane, different proteolipid nanodomains possess distinct biophysical properties and respond to membrane perturbations in distinct manners. Diverse changes in lipid packing and lateral diffusion of plasma membrane domains alter the spatiotemporal organization of RAS isoforms, which in turn perturb effector recruitment and signal intracellular transmission.

mislocalized oncogenic mutant KRAS4B from the PM and disrupted its nanoclustering and signaling (van der Hoeven et al., 2013; Cho et al., 2015; van der Hoeven & et al., 2017). ASM converts sphingomyelin (SM) to ceramide (Cer) (Santana et al., 1996). The SM/Cer equilibrium contributes to the vesicular trafficking between the PM and the recycling endosomes that are highly enriched with PS (Chatterjee et al., 2001). The fendiline-disrupted spatiotemporal organization and signaling of oncogenic mutant KRAS4B were selectively restored by the acute addback of natural extracts of PS, but not the natural extracts of other lipids tested including PIP_2, PC or phosphatidylethanolamine (PE) (Cho et al., 2015). Effects of fendiline on the MAPK-regulated cell proliferation were more pronounced on the oncogenic mutant KRAS4B-transformed tumor cells, but not tumor cells that were independent of oncogenic KRAS4B activities (Cho et al., 2015; van der Hoeven et al., 2013; van der Hoeven & et al., 2017). Fendiline treatment also effectively reduced the sizes of tumors in xenografts composed of tumor cells transformed by mutant KRAS4B, but not those independent of mutant KRAS4B (van der Hoeven & et al., 2017). Taken together, by disrupting PS trafficking from recycling endosomes to the PM, fendiline effectively depletes the PS content in the PM and compromises the spatiotemporal organization, signaling and oncogenic activities of mutant KRAS4B.

Proper intracellular transport of PS can also be blocked or attenuated by staurosporine, an alkaloid isolated from bacterium *Streptomyces* staurosporeus, and analogs. These small molecules include 7-oxostaurosporine (OSS), UCN-01 and UCN-02. Treatment of cells by staurosporines effectively mislocalized PS from the PM to endosomes (Cho et al., 2012). As a result, these staurosporine analogs effectively mislocalized mutant KRAS4B from the PM and disrupted the nanoclustering of KRAS4B left on the PM, which in turn inhibited the mutant KRAS4B-dependent MAPK signaling (Cho et al., 2012). Additional strategies for interfering with the PS transport involve perturbing the exchange of PS between the PM and the endoplasmic reticulum (ER), via altering the expression of oxysterol-related binding proteins, ORP5 and ORP8. ORP5 and ORP8 regulate the exchange of phosphoinositol 4-monophosphate (PI_4P) in the PM and PS in the ER (Moser von Filseck et al., 2015; Moser von Filseck and et al., 2015; Sohn et al., 2016). Concordantly, treatment by a selective inhibitor of PI4-kinase IIIα (PI4KIIIα) that converts phosphoinositol (PI) to PI_4P (Waring et al., 2014; Boura and Nencka, 2015; Raubo et al., 2015), called compound 7, depleted the PS levels in the PM by reducing the PI_4P/PS exchange (Kattan et al., 2019). Indeed, Compound 7 effectively mislocalized oncogenic mutant KRAS4B from the PM and disrupted the nanoclustering of mutant KRAS4B (Kattan and et al., 2019).

Compound 7 also selectively compromised the proliferation of human tumor cell lines transformed by mutant KRAS4B, but not those independent of KRAS4B (Kattan and et al., 2019). Taken together, pharmacologically targeting the PS transport between endomembranes and the PM effectively and selectively perturbs the oncogenic activities of mutant KRAS4B.

As described above, phosphorylation of Ser181 mislocalizes KRAS4B from the PM and decreasing its clustering on the PM (Bivona et al., 2006; Cho et al., 2016). This is correlated with the switch of lipid sorting preference from PS to the relatively less abundant anionic phospholipid PIP_2 (Zhou et al., 2017). Protein kinase C (PKC) and protein kinase G (PKG) directly phosphorylate KRAS4B at Ser181, resulting in changes in the spatiotemporal organization of oncogenic mutant KRAS4B and inhibition of mutant KRAS4B-dependent MAPK signaling (Bivona et al., 2006; Cho et al., 2016). Several groups of compounds have been shown to promote the phosphorylation of Ser181 of KRAS4B and perturb oncogenic KRAS4B activities. Specifically, the PKC activator, bryostatin-1, mislocalized oncogenic mutant KRAS4B from the PM and induced apoptosis (Bivona et al., 2006). Additionally, a number of small molecules have been shown to activate the AMP-activated protein kinase (AMPK) → eNOS → soluble guanylyl cyclase (sGC) → cyclic GMP (cGMP) → PKG cascade and promote the phosphorylation of Serine 181 of KRAS4B (Cho et al., 2016). These PKG-activating molecules include AMPK activators oligomycin A, neoantimycin, antidiabetic drug metformin and aminoimidazole-4-carboxamide riboside (AICAR) (Cho et al., 2016). Nitric oxide donor, diethylamine nitric oxide (DEA-NO), promotes the generation of sGC in the production of cGMP, the main substrate of PKG. Sildenafil inhibits PDE5 hydrolyze cGMP and lead to the further accumulation of cGMP (Cho et al., 2016). These PKG activators attenuated the PM localization and nanoclustering of oncogenic mutant KRAS4B on the PM, and inhibited the mutant KRAS4B-dependent MAPK signaling (Cho et al., 2016). Thus, altering the selective lipid sorting of KRAS4B by inducing phosphorylation of Serine 181 effectively attenuates the oncogenic activities of mutant KRAS4B.

Monobodies and ankyrin repeat proteins (DARPins) have also been utilized to directly target KRAS4B dimers. Specifically, integration of NMR spectroscopy, X-ray diffraction of crystal structures, fluorescence imaging of intact cells, EM-spatial analysis, as well as signaling and functional assays have revealed that a monobody called NS1 bound to the α4, β5 and α5 interface of HRAS and KRAS and disrupted their dimerization and nanoclustering. As a result, NS1 perturbed effector binding, inhibited MAPK signaling and cell proliferation regulated by oncogenic mutants of HRAS and KRAS (Spencer-Smith et al., 2017). Similarly, several DARPins have been shown to bind the i1 dimer interface involving helices α3, α4 and loop 7 or the switch 1 region and inhibited KRAS signaling and RAS-dependent proliferation (Guillard et al., 2017; Bery et al., 2019). Taken together, existing data suggest that directly targeting dimer interfaces of RAS is also an effective strategy for compromising the oncogenic activities of RAS.

CONCLUSION

We have discussed how different RAS isoforms undergo spatial segregation on the plasma membrane for efficient signal transduction and function. More specifically, we have focused on the intricate capabilities of RAS proteins to selectively sort lipids in a headgroup- and acyl chain structure-dependent manner. This specific lipid sorting capability not only allows RAS proteins to recruit effectors in an isoform-specific manner, but also allows RAS nanoclusters to sense and respond to various membrane perturbations in distinct manners (summarized in **Figure 5**). This is because plasma membrane domains that vary in lipid and protein content as well as mechanical and electrostatic properties respond to membrane perturbations in distinct manners. We therefore propose that RAS/lipid nanoclusters act as important transition hubs on the cell surface, where extracellular mechanical and electrostatic stimuli are relayed to distinct intracellular signal output. These nanometer-sized transition hubs intricately connect extracellular stimuli with intracellular signaling networks and may contribute to mechanosensing and mechanotransduction.

AUTHOR CONTRIBUTIONS

YZ, AG and JH co-wrote and co-edited the manuscript.

FUNDING

This work was in part supported by grants from the NIH National Institute of General Medical Sciences R01GM138668 (YZ) and R01GM124233 (AG and JH).

REFERENCES

Abankwa, D., and Gorfe, A. A. (2021). Mechanisms of Ras Membrane Organization and Signaling: Ras Rocks Again. *Biomolecules* 10 (11).

Abankwa, D., Gorfe, A. A., and Hancock, J. F. (2007). Ras Nanoclusters: Molecular Structure and Assembly. *Semin. Cel. Dev. Biol.* 18 (5), 599–607. doi:10.1016/j.semcdb.2007.08.003

Abankwa, D., Gorfe, A. A., Inder, K., and Hancock, J. F. (2010). Ras Membrane Orientation and Nanodomain Localization Generate Isoform Diversity. *Proc. Natl. Acad. Sci.* 107 (3), 1130–1135. doi:10.1073/pnas.0903907107

Abankwa, D., Hanzal-Bayer, M., Ariotti, N., Plowman, S. J., Gorfe, A. A., Parton, R. G., et al. (2008). A Novel Switch Region Regulates H-Ras Membrane Orientation and Signal Output. *EMBO J.* 27 (5), 727–735. doi:10.1038/emboj.2008.10

Ahearn, I. M., Tsai, F. D., Court, H., Zhou, M., Jennings, B. C., Ahmed, M., et al. (2011). FKBP12 Binds to Acylated H-Ras and Promotes Depalmitoylation. *Mol. Cel.* 41 (2), 173–185. doi:10.1016/j.molcel.2011.01.001

Ambrogio, C., Köhler, J., Zhou, Z.-W., Wang, H., Paranal, R., Li, J., et al. (2018). KRAS Dimerization Impacts MEK Inhibitor Sensitivity and Oncogenic Activity of Mutant KRAS. *Cell* 172 (4), 857–868. doi:10.1016/j.cell.2017.12.020

Amendola, C. R., Mahaffey, J. P., Parker, S. J., Ahearn, I. M., Chen, W.-C., Zhou, M., et al. (2019). KRAS4A Directly Regulates Hexokinase 1. *Nature* 576 (7787), 482–486. doi:10.1038/s41586-019-1832-9

Ariotti, N., Fernández-Rojo, M. A., Zhou, Y., Hill, M. M., Rodkey, T. L., Inder, K. L., et al. (2014). Caveolae Regulate the Nanoscale Organization of the Plasma Membrane to Remotely Control Ras Signaling. *J. Cel. Biol.* 204 (5), 777–792. doi:10.1083/jcb.201307055

Baumgart, T., Capraro, B. R., Zhu, C., and Das, S. L. (2011). Thermodynamics and Mechanics of Membrane Curvature Generation and Sensing by Proteins and Lipids. *Annu. Rev. Phys. Chem.* 62, 483–506. doi:10.1146/annurev.physchem.012809.103450

Baumgart, T., Hess, S. T., and Webb, W. W. (2003). Imaging Coexisting Fluid Domains in Biomembrane Models Coupling Curvature and Line Tension. *Nature* 425 (6960), 821–824. doi:10.1038/nature02013

Belanis, L., Plowman, S. J., Rotblat, B., Hancock, J. F., and Kloog, Y. (2008). Galectin-1 Is a Novel Structural Component and a Major Regulator of H-Ras Nanoclusters. *MBoC* 19 (4), 1404–1414. doi:10.1091/mbc.e07-10-1053

Bery, N., Legg, S., Debreczeni, J., Breed, J., Embrey, K., Stubbs, C., et al. (2019). KRAS-specific Inhibition Using a DARPin Binding to a Site in the Allosteric Lobe. *Nat. Commun.* 10 (1), 2607. doi:10.1038/s41467-019-10419-2

Bigay, J., and Antonny, B. (2012). Curvature, Lipid Packing, and Electrostatics of Membrane Organelles: Defining Cellular Territories in Determining Specificity. *Dev. Cel.* 23 (5), 886–895. doi:10.1016/j.devcel.2012.10.009

Bivona, T. G., Quatela, S. E., Bodemann, B. O., Ahearn, I. M., Soskis, M. J., Mor, A., et al. (2006). PKC Regulates a Farnesyl-Electrostatic Switch on K-Ras that Promotes its Association with Bcl-XL on Mitochondria and Induces Apoptosis. *Mol. Cel.* 21 (4), 481–493. doi:10.1016/j.molcel.2006.01.012

Blackiston, D. J., McLaughlin, K. A., and Levin, M. (2009). Bioelectric Controls of Cell Proliferation: Ion Channels, Membrane Voltage and the Cell Cycle. *Cell Cycle* 8 (21), 3519–3528. doi:10.4161/cc.8.21.9888

Blazevits, O., Mideksa, Y. G., solman, M, Ligabue, A., Ariotti, N., Nakhaeizadeh, H., et al. (2016). Galectin-1 Dimers Can Scaffold Raf-Effectors to Increase H-Ras Nanoclustering. *Sci. Rep.* 6, 24165.

Boura, E., and Nencka, R. (2015). Phosphatidylinositol 4-kinases: Function, Structure, and Inhibition. *Exp. Cel. Res.* 337 (2), 136–145. doi:10.1016/j.yexcr.2015.03.028

Boyartchuk, V. L., Ashby, M. N., and Rine, J. (1997). Modulation of Ras and A-Factor Function by Carboxyl-Terminal Proteolysis. *Science* 275 (5307), 1796–1800. doi:10.1126/science.275.5307.1796

Chandra, A., Grecco, H. E., Pisupati, V., Perera, D., Cassidy, L., Skoulidis, F., et al. (2012). The GDI-like Solubilizing Factor PDEδ Sustains the Spatial Organization and Signalling of Ras Family Proteins. *Nat. Cel. Biol.* 14 (2), 148–158. doi:10.1038/ncb2394

Chatterjee, S., Smith, E. R., Hanada, K., Stevens, V. L., and Mayor, S. (2001). GPI Anchoring Leads to Sphingolipid-dependent Retention of Endocytosed Proteins in the Recycling Endosomal Compartment. *EMBO J.* 20 (7), 1583–1592. doi:10.1093/emboj/20.7.1583

Cho, K.-j., Casteel, D. E., Prakash, P., Tan, L., van der Hoeven, D., Salim, A. A., et al. (2016). AMPK and Endothelial Nitric Oxide Synthase Signaling Regulates K-Ras Plasma Membrane Interactions via Cyclic GMP-dependent Protein Kinase 2. *Mol. Cel. Biol.* 36 (24), 3086–3099. doi:10.1128/mcb.00365-16

Cho, K.-j., Park, J.-H., Piggott, A. M., Salim, A. A., Gorfe, A. A., Parton, R. G., et al. (2012). Staurosporines Disrupt Phosphatidylserine Trafficking and Mislocalize Ras Proteins. *J. Biol. Chem.* 287 (52), 43573–43584. doi:10.1074/jbc.m112.424457

Cho, K. J., van der Hoeven, D., Zhou, Y., Maekawa, M., Ma, X., Chen, W., et al. (2015). Inhibition of Acid Sphingomyelinase Depletes Cellular Phosphatidylserine and Mislocalizes K-Ras from the Plasma Membrane. *Mol. Cel. Biol.* 36 (2), 363–374. doi:10.1128/MCB.00719-15

Cox, A. D., Der, C. J., and Philips, M. R. (2015). Targeting RAS Membrane Association: Back to the Future for Anti-RAS Drug Discovery? *Clin. Cancer Res.* 21 (8), 1819–1827. doi:10.1158/1078-0432.ccr-14-3214

Cox, A. D., Fesik, S. W., Kimmelman, A. C., Luo, J., and Der, C. J. (2014). Drugging the Undruggable RAS: Mission Possible? *Nat. Rev. Drug Discov.* 13 (11), 828–851. doi:10.1038/nrd4389

Dai, Q., Choy, E., Chiu, V., Romano, J., Slivka, S. R., Steitz, S. A., et al. (1998). Mammalian Prenylcysteine Carboxyl Methyltransferase Is in the Endoplasmic Reticulum. *J. Biol. Chem.* 273 (24), 15030–15034. doi:10.1074/jbc.273.24.15030

Diggle, P. J., Mateu, J., and Clough, H. E. (2000). A Comparison between Parametric and Non-parametric Approaches to the Analysis of Replicated Spatial point Patterns. *Adv. Appl. Probab.* 32, 331–343. doi:10.1017/s0001867800009952

Diggle, P. J. (1979). On Parameter Estimation and Goodness-Of-Fit Testing for Spatial Point Patterns. *Biometrics* 35 (1), 87–101. doi:10.2307/2529938

Downward, J. (2003). Targeting RAS Signalling Pathways in Cancer Therapy. *Nat. Rev. Cancer* 3 (1), 11–22. doi:10.1038/nrc969

Drosten, M., Dhawahir, A., Sum, E. Y. M., Urosevic, J., Lechuga, C. G., Esteban, L. M., et al. (2010). Genetic Analysis of Ras Signalling Pathways in Cell Proliferation, Migration and Survival. *EMBO J.* 29 (6), 1091–1104. doi:10.1038/emboj.2010.7

Elad-Sfadia, G., Haklai, R., Balan, E., and Kloog, Y. (2004). Galectin-3 Augments K-Ras Activation and Triggers a Ras Signal that Attenuates ERK but Not Phosphoinositide 3-kinase Activity. *J. Biol. Chem.* 279 (33), 34922–34930. doi:10.1074/jbc.m312697200

Fehrenbacher, N., Tojal da Silva, I., Ramirez, C., Zhou, Y., Cho, K. J., Kuchay, S., et al. (2017). The G Protein-Coupled Receptor GPR31 Promotes Membrane Association of KRAS. *J. Cell Biol.* 216 (8), 2329–2338. doi:10.1083/jcb.201609096

Ghosh, S., Strum, J. C., Sciorra, V. A., Daniel, L., and Bell, R. M. (1996). Raf-1 Kinase Possesses Distinct Binding Domains for Phosphatidylserine and Phosphatidic Acid. *J. Biol. Chem.* 271 (14), 8472–8480. doi:10.1074/jbc.271.14.8472

Ghosh, S., Xie, W. Q., Quest, A. F., Mabrouk, G. M., Strum, J. C., and Bell, R. M. (1994). The Cysteine-Rich Region of Raf-1 Kinase Contains Zinc, Translocates to Liposomes, and Is Adjacent to a Segment that Binds GTP-Ras. *J. Biol. Chem.* 269 (13), 10000–10007. doi:10.1016/s0021-9258(17)36981-8

Gorfe, A. A., Babakhani, A., and McCammon, J. A. (2007a). H-ras Protein in a Bilayer: Interaction and Structure Perturbation. *J. Am. Chem. Soc.* 129 (40), 12280–12286. doi:10.1021/ja073949v

Gorfe, A. A., Hanzal-Bayer, M., Abankwa, D., Hancock, J. F., and McCammon, J. A. (2007b). Structure and Dynamics of the Full-Length Lipid-Modified H-Ras Protein in a 1,2-Dimyristoylglycero-3-Phosphocholine Bilayer. *J. Med. Chem.* 50 (4), 674–684. doi:10.1021/jm061053f

Gorfe, A. A., and McCammon, J. A. (2008). Similar Membrane Affinity of Mono- and Di-S-acylated Ras Membrane Anchors: a New Twist in the Role of Protein Lipidation. *J. Am. Chem. Soc.* 130 (38), 12624–12625. doi:10.1021/ja805110q

Gorfe, A. A., Pellarin, R., and Caflisch, A. (2004). Membrane Localization and Flexibility of a Lipidated Ras Peptide Studied by Molecular Dynamics Simulations. *J. Am. Chem. Soc.* 126 (46), 15277–15286. doi:10.1021/ja046607n

Guillard, S., Kolasinska-Zwierz, P., Debreczeni, J., Breed, J., Zhang, J., Bery, N., et al. (2017). Structural and Functional Characterization of a DARPin Which Inhibits Ras Nucleotide Exchange. *Nat. Commun.* 8, 16111. doi:10.1038/ncomms16111

Gulbins, E., Palmada, M., Reichel, M., Lüth, A., Böhmer, C., Amato, D., et al. (2013). Acid Sphingomyelinase-Ceramide System Mediates Effects of Antidepressant Drugs. *Nat. Med.* 19 (7), 934–938. doi:10.1038/nm.3214

Güldenhaupt, J., Rudack, T., Bachler, P., Mann, D., Triola, G., Waldmann, H., et al. (2012). N-ras Forms Dimers at POPC Membranes. *Biophysical J.* 103 (7), 1585–1593. doi:10.1016/j.bpj.2012.08.043

Ha, T. S., Xia, R., Zhang, H., Jin, X., and Smith, D. P. (2014). Lipid Flippase Modulates Olfactory Receptor Expression and Odorant Sensitivity in Drosophila. *Proc. Natl. Acad. Sci.* 111 (21), 7831–7836. doi:10.1073/pnas.1401938111

Hancock, J. F., Cadwallader, K., and Marshall, C. J. (1991). Methylation and Proteolysis Are Essential for Efficient Membrane Binding of Prenylated p21K-Ras(B). *EMBO J.* 10 (3), 641–646. doi:10.1002/j.1460-2075.1991.tb07992.x

Hancock, J. F., Cadwallader, K., Paterson, H., and Marshall, C. J. (1991). A CAAX or a CAAL Motif and a Second Signal Are Sufficient for Plasma Membrane Targeting of Ras Proteins. *EMBO J.* 10 (13), 4033–4039. doi:10.1002/j.1460-2075.1991.tb04979.x

Hancock, J. F. (2006). Lipid Rafts: Contentious Only from Simplistic Standpoints. *Nat. Rev. Mol. Cel. Biol.* 7 (6), 456–462. doi:10.1038/nrm1925

Hancock, J. F., Magee, A. I., Childs, J. E., and Marshall, C. J. (1989). All Ras Proteins Are Polyisoprenylated but Only Some Are Palmitoylated. *Cell* 57 (7), 1167–1177. doi:10.1016/0092-8674(89)90054-8

Hancock, J. F. (2003). Ras Proteins: Different Signals from Different Locations. *Nat. Rev. Mol. Cel. Biol.* 4 (5), 373–385. doi:10.1038/nrm1105

Hemmings, B. A., and Restuccia, D. F. (2012). PI3K-PKB/Akt Pathway. *Cold Spring Harbor Perspect. Biol.* 4 (9), a011189. doi:10.1101/cshperspect.a011189

Hrycyna, C. A., Sapperstein, S. K., Clarke, S., and Michaelis, S. (1991). The *Saccharomyces cerevisiae* STE14 Gene Encodes a Methyltransferase that Mediates C-Terminal Methylation of A-Factor and RAS Proteins. *EMBO J.* 10 (7), 1699–1709. doi:10.1002/j.1460-2075.1991.tb07694.x

Inder, K., and Hancock, J. F. (2008). System Output of the MAPK Module Is Spatially Regulated. *Communicative Integr. Biol.* 1 (2), 178–179. doi:10.4161/cib.1.2.7197

Inder, K., Harding, A., Plowman, S. J., Philips, M. R., Parton, R. G., and Hancock, J. F. (2008). Activation of the MAPK Module from Different Spatial Locations Generates Distinct System Outputs. *MBoC* 19 (11), 4776–4784. doi:10.1091/mbc.e08-04-0407

Inder, K. L., Hill, M. M., and Hancock, J. F. (2010). Nucleophosmin and Nucleolin Regulate K-Ras Signaling. *Communicative Integr. Biol.* 3 (2), 188–190. doi:10.4161/cib.3.2.10923

Inder, K. L., Lau, C., Loo, D., Chaudhary, N., Goodall, A., Martin, S., et al. (2009). Nucleophosmin and Nucleolin Regulate K-Ras Plasma Membrane Interactions and MAPK Signal Transduction. *J. Biol. Chem.* 284 (41), 28410–28419. doi:10.1074/jbc.m109.001537

Janosi, L., and Gorfe, A. A. (2010). Segregation of Negatively Charged Phospholipids by the Polycationic and Farnesylated Membrane Anchor of Kras. *Biophysical J.* 99 (11), 3666–3674. doi:10.1016/j.bpj.2010.10.031

Janosi, L., Li, Z., Hancock, J. F., and Gorfe, A. A. (2012). Organization, Dynamics, and Segregation of Ras Nanoclusters in Membrane Domains. *Proc. Natl. Acad. Sci.* 109 (21), 8097–8102. doi:10.1073/pnas.1200773109

Kattan, W. E., Chen, W., Ma, X., Lan, T. H., van der Hoeven, D., van der Hoeven, R., et al. (2019). Targeting Plasma Membrane Phosphatidylserine Content to Inhibit Oncogenic KRAS Function. *Life Sci. Alliance* 2 (5). doi:10.26508/lsa.201900431

Kholodenko, B. N., Hancock Jf Fau - Kolch, W., and Kolch, W. (2010). Signalling Ballet in Space and Time. *Nat. Rev. Mol. Cel. Biol.* 11, 414–426. doi:10.1038/nrm2901

Kim, E., Ambroziak, P., Otto, J. C., Taylor, B., Ashby, M., Shannon, K., et al. (1999). Disruption of the Mouse Rce1 Gene Results in Defective Ras Processing and Mislocalization of Ras within Cells. *J. Biol. Chem.* 274 (13), 8383–8390. doi:10.1074/jbc.274.13.8383

Ledford, H. (2015). Cancer: The Ras Renaissance. *Nature* 520 (7547), 278–280. doi:10.1038/520278a

Lee, K. Y., Fang, Z., Enomoto, M., Gasmi-Seabrook, G., Zheng, L., Koide, S., et al. (2020). Two Distinct Structures of Membrane-Associated Homodimers of GTP- and GDP-Bound KRAS4B Revealed by Paramagnetic Relaxation Enhancement. *Angew. Chem. Int. Ed.* 59 (27), 11037–11045. doi:10.1002/anie.202001758

Lee, S., Uchida, Y., Emoto, K., Umeda, M., Kuge, O., Taguchi, T., et al. (2012). Impaired Retrograde Membrane Traffic through Endosomes in a Mutant CHO Cell Defective in Phosphatidylserine Synthesis. *Genes Cells* 17 (8), 728–736. doi:10.1111/j.1365-2443.2012.01622.x

Li, H., and Gorfe, A. A. (2013). Aggregation of Lipid-Anchored Full-Length H-Ras in Lipid Bilayers: Simulations with the MARTINI Force Field. *PLoS One* 8 (7), e71018. doi:10.1371/journal.pone.0071018

Li, H., and Gorfe, A. A. (2014). Membrane Remodeling by Surface-Bound Protein Aggregates: Insights from Coarse-Grained Molecular Dynamics Simulation. *J. Phys. Chem. Lett.* 5 (8), 1457–1462. doi:10.1021/jz500451a

Li, L., Herzog, M., Möbitz, S., and Winter, R. (2021). Liquid Droplets of Protein LAF1 Provide a Vehicle to Regulate Storage of the Signaling Protein K-Ras4B and its Transport to the Lipid Membrane. *Phys. Chem. Chem. Phys.* 23 (9), 5370–5375. doi:10.1039/d1cp00007a

Li, Z.-L., Prakash, P., and Buck, M. (2018). A "Tug of War" Maintains a Dynamic Protein-Membrane Complex: Molecular Dynamics Simulations of C-Raf RBD-CRD Bound to K-Ras4B at an Anionic Membrane. *ACS Cent. Sci.* 4 (2), 298–305. doi:10.1021/acscentsci.7b00593

Li, Z., and Gorfe, A. A. (2013). Deformation of a Two-Domain Lipid Bilayer Due to Asymmetric Insertion of Lipid-Modified Ras Peptides. *Soft Matter* 9 (47). doi:10.1039/c3sm51388b

Li, Z., and Gorfe, A. A. (2014). Modulation of a Small Two-Domain Lipid Vesicle by Linactants. *J. Phys. Chem. B* 118 (30), 9028–9036. doi:10.1021/jp5042525

Li, Z., Janosi, L., and Gorfe, A. A. (2012). Formation and Domain Partitioning of H-Ras Peptide Nanoclusters: Effects of Peptide Concentration and Lipid Composition. *J. Am. Chem. Soc.* 134 (41), 17278–17285. doi:10.1021/ja307716z

Liang, H., Mu, H., Jean-Francois, F., Lakshman, B., Sarkar-Banerjee, S., Zhuang, Y., et al. (2019). Membrane Curvature Sensing of the Lipid-Anchored K-Ras Small GTPase. *Life Sci. Alliance* 2 (4). doi:10.26508/lsa.201900343

Lin, X., Li, Z., and Gorfe, A. A. (2015). Reversible Effects of Peptide Concentration and Lipid Composition on H-Ras Lipid Anchor Clustering. *Biophysical J.* 109 (12), 2467–2470. doi:10.1016/j.bpj.2015.11.009

Mazhab-Jafari, M. T., Marshall, C. B., Smith, M. J., Gasmi-Seabrook, G. M. C., Stathopulos, P. B., Inagaki, F., et al. (2015). Oncogenic and RASopathy-Associated K-RAS Mutations Relieve Membrane-dependent Occlusion of the Effector-Binding Site. *Proc. Natl. Acad. Sci. USA* 112 (21), 6625–6630. doi:10.1073/pnas.1419895112

McMahon, H. T., and Boucrot, E. (2015). Membrane Curvature at a Glance. *J. Cel. Sci.* 128 (6), 1065–1070. doi:10.1242/jcs.114454

Moser von Filseck, J., Vanni, S., Mesmin, B., Antonny, B., and Drin, G. (2015). A Phosphatidylinositol-4-Phosphate Powered Exchange Mechanism to Create a Lipid Gradient between Membranes. *Nat. Commun.* 6, 6671. doi:10.1038/ncomms7671

Moser von Filseck, J., opi , A., Delfosse, V., Vanni, S., Jackson, C. L., Bourguet, W., et al. (2015). Phosphatidylserine Transport by ORP/Osh Proteins Is Driven by Phosphatidylinositol 4-phosphate. *Science* 349 (6246), 432–436. doi:10.1126/science.aab1346

Murakoshi, H., Iino, R., Kobayashi, T., Fujiwara, T., Ohshima, C., Yoshimura, A., et al. (2004). Single-molecule Imaging Analysis of Ras Activation in Living Cells. *Proc. Natl. Acad. Sci.* 101 (19), 7317–7322. doi:10.1073/pnas.0401354101

Muratcioglu, S., Chavan, T. S., Freed, B. C., Jang, H., Khavrutskii, L., Freed, R. N., et al. (2015). GTP-dependent K-Ras Dimerization. *Structure* 23 (7), 1325–1335. doi:10.1016/j.str.2015.04.019

Nan, X., Tamgüney, T. M., Collisson, E. A., Lin, L.-J., Pitt, C., Galeas, J., et al. (2015). Ras-GTP Dimers Activate the Mitogen-Activated Protein Kinase (MAPK) Pathway. *Proc. Natl. Acad. Sci. USA* 112 (26), 7996–8001. doi:10.1073/pnas.1509123112

Neale, C., and García, A. E. (2020). The Plasma Membrane as a Competitive Inhibitor and Positive Allosteric Modulator of KRas4B Signaling. *Biophysical J.* 118 (5), 1129–1141. doi:10.1016/j.bpj.2019.12.039

Nicolini, C., Baranski, J., Schlummer, S., Palomo, J., Lumbierres-Burgues, M., Kahms, M., et al. (2006). Visualizing Association of N-Ras in Lipid Microdomains: Influence of Domain Structure and Interfacial Adsorption. *J. Am. Chem. Soc.* 128 (1), 192–201.

Packer, M. R., Parker, J. A., Chung, J. K., Li, Z., Lee, Y. K., Cookis, T., et al. (2021). Raf Promotes Dimerization of the Ras G-Domain with Increased Allosteric Connections. *Proc. Natl. Acad. Sci. USA* 118 (10). doi:10.1073/pnas.2015648118

Paulusma, C. C., Folmer, D. E., Ho-Mok, K. S., de Waart, D. R., Hilarius, P. M., Verhoeven, A. J., et al. (2008). ATP8B1 Requires an Accessory Protein for Endoplasmic Reticulum Exit and Plasma Membrane Lipid Flippase Activity. *Hepatology* 47 (1), 268–278. doi:10.1002/hep.21950

Plowman, S. J., Muncke, C., Parton, R. G., and Hancock, J. F. (2005). H-ras, K-Ras, and Inner Plasma Membrane Raft Proteins Operate in Nanoclusters with Differential Dependence on the Actin Cytoskeleton. *Proc. Natl. Acad. Sci.* 102 (43), 15500–15505. doi:10.1073/pnas.0504114102

Posada, I. M. D., Lectez, B., Sharma, M., Oetken-Lindholm, C., Yetukuri, L., Zhou, Y., et al. (2017). Rapalogs Can Promote Cancer Cell Stemness *In Vitro* in a Galectin-1 and H-ras-dependent Manner. *Oncotarget* 8 (27), 44550–44566. doi:10.18632/oncotarget.17819

Posada, I. M., Serulla, M., Zhou, Y., Oetken-Lindholm, C., Abankwa, D., Lectez, B., et al. (2016). ASPP2 Is a Novel Pan-Ras Nanocluster Scaffold. *PLoS One* 11 (7), e0159677. doi:10.1371/journal.pone.0159677

Prakash, P., Sayyed-Ahmad, A., Cho, K. J., Dolino, D. M., Chen, W., Li, H., et al. (2017). Computational and Biochemical Characterization of Two Partially Overlapping Interfaces and Multiple Weak-Affinity K-Ras Dimers. *Sci. Rep.* 7, 40109. doi:10.1038/srep40109

Prakash, P., and Gorfe, A. A. (2019). Probing the Conformational and Energy Landscapes of KRAS Membrane Orientation. *J. Phys. Chem. B* 123 (41), 8644–8652. doi:10.1021/acs.jpcb.9b05796

Prakash, P., Litwin, D., Liang, H., Sarkar-Banerjee, S., Dolino, D., Zhou, Y., et al. (2019). Dynamics of Membrane-Bound G12V-KRAS from Simulations and Single-Molecule FRET in Native Nanodiscs. *Biophysical J.* 116 (2), 179–183. doi:10.1016/j.bpj.2018.12.011

Prakash, P., Sayyed-Ahmad, A., Zhou, Y., Volk, D. E., Gorenstein, D. G., Dial, E., et al. (2012). Aggregation Behavior of Ibuprofen, Cholic Acid and Dodecylphosphocholine Micelles. *Biochim. Biophys. Acta (Bba) - Biomembranes* 1818 (12), 3040–3047. doi:10.1016/j.bbamem.2012.07.029

Prakash, P., Zhou, Y., Liang, H., Hancock, J. F., and Gorfe, A. A. (2016). Oncogenic K-Ras Binds to an Anionic Membrane in Two Distinct Orientations: A Molecular Dynamics Analysis. *Biophysical J.* 110 (5), 1125–1138. doi:10.1016/j.bpj.2016.01.019

Prior, I. A., Hood, F. E., and Hartley, J. L. (2020). The Frequency of Ras Mutations in Cancer. *Cancer Res.* 80 (14), 2969–2974. doi:10.1158/0008-5472.can-19-3682

Prior, I. A., Muncke, C., Parton, R. G., and Hancock, J. F. (2003). Direct Visualization of Ras Proteins in Spatially Distinct Cell Surface Microdomains. *J. Cel. Biol.* 160, 165–170. doi:10.1083/jcb.200209091

Prior, I. A., Parton, R. G., and Hancock, J. F. (2003). Observing Cell Surface Signaling Domains Using Electron Microscopy. *Sci. Signaling* 2003 (177), PL9. doi:10.1126/stke.2003.177.pl9

Raubo, P., Andrews, D. M., McKelvie, J. C., Robb, G. R., Smith, J. M., Swarbrick, M. E., et al. (2015). Discovery of Potent, Selective Small Molecule Inhibitors of α-subtype of Type III Phosphatidylinositol-4-Kinase (PI4KIIIα). *Bioorg. Med. Chem. Lett.* 25 (16), 3189–3193. doi:10.1016/j.bmcl.2015.05.093

Reiss, Y., Goldstein, J. L., Seabra, M. C., Casey, P. J., and Brown, M. S. (1990). Inhibition of Purified P21ras Farnesyl:protein Transferase by Cys-AAX Tetrapeptides. *Cell* 62 (1), 81–88. doi:10.1016/0092-8674(90)90242-7

Ripley, B. D. (1977). Modelling Spatial Patterns. *J. R. Stat. Soc. Ser. B (Methodological)* 39, 172–192. doi:10.1111/j.2517-6161.1977.tb01615.x

Rotblat, B., Niv, H., André, S., Kaltner, H., Gabius, H.-J., and Kloog, Y. (2004). Galectin-1(L11A) Predicted from a Computed Galectin-1 Farnesyl-Binding Pocket Selectively Inhibits Ras-GTP. *Cancer Res.* 64 (9), 3112–3118. doi:10.1158/0008-5472.can-04-0026

Roy, S., Plowman, S., Rotblat, B., Prior, I. A., Muncke, C., Grainger, S., et al. (2005). Individual Palmitoyl Residues Serve Distinct Roles in H-Ras Trafficking, Microlocalization, and Signaling. *Mcb* 25 (15), 6722–6733. doi:10.1128/mcb.25.15.6722-6733.2005

Rudack, T., Teuber, C., Scherlo, M., Güldenhaupt, J., Schartner, J., Lübben, L. B., et al. (2021). *The Ras Dimer Structure* [Epub ahead of print]. ChemRxiv. doi:10.1039/d1sc00957e

Santana, P., Peña, L. A., Haimovitz-Friedman, A., Martin, S., Green, D., McLoughlin, M., et al. (1996). Acid Sphingomyelinase-Deficient Human Lymphoblasts and Mice Are Defective in Radiation-Induced Apoptosis. *Cell* 86 (2), 189–199. doi:10.1016/s0092-8674(00)80091-4

Sarkar-Banerjee, S., Sayyed-Ahmad, A., Prakash, P., Cho, K.-J., Waxham, M. N., Hancock, J. F., et al. (2017). Spatiotemporal Analysis of K-Ras Plasma Membrane Interactions Reveals Multiple High Order Homo-Oligomeric Complexes. *J. Am. Chem. Soc.* 139 (38), 13466–13475. doi:10.1021/jacs.7b06292

Sayyed-Ahmad, A., Cho, K.-J., Hancock, J. F., and Gorfe, A. A. (2016). Computational Equilibrium Thermodynamic and Kinetic Analysis of K-Ras Dimerization through an Effector Binding Surface Suggests Limited Functional Role. *J. Phys. Chem. B* 120 (33), 8547–8556. doi:10.1021/acs.jpcb.6b02403

Schmick, M., Kraemer, A., and Bastiaens, P. I. H. (2015). Ras Moves to Stay in Place. *Trends Cel. Biol.* 25 (4), 190–197. doi:10.1016/j.tcb.2015.02.004

Schmick, M., Vartak, N., Papke, B., Kovacevic, M., Truxius, D. C., Rossmannek, L., et al. (2014). KRas Localizes to the Plasma Membrane by Spatial Cycles of Solubilization, Trapping and Vesicular Transport. *Cell* 157 (2), 459–471. doi:10.1016/j.cell.2014.02.051

Shalom-Feuerstein, R., Plowman, S. J., Rotblat, B., Ariotti, N., Tian, T., Hancock, J. F., et al. (2008). K-ras Nanoclustering Is Subverted by Overexpression of the Scaffold Protein Galectin-3. *Cancer Res.* 68 (16), 6608–6616. doi:10.1158/0008-5472.can-08-1117

Simons, K., and Gerl, M. J. (2010). Revitalizing Membrane Rafts: New Tools and Insights. *Nat. Rev. Mol. Cel. Biol.* 11 (10), 688–699. doi:10.1038/nrm2977

Simons, K., and Ikonen, E. (1997). Functional Rafts in Cell Membranes. *Nature* 387 (6633), 569–572. doi:10.1038/42408

Simons, K., and Toomre, D. (2000). Lipid Rafts and Signal Transduction. *Nat. Rev. Mol. Cel. Biol.* 1 (1), 31–39. doi:10.1038/35036052

Simons, K., and Vaz, W. L. C. (2004). Model Systems, Lipid Rafts, and Cell Membranes. *Annu. Rev. Biophys. Biomol. Struct.* 33, 269–295. doi:10.1146/annurev.biophys.32.110601.141803

Sohn, M., Ivanova, P., Brown, H. A., Toth, D. J., Varnai, P., Kim, Y. J., et al. (2016). Lenz-Majewski Mutations in PTDSS1 Affect Phosphatidylinositol 4-phosphate Metabolism at ER-PM and ER-Golgi Junctions. *Proc. Natl. Acad. Sci. USA* 113 (16), 4314–4319. doi:10.1073/pnas.1525719113

Spencer-Smith, R., Koide, A., Zhou, Y., Eguchi, R. R., Sha, F., Gajwani, P., et al. (2017). Inhibition of RAS Function through Targeting an Allosteric Regulatory Site. *Nat. Chem. Biol.* 13 (1), 62–68. doi:10.1038/nchembio.2231

Stokoe, D., Macdonald, S., Cadwallader, K., Symons, M., and Hancock, J. (1994). Activation of Raf as a Result of Recruitment to the Plasma Membrane. *Science* 264 (5164), 1463–1467. doi:10.1126/science.7811320

Sundelacruz, S., Levin, M., and Kaplan, D. L. (2009). Role of Membrane Potential in the Regulation of Cell Proliferation and Differentiation. *Stem Cel. Rev. Rep.* 5 (3), 231–246. doi:10.1007/s12015-009-9080-2

Tian, T., Harding, A., Inder, K., Plowman, S., Parton, R. G., and Hancock, J. F. (2007). Plasma Membrane Nanoswitches Generate High-Fidelity Ras Signal Transduction. *Nat. Cel. Biol.* 9 (8), 905–914. doi:10.1038/ncb1615

Tian, T., Plowman, S. J., Parton, R. G., Kloog, Y., and Hancock, J. F. (2010). Mathematical Modeling of K-Ras Nanocluster Formation on the Plasma Membrane. *Biophysical J.* 99 (2), 534–543. doi:10.1016/j.bpj.2010.04.055

Tsai, F. D., Lopes, M. S., Zhou, M., Court, H., Ponce, O., Fiordalisi, J. J., et al. (2015). K-Ras4A Splice Variant Is Widely Expressed in Cancer and Uses a Hybrid Membrane-Targeting Motif. *Proc. Natl. Acad. Sci. USA* 112 (3), 779–784. doi:10.1073/pnas.1412811112

van der Hoeven, D., Cho, K.-j., Ma, X., Chigurupati, S., Parton, R. G., and Hancock, J. F. (2013). Fendiline Inhibits K-Ras Plasma Membrane Localization and Blocks K-Ras Signal Transmission. *Mol. Cell Biol.* 33 (2), 237–251. doi:10.1128/mcb.00884-12

van der Hoeven, D., Cho, K. J., Zhou, Y., Ma, X., Chen, W., Naji, A., et al. (2017). Sphingomyelin Metabolism Is a Regulator of KRAS Function. *Mol. Cel. Biol.* 38 (3), e00373–17. doi:10.1128/MCB.00373-17

Van, Q. N., Prakash, P., Shrestha, R., Balius, T. E., Turbyville, T. J., Stephen, A. G., et al. (2021). RAS Nanoclusters: Dynamic Signaling Platforms Amenable to Therapeutic Intervention. *Biomolecules* 11 (3). doi:10.3390/biom11030377

Veatch, S. L., and Keller, S. L. (2002). Organization in Lipid Membranes Containing Cholesterol. *Phys. Rev. Lett.* 89 (26), 268101. doi:10.1103/physrevlett.89.268101

Veatch, S. L., and Keller, S. L. (2003). Separation of Liquid Phases in Giant Vesicles of Ternary Mixtures of Phospholipids and Cholesterol. *Biophysical J.* 85 (5), 3074–3083. doi:10.1016/s0006-3495(03)74726-2

Veatch, S. L., Soubias, O., Keller, S. L., and Gawrisch, K. (2007). Critical Fluctuations in Domain-Forming Lipid Mixtures. *Proc. Natl. Acad. Sci.* 104 (45), 17650–17655. doi:10.1073/pnas.0703513104

Waring, M. J., Andrews, D. M., Faulder, P. F., Flemington, V., McKelvie, J. C., Maman, S., et al. (2014). Potent, Selective Small Molecule Inhibitors of Type III Phosphatidylinositol-4-Kinase α- but Not β-inhibit the Phosphatidylinositol Signaling cascade and Cancer Cell Proliferation. *Chem. Commun.* 50 (40), 5388–5390. doi:10.1039/c3cc48391f

Weise, K., Kapoor, S., Denter, C., Nikolaus, J., Opitz, N., Koch, S., et al. (2011). Membrane-mediated Induction and Sorting of K-Ras Microdomain Signaling Platforms. *J. Am. Chem. Soc.* 133 (4), 880–887. doi:10.1021/ja107532q

Weise, K., Triola, G., Brunsveld, L., Waldmann, H., and Winter, R. (2009). Influence of the Lipidation Motif on the Partitioning and Association of N-Ras in Model Membrane Subdomains. *J. Am. Chem. Soc.* 131 (4), 1557–1564. doi:10.1021/ja808691r

Werkmüller, A., Triola, G., Waldmann, H., and Winter, R. (2013). Rotational and Translational Dynamics of Ras Proteins upon Binding to Model Membrane Systems. *ChemPhysChem* 14 (16), 3698–3705. doi:10.1002/cphc.201300617

Zhou, Y., Cho, K.-J., Plowman, S. J., and Hancock, J. F. (2012). Nonsteroidal Anti-inflammatory Drugs Alter the Spatiotemporal Organization of Ras Proteins on the Plasma Membrane. *J. Biol. Chem.* 287 (20), 16586–16595. doi:10.1074/jbc.m112.348490

Zhou, Y., Prakash, P., Liang, H., Cho, K. J., Gorfe, A. A., and Hancock, J. F. (2017). Lipid-Sorting Specificity Encoded in K-Ras Membrane Anchor Regulates Signal Output. *Cell* 168 (1–2), 239–251. e16. doi:10.1016/j.cell.2016.11.059

Zhou, Y., Prakash, P., Liang, H., Gorfe, A. A., Hancock, J. F., et al. (2021). The KRAS and Other Prenylated PBD Membrane Anchors Recognize Phosphatidylserine Acyl Chain Structure. *Proc. Natl. Acad. Sci. USA* 118 (6). doi:10.1073/pnas.2014605118

Zhou, Y., and Hancock, J. F. (2017). *Deciphering Lipid Codes: K-Ras as a Paradigm*. Traffic.

Zhou, Y., and Hancock, J. F. (2015). Ras Nanoclusters: Versatile Lipid-Based Signaling Platforms. *Biochim. Biophys. Acta (Bba) - Mol. Cel. Res.* 1853 (4), 841–849. doi:10.1016/j.bbamcr.2014.09.008

Zhou, Y., Liang, H., Rodkey, T., Ariotti, N., Parton, R. G., and Hancock, J. F. (2014). Signal Integration by Lipid-Mediated Spatial Cross Talk between Ras Nanoclusters. *Mol. Cel. Biol.* 34 (5), 862–876. doi:10.1128/mcb.01227-13

Zhou, Y., Wong, C.-O., Cho, K.-j., van der Hoeven, D., Liang, H., Thakur, D. P., et al. (2015). Membrane Potential Modulates Plasma Membrane Phospholipid Dynamics and K-Ras Signaling. *Science* 349 (6250), 873–876. doi:10.1126/science.aaa5619

Conflict of Interest: The authors declare that the research was conducted in the absence of any commercial or financial relationships that could be construed as a potential conflict of interest.

frontiers in Molecular Biosciences

ORIGINAL RESEARCH
published: 21 June 2021
doi: 10.3389/fmolb.2021.677979

Molecular Associations and Clinical Significance of RAPs in Hepatocellular Carcinoma

Sarita Kumari[1†], Mohit Arora[2†], Jay Singh[1], Lokesh K. Kadian[2], Rajni Yadav[3], Shyam S. Chauhan[2] and Anita Chopra[1*]*

[1]*Laboratory Oncology Unit, Dr. BRA-IRCH, All India Institute of Medical Sciences, New Delhi, India,* [2]*Department of Biochemistry, All India Institute of Medical Sciences, New Delhi, India,* [3]*Department of Pathology, All India Institute of Medical Sciences, New Delhi, India*

Hepatocellular carcinoma (HCC) is an aggressive gastrointestinal malignancy with a high rate of mortality. Multiple studies have individually recognized members of RAP gene family as critical regulators of tumor progression in several cancers, including hepatocellular carcinoma. These studies suffer numerous limitations including a small sample size and lack of analysis of various clinicopathological and molecular features. In the current study, we utilized authoritative multi-omics databases to determine the association of RAP gene family expression and detailed molecular and clinicopathological features in hepatocellular carcinoma (HCC). All five RAP genes were observed to harbor dysregulated expression in HCC compared to normal liver tissues. RAP2A exhibited strongest ability to differentiate tumors from the normal tissues. RAP2A expression was associated with progressive tumor grade, *TP53* and *CTNNB1* mutation status. Additionally, RAP2A expression was associated with the alteration of its copy numbers and DNA methylation. RAP2A also emerged as an independent marker for patient prognosis. Further, pathway analysis revealed that RAP2A expression is correlated with tumor-infiltrating immune cell composition and oncogenic molecular pathways, such as cell cycle and cellular metabolism.

Keywords: hepatocellular carcinoma, liver, RAP, TCGA, prognosis, biomarker 3

OPEN ACCESS

Edited by:
Veronica Aran,
Instituto Estadual do Cérebro Paulo Niemeyer (IECPN), Brazil

Reviewed by:
Pooja Panwalkar,
Weill Cornell Medicine, United States
Jasminka Omerovic,
University of Split, Croatia

****Correspondence:***
Anita Chopra
chopraanita2005@gmail.com
Shyam S. Chauhan
s_s_chauhan@hotmail.com

†These authors have contributed equally to this work

Specialty section:
This article was submitted to Molecular Diagnostics and Therapeutics, a section of the journal Frontiers in Molecular Biosciences

Received: *08 March 2021*
Accepted: *26 May 2021*
Published: *21 June 2021*

Citation:
Kumari S, Arora M, Singh J, Kadian LK, Yadav R, Chauhan SS and Chopra A (2021) Molecular Associations and Clinical Significance of RAPs in Hepatocellular Carcinoma. Front. Mol. Biosci. 8:677979. doi: 10.3389/fmolb.2021.677979

INTRODUCTION

Hepatocellular carcinoma (HCC) is the sixth leading cancer in incidence and the fourth most common cause of cancer mortality in the world (Bray et al., 2018). It is the most common type of primary liver cancer that usually arises on the background of chronic liver disease, hepatitis B or C virus infection, or nonalcoholic steatohepatitis (Bruix et al., 2011; Villanueva, 2019). For locally advanced cancers without cirrhosis, the 5-years survival rate of patients is only 36–70% and 60–70% with successful surgical resection or liver transplantation, respectively. Further, postoperative recurrence and metastasis are common in HCC, which pose a challenge in the management of this disease. Therefore, biomarkers to predict prognosis in HCC are highly needed. The common indicators of prognosis of HCC include tumor size, degree of cirrhosis, tumor differentiation and microvascular invasion (Villanueva, 2019). The recent emergence of high throughput sequencing data by multiple studies has enabled researchers to describe molecular features of HCC in detail and has provided several potential biomarkers for the prediction of patient prognosis (Wheeler and Roberts, 2017).

RAP proteins (Ras proximate proteins) are members of the Ras GTP binding family sharing 50–60% sequence homology with the Ras family. The diversity and specificity of Ras and RAP proteins are contributed by different sets of GEFs (guanine nucleotide exchange factors) and GAPs (GTPase-activating proteins). Five different genes of the RAP family, RAP1A, RAP1B, RAP2A, RAP2B, and RAP2C have been identified in the human genome (Bokoch, 1993). RAP proteins primarily function in cell adhesion, migration, and polarity (Bokoch, 1993; Ehrhardt et al., 2002; Di et al., 2015b; Qu et al., 2016; Meng et al., 2018). The effect of RAP activation depends on the context-specific interaction of RAP with their regulators and downstream effectors.

Oncogenic functions of RAP proteins have been well established in multiple cancer types, such as breast (Di et al., 2015a), lung (Fu et al., 2009; Wu et al., 2014; Xie et al., 2015; Peng et al., 2016), ovary (Che et al., 2015; Lu et al., 2016), stomach (Zhang J. et al., 2020), cervix (Li et al., 2018), prostate (Bigler et al., 2007) and brain (Wang et al., 2017). Accumulating evidence suggests that RAP proteins also play critical roles in hepatocellular carcinogenesis and tumor progression. Single nucleotide polymorphism (SNPs) in RAP1A gene rs494453 has been shown to associate with higher incidence and recurrence after liver transplantation (Mo et al., 2018; Zhang R. et al., 2020). Further, higher activity of the NF-κB/RAP1 signaling pathway is associated with tumorigenicity in HCC cells (Mo et al., 2018). Some studies have also provided strong links between RAP1A expression and liver inflammation, a risk factor for liver carcinogenesis. RAPGEF1, the GEF for RAP1A has also been shown to be overexpressed in HCC (Sequera et al., 2018). A previous study reported that HBV replication promotes liver carcinogenesis through upregulation of RAP1B (Sheng et al., 2014). Further, overexpression of RAP1B enhances the proliferation and migration of HCC cells by regulating Twist-1 gene expression (Tang et al., 2018). Overexpression of RAB2B has also been reported in HCC and its inhibition reduces cell proliferation and invasion (Zhang et al., 2017). Recently, Zheng et al. reported that HCC tissues exhibit significantly higher mRNA and protein expression of RAP2A, which is associated with tumor size, metastasis, pathological differentiation, and vascular invasion (Zheng et al., 2017). Furthermore, they also demonstrated that higher protein levels of RAP2A are independently associated with poor overall survival in HCC.

While the current literature suggests that RAP genes might play critical roles in the pathophysiology of HCC, these studies are limited by determining individual genes of the RAP signaling pathway, limited number of clinical samples used in different studies. Further, studies focused on determining the association of RAP genes with genetic alteration and molecular alterations remain limited. In the current study, we utilized authoritative multi-omics databases to determine the association of RAP gene family expression and detailed molecular and clinicopathological features. Furthermore, we also determined their association with multiple survival parameters to determine their prognostic value.

TABLE 1 | Patient charcterstics in TCGA-LIHC dataset.

Characterstics		Total (370)	%
Age (years)	≤50	75	20.67
	>50	288	79.33
Gender	Male	245	67.30
	Female	119	32.7
Stage	I + II	253	73.76
	III + IV	90	26.24
Grade	I + II	227	63.23
	III + IV	132	36.77
AFP levels	⩽ 400	212	76.81
	> 400	64	23.19
History of alcohol consumption	No	233	66.57
	Yes	117	33.43
Postoperative ablation embolization	No	317	91.88
	Yes	28	8.12
Radiation therapy	No	336	97.67
	Yes	8	2.33
TP53 mutation	No	252	70.19
	Yes	107	29.81
CTNNB1 mutation	No	266	74.09
	Yes	93	25.91
PCLO mutation	No	320	89.13
	Yes	39	10.87
ALB mutation	No	315	87.74
	Yes	44	12.26

MATERIALS AND METHODS

Data Retrieval

For mRNA expression analysis, RNA seq data of TCGA-LIHC dataset, which was originally sourced from Broad GDAC Firehose (http://gdac.broadinstitute.org/) (Wheeler and Roberts, 2017) was extracted using UCSC XENA webserver (Goldman et al., 2020). Clinicopathological and molecular characterstics of the TCGA-LIHC dataset has been given in **Table 1**. Microarray gene expression data from multiple studies was accessed through the TNMplot webserver (Bartha and Győrffy, 2020). This web server hosts data from multiple HCC studies, where gene expression data has been normalized for all available studies and can be used for comparison between the collective groups of all normal samples with tumor samples. Multi-Omics dataset of hepatocellular carcinoma released by Clinical Proteomic Tumor Analysis Consortium (CPTAC) (https://cptac-data-portal.georgetown.edu/cptacPublic/) was utilized to analyze both mRNA and protein levels of RAP genes.

DNA Methylation Analysis

DNA methylation of RAP genes in TCGA cancer dataset was estimated and visualized using MEXPRESS web server (https://mexpress.be) (Koch et al., 2015; Koch et al., 2019) and TCGA Wanderer (Díez-Villanueva et al., 2015). The MEXPRESS web server uses DNA methylation data of cancer and normal tissues from TCGA datasets, which were originally developed on the Illumina Human Methylation 450 BeadChip platform. The predesignated methylation probes for each gene were taken into consideration.

Survival Analysis

Kaplan-Meier survival analysis was performed using the tool available in the KM-plotter (Nagy et al., 2018). For Kaplan-Meier analysis, patients were distributed in high and low expression groups based on median expression value as a cut-off point for each gene. For survival analysis using univariate and multivariate Cox proportionate hazard model, RAP2A gene expression was taken as a continuous variable with multiple survival parameters for the TCGA-LIHC dataset, as recommended (Liu et al., 2018).

Correlation and Pathway Enrichment Analysis

Similarly, whole transcriptome correlations of RAP2A in the TCGA-LIHC study were downloaded from the cBioPortal website (https://www.cbioportal.org/) (Cerami et al., 2012; Gao et al., 2013). After applying a filter for a cutoff of FDR corrected p-value of 0.05 for Spearman's r-value, 10,980 genes with Spearman's correlation q value <0.05 were filtered and used for gene set enrichment analysis in GSEA software (Broad Institute, http://www.broad.mit.edu/gsea/). Hallmark gene set (version 7.1) (Subramanian et al., 2005) from predefined molecular signature database was used as a reference gene set for pathway enrichment (Liberzon et al., 2015).

Tumor Immunity Associations

Tumor immune estimation score (TIMER) webserver (https://cistrome.shinyapps.io/timer/), which utilizes the RNA sequencing data from TCGA for estimation of correlation between gene expression and level of immune cells, present in the tumor samples (Li et al., 2017). We utilized TIMER to calculate the association between RAP2A gene expression with infiltration of six immune cells including B cells, CD4+ T cells, CD8+ T cells, neutrophils, macrophages, and dendritic cells in TCGA-LIHC datasets. Default parameters were used in the TIMER database for the gene-specific analysis module.

Further, CIBERSORT (Cell-type Identification By Estimating Relative Subsets Of RNA Transcripts) analysis data of TCGA-LIHC were extracted from a previously published study (Chen et al., 2018; Thorsson et al., 2018). This provided relative fractions of 22 different immune cells from a mixture of gene expression profiles (TCGA-LIHC study) and was used to correlate with RAP2A expression using Spearman's correlation test. A total of 360 HCC samples were available with both gene expression data and CIBERSORT analysis estimated fractions of immune cells. Heatmap of the immune cell profiling data was generated along with hierarchical clustering using HemI (Deng et al., 2014). The default parameters of hierarchical clustering using the average linkage method and Pearson distance were used.

Statistical Analysis

Data analysis was performed using Graphpad (version 6) and Stata software (version 11). Mann-Whitney U-test was used for comparison among histological subtypes, molecular subtype and grades (***$p < 0.001$; **$p < 0.01$; *$p < 0.05$; ns, $p > 0.05$). Pearson correlation analysis was used to determine the association of DNA methylation of RAP2A to its expression in the TCGA-LIHC dataset. Kaplan-Meier survival analysis was performed using the log-rank test. A p-value < 0.05 was considered statistically significant.

RESULTS

Expression Pattern of RAPs in HCC

Further, RNA sequencing data from TCGA-LIHC study was utilized to compare RAP gene expression in tumor tissues with both tumor adjacent normal tissues from the same dataset and with non-tumor associated normal hepatic tissue. RAP1A, RAP1B, RAP2A and RAP2B exhibited significant higher expression in tumors compared to other two groups (**Figures 1A,C,E,G**). Although RAP2C expression was higher in tumors compared to adjacent normal tissues, but both these groups exhibited lower expression of RAP2C compared to normal tissues from GTEx (**Figure 1I**). Furthermore, tumor adjacent normal tissues also exhibited higher expression of RAP1A and RAP2B, while no difference was observed for RAP1B and RAP2A. Comparison between 50 paired normal and tumor tissues from TCGA-LIHC also revealed that all RAP genes exhibit higher expression in tumor tissues compared to tumor adjacent normal tissues (**Figures 1B,D,F,H,J**). Among all RAPs, RAP2A displayed most robust upregulation in tumor tissues in TCGA dataset (**Figure 1F**). Further, we utilized multiomics data of hepatocellular carcinoma developed by CPTAC study, where both mRNA and proteomic data was available. The expression analysis in CPTAC data also suggested that expression of RAP genes differ between normal and tumor tissues both at the mRNA and protein level. In CPTAC data also, RAP2A exhibited most robust upregulation of mRNA and protein levels in tumor tissues compared to normal tissues, while expression of RAP2C was found to be reduced in tumor tissues compared to normal tissues (**Supplementary Figure S1**).

We further performed receiver operating characteristic (ROC) curve analysis to determine potential of RAP gene expression in differentiating tumor tissues from normal liver tissues. Interestingly, among five RAP genes, RAP2A exhibited highest area under curve (AUC) of 0.8676 in TCGA-LIHC mRNA data (**Figure 2A**). Similarly, analysis of CPTAC mRNA data also suggested highest AUC of RAP2A (AUC: 0.9173, **Figure 2B**) compared to other RAP genes. Interestingly, analysis of AUC in CPTAC protein expression data revealed that RAP2C exhibit highest AUC of 0.8445 followed by RAP2A with AUC of 0.8172 (**Figure 2C**).

Furthermore, expression data of RAP gene family in hepatocellular carcinoma tissues and normal tissues from multiple other datasets was assessed through TNMplot web server. The analysis revealed that RAP1A, RAP1B, RAP2A, and RAP2B genes exhibit significantly higher expression in HCC tissues compared to normal tissues in comparison of both available paired (**Supplementary Figure S2**, left panel) and unpaired tissues (**Supplementary Figure S2**, right panel). However, RAP2C did not exhibit significant difference in expression in paired tissue analysis (**Supplementary Figures S2J**). Considering robust upregulation of RAP2A in tumors,

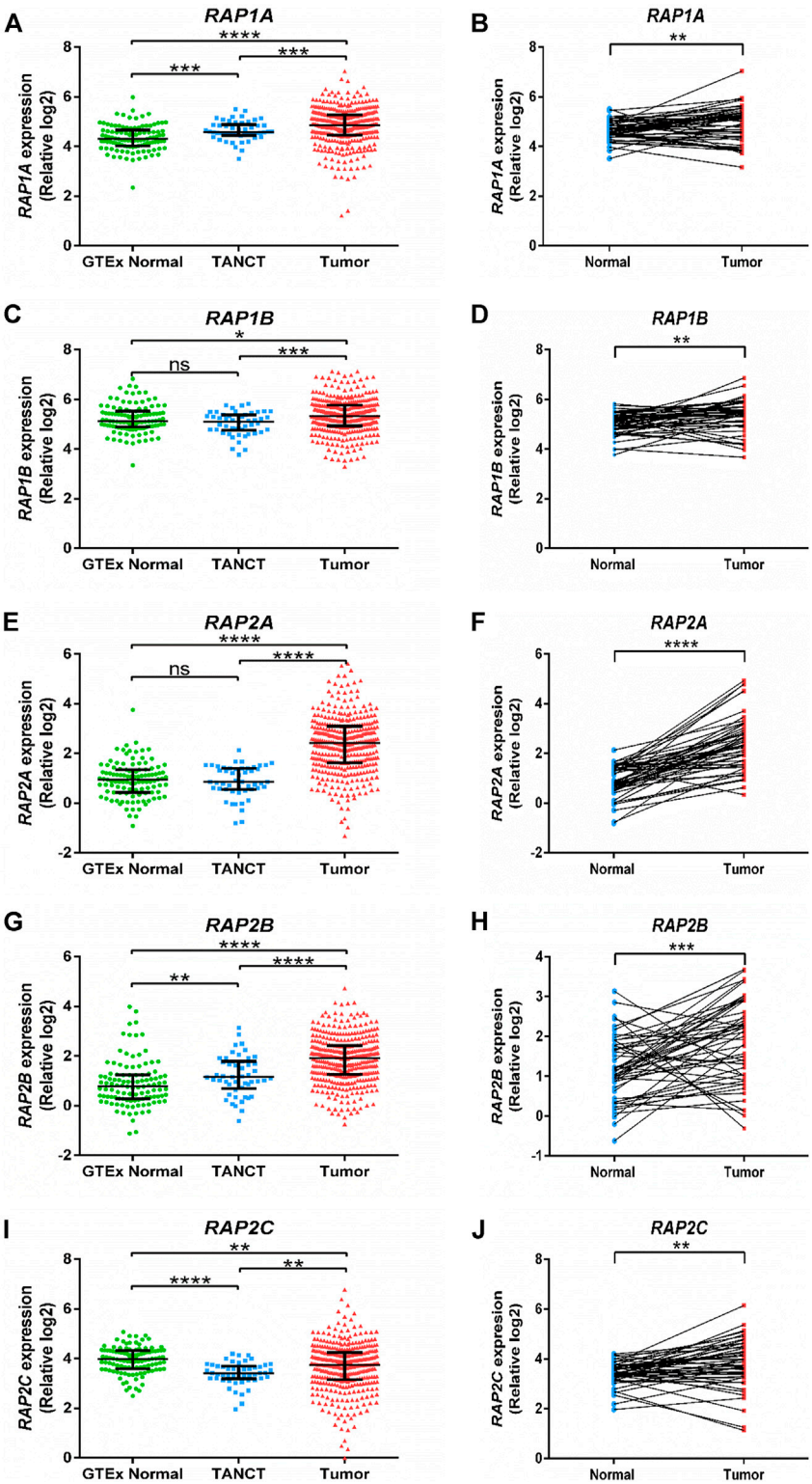

FIGURE 1 | Expression of RAP genes in tumor tissues compared with adjacent normal tissues and normal tissues from GTEx study. GTEx, Genotype-Tissue Expression project; TANCT, tumor adjacent non-cancerous tissue. ****$p < 0.0001$; ***$p < 0.001$; **$p < 0.01$; *$p < 0.05$; ns, $p > 0.05$.

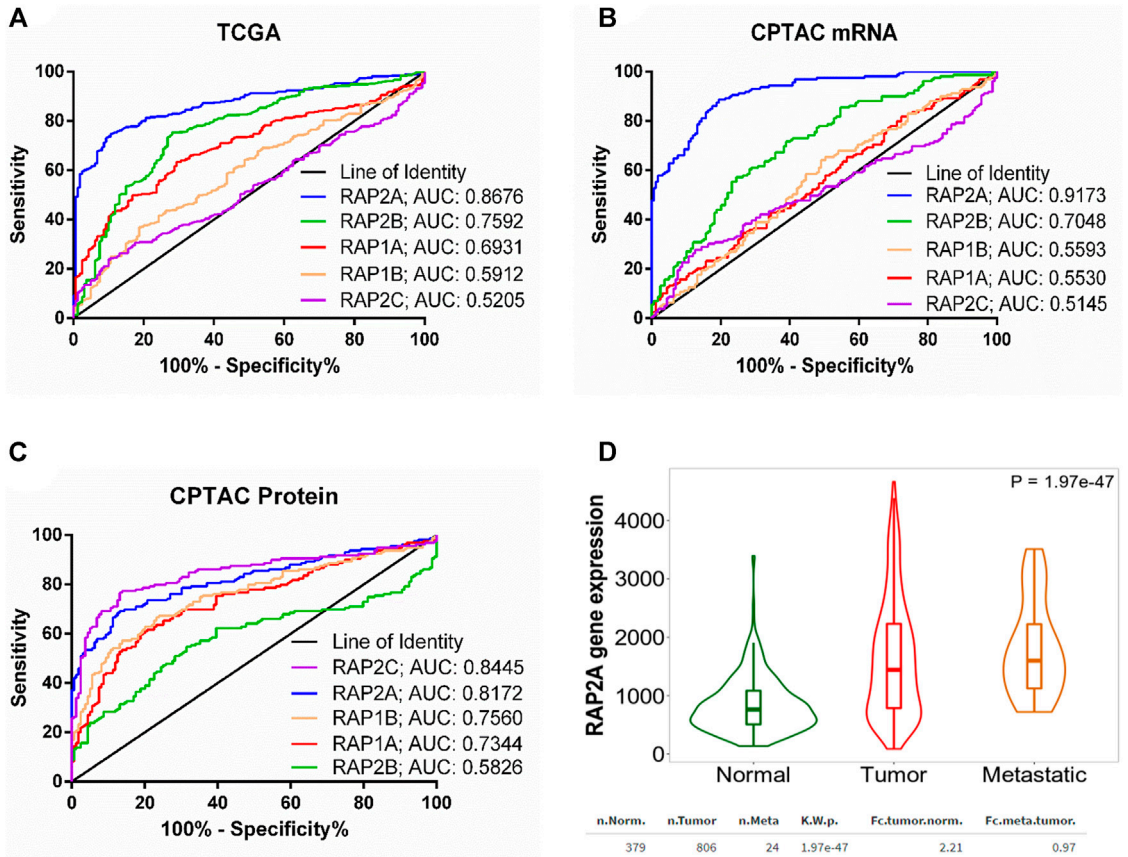

FIGURE 2 | (A) ROC curve for the utility of RAP gene expression to differentiate between liver tumor tissues and normal tissue group in **(A)** TCGA mRNA data **(B)** CPTAC mRNA data, and **(C)** CPTAC protein expression data. For **(A)**, normal tissue group consisted of tumor-adjacent normal tissues from TCGA study and normal tissues from non-disease controls from the GTEx study. **(D)** Comparison of RAP2A gene expression among normal tissue, tumor tissue, and metastatic tissues assessed through TNM webtool.

and its established involvement in cell migration, we compared expression of RAP2A in metastatic tissues with both normal and primary tissues, which revealed highest expression of RAP2A in metastatic tissues compared to other two groups (**Figure 2D**).

Association of RAP Family Expression and Clinicopathological Features in HCC

We further assessed the association of RAP genes with clinicopathological including pathological age, gender, stage, tumor grade, blood *AFP* levels. Among all RAP genes, higher expression of RAP1B was associated with advanced-stage (**Figure 3A**). Higher expression of RAP2A and RAP2B, and low expression of RAP1A was associated with advanced grade (**Figure 3B**). High RAP2A expression was associated with younger age (<50 years, **Supplementary Figure S3A**) and female gender (**Supplementary Figure S3B**). Higher expression of RAP2A was also associated with increased AFP levels (**Figure 4A**). A history of alcohol consumption was associated with lower levels of RAP2A and RAP2C expression (**Figure 4B**).

Association of RAP Family Expression and Genetic and Epigenetic Alterations in HCC

To further determine whether the expression of RAP genes is associated with genetic alterations in HCC, we compared their expression in tumors with mutated or wild type *TP53*, *CTNNB1*, *ALB*, *PCLO*, and *LRP1B*. *TP53* mutation was observed to be associated with higher expression of RAP1A, RAP1B, RAP2A, and RAP2B (**Figure 5A**). Further, *CTNNB1* mutation was significantly associated with reduced levels of RAP1B, RAP2A, and RAP2B expression (**Figure 5B**). No RAP gene exhibited association with *PCLO* and *ALB* mutation status (**Supplementary Figures S4A,B** respectively), while higher expression of RAP1A was associated with *LRPB1* mutant tumors (**Supplementary Figure S5**).

To determine the potential role of copy number alterations and DNA methylation in the regulation of RAP2A expression in HCC, we utilized a TCGA-LIHC study where copy number variation, DNA methylation, and gene expression data were available. The DNA methylation data in TCGA study was developed on "Illumina HumanMethylation450 Beadchip" platform, where representative CpG sites from different regions of most genes

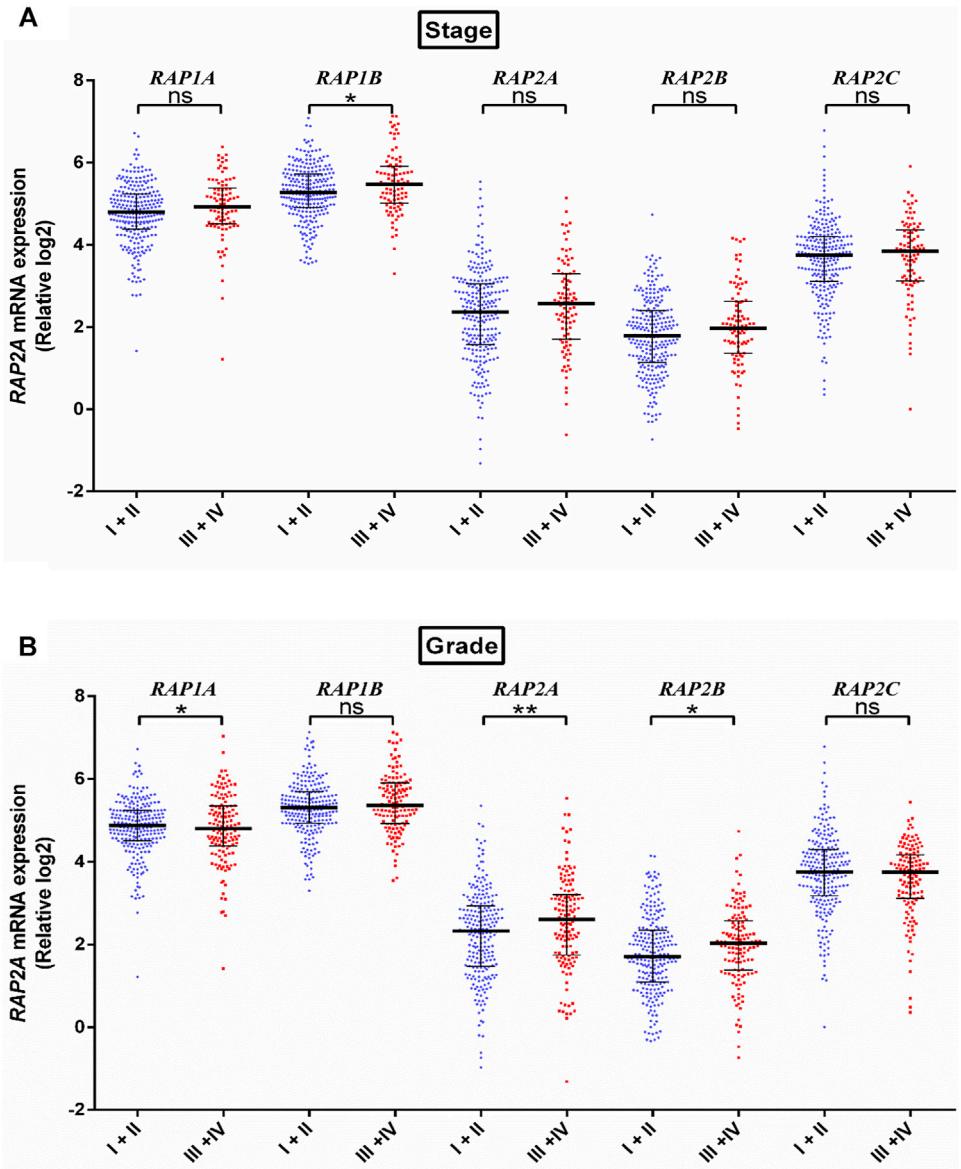

FIGURE 3 | Expression of RAP genes in tumor tissues compared between different stage **(A)** and grade **(B)**. ****$p < 0.0001$; ***$p < 0.001$; **$p < 0.01$; *$p < 0.05$; ns, $p > 0.05$.

are captured. Interestingly, RAP2A gene expression was reduced in tumor tissues and exhibited a negative correlation with DNA methylation at several sites within the RAP2A promoter regions and gene body (**Figures 6A,B**). A similar association was also observed for normal liver tissues (**Supplementary Figure S6**). We observed that in both normal and tumor tissues, DNA methylation at an intragenic region represented by cg03608515 was most negatively correlated with gene expression, suggesting this region, but not promoter region is the major regulatory site for the expression (**Figure 6C**). Furthermore, a comparison of 47 paired normal and tumor tissue also revealed significantly reduced methylation levels of cg03608515 in tumor tissues., these results strongly suggest the role of DNA methylation in aberrant expression of RAP2A in HCC. Additionally, the expression of RAP2A was also positively correlated with its copy number (r = 0.450, $p < 0.001$). Further, analysis of CNV data revealed frequent alterations in RAP2A copy number in HCC tissues was associated with its higher expression with copy number gain (**Figure 6D**, Kruskal-Wallis test, $p < 0.0001$).

Prognostic Significance of RAP Genes in Hepatocellular Carcinoma

To determine the association of RAP gene family expression with patient prognosis, we utilized the TCGA-LIHC dataset where information for overall survival (OS), disease-specific survival

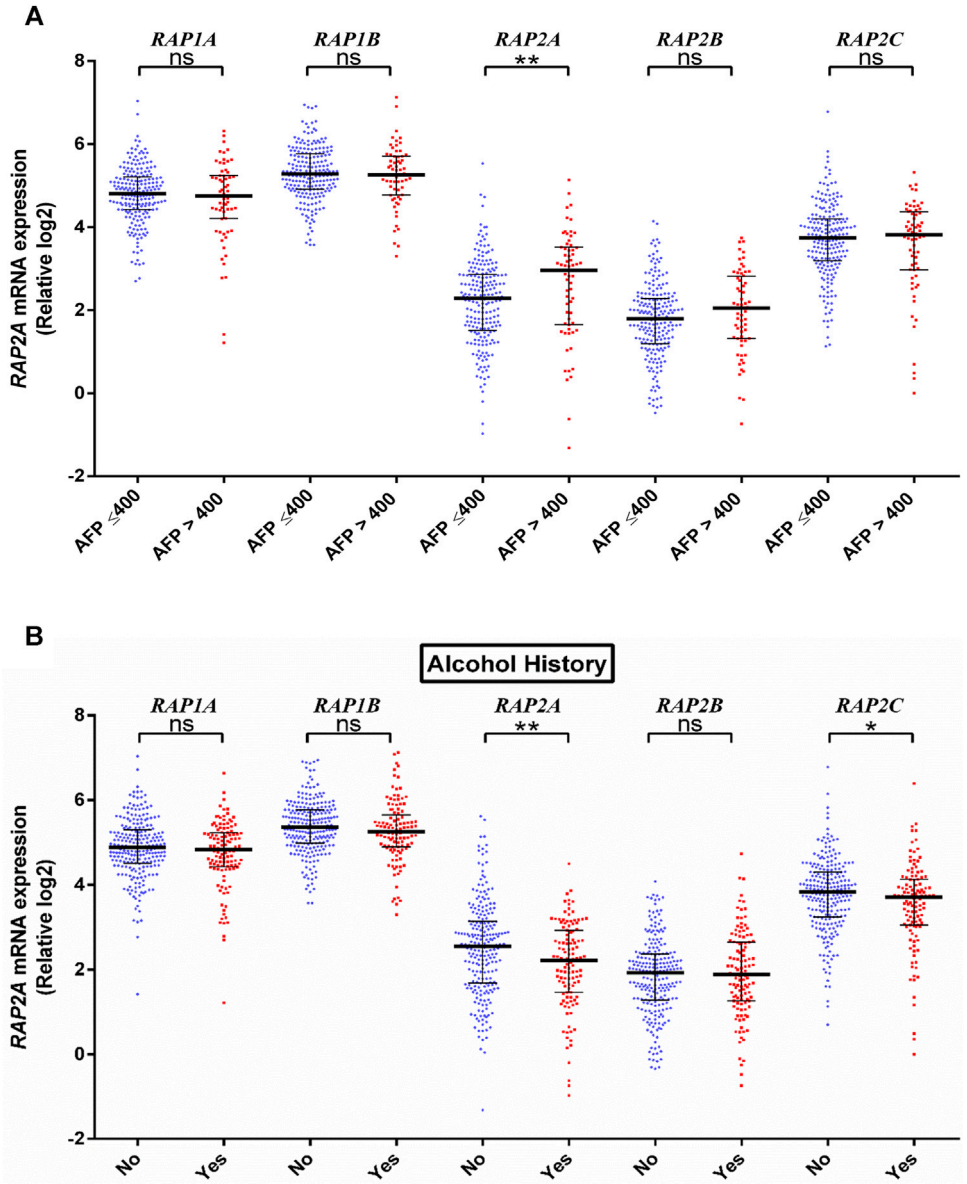

FIGURE 4 | Association of RAP expression in TCGA-KIRC dataset with **(A)** AFP levels, and **(B)** alcohol history. ****$p < 0.0001$; ***$p < 0.001$; **$p < 0.01$; *$p < 0.05$; ns, $p > 0.05$.

(DSS), disease-free interval (DFI), and progression-free interval (PFI) was available. We performed survival analysis by constructing a Kaplan-Meier plot for all RAP genes using median expression levels for allotting patients into high and low groups. We observed that higher expression of RAP2A was significantly associated with poor OS (HR = 1.72, CI = 1.21–2.45, $p = 0.0023$, **Figure 7A**) and DSS (HR = 1.9, CI = 1.2–2.99, $p = 0.005$, **Figure 7B**), while no significant association was observed with DFI and PFI (**Figures 7C,D**, respectively). In light of the high positive correlation of RAP2A with other RAP genes, we also assessed their association with patient survival (**Supplementary Figure S7**). Among other RAPs, higher expression of RAP1A and RAP1B was also associated with poor overall survival (**Supplementary Figures S7A,B**). We further performed univariate and multivariate survival analysis for RAP2A expression and other clinicopathological features, such as age, gender, stage, grade, alcohol intake history, radiotherapy status, and embolization status using Cox proportionate hazard model. Interestingly, higher RAP2A expression was also associated with poor OS, DSS, and PFI in both univariate and multivariate survival analysis (**Tables 2**,

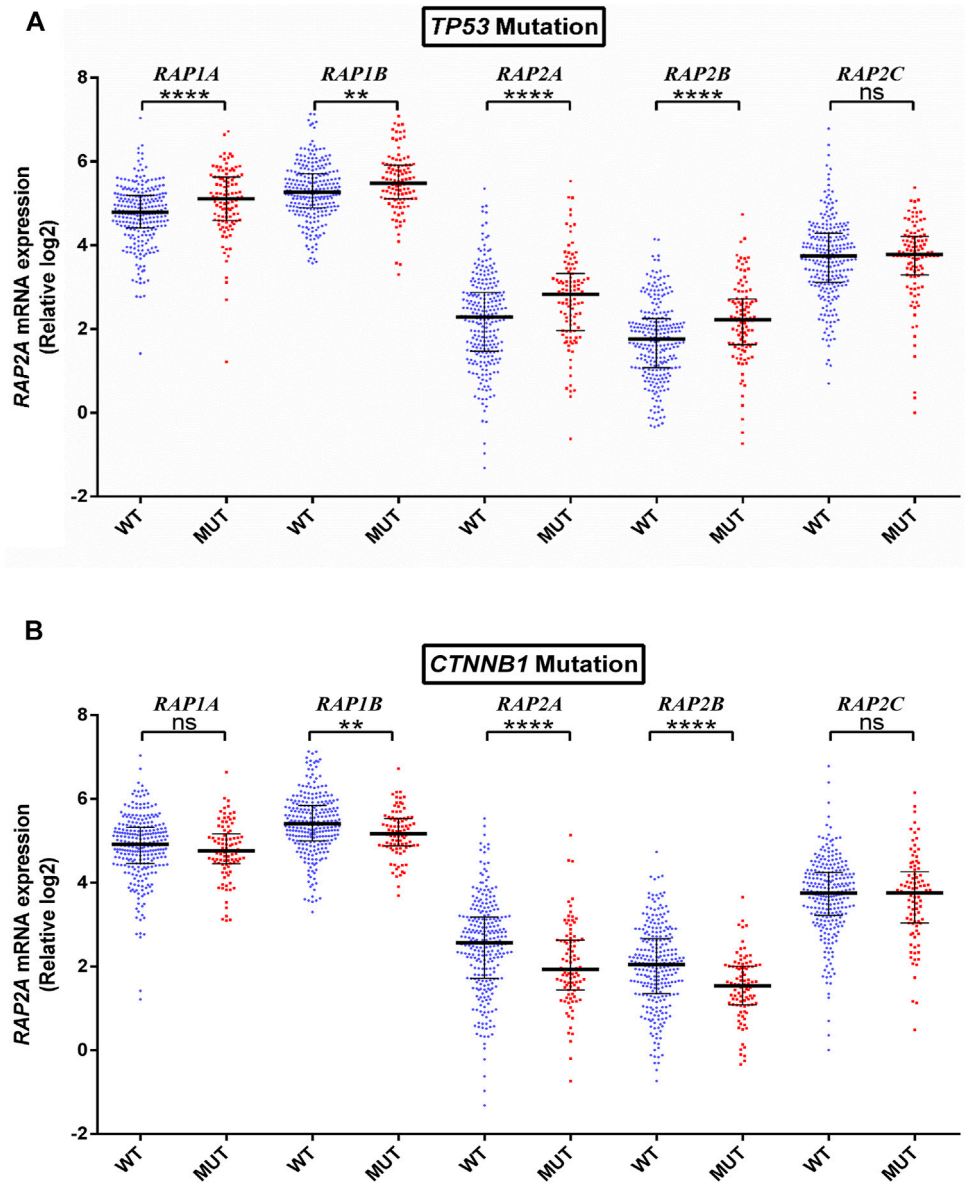

FIGURE 5 | Association of RAP expression in TCGA-KIRC dataset with **(A)** TP53 mutation, and **(B)** CTNNB1 mutation. ****$p < 0.0001$; ***$p < 0.001$; **$p < 0.01$; *$p < 0.05$; ns, $p > 0.05$.

3, respectively). This suggested that RAP2A expression is independently associated with poor outcome in HCC patients.

RAP2A Associated Cellular Pathways in Hepatocellular Carcinoma

To determine RAP2A associated cancer-related pathways, gene expression data of the TCGA-LIHC study was used. GSEA analysis revealed that RAP2A expression is positively correlated with cell cycle associated pathways such as mitotic spindle (**Figure 8A**), G2M checkpoint (**Figure 8B**), and E2F targets (**Figure 8C**) besides protein secretion (**Figure 8D**). Further, negatively correlated genes were enriched in metabolism associated pathways, such as oxidative phosphorylation (**Figure 8E**), xenobiotic metabolism (**Figure 8F**), fatty acid metabolism (**Figure 8G**), bile acid metabolism (**Figure 8H**), adipogenesis (**Figure 8I**), reactive oxygen species (**Figure 8J**) and others such as coagulation (**Figure 8K**), peroxisome (**Figure 8L**), interferon-alpha response (**Figure 8M**), DNA repair (**Figure 8N**) and Myc target genes (**Figure 8O**).

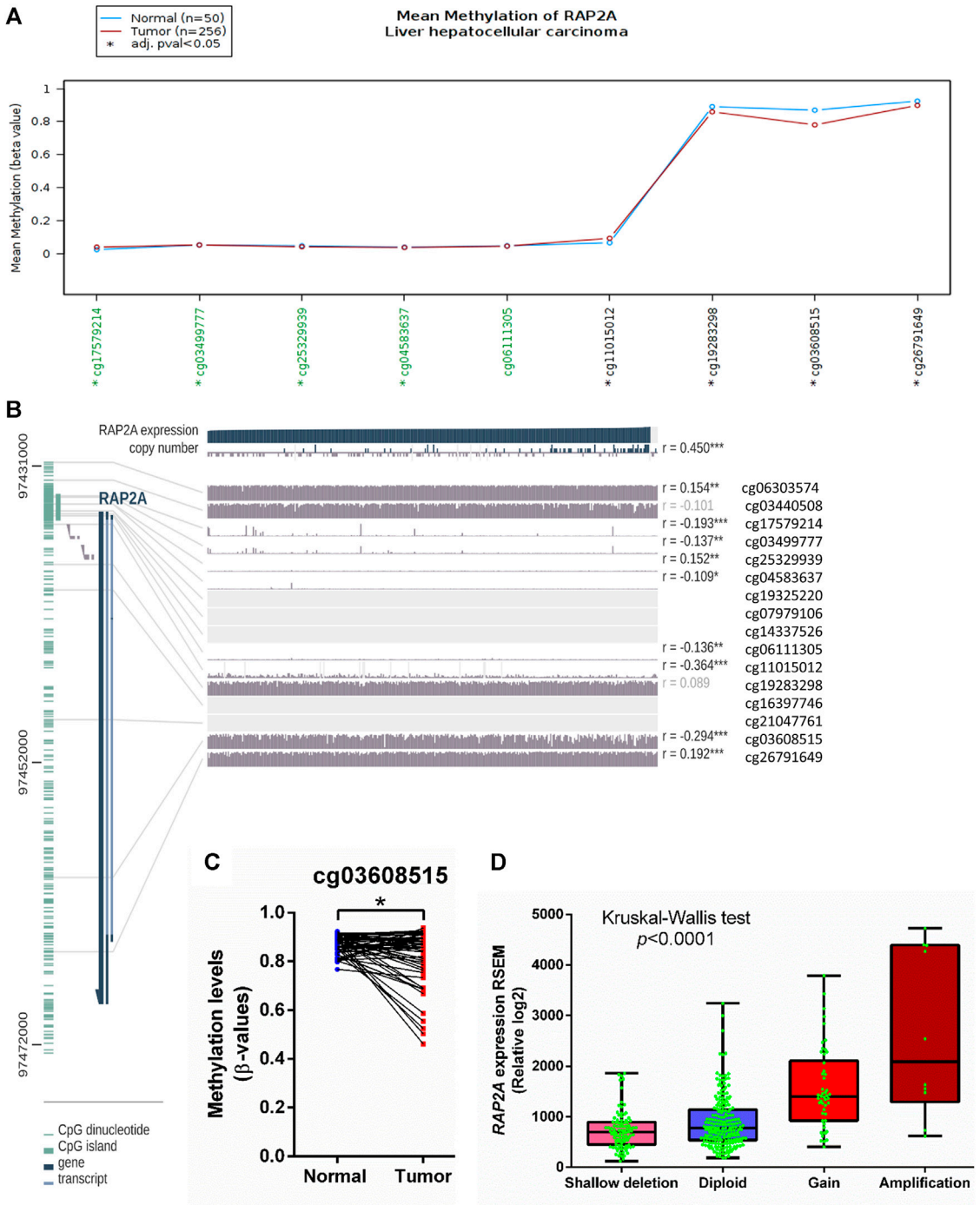

FIGURE 6 | Association of mRNA expression of RAP2A with its copy number variation and DNA methylation in TCGA-LIHC dataset. **(A)** Comparison of DNA methylation level of RAP2A between tumor tissues and normal tissues. **(B)** Correlation of RAP2A mRNA expression of RAP2A with its copy number variation and DNA methylation in tumor tissues. **(C)** Comparison of DNA methylation level of RAP2A at an intragenic site associated probe cg03608515. **(D)** Comparison of RAP2A gene expression among different copy number based groups in TCGA-LIHC dataset. ***$p < 0.001$; **$p < 0.01$; *$p < 0.05$. Insignificant associations ($p > 0.05$), are faded.

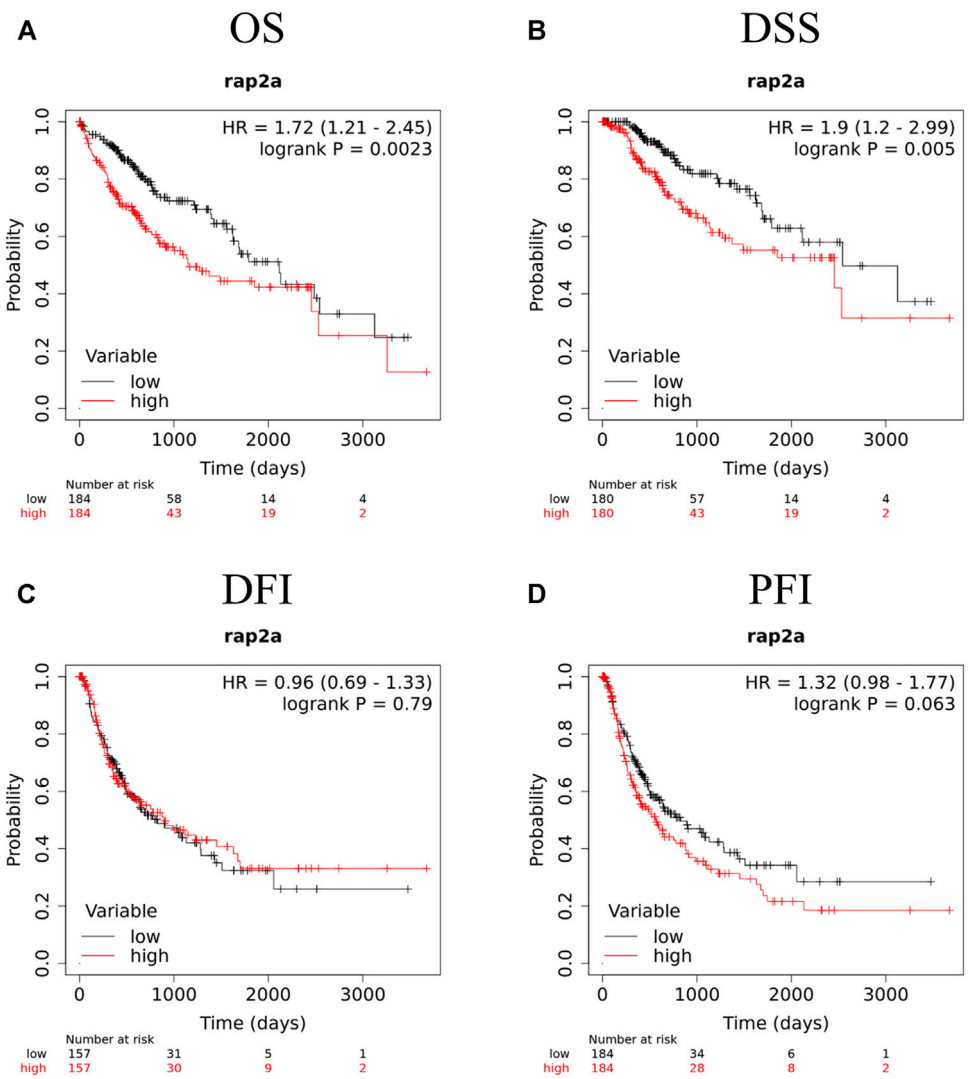

FIGURE 7 | Kaplan-Meier survival analysis of RAP2A in TCGA-LIHC dataset, including **(A)** OS, overall survival **(B)** DSS, disease specific survival **(C)** DFI, disease free interval and **(D)** PFI, progression free interval. HR, hazard ratio; ****$p < 0.0001$; ***$p < 0.001$; **$p < 0.01$; *$p < 0.05$; ns, $p > 0.05$.

Association of RAP2A Expression With Tumor Immunity

Considering the previously described role of RAP genes in immune cell functions (Carvalho et al., 2019a), we analyzed the association of RAP2A expression with the level of immune cell infiltration. Using the TIMER tool, we determine tumor purity normalized spearman correlation of RAP2A expression with infiltration level of six different immune cells. This analysis revealed a positive correlation between RAP2A expression with B cells (r = 0.3, p = 1.37e-08), CD8+ T cells (r = 0.237, p = 9.06e-06), CD4+ T cells (r = 0.474, p = 1.16e-20), macrophages (r = 0.469, p = 4.56e-20), neutrophils (r = 0.374, p = 7.19e-13), and dendritic cells (r = 0.401, p = 1.36e-14) in HCC (**Figure 9A**). Furthermore, we utilized CIBERSORT analysis to determine the association of RAP2A gene expression with the relative abundance of 22 different types of immune cells in the TCGA-LIHC dataset (**Figure 9B**, **Supplementary Table S2**). Among immune cells, RAP2A expression was positively correlated to CD4 Memory Resting T cells, resting dendritic cells, neutrophils, M0 type macrophages, and naïve B cells, while it exhibited negative correlations to monocytes, activated NK cells, CD4 naïve T cells, CD8 T cells.

DISCUSSION

HCC is one of the leading causes of cancer-related deaths worldwide. Significant advancement has been made in the treatment of this malignancy over the past decade, however, clinical response is highly heterogeneous. Further, treatment strategies have been highly adapted to be based on the progression of the disease at the time of diagnosis.

TABLE 2 | Univariate analysis for association of RAP2A expression with patient prognosis in HCC.

	OS			DSS			DFI			PFI		
	Haz. ratio	**P**	**[95% Conf. interval]**	**Haz. ratio**	**P**	**[95% Conf. interval]**	**Haz. ratio**	**P**	**[95% Conf. interval]**	**Haz. ratio**	**P**	**[95% Conf. interval]**
Age	1.014	0.056	1.000–1.028-	1.007	0.419	0.990–1.025	0.998	0.742	0.985–1.011	0.996	0.449	0.984–1.007
Gender	1.229	0.259	0.859–1.758	1.243	0.353	0.786–1.965	0.891	0.525	0.625–1.272	1.072	0.662	0.785–1.465
Stage 1		(Ref.)			(Ref.)			(Ref.)			(Ref.)	
2	1.535	0.086	0.941–2.504	1.734	0.118	0.869–3.462	1.708	0.014	1.116–2.614	1.943	0.001	1.321–2.857
3	2.728	0.000	1.774–4.193	4.169	0.000	2.342–7.424	2.829	0.000	1.876–4.265	2.721	0.000	1.874–3.952
4	5.318	0.002	1.892–14.950	9.331	0.000	2.731–31.878	23.214	0.002	3.055–176.362	6.951	0.000	2.483–19.456
Grade 1		(Ref.)			(Ref.)			(Ref.)			(Ref.)	
2	1.269	0.387	0.740–2.175	1.316	0.443	0.653–2.653	1.489	0.156	0.859–2.582	1.189	0.451	0.758–1.865
3	1.268	0.409	0.721–2.230	1.413	0.351	0.683–2.924	1.724	0.056	0.986–3.015	1.347	0.209	0.846–2.142
4	1.514	0.458	0.507–4.519	0.689	0.724	0.088–5.411	1.002	0.998	0.291–3.446	0.920	0.877	0.320–2.647
Embolization	0.859	0.633	0.461–1.602	1.350	0.361	0.709–2.568	2.302	0.000	1.443–3.674	2.218	0.000	1.457– 3.375
Radiation	0.959	0.943	0.304–3.021	0.986	0.984	0.241–4.024	1.590	0.310	0.649–3.892	1.544	0.297	0.683–3.494
Alcohol history	1.050	0.799	0.719–1.535	1.466	0.099	0.930–2.311	1.130	0.502	0.791–1.616	1.043	0.794	0.760–1.432
RAP2A	**1.325**	**0.000**	1.132–1.550	**1.429**	**0.001**	1.166–1.750	1.099	0.216	0.946–1.276	**1.189**	**0.011**	1.040–1.359

OS, overall survival; DSS, disease-specific survival; DFI, disease-free interval; PFI, progression-free interval; HR, hazard ratio; CI, confidence interval.

TABLE 3 | Multivariate analysis for association of RAP2A expression with patient prognosis in HCC.

	OS			DSS			DFI			PFI		
	Haz. ratio	**P**	**[95% Conf. interval]**	**Haz. ratio**	**P**	**[95% Conf. interval]**	**Haz. ratio**	**P**	**[95% Conf. interval]**	**Haz. ratio**	**P**	**[95% Conf. interval]**
Age	1.028	0.003	1.009–1.047	1.009	0.410	0.987–1.032	1.002	0.809	0.986–1.018	1.000	0.982	0.987–1.013
Gender	0.971	0.899	0.611–1.542	1.136	0.679	0.622–2.073	0.873	0.540	0.564–1.349	0.980	0.918	0.662–1.449
Stage 1		(Ref.)			(Ref.)			(Ref.)			(Ref.)	
2	1.615	0.096	0.918–2.839	2.143	0.047	1.012–4.538	1.895	0.010	1.165–3.082	2.100	0.001	1.358–3.246
3	2.851	0.000	1.775–4.581	4.439	0.000	2.405–8.193	3.901	0.000	2.451–6.210	3.311	0.000	2.193–5.000
4	5.230	0.030	1.176–23.267	7.137	0.012	1.532–33.252	33.053	0.001	4.123–265.000	8.346	0.001	2.362–29.483
Grade 1		(Ref.)			(Ref.)			(Ref.)			(Ref.)	
2	1.126	0.726	0.580–2.185	1.849	0.191	0.736–4.648	1.505	0.211	0.793–2.855	1.173	0.568	0.678–2.028
3	1.323	0.418	0.672–2.603	1.837	0.209	0.712–4.741	1.837	0.067	0.957–3.527	1.224	0.484	0.695–2.154
4	1.593	0.487	0.429–5.924	1.479	0.725	0.168–13.052	0.979	0.978	0.214–4.487	0.886	0.850	0.253–3.101
Embolization	1.017	0.966	0.470–2.203	1.661	0.224	0.733–3.766	3.658	0.000	2.075–6.446	2.966	0.000	1.746–5.037
Radiation	1.057	0.928	0.319–3.498	1.031	0.967	0.239–4.448	0.996	0.993	0.388–2.556	1.185	0.698	0.503–2.789
Alcohol history	0.955	0.849	0.597–1.529	1.682	0.085	0.931–3.040	1.077	0.740	0.696–1.667	1.244	0.270	0.844–1.834
RAP2A	**1.296**	**0.011**	1.062–1.581	**1.334**	**0.028**	1.032–1.724	1.063	0.528	0.879–1.287	**1.199**	**0.037**	1.011–1.423

OS, overall survival; DSS, disease-specific survival; DFI, disease-free interval; PFI, progression-free interval; HR, hazard ratio; CI, confidence interval.

Nevertheless, several molecular biomarkers have been determined with high prognostic value and future studies are required to determine novel molecular features as therapeutic targets and prognostic biomarkers. In the current study, we uncovered distinct genomic and epigenomic features of RAP family genes in HCC. Our study revealed that among five RAP genes, RAP2A expression is highly altered in HCC and is associated with multiple oncogenic features in HCC.

Little is known about the specific roles of RAP2A; in its active form RAP2A interacts with several effectors including MINK1, TNIK, and MAP4K4 and activates various signaling pathways involved in cytoskeletal rearrangements, cell migration, cell adhesion, and cell proliferation (Mittal and Linder, 2006). RAP2A interacts directly with upstream MAPK signaling element MAP4K4, and thus, increased RAP2A activity can enable downstream signaling (Machida et al., 2004). So far, the role of RAP2A in human malignancies remains controversial, with some suggesting it as a tumor suppressor gene while other studies refer to it as an oncogene. Upregulation of RAP2A has been observed in several human malignancies such as follicular thyroid cancer (Prabakaran et al., 2011), prostate cancer (Bigler et al., 2007), renal cancer (Wu et al., 2017), gastric cancer (Zhang J. et al., 2020) and bladder cancer (Wang et al., 2020).

In prostate cancer cells, RAP2A promotes androgen hypersensitivity and cell growth (Bigler et al., 2007). In lung cancer cells, ectopic expression of RAP2A enhances the migration and invasion of the cells (Wu et al., 2014). In bladder cancer cells, the expression of RAP2a was found significantly higher as compared to normal cells. The proliferation and invasion of cells were repressed by miR-3127 through directly targeting

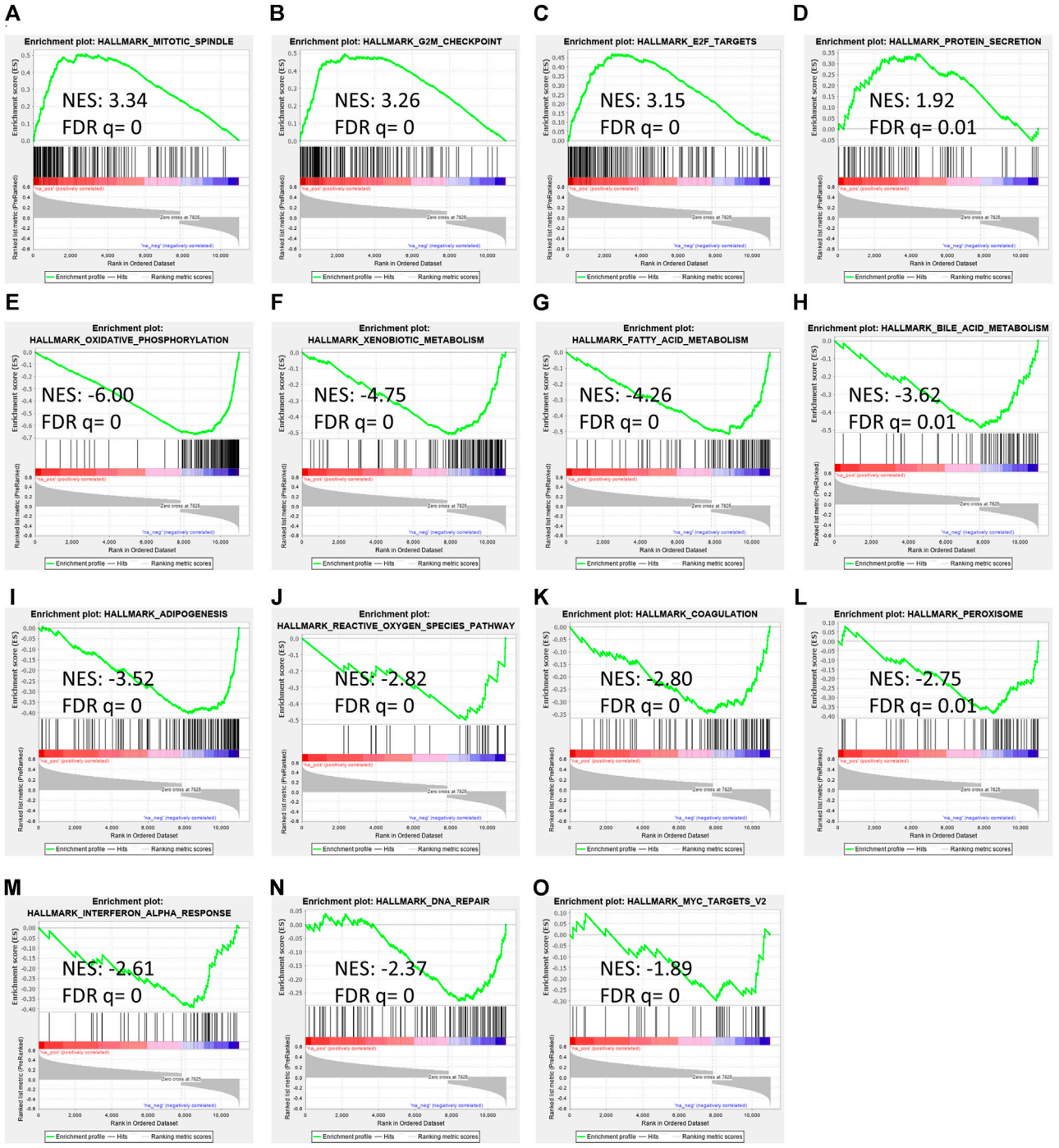

FIGURE 8 | Gene set enrichment analysis of RAP2A correlated genes in TCGA-LIHC dataset. **(A–D)** depicts positively enriched pathways **(E–L)** depicts negatively enriched pathways with normalized enrichment score (NES), false discovery rate (FDR), and *p*-value depicted inside the respective pathway.

the 3′-UTR of RAP2A and associated with poor overall survival in bladder cancer patients (Wang et al., 2020). In gastric cancer, the role of RAP2A was also observed in drug resistance where expression of RAP2A increased the viability, migration, and metastasis of cells by suppressing apoptosis and DNA damage (Zhang J. et al., 2020). In renal cancer, overexpression of RAP2A enhances the protein levels of p-Akt and promotes migration and invasion of cells by increasing p-Akt expression (Wu et al., 2017). Contrary to these, RAP2A seems to play tumor suppressor functions in glioma as its downregulation is associated with glioma progression and its inhibition in the glioma cell line reduces migration and invasion (Wang et al., 2014). Results of

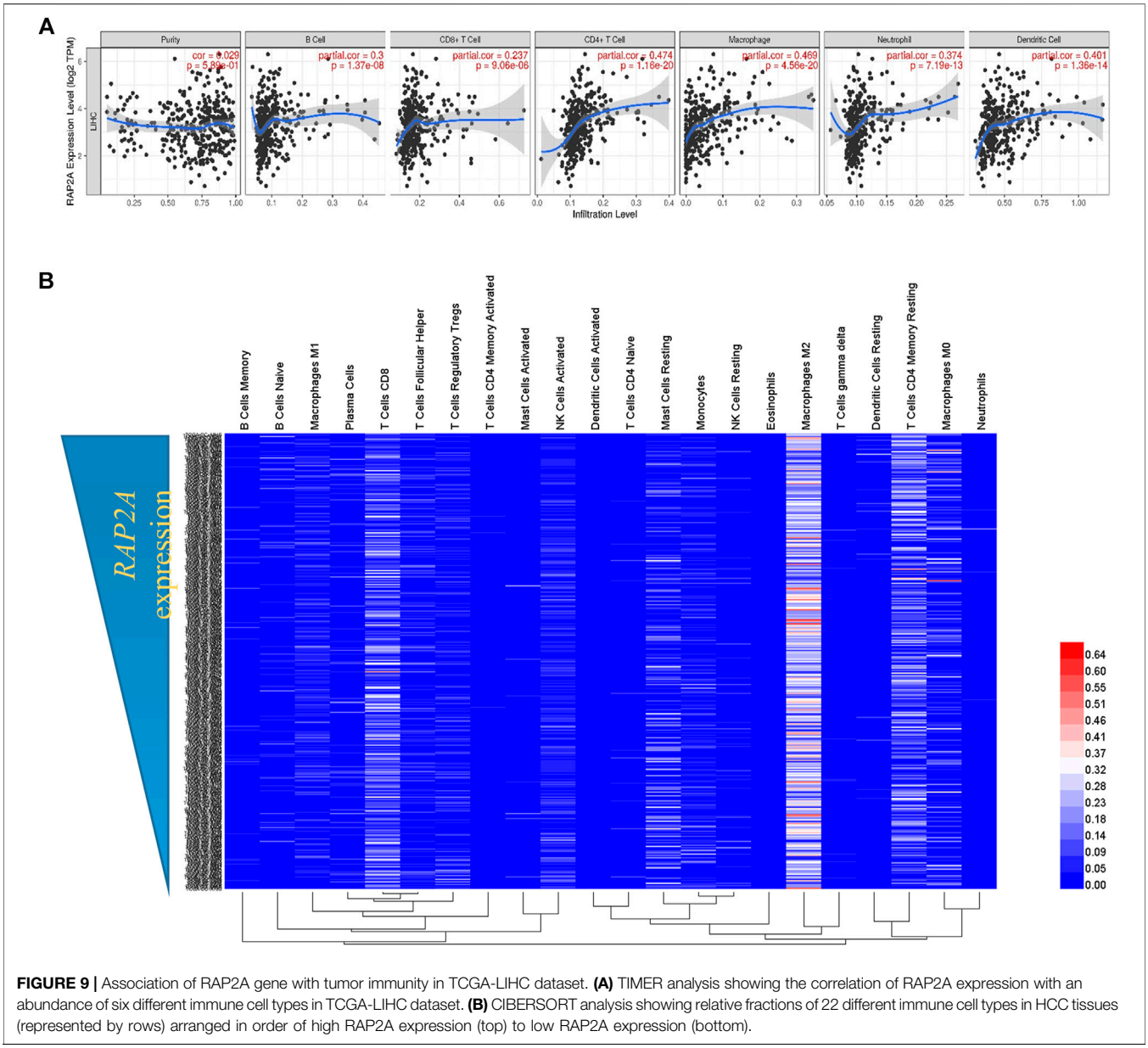

FIGURE 9 | Association of RAP2A gene with tumor immunity in TCGA-LIHC dataset. **(A)** TIMER analysis showing the correlation of RAP2A expression with an abundance of six different immune cell types in TCGA-LIHC dataset. **(B)** CIBERSORT analysis showing relative fractions of 22 different immune cell types in HCC tissues (represented by rows) arranged in order of high RAP2A expression (top) to low RAP2A expression (bottom).

the current study indicate that in hepatocellular carcinoma, RAP2A may act as an important oncogene and its mRNA expression is strongly associated with patient prognosis in HCC. Furthermore, other RAP genes also exhibit a strong positive correlation with RAP2A expression. This might be due to the conservation of regulatory sequences during evolution. We were further interested in whether RAP genes share common features for association with molecular characteristics in HCC.

It was recently demonstrated that RAP2A expression is regulated by p53 and RAP2A mediated cell migration and invasive properties are driven by downstream activation of the matrix metalloproteinases (MMP) MMP2 and MMP9 via phosphorylation of AKT (Wu et al., 2015). Consistent with this, we observed higher expression of multiple RAP genes, including RAP2A in p53 mutant HCC. Further, we also observed that expression of RAP1A, RAP1B, RAP2A, and RAP2B were reduced in HCC tissues which harbor a mutation in *CTNNB1*, the gene encoding for beta-catenin protein. This is contrary with the previous report where RAP1B has shown to activate Wnt/beta-catenin signaling in esophageal squamous cell carcinoma (Jia et al., 2017). Further, RAPGEF2, a guanine nucleotide exchange factor for RAP1, was shown to regulate adherence junction (AJ) formation in radial glial cells through ERK-mediated upregulation of β-catenin (Farag et al., 2017). While *CTNNB1* mutations in HCC are associated with higher activity of Wnt-beta catenin signaling (Tornesello et al., 2013), its association with RAP signaling appears to be negatively related in this case. Therefore, our results suggested potential crosstalk of Wnt-beta catenin signaling in RAP signaling in HCC tissues.

In light of its aberrant overexpression in HCC, we explored whether the expression of RAP2A is driven by copy number alteration and DNA methylation in HCC. Our results collectively demonstrated that the RAP2A harbors alterations in both of the abovementioned features. Our results highlighted a specific intragenic region in the RAP2A where DNA methylation was highly reduced in tumor tissues compared to normal liver tissues. Further, DNA methylation at this region is negatively correlated to RAP2A gene expression in both tumor and normal tissues. DNA methylation of RAP2A has not been previously studied in cancer, therefore, epigenetic regulation of RAP signaling requires detailed exploration.

While our study is based on mRNA expression, a recent study by, Zheng et al. has also demonstrated that RAP2A protein expression is associated with oncogenic features in HCC (Zheng et al., 2017). Therefore, our findings further provide a detailed understanding of the role of all five members of this gene family involvement in HCC. Among all five RAPs, RAP2A expression exhibited a strong ability to differentiate tumor tissues from normal tissues. Further, its higher expression also exhibited association with higher tumor grade, metastasis, increased AFP levels, and poor patient prognosis. Furthermore, our multivariate survival analysis including major clinical and pathological features revealed that the RAP2A expression is independently associated with poor overall survival, disease-specific survival, and progression-free interval in HCC.

Pathway analysis revealed strong associations of RAP2A expression in HCC with several HCC relevant pathways, including cell cycle-related pathways and metabolic pathways. Interestingly, RAP1A expression has previously been shown to be regulated during the cell cycle (Cruise et al., 1997). The causal relationship between RAP2A expression and these pathways requires further validation. We also analyzed the immunological association of RAP2A expression in HCC, which revealed that its expression is highly associated with the immune composition of HCC tumors. While, the role of RAP2A has been previously demonstrated in the regulation of lipopolysaccharide induced innate cell functions (Carvalho et al., 2019a; Carvalho et al., 2019b), detailed role of RAP2A in the modulation of tumor immunity remains to be studied in detail. Conclusively, the current study provides detailed molecular and clinical features associated with the expression of RAP genes in HCC, however, some of these associations require further exploration for the causal relationships. Further, these results support the potential of RAP2A as a therapeutic target and prognostic biomarker in this malignancy.

DATA AVAILABILITY STATEMENT

The datasets presented in this study can be found in online repositories. The names of the repository/repositories and accession number(s) can be found in the article/ **Supplementary Material**.

ETHICS STATEMENT

Ethical review and approval was not required for the study on human participants in accordance with the local legislation and institutional requirements. Written informed consent for participation was not required for this study in accordance with the national legislation and the institutional requirements.

AUTHOR CONTRIBUTIONS

Conceptualization, SC and MA; supervision and resources, SC, RY, and AC; experimentation, MA, SK, and JS; Manuscript writing, MA and LK; manuscript editing, SC, RY, and AC. All authors have approved the final version of the submitted manuscript.

ACKNOWLEDGMENTS

MA acknowledges financial support as a fellowship from the Council of Scientific and Industrial Research, Government of India. SK acknowledges financial support as a fellowship from the Department of Health Research, Government of India. JS acknowledges financial support as a fellowship from the Department of Biotechnology, Government of India.

SUPPLEMENTARY MATERIAL

The Supplementary Material for this article can be found online at: https://www.frontiersin.org/articles/10.3389/fmolb.2021.677979/full#supplementary-material

REFERENCES

Bartha, Á., and Győrffy, B. (2021). TNMplot.com: A Web Tool for the Comparison of Gene Expression in Normal, Tumor and Metastatic Tissues. *Int. J. Mol. Sci.*, 22. doi:10.3390/ijms22052622

Bigler, D., Gioeli, D., Conaway, M. R., Weber, M. J., and Theodorescu, D. (2007). Rap2 Regulates Androgen Sensitivity in Human Prostate Cancer Cells. *Prostate* 67, 1590–1599. doi:10.1002/pros.20644

Bokoch, G. M. (1993). Biology of the RAP Proteins, Members of the Ras Superfamily of GTP-Binding Proteins. *Biochem. J.* 289 (Pt 1), 17–24. doi:10.1042/bj2890017

Bray, F., Ferlay, J., Soerjomataram, I., Siegel, R. L., Torre, L. A., and Jemal, A. (2018). Global Cancer Statistics 2018: GLOBOCAN Estimates of Incidence and Mortality Worldwide for 36 Cancers in 185 Countries. *CA: A Cancer J. Clinicians* 68, 394–424. doi:10.3322/caac.21492

Bruix, J., and Sherman, M.American Association for the Study of Liver Diseases (2011). Management of Hepatocellular Carcinoma: an Update. *Hepatology* 53, 1020–1022. doi:10.1002/hep.24199

Carvalho, B. C., Oliveira, L. C., Rocha, C. D., Fernandes, H. B., Oliveira, I. M., Leão, F. B., et al. (2019a). Data in Support of RAP2A GTPase Expression, Activation and Effects in LPS-Mediated Innate Immune Response and NF-κB Activation. *Data in Brief* 24, 103965. doi:10.1016/j.dib.2019.103965

Carvalho, B. C., Oliveira, L. C., Rocha, C. D., Fernandes, H. B., Oliveira, I. M., Leão, F. B., et al. (2019b). Both knock-down and Overexpression of RAP2A Small GTPase in Macrophages Result in Impairment of NF-κB Activity and Inflammatory Gene Expression. *Mol. Immunol.* 109, 27–37. doi:10.1016/j.molimm.2019.02.015

Cerami, E., Gao, J., Dogrusoz, U., Gross, B. E., Sumer, S. O., Aksoy, B. A., et al. (2012). The cBio Cancer Genomics Portal: An Open Platform for Exploring Multidimensional Cancer Genomics Data: Figure 1. *Cancer Discov.* 2, 401–404. doi:10.1158/2159-8290.CD-12-0095

Che, Y.-L., Luo, S.-J., Li, G., Cheng, M., Gao, Y.-M., Li, X.-M., et al. (2015). The C3G/RAP1 Pathway Promotes Secretion of MMP-2 and MMP-9 and Is Involved in Serous Ovarian Cancer Metastasis. *Cancer Lett.* 359, 241–249. doi:10.1016/j.canlet.2015.01.019

Chen, B., Khodadoust, M. S., Liu, C. L., Newman, A. M., and Alizadeh, A. A. (2018). Profiling Tumor Infiltrating Immune Cells with CIBERSORT. *Methods Mol. Biol. Clifton NJ* 1711, 243–259. doi:10.1007/978-1-4939-7493-1_12

Cruise, J. L., Rafferty, M. P., and Riehle, M. M. (1997). Cell-cycle Regulated Expression of RAP1 in Regenerating Liver. *Biochem. Biophysical Res. Commun.* 230, 578–581. doi:10.1006/bbrc.1996.6003

Deng, W., Wang, Y., Liu, Z., Cheng, H., and Xue, Y. (2014). HemI: A Toolkit for Illustrating Heatmaps. *PLoS One* 9, e111988. doi:10.1371/journal.pone.0111988

Di, J., Huang, H., Qu, D., Tang, J., Cao, W., Lu, Z., et al. (2015a). RAP2B Promotes Proliferation, Migration and Invasion of Human Breast Cancer through Calcium-Related ERK1/2 Signaling Pathway. *Sci. Rep.* 5, 12363. doi:10.1038/srep12363

Di, J., Huang, H., Wang, Y., Qu, D., Tang, J., Cheng, Q., et al. (2015b). p53 Target Gene RAP2B Regulates the Cytoskeleton and Inhibits Cell Spreading. *J. Cancer Res. Clin. Oncol.* 141, 1791–1798. doi:10.1007/s00432-015-1948-8

Díez-Villanueva, A., Mallona, I., and Peinado, M. A. (2015). Wanderer, an Interactive Viewer to Explore DNA Methylation and Gene Expression Data in Human Cancer. *Epigenet. Chromatin* 8, 22. doi:10.1186/s13072-015-0014-8

Ehrhardt, A., Ehrhardt, G., Guo, X., and Schrader, J. (2002). Ras and Relatives-Job Sharing and Networking Keep an Old Family Together. *Exp. Hematol.* 30, 1089–1106. doi:10.1016/s0301-472x(02)00904-9

Farag, M. I., Yoshikawa, Y., Maeta, K., and Kataoka, T. (2017). RAPGEF2, a Guanine Nucleotide Exchange Factor for RAP1 Small GTPases, Plays a Crucial Role in Adherence junction (AJ) Formation in Radial Glial Cells through ERK-Mediated Upregulation of the AJ-Constituent Protein Expression. *Biochem. Biophys. Res. Commun.* 493, 139–145. doi:10.1016/j.bbrc.2017.09.062

Fu, G., Liu, Y., Yuan, J., Zheng, H., Shi, T., Lei, W., et al. (2009). [Identification and Functional Analysis of A Novel Candidate Oncogene RAP2B in Lung Cancer.]. *Zhongguo Fei Ai Za Zhi* 12, 273–276. doi:10.3779/j.issn.1009-3419.2009.04.03

Gao, J., Aksoy, B. A., Dogrusoz, U., Dresdner, G., Gross, B., Sumer, S. O., et al. (2013). Integrative Analysis of Complex Cancer Genomics and Clinical Profiles Using the cBioPortal. *Sci. Signaling* 6, pl1. doi:10.1126/scisignal.2004088

Goldman, M. J., Craft, B., Hastie, M., Repečka, K., McDade, F., Kamath, A., et al. (2020). Visualizing and Interpreting Cancer Genomics Data via the Xena Platform. *Nat. Biotechnol.* 38, 675–678. doi:10.1038/s41587-020-0546-8

Jia, Z., Yang, Y., Dengyan, Z., Chunyang, Z., Donglei, L., Kai, W., et al. (2017). RAP1B, a DVL2 Binding Protein, Activates Wnt/beta-Catenin Signaling in Esophageal Squamous Cell Carcinoma. *Gene* 611, 15–20. doi:10.1016/j.gene.2017.01.021

Koch, A., De Meyer, T., Jeschke, J., and Van Criekinge, W. (2015). MEXPRESS: Visualizing Expression, DNA Methylation and Clinical TCGA Data. *BMC Genomics* 16, 636. doi:10.1186/s12864-015-1847-z

Koch, A., Jeschke, J., Van Criekinge, W., van Engeland, M., and De Meyer, T. (2019). MEXPRESS Update 2019. *Nucleic Acids Res.* 47, W561–W565. doi:10.1093/nar/gkz445

Li, T., Fan, J., Wang, B., Traugh, N., Chen, Q., Liu, J. S., et al. (2017). TIMER: A Web Server for Comprehensive Analysis of Tumor-Infiltrating Immune Cells. *Cancer Res.* 77, e108–e110. doi:10.1158/0008-5472.CAN-17-0307

Li, Y., Li, S., and Huang, L. (2018). Knockdown of RAP2B, a Ras Superfamily Protein, Inhibits Proliferation, Migration, and Invasion in Cervical Cancer Cells via Regulating the ERK1/2 Signaling Pathway. *Oncol. Res.* 26, 123–130. doi:10.3727/096504017X14912172235777

Liberzon, A., Birger, C., Thorvaldsdóttir, H., Ghandi, M., Mesirov, J. P., and Tamayo, P. (2015). The Molecular Signatures Database Hallmark Gene Set Collection. *Cel. Syst.* 1, 417–425. doi:10.1016/j.cels.2015.12.004

Liu, J., Lichtenberg, T., Hoadley, K. A., Poisson, L. M., Lazar, A. J., Cherniack, A. D., et al. (2018). An Integrated TCGA Pan-Cancer Clinical Data Resource to Drive High-Quality Survival Outcome Analytics. *Cell* 173, 400–e11. doi:10.1016/j.cell.2018.02.052

Lu, L., Wang, J., Wu, Y., Wan, P., and Yang, G. (2016). RAP1A Promotes Ovarian Cancer Metastasis via Activation of ERK/p38 and Notch Signaling. *Cancer Med.* 5, 3544–3554. doi:10.1002/cam4.946

Machida, N., Umikawa, M., Takei, K., Sakima, N., Myagmar, B.-E., Taira, K., et al. (2004). Mitogen-activated Protein Kinase Kinase Kinase Kinase 4 as a Putative Effector of RAP2 to Activate the C-Jun N-Terminal Kinase. *J. Biol. Chem.* 279, 15711–15714. doi:10.1074/jbc.C300542200

Meng, Z., Qiu, Y., Lin, K. C., Kumar, A., Placone, J. K., Fang, C., et al. (2018). RAP2 Mediates Mechanoresponses of the Hippo Pathway. *Nature* 560, 655–660. doi:10.1038/s41586-018-0444-0

Mittal, V., and Linder, M. E. (2006). Biochemical Characterization of RGS14: RGS14 Activity towards G-Protein α Subunits Is Independent of its Binding to RAP2A. *Biochem. J.* 394, 309–315. doi:10.1042/BJ20051086

Mo, S.-J., Hou, X., Hao, X.-Y., Cai, J.-P., Liu, X., Chen, W., et al. (2018). EYA4 Inhibits Hepatocellular Carcinoma Growth and Invasion by Suppressing NF-κB-dependent RAP1 Transactivation. *Cancer Commun.* 38, 9. doi:10.1186/s40880-018-0276-1

Nagy, Á., Lánczky, A., Menyhárt, O., and Győrffy, B. (2018). Validation of miRNA Prognostic Power in Hepatocellular Carcinoma Using Expression Data of Independent Datasets. *Sci. Rep.* 8, 9227. doi:10.1038/s41598-018-27521-y

Peng, Y.-G., Zhang, Z.-Q., Chen, Y.-b., and Huang, J.-A. (2016). RAP2b Promotes Proliferation, Migration, and Invasion of Lung Cancer Cells. *J. Receptors Signal Transduction* 36, 459–464. doi:10.3109/10799893.2015.1122044

Prabakaran, I., Grau, J. R., Lewis, R., Fraker, D. L., and Guvakova, M. A. (2011). RAP2AIs Upregulated in Invasive Cells Dissected from Follicular Thyroid Cancer. *J. Thyroid Res.* 2011, 1–6. doi:10.4061/2011/979840

Qu, D., Huang, H., Di, J., Gao, K., Lu, Z., and Zheng, J. (2016). Structure, Functional Regulation and Signaling Properties of RAP2B. *Oncol. Lett.* 11, 2339–2346. doi:10.3892/ol.2016.4261

Sequera, C., Manzano, S., Guerrero, C., and Porras, A. (2018). How RAP and its GEFs Control Liver Physiology and Cancer Development. C3G Alterations in Human Hepatocarcinoma. *Hepatic Oncol.* 5, HEP05. doi:10.2217/hep-2017-0026

Sheng, Y., Ding, S., Chen, K., Chen, J., Wang, S., Zou, C., et al. (2014). Functional Analysis of miR-101-3p and RAP1B Involved in Hepatitis B Virus-Related Hepatocellular Carcinoma Pathogenesis. *Biochem. Cel. Biol.* 92, 152–162. doi:10.1139/bcb-2013-0128

Tang, Z., Peng, H., Chen, J., Liu, Y., Yan, S., Yu, G., et al. (2018). RAP1B Enhances the Invasion and Migration of Hepatocellular Carcinoma Cells by Up-Regulating Twist 1. *Exp. Cel. Res.* 367, 56–64. doi:10.1016/j.yexcr.2018.03.019

Thorsson, V., Gibbs, D. L., Brown, S. D., Wolf, D., Bortone, D. S., Ou Yang, T. H., et al. (2018). The Immune Landscape of Cancer. *Immunity* 48, 812–e14. doi:10.1016/j.immuni.2018.03.023

Tornesello, M. L., Buonaguro, L., Tatangelo, F., Botti, G., Izzo, F., and Buonaguro, F. M. (2013). Mutations in TP53, CTNNB1 and PIK3CA Genes in Hepatocellular Carcinoma Associated with Hepatitis B and Hepatitis C Virus Infections. *Genomics* 102, 74–83. doi:10.1016/j.ygeno.2013.04.001

Villanueva, A. (2019). Hepatocellular Carcinoma. *N. Engl. J. Med.* 380, 1450–1462. doi:10.1056/NEJMra1713263

Wang, L., Zhan, W., Xie, S., Hu, J., Shi, Q., Zhou, X., et al. (2014). Over-expression of RAP2A Inhibits Glioma Migration and Invasion by Down-Regulating P-AKT. *Cell Biol. Int.* 38, 326–334. doi:10.1002/cbin.10213

Wang, L., Zhu, B., Wang, S., Wu, Y., Zhan, W., Xie, S., et al. (2017). Regulation of Glioma Migration and Invasion via Modification of RAP2A Activity by the Ubiquitin Ligase Nedd4-1. *Oncol. Rep.* 37, 2565–2574. doi:10.3892/or.2017.5572

Wang, X., Meng, R., and Hu, Q.-M. (2020). LINC00319-Mediated miR-3127 Repression Enhances Bladder Cancer Progression through Upregulation of RAP2A. *Front. Genet.* 11, 180. doi:10.3389/fgene.2020.00180

Wheeler, D. A., and Roberts, L. R. (2017). Comprehensive and Integrative Genomic Characterization of Hepatocellular Carcinoma. *Cell* 169, 1327–e23. doi:10.1016/j.cell.2017.05.046

Wu, J., Sang, M., Cao, W., Zheng, J., and Pei, D. (2014). [Identification Analysis of Eukaryotic Expression Plasmid RAP2A and its Effect on the Migration of Lung Cancer Cells]. *Zhongguo Fei Ai Za Zhi* 17, 643–648. doi:10.3779/j.issn.1009-3419.2014.09.01

Wu, J.-X., Zhang, D.-G., Zheng, J.-N., and Pei, D.-S. (2015). RAP2A Is a Novel Target Gene of P53 and Regulates Cancer Cell Migration and Invasion. *Cell Signal.* 27, 1198–1207. doi:10.1016/j.cellsig.2015.02.026

Wu, J.-X., Du, W.-Q., Wang, X.-C., Wei, L.-L., Huo, F.-C., Pan, Y.-J., et al. (2017). RAP2A Serves as a Potential Prognostic Indicator of Renal Cell Carcinoma and Promotes its Migration and Invasion through Up-Regulating P-Akt. *Sci. Rep.* 7, 6623. doi:10.1038/s41598-017-06162-7

Xie, X., Liu, H., Wang, M., Ding, F., Xiao, H., Hu, F., et al. (2015). miR-342-3p Targets RAP2B to Suppress Proliferation and Invasion of Non-small Cell Lung Cancer Cells. *Tumor Biol.* 36, 5031–5038. doi:10.1007/s13277-015-3154-3

Zhang, L., Duan, H.-b., and Yang, Y.-s. (2017). Knockdown of RAP2B Inhibits the Proliferation and Invasion in Hepatocellular Carcinoma Cells. *Oncol. Res.* 25, 19–27. doi:10.3727/096504016X14685034103914

Zhang, J., Wei, Y., Min, J., Wang, Y., Yin, L., Cao, G., et al. (2020). Knockdown of RAP2A Gene Expression Suppresses Cisplatin Resistance in Gastric Cancer Cells. *Oncol. Lett.* 19, 350–358. doi:10.3892/ol.2019.11086

Zhang, R., Wu, J., Yang, Y., Xia, D., Li, J., Quan, H., et al. (2020). Donor Polymorphisms of RAP1A Rs494453 Contribute to a Higher Risk of Hepatocellular Carcinoma Recurrence Following Liver Transplantation. *J. Cancer* 11, 3082–3088. doi:10.7150/jca.39712

Zheng, X., Zhao, W., Ji, P., Zhang, K., Jin, J., Feng, M., et al. (2017). High Expression of RAP2A Is Associated with Poor Prognosis of Patients with Hepatocellular Carcinoma. *Int. J. Clin. Exp. Pathol.* 10, 9607–9613.

Conflict of Interest: The authors declare that the research was conducted in the absence of any commercial or financial relationships that could be construed as a potential conflict of interest.

frontiers in Molecular Biosciences

REVIEW
published: 08 July 2021
doi: 10.3389/fmolb.2021.707439

Divergent Mechanisms Activating RAS and Small GTPases Through Post-translational Modification

*Natsuki Osaka[1], Yoshihisa Hirota[2,3], Doshun Ito[4,5], Yoshiki Ikeda[6], Ryo Kamata[1], Yuki Fujii[2,7], Venkat R. Chirasani[8], Sharon L. Campbell[8], Koh Takeuchi[9], Toshiya Senda[4,10,11] and Atsuo T. Sasaki[1,2,12,13]**

[1]Institute for Advanced Biosciences, Keio University, Tsuruoka, Japan, [2]Division of Hematology and Oncology, Department of Internal Medicine, University of Cincinnati College of Medicine, Cincinnati, OH, United States, [3]Department of Bioscience and Engineering, College of Systems Engineering and Science, Shibaura Institute of Technology, Saitama, Japan, [4]Structural Biology Research Center, Institute of Materials Structure Science, High Energy Accelerator Research Organization (KEK), Tsukuba, Japan, [5]Faculty of Environment and Information Studies, Keio University, Fujisawa, Japan, [6]Department of Molecular Genetics, Institute of Biomedical Science, Kansai Medical University, Osaka, Japan, [7]Graduate School of Science, Osaka City University, Osaka, Japan, [8]Department of Biochemistry and Biophysics and Lineberger Comprehensive Cancer Center, University of North Carolina at Chapel Hill, Chapel Hill, NC, United States, [9]Cellular and Molecular Biotechnology Research Institute, National Institute of Advanced Science and Technology, Tokyo, Japan, [10]Department of Accelerator Science, School of High Energy Accelerator Science, SOKENDAI (The Graduate University for Advanced Studies), Tsukuba, Japan, [11]Faculty of Pure and Applied Sciences, University of Tsukuba, Tsukuba, Japan, [12]Department of Cancer Biology, University of Cincinnati College of Medicine, Columbus, OH, United States, [13]Department of Neurosurgery, Brain Tumor Center at UC Gardner Neuroscience Institute, Cincinnati, OH, United States

OPEN ACCESS

Edited by:
Kwang-jin Cho,
Wright State University, United States

Reviewed by:
Katalin Szaszi,
St. Michael's Hospital, Canada
Yuqi Wang,
Saint Louis University, United States
Daniel Dempsey,
Harvard Medical School, United States

***Correspondence:**
Atsuo T. Sasaki
atsuo.sasaki@uc.edu

Specialty section:
This article was submitted to Cellular Biochemistry, a section of the journal Frontiers in Molecular Biosciences

Received: *10 May 2021*
Accepted: *22 June 2021*
Published: *08 July 2021*

Citation:
Osaka N, Hirota Y, Ito D, Ikeda Y, Kamata R, Fujii Y, Chirasani VR, Campbell SL, Takeuchi K, Senda T and Sasaki AT (2021) Divergent Mechanisms Activating RAS and Small GTPases Through Post-translational Modification. Front. Mol. Biosci. 8:707439. doi: 10.3389/fmolb.2021.707439

RAS is a founding member of the RAS superfamily of GTPases. These small 21 kDa proteins function as molecular switches to initialize signaling cascades involved in various cellular processes, including gene expression, cell growth, and differentiation. RAS is activated by GTP loading and deactivated upon GTP hydrolysis to GDP. Guanine nucleotide exchange factors (GEFs) and GTPase-activating proteins (GAPs) accelerate GTP loading and hydrolysis, respectively. These accessory proteins play a fundamental role in regulating activities of RAS superfamily small GTPase *via* a conserved guanine binding (G)-domain, which consists of five G motifs. The Switch regions lie within or proximal to the G2 and G3 motifs, and undergo dynamic conformational changes between the GDP-bound "OFF" state and GTP-bound "ON" state. They play an important role in the recognition of regulatory factors (GEFs and GAPs) and effectors. The G4 and G5 motifs are the focus of the present work and lie outside Switch regions. These motifs are responsible for the recognition of the guanine moiety in GTP and GDP, and contain residues that undergo post-translational modifications that underlie new mechanisms of RAS regulation. Post-translational modification within the G4 and G5 motifs activates RAS by populating the GTP-bound "ON" state, either through enhancement of intrinsic guanine nucleotide exchange or impairing GAP-mediated down-regulation. Here, we provide a comprehensive review of post-translational modifications in the RAS G4 and G5 motifs, and describe the role of these modifications in RAS activation as well as potential applications for cancer therapy.

Keywords: RAS, post-translational modification, G-domain, ubiquitylation (ubiquitination), lysine modification, cysteine oxydation, cancer, RAS superfamily GTPase

INTRODUCTION

RAS superfamily small GTPases consist of more than 170 members. They act as molecular switches cycling between GTP-bound "ON"- and GDP-bound "OFF"-states and play a crucial role in transducing signals that direct various cellular activities (Wennerberg et al., 2005). The RAS superfamily and other GTPase families (e.g., heterotrimeric G-proteins, elongation factors) contain a core guanine binding (G)-domain that possesses a Rossman fold. This structural unit enables high-affinity binding to GTP and GDP, as well as the ability to hydrolyze GTP (**Figure 1A**). RAS proteins have been the subject of intense investigation, as they are the most prevalent oncoprotein in human cancer. In this review, we will focus on the RAS G-protein and introduce a new layer of the regulation by post-translational modifications outside the canonical Switch regions. We will also discuss potential applications for cancer therapy.

THE OVERVIEW OF RAS STRUCTURE AND REGULATION

The Conserved G-Motif Is Required for High-Affinity GTP and GDP Binding of RAS

The core G-domain of RAS superfamily small GTPases consists of a six-stranded β-sheet and five α-helices, which contain five functional motifs, G1-G5 motifs (**Figures 1A,C**; Wennerberg et al., 2005; Wittinghofer and Vetter, 2011). The G1 motif is also referred to as P-loop or Walker A/phosphate-binding loop.

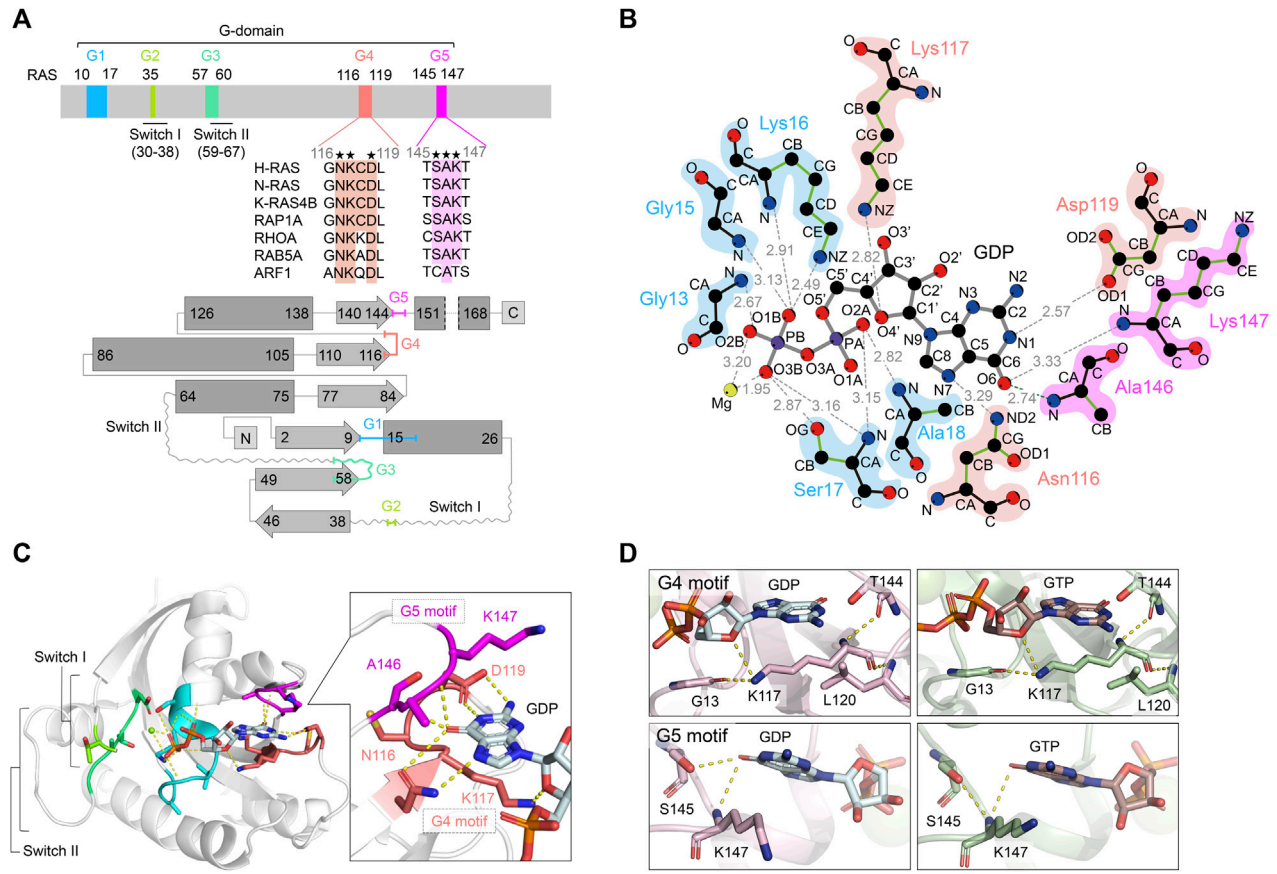

FIGURE 1 | Overview of RAS structures and the guanine nucleotide-dependent interactions of G4 and G5 motifs. **(A)** A schematic diagram of the RAS G-domain. Upper: Multiple sequence alignment of the RAS isotype G4 and G5 motifs and representative RAS superfamily members are shown. Conserved residues are annotated by asterisks. Lower: the secondary structures and topology of RAS. α-helices and β-sheets are shown in rectangle and arrow shape, respectively. Color theme for each G motif (G1: cyan, G2: light green, G3: green, G4: coral pink, G5: magenta) are consistent throughout the figures. **(B)** Interaction of H-RAS G-motifs with GDP (PDB: 4Q21) with hydrogen bonds. The plots were generated by LigPlot (Wallace et al., 1995) and the modified for clarity. The hydrogen bonds are shown in gray dotted lines with the distance between atoms. For amino acid residues, the main chains are shown in black, and the side chains are shown in green. Each atom is shown in a sphere and colored as follows: carbon, black; oxygen, red; nitrogen, blue; phosphorous, purple; magnesium, lime yellow. **(C)** The crystal structure of GDP-bound H-RAS (PDB: 4Q21). The hydrogen bonds are shown as dotted lines and Mg^{2+} ion as a purple sphere. Protein is shown as gray helix and the interacting residues of G4 and G5 motifs with the guanine moiety are shown in licorice representation in the inset. **(D)** Interactions of Lys117 within the G4 motif (upper panels) and Lys147 within the G5 motif (lower panels) with GDP-bound K-RAS (PDB: 6MBT) (left panels) and GTP-bound K-RAS (PDB: 5VQ2) (right panels). Hydrogen bond interactions are shown as dotted lines. Protein is rendered as cartoon and residues interacting with Lys117 or Lys147 are shown in licorice representation.

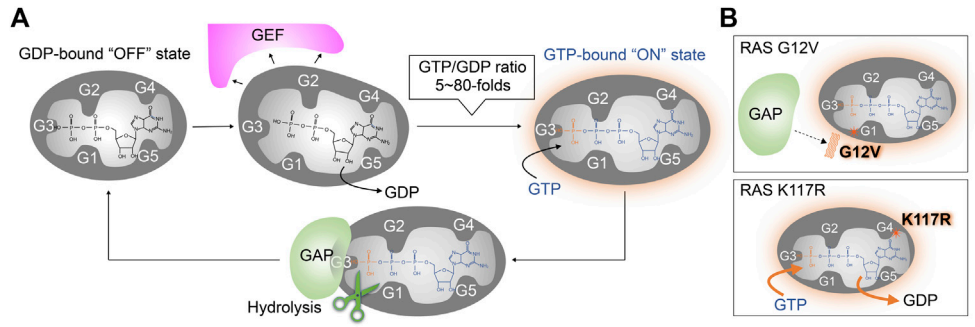

FIGURE 2 | Wild type and oncogenic RAS regulation by GEFs and GAPs. **(A)** The RAS nucleotide cycling regulated by GEF and GAP. GEFs bind to RAS, inducing conformation changes that reduce the RAS affinity for guanine nucleotide ligands. This leads to the dissociation of GDP and the formation of the nucleotide-free apo-form of RAS from the GDP-bound "OFF" state. Stochastic GTP loading to the apo-form of RAS facilitating the GTP-bound "ON" state, due to the higher GTP/GDP ratios in the cell. GAPs bind to the GTP-bound RAS and increases its intrinsic GTPase activity for GTP hydrolysis. **(B)** Activation mechanism of oncogenic RAS mutant. Upper: The RAS G12V oncogenic mutant impairs both intrinsic GTPase activity and GAP-dependent GTP hydrolysis. Lower: the RAS K117R mutant maintains intrinsic GTPase activity and GAP-dependent GTP-hydrolysis, but decreases the nucleotide affinity, leading to an increased GTP/GDP exchange.

The G2 and G3 motifs contain regions termed Switch I and Switch II (collectively referred to as Switch regions). The P-loop and Switch regions form interactions with the β- and γ-phosphate groups of GTP, GDP and Mg^{2+}. The Switch regions differ in conformation between the GDP-bound "OFF" state to the GTP-bound "ON" state (Kinoshita et al., 1999; Wittinghofer and Vetter, 2011). The GTP-bound "ON" state is considered the active state as it adopts a conformation that leads to increased affinity for downstream effectors (e.g., RAFs, class I PI3Ks), thereby transmitting signals. For example, the affinity of the GTP-bound RAS for RAF1 (CRAF) is approximately 1000-fold higher than that of GDP-bound RAS (Herrmann et al., 1995; Kiel et al., 2009).

The G4 and G5 motifs—the focus of this review—play a critical role in the high-affinity binding of RAS to GTP and GDP through guanine base and ribose recognition (Vetter and Wittinghofer, 2001; Wittinghofer and Vetter, 2011). In fact, the substitution of Lys117 or Asp119 in the G4 motif significantly reduces guanine ligand binding, leading to greatly enhanced guanine nucleotide dissociation (Feig et al., 1986; Denayer et al., 2008; Baker et al., 2013b). In the RAS superfamily, the G4 motif contains an "N-K-X-D" sequence (X denotes any amino acid, ^{116}NKCD^{119} in human RAS) and is a major determinant of guanine nucleotide specificity. The amino acid residues in the G4 motif are strictly conserved, except for the third position (X). In the structure of the GDP-bound RAS, Lys117 in the G4 motif interacts with Gly13 of the G1 motif and the guanine nucleotide ribose sugar (**Figures 1B**,**D**). Since Lys117 and Asp119 are highly conserved residues present in the guanine-specificity region of all guanine-nucleotide-binding proteins, mutations at these residues significantly alter the nucleotide exchange rates. Mutations in Lys117 drastically reduce the nucleotide-binding affinity and influence interactions with P-loop residues. As Asp119 makes a key hydrogen bond interaction with the guanine N1 atom (**Figures 1B**,**D**; Pai et al., 1989), mutations in Asp119 will also influence nucleotide binding affinity (Cool et al., 1999). The influence of Asp119 mutations on nucleotide-binding affinity is significantly lower than that of Lys117 mutations. The G5 motif has an "S-A-X" sequence (X denotes any amino acid, ^{145}SAK^{147} in human RAS), which also interacts with the guanine moiety and is required for selective and high-affinity binding of RAS to guanine nucleotides (**Figure 1B**). The amino group of Ala146 forms a hydrogen bond with the O6 atom of the guanine ring, and the amino group of Lys147 forms a hydrogen bond with the N2 atom of the guanine ring (**Figure 1D**; Pai et al., 1989).

RAS Regulation by GEFs and GAPs

In mammalian cells, three families of GEFs and six families of GAPs have been identified that act on RAS (Vigil et al., 2010; Henning et al., 2015; Li et al., 2018; Gray et al., 2020; Stalnecker and Der., 2020). Similarly, there are multiple GEFs and GAPs associated with other RAS superfamily small GTPases (Bos et al., 2007; Cherfils and Zeghouf, 2013). GEFs are regulated by kinase-mediated phosphorylation and interactions with second messengers (e.g., Ca^{2+}, diacylglycerol, cAMP), which is often coupled with changes in subcellular localization (Bos et al., 2007; Vigil et al., 2010; Cherfils and Zeghouf, 2013). In unstimulated cells, RAS exists predominately in the GDP-bound "OFF" state. Once the GEF is activated or co-localized with RAS, the GEF binds to RAS and interferes with the RAS/guanine ligand. This leads to the dissociation of GDP from RAS. As the affinity of RAS to GTP and GDP is similar (Feuerstein et al., 1987; John et al., 1993; Ford et al., 2009), the frequency of RAS activation reflects the intracellular GTP/GDP ratio (5~80 fold) in mammalian cells (Traut, 1994), to promote the population of RAS in the GTP-bound "ON" state *via* a stochastic GTP loading (**Figure 2A**). RAS is deactivated upon hydrolysis of the phosphate bond between the β- and γ-phosphate of GTP. Although the rate of intrinsic GTP hydrolysis activity is slow, RAS GAPs bind to GTP-bound RAS and stimulate GTP hydrolysis. In the structure of RAS GAPs (p120 RASGAP) and NF1-bound RAS, GAP binding stabilizes the active site and provides an arginine finger, which directly interacts with the β- and γ-phosphate of GTP, to greatly enhance the GTP hydrolysis rate of RAS (**Figure 2A**; Scheffzek et al., 1997; Kötting et al., 2008).

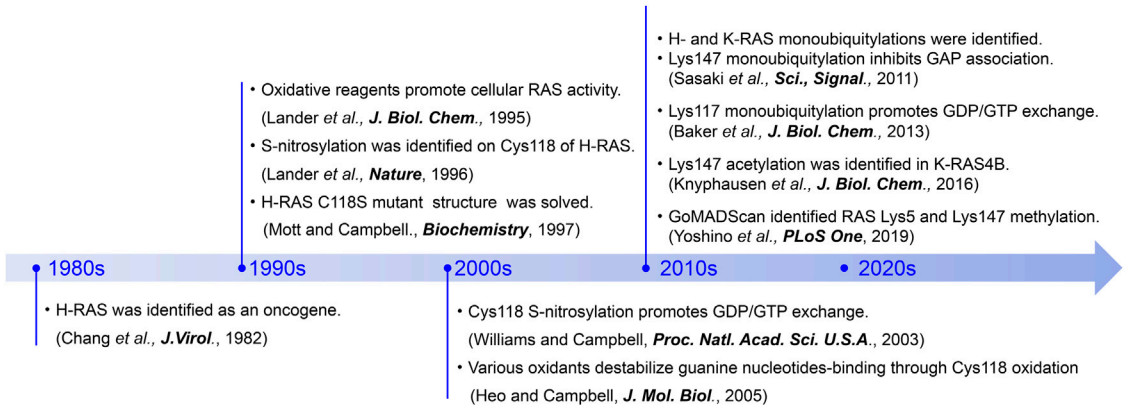

FIGURE 3 | A chronicle of RAS-related discoveries highlighted in this review.

Oncogenic Mutation Within the G4 and G5 Motifs

In mammalian cells, there are three isotypes of RAS, named H-RAS, K-RAS, and N-RAS. Single point mutations in RAS that promote constitutive RAS activation and tumorigenesis (Bos, 1989; Downward, 2003; Malumbres and Barbacid, 2003; Karnoub and Weinberg, 2008; Pylayeva-Gupta et al., 2011; Ratner and Miller, 2015) and developmental disorders (Tidyman and Rauen, 2009; Rauen, 2013; Borrie et al., 2017; Simanshu et al., 2017) were first identified in the early 1980s (**Figure 3**; Chang et al., 1982). These were later found to be present in approximately 25% of human cancers (Forbes et al., 2010; Prior et al., 2012; Prior et al., 2020), and over 100 oncogenic mutations have since been identified in human RAS. Among them, the K-RAS G12C oncogenic mutation is present in about 3–14% of cancer patients (Prior et al., 2012; Prior et al., 2020; Nassar et al., 2021) and has been targeted for drug discovery efforts (Ostrem et al., 2013; Lito et al., 2016; Janes et al., 2018; Hallin et al., 2020; Moore et al., 2020). However, the K-RAS G12C inhibitors do not act on other oncogenic mutants as they lack the reactive cysteine at position 12 needed for covalent ligation and inhibition. Thus, further understanding of RAS regulatory mechanisms is critical to developing new therapeutic approaches for targeting RAS-driven cancers and developmental disorders.

Gly12 and Gly13 in the G1 motif and Gln61 in the G3 motif are known as hot spots for RAS oncogenic mutations (Moore et al., 2020; Prior et al., 2020). One common feature of these mutants is that they are impaired in GTP hydrolysis and thus populated in the GTP-bound "ON" state (**Figure 2B** upper panel) (Gideon et al., 1992). In addition to the impaired GTP hydrolysis, the G13D and Q61L mutants are unique in that they also display enhanced intrinsic guanine nucleotide exchange (Smith et al., 2013). The improvements in sequencing technology in the 2000s have uncovered additional point mutations in the G4 (e.g., K117N) and G5 (e.g., A146T) motifs (Edkins et al., 2006; Denayer et al., 2008; Wójcik et al., 2008; Smith et al., 2010; Gremer et al., 2011; Niihori et al., 2011) that promote RAS activation.

These oncogenic mutations in the G4 and G5 motifs of RAS retain GTP hydrolytic activity but greatly accelerate the guanine nucleotide exchange rate that renders the GTPase less sensitive to GEF-regulation (Denayer et al., 2008; Janakiraman et al., 2010; **Figure 2B** lower panel). As indicated in the previous section "The Conserved G-Motif is Required for High-Affinity GTP and GDP Binding of RAS," a subset of amino acids in the G4 and G5 motifs are highly conserved as they directly interact with the guanine ring and are important for the high affinity and specificity of the guanine nucleotide. For example, even conservative mutations, such as K117N, K117R, and K147R, can significantly increase nucleotide exchange rate and populate RAS in the GTP-bound "ON" state (Sasaki et al., 2011; **Figure 2B** lower panel). X-ray structural analysis indicates that the guanidium group of Arg117 associated with the K-RAS K117R mutant forms an additional interaction with the amide group of Asn85, resulting in destabilization of key nucleotide ligand interactions with the G4 motif (Lys117) and P-loop (Gly13) (Denayer et al., 2008; **Figure 1D**). These observations suggest that the conserved amino acids in the G4 and G5 motifs are critical for guanine nucleotide-binding—i.e., perturbations in these key residues may promote RAS activation.

Post-translational Modifications Outside the Switch Regions

While missense mutations within the key residues in G4 and G5 motifs can promote RAS activation, post-translational modification (PTM) of these residues is yet another mechanism that can alter guanine nucleotide interactions and RAS activity. PTMs of proteins are key regulatory events in many cellular processes. Eukaryotic cells possess a variety of enzymes responsible for PTMs, such as Ser/Thr/Tyr kinases, methyltransferases, acetyltransferases, and ubiquitin ligases. PTMs by these enzymes are dynamic and, in most cases, reversible. It is well-known that the G-domain and C-terminal region of RAS is regulated by various PTMs (Ahearn et al., 2018). Furthermore, accumulating evidence indicates that RAS undergoes S-nitrosylation of select cysteine residues, as well as acetylation, methylation, and ubiquitylation of lysine residues within the G4 and G5 motifs (Lander et al., 1995; Sasaki et al., 2011; Knyphausen

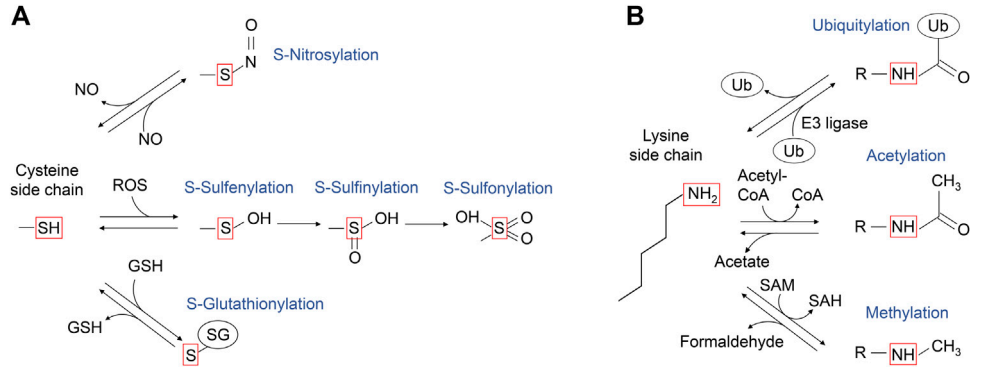

FIGURE 4 | A schematic diagram of the post-translational modifications of cysteine and lysine side chains. **(A)** The sulfur atom of cysteine side chain can undergo several oxidative modifications, including those shown in the red box. S-nitrosylation can be generated upon reaction with nitric oxide (NO). Upon the reaction with reactive oxygen species (ROS), the sulfur atom of cysteine side chain can undergo S-sulfenylation, and further oxidation to S-sulfinic and S-sulfonic states. The cysteine side chain can also form mixed disulfides, including reaction with glutathione (GSH) to undergo reversible S-glutathionylation. **(B)** The ε-amino group of lysine side chain can undergo several modifications as shown in the red box. The portion of modified lysine side chains is shown as "R-NH". Ubiquitylation is mediated by ubiquitin E3 ligase, while deubiquitylation is mediated by deubiquitylases. Lysine acetyltransferases use acetyl-CoA as the acetyl-donor for lysine acetylation, which can be reversed by acetylated lysine deacetylases. Lysine methyltransferases use S-adenosylmethionine as a methyl donor for lysine methylation, which is reversed by methylated lysine demethylase, coproducing formaldehyde.

et al., 2016; Yoshino et al., 2019; **Figure 3**). These PTMs can upregulate RAS activity by increasing the guanine nucleotide exchange rate and/or inhibiting GAP-mediated GTP hydrolysis.

PTM WITHIN THE RAS G4 MOTIF (^{116}NKCD^{119})

S-Oxidation and S-Nitrosylation of Cys118 in the G4 Motif

Cells are often exposed to various stresses, such as increased reactive oxygen species (ROS). ROS are continuously generated through the mitochondrial electron transport chain, peroxidases, xanthine oxidase, lipoxygenase, NADPH oxidases, and heme-enzyme reactions. ROS can be generated by exogenous stimuli, such as UV and ionizing radiation, ethanol intake, oxidized food, metal ion overload (e.g., Fe and Cu), and smoking. Also, nitric oxide (NO) is generated endogenously by nitric oxide synthases (NOS) and exogenously by nitrogen oxides in air pollution (NO_X) (e.g., car exhaust) and nitro compounds (Davies, 2016).

Cysteine is a key amino acid in proteins for maintaining redox balance. Cysteine has a reactive thiol side chain (Cys-SH), which can undergo one- and two-electron oxidation reactions. Also, cysteine can undergo several reversible oxidative modifications, including S-sulfenylation (Cys-SOH), S-nitrosylation (Cys-SNO), and S-glutathionylation (Cys-SSG) (**Figure 4A**; Paulsen and Carroll, 2013). In addition, some cysteine residues in proteins are more redox-sensitive than others because of changes in the side chain orientation, charge, and altered exposure to ROS, affecting the efficiency of modification. For example, PTEN, a lipid phosphatase that antagonizes class I PI3K signaling by dephosphorylation of PI(3,4,5)P_3, has a redox-sensitive cysteine residue in its catalytic center, which undergoes S-sulfenylation, leading to PTEN inactivation and increased class I PI3K signaling (Lee et al., 2002; Leslie et al., 2003; Zhang et al., 2017). The RAS GTPases are also regulated by cysteine oxidation, with the history of the RAS cysteine oxidation research tracked back to 1995 (**Figure 3**).

Novogrodsky's group at the Tel Aviv University found that treatment of RAS with a variety of oxidative reagents, including hydrogen peroxide (H_2O_2), hemin, Hg^{2+}, and NO, increases cellular RAS activity (Lander et al., 1995). Further, Cys118 was identified as the primary S-nitrosylation site in H-RAS. Cys118 is the most exposed solvent-accessible cysteine amongst three cysteine residues within the G-domain (Lander et al., 1996). Biochemical and structural studies of Cys118-nitrosylated H-RAS and a redox insensitive H-RAS variant (C118S) revealed that neither nitrosylation at this solvent-exposed site or mutation perturbs RAS structure, nucleotide cycling, or association with the RAS binding domain of CRAF (Mott et al., 1997; Williams et al., 2003). Subsequent functional analysis revealed that treatment with S-nitrosocysteine (CysNO), an NO donor, increases the GDP dissociation rate by ~200-fold, resulting in the increased guanine nucleotide exchange rate, in the absence of a GEF (Williams et al., 2003; Heo and Campbell, 2004; Heo et al., 2005; **Figure 5**). Biochemical analysis revealed that various oxidants (e.g., superoxide, CysNO), but not H_2O_2, which produce a Cys118 thiol radical intermediate, can cause oxidation of the guanine nucleotide and destabilize guanine nucleotide-binding (Heo and Campbell, 2005), leading to enhanced guanine nucleotide exchange.

Conservation of Cys118 Within RAS Superfamily Members

About 20% of small GTPases possess a cysteine residue at the position equivalent to Cys118 in the RAS superfamily. Within the RAS and RAB sub-classes, 25 and 30% of these retain the Cys118 (RAS isotypes numbering) (**Figure 6**; Wennerberg et al., 2005), respectively. Similar to H-RAS, a RAS sub-class member RAP1A and a RAB sub-class member RAB3 undergo cysteine S-nitrosylation at

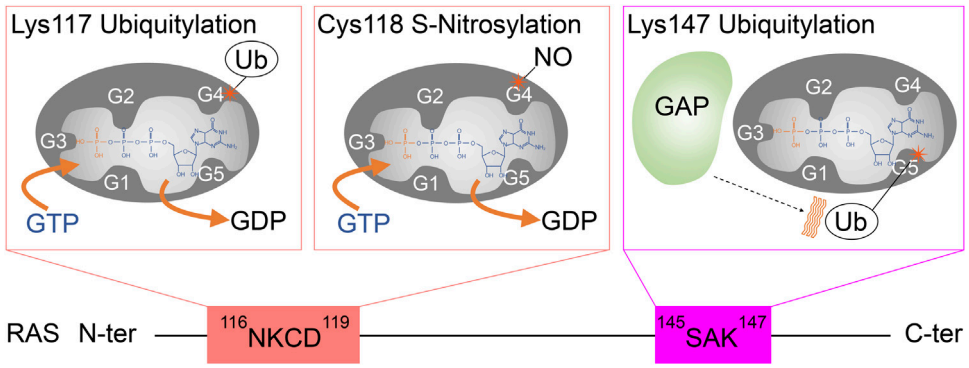

FIGURE 5 | A schematic diagram highlighting the role of G4 and G5 post-translational modifications in RAS activation. Monoubiquitylation of RAS at Lys117, as well as S-nitrosylation of RAS at Cys118, increases GDP dissociation, leading to an increased GTP/GDP exchange rate. In contrast, monoubiquitylation of RAS at Lys147 impedes GAP-mediated GTP hydrolysis, which populates the active RAS GTP-bound "ON" state.

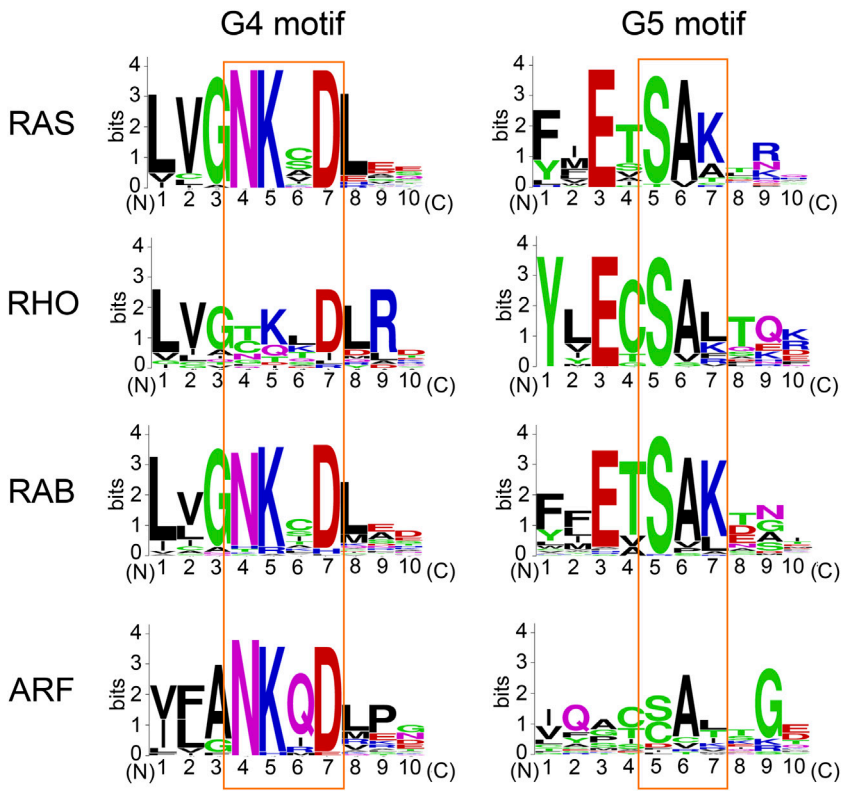

FIGURE 6 | The conservation of amino acids within the G4 and G5 motifs. Sequence alignment performed using Clustal Omega (https://www.ebi.ac.uk/Tools/msa/clustalo/). The amino acid sequence logo for the G4 and G5 motifs was created using WebLogo (https://weblogo.berkeley.edu/logo.cgi).

the cysteine residue in the G4 motif, leading to enhanced guanine nucleotide exchange resulting in elevated RAS activity (Heo and Campbell, 2005; Heo et al., 2005). Thus, the role of Cys118 oxidation in regulation of GTPase activity appears to be conserved in several RAS and RAB sub-class GTPases, and possibly in the other small GTPases with the cysteine residue equivalent to RAS Cys118 (Raines et al., 2007; Lim et al., 2008; Davis et al., 2011; Mitchell et al., 2013).

Ubiquitylation of Lys117 in G4 Motif

Lysine is a positively charged amino acid containing a long aliphatic sidechain and can undergo several post-translational modifications, such as acetylation, methylation, and ubiquitylation (**Figure 4B**). Ubiquitylation is a large lysine PTM, in which the 76 amino acid residue protein ubiquitin is conjugated to the ε-amine of the lysine residue in the target

protein through an isopeptide bond formation to its carboxyl group of C-terminal glycine. The conjugated ubiquitin can be further polyubiquitylated. Lys48-linked polyubiquitylation induces proteasome-dependent protein degradation (Heride et al., 2014). This process typically requires four or more polyubiquitin chains (Thrower et al., 2000; Miller and Gordon, 2005). Protein monoubiquitylation, on the other hand, does not promote protein degradation but regulates other cell functions such as endocytic trafficking (Haglund et al., 2003; Mosesson et al., 2003) and DNA damage response (Uckelmann and Sixma, 2017).

In 2011, RAS was identified as a target for monoubiquitylation (**Figure 3**; Sasaki et al., 2011). Cell biology experiments conducted in HEK293T cells determined that both H- and K-RAS are targets for monoubiquitylation. Monoubiquitylation of H- and K-RAS appeared to promote RAS activation, as the ubiquitylated RAS were more populated in GTP-bound "ON" state and showed enhanced association with RAS effectors compared to the non-modified RAS. These findings suggest that the monoubiquitylation of RAS is linked to RAS activation (Sasaki et al., 2011). Tandem affinity purification of ubiquitylated H- and K-RAS4B (hereafter K-RAS) followed by mass spectrometry analysis identified Lys117 and Lys147 as major sites for monoubiquitylation, respectively. NMR analysis and cell biology experiments showed that monoubiquitylation of Lys117 stimulates nucleotide exchange in the absence of RAS GEF and thereby induces GTP loading and RAS activation (Baker et al., 2013b; **Figure 5**).

Conservation of Lys117 Within RAS Superfamily Members

The lysine residue within the "N-K-X-D" G4 motif is highly conserved within the RAS superfamily (**Figure 6**). Within the RAS, RAB, and ARF sub-classes, almost all of these retain Lys117 (RAS isotypes numbering), while a few exceptions exist within the RHO sub-class GTPases (e.g., CDC42, TCL, RHOH) (Wennerberg et al., 2005). Furthermore, the lysine residue within the G4 motif is also highly conserved within the other G-protein families (Dever et al., 1987). Hence, it is considered that the GEF-independent activation via Lys117 monoubiquitylation may be a fundamental mechanism to regulate the activity of small GTPases and perhaps the other G-proteins as well.

PTM WITHIN RAS G5 MOTIF (^{145}SAK^{147})

Ubiquitylation of RAS Lys147 in the G5 Motif

Lys147 monoubiquitylation upregulates RAS activity in a manner distinct from Lys117 monoubiquitylation (**Figure 5**). Lys147 lies outside the Switch regions (**Figures 1A**,**C**). Using ubiquitin-conjugated K-RAS, our group discovered that Lys147 monoubiquitylation alters conformational dynamics of the Switch I and II regions and interferes with association of and downregulation by RAS GAPs while slightly altering GEF-dependent GDP/GTP exchange (Baker et al., 2013a; **Figure 5**). Biochemical, NMR, and computational analyses indicated that ubiquitin makes dynamic non-specific contacts with RAS, yet since the modification is large (~8 kDa), it alters the conformation of Switch regions and dynamics of RAS structure (Baker et al., 2013a; Hobbs et al., 2013). This, in turn, alters recognition by GAP and effector proteins. In particular, the Lys147 monoubiquitylation enhances the association with the specific K-RAS effectors: CRAF, BRAF, and class I PI3K in HEK293T cells, while binding affinity appears unaffected with other effectors, such as phospholipase C (PLC) and calmodulin. These findings revealed a new function for ubiquitylation in modulating signaling through specific downstream pathways (Sasaki et al., 2011). While Lys147 monoubiquitylation of GDP-bound K-RAS significantly enhances the affinity to CRAF (more than 40-fold), monoubiquitylated GTP-bound K-RAS shows attenuated binding affinity for the RAS binding domain of certain RAS effectors (CRAF, RALGDS, and PI3Ks) (Thurman et al., 2017). These results suggest that monoubiquitylation in K-RAS Lys147 facilitates RAF association and promotes signaling in a GTP-independent manner. Also, further analysis showed that the linker length (at least seven to eight residues) and protein ligation size of ubiquitin are critical for the GAP defect (Hobbs et al., 2013).

Consistent with these results, cell biological analysis indicated that Lys147 monoubiquitylation promotes GTP loading of K-RAS. In mouse xenograft assays, a K-RAS G12V/K147L double mutant that cannot be ubiquitylated showed significantly decreased tumor mass and volume, compared to oncogenic K-RAS G12V expressing isogenic control cells, suggesting a critical role of Lys147 monoubiquitylation, or possibly through other modifications (e.g., acetylation, methylation), in tumor progression (Sasaki et al., 2011).

Acetylation of RAS Lys147 in the G5 Motif

Lysine acetylation is a prevalent post-translational modification in eukaryotes and bacteria, and is mediated by the transfer of an acetyl CoA acetyl group by a cognate lysine acetyltransferase (Ali et al., 2018; Nakayasu et al., 2017). Acetylation of lysine decreases the overall positive charge of lysine residues and can create a docking site for other proteins (**Figure 4B**). Beyond its well-characterized role in regulating gene transcription through histone modification, lysine acetylation regulates diverse cellular processes through non-histone proteins (Ali et al., 2018).

Recent studies have shown that Lys147 in K-RAS also undergoes acetylation (Knyphausen et al., 2016; Song et al., 2016). The K-RAS K147Q mutation, which was generated to mimic Lys147-acetylation, increased the rate of guanine nucleotide exchange approximately three-fold higher than wild-type K-RAS (Song et al., 2016), which implies that acetylation of Lys147 in K-RAS may be involved in regulating guanine nucleotide exchange. However, the K147Q mutant may not mimic lysine acetylation as substitution of Lys147 with glutamine may disrupt a key interaction(s) important for guanine nucleotide-binding. Indeed, it has been shown that Lys147 acetylation did not affect the intrinsic and the GEF-dependent guanine nucleotide exchange (Knyphausen et al.,

2016). Further studies are warranted to define the role of Lys147 acetylation in K-RAS functions.

Methylation of RAS Lys147 in the G5 Motif

Protein methylation also occurs on side chain nitrogen atoms of lysine, arginine, and histidine residues. In contrast to the long-studied lysine acetylation, the roles of lysine-methylations beyond chromatin regulation are less well characterized, despite its earlier discovery in *Salmonella typhimurium* flagellin protein in 1959 (Ambler and Rees, 1959). Lysine modifications are more diverse than acetylation and can involve the transfer of one, two, or three methyl groups to the ε-amine of a lysine side chain through the conjugation of a methyl group from S-adenosyl methionine (SAM) by a lysine methyltransferase (**Figure 4B**). Unlike ubiquitylation and acetylation, lysine methylation maintains its overall positive charge. It is thus believed that the major function of lysine methylation is to provide a docking site for the proteins that recognize and bind methylated lysine (e.g., MBT and Tudor domains) (Lanouette et al., 2014; Teske and Hadden, 2017).

In 2019, mass spectrometry analysis of the immunoprecipitated endogenous RAS identified dimethylation at Lys5, adjacent to the G1 motif, as well as monomethylation at Lys147 in H-RAS (**Figure 3**) (Yoshino et al., 2019). While it is currently unclear whether Lys5 dimethylation is specific for all RAS isotypes, Lys147 is unique to the H-RAS. Given that substitutions at Lys147 to alanine, cysteine, or leucine do not significantly alter RAS activity (Sasaki et al., 2011; Baker et al., 2013a), it has been speculated that methylation of Lys147 does not alter RAS structure and that methylation of Lys147 may affect the H-RAS function by creating a docking site or blocking other PTMs. It is worth noting that methylation can prevent protein degradation by antagonizing ubiquitylation at the same targeted lysine residue (Lanouette et al., 2014); in yeast, 43% of methylated lysine residues are predicted to undergo ubiquitylation as well (Pang et al., 2010). Given that Lys147 in K-RAS undergoes monoubiquitylation, Lys147 methylation may negatively regulate RAS activation and monoubiquitylation-mediated effector switching.

Conservation of Lys147 Within RAS Superfamily Members

The lysine residue within the "S-A-K" G5 motif is conserved in about 45% of RAS superfamily members (**Figure 6**; Wennerberg et al., 2005). The adjacent serine and alanine residues within the G5 motif are also highly conserved in each sub-class (**Figure 6**). Thus, the PTM of Lys147 (RAS isotypes numbering) may not be limited to RAS but present in other RAS superfamily GTPases. The G5 motif within some of the RHO, RAB, and ARF sub-classes contain "S-A-L," "S-A-T," "C-A-L," and "C-A-T" sequences (**Figure 6**), and may undergo different PTMs within the G5 motif (e.g., phosphorylation at threonine residue of "S-A-T" motif and S-oxidation or S-nitrosylation at cysteine residue of "C-A-L" motif). Of note, the G5 motif is absent in several other G-proteins (e.g., heterotrimeric G-proteins and elongation factors). Whether the diverse sequences associated with the G5 motif in comparison to the more conserved G4 motif contribute to the functional difference of these RAS sub-classes remains unknown.

POTENTIAL THERAPEUTIC APPLICATION

Oncogenic RAS Specific Inhibitors

Although RAS has been considered "undruggable" (Gysin et al., 2011; Samatar and Poulikakos, 2014; Stephen et al., 2014; Papke and Der, 2017; Welsch et al., 2017), recent discoveries identified covalent inhibitors that target Cys12 which is the reactive cysteine within the K-RAS G12C oncogenic mutant by designed peptide mimetics (Ostrem et al., 2013; Yoo et al., 2020). These inhibitors are shown to suppress tumor progression (Lito et al., 2016; Janes et al., 2018). Recently, Sotorasib, a K-RAS G12C inhibitor, has been granted accelerated approval by the Food and Drug Administration (FDA) (Canon et al., 2019; Hong et al., 2020) for the treatment of non-small-cell lung cancer (NSCLC). In addition, other K-RAS G12C inhibitors are now in multiple clinical trials, including phase II and phase III studies (Clinical Trial number: NCT04613596; NCT04685135; NCT04793958; NCT04449874; NCT04699188) (Hallin et al., 2020). While most K-RAS mutations occur at codon 12 (e.g., G12V, G12D), G12C is only one of the mutations that can lead to oncogenic RAS activation at this position. Hence, there is a need to develop therapeutics effective for other RAS mutant-driven cancers.

Targeting the Enzymes Responsible for RAS PTMs

Given that the post-translational modifications identified in the G4 and G5 motifs are mediated by enzymes, we postulate that further mechanistic understanding of RAS regulation by PTMs of G4 and G5 motifs may unveil new approaches to suppress the RAS oncogenic activity that targets these modification enzymes (**Figure 7**). While the enzymes involved in RAS methylation remain unclear, several enzymes for RAS ubiquitylation and acetylation have been identified. Lysine deacetylases, HDAC6 and SIRT2, are suggested to negatively regulate K-RAS acetylation in cancer cells (Yang et al., 2013; Knyphausen et al., 2016). RABEX5, an E3 Ubiquitin ligase, catalyzes mono- and di-ubiquitylation of H- and N-RAS, but not K-RAS, which downregulates RAS activity (Xu et al., 2010; Yan et al., 2010; Washington et al., 2020). The ubiquitylation site(s) by RABEX5 remains unclear. A deubiquitinase OTUB1 has been identified as a negative regulator of RAS through a mammalian protein-protein interaction screening using H-RAS G12V mutant as the bait (Baietti et al., 2016). As Lys117 or Lys147 ubiquitylation upregulates RAS activity, it is unlikely that RABEX5 and OTUB1 modulate ubiquitylation of either Lys 117 or Lys147 in the G4 and G5 motifs. Hence, further studies exploring enzymes responsible for RAS ubiquitylation are required.

A promising new strategy to antagonize aberrant RAS signaling involves RAS degradation through ubiquitylation. These proteolysis-targeting chimera (PROTAC) approaches have proven to be an effective strategy for inhibiting specific protein

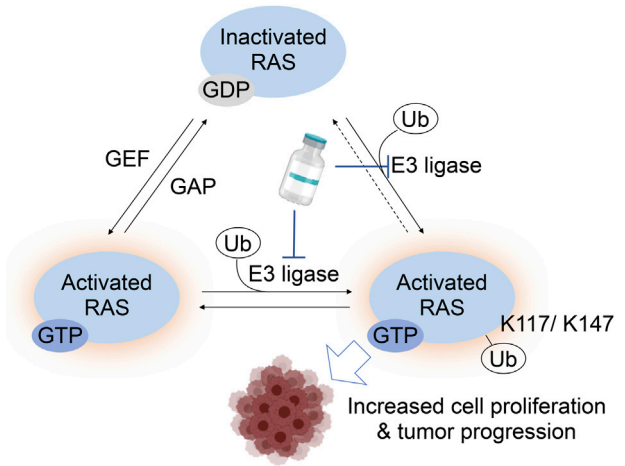

FIGURE 7 | A RAS activation model by monoubiquitylation at Lys117 and Lys147. For RAS Lys117 ubiquitylation, a current working model is that Lys117 monoubiquitylation increase GTP-bound RAS by increased GTP/GDP exchange. The Lys147 monoubiquitylation inhibits the RAS GAP binding to RAS, which leads to the increased GTP-bound RAS. Hence, targeting the E3 ligase responsible for Lys117 and/or Lys147 monoubiquitylation is expected to suppress the RAS activation and possibly decrease tumorigenic activity or progression of cancer.

targets (Churcher, 2017; Coleman and Crews, 2018). PROTACs induce proteolysis of a target protein by linking a target protein to the specific E3 ubiquitin ligase *via* a chemical tag (Khan et al., 2020). Importantly, PROTACs specifically targeting K-RAS or the K-RAS G12C mutant have recently been developed (Bery et al., 2020; Bond et al., 2020). Identifying RAS E3 ligases could aid in the application of PROTAC approaches for therapeutic inhibition of RAS as RAS-specific ligases may facilitate spatial/temporal localization needed for efficient RAS degradation. Clarifying which enzymes are responsible for RAS acetylation and methylation may provide another indirect way to suppress RAS activity by modulating these PTMs.

CONCLUDING REMARKS

Post-translational modifications contribute to the diversification of protein function as well as the robustness to intra- and extracellular stress for maintaining cellular functions. Among the many post-translational modifications, S-oxygenation, S-nitrosylation, monoubiquitylation, acetylation, and methylation described in this review reflect reversible modifications that can modulate the function of RAS proteins. Divergent mechanisms involved in RAS activation through PTMs of the G4 and G5 motifs are likely to enable RAS to function at the distinctive subcellular localization, timing, and kinetics, apart from the canonical RAS regulatory pathway by GEFs and GAPs. Thus, RAS PTMs may play an important role in developing a new therapeutic approach for RAS-driven cancers. One of the next important steps will be to identify enzymes responsible for RAS PTMs as well as to clarify the physiological significance of these modifications in developmental processes, homeostasis, and disease states. PTMs associated with RAS G4 and G5 motifs may represent novel "Achille's heels" for new anti-RAS approaches. Further understanding of these mechanisms might shed light on the development of effective therapeutic approaches.

AUTHOR CONTRIBUTIONS

NO and AS organized and wrote the manuscript. YH, DI, RK, and VC projected to draw the illustration. NO, AS, YH, DI, YI, RK, and YF conceptualized. NO, AS, TS, KT, and SC edited the manuscript. All authors contributed to the article and approved the submitted version.

FUNDING

The work is supported in part by the MTP UC-Brain Tumor Center grant and NIH grants R21NS100077 and R01NS089815 to AS. Support is also provided by Project for Cancer Research and Therapeutic Evolution (P-CREATE; JP20cm0106173 to AS, TS, and KT) from Japan Agency for Medical Research and Development (AMED). NO is supported by the Japan Society for the Promotion of Science (JSPS), KAKENHI grant number JP20H03165 and the Japan Science and Technology (JST) grant number JP20356709. YH is supported, in part, by JSPS KAKENHI grant number JP18KK0455 and JP 21K11709. DI is supported by JSPS KAKENHI grant number 21J00755. YI is supported by JSPS KAKENHI grant number JP20K07624. RK is supported by JSPS KAKENHI grant number 21K15019. SC is supported in part by NIH grants 3R35GM134962 and P01CA203567. TS is supported by the Platform Project for Supporting Drug Discovery and Life Science Research (Basis for Supporting Innovative Drug Discovery and Life Science Research (BINDS)) from AMEDunder Grant Numbers JP19am0101071. This work was also supported in part by research funds from the Sumitomo Foundation, and the Yamagata prefectural government, and the City of Tsuruoka.

REFERENCES

Ahearn, I., Zhou, M., and Philips, M. R. (2018). Posttranslational Modifications of RAS Proteins. *Cold Spring Harb. Perspect. Med.* 8, a031484. doi:10.1101/cshperspect.a031484

Ali, I., Conrad, R. J., Verdin, E., and Ott, M. (2018). Lysine Acetylation Goes Global: From Epigenetics to Metabolism and Therapeutics. *Chem. Rev.* 118, 1216–1252. doi:10.1021/acs.chemrev.7b00181

Ambler, R. P., and Rees, M. W. (1959). ε-N-Methyl-lysine in Bacterial Flagellar Protein. *Nature* 184, 56–57. doi:10.1038/184056b0

Baietti, M. F., Simicek, M., Abbasi Asbagh, L., Radaelli, E., Lievens, S., Crowther, J., et al. (2016). OTUB 1 Triggers Lung Cancer Development by Inhibiting RAS Monoubiquitination. *EMBO Mol. Med.* 8, 288–303. doi:10.15252/emmm.201505972

Baker, R., Lewis, S. M., Sasaki, A. T., Wilkerson, E. M., Locasale, J. W., Cantley, L. C., et al. (2013a). Site-specific Monoubiquitination Activates Ras by Impeding GTPase-Activating Protein Function. *Nat. Struct. Mol. Biol.* 20, 46–52. doi:10.1038/nsmb.2430

Baker, R., Wilkerson, E. M., Sumita, K., Isom, D. G., Sasaki, A. T., Dohlman, H. G., et al. (2013b). Differences in the Regulation of K-Ras and H-Ras Isoforms by Monoubiquitination. *J. Biol. Chem.* 288, 36856–36862. doi:10.1074/jbc.C113.525691

Bery, N., Miller, A., and Rabbitts, T. (2020). A Potent KRAS Macromolecule Degrader Specifically Targeting Tumours with Mutant KRAS. *Nat. Commun.* 11, 3233. doi:10.1038/s41467-020-17022-w

Bond, M. J., Chu, L., Nalawansha, D. A., Li, K., and Crews, C. M. (2020). Targeted Degradation of Oncogenic KRASG12C by VHL-Recruiting PROTACs. *ACS Cent. Sci.* 6, 1367–1375. doi:10.1021/acscentsci.0c00411

Borrie, S. C., Brems, H., Legius, E., and Bagni, C. (2017). Cognitive Dysfunctions in Intellectual Disabilities: The Contributions of the Ras-MAPK and PI3K-AKT-mTOR Pathways. *Annu. Rev. Genom. Hum. Genet.* 18, 115–142. doi:10.1146/annurev-genom-091416-035332

Bos, J. L. (1989). Ras Oncogenes in Human Cancer: a Review. *Cancer Res.* 49, 4682–4689.

Bos, J. L., Rehmann, H., and Wittinghofer, A. (2007). GEFs and GAPs: Critical Elements in the Control of Small G Proteins. *Cell* 129, 865–877. doi:10.1016/j.cell.2007.05.018

Canon, J., Rex, K., Saiki, A. Y., Mohr, C., Cooke, K., Bagal, D., et al. (2019). The Clinical KRAS(G12C) Inhibitor AMG 510 Drives Anti-tumour Immunity. *Nature* 575, 217–223. doi:10.1038/s41586-019-1694-1

Chang, E. H., Gonda, M. A., Ellis, R. W., Scolnick, E. M., and Lowy, D. R. (1982). Human Genome Contains Four Genes Homologous to Transforming Genes of Harvey and Kirsten Murine Sarcoma Viruses. *Proc. Natl. Acad. Sci.* 79, 4848–4852. doi:10.1073/pnas.79.16.4848

Cherfils, J., and Zeghouf, M. (2013). Regulation of Small GTPases by GEFs, GAPs, and GDIs. *Physiol. Rev.* 93, 269–309. doi:10.1152/physrev.00003.2012

Churcher, I. (2017). Protac-induced Protein Degradation in Drug Discovery: Breaking the Rules or Just Making New Ones? *J. Med. Chem.* 61, 444–452. doi:10.1021/acs.jmedchem.7b01272

Coleman, K. G., and Crews, C. M. (2018). Proteolysis-targeting Chimeras: Harnessing the Ubiquitin-Proteasome System to Induce Degradation of Specific Target Proteins. *Annu. Rev. Cancer Biol.* 2, 41–58. doi:10.1146/annurev-cancerbio-030617-050430

Cool, R. H., Schmidt, G., Lenzen, C. U., Prinz, H., Vogt, D., and Wittinghofer, A. (1999). The Ras Mutant D119N Is Both Dominant Negative and Activated. *Mol. Cel. Biol.* 19, 6297–6305. doi:10.1128/mcb.19.9.6297

Davies, M. J. (2016). Protein Oxidation and Peroxidation. *Biochem. J.* 473, 805–825. doi:10.1042/BJ20151227

Davis, M. F., Vigil, D., and Campbell, S. L. (2011). Regulation of Ras Proteins by Reactive Nitrogen Species. *Free Radic. Biol. Med.* 51, 565–575. doi:10.1016/j.freeradbiomed.2011.05.003

Denayer, E., Parret, A., Chmara, M., Schubbert, S., Vogels, A., Devriendt, K., et al. (2008). Mutation Analysis in Costello Syndrome: Functional and Structural Characterization of theHRASp.Lys117Arg Mutation. *Hum. Mutat.* 29, 232–239. doi:10.1002/humu.20616

Dever, T. E., Glynias, M. J., and Merrick, W. C. (1987). GTP-binding Domain: Three Consensus Sequence Elements with Distinct Spacing. *Proc. Natl. Acad. Sci.* 84, 1814–1818. doi:10.1073/pnas.84.7.1814

Downward, J. (2003). Targeting RAS Signalling Pathways in Cancer Therapy. *Nat. Rev. Cancer* 3, 11–22. doi:10.1038/nrc969

Edkins, S., O'Meara, S., Parker, A., Stevens, C., Reis, M., Jones, S., et al. (2006). Recurrent KRAS Codon 146 Mutations in Human Colorectal Cancer. *Cancer. Biol. Ther.* 5, 928–932. doi:10.4161/cbt.5.8.3251

Feig, L. A., Pan, B. T., Roberts, T. M., and Cooper, G. M. (1986). Isolation of Ras GTP-Binding Mutants Using an *In Situ* colony-binding Assay. *Proc. Natl. Acad. Sci.* 83, 4607–4611. doi:10.1073/pnas.83.13.4607

Feuerstein, J., Goody, R. S., and Wittinghofer, A. (1987). Preparation and Characterization of Nucleotide-free and Metal Ion-free P21 "apoprotein". *J. Biol. Chem.* 262, 8455–8458. doi:10.1016/s0021-9258(18)47433-9

Forbes, S. A., Bindal, N., Bamford, S., Cole, C., Kok, C. Y., Beare, D., et al. (2010). COSMIC: Mining Complete Cancer Genomes in the Catalogue of Somatic Mutations in Cancer. *Nucleic Acids Res.* 39, D945–D950. doi:10.1093/nar/gkq929

Ford, B., Boykevisch, S., Zhao, C., Kunzelmann, S., Bar-Sagi, D., Herrmann, C., et al. (2009). Characterization of a Ras Mutant with Identical GDP- and GTP-Bound Structures,. *Biochemistry* 48, 11449–11457. doi:10.1021/bi901479b

Gideon, P., John, J., Frech, M., Lautwein, A., Clark, R., Scheffler, J. E., et al. (1992). Mutational and Kinetic Analyses of the GTPase-Activating Protein (GAP)-p21 Interaction: the C-Terminal Domain of GAP Is Not Sufficient for Full Activity. *Mol. Cel. Biol.* 12, 2050–2056. doi:10.1128/mcb.12.5.2050

Gray, J. L., Delft, F., and Brennan, P. E. (2020). Targeting the Small GTPase Superfamily through Their Regulatory Proteins. *Angew. Chem. Int. Ed.* 59, 6342–6366. doi:10.1002/anie.201900585

Gremer, L., Merbitz-Zahradnik, T., Dvorsky, R., Cirstea, I. C., Kratz, C. P., Zenker, M., et al. (2011). Germline KRAS Mutations Cause Aberrant Biochemical and Physical Properties Leading to Developmental Disorders. *Hum. Mutat.* 32, 33–43. doi:10.1002/humu.21377

Gysin, S., Salt, M., Young, A., and McCormick, F. (2011). Therapeutic Strategies for Targeting Ras Proteins. *Genes & Cancer* 2, 359–372. doi:10.1177/1947601911412376

Haglund, K., Di Fiore, P. P., and Dikic, I. (2003). Distinct Monoubiquitin Signals in Receptor Endocytosis. *Trends Biochem. Sci.* 28, 598–604. doi:10.1016/j.tibs.2003.09.005

Hallin, J., Engstrom, L. D., Hargis, L., Calinisan, A., Aranda, R., Briere, D. M., et al. (2020). The KRAS G12CInhibitor MRTX849 Provides Insight toward Therapeutic Susceptibility of KRAS-Mutant Cancers in Mouse Models and Patients. *Cancer Dis.* 10, 54–71. doi:10.1158/2159-8290.CD-19-1167

Hennig, A., Markwart, R., Esparza-Franco, M. A., Ladds, G., and Rubio, I. (2015). Ras Activation Revisited: Role of GEF and GAP Systems. *Biol. Chem.* 396, 831–848. doi:10.1515/hsz-2014-0257

Heo, J., and Campbell, S. L. (2004). Mechanism of p21RasS-Nitrosylation and Kinetics of Nitric Oxide-Mediated Guanine Nucleotide Exchange†. *Biochemistry* 43, 2314–2322. doi:10.1021/bi035275g

Heo, J., and Campbell, S. L. (2005). Superoxide Anion Radical Modulates the Activity of Ras and Ras-Related GTPases by a Radical-Based Mechanism Similar to that of Nitric Oxide. *J. Biol. Chem.* 280, 12438–12445. doi:10.1074/jbc.M414282200

Heo, J., Prutzman, K. C., Mocanu, V., and Campbell, S. L. (2005). Mechanism of Free Radical Nitric Oxide-Mediated Ras Guanine Nucleotide Dissociation. *J. Mol. Biol.* 346, 1423–1440. doi:10.1016/j.jmb.2004.12.050

Heride, C., Urbé, S., and Clague, M. J. (2014). Ubiquitin Code Assembly and Disassembly. *Curr. Biol.* 24, R215–R220. doi:10.1016/j.cub.2014.02.002

Herrmann, C., Martin, G. A., and Wittinghofer, A. (1995). Quantitative Analysis of the Complex between P21 and the Ras-Binding Domain of the Human Raf-1 Protein Kinase. *J. Biol. Chem.* 270, 2901–2905. doi:10.1074/jbc.270.7.2901

Hobbs, G. A., Gunawardena, H. P., Baker, R., Chen, X., and Campbell, S. L. (2013). Site-specific Monoubiquitination Activates Ras by Impeding GTPase-Activating Protein Function. *Small GTPases* 4, 186–192. doi:10.4161/sgtp.26270

Hong, D. S., Fakih, M. G., Strickler, J. H., Desai, J., Durm, G. A., Shapiro, G. I., et al. (2020). KRASG12C Inhibition with Sotorasib in Advanced Solid Tumors. *N. Engl. J. Med.* 383, 1207–1217. doi:10.1056/NEJMoa1917239

Janakiraman, M., Vakiani, E., Zeng, Z., Pratilas, C. A., Taylor, B. S., Chitale, D., et al. (2010). Genomic and Biological Characterization of Exon 4 KRAS Mutations in Human Cancer. *Cancer Res.* 70, 5901–5911. doi:10.1158/0008-5472.CAN-10-0192

Janes, M. R., Zhang, J., Li, L.-S., Hansen, R., Peters, U., Guo, X., et al. (2018). Targeting KRAS Mutant Cancers with a Covalent G12C-specific Inhibitor. *Cell* 172, 578–589. doi:10.1016/j.cell.2018.01.006

John, J., Rensland, H., Schlichting, I., Vetter, I., Borasio, G. D., Goody, R. S., et al. (1993). Kinetic and Structural Analysis of the Mg(2+)-Binding Site of the Guanine Nucleotide-Binding Protein p21H-Ras. *J. Biol. Chem.* 268, 923–929. doi:10.1016/s0021-9258(18)54022-9

Karnoub, A. E., and Weinberg, R. A. (2008). Ras Oncogenes: Split Personalities. *Nat. Rev. Mol. Cel Biol.* 9, 517–531. doi:10.1038/nrm2438

Khan, S., He, Y., Zhang, X., Yuan, Y., Pu, S., Kong, Q., et al. (2020). PROteolysis TArgeting Chimeras (PROTACs) as Emerging Anticancer Therapeutics. *Oncogene* 39, 4909–4924. doi:10.1038/s41388-020-1336-y

Kiel, C., Filchtinski, D., Spoerner, M., Schreiber, G., Kalbitzer, H. R., and Herrmann, C. (2009). Improved Binding of Raf to Ras·GDP Is Correlated with Biological Activity. *J. Biol. Chem.* 284, 31893–31902. doi:10.1074/jbc.M109.031153

Kinoshita, K., Sadanami, K., Kidera, A., and Go, N. (1999). Structural Motif of Phosphate-Binding Site Common to Various Protein Superfamilies: All-

Against-All Structural Comparison of Protein-Mononucleotide Complexes. *Protein Eng.* 12, 11–14. doi:10.1093/protein/12.1.11

Knyphausen, P., Lang, F., Baldus, L., Extra, A., and Lammers, M. (2016). Insights into K-Ras 4B Regulation by post-translational Lysine Acetylation. *Biol. Chem.* 397, 1071–1085. doi:10.1515/hsz-2016-0118

Kötting, C., Kallenbach, A., Suveyzdis, Y., Wittinghofer, A., and Gerwert, K. (2008). The GAP Arginine finger Movement into the Catalytic Site of Ras Increases the Activation Entropy. *Proc. Natl. Acad. Sci.* 105, 6260–6265. doi:10.1073/pnas.0712095105

Lander, H. M., Milbank, A. J., Tauras, J. M., Hajjar, D. P., Hempstead, B. L., Schwartz, G. D., et al. (1996). Redox Regulation of Cell Signalling. *Nature* 381, 380–381. doi:10.1038/381380a0

Lander, H. M., Ogiste, J. S., Teng, K. K., and Novogrodsky, A. (1995). p21 as a Common Signaling Target of Reactive Free Radicals and Cellular Redox Stress. *J. Biol. Chem.* 270, 21195–21198. doi:10.1074/jbc.270.36.21195

Lanouette, S., Mongeon, V., Figeys, D., and Couture, J. F. (2014). The Functional Diversity of Protein Lysine Methylation. *Mol. Syst. Biol.* 10, 724. doi:10.1002/msb.134974

Lee, S.-R., Yang, K.-S., Kwon, J., Lee, C., Jeong, W., and Rhee, S. G. (2002). Reversible Inactivation of the Tumor Suppressor PTEN by H2O2. *J. Biol. Chem.* 277, 20336–20342. doi:10.1074/jbc.M111899200

Leslie, N. R., Bennett, D., Lindsay, Y. E., Stewart, H., Gray, A., and Downes, C. P. (2003). Redox Regulation of PI 3-kinase Signalling via Inactivation of PTEN. *EMBO J.* 22, 5501–5510. doi:10.1093/emboj/cdg513

Li, S., Balmain, A., and Counter, C. M. (2018). A Model for RAS Mutation Patterns in Cancers: Finding the Sweet Spot. *Nat. Rev. Cancer* 18, 767–777. doi:10.1038/s41568-018-0076-6

Lim, K.-H., Ancrile, B. B., Kashatus, D. F., and Counter, C. M. (2008). Tumour Maintenance Is Mediated by eNOS. *Nature* 452, 646–649. doi:10.1038/nature06778

Lito, P., Solomon, M., Li, L.-S., Hansen, R., and Rosen, N. (2016). Allele-specific Inhibitors Inactivate Mutant KRAS G12C by a Trapping Mechanism. *Science* 351, 604–608. doi:10.1126/science.aad6204

Malumbres, M., and Barbacid, M. (2003). RAS Oncogenes: the First 30 Years. *Nat. Rev. Cancer* 3, 459–465. doi:10.1038/nrc1097

Miller, J., and Gordon, C. (2005). The Regulation of Proteasome Degradation by Multi-Ubiquitin Chain Binding Proteins. *FEBS Lett.* 579, 3224–3230. doi:10.1016/j.febslet.2005.03.042

Mitchell, L., Hobbs, G. A., Aghajanian, A., and Campbell, S. L. (2013). Redox Regulation of Ras and Rho GTPases: Mechanism and Function. *Antioxid. Redox Signaling* 18, 250–258. doi:10.1089/ars.2012.4687

Moore, A. R., Rosenberg, S. C., McCormick, F., and Malek, S. (2020). RAS-targeted Therapies: Is the Undruggable Drugged?. *Nat. Rev. Drug Discov.* 19, 533–552. doi:10.1038/s41573-020-0068-6

Mosesson, Y., Shtiegman, K., Katz, M., Zwang, Y., Vereb, G., Szollosi, J., et al. (2003). Endocytosis of Receptor Tyrosine Kinases Is Driven by Monoubiquitylation, Not Polyubiquitylation. *J. Biol. Chem.* 278, 21323–21326. doi:10.1074/jbc.C300096200

Mott, H. R., Carpenter, J. W., and Campbell, S. L. (1997). Structural and Functional Analysis of a Mutant Ras Protein that Is Insensitive to Nitric Oxide Activation†. *Biochemistry* 36, 3640–3644. doi:10.1021/bi962790o

Nakayasu, E. S., Burnet, M. C., Walukiewicz, H. E., Wilkins, C. S., Shukla, A. K., Brooks, S., et al. (2017). Ancient Regulatory Role of Lysine Acetylation in Central Metabolism. *mBio* 8, 1395. doi:10.1128/mBio.01894-17

Nassar, A. H., Adib, E., and Kwiatkowski, D. J. (2021). Distribution of KRASG12C Somatic Mutations across Race, Sex, and Cancer Type. *N. Engl. J. Med.* 384, 185–187. doi:10.1056/NEJMc2030638

Niihori, T., Aoki, Y., Okamoto, N., Kurosawa, K., Ohashi, H., Mizuno, S., et al. (2011). HRAS Mutants Identified in Costello Syndrome Patients Can Induce Cellular Senescence: Possible Implications for the Pathogenesis of Costello Syndrome. *J. Hum. Genet.* 56, 707–715. doi:10.1038/jhg.2011.85

Ostrem, J. M., Peters, U., Sos, M. L., Wells, J. A., and Shokat, K. M. (2013). K-Ras(G12C) Inhibitors Allosterically Control GTP Affinity and Effector Interactions. *Nature* 503, 548–551. doi:10.1038/nature12796

Pai, E. F., Kabsch, W., Krengel, U., Holmes, K. C., John, J., and Wittinghofer, A. (1989). Structure of the Guanine-Nucleotide-Binding Domain of the Ha-Ras Oncogene Product P21 in the Triphosphate Conformation. *Nature* 341, 209–214. doi:10.1038/341209a0

Pang, C., Gasteiger, E., and Wilkins, M. R. (2010). Identification of Arginine- and Lysine-Methylation in the Proteome of *Saccharomyces cerevisiae* and its Functional Implications. *BMC Genomics* 11, 92. doi:10.1186/1471-2164-11-92

Papke, B., and Der, C. J. (2017). Drugging RAS: Know the Enemy. *Science* 355, 1158–1163. doi:10.1126/science.aam7622

Paulsen, C. E., and Carroll, K. S. (2013). Cysteine-Mediated Redox Signaling: Chemistry, Biology, and Tools for Discovery. *Chem. Rev.* 113, 4633–4679. doi:10.1021/cr300163e

Prior, I. A., Hood, F. E., and Hartley, J. L. (2020). The Frequency of Ras Mutations in Cancer. *Cancer Res.* 80, 2969–2974. doi:10.1158/0008-5472.CAN-19-3682

Prior, I. A., Lewis, P. D., and Mattos, C. (2012). A Comprehensive Survey of Ras Mutations in Cancer. *Cancer Res.* 72, 2457–2467. doi:10.1158/0008-5472.CAN-11-2612

Pylayeva-Gupta, Y., Grabocka, E., and Bar-Sagi, D. (2011). RAS Oncogenes: Weaving a Tumorigenic Web. *Nat. Rev. Cancer* 11, 761–774. doi:10.1038/nrc3106

Raines, K., Bonini, M., and Campbell, S. (2007). Nitric Oxide Cell Signaling: S-Nitrosation of Ras Superfamily GTPases. *Cardiovasc. Res.* 75, 229–239. doi:10.1016/j.cardiores.2007.04.013

Ratner, N., and Miller, S. J. (2015). A RASopathy Gene Commonly Mutated in Cancer: the Neurofibromatosis Type 1 Tumour Suppressor. *Nat. Rev. Cancer* 15, 290–301. doi:10.1038/nrc3911

Rauen, K. A. (2013). The RASopathies. *Annu. Rev. Genom. Hum. Genet.* 14, 355–369. doi:10.1146/annurev-genom-091212-153523

Samatar, A. A., and Poulikakos, P. I. (2014). Targeting RAS-ERK Signalling in Cancer: Promises and Challenges. *Nat. Rev. Drug Discov.* 13, 928–942. doi:10.1038/nrd4281

Sasaki, A. T., Carracedo, A., Locasale, J. W., Anastasiou, D., Takeuchi, K., Kahoud, E. R., et al. (2011). Ubiquitination of K-Ras Enhances Activation and Facilitates Binding to Select Downstream Effectors. *Sci. Signaling* 4, ra13. doi:10.1126/scisignal.2001518

Scheffzek, K., Ahmadian, M. R., Kabsch, W., Wiesmüller, L., Lautwein, A., Schmitz, F., et al. (1997). The Ras-RasGAP Complex: Structural Basis for GTPase Activation and its Loss in Oncogenic Ras Mutants. *Science* 277, 333–338. doi:10.1126/science.277.5324.333

Simanshu, D. K., Nissley, D. V., and McCormick, F. (2017). RAS Proteins and Their Regulators in Human Disease. *Cell* 170, 17–33. doi:10.1016/j.cell.2017.06.009

Smith, G., Bounds, R., Wolf, H., Steele, R. J. C., Carey, F. A., and Wolf, C. R. (2010). Activating K-Ras Mutations Outwith 'hotspot' Codons in Sporadic Colorectal Tumours - Implications for Personalised Cancer Medicine. *Br. J. Cancer* 102, 693–703. doi:10.1038/sj.bjc.6605534

Smith, M. J., Neel, B. G., and Ikura, M. (2013). NMR-based Functional Profiling of RASopathies and Oncogenic RAS Mutations. *Proc. Natl. Acad. Sci.* 110, 4574–4579. doi:10.1073/pnas.1218173110

Song, H. Y., Biancucci, M., Kang, H.-J., O'Callaghan, C., Park, S.-H., Principe, D. R., et al. (2016). SIRT2 Deletion Enhances KRAS-Induced Tumorigenesis *In Vivo* by Regulating K147 Acetylation Status. *Oncotarget* 7, 80336–80349. doi:10.18632/oncotarget.12015

Stalnecker, C. A., and Der, C. J. (2020). RAS, Wanted Dead or Alive: Advances in Targeting RAS Mutant Cancers. *Sci. Signal.* 13, eaay6013. doi:10.1126/scisignal.aay6013

Stephen, A. G., Esposito, D., Bagni, R. K., and McCormick, F. (2014). Dragging Ras Back in the Ring. *Cancer Cell* 25, 272–281. doi:10.1016/j.ccr.2014.02.017

Teske, K. A., and Hadden, M. K. (2017). Methyllysine Binding Domains: Structural Insight and Small Molecule Probe Development. *Eur. J. Med. Chem.* 136, 14–35. doi:10.1016/j.ejmech.2017.04.047

Thrower, J. S., Hoffman, L., Rechsteiner, M., and Pickart, C. M. (2000). Recognition of the Polyubiquitin Proteolytic Signal. *EMBO J.* 19, 94–102. doi:10.1093/emboj/19.1.94

Thurman, R., Siraliev-Perez, E., and Campbell, S. L. (2020). RAS Ubiquitylation Modulates Effector Interactions. *Small GTPases* 11, 180–185. doi:10.1080/21541248.2017.1371267

Tidyman, W. E., and Rauen, K. A. (2009). The RASopathies: Developmental Syndromes of Ras/MAPK Pathway Dysregulation. *Curr. Opin. Genet. Develop.* 19, 230–236. doi:10.1016/j.gde.2009.04.001

Traut, T. W. (1994). Physiological Concentrations of Purines and Pyrimidines. *Mol. Cel. Biochem.* 140, 1–22. doi:10.1007/BF00928361

Uckelmann, M., and Sixma, T. K. (2017). Histone Ubiquitination in the DNA Damage Response. *DNA Repair* 56, 92–101. doi:10.1016/j.dnarep.2017.06.011

Vetter, I. R., and Wittinghofer, A. (2001). The Guanine Nucleotide-Binding Switch in Three Dimensions. *Science* 294, 1299–1304. doi:10.1126/science.1062023

Vigil, D., Cherfils, J., Rossman, K. L., and Der, C. J. (2010). Ras Superfamily GEFs and GAPs: Validated and Tractable Targets for Cancer Therapy? *Nat. Rev. Cancer* 10, 842–857. doi:10.1038/nrc2960

Wallace, A. C., Laskowski, R. A., and Thornton, J. M. (1995). LIGPLOT: a Program to Generate Schematic Diagrams of Protein-Ligand Interactions. *Protein Eng. Des. Sel* 8, 127–134. doi:10.1093/protein/8.2.127

Washington, C., Chernet, R., Gokhale, R. H., Martino-Cortez, Y., Liu, H.-Y., Rosenberg, A. M., et al. (2020). A Conserved, N-Terminal Tyrosine Signal Directs Ras for Inhibition by Rabex-5. *Plos Genet.* 16, e1008715. doi:10.1371/journal.pgen.1008715

Welsch, M. E., Kaplan, A., Chambers, J. M., Stokes, M. E., Bos, P. H., Zask, A., et al. (2017). Multivalent Small-Molecule Pan-RAS Inhibitors. *Cell* 168, 878–889. doi:10.1016/j.cell.2017.02.006

Wennerberg, K., Rossman, K. L., and Der, C. J. (2005). The Ras Superfamily at a Glance. *J. Cel Sci.* 118, 843–846. doi:10.1242/jcs.01660

Williams, J. G., Pappu, K., and Campbell, S. L. (2003). Structural and Biochemical Studies of p21Ras S-Nitrosylation and Nitric Oxide-Mediated Guanine Nucleotide Exchange. *Proc. Natl. Acad. Sci.* 100, 6376–6381. doi:10.1073/pnas.1037299100

Wittinghofer, A., and Vetter, I. R. (2011). Structure-function Relationships of the G Domain, a Canonical Switch Motif. *Annu. Rev. Biochem.* 80, 943–971. doi:10.1146/annurev-biochem-062708-134043

Wójcik, P., Kulig, J., Okoń, K., Zazula, M., Możdzioch, I., Niepsuj, A., et al. (2008). KRAS Mutation Profile in Colorectal Carcinoma and Novel Mutation-Iinternal Tandem Duplication in KRAS. *Pol. J. Pathol.* 59, 93–96.

Xu, L., Lubkov, V., Taylor, L. J., and Bar-Sagi, D. (2010). Feedback Regulation of Ras Signaling by Rabex-5-Mediated Ubiquitination. *Curr. Biol.* 20, 1372–1377. doi:10.1016/j.cub.2010.06.051

Yan, H., Jahanshahi, M., Horvath, E. A., Liu, H-Y., and Pfleger, C. M. (2010). Rabex-5 Ubiquitin Ligase Activity Restricts Ras Signaling to Establish Pathway Homeostasis in Drosophila. *Curr. Biol.* 20, 1378–1382. doi:10.1016/j.cub.2010.06.058

Yang, M. H., Laurent, G., Bause, A. S., Spang, R., German, N., Haigis, M. C., et al. (2013). HDAC6 and SIRT2 Regulate the Acetylation State and Oncogenic Activity of Mutant K-RAS. *Mol. Cancer Res.* 11, 1072–1077. doi:10.1158/1541-7786.MCR-13-0040-T

Yoo, D. Y., Hauser, A. D., Joy, S. T., Bar-Sagi, D., and Arora, P. S. (2020). Covalent Targeting of Ras G12C by Rationally Designed Peptidomimetics. *ACS Chem. Biol.* 15, 1604–1612. doi:10.1021/acschembio.0c00204

Yoshino, H., Yin, G., Kawaguchi, R., Popov, K. I., Temple, B., Sasaki, M., et al. (2019). Identification of Lysine Methylation in the Core GTPase Domain by GoMADScan. *PLoS One* 14, e0219436–17. doi:10.1371/journal.pone.0219436

Zhang, Y., Han, S.-J., Park, I., Kim, I., Chay, K.-O., Kim, S., et al. (2017). Redox Regulation of the Tumor Suppressor PTEN by Hydrogen Peroxide and Tert-Butyl Hydroperoxide. *Int. J. Mol. Sci.* 18, 982–. doi:10.3390/ijms18050982

Conflict of Interest: The authors declare that the research was conducted in the absence of any commercial or financial relationships that could be construed as a potential conflict of interest.

frontiers in Cell and Developmental Biology

ORIGINAL RESEARCH
published: 08 July 2021
doi: 10.3389/fcell.2021.665673

A Covalent Calmodulin Inhibitor as a Tool to Study Cellular Mechanisms of K-Ras-Driven Stemness

*Sunday Okutachi[1], Ganesh Babu Manoharan[1], Alexandros Kiriazis[2], Christina Laurini[1], Marie Catillon[1], Frank McCormick[3,4], Jari Yli-Kauhaluoma[2] and Daniel Abankwa[1]**

[1] Cancer Cell Biology and Drug Discovery Group, Department of Life Sciences and Medicine, University of Luxembourg, Esch-sur-Alzette, Luxembourg, [2] Drug Research Program, Division of Pharmaceutical Chemistry and Technology, Faculty of Pharmacy, University of Helsinki, Helsinki, Finland, [3] Helen Diller Family Comprehensive Cancer Center, University of California, San Francisco, San Francisco, CA, United States, [4] Frederick National Laboratory for Cancer Research, Cancer Research Technology Program, Leidos Biomedical Research, Inc., National Cancer Institute RAS Initiative, Frederick, MD, United States

OPEN ACCESS

Edited by:
Jin Rui Liang, ETH Zürich, Switzerland

Reviewed by:
Ken Westover, University of Texas Southwestern Medical Center, United States
Vadim Gaponenko, University of Illinois at Chicago, United States

***Correspondence:**
Daniel Abankwa
daniel.abankwa@uni.lu

Specialty section:
This article was submitted to Cellular Biochemistry, a section of the journal Frontiers in Cell and Developmental Biology

Received: *08 February 2021*
Accepted: *04 June 2021*
Published: *08 July 2021*

Citation:
Okutachi S, Manoharan GB, Kiriazis A, Laurini C, Catillon M, McCormick F, Yli-Kauhaluoma J and Abankwa D (2021) A Covalent Calmodulin Inhibitor as a Tool to Study Cellular Mechanisms of K-Ras-Driven Stemness. Front. Cell Dev. Biol. 9:665673. doi: 10.3389/fcell.2021.665673

Recently, the highly mutated oncoprotein K-Ras4B (hereafter K-Ras) was shown to drive cancer cell stemness in conjunction with calmodulin (CaM). We previously showed that the covalent CaM inhibitor ophiobolin A (OphA) can potently inhibit K-Ras stemness activity. However, OphA, a fungus-derived natural product, exhibits an unspecific, broad toxicity across all phyla. Here we identified a less toxic, functional analog of OphA that can efficiently inactivate CaM by covalent inhibition. We analyzed a small series of benzazulenones, which bear some structural similarity to OphA and can be synthesized in only six steps. We identified the formyl aminobenzazulenone **1**, here named Calmirasone1, as a novel and potent covalent CaM inhibitor. Calmirasone1 has a 4-fold increased affinity for CaM as compared to OphA and was active against K-Ras in cells within minutes, as compared to hours required by OphA. Calmirasone1 displayed a 2.5–4.5-fold higher selectivity for KRAS over BRAF mutant 3D spheroid growth than OphA, suggesting improved relative on-target activity. Importantly, Calmirasone1 has a 40–260-fold lower unspecific toxic effect on HRAS mutant cells, while it reaches almost 50% of the activity of novel K-RasG12C specific inhibitors in 3D spheroid assays. Our results suggest that Calmirasone1 can serve as a new tool compound to further investigate the cancer cell biology of the K-Ras and CaM associated stemness activities.

Keywords: K-Ras, calmodulin, covalent inhibitor, cancer stem cell (CSC), BRET

INTRODUCTION

Calmodulin (CaM) is a small (17 kDa) dumbbell-shaped signaling adapter, with hundreds of protein interactions and widespread functions in cellular signaling (Tidow and Nissen, 2013). Its two N- and C-terminal lobes each contain two EF-hands that can coordinate altogether four Ca^{2+} ions. Ca^{2+}/CaM classically recognizes with high, nanomolar affinity approximately 20-residue long peptides with bulky hydrophobic and basic residues that become encased in the hydrophobic pocket formed by the two lobes. This leads to a significant conformational change of CaM with loss of the central helical structure (Tidow and Nissen, 2013). Non-canonical CaM binders typically

possess a polybasic N- or C-terminus with a single lipid modification, which can bind to either or both of the hydrophobic pockets on the N- and C-lobes (Grant et al., 2020b).

CaM has been pursued as a cancer drug target in the 1980s due to its significant role in activating CDKs in the cell cycle (Hait and Lazo, 1986). CaM levels increase during the cell cycle, peaking at G2/M, with a drop-off thereafter (Berchtold and Villalobo, 2014). In addition, CaM seems to be indirectly important for the activation of CDKs that are active in G1 (Taules et al., 1998). CaM distribution is furthermore tightly associated with cell division, as it co-distributes with major structures of the mitotic machinery, such as the central spindle, centrosomes, and the cleavage furrow (Li et al., 1999; Yu et al., 2004). In line with this, CaM inhibitors have been demonstrated to block tumor growth, such as, for example, in multiple myeloma cell line xenografts (Yokokura et al., 2014).

Several non-covalent CaM inhibitors have been developed including the frequently used calmidazolium (Sunagawa et al., 1999) and the highly water-soluble and cell-penetrating naphthalenesulfonamides, such as W-7 (Hidaka et al., 1981; Sengupta et al., 2007). However, the latter can also inhibit CaM targets, such as Ca^{2+}/CaM-dependent cyclic nucleotide phosphodiesterase at concentrations > 100 μM (Itoh and Hidaka, 1984; Zimmer and Hofmann, 1984).

Ophiobolin A (OphA) is a potent, covalent CaM inhibitor (Leung et al., 1984). It is a naturally occurring fungal 5-8-5 tricyclic sesterterpene metabolite with broad toxicity against plants, microbes, and cancer cells (Au et al., 2000). It forms an irreversible covalent adduct via C5, C21-dicarbonyl functionalities after intermediate Schiff base formation with Lys 75 or Lys 77 and Lys 148 of CaM (**Supplementary Scheme 1**). Thus, OphA can react with CaM at a 2:1 ratio, similar to covalent phenothiazine derivatives, which also react with the same lysines (Faust et al., 1987). Despite its potency against CaM, OphA appears to have several other targets, such as phosphatidylethanolamine (Chidley et al., 2016). Together with its broad toxicity across most phyla, this suggests a problematic toxicity spectrum of OphA.

We previously identified OphA as a K-Ras4B (hereafter K-Ras) but not an H-Ras selective inhibitor (Najumudeen et al., 2016). OphA disrupts membrane organization of K-Ras in a CaM-dependent manner and blocked the growth of cancer stem cell enriched spheroids derived from breast cancer cell lines. Up to two K-Ras proteins can directly bind to the two lobes of Ca^{2+}/CaM (Agamasu et al., 2019; Grant et al., 2020a). Interestingly, K-Ras has a higher affinity to the C-terminal lobe (K_D = 0.5 μM) than to the N-terminal lobe (K_D = 4 μM). Complementary to this, the C-terminal lobe of CaM binds Ca^{2+} with higher affinity compared to the N-terminal lobe (Teleman et al., 1986). This affinity constellation may underpin a Ca^{2+}-mediated K-Ras release mechanism. Binding of K-Ras is nucleotide-independent but dependent on the farnesylated C-terminus, while also geranylgeranylation mediates binding albeit with an almost 10-fold lower affinity (Wu et al., 2011; Agamasu et al., 2019; Grant et al., 2020a). In addition, basic residues of the hypervariable region of K-Ras may contribute to the interaction; however, interaction with the prenyl moiety provides the core affinity (Jang et al., 2019; Grant et al., 2020a). In contrast to these more recently established binding determinants, a preference of CaM binding to GTP-K-Ras was previously observed (Villalonga et al., 2001; Abraham et al., 2009).

Experimental data show that palmitoylated Ras isoforms do not interact with CaM (Villalonga et al., 2001) probably because the palmitoyl-moiety would hinder binding to CaM sterically. Thus, its client selectivity could resemble that of PDE6D (PDEδ), a trafficking chaperone that is important for K-Ras plasma membrane localization (Chandra et al., 2011). Indeed, evidence suggests that Ca^{2+}/CaM can act as a trafficking chaperone for K-Ras (Fivaz and Meyer, 2005; Grant et al., 2020a), which at high concentration could sequester K-Ras from the membrane as it binds with a lower affinity (K_D = 4 μM) to nanodiscs than to Ca^{2+}/CaM (Gillette et al., 2015). Given that Ca^{2+}/CaM has a different K-Ras affinity, release mechanism, cellular distribution, and probably client spectrum than PDE6D, it can be expected that these proteins have overlapping, yet non-redundant chaperone functions. The interaction of CaM with K-Ras is inhibited by the phosphorylation of Ser181 in the C-terminus of K-Ras, while vice versa CaM binding prevents phosphorylation (Alvarez-Moya et al., 2010). Intriguingly, the phosphomimetic S181D has a reduced stemness potential (Wang et al., 2015b). Consistently, the atypical PKC agonist prostratin reduced the growth in several murine tumor models, including pancreatic cancer cell line derived xenografts (Wang et al., 2015b).

Thus, a novel rationale for the development of CaM inhibitors has emerged, which is tied to the K-Ras-dependent induction of cancer cell stemness. While this K-Ras and cancer stemness association may rekindle CaM inhibitor drug development, further dissection of the molecular mechanism is hampered by the fact that three transcribed copies of CaM genes exist (*CALM1-3*) in the human genome (Toutenhoofd and Strehler, 2000). CaM cell biology is therefore difficult to dissect genetically.

Here we describe the identification of the formyl aminobenzazulenone **1**, later named Calmirasone1, as a novel, covalent CaM inhibitor. The compound is synthetically readily accessible in a six-step synthesis from commercially available guaiazulene. Its higher CaM affinity, fast K-Ras directed cellular activity, and > 40-fold reduced unspecific cell toxicity as compared to OphA allow the utilization of Calmirasone1 in acute cell biological experiments.

RESULTS

Phenotypic Assessment of Amino Benzazulenones vs. Ophiobolin A

OphA is a potent CaM inhibitor that covalently inactivates its target. We previously showed that it selectively inhibits the functional membrane organization of oncogenic K-Ras. This enabled the inhibition of cancer stem cell features by an as yet not fully defined cellular mechanism (Najumudeen et al., 2016). However, the broad toxicity of OphA limits its application (Chidley et al., 2016).

In order to identify a less toxic functional analog of OphA for application in cell biological studies, we chose the azulene-derived aromatic benzazulen-3-one scaffold, which is distantly related to the non-aromatic 5-8-5 tricyclic ring framework of OphA. This choice was based only on the chemical similarity, and no additional compound-design or -screening efforts were made. We prepared two series of synthetically easily accessible compounds, formylated and matching non-formylated aminobenzazulenones, containing two or one electrophilic functionality for covalent binding (**Scheme 1**). The *ortho*-quinone methide electrophile is part of the ring structure and was shown to react readily with primary amines in a nucleophilic aromatic substitution reaction (Kiriazis et al., 2017; **Supplementary Data 1**); however, other nucleophiles could also react with it. In addition, formyl aminobenzazulenones can undergo a typical Schiff base reaction with amines via their C1-formyl, similar to OphA.

Given that toxicity was the major obstacle to overcome, we first characterized the effects of the compounds in phenotypic assays. Clonogenic growth of breast cancer cell derived 3D tumor spheroids under low adherent conditions is a well-established assay for cancer stem cell properties (Dontu et al., 2003). We were interested in compounds with high K-Ras selectivity in 3D spheroid assays, but low general toxicity in 2D proliferation assays. Consistent with their Ras mutation status, MDA-MB-231 (K-RasG13D) and Hs 578T (H-RasG12D) spheroids were selectively sensitive to KRAS and HRAS knockdown, respectively (**Supplementary Figures 1A–D**), as shown previously (Siddiqui et al., 2020).

Compounds showed varying potencies in 3D spheroids with IC_{50} values between 12 and > 40 μM in MDA-MB-231, and 5.2 and > 40 μM in Hs 578T, as compared to 0.3 and 1.8 μM, respectively, for OphA (**Table 1** and **Supplementary Figures 1E–H**). In order to have a more robust descriptor of the compound effect on the clonogenic sphere forming ability of these cells, we used the drug sensitivity score, DSS_3, which is a normalized area under the dose-response curve value with superior accuracy over IC_{50} determination (**Figures 1A,B**; Yadav et al., 2014). Thus, it became clear that some compounds had a selectivity for the

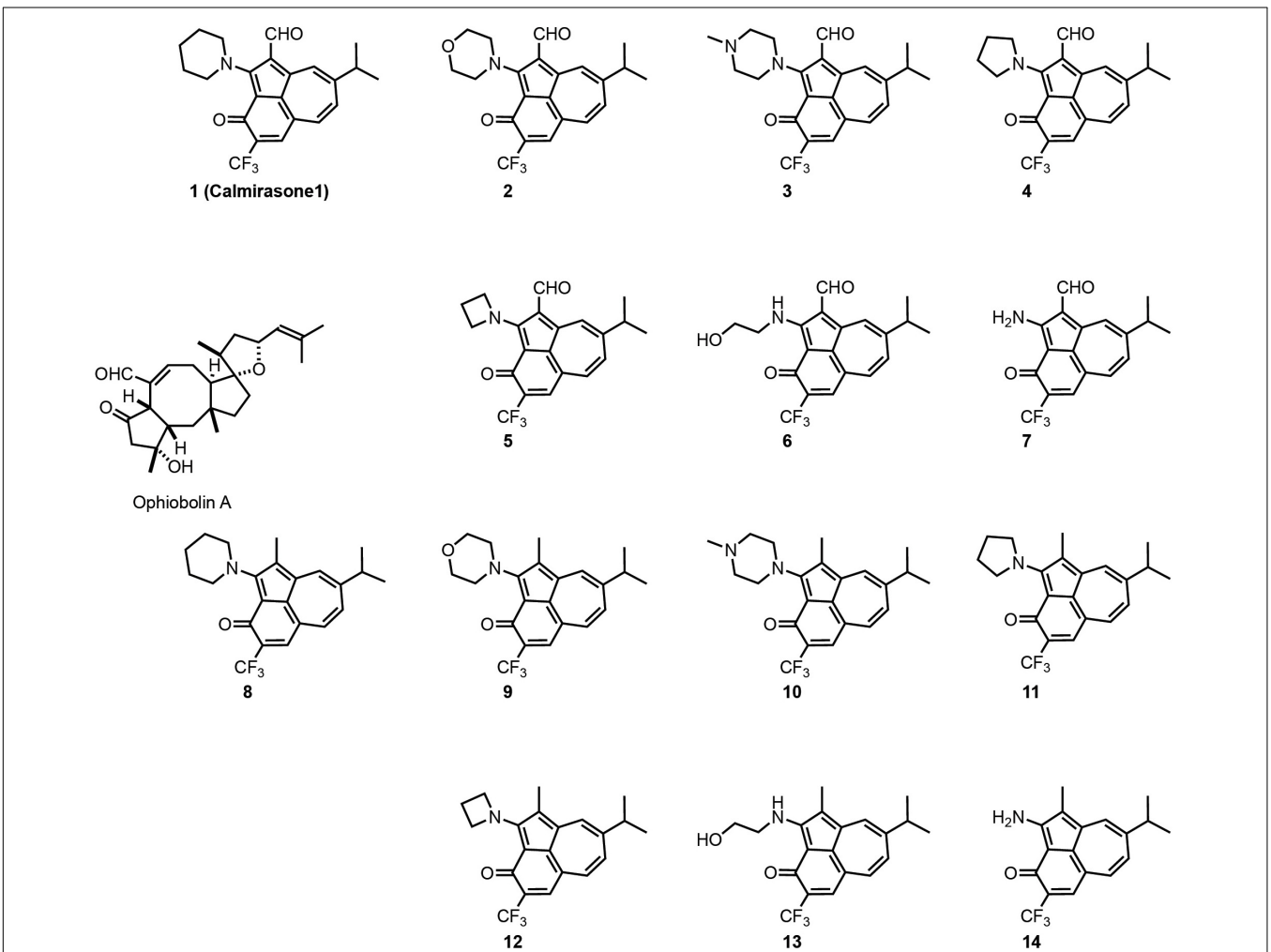

SCHEME 1 | Structures of OphA and the synthetic formyl aminobenzazulenones **(1–7)** and matching aminobenzazulenones **(8–14)**.

TABLE 1 | IC_{50} values of benzazulenones tested on 3D tumorosphere assay.

	MDA-MB-231		Hs 578T	
Compound	**IC_{50}/μM**	**logIC_{50} ± SD**	**IC_{50}/μM**	**logIC_{50} ± SD**
1	12	−4.92 ± 0.03	22.5	−4.65 ± 0.04
2	22.8	−4.64 ± 0.06	24.9	−4.61 ± 0.05
3	35	−4.46 ± 0.05	25.8	−4.6 ± 0.1
4	>40	Inconclusive	>40	Inconclusive
5	34.5	−4.46 ± 0.05	13.2	−4.88 ± 0.04
6	>40	Inconclusive	>40	Inconclusive
7	>40	Inconclusive	>40	Inconclusive
8	32.4	−4.5 ± 0.5	10.6	−4.98 ± 0.03
9	19.6	−4.71 ± 0.03	17.4	−4.76 ± 0.01
10	>40	Inconclusive	23.1	−4.64 ± 0.04
11	15.4	−4.81 ± 0.05	5.2	−5.23 ± 0.04
12	>40	Inconclusive	8.5	−5.1 ± 0.1
13	>40	Inconclusive	>40	Inconclusive
14	>40	Inconclusive	>40	Inconclusive
OphA	0.3	−6.54 ± 0.02	1.8	−5.75 ± 0.02

*Data represent mean of three biological repeats (**Supplementary Figures 1E–H**).*

KRAS-dependent MDA-MB-231 spheroids that was similar to or better than that of OphA.

Next we compared the general cytotoxicity (**Figures 1C,D**) and antiproliferative activity in cells grown in 2D at 10 μM compound concentration (**Supplementary Figures 1I,J**). Higher toxicities and antiproliferative effects with selectivity for MDA-MB-231 were generally observed for the formyl aminobenzazulenones. However, none of the compounds tested at 10 μM was as non-specifically toxic as OphA at only 1 μM against HRAS-dependent Hs 578T cells.

Several Benzazulenones Have a Higher Affinity to CaM Than OphA

High affinity to the target typically reduces off-target toxicities (Bedard et al., 2020). We therefore next determined the *in vitro* affinity of the 14 compounds to the intended target CaM using a fluorescence polarization assay previously developed by us (Manoharan et al., 2019). This assay measures the displacement of a fluorescein-labeled CaM-binding peptide, here derived from plasma membrane calcium-ATPase (PMCA), from purchased CaM by the inhibitors (**Table 2** and **Supplementary Figures 2A,B**).

Compounds **2** and **3** showed the highest affinity (15-fold higher affinity than OphA) and **1** being third best (fourfold higher affinity) after 24-h incubation. The fact that OphA had a significantly higher cytotoxic and antiproliferative activity (**Figures 1C,D** and **Supplementary Figures 1I,J**), despite lower affinity than six of the compounds, confirms its problematic off-target toxicity (Chidley et al., 2016).

Based on these *in vitro* and the phenotypic data, we calculated a customized *composite drug activity score* to select compounds with most favorable properties in each series, i.e., high overall activity in the 3D spheroid assay, high MDA-MB-231 KRAS-mutant cell line selectivity in 3D spheroid assays, low relative 2D growth toxicity against Hs 578T cells relatively to MDA-MB-231, and high affinity (**Supplementary Figures 2E,F**). Thus, we selected **1**, **2, 3, 8, 9**, and **11** for further analysis.

Of note, the binding affinity of OphA increased over several hours, consistent with the slow covalent Schiff base bond formation and the additional pyrrole adduct formation (**Figures 2A,B** and **Supplementary Scheme 1**). By contrast, most benzazulenones immediately showed high IC_{50} ranging from submicromolar to tens of micromolar.

The potency and selectivity of covalent inhibitors are governed by two parameters, namely K_i, the dissociation constant of the initial non-covalent complex, and k_2, the rate of subsequent covalent bond formation (Singh et al., 2011). The latter cannot be too high to avoid non-specific reactivity. Analysis of the reactivity of the top six compounds revealed that formyl aminobenzazulenonens had lower K_i as compared to non-formylated compounds, suggesting that the formyl moiety increases the non-covalent affinity component (**Table 3** and **Supplementary Figures 2G,H**). This is inconsistent with the hydrophobic binding sites on CaM. However, k_2 increased for **1** and **2**, as well as **8** and **9**, with both **2** and **9** having a covalent bond rate constant as high as that of OphA, which also showed an intermediate K_i value.

Cellular BRET Experiments Confirm K-Ras Selectivity of Top Compound 1

Ras proteins are tightly packed into proteo-lipid membrane signaling complexes called nanoclusters (Abankwa et al., 2007). Fluorescent tagging of Ras proteins with a pair of FRET-enabling fluorophores thus leads to the emergence of nanoclustering-dependent FRET. Loss of this FRET signal reports, however, not only on the loss of nanoclustering but also on any upstream processes, i.e., proper Ras plasma membrane trafficking or lipid modifications (Kohnke et al., 2012).

Here we established an analogous nanoclustering-BRET assay by tagging RasG12V proteins with Rluc8, enabling donor emission, and GFP2 as an acceptor. As expected, treatment with mevastatin, which blocks prenyl synthesis, reduced nanoclustering-BRET of both Ras isoforms fairly indiscriminately, while treatment with a farnesyl transferase inhibitor (FTI-277) selectively (1.4-fold) decreased H-Ras nanoclustering-BRET (**Figures 3A,B**), due to the alternative prenylation of K-Ras, as described before (Kohnke et al., 2012).

The inhibition of the trafficking chaperone PDE6D, which facilitates plasma membrane trafficking, in particular of K-Ras, decreases selectively K-Ras nanoclustering-FRET (Siddiqui et al., 2020). In agreement with CaM acting as a trafficking chaperone that can likewise promote forward trafficking to the plasma membrane, we observed a K-Ras selective reduction of nanoclustering-BRET after CaM inhibition with calmidazolium (1.5-fold) and OphA (1.2-fold). The atypical PKC agonist prostratin, which would stimulate K-Ras-Ser181 phosphorylation and thus block CaM binding, had a similar selectivity (1.5-fold) as the CaM inhibitors.

We then tested the top six compounds in this assay in order to directly assess their in cellulo K-Ras selectivity. While most compounds appeared to show some level of K-Ras selectivity

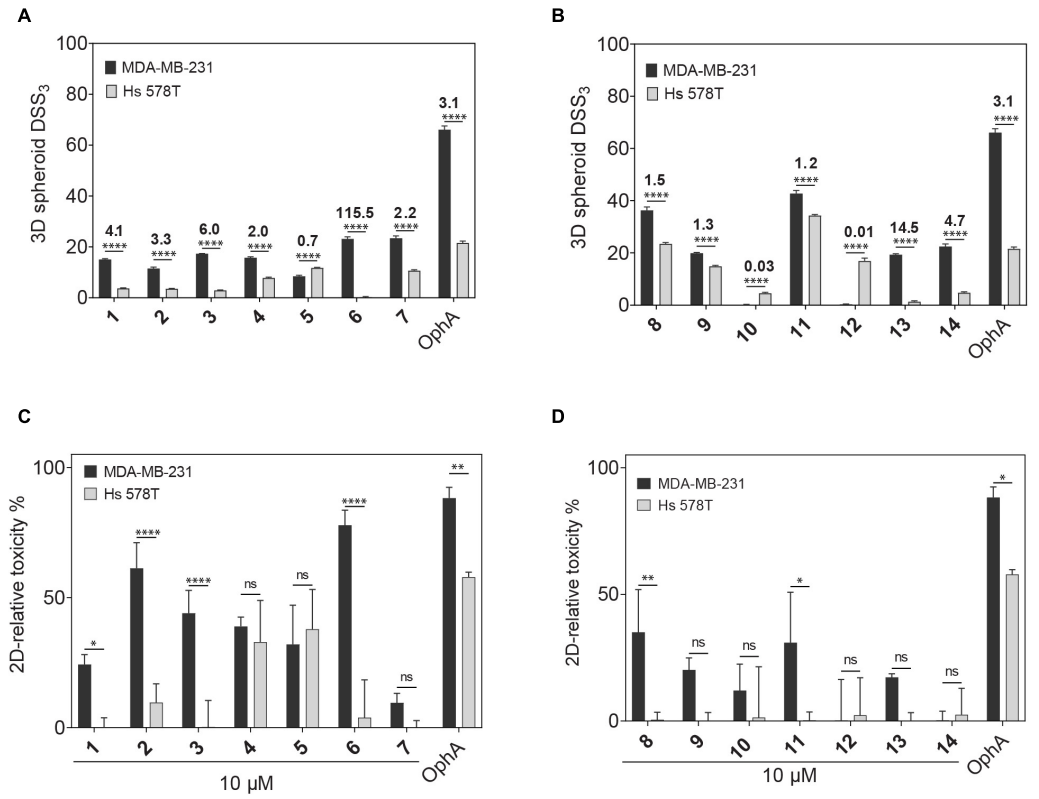

FIGURE 1 | Phenotypic assessment of anticlonogenic and cytotoxic activities of compounds. **(A,B)** A higher DSS_3 reflects a more potent effect of formyl aminobenzazulenones **(A)** and aminobenzazulenones **(B)** tested at a concentration range of 0.6–40 μM on KRAS-mutant MDA-MB-231 and HRAS-mutant Hs 578T 3D spheroid formation in low attachment condition without serum. Data represent mean values ± SD, $n \geq 3$. Numbers above the bars indicate the KRAS/HRAS mutant cell line DSS_3 ratios. **(C,D)** The relative toxicity of formyl aminobenzazulenones **(C)** and aminobenzazulenones **(D)** was assessed in the CellTox Green assay. Cells were grown as 2D adherent monolayers overnight and then treated for 72 h with 1 μM OphA or 10 μM of the indicated benzazulenones. Data represent mean values ± SD, $n \geq 2$. The statistical significance levels are annotated as $^{*}p < 0.05$; $^{**}p < 0.01$; $^{****}p < 0.0001$, or ns, not significant.

TABLE 2 | CaM-binding affinity of compounds after 24-h incubation.

Formyl aminobenzazulenones		Aminobenzazulenones	
Compound	**K_d ± SD/μM**	**Compound**	**K_d ± SD/μM**
1	0.87 ± 0.02	8	3.1 ± 0.3
2	0.23 ± 0.01	9	1.44 ± 0.03
3	0.25 ± 0.02	10	Inconclusive
4	39 ± 12	11	0.81 ± 0.03
5	29 ± 7	12	6.1 ± 0.3
6	31 ± 10	13	62 ± 26
7	45 ± 4	14	21.4 ± 0.6

*A fluorescence polarization assay with the fluorescently labeled PMCA peptide as probe was performed. For comparison K_d(OphA) = 3.5 ± 0.2 μM. While some compounds showed faint autofluorescence under the polarization assay conditions, their emission was too weak as compared to that of fluorescein to interfere with the measurements (**Supplementary Figures 2C,D**).*

(all < 1.3-fold) when compared at 20 μM and 24-h exposure (**Figures 3A,B**), testing over a wider concentration range revealed distinct potencies and selectivities (**Supplementary Figures 3A,B**). We employed the DSS analysis adapted to BRET-data (BRET-DSS_3) to quantify these activities (**Figure 3C**). While, again, overall BRET-activity was highest for OphA, K-Ras selectivity was highest for **1**. All other compounds had lower and non-significant selectivities. By doing a BRET donor saturation titration analysis, we further confirmed that **1** has a similar K-Ras vs. H-Ras selectivity as OphA (**Figures 3 D,E** and **Supplementary Figures 3C–F**).

Compound **1** affinity to CaM changes less over time than that of OphA, suggesting that it assumes its full activity faster (**Figure 2**), which could be advantageous if true also in cellular applications. We therefore tested this property in cells using the K-Ras BRET biosensor. In order to see clear effects at short exposure times, all compound concentrations were increased. OphA showed no significant BRET change during the 2-h treatment timeframe, consistent with the significant time it requires for high affinity binding (**Figure 2**). Likewise, mevastatin did not cause any reduction in the BRET signal, as it has to block metabolic pathways for farnesyl- and geranylgeranyl-pyrophosphate synthesis and therefore acts slowly after protein turnover. In agreement with the *in vitro* data, **1** showed a 38% reduction in the BRET signal within 10 min of treatment (**Figure 3F**). It was therefore even more active acutely in cells than

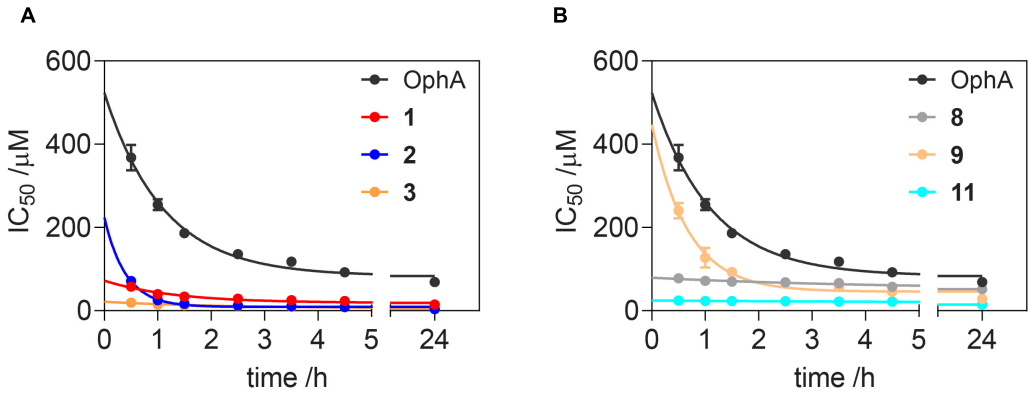

FIGURE 2 | Benzazulenones have higher IC_{50} with less change over time as compared to OphA. Change of effective CaM-binding affinity over time of OphA and formyl aminobenzazulenones **(A)** and aminobenzazulenones **(B)** as measured in the fluorescence polarization assay using F-PMCA peptide as the fluorescent probe. Data represent mean values ± SD, $n = 2$. Binding curves are plotted in **Supplementary Figures 2A,B**. Derived rate analysis plots are in **Supplementary Figures 2G,H**.

TABLE 3 | Analysis of K_i and k_2 and the second-order rate constant k_2/K_i from data plotted in **Figure 2** and processed as described.

Compound	$k_2 \pm$ SD/h^{-1}	$K_i \pm$ SD/µM	$k_2/K_i/M^{-1}\ h^{-1}$
OphA	1.09 ± 0.04	79 ± 8	14×10^3
1	0.51 ± 0.09	52 ± 29	10×10^3
2	1.18 ± 0.09	13 ± 4	93×10^3
3	0.45 ± 0.07	11 ± 6	42×10^3
8	0.35 ± 0.03	39 ± 10	9×10^3
9	1.3 ± 0.2	229 ± 67	6×10^3
11	0.29 ± 0.05	78 ± 34	4×10^3

the non-covalent CaM inhibitor trifluoperazine (K_d = 1.35 µM) or calmidazolium (K_d = 13.5 nM) (Manoharan et al., 2019).

BRET Experiments Confirm K-Ras/CaM Disrupting on-Target Activity in Cells

Previously, a preference of CaM binding to active GTP-K-Ras was observed (Villalonga et al., 2001; Abraham et al., 2009). In agreement with these data, we observed in cells a higher BRET of N-terminally Rluc8-tagged K-RasG12V with GFP2-CaM than that of non-oncogenic K-Ras (**Figure 4A** and **Supplementary Figure 4**). Likewise, higher BRET levels were confirmed with three additional oncogenic mutants of K-Ras (**Figure 4B** and **Supplementary Figures 4A,B**). Furthermore, in line with previous reports (Villalonga et al., 2001), K-RasG12V ($BRET_{max}$ = 0.35 ± 0.02) displayed a significantly (p = 0.001, unpaired t-test) higher cellular BRET ratio with GFP2-CaM than H-RasG12V did ($BRET_{max}$ = 0.20 ± 0.02), which remained at or below control levels (**Figure 4C** and **Supplementary Figure 4**). This could explain the preferential effect on K-Ras nanoclustering-BRET by CaM inhibitors (**Figure 3**).

In order to have a high dynamic range of the BRET signal, we used the Rluc8-K-RasG12V/GFP2-CaM BRET pair to directly assess the effect of modulators of the K-Ras/CaM interaction. Both CaM inhibitor calmidazolium and OphA significantly reduced the BRET signal. Surprisingly, prostratin did not have an effect at the tested concentration (**Figure 4D**).

To further delineate the structural requirements for the on-target, K-RasG12V/CaM disrupting activity, we tested formyl aminobenzazulenone **1** in comparison to the closely related, but less active aminobenzazulenone derivative **8**, which lacks the C1-formyl group. Compound **1** (IC_{50} = 31 ± 2 µM) was significantly more active than **8** (IC_{50} = 70 ± 11 µM; p = 0.03), also when tested over a wider concentration range (**Figure 4E**). Yet, OphA remained the most effective compound in this cellular assay after a 24-h-long exposure (IC_{50} = 12 ± 2 µM).

Dependence of the Activity of top Compound 1 on Lysines 75, 77, and 148 of CaM

We previously showed that the K-Ras directed effect of OphA is abolished if a lysine mutant of CaM is expressed to rescue the knockdown of endogenous CaM (Najumudeen et al., 2016). In this mutant CaM (mutCaM), lysines 75, 77, and 148 were replaced by glutamine, i.e., those residues that were reported to be modified by OphA (Kong Au and Chow Leung, 1998). To assess the dependence of compound **1** binding to CaM on these lysine residues, we again employed a fluorescence polarization assay using in-house purified, His-tagged CaM or mutCaM. Both variants bound to the fluorescein-labeled peptide of Ca^{2+}/calmodulin-dependent kinase II (CaMKII) (Manoharan et al., 2019). As observed before (**Figure 2**), the affinity of OphA to wild-type (wt) CaM increased over several hours, while no binding was observed to mutCaM (**Figure 5A** and **Supplementary Figures 5A,B**), as reported previously (Najumudeen et al., 2016; Manoharan et al., 2019). By contrast, compound **1** also displayed binding to mutCaM; however, as compared to wt CaM, the affinity did not increase over time (**Figure 5B** and **Supplementary Figures 5E,F**). This was different for the non-formylated counterpart **8**, which showed the same binding affinity for wt CaM and mutCaM over time (**Figure 5C** and **Supplementary Figures 5E,F**). The comparison of the

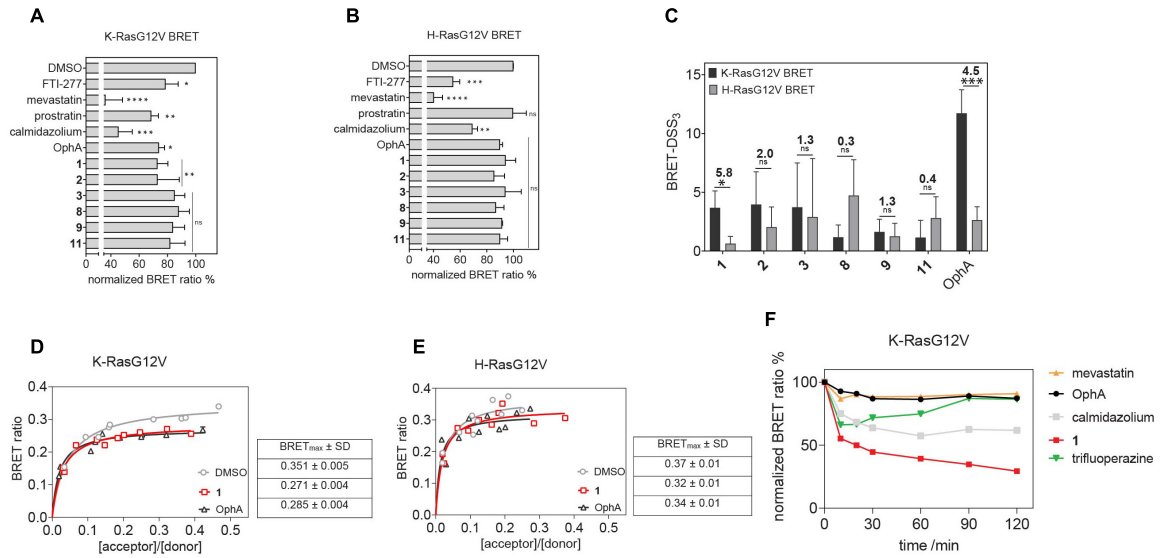

FIGURE 3 | Nanoclustering-BRET assays confirm K-Ras selectivity and fast intracellular activity of compound 1 in cells. **(A,B)** Testing of top six benzazulenones at 20 μM and 24-h exposure in K-RasG12V **(A)** and H-RasG12V **(B)** nanoclustering-BRET assays. Controls are FTI-277 (1 μM), OphA (2.5 μM), mevastatin (10 μM), calmidazolium (20 μM), and prostratin (10 μM). The acceptor/donor (A/D) plasmid ratio of GFP2- and Rluc8-tagged RasG12V was 4/1. Data represent mean values ± SD, $n = 3$. **(C)** BRET-DSS_3 values for selected six benzazulenones and OphA, derived from dose response analysis of benzazulenones (0.1–80 μM) and OphA (0.3–20 μM) on K-RasG12V and H-RasG12V nanoclustering-BRET data (**Supplementary Figures 3A,B**). Numbers above the bars indicate the K-RasG12V/H-RasG12V BRET-DSS_3 ratios. The A/D plasmid ratio was 4/1. Data represent mean values ± SD, $n \geq 3$. **(D)** K-RasG12V and **(E)** H-RasG12V nanoclustering-BRET donor saturation titration curves showing the effect of OphA (2.5 μM), **1** (20 μM), and vehicle control. Data represent mean values ± SD, $n = 2$. Note that error bars are very small and may not be recognizable. $BRET_{max}$ data represent mean values ± SD, $n = 2$. **(F)** Time-dependent change of K-RasG12V nanoclustering-BRET signal after treatment with **1** (50 μM), OphA (10 μM), mevastatin (10 μM), trifluoperazine (20 μM), and calmidazolium (20 μM). The A/D plasmid ratio was 4/1. Data represent mean values ± SD, $n \geq 2$. The statistical significance levels are annotated as $^*p < 0.05$; $^{**}p < 0.01$; $^{***}p < 0.001$; $^{****}p < 0.0001$, or ns, not significant.

activities of all three compounds suggests that the K75Q, K77Q, and K148Q mutations in the mutCaM have rendered CaM partially insensitive to **1** and **8** binding. It furthermore shows that the lysine-dependent increase in affinity over time of compound **1** depends on the C1-formyl, which could form a Schiff base bond in a slow reaction.

Activity in Cell Proliferation Assays Correlates With the K-Ras Dependence of Cancer Cell Lines

Unspecific, broad toxicity against KRAS (MDA-MB-231, MIA PaCa-2) and HRAS mutant (Hs 578T, T24) cancer cell lines, as well as HEK293-EBNA cells, is a major issue of OphA (**Figure 6A**). This broad toxicity appears to greatly contribute to the high "anti-cancer cell activity" that is observed with this compound and clearly contrasts to the KRAS mutant cancer cell line selectivity seen with calmidazolium and **1** (**Figure 6B** and **Supplementary Figures 6A–E**). Of note, the latter has a background activity against HRAS mutant cancer cells that was as low as that of the covalent K-RasG12C inhibitor AMG-510.

When compounds were compared in 3D spheroid growth assays, the significant potency difference between clinical compounds and **1** became, however, more obvious than in 2D assays. Both AMG-510 and vemurafenib selectively and potently abolished the growth of the K-RasG12C- and BRAF-V600E-mutant cancer cell 3D spheroids, respectively, with basically no activity against other cancer cell spheroids (**Figure 6C** and **Supplementary Figures 6F–I**). Compound **1** had a visibly lower activity, yet the activity profile seemed to correlate with the KRAS dependence of the cancer cell lines (**Figures 6C,D**). Again, OphA appeared highly potent, yet clearly at the cost of its broad toxicity (**Figures 6A,C**). These data are in line with a much improved on-target activity of **1** as compared to OphA.

The Best Tool Compound 1 Can Be Utilized in Cell Biological Experiments

Given the significantly reduced unspecific toxicity of **1** as compared to OphA, we tested its application in cell biological experiments. CaM dynamically localizes to centrosomes, spindle, and other structures during mitosis, and its inhibition is known to affect proper cleavage furrow formation, which can lead to multipolarity (Yu et al., 2004; Wu et al., 2010).

In order to track this phenotype and the CaM distribution, we transfected HeLa cells with a mCherry-CaM construct, which primarily localized to centrosomes in mitotic cells (**Figure 7A**). When these cells were synchronized and treated with the potent, non-covalent CaM inhibitor calmidazolium, an increased fraction of multipolar cells with multiple mCherry-CaM-positive centrosomes was observed. As expected from the faster in-cell activity observed in BRET experiments (**Figure 3F**), this phenotype was significantly pronounced with **1** (**Figure 7B**), confirming its utility in cell biological experiments. Finally,

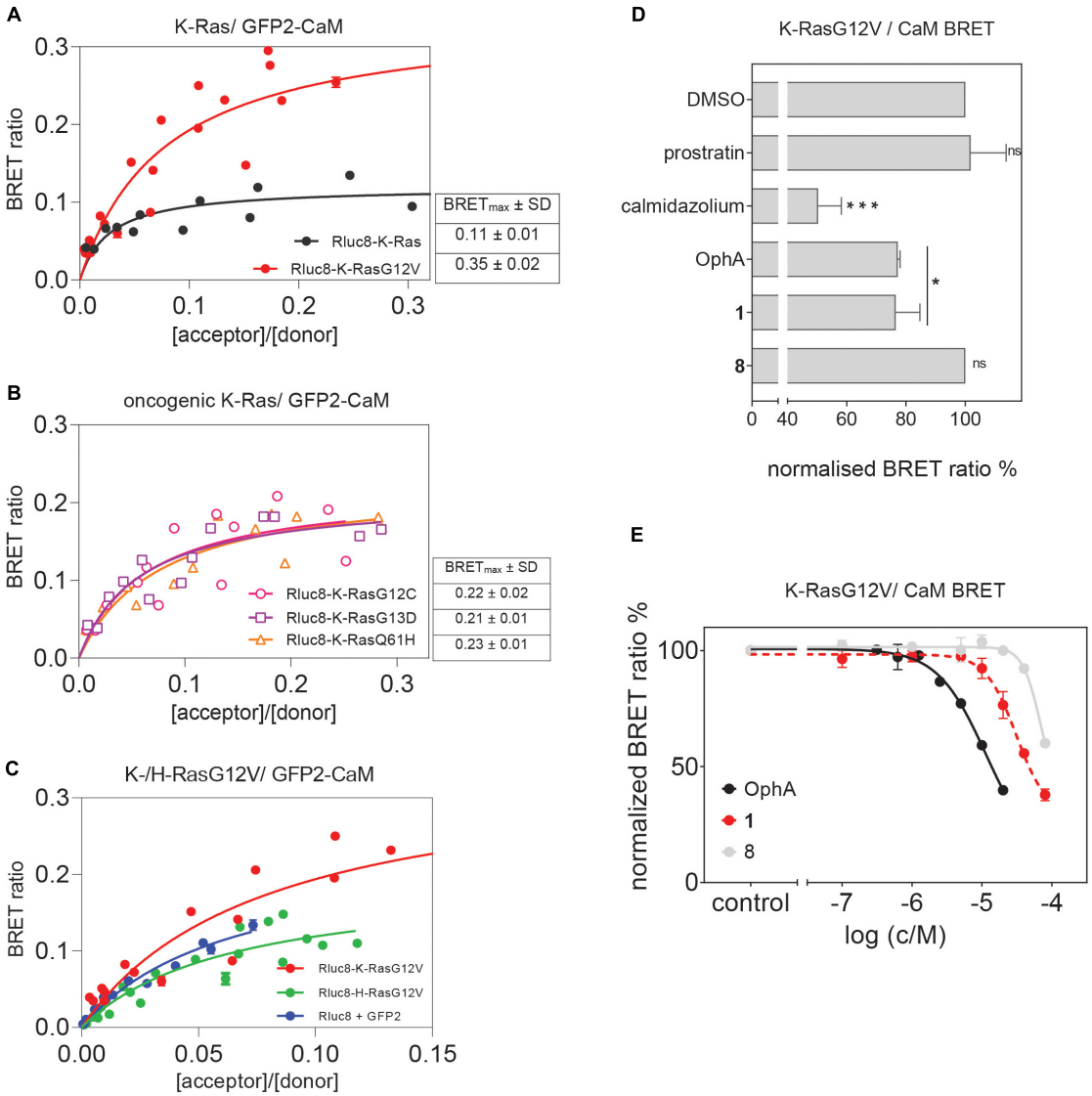

FIGURE 4 | Cellular K-RasG12V/CaM interaction BRET confirms on-target activity of compound 1 in cells. **(A)** BRET donor saturation titration curves between Rluc8-K-Ras or Rluc8-K-RasG12V and N-terminally GFP2-tagged CaM. **(B)** BRET donor saturation titration curves between the Rluc8-tagged K-Ras oncogenic mutants (K-RasG12C, K-RasG13D, and K-RasQ61H) with GFP2-CaM. The $BRET_{max}$ data represent mean values ± SD, $n \geq 2$. **(C)** BRET donor saturation titration curves between Rluc8-K-RasG12V or Rluc8-H-RasG12V and GFP2-CaM. Plasmids expressing Rluc8 and GFP2 proteins alone were used as controls for non-specific interaction. **(D)** Compounds calmidazolium (20 μM), prostratin (20 μM), or OphA (5 μM), as well as formyl aminobenzazulenone **1** (20 μM) or non-formylated counterpart aminobenzazulenone **8** (20 μM) were tested using the Rluc8-K-RasG12V/GFP2-CaM BRET reporter. The A/D plasmid ratio was 9/1. Data represent mean values ± SD, $n \geq 2$. **(E)** Dose-response analysis of compound **1** and its non-formylated derivative **8** as compared to OphA using Rluc8-K-RasG12V/GFP2-CaM BRET signal. The A/D plasmid ratio was 9/1. Data represent mean values ± SD, $n \geq 2$. The statistical significance levels are annotated as $^{*}p < 0.05$; $^{***}p < 0.001$, or ns, not significant.

we named compound **1**, the best performing tool compound, **Calmirasone1**.

DISCUSSION

We have here identified compound **1**, which we named **Calmirasone1,** a synthetically well-accessible, high affinity covalent CaM inhibitor with fast cellular K-Ras selectivity and significantly lower toxicity than the natural product counterpart OphA. While the current potency and properties of **Calmirasone1** do not fit for a compound with future medical applications, our data support its intended utility as a tool compound in cell biological applications to study CaM-dependent cellular processes. Such tool compounds are important also for drug development, as they can foreshadow some on-target issues and reveal crucial mechanistic features of actual drug candidates.

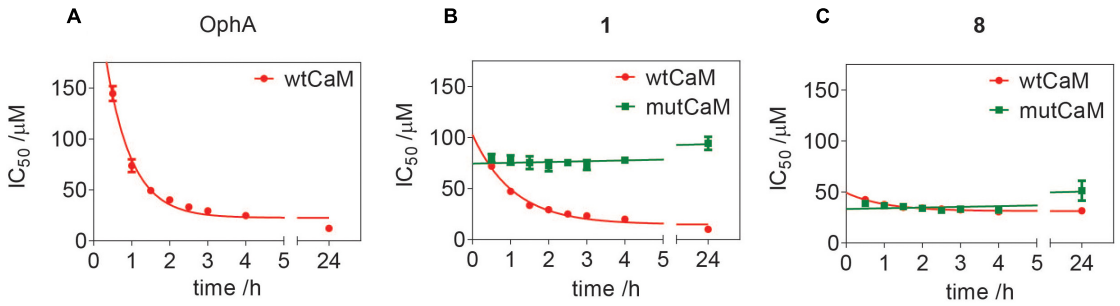

FIGURE 5 | Assessment of lysine-dependent CaM-binding activity of OphA, formyl aminobenzazulenone **1**, and aminobenzazulenone **8**. Time course of lysine-dependent CaM-binding activity of OphA **(A)**, compound **1 (B)**, and compound **8 (C)** as measured in the fluorescence polarization assay using F-CaMKII peptide as the fluorescent probe. OphA displayed negligible binding with mutCaM compared to wtCaM; hence, no IC_{50} values could be derived (**Supplementary Figures 5A,B**).

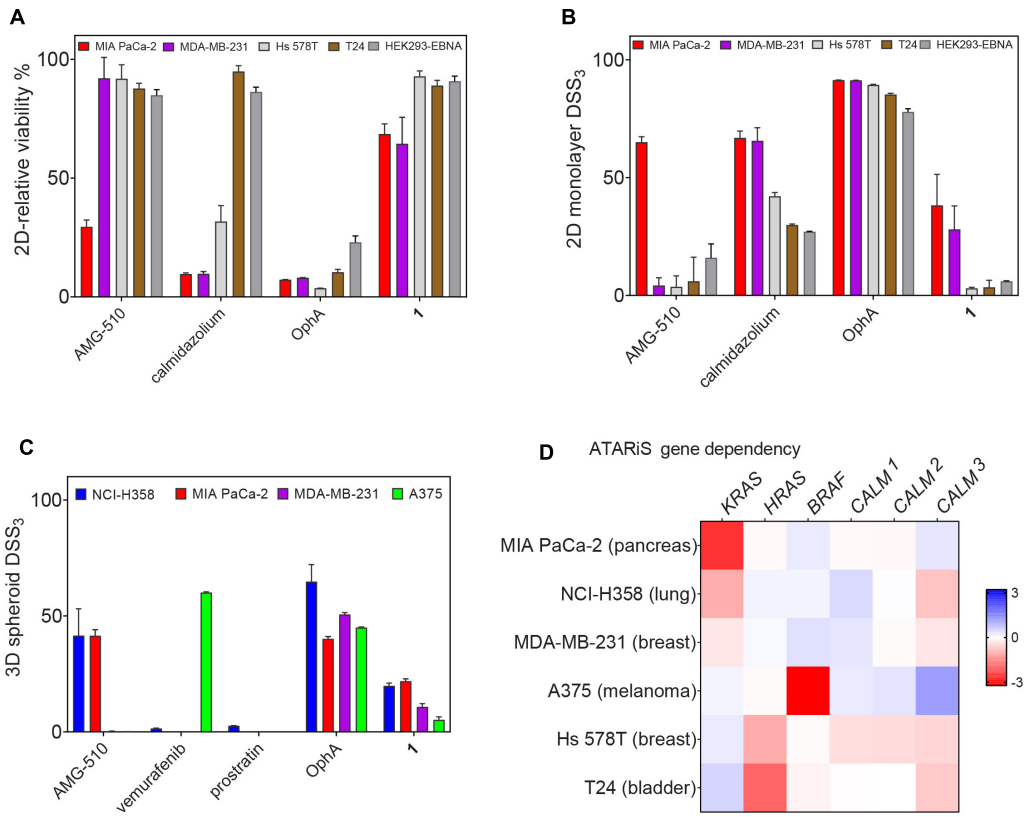

FIGURE 6 | Benchmarking of top compound 1 in several cancer cell lines. **(A)** The relative 2D viability of various cell lines following single dose treatment with AMG-510 (1 µM), calmidazolium (2.5 µM), OphA (1 µM), and **1** (10 µM) was assessed using the alamarBlue assay. Cells were grown as 2D adherent monolayers overnight and then treated for 72 h with indicated compounds. Data represent mean values ± SD, $n \geq 3$. **(B)** DSS_3 measuring the effects of AMG-510 (0.003–40 µM), calmidazolium (0.3–40 µM), OphA (0.3–40 µM), and **1** (0.6–80 µM). Cells were grown as 2D adherent monolayers overnight and then treated for 72 h. Results represent mean values ± SD, $n = 3$. **(C)** DSS_3 measuring the effects of AMG-510 (0.6–40 µM), vemurafenib (0.3–20 µM), prostratin (0.6–80 µM), OphA (0.3–20 µM), and **1** (1.3–80 µM). Cells were grown as 3D spheroids for 72 h then treated with compounds for another 72 h before alamarBlue viability measurements. Data represent mean values ± SD, $n \geq 2$. **(D)** Heatmap of ATARiS gene sensitivity scores obtained from the project DRIVE database for KRAS-dependent cell lines (MIA PaCa-2, NCI H358, and MDA-MB-231) and HRAS-dependent cell lines (Hs 578T and T24). Negative values (red) indicate sensitivity of the cell line proliferation to the knockdown of shown genes, while positive (blue) indicates the opposite.

Several of our compounds bound to CaM with submicromolar affinity, with **Calmirasone1** binding four times better than OphA. Comparison of **Calmirasone1** and **8** affinities with purified wt and mutant CaM suggests that the affinity binding component that remained constant over time was independent of the C1-formyl (**Figure 5**). This immediate high affinity

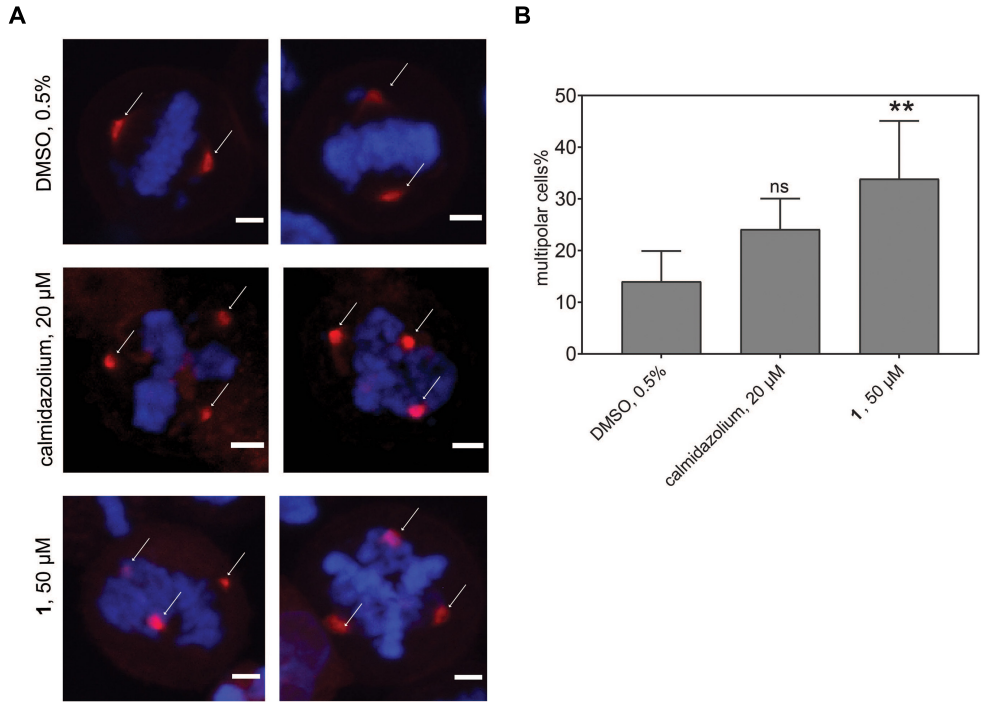

FIGURE 7 | Phenotypic effects of CaM inhibitors on centrosome numbers. **(A)** Representative images for bipolar normal (DMSO 0.5%, top) and multipolar centrosomes in HeLa cells after acute treatment for 2 h with calmidazolium (20 μM, middle) **1** (50 μM, bottom). Hela cells expressing mCherry-wtCaM (red) cells were synchronized with nocodazole to the G2/M phase for 16 h. Then cells were treated with compounds and simultaneously with the protease inhibitor MG132 (10 μM). Arrows indicate predominant localization of mCherry-wtCaM on the centrosomes during mitosis. DNA was stained with DAPI (blue). Scale bar, 5 μm. **(B)** The multipolar phenotype was quantified for each treatment from images containing 35 to 70 cells per condition. Data represent mean values ± SD, $n = 3$. Statistical significance was evaluated with Fisher's exact test. The statistical significance levels are annotated as $^{**}p < 0.01$, or ns, not significant.

could have been of non-covalent or actually also of covalent nature. Given that a second reactive group with covalent binding potential (*ortho* quinone-methide, *o*-QM) is present in both **Calmirasone1** and **8**, it is possible that this electrophile mediates additional covalent binding to lysine residues other than those three mutated lysines in mutCaM (**Supplementary Data 1**), or alternatively cysteines. However, nucleophilic cysteines are not present in the studied CaM variants. Based on previous synthetic studies, the *o*-QM reactivity toward nucleophiles (amino or thiol) can be very fast (within minutes) and proceeds via a nucleophilic aromatic substitution (S_NAr-type) reaction (Kiriazis et al., 2017). We currently lack evidence whether this second electrophile is also engaged covalently.

Our rate analysis (**Table 3**) shows that the compound with the highest second order rate constant was **2**, followed by **3**. However, as our cellular BRET-data in **Figure 3C** indicate, this increased reactivity appears to come at the cost of selectivity. We see a maximal selectivity for K-RasG12V vs. H-RasG12V for **1**, which has intermediate parameters, in agreement with a balance between sufficient affinity and a moderate reactivity. In agreement with the slow Schiff-bond formation, we find rate constants that are several thousand-fold lower than those of Lys-reactive compounds with a vinyl sulfone as warhead, such as the CDK2-inhibitor NU600 ($k_2/K_i = 5.0 \times 10^3$ M^{-1} s^{-1}) (Anscombe et al., 2015). However, the α-hemoglobin targeting compound GBT440 (Voxelotor) with a formyl warhead similar to our compounds has a second-order rate constant comparable to what we found for our benzazulenones ($k_2/K_i = 15 \times 10^3$ M^{-1} h^{-1}) (Center for Drug Evaluation and Research, 2017; Metcalf et al., 2017).

We speculate that the formyl-independent binding component significantly improves the unspecific toxicity of compounds **Calmirasone1** and **8** (**Figures 1C,D**). However, the major, slower affinity increase stems from the C1-formyl and depends on mutated lysines 75, 77, and 148. This is consistent with the formyl as a hard electrophile reacting with lysine as a hard nucleophile. The typically slow Schiff base formation may, therefore, explain the slow increase in the effective affinity (**Figure 5B**). The formyl substituent is furthermore beneficial, as it lowers the relatively high clogP, thus potentially increasing water solubility of these not very drug-like molecules. However, drug entry into cells can be an active process that depends on transporters from the solute carrier protein (SLC) family (Girardi et al., 2020). In addition, passive entry is typically characterized by the compound specific partitioning coefficients. Both passive and active entry may explain why we observed distinct time courses for the inhibitors to become active in cells against K-RasG12V membrane anchorage (**Figure 3F**).

Currently, the structural basis for CaM inhibition by OphA is not known. However, similar to other non-covalent inhibitors,

such as trifluoperazine, the conformational dynamics of CaM may change dramatically upon inhibitor binding, collapsing the original dumbbell-shaped molecule into a compact globular structure (Vandonselaar et al., 1994). We speculate that covalent inhibitors such as OphA and the here tested compounds would have a similar effect on the conformation and therefore activity of CaM to bind its canonical and non-canonical clients, such as K-Ras.

The Ras nanoclustering-dependent BRET assay that we used before successfully in the FRET format to assess the Ras selectivity close to the mechanistic target K-Ras (Najumudeen et al., 2016; Posada et al., 2016) is sensitive to the disruption of Ras membrane anchorage and correct plasma membrane trafficking. CaM was recently established as a K-Ras trafficking chaperone, which can essentially act as a solubilizing factor to shield the farnesyl tail from the aqueous environment of the cytoplasm (Grant et al., 2020a). Therefore, the drop in K-Ras nanoclustering-BRET with CaM inhibitors is consistent with CaM being a trafficking chaperone for K-Ras (Grant et al., 2020b).

We have previously demonstrated similar changes in membrane anchorage of K-Ras with the inhibition of PDE6D, another prominent trafficking chaperone of K-Ras (Siddiqui et al., 2020). For PDE6D, clients such as H-Ras that are in addition palmitoylated cannot bind as long as they are palmitoylated (Chandra et al., 2011; Dharmaiah et al., 2016). This establishes an effective K-Ras over H-Ras selectivity for PDE6D inhibition-induced cell growth effects (Siddiqui et al., 2020). Grant et al. (2020a) recently derived singly lipidated polybasic termini of proteins as non-canonical CaM interaction sequences. Consistently, K-Ras but not H-Ras or N-Ras bind to CaM (Villalonga et al., 2001). It can be speculated that any additional palmitoylation would sterically hinder access to CaM, making palmitoylated Ras isoform clients only if they are in their non-palmitoylated state (Agamasu et al., 2019). This would explain why the potent CaM inhibitor calmidazolium decreased the BRET signal of H-Ras, albeit to a lesser extent than that of K-Ras (**Figures 3A,B**).

The highly potent calmidazolium, as well as the covalent inhibitors OphA and **Calmirasone1**, significantly disrupted K-Ras/CaM-BRET in cells. By contrast, the PKC agonist prostratin had no effect on K-Ras/CaM-BRET, but on K-RasG12V nanoclustering BRET. It may therefore be that prostratin exerts its K-Ras selectivity by a different mechanistic route than the inhibition of K-Ras/CaM interaction. Interestingly, prostratin had almost no effect on cell growth in 3D spheroid assays (**Figure 6C**).

Clonogenic 3D spheroid growth depends on stemness associated asymmetric and symmetric division processes of cancer cells with stemness traits (Cicalese et al., 2009). Accordingly, **Calmirasone1** demonstrates an efficacy against 3D spheroid growth that correlates with the KRAS dependence of the tested cell lines. In this regard, it is noteworthy that the DSS_3 potency of **Calmirasone1** reaches already approximately 50% of AMG-510, the K-RasG12C inhibitor that is currently being evaluated in the clinic (Hong et al., 2020). However, a much larger number of cell lines would have to be tested to demonstrate a correlation between compound activity and anticipated K-Ras/CaM targeting mechanism. For instance, both cell lines that were employed here also carry mutations in BRAF (MDA-MB-231) or in TP53 (both MDA-MB-231 and Hs578T). For both B-Raf and p53, connections to CaM signaling have been reported (Ren et al., 2008; Taylor et al., 2020); hence, the cell killing activity may relate to multiple pathways that are affected downstream of CaM.

In addition, we could demonstrate the benefits of using **Calmirasone1** as a tool compound in cell biological experiments, which are not possible with OphA due to its high toxicity. We observed the induction of multipolar cells by CaM inhibitor treatment. Inhibition of CaM affects multiple processes during cell division, notably cleavage furrow formation (Yu et al., 2004). While failure of cytokinesis can lead to chromosomal instability and therefore a hallmark of cancer cells, the exact nature of the multipolar phenotype and additional effects could also play a role in the ultimately cell growth inhibiting effect of CaM inhibition (Wu et al., 2010). Interestingly, a different compound that induces multipolar acentrosomal spindles was found to selectively kill tumor cells (Wang et al., 2015a). In our cell biological experiments, **Calmirasone1** (K_d = 0.87 ± 0.02 μM) can be considered more effective than non-covalent calmidazolium (K_d = 13.5 nM) (**Figures 3F**, **7B**). While **Calmirasone1** was used at 2.5-fold higher concentration, the 64-fold affinity difference between these two compounds suggests a > 25-fold higher effectivity of **Calmirasone1**. Therefore, **Calmirasone1** can be used to acutely (within 30–60 min) perform a chemical knockdown of CaM in cells in a more efficient manner than with the most potent non-covalent inhibitor calmidazolium.

Covalent inhibitors have experienced a renaissance in the past few years (Singh et al., 2011). Our novel covalent CaM inhibitor **Calmirasone1** will add to the arsenal of covalent tool compounds to study in particular the cell biology of K-Ras/CaM-driven stemness processes.

MATERIALS AND METHODS

Compound Synthesis

Synthesis of chemical compounds and their analytical information are given in **Supplementary Data 1**.

Expression Constructs and siRNA

Most expression constructs described in the study were produced by multisite gateway cloning as described (Wall et al., 2014; **Supplementary Table 1**). For plasmids used in the BRET assay, three entry clones, with compatible LR recombination sites, encoding the CMV promoter, Rluc8, or GFP2 tag, and the gene of interest were recombined with a destination vector, pDest-305 or pDest-312, using the Gateway LR Clonase II enzyme mix (cat. no. 11791020, Thermo Fisher Scientific). The reaction mix was transformed into the ccdB-sensitive *E. coli* strain DH10B (cat. no. EC0113, Thermo Fisher Scientific), and positive clones were selected using ampicillin. pDest527-His-wtCaM and pDest527-His-mutCaM were produced from the LR reaction between the pDest-527 vector with either entry clone pDONR221-wtCaM or pDONR221-mutCaM. The

N-terminally GFP2-tagged CaM plasmid pDest-CMV-GFP2-CaM was cloned at Genecust (France) and amplified in the *E. coli* CopyCutter EPI-400 strain (cat. no. C400CH10, Lucigen) according to the instruction of the manufacturer. All the plasmids were verified by sequencing. Expression and localization of the Ras and CaM fusion proteins were confirmed by confocal microscopy (**Supplementary Figure 7**). Protein sequences of all expression constructs are given in the Supplementary Material section. pmCherry-wtCaM was previously described (Manoharan et al., 2019).

Knockdown of CALM1 was done using a master mix of multiple siRNA against the CALM1 transcript [QIAGEN Hs_CALM1, siRNAs: SI00092925 (CALM1_4), SI02224215 (CALM1_5), SI02224222 (CALM1_6), and SI03649268 (CALM1_8)]. For the knockdown of specific Ras isoforms, we used KRAS (K-Ras4A + K-Rras4B- L-005069-00) and HRAS (L-004142-00) Dharmacon On-Target plus siRNA SMARTpools. Scrambled siRNA control was from QIAGEN (cat. no. 102276).

Commercial Chemical Inhibitors

Fluorescein-labeled CaMKII and PMCA peptide were from Pepmic, China, and Genscript, United States, respectively (Manoharan et al., 2019). DMSO was from PanReac-AppliChem (cat. no. A3672, ITW Reagents). Sources of the inhibitors used in the study are listed below.

Compound	Source	Catalog number
Ophiobolin A	Santa Cruz	sc-202266
Mevastatin	Alfa Aesar	J61357
FTI-277	BioVision	2874
Prostratin	Sigma-Aldrich	P0077
Calmidazolium	Santa Cruz	sc-201494
AMG-510	MedChem Express	HY-114277
Vemurafenib	Selleckchem	S1267
Trifluoperazine	Cayman	15068
Benzethonium chloride	Sigma-Aldrich	53751

RT-qPCR Analysis of Gene Transcript Knockdown

MDA-MB-231 and Hs 578T cells were seeded in 12-well plates and transfected with indicated amounts of siRNAs. Where required, siRNA was transfected into cells using a Lipofectamine RNAiMAX (cat. no. 13778075, Thermo Fisher Scientific) reagent according to the instruction of the manufacturer. After 24 h of transfection, total RNA was isolated using NucleoZol (cat. no. 7040404, Macherey-Nagel) according to the manufacturer protocol. Reverse transcription was performed with 1 μg of total RNA using SuperScript III Reverse Transcriptase (cat. no. 18080093, Thermo Fisher Scientific). The knockdowns of KRAS, HRAS, and CALM1 gene transcripts were analyzed by real-time qPCR using SsoAdvanced Universal SYBR Green Supermix (cat. no. 1725274, BIO-RAD) on the CFX-connect real-time PCR instrument (BIO-RAD). The transcripts were selectively amplified using specific primers producing amplicons for total KRAS (both KRAS4A and KRAS4B), HRAS, and CALM1. The gene transcript ACTB encoding for β-actin was used as reference. The following primers were used (Tsai et al., 2015): for total KRAS, forward 5′-tacagtgcaatgagggacca-3′, reverse 5′-tcctgagcctgttttgtgtct-3′ (amplicon 206 bp); for HRAS, forward 5′-ctgaccatccagctgatcca-3′, reverse 5′-tggcaaacacacacaggaag-3′ (amplicon 196 bp); for ACTB, forward 5′-ggggtgttgaaggtctcaaa-3′; reverse 5′- ggcatcctcaccctgaagta-3′ (amplicon 203 bp); for CALM1, forward 5′-gctcgcaccatggctgat-3′, reverse 5′- tgttggg ttctgacccagtg-3′ (amplicon 144 bp).

3D Spheroid Assays

3D spheroid formation assays were performed in 96-well low-attachment, suspension culture plates (cat. no. 655185, Cellstar, Greiner Bio-One) under serum-free condition. About 1,000 (MDA-MB-231, NCI-H358, and MIA PaCa-2) or 2,500 (Hs 578T) cells per well were seeded in 50 μl of either an RPMI medium (cat. no. 52400-025, Gibco, Thermo Fisher Scientific) (MDA-MB-231, A375, and NCI-H358) or DMEM (cat. no. 41965-039, Gibco, Thermo Fisher Scientific) (Hs 578T and MIA PaCa-2), containing 0.5% MethoCult (cat. no. SF H4636, Stemcell technologies), 1x B27 (cat. no. 17504044, Gibco, Thermo Fisher Scientific), 25 ng/ml EGF (cat. no. E9644, Sigma-Aldrich), and 25 ng/ml FGF (cat. no. RP-8628, Thermo Fisher Scientific). Cells were cultured for 3 days and then treated with compounds or vehicle control (DMSO 0.1% v/v in growth medium) for another 3 days. The cells were supplemented with a fresh growth medium on the third day together with the drug treatment. For knockdown experiments, cells were seeded in 12-well plates and treated with either 50 nM scrambled siRNA (cat. no. 1022076, QIAGEN) or indicated concentrations of siRNAs. Next day, cells were collected by trypsinization and re-plated into 96-well plates for 3D spheroid suspension culture.

Spheroid formation efficiency was analyzed by an alamarBlue assay reagent (cat. no. DAL1100, Thermo Fisher Scientific). A 10% final volume of the alamarBlue reagent was added to each well of the plate and incubated for 4 h at 37°C. Then the fluorescence intensity was measured using the FLUOstar OPTIMA plate reader (BMG Labtech, Germany) with an excitation wavelength of 560 ± 5 nm and an emission wavelength of 590 ± 5 nm. The obtained fluorescence intensity data were normalized to vehicle control corresponding to 100% sphere formation and the signal after 100 μM benzethonium chloride treatment, which killed all cells (i.e., maximum inhibition of sphere formation).

Drug Sensitivity Score (DSS) Analysis

To quantitatively profile the drug sensitivity with a more robust parameter than the IC_{50} or EC_{50} values, the drug sensitivity score (DSS) analysis was employed. DSS values are essentially normalized area under the curve (AUC) measures of dose-response inhibition data (Yadav et al., 2014). Drug response data files (in Excel) ready for online analysis were prepared according to the example file obtained from the DSS pipeline website, called

Breeze[1] (Potdar et al., 2020). Either raw fluorescence intensity measurements or normalized % inhibition data (for BRET assay analysis) were uploaded.

The output file provides several drug sensitivity measures including EC_{50} and AUC. We plotted the DSS_3 value (Yadav et al., 2014), which was calculated as

$$DSS_3 = DSS_2 \frac{x_2 - x_1}{C_{max} - C_{min}}$$

where DSS_2 is given by the equation $DSS_2 = \frac{DSS_1}{\log a}$ and DSS_1 is given by the equation $DSS_1 = \frac{AUC - t(x_2 - x_1)}{(100-t)(C_{max} - C_{min})}$

DSS_3 was employed to emphasize drugs that obtain their response area over a relatively wide dose window, as compared to drugs that show increased response only at the higher end of the concentration range. After logistic fitting of the dose-response inhibition data, the area under the curve (AUC) was determined as the exact solution. A 10% minimal activity threshold (t) was set. The maximum (C_{max}) and minimum (C_{min}) concentrations were used for screening of the inhibitors, with $C_{max} = x_2$ and x_1 concentration with minimal activity t. The parameter a is the value of the top asymptote, which can be different from 100% inhibition as obtained from 100 μM benzethonium chloride treatment.

2D Cell Toxicity and Viability Assays

Hs 578T and MDA-MB-23 cells cultured in complete DMEM and RPMI medium [i.e., supplemented with 10% FBS (cat. no. 10270–098, Gibco, Thermo Fisher Scientific), 2 mM L-glutamine (cat. no. 25030-024, Thermo Fisher Scientific)], respectively, were plated onto 96-well F-bottom cell culture plates (cat. no. 655180, Cellstar, Greiner Bio-One) at a density of 1,000 cells (MDA-MB-231, MIA-PaCa-2, T24, and HEK293-EBNA) and 2,500 cells (Hs 578T) per well grown for 24 h. Freshly thawed aliquots of test compounds were then added at indicated concentrations. DMSO 0.2% v/v in a growth medium was used as the vehicle control. Plates were further incubated for 72 h. The cell viability and cell toxicity effects were analyzed by alamarBlue and CellTox Green (cat. no. G8743, Promega) assays, respectively. A 10% final volume of the alamarBlue reagent was added to each well of the plate and incubated for 4 h at 37°C. Then the fluorescence intensity was measured using the FLUOstar OPTIMA plate reader (BMG Labtech) with an excitation wavelength of 560 ± 5 nm and an emission wavelength of 590 ± 5 nm. The obtained fluorescence intensity data were normalized to vehicle control (100% viability).

For the CellTox Green assay, 100 μl of the 2× CellTox Green reagent was added to each well of a 96-well plate containing 100 μl of the medium. The plate was protected from light and incubated for 15 min at 37°C, then orbitally shaken for 1 min at 700–900 rpm. The fluorescence intensity was measured using the Clariostar plate reader (BMG Labtech) with an excitation wavelength of 485 ± 4 nm and an emission wavelength of 530 ± 4 nm. The obtained fluorescence intensity data were normalized to vehicle control (0% toxicity).

[1]https://breeze.fimm.fi/

Protein Purification

Our numbering of CaM follows (Kong Au and Chow Leung, 1998) with Ala being the first amino acid in human CaM, as the N-terminal methionine of CaM is removed in most organisms (Halling et al., 2016). His-wtCaM and His-mutCaM were expressed in *E. coli* BL21 Star (DE3)pLysS (cat. no. C602003, Thermo Fisher Scientific). pDest527-His-wtCaM and pDest527-His-mutCaM plasmids encoding wild-type human CaM and CaM with K75Q, K77Q, and K148Q mutations, respectively, were transformed into *E. coli* BL21 Star (DE3)pLysS and grown in a Luria Broth medium supplemented with ampicillin (100 μg/ml). At A_{600} of 0.6–0.8, the culture was induced with 0.5 mM of isopropyl β-D-thiogalactopyranoside and expressed for 16 h at 25°C. Cells were collected by centrifugation and incubated on ice for 30 min. The cell suspension was sonicated in a lysis buffer (20 mM HEPES, pH 7.6, 150 mM NaCl, 5 mM $MgCl_2$, 0.5 mg/ml lysozyme, and DNase I). The lysates were clarified by centrifugation at 18,000 *g* for 30 min at 4°C. The soluble fractions were subjected to protein purification.

The His-tagged proteins were purified on HisTrap™ HP Prepacked Columns (GE Healthcare) using the chromatography system ÄKTAprime plus (GE Healthcare). The columns were equilibrated in a buffer composed of 50 mM Tris HCl, pH 7.5, 150 mM NaCl, and 35 mM imidazole, and the His-tagged proteins were eluted in an elution buffer containing 250 mM of imidazole. The eluted fractions were dialyzed for 16 h at 4 °C in a buffer composed of 50 mM Tris HCl, pH 7.5, 150 mM NaCl, and 2 mM $CaCl_2$. Protein concentration was measured using a NanoDrop 2000c Spectrophotometer (Thermo Fisher Scientific), and purified proteins were analyzed on a 4–12% NuPAGE gel (cat. no. NP0321, Thermo Fisher Scientific) (**Supplementary Figure 8**).

Fluorescence Polarization Assay

Fluorescence polarization (FP) assays were performed as described (Manoharan et al., 2019). The IC_{50} of compounds were determined in a binding/displacement assay using fluorescein-labeled PMCA peptide (derived from plasma membrane Ca^{2+} transporting ATPase, a CaM binding protein) as the probe and recombinant bovine calmodulin (cat. no. 208690, Merck), which has an amino acid sequence identical to the human isoform. The F-CaMKII peptide was used at 5 nM concentration with 50 nM of His-tagged wt and mutCaM. FP assays were carried out in a black low volume round bottom 384-well plate (cat. no. 4514, Corning) with a reaction volume of 20 μl. Compounds were threefold-diluted in an assay buffer (20 mM Tris Cl pH 7.5, 50 mM NaCl, 1 mM $CaCl_2$, and 0.005% Tween 20), and a complex of 100 nM CaM and 10 nM F-PMCA peptide was added. The FP signals were recorded on the Clariostar (BMG labtech) plate reader with excitation at 482 ± 8 nm and emission at 530 ± 20 nm at 25°C, after 30–60-min interval for up to 5 h. Then the plate was incubated overnight at 4°C, and the next day, final readings were taken after a total of 24 h incubation. The fluorescence anisotropy was calculated and plotted against the logarithm of the compound concentration and fit to the log inhibitor vs. response–variable slope (four parameters) equation in Prism (GraphPad). The IC_{50}

of the inhibitor was converted into K_d as described in Sinijarv et al. (2017) using the equation

$$K_d = \frac{[I]_{50}}{1 + \frac{[P]_{50}}{K_{D,probe}} + \frac{[E]_0}{K_{D,probe}}}$$

where $[I]_{50}$ is the concentration of the free inhibitor at 50% displacement, given as $[I]_{50} = IC_{50} - [EI]_{50}$, where $[EI]_{50}$ is the concentration of the CaM:inhibitor complex in case of 50% displacement; $[P]_{50}$ is the concentration of the free probe at 50% displacement; $[E]_0$ is the concentration of free CaM at 0% displacement; and $K_{D,probe}$ is the dissociation constant of the complex of the probe and CaM. The K_D of the probe, F-PMCA to CaM, is 6 nM (Manoharan et al., 2019).

The potency of the irreversible covalent inhibitors was assessed as described in Singh et al. (2011). The potency and selectivity of a covalent inhibitor are governed by two parameters, namely, K_i, the dissociation constant of the initial non-covalent complex, and k_2, the rate of the subsequent covalent bond-forming reaction as given in the chemical equation

$$E + I \underset{}{\overset{K_i}{\rightleftharpoons}} E \cdot I \overset{k_2}{\rightleftharpoons} E - I \quad (k_{-2})$$

E and I denote a protein target and its covalent inhibitor, respectively. E · I is the initial non-covalent complex, and E – I is the final covalent complex. To obtain the K_i and k_2 rates, the fluorescence polarization signal after inhibitor treatment was plotted against the incubation time and fit using a one-phase decay function to obtain the observed rate constant, k_{obs}. This was repeated for several inhibitor concentrations. Then, k_{obs} was plotted against the concentration of the inhibitor, and the data were fit to a hyperbolic equation $k_{obs} = \frac{k_2 \times [I]}{K_i + [I]}$ to obtain K_i and k_2. The ratio of k_2/K_i represents the second-order rate constant of the reaction of the covalent inhibitor with the target.

Composite Drug Activity Score

The composite drug activity score was obtained by computing the activity of the compounds across various assays performed. The desired properties taken into consideration are a high activity in the spheroid assay, a higher selectivity for MDA-MB-231 over Hs 578T in the spheroid assay, a lower toxicity in the 2D assay against Hs 578T as compared to MDA-MB-231 cells, and a higher affinity to CaM. The final score is obtained using the equation below:

$$composite\ drug\ activiy\ score = \frac{DSS_{(MDA-MB-231)}{}^2}{DSS_{(Hs\ 578T)}} \times \frac{2D_{toxicity(Hs\ 578T)}}{2D_{toxicity(MDA-MB-231)}} \times \frac{1}{K_d}$$

BRET Assays

BRET assays were essentially performed as described by others (Lavoie et al., 2013; Bery et al., 2018). About 100,00–150,000 HEK293-EBNA (Meissner et al., 2001) cells were seeded per well of a 12-well plate in 1 ml of DMEM containing 10% FBS and 2 mM L-glutamine and were grown for 24 h. Next day, Rluc8-tagged donor and GFP2-tagged acceptor constructs were transfected into cells using a jetPRIME transfection reagent (cat. no. 114-75, Polyplus). Each well was transfected with about 1 μg of plasmid DNA using 3 μl of the jetPRIME reagent. For BRET donor saturation titration experiments, the concentration of donor plasmid (25 ng) was kept constant, and the concentration of acceptor plasmid was increased from 0 to 500 ng for RasG12V BRET pairs and 0–1,000 ng for K-Ras/CaM BRET pairs. The empty pcDNA3.1(-) plasmid was used to top-up the total DNA load per transfection. After 24 h of transfection, cells were treated with compounds or vehicle control (DMSO 0.2% v/v in a growth medium) at the specified concentration for 24 h or the stipulated time period in case of the time-course experiments. The cells from one well of a 12-well plate were collected, washed, and re-plated in PBS (cat. no. 14190-094, Gibco, Thermo Fisher Scientific) on flat bottom, white 96-well plates (cat. no. 236108, Nunc, Thermo Fisher Scientific) as four technical replicates containing 90 μl of cell suspension per well. Then fluorescence intensity followed by BRET readings were carried out on a Clariostar (BMG Labtech) plate reader at 25°C. The fluorescence intensity (RFU) of GFP2 was measured with excitation at 405 ± 10 nm and emission 515 ± 10 nm; it is proportional to the acceptor concentration [acceptor]. BRET readings were taken well by well by adding 10 μl of 100 μM coelenterazine 400a (cat. no. C-320, GoldBio), the Rluc8 substrate to each well (final concentration of 10 μM) using the injector present in the plate reader. Luminescence emission intensities were simultaneously recorded at 410 ± 40 nm (RLU, proportional to [donor]) and 515 ± 15 nm (BRET signal).

The raw BRET ratio was calculated as the BRET signal measured at 515 nm divided by the emission signal measured at 410 nm (RLU). The BRET ratio was obtained by subtracting the raw BRET ratio by a background BRET signal measured for cells expressing only the donor (Bacart et al., 2008) as indicated in the formula below:

$$BRET\ ratio = \frac{\lambda em\ 515\ nm_{(donor + acceptor)}}{\lambda em\ 410\ nm_{(donor + acceptor)}} - \frac{\lambda em\ 515\ nm_{(donor\ only)}}{\lambda em\ 410\ nm_{(donor\ only)}}$$

with *donor+acceptor* denoting cells transfected with the BRET pair and *donor only* being cells expressing only the donor.

The expression of the acceptor relative to the donor ([acceptor]/[donor]) was determined as $relative\ expression = \frac{RFU}{RLU}$.

For BRET donor saturation titration experiments, the BRET ratio was plotted against the [acceptor]/[donor] ratio. Technical repeat data points were averaged, and data points from all biological repeats were collected into one graph for subsequent fitting. The BRET ratio vs. relative expression data were fitted using a binding saturation equation in the Prism (GraphPad) software to obtain $BRET_{max}$ and $BRET_{50}$ using the equation $y = \frac{BRET_{max} \times x}{BRET_{50} + x}$, where x is the relative expression and y is the BRET ratio. $BRET_{max}$ represents the maximum saturation BRET signal and depends on the structural parameters (distance, orientation) of the BRET complex. $BRET_{50}$ corresponds to the ratio of the acceptor construct over the donor construct required to attain 50% of the maximum BRET signal and is a measure of

the effective relative affinity between the interacting BRET pair (Marullo and Bouvier, 2007).

When applying the DSS analysis to nanoclustering-BRET data, we used mevastatin (10 μM) to obtain the asymptote parameter (a) for the maximal inhibition effect, as it prevents the prenylation of Ras proteins, their plasma membrane trafficking, and therefore nanoclustering. Otherwise, normalized BRET ratio data were converted to % inhibition and then subsequently uploaded onto the Breeze site (see text footnote 1).

Using BRET donor saturation data, the A/D plasmid ratio at which the BRET ratio changes most linearly with the relative expression was determined for each BRET sensor and then used for testing compound treatments.

ATARiS Gene Dependence Score

To generate the ATARiS sensitivity plots, Excel files corresponding to the normalized viability data for the siRNA knockdown of each gene of interest were downloaded from the publicly available database of the project DRIVE[2] (McDonald et al., 2017). The Project DRIVE study is a large-scale RNAi screen in which 2D viability effects of mRNA knockdown were assessed (McDonald et al., 2017). The ATARiS algorithm was used in this study to aggregate consistent shRNA activity to gene level activity (Shao et al., 2013). From the Excel files of each gene of interest, the sensitivity score data were extracted, and a double gradient heatmap plot was generated using Prism (GraphPad). Higher gene dependence (of 2D viability) is indicated by a negative score, while scores zero or above represent no or neutral effects.

Confocal Imaging

The localization of Ras and CaM fusion proteins was visualized by confocal microscopy. For imaging, MDCK cells were cultured in DMEM supplemented with 10% FBS and 2 mM L-glutamine at 37 °C with 5% CO_2. Cells were seeded on glass coverslips 1.5H (cat. no. LH22.1, Carl Roth) in 6-well plates (cat. no. 657160, Cellstar, Greiner Bio-One), and plasmids were transiently transfected with jetPRIME. Cells were fixed 48 h after the transfection with 4% paraformaldehyde (cat. no. 43368, Alfa Aesar) in PBS for 10 min at ambient temperature. After washing with PBS-Tween 0.05% (cat. no. 9127.1, Carl Roth), DNA was stained with a 1 μg/ml solution of DAPI (cat. no. D1306, Thermo Fisher Scientific) diluted in PBS for 10 min. The coverslips were mounted onto glass slides using Vectashield (cat. no. H-1000, Vector Laboratories). Images were captured on a spinning disk confocal microscope (Andor, Oxford Instruments), fitted with a Zyla 5.5 sCMOS camera (Andor, Oxford Instruments), using a plan APO 60 × /1.40 Ph3 DM oil immersion objective (Nikon) and NIS-Elements Imaging Software (Nikon).

To evaluate the effect of compounds on centrosome numbers during mitosis, HeLa cells were seeded in 6-well plates onto sterile coverslips and cotransfected with 0.5 μg of pmCherry-CaM and 1.5 μg pEGFP-Centrin1 plasmids using 4 μl of jetPRIME. Twenty-four hours after the transfection, cells were synchronized with 60 ng/ml of nocodazole for 16 h. After the removal of nocodazole, the cells were treated with the protease inhibitor MG132 (10 μM) to block the cells in metaphase and either calmidazolium (20 μM), **1** (50 μM), or DMSO (0.5%) for 2 h. Cells were then fixed with 4% paraformaldehyde in PBS for 10 min at ambient temperature. After washing with PBS-Tween 0.05%, DNA was stained with a 1 μg/ml solution of DAPI diluted in PBS for 10 min. Coverslips were mounted on glass slides using Vectashield, and images were captured on a spinning disk confocal microscope. Images were analyzed with the ImageJ software, and the number of transfected mitotic cells with multipolar and normal bipolar phenotypes was counted (between 35 and 70 cells per test condition). The percentage multipolar vs. bipolar cells was computed to generate the plot using the Prism software.

Data Analysis

All data analysis was performed using Prism (GraphPad) version 9 unless otherwise indicated. The number of independent biological repeats, n, for each data set is provided in the relevant figure legend. Unless otherwise stated, statistical significance was evaluated using one-way ANOVA. A p-value < 0.05 is considered statistically significant, and the statistical significance levels are annotated as follows: $^{*}p < 0.05$; $^{**}p < 0.01$; $^{***}p < 0.001$; $^{****}p < 0.0001$, or ns = not significant.

DATA AVAILABILITY STATEMENT

The original contributions presented in the study are included in the article/**Supplementary Material**, further inquiries can be directed to the corresponding author/s.

AUTHOR CONTRIBUTIONS

SO designed and performed the 3D spheroid assay, 2D cell viability and toxicity studies, BRET assays, and DSS analysis, and performed the RT-qPCR experiments and cloning together with MC. GM developed the BRET assay, designed and performed FP assays, and performed cloning. AK synthesized the compounds and curated the analytical data. CL performed microscopy. MC together with GM implemented the gateway cloning system and performed cloning, protein purification, and RT-qPCR. FM contributed reagents and funding support. JY-K collaboratively designed the compounds with AK. SO and GM analyzed all the data. DA conceived the study, designed the experiments, interpreted the results, and wrote the manuscript together with SO, GM, AK, and JY-K. All authors commented on the manuscript.

FUNDING

This work was supported by the Finnish Funding Agency for Innovation, Tekes, 3iRegeneration, project 40395/13) and Jane and Aatos Erkko Foundation to JY-K. DA received funding from

[2]https://oncologynibr.shinyapps.io/drive/

the Academy of Finland (Key Project # 304638) and core funding support by the University of Luxembourg.

ACKNOWLEDGMENTS

We are thankful to Dominic Esposito and Vanessa Wall (Frederick National Laboratory for Cancer Research, Frederick, MD, United States) for providing the entry clones and destination vectors for multisite gateway cloning. Nina Sipari from the Viikki Metabolomics Unit (Helsinki Institute of Life Science, University of Helsinki; Biocenter Finland) is thanked for her expertise with the LC-MS analyses.

SUPPLEMENTARY MATERIAL

The Supplementary Material for this article can be found online at: https://www.frontiersin.org/articles/10.3389/fcell.2021.665673/full#supplementary-material

REFERENCES

Abankwa, D., Gorfe, A. A., and Hancock, J. F. (2007). Ras nanoclusters: molecular structure and assembly. *Semin. Cell Dev. Biol.* 18, 599–607. doi: 10.1016/j.semcdb.2007.08.003

Abraham, S. J., Nolet, R. P., Calvert, R. J., Anderson, L. M., and Gaponenko, V. (2009). The hypervariable region of K-Ras4B is responsible for its specific interactions with calmodulin. *Biochemistry* 48, 7575–7583. doi: 10.1021/bi900769j

Agamasu, C., Ghirlando, R., Taylor, T., Messing, S., Tran, T. H., Bindu, L., et al. (2019). KRAS prenylation is required for bivalent binding with calmodulin in a nucleotide-independent manner. *Biophys. J.* 116, 1049–1063. doi: 10.1016/j.bpj.2019.02.004

Alvarez-Moya, B., Lopez-Alcala, C., Drosten, M., Bachs, O., and Agell, N. (2010). K-Ras4B phosphorylation at Ser181 is inhibited by calmodulin and modulates K-Ras activity and function. *Oncogene* 29, 5911–5922. doi: 10.1038/onc.2010.298

Anscombe, E., Meschini, E., Mora-Vidal, R., Martin, M. P., Staunton, D., Geitmann, M., et al. (2015). Identification and characterization of an irreversible inhibitor of CDK2. *Chem. Biol.* 22, 1159–1164. doi: 10.1016/j.chembiol.2015.07.018

Au, T. K., Chick, W. S., and Leung, P. C. (2000). The biology of ophiobolins. *Life Sci.* 67, 733–742. doi: 10.1016/s0024-3205(00)00668-8

Bacart, J., Corbel, C., Jockers, R., Bach, S., and Couturier, C. (2008). The BRET technology and its application to screening assays. *Biotechnol. J.* 3, 311–324. doi: 10.1002/biot.200700222

Bedard, P. L., Hyman, D. M., Davids, M. S., and Siu, L. L. (2020). Small molecules, big impact: 20 years of targeted therapy in oncology. *Lancet* 395, 1078–1088. doi: 10.1016/s0140-6736(20)30164-1

Berchtold, M. W., and Villalobo, A. (2014). The many faces of calmodulin in cell proliferation, programmed cell death, autophagy, and cancer. *Biochim. Biophys. Acta* 1843, 398–435. doi: 10.1016/j.bbamcr.2013.10.021

Bery, N., Cruz-Migoni, A., Bataille, C. J., Quevedo, C. E., Tulmin, H., Miller, A., et al. (2018). BRET-based RAS biosensors that show a novel small molecule is an inhibitor of RAS-effector protein-protein interactions. *Elife* 7:e37122.

Center for Drug Evaluation and Research (2017). *US FDA*. Available online at: https://www.accessdata.fda.gov/drugsatfda_docs/nda/2019/213137Orig1s000Multidiscipline.pdf (accessed 02 June 2021)

Chandra, A., Grecco, H. E., Pisupati, V., Perera, D., Cassidy, L., Skoulidis, F., et al. (2011). The GDI-like solubilizing factor PDEdelta sustains the spatial organization and signalling of Ras family proteins. *Nat. Cell Biol.* 14, 148–158. doi: 10.1038/ncb2394

Chidley, C., Trauger, S. A., Birsoy, K., and O'shea, E. K. (2016). The anticancer natural product ophiobolin A induces cytotoxicity by covalent modification of phosphatidylethanolamine. *Elife* 5:e14601.

Cicalese, A., Bonizzi, G., Pasi, C. E., Faretta, M., Ronzoni, S., Giulini, B., et al. (2009). The tumor suppressor p53 regulates polarity of self-renewing divisions in mammary stem cells. *Cell* 138, 1083–1095. doi: 10.1016/j.cell.2009.06.048

Dharmaiah, S., Bindu, L., Tran, T. H., Gillette, W. K., Frank, P. H., Ghirlando, R., et al. (2016). Structural basis of recognition of farnesylated and methylated KRAS4b by PDEdelta. *Proc. Natl. Acad. Sci. U.S.A.* 113, E6766–E6775.

Dontu, G., Abdallah, W. M., Foley, J. M., Jackson, K. W., Clarke, M. F., Kawamura, M. J., et al. (2003). In vitro propagation and transcriptional profiling of human mammary stem/progenitor cells. *Genes Dev.* 17, 1253–1270. doi: 10.1101/gad.1061803

Faust, F. M., Slisz, M., and Jarrett, H. W. (1987). Calmodulin is labeled at lysine 148 by a chemically reactive phenothiazine. *J. Biol. Chem.* 262, 1938–1941. doi: 10.1016/s0021-9258(18)61599-6

Fivaz, M., and Meyer, T. (2005). Reversible intracellular translocation of KRas but not HRas in hippocampal neurons regulated by Ca2+/calmodulin. *J. Cell Biol.* 170, 429–441. doi: 10.1083/jcb.200409157

Gillette, W. K., Esposito, D., Abreu Blanco, M., Alexander, P., Bindu, L., Bittner, C., et al. (2015). Farnesylated and methylated KRAS4b: high yield production of protein suitable for biophysical studies of prenylated protein-lipid interactions. *Sci. Rep.* 5:15916.

Girardi, E., Cesar-Razquin, A., Lindinger, S., Papakostas, K., Konecka, J., Hemmerich, J., et al. (2020). A widespread role for SLC transmembrane transporters in resistance to cytotoxic drugs. *Nat. Chem. Biol.* 16, 469–478. doi: 10.1038/s41589-020-0483-3

Grant, B. M. M., Enomoto, M., Back, S. I., Lee, K. Y., Gebregiworgis, T., Ishiyama, N., et al. (2020a). Calmodulin disrupts plasma membrane localization of farnesylated KRAS4b by sequestering its lipid moiety. *Sci. Signal.* 13:eaaz0344. doi: 10.1126/scisignal.aaz0344

Grant, B. M. M., Enomoto, M., Ikura, M., and Marshall, C. B. (2020b). A non-canonical calmodulin target motif comprising a polybasic region and lipidated terminal residue regulates localization. *Int. J. Mol. Sci.* 21:2751. doi: 10.3390/ijms21082751

Hait, W. N., and Lazo, J. S. (1986). Calmodulin: a potential target for cancer chemotherapeutic agents. *J. Clin. Oncol.* 4, 994–1012. doi: 10.1200/jco.1986.4.6.994

Halling, D. B., Liebeskind, B. J., Hall, A. W., and Aldrich, R. W. (2016). Conserved properties of individual Ca2+-binding sites in calmodulin. *Proc. Natl. Acad. Sci. U.S.A.* 113, E1216–E1225.

Hidaka, H., Sasaki, Y., Tanaka, T., Endo, T., Ohno, S., Fujii, Y., et al. (1981). N-(6-aminohexyl)-5-chloro-1-naphthalenesulfonamide, a calmodulin antagonist, inhibits cell proliferation. *Proc. Natl. Acad. Sci. U.S.A.* 78, 4354–4357. doi: 10.1073/pnas.78.7.4354

Hong, D. S., Fakih, M. G., Strickler, J. H., Desai, J., Durm, G. A., Shapiro, G. I., et al. (2020). KRAS(G12C) inhibition with sotorasib in advanced solid tumors. *N. Engl. J. Med.* 383, 1207–1217.

Itoh, H., and Hidaka, H. (1984). Direct interaction of calmodulin antagonists with Ca2+/calmodulin-dependent cyclic nucleotide phosphodiesterase. *J. Biochem.* 96, 1721–1726. doi: 10.1093/oxfordjournals.jbchem.a135004

Jang, H., Banerjee, A., Marcus, K., Makowski, L., Mattos, C., Gaponenko, V., et al. (2019). The structural basis of the farnesylated and methylated KRas4B interaction with calmodulin. *Structure* 27:e1644.

Kiriazis, A., Aumuller, I. B., Arnaudova, R., Brito, V., Ruffer, T., Lang, H., et al. (2017). Nucleophilic substitution of hydrogen facilitated by quinone methide moieties in benzo[cd]azulen-3-ones. *Org. Lett.* 19, 2030–2033. doi: 10.1021/acs.orglett.7b00588

Kohnke, M., Schmitt, S., Ariotti, N., Piggott, A. M., Parton, R. G., Lacey, E., et al. (2012). Design and application of in vivo FRET biosensors to identify protein prenylation and nanoclustering inhibitors. *Chem. Biol.* 19, 866–874. doi: 10.1016/j.chembiol.2012.05.019

Kong Au, T., and Chow Leung, P. (1998). Identification of the binding and inhibition sites in the calmodulin molecule for ophiobolin A by site-directed mutagenesis. *Plant Physiol.* 118, 965–973. doi: 10.1104/pp.118.3.965

Lavoie, H., Thevakumaran, N., Gavory, G., Li, J. J., Padeganeh, A., Guiral, S., et al. (2013). Inhibitors that stabilize a closed RAF kinase domain conformation induce dimerization. *Nat. Chem. Biol.* 9, 428–436. doi: 10.1038/nchembio.1257

Leung, P. C., Taylor, W. A., Wang, J. H., and Tipton, C. L. (1984). Ophiobolin A. A natural product inhibitor of calmodulin. *J. Biol. Chem.* 259, 2742–2747. doi: 10.1016/s0021-9258(17)43208-x

Li, C. J., Heim, R., Lu, P., Pu, Y., Tsien, R. Y., and Chang, D. C. (1999). Dynamic redistribution of calmodulin in HeLa cells during cell division as revealed by a GFP-calmodulin fusion protein technique. *J. Cell Sci.* 112, 1567–1577. doi: 10.1242/jcs.112.10.1567

Manoharan, G. B., Kopra, K., Eskonen, V., Härmä, H., and Abankwa, D. (2019). High-throughput amenable fluorescence-assays to screen for calmodulin-inhibitors. *Anal. Biochem.* 572, 25–32. doi: 10.1016/j.ab.2019.02.015

Marullo, S., and Bouvier, M. (2007). Resonance energy transfer approaches in molecular pharmacology and beyond. *Trends Pharmacol. Sci.* 28, 362–365. doi: 10.1016/j.tips.2007.06.007

McDonald, E. R. III, De Weck, A., Schlabach, M. R., Billy, E., Mavrakis, K. J., Hoffman, G. R., et al. (2017). Project DRIVE: a compendium of cancer dependencies and synthetic lethal relationships uncovered by large-scale, deep RNAi Screening. *Cell* 170:e510.

Meissner, P., Pick, H., Kulangara, A., Chatellard, P., Friedrich, K., and Wurm, F. M. (2001). Transient gene expression: recombinant protein production with suspension-adapted HEK293-EBNA cells. *Biotechnol. Bioeng.* 75, 197–203. doi: 10.1002/bit.1179

Metcalf, B., Chuang, C., Dufu, K., Patel, M. P., Silva-Garcia, A., Johnson, C., et al. (2017). Discovery of GBT440, an orally bioavailable R-State stabilizer of sickle cell hemoglobin. *ACS Med. Chem. Lett.* 8, 321–326. doi: 10.1021/acsmedchemlett.6b00491

Najumudeen, A. K., Jaiswal, A., Lectez, B., Oetken-Lindholm, C., Guzman, C., Siljamaki, E., et al. (2016). Cancer stem cell drugs target K-ras signaling in a stemness context. *Oncogene* 35, 5248–5262. doi: 10.1038/onc.2016.59

Posada, I. M., Serulla, M., Zhou, Y., Oetken-Lindholm, C., Abankwa, D., and Lectez, B. (2016). ASPP2 is a novel pan-ras nanocluster scaffold. *PLoS One* 11:e0159677. doi: 10.1371/journal.pone.0159677

Potdar, S., Ianevski, A., Mpindi, J. P., Bychkov, D., Fiere, C., Ianevski, P., et al. (2020). Breeze: an integrated quality control and data analysis application for high-throughput drug screening. *Bioinformatics* 36, 3602–3604. doi: 10.1093/bioinformatics/btaa138

Ren, J. G., Li, Z., and Sacks, D. B. (2008). IQGAP1 integrates Ca2+/calmodulin and B-Raf signaling. *J. Biol. Chem.* 283, 22972–22982. doi: 10.1074/jbc.m804626200

Sengupta, P., Ruano, M. J., Tebar, F., Golebiewska, U., Zaitseva, I., Enrich, C., et al. (2007). Membrane-permeable calmodulin inhibitors (e.g. W-7/W-13) bind to membranes, changing the electrostatic surface potential: dual effect of W-13 on epidermal growth factor receptor activation. *J. Biol. Chem.* 282, 8474–8486. doi: 10.1074/jbc.m607211200

Shao, D. D., Tsherniak, A., Gopal, S., Weir, B. A., Tamayo, P., Stransky, N., et al. (2013). ATARiS: computational quantification of gene suppression phenotypes from multisample RNAi screens. *Genome Res.* 23, 665–678. doi: 10.1101/gr.143586.112

Siddiqui, F. A., Alam, C., Rosenqvist, P., Ora, M., Sabt, A., Manoharan, G. B., et al. (2020). PDE6D inhibitors with a new design principle selectively block K-Ras Activity. *ACS Omega* 5, 832–842. doi: 10.1021/acsomega.9b03639

Singh, J., Petter, R. C., Baillie, T. A., and Whitty, A. (2011). The resurgence of covalent drugs. *Nat. Rev. Drug Discov.* 10, 307–317. doi: 10.1038/nrd3410

Sinijarv, H., Wu, S., Ivan, T., Laasfeld, T., Viht, K., and Uri, A. (2017). Binding assay for characterization of protein kinase inhibitors possessing sub-picomolar to sub-millimolar affinity. *Anal. Biochem.* 531, 67–77. doi: 10.1016/j.ab.2017.05.017

Sunagawa, M., Yokoshiki, H., Seki, T., Nakamura, M., Laber, P., and Sperelakis, N. (1999). Direct block of Ca2+ channels by calmidazolium in cultured vascular smooth muscle cells. *J. Cardiovasc. Pharmacol.* 34, 488–496. doi: 10.1097/00005344-199910000-00003

Taules, M., Rius, E., Talaya, D., Lopez-Girona, A., Bachs, O., and Agell, N. (1998). Calmodulin is essential for cyclin-dependent kinase 4 (Cdk4) activity and nuclear accumulation of cyclin D1-Cdk4 during G1. *J. Biol. Chem.* 273, 33279–33286. doi: 10.1074/jbc.273.50.33279

Taylor, A. M., Macari, E. R., Chan, I. T., Blair, M. C., Doulatov, S., Vo, L. T., et al. (2020). Calmodulin inhibitors improve erythropoiesis in Diamond-Blackfan anemia. *Sci. Transl. Med.* 12:eabb5831. doi: 10.1126/scitranslmed.abb5831

Teleman, A., Drakenberg, T., and Forsen, S. (1986). Kinetics of Ca2+ binding to calmodulin and its tryptic fragments studied by 43Ca-NMR. *Biochim. Biophys. Acta* 873, 204–213. doi: 10.1016/0167-4838(86)90047-6

Tidow, H., and Nissen, P. (2013). Structural diversity of calmodulin binding to its target sites. *FEBS J.* 280, 5551–5565. doi: 10.1111/febs.12296

Toutenhoofd, S. L., and Strehler, E. E. (2000). The calmodulin multigene family as a unique case of genetic redundancy: multiple levels of regulation to provide spatial and temporal control of calmodulin pools? *Cell Calcium.* 28, 83–96. doi: 10.1054/ceca.2000.0136

Tsai, F. D., Lopes, M. S., Zhou, M., Court, H., Ponce, O., Fiordalisi, J. J., et al. (2015). K-Ras4A splice variant is widely expressed in cancer and uses a hybrid membrane-targeting motif. *Proc. Natl. Acad. Sci. U.S.A.* 112, 779–784. doi: 10.1073/pnas.1412811112

Vandonselaar, M., Hickie, R. A., Quail, J. W., and Delbaere, L. T. (1994). Trifluoperazine-induced conformational change in Ca(2+)-calmodulin. *Nat. Struct. Biol.* 1, 795–801. doi: 10.1038/nsb1194-795

Villalonga, P., Lopez-Alcala, C., Bosch, M., Chiloeches, A., Rocamora, N., Gil, J., et al. (2001). Calmodulin binds to K-Ras, but not to H- or N-Ras, and modulates its downstream signaling. *Mol. Cell Biol.* 21, 7345–7354. doi: 10.1128/mcb.21.21.7345-7354.2001

Wall, V. E., Garvey, L. A., Mehalko, J. L., Procter, L. V., and Esposito, D. (2014). Combinatorial assembly of clone libraries using site-specific recombination. *Methods Mol. Biol.* 1116, 193–208. doi: 10.1007/978-1-62703-764-8_14

Wang, J., Li, J., Santana-Santos, L., Shuda, M., Sobol, R. W., Van Houten, B., et al. (2015a). A novel strategy for targeted killing of tumor cells: induction of multipolar acentrosomal mitotic spindles with a quinazolinone derivative mdivi-1. *Mol. Oncol.* 9, 488–502. doi: 10.1016/j.molonc.2014.10.002

Wang, M. T., Holderfield, M., Galeas, J., Delrosario, R., To, M. D., Balmain, A., et al. (2015b). K-Ras promotes tumorigenicity through suppression of non-canonical wnt signaling. *Cell* 163, 1237–1251. doi: 10.1016/j.cell.2015.10.041

Wu, L. J., Xu, L. R., Liao, J. M., Chen, J., and Liang, Y. (2011). Both the C-terminal polylysine region and the farnesylation of K-RasB are important for its specific interaction with calmodulin. *PLoS One* 6:e21929. doi: 10.1371/journal.pone.0021929

Wu, Q., Sahasrabudhe, R. M., Luo, L. Z., Lewis, D. W., Gollin, S. M., and Saunders, W. S. (2010). Deficiency in myosin light-chain phosphorylation causes cytokinesis failure and multipolarity in cancer cells. *Oncogene* 29, 4183–4193. doi: 10.1038/onc.2010.165

Yadav, B., Pemovska, T., Szwajda, A., Kulesskiy, E., Kontro, M., Karjalainen, R., et al. (2014). Quantitative scoring of differential drug sensitivity for individually optimized anticancer therapies. *Sci. Rep.* 4:5193.

Yokokura, S., Yurimoto, S., Matsuoka, A., Imataki, O., Dobashi, H., Bandoh, S., et al. (2014). Calmodulin antagonists induce cell cycle arrest and apoptosis *in vitro* and inhibit tumor growth *in vivo* in human multiple myeloma. *BMC Cancer* 14:882. doi: 10.1186/1471-2407-14-882

Yu, Y. Y., Chen, Y., Dai, G., Chen, J., Sun, X. M., Wen, C. J., et al. (2004). The association of calmodulin with central spindle regulates the initiation of cytokinesis in HeLa cells. *Int. J. Biochem. Cell Biol.* 36, 1562–1572. doi: 10.1016/j.biocel.2003.12.016

Zimmer, M., and Hofmann, F. (1984). Calmodulin antagonists inhibit activity of myosin light-chain kinase independent of calmodulin. *Eur. J. Biochem.* 142, 393–397. doi: 10.1111/j.1432-1033.1984.tb08300.x

Conflict of Interest: FM was employed by company Leidos Biomedical Research, Inc.

The remaining authors declare that the research was conducted in the absence of any commercial or financial relationships that could be construed as a potential conflict of interest.

frontiers in Molecular Biosciences

REVIEW
published: 16 August 2021
doi: 10.3389/fmolb.2021.706650

Lipid Metabolism Regulates Oxidative Stress and Ferroptosis in RAS-Driven Cancers: A Perspective on Cancer Progression and Therapy

*Caterina Bartolacci†, Cristina Andreani†, Yasmin El-Gammal and Pier Paolo Scaglioni**

Department of Internal Medicine, University of Cincinnati College of Medicine, Cincinnati, OH, United States

HRAS, *NRAS* and *KRAS*, collectively referred to as oncogenic RAS, are the most frequently mutated driver proto-oncogenes in cancer. Oncogenic RAS aberrantly rewires metabolic pathways promoting the generation of intracellular reactive oxygen species (ROS). In particular, lipids have gained increasing attention serving critical biological roles as building blocks for cellular membranes, moieties for post-translational protein modifications, signaling molecules and substrates for ß-oxidation. However, thus far, the understanding of lipid metabolism in cancer has been hampered by the lack of sensitive analytical platforms able to identify and quantify such complex molecules and to assess their metabolic flux *in vitro* and, even more so, in primary tumors. Similarly, the role of ROS in RAS-driven cancer cells has remained elusive. On the one hand, ROS are beneficial to the development and progression of precancerous lesions, by upregulating survival and growth factor signaling, on the other, they promote accumulation of oxidative by-products that decrease the threshold of cancer cells to undergo ferroptosis. Here, we overview the recent advances in the study of the relation between RAS and lipid metabolism, in the context of different cancer types. In particular, we will focus our attention on how lipids and oxidative stress can either promote or sensitize to ferroptosis RAS driven cancers. Finally, we will explore whether this fine balance could be modulated for therapeutic gain.

Keywords: lipid metabolism, ferroptosis, tumorigenesis, oxidative stress, RAS oncogenes

OPEN ACCESS

Edited by:
Veronica Aran, Instituto Estadual do Cérebro Paulo Niemeyer (IECPN), Brazil

Reviewed by:
Alessandro Fanzani, University of Brescia, Italy
Jasminka Omerovic, University of Split, Croatia

****Correspondence:***
Pier Paolo Scaglioni
scaglipr@ucmail.uc.edu

†These authors have contributed equally to this work

Specialty section:
This article was submitted to Molecular Diagnostics and Therapeutics, a section of the journal Frontiers in Molecular Biosciences

Received: *07 May 2021*
Accepted: *02 August 2021*
Published: *16 August 2021*

Citation:
Bartolacci C, Andreani C, El-Gammal Y and Scaglioni PP (2021) Lipid Metabolism Regulates Oxidative Stress and Ferroptosis in RAS-Driven Cancers: A Perspective on Cancer Progression and Therapy. Front. Mol. Biosci. 8:706650. doi: 10.3389/fmolb.2021.706650

CLINICAL SIGNIFICANCE OF RAS MUTATIONS

The three *RAS* genes (*HRAS*, *NRAS* and *KRAS*), hereafter collectively referred to as oncogenic RAS, are the most frequently mutated driver proto-oncogenes in cancer, with *KRAS* being the most prevalent. Notably, mutant KRAS is present in more than 90% of pancreatic ductal adenocarcinoma (PDAC) where it is the most frequent and earliest genetic alteration, as it is found in more than 90% of neoplastic precursor lesions (*e.g.* pancreatic intraepithelial neoplasia, PanINs) (Kanda et al., 2012; Eser et al., 2014). Similarly, mutant KRAS is present in 30–40% of colorectal cancers (CRC) and almost 25% of patients with Non-Small Cell Lung Cancer (NSCLC), where it correlates with poor prognosis and high risk of recurrence (Stephen et al., 2014).

While much of the early work had focused on the signal transduction related to cell proliferation, it is now understood the RAS oncogene has yet other crucial roles in tumorigenesis. For instance, it orchestrates the reprogramming of lipid metabolism and promotes the generation of intracellular

reactive oxygen species (ROS). Since these metabolic changes are critical for ferroptosis, a unique form of iron-dependent programed cell death, and are dependent on the presence of oncogenic RAS, they might offer new therapeutic opportunities.

AN INTRODUCTION TO FERROPTOSIS AND LIPID PEROXIDATION

Ferroptosis (extensively reviewed in (Dixon and Stockwell, 2019; Zheng and Conrad, 2020) is a unique form of iron-dependent programed cell death defined by the existence of substantial oxidative stress and lipid peroxidation (LPO). It differs from other well-characterized types of cell death as apoptosis, pyroptosis, necroptosis or autophagy in morphology, biochemistry, and genetics. Accordingly, inhibitors for apoptosis, necrosis or autophagy are all ineffective against ferroptosis (Dixon et al., 2012).

Even if preliminary observations were reported as early as in the 70s (Maellaro et al., 1990), only in 2012 the term "ferroptosis" was first introduced by the group of Dr. Stockwell (Dixon et al., 2012) to finally provide a rational explanation for the long-lasting query regarding the nature of LPO-induced cell death.

LPO was first studied in relation to damage to alimentary oils and fats in meat and meat products (Dianzani and Barrera, 2008), but was soon implicated in numerous pathological states, including cancer. It can be generally described as a complex process whereby oxidants, free radicals or nonradical species, attack lipids containing carbon-carbon double bond(s), resulting in the formation/propagation of lipid hydroperoxides (LOOH) and peroxyl radicals, which in turn generate secondary products with prolonged half-life.

Thus, understanding LPO entails a detailed knowledge of lipids and oxidative stress, which we will briefly address with particular attention to their relationship with oncogenic RAS.

It is now well-established that LPO plays a central role in the initiation and execution of ferroptosis and that LPO-induced toxic species, such as lipid derived toxic aldehydes, are biomarkers of ferroptosis. However, the identification of the lipid species that are essential for the regulation, initiation and execution of ferroptosis remain poorly understood. Even more so, analyzing ferroptosis *in vivo* remains challenging. Indeed, exploring ferroptosis requires lipidomic and redox analyses that are technically demanding, giving the huge diversity and biochemical complexity of lipids. In addition, none of the biomarkers or gene products identified to date is entirely specific to ferroptosis. The unambiguous demonstration of the occurrence of ferroptosis requires the simultaneous detection of biochemical markers of LPO, redox-active iron, and deficiency in the repair of the lipid peroxides (Dixon and Stockwell, 2019).

Today, ferroptosis is the subject of intense investigation and its clinical relevance has started to being recognized. Indeed, various compounds, some of which are FDA-approved drugs, have been identified as ferroptosis inducers in cancer cells (Shen et al., 2018; Hassannia et al., 2019).

Ferroptosis was initially found to be induced by a set of small molecules identified in a screen for compounds able to selectively induce cell death in isogenic cancer cell lines tumors carrying a mutant form of RAS, suggesting a connection between RAS oncogene and ferroptosis (Dolma et al., 2003; Yagoda et al., 2007; Yang and Stockwell, 2008). However, subsequent studies have questioned the selective lethality of these compounds on RAS-mutated cell lines (Yang and Stockwell, 2008). Moreover, while cancer cells display high levels of oxidative stress, increased levels of LPO products are detected only in some cancer types, depending on the lipid composition of cellular membranes, presence of inflammation and the level of enzymes able to metabolize LPO products (Canuto et al., 1993; Hammer et al., 1997). Thus, the relationship among cancer, RAS-driven cancers in particular, LPO and ferroptosis still remains controversial.

Here, we will briefly review the mechanisms of oxidative stress, lipid metabolism and LPO and the current understanding of how RAS oncogene regulates these processes to escape ferroptosis, highlighting questions still open for future studies.

LIPID METABOLISM: A BROAD PICTURE

Fatty acids (FA) serve essential roles in cancer cells as they provide constituents for cellular membranes and substrates for energy metabolism to meet the demand for high-rate proliferation. Moreover, FA come in many different flavors, and specific FA are essential to support tumorigenesis and cancer progression.

It is well known that the biosynthesis of saturated FA (SFA) and monounsaturated FA (MUFA) starts from palmitate (PA, C16:0), formed by the 250–270 kDa multifunctional, homodimeric fatty acid synthase (FASN) (Chirala and Wakil, 2004; Asturias et al., 2005; Maier et al., 2006). FASN synthesizes long-chain FA, mainly PA, using acetyl-CoA as a primer, malonyl-CoA as a two-carbon donor, and NADPH as a reducing equivalent. PA is further elongated to stearic acid (SA, C18:0) and/or desaturated to palmitoleic (C16:1n-9) and oleic (OA, C18:1n-9) acids, with the latter being further elongated to eicosatrienoic acid (EA, C20:3n-9) (Miyazaki and Ntambi, 2008) (**Figure 1**).

However, Δ-6 desaturase shows strong preference for the two essential polyunsaturated fatty acids (PUFA) linoleic acid (LA, C18:2n-6) and α-linolenic acid (LA, C18:3n-3) over OA (Sprecher et al., 1995). Hence, eukaryotic cells rely on dietary LA and ALA to synthetize n-6 long chain PUFA (*e.g.* arachidonic acid, AA, C20:4n-6), and n-3 long chain-PUFA (*e.g.* eicosapentaenoic and docosahexaenoic acids, EPA, C20:5n-3, DHA, C22:6n-3), respectively through the "Sprecher pathway" (Voss et al., 1991; Sprecher et al., 1995) (**Figure 1**).

FA, either *de novo* synthetized or deriving from exogenous sources (i.e. diet), can be broken down into acetyl-CoA, which then enters the tricarboxylic acid (TCA) cycle to aid ATP generation. Alternatively, FA can be incorporated into more complex lipids such as triglycerides (TAG), phospholipids (PL) or cholesteryl esters (CE). Yet, these two distinct pathways require a common initial step known as FA activation by acyl-CoA synthetase (ACS) enzymes (Ellis et al., 2010). FASN is very active during embryogenesis and in fetal lungs, where FA are

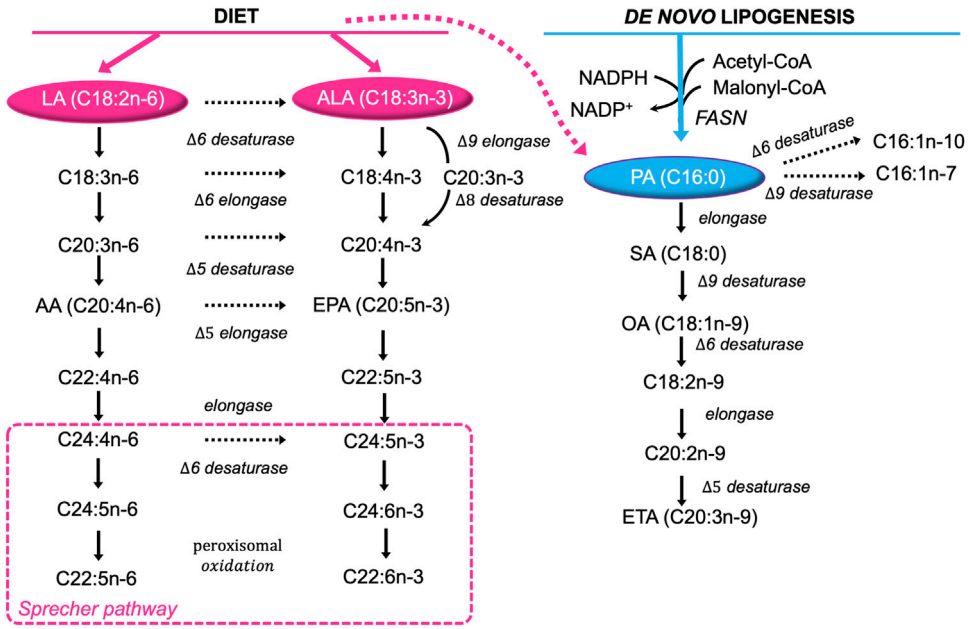

FIGURE 1 | Major pathways of FA desaturation and chain elongation in eukaryotic cells. Both exogenous (diet, pink) and endogenously synthetized FA (blue) are extensively desaturated and elongated giving rise to the huge diversity found in lipid molecules. Note the alternating sequence of desaturation in the horizontal direction and chain elongation in the vertical direction in the formation of polyunsaturated fatty acids from dietary essential fatty acids. LA, linoleic acid; ALA, α-linolenic acid; C18:4n-3, stearidonic acid; C18:3n-6, γ-linolenic acid; C20:3n-3, eicosatrienoic acid; C20:3n-6, dihomo-γ-linolenic acid; C20:4n-3, eicosatetraenoic acid; AA, arachidonic acid; EPA, eicosapentaenoic acid; C22:4n-6, adrenic acid; C22:5n-3, docosapentaenoic acid; C24:4n-6, tetracosatetraenoic acid; C24:5n-6, etracosapentaenoic acid; C24:5n-3, tetracosapentaenoic acid; C24:6n-3, tetracosahexaenoic acid; C22:5n-6, docosapentanoic acid; C22:6n-3, docosahexaenoic acid; PA, palmitic acid; C16:1n-10, sapienic acid; C16:1n-7, palmitoleic acid; OA, oleic acid; SA, stearic acid; C18:2n-9, trans linoleic acid; C20:2n-9, 5,11-eicosadienoic acid; ETA, cis-5,8,11-eicosatrienoic acid.

used for the production of lung surfactant (Wagle et al., 1999). However, in well-nourished adults FASN is less active, as non-transformed cells generally rely on the uptake of lipids from the circulation. By contrast, cancer cells aberrantly activate *de novo* lipid synthesis: in 1953 Medes *et al.* already used *in vivo* labelling with ^{14}C-glucose tracer to demonstrate that most of the esterified FA in tumor models were derived from *de novo* synthesis (Medes et al., 1953). The mechanisms underlying the switch of cancer cells to *de novo* lipogenesis remain an area of intense research. (Menendez and Lupu, 2007; Padanad et al., 2016; Rozeveld et al., 2020; Ferraro et al., 2021).

ONCOGENIC RAS AND LIPID METABOLISM: A FAT ADDICTION

According to the literature, the relationship between oncogenic RAS and lipids is intertwined and multifaceted. Firstly, all the RAS proteins (HRAS, NRAS, KRAS4A, and KRAS4B) are modified by lipids through lipidation which reversibly regulates their membrane localization and function. A RAS plasma membrane anchor consists of two components: a C-terminal S-farnesyl cysteine carboxylmethyl ester, common to all isoforms; and a second signal that comprises mono-palmitoylation of NRAS, duo-palmitoylation of HRAS and a polybasic domain (PBD) of six contiguous lysines in KRAS4B, the predominantly expressed splice variant of KRAS, hereafter referred to as KRAS. Evidence from the Hancock laboratory showed that the anchor of mutant KRAS^{G12V} exhibits remarkable specificity for distinct subclasses of phosphatidylserine (PS). In particular, only in presence of monounsaturated PS, KRAS^{G12V} is assembled into membrane nanoclusters, that are considered to be the hotspots of KRAS activation. On the other hand, KRAS^{G12V} does not interact with fully saturated PS at all, whereas mono- and di-unsaturated PS can support KRAS^{G12V} binding to the plasma membrane, but cannot be assembled into nanoclusters (Zhou et al., 2017). Moreover, full-length KRAS, or its minimal membrane anchor, localizes preferentially to cholesterol-depleted liquid-disordered domains in synthetic model bilayers and KRAS^{G12V} is typically excluded from cholesterol-rich domains, as these domains are suboptimal for Raf activation (Prior et al., 2001; Inder et al., 2008). In agreement, nanoclustering of KRAS (either GDP or GTP-loaded) is insensitive to acute cholesterol depletion (Prior et al., 2003).

The fact that lipid availability and lipid composition of the membrane can deeply impact KRAS localization and function is just the tip of the iceberg. Besides acting as building blocks for membrane assembly, signaling molecules and energy storage, FA have recently been found to serve a pivotal role in coping with oncogenic stress. Our lab and others described that mutant KRAS activation/extinction in preclinical lung cancer (LC) models directly controls the expression of genes involved in

β-oxidation and *de novo* lipogenesis, and that this can be exploited for therapeutic gain (Padanad et al., 2016; Gouw et al., 2017; Bartolacci et al., 2021). The role of mutant KRAS in FA oxidation has been reported in a transgenic mouse model that expresses the doxycycline (doxy)-inducible KRAS transgene ($KRAS^{G12D}$) in the respiratory epithelium (Padanad et al., 2016). These mice, when fed with doxy, develop lung tumors that completely regress when doxy is removed with concomitant significant decrease in the expression of lipid metabolism genes (Padanad et al., 2016). In this regard, Acyl-coenzyme A synthetase long chain family member 3 and 4 (*Acsl3* and *Acsl4*) are significantly down regulated in tumors undergoing $KRAS^{G12D}$ extinction and ACSL3 contributes the most to the oncogenic phenotype both *in vitro* and *in vivo*. ACSL enzymes conjugate long-chain FA (12–20 C atoms) with Coenzyme A (CoA) to produce acyl-CoA. While genetic deletion of *Acsl3* in mice does not cause any morphological defects neither during development nor in adult life, it impairs KRAS-driven tumorigenesis (Padanad et al., 2016). Therefore, it may represent a good therapeutic target. Even though a specific inhibitor of ACSL3 is not available, yet, evidence indicates that inhibition of FASN has effects similar to *ACSL3* silencing, opening to new possible therapeutic strategies in NSCLC (Bartolacci et al., 2017, 2021). The role of KRAS in inducing lipogenesis is highlighted by the upregulation of FASN along with other enzymes that control FA metabolism, such as ATP citrate lyase (ACLY) and acetyl-coenzyme A carboxylase (ACC) in the $KRAS^{G12D}$ LC model. Overexpression of both *ACLY* and *FASN* correlates with poor survival and with increased lipogenesis as shown by the higher levels of newly synthetized SFA and MUFA, such as PA and OA (Bartolacci et al., 2017; Singh et al., 2018).

The liaison between oncogenic RAS and lipids seems to consistently occur in cancers other than LC. Indeed, it has been shown that oncogenic KRAS downregulates hormone-sensitive lipase (HSL) in pancreatic cancer, modulating invasion and metastasis (Rozeveld et al., 2020). Pancreatic cancer cells accumulate fat into lipid droplets, which is then used to fuel catabolism during metastasis and invasion. Indeed, blocking the KRAS–HSL axis lowers lipid storage into lipid droplets, effectively reducing invasive capacity of KRAS-mutant pancreatic cancer (Rozeveld et al., 2020). A positive association between high cholesterol:high-density lipoprotein (chol:HDL) ratio and KRAS mutation has been found also in a subset of metastatic CRC (Tabuso et al., 2020). In addition, in murine models of MYC/KRAS breast cancer, FA metabolism genes are upregulated in tumors treated with neoadjuvant therapy, suggesting that this is feature of therapy resistance and recurrence (Havas et al., 2017).

OXIDATIVE STRESS AND ONCOGENIC RAS: THE REDOX PARADOX

Cancer cell metabolism and redox signaling are intimately coupled and mutually regulated (Holmström and Finkel, 2014; Wang et al., 2019a): on the one hand, ROS accumulate as by-products of cellular metabolism, on the other, increased ROS and lactate quantities enhance metabolic rate and act as mitogenic signaling molecules, sustaining tumorigenesis (Lee et al., 1999; Ogrunc et al., 2014). However, excessive ROS can cause oxidative damage to macromolecules (*e.g.* DNA and lipids) and can alter intracellular signal transduction (*e.g.* through NF-κB). This is especially true in RAS-driven tumorigenesis: if oncogenic RAS induces ROS accumulation, then ROS scavenging mechanisms must be put in place to reduce cellular senescence and support tumorigenesis (Lee et al., 1999) (**Figure 2**).

In mutant-RAS cancer cells, high ROS levels can result from increased metabolic activity of peroxisomes, oxidases, cyclooxygenases (COX), lipoxygenases (LOX), from mitochondrial dysfunction, or they can derive from the cross-talk with infiltrating immune cells and other components of the tumor microenvironment (TME) (Szatrowski and Nathan, 1991; Babior, 1999; Storz, 2005).

Oncogenic RAS promotes the direct activation or induction of ROS-producing enzymes. For instance, in murine peripheral lung epithelial cells, mutant $KRAS^{G12V}$ increases levels of intracellular ROS through COX2, which produces hydrogen peroxide (H_2O_2) as a by-product of prostaglandin-E2 synthesis (Maciag et al., 2004) (**Figure 2A**). Several investigations determined that oncogenic RAS increases protein level and activity of NADPH oxidase (NOX), the enzyme responsible for the catalytic one-electron transfer of oxygen at the cell membrane to generate superoxide anion ($O_2^{-\bullet}$) (Kong et al., 2013; Ogrunc et al., 2014) (**Figure 2B**). In particular, RAS-driven induction of NOX1 and RAC1 was found to be mediated by the MAPK pathway (Mitsushita et al., 2004). Accordingly, *Nox1* abrogation hampers $O_2^{-\bullet}$ generation and oncogenic RAS-driven tumorigenesis, NIH3T3 fibroblasts ectopically expressing $HRAS^{G12V}$ have higher amounts of $O_2^{-\bullet}$ in a Rac1-dependent way as they progress through the cell cycle (Irani et al., 1997). Consistently, in PanIN1b)/PanIN2 stage of pancreatic carcinogenesis, concomitant deletion of tumor protein p53-induced nuclear protein 1 (TP53INP1) and activation $KRAS^{G12D}$, activate Rac1, accelerate PanIN formation and increase pancreatic injury (Al Saati et al., 2013). Active Rac1 was further implicated to induce 5-Lipoxigenase (5-LOX)-mediated generation of H_2O_2 and c-Met-triggered $O_2^{-\bullet}$ production (Shin et al., 1999; Ferraro et al., 2006) (**Figure 2B**).

In addition, oncogenic RAS was reported to modulate mitochondrial metabolism, hence ROS generation, suppressing the respiratory chain complex I and III (Weinberg et al., 2010; Hu et al., 2012; Liou et al., 2016), regulating hypoxia-inducible factors (HIFs), HIF-1α and HIF-2α (Chun et al., 2010), or the transferrin receptor (TfR1) (Jeong et al., 2016) in CRC and PDA (**Figure 2C**).

Induction of growth factor- and cytokine-signaling, autophagy-specific genes 5 and 7 (*ATG5, ATG7*) (Kim et al., 2011) or expression of micro RNAs such as miR-155 (Wang et al., 2015) are other ROS-producing mechanisms exploited by RAS. Interestingly, RAS can attain and sustain a prooxidant environment also repressing sestrins (SESN1, 2, and 3), which mediate the regeneration of cytosolic peroxiredoxins (PRXDs), the enzymatic antioxidants involved in the decomposition of endogenously produced H_2O_2 (**Figure 2D**). In MDAH041 immortalized fibroblasts, expression of activated RAS

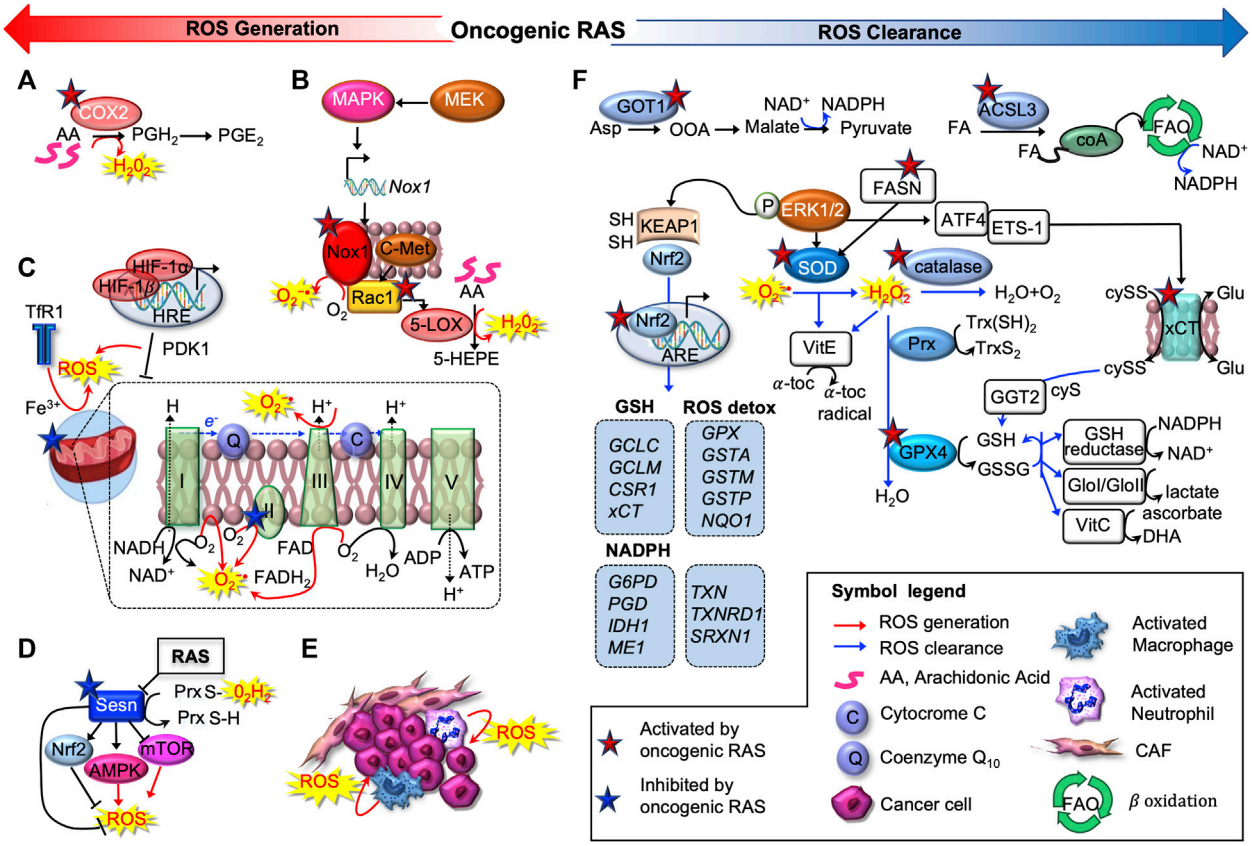

FIGURE 2 | Oncogenic RAS induces pro-oxidant and anti-oxidant programs. Oncogenic RAS promotes ROS production exploiting several strategies, as activation of cyclooxygenase-2 (COX2) **(A)**, subunits of the NADPH oxidase complex (NOX1/4) **(B)**, regulating mitochondrial activity **(C)** or inactivating sestrin 1 (SESN1) **(D)**. The tumor microenvironment (TME) can also produce ROS, contributing to maintain oxidative, pro-tumorigenic conditions **(E)**. Oncogenic RAS drives multiple antioxidant programs as well **(F)**. First, it can upregulate the main antioxidant enzymes superoxide dismutases (SOD); catalase and peroxidases, of which GPX4 is the main member. Oncogenic RAS can drive NADPH production through an alternative glutamine metabolic pathway mediated by aspartate aminotransferase (GOT1), or potentially via a fatty acid oxidation pathway mediated by acyl-coenzyme A (CoA) synthetase long-chain family member 3 (ACSL3). In addition, oncogenic RAS upregulates several key antioxidant proteins, including the light-chain subunit of the system xc−transporter (xCT), nuclear factor, erythroid 2-like 2 (NRF2), and gamma-glutamyltransferase 2 (GGT2).

($HRAS^{G12V}$ and $NRAS^{G13D}$) transcriptionally repressed *SESN* family genes, thus increasing intracellular ROS production (Lee et al., 1999; Kopnin et al., 2007; Zamkova et al., 2013). Finally, many cancers arise from sites of chronic irritation, infection or inflammation. Apart from cancer cells, also various tumor-associated cell types (*e.g.* activated macrophages and neutrophils) produce ROS contributing to maintain an oxidative, pro-tumorigenic TME (Marumo et al., 1997; Basuroy et al., 2009; Edderkaoui et al., 2011) (**Figure 2E**).

On the other hand, detoxification from ROS can be achieved by the complex battery of antioxidant systems shown in **Figure 2F**, including both antioxidant enzymes, which specifically scavenge different kinds of ROS, and non-enzymatic molecules, i.e. GSH, flavonoids, and vitamins A (ascorbic acid), C (ascorbic acid) and E (α-tocopherol). RAS-transformed cells upregulate all the three major types of primary intracellular antioxidant enzymes found in mammalian cells: superoxide dismutases (SOD), catalase and peroxidases.

KRAS stably expressed in NIH 3T3 cells, or transiently transfected in COS7 cells, was found to stimulate the scavenging of ROS by posttranscriptionally activating manganese (Mn)SOD, via an ERK1/2-dependent pathway (Santillo et al., 2001). Similarly, HRAS–transduced human keratinocyte HaCaT cells have higher SOD than control cells (Yang et al., 1999). Numerous proteomic analyses performed after RAS-mediated transformation revealed changes in other proteins involved either directly in metabolizing ROS or in maintaining the redox balance, such as Peroxiredoxin 3 and 4, thioredoxin peroxidases, NADH dehydrogenase ubiquinone Fe/S protein, glyoxyalase I, selenophosphate synthetase, and gamma-glutamyltransferase 2 (GGT2) (Young et al., 2004; Recktenwald et al., 2008; Moon et al., 2012). Increased expression of these enzymes was paralleled by an elevated tolerance of KRAS mutants against the cytotoxic potential of H_2O_2 and formaldehyde.

Mechanistically, oncogenic RAS activates expression of antioxidant genes predominantly trough the nuclear factor, erythroid derived 2, like 2 (NFE2L2, also known as NRF2),

which is widely regarded as the master regulator of antioxidant response (**Figure 2F**). NRF2 binds to the antioxidant response elements (ARE) within promoters of genes encoding antioxidant enzymes, such as glutathione S-transferase A2 (GSTA2) and NADPH quinone oxidoreductase 1 (NQO1) (Nguyen et al., 2009). For example, $KRAS^{G12D}$ raised mRNA and protein levels of *Nrf2* and its target genes, *e.g. Nqo1*, and decreased immunoreactivity for 7,8-dihydro-8-oxo-2′-deoxyguanosine (8-oxo-dGuo), one of the major products of DNA oxidation *in vitro* (Denicola et al., 2011). Importantly, such activation was validated *in vivo*, when comparing $KRAS^{G12D/+}$ pancreatic cancer cells to $KRAS^{LSL/+}$ epithelial cells in murine KRAS PanIN and PDA. Consistently, Nrf2-deficient murine PanIN were negative for Nqo1 and demonstrated similar levels of 8-oxo-dGuo and MDA in PanIN compared to neighboring normal ductal cells (Denicola et al., 2011).

Moreover, NRF2 activity is regulated by a coordinated protein complex consisting of Kelch-like ECH-associated protein 1 (KEAP1), CLLIN3 (CUL3), ubiquitin ligase, and other factors (Taguchi et al., 2011) (**Figure 2F**). Under normal conditions, this complex mediates the protein degradation of NRF2, preventing its translocation to the nucleus. However, oncogenic RAS can induce conformational changes in KEAP1, resulting in the upregulation of NRF2 target gene transcription and the following cytoprotection (Taguchi et al., 2011).

Noteworthy, all the enzymatic antioxidant activities responsible for ROS detoxification consume GSH and ultimately NADPH. Not only GSH directly scavenges hydroxyl radical ($HO^{\bullet}$) and $O_2^{-\bullet}$, but it acts as cofactor in antioxidant systems, and it regenerates the active forms of vitamin C and E. Once oxidized, glutathione (GSSG) can be converted back to its reduced form by glutathione reductase (GSR). Thus, the GSH/GSSG ratio can be assumed as an index of the redox buffering capacity of the cell. In order to increase intracellular GSH levels, oncogenic KRAS controls *xCT* transcription by downstream activation of ETS-1 which synergizes with Activating Transcription 4 (ATF4) (Lim et al., 2019) (**Figure 2F**). xCT (encoded by the gene *SLC7A11*) is the subunit of the system xc^-transporter, responsible for the exchange of intracellular glutamate for extracellular cystine, which, once inside the cell, is rapidly reduced to cysteine, the rate-limiting precursor in the synthesis GSH (Sato et al., 1999).

Given that NADPH is required to reduce GSSG and is thus the predominant source of reducing power, generation and maintenance of intracellular GSH and NADPH pools is crucial for redox homeostasis and potentially for oncogenesis. This can be achieved by rewiring cellular metabolic circuitries, as glutamine and glucose metabolism. In PDA, mutant KRAS was found to upregulate transcriptionally the aspartate transaminase (GOT1) (Son et al., 2013): in this way, GOT1 converts glutamine-derived aspartate into oxaloacetate, which fuels malate and then pyruvate synthesis, thus increasing the $NADPH/NADP^+$ ratio (**Figure 2F**). In LC cell lines, as well as in lung tumors, $KRAS^{G12D}$ enhances glucose metabolism providing the metabolites to be channeled into the TCA cycle, increasing NADPH levels and ultimately leading to ROS detoxification (Kerr et al., 2016). Moreover, in human LC cells and in lung tumors, mutant KRAS promotes FA oxidation (Padanad et al., 2016), a process that generates acetyl-CoA, which is metabolized to produce NADPH (Carracedo et al., 2013), especially under conditions of glucose scarcity (**Figure 2F**). Besides the generation of NADPH as a byproduct of FA oxidation, a direct link between lipid metabolism and oxidative stress was suggested by Yun et al., who showed that *FASN* knockdown decreased *SOD* expression, increased ROS production and sensitivity to H_2O_2. This report demonstrates how FASN regulates H_2O_2-induced cytotoxicity in CRC SNU-C4 ($KRAS^{G12C}$) human cancer cells (Yun et al., 2017).

LIPID PEROXIDES AT THE CROSS NODE BETWEEN LIPIDS AND OXIDATIVE STRESS

At physiological levels, lipid peroxides (LOOH) have beneficial effects: they induce cellular adaptive responses and enhance tolerance against subsequent oxidative stress through upregulation of antioxidant compounds and enzymes (Gaschler and Stockwell, 2017). However, their uncontrolled generation finally results in the initiation and execution of ferroptosis. LOOH production preferentially occurs in cell membranes due to the high solubility of molecular oxygen and it can be carried out either in an enzymatic or non-enzymatic manner. Yet, the two LPO mechanisms share the same substrate: PUFA.

PUFA, as LA, AA, DHA, and EPA are defined as long chain FA with two or more carbon-carbon double bonds. PUFA, as free FA or esterified into the sn-2 position of PL, are the preferential substrate of LPO, whereas acyl of the sn-1 position hardly participate in oxidation reactions (Davies and Guo, 2014). Other unsaturated lipids, such as cholesterol, can be oxidized to hydroperoxides too, but to a minor extent (Smith, 1987). Indeed, the bis-allylic hydrogen with a (1Z, 4Z) pentadiene moiety makes the C-H bond in PUFA weaker and the hydrogen more susceptible to abstraction (Gaschler and Stockwell, 2017). As elegantly shown by Yang *et al.*, replacing natural PUFA with deuterated PUFA (dPUFA) which have deuterium in place of the bis-allylic hydrogens, reduced oxidative stress and prevented cell death induced by Erastin or RSL3 -two potent ferroptosis inducers-in HT-1080 fibrosarcoma cancer cells (which harbor $NRAS^{Q61A}$) (Yang et al., 2016). Further, direct evidence for the oxidation of PUFA during ferroptosis was provided by incubating HT-1080 cells with alkyne-labeled LA, followed by copper-catalyzed cycloaddition (Click)-labeling reaction. Treatment with Erastin induced the accumulation of oxidative breakdown products of LA, which could be prevented by cotreatment with Ferrostatin-1 (Fer-1), a potent and selective inhibitor of ferroptosis (Skouta et al., 2014). Consistently with this concept, addition of AA or other PUFA was reported to increase ferroptosis sensitivity, possibly due to their increased incorporation into PL (PUFA-PL) (Conrad et al., 2018). Similarly, Fuentes et al., found that n-3 PUFA specifically suppress oncogenic KRAS-driven CRC by 1) incorporating into plasma membrane PL, 2) modifying KRAS nanoscale proteolipid composition, 3) disrupting oncogenic KRAS driven signaling, and

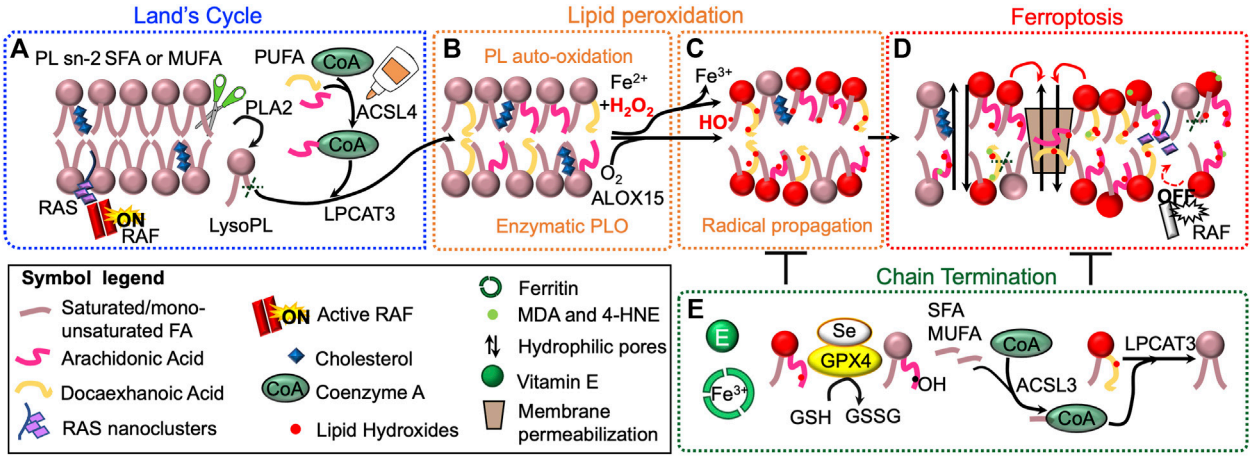

FIGURE 3 | Lipid peroxidation drives ferroptosis. Phospholipid (PL) acyl chain remodeling (Land's cycle) is responsible for the enrichment of membranes with polyunsaturated fatty acids (PUFA), when monounsaturated (MUFA) and saturated (SFA) FA become limiting. Phospholipase A2 (PLA2) removes acyl chain at sn-2 position. Lysophosphatydilcholine-acyltransferase-3 (LPCAT3) re-esterifies the position using PUFA-CoA, generated by acyl-CoA long-chain family member 4 (ACSL4) **(A)**. Membranes PL enriched with PUFA are prone to undergo iron–dependent lipid peroxidation (LPO) possibly via Fenton chemistry or enzymatic oxygenation (*e.g.* ALOX15) **(B)**. Once produced, lipid hydroxides (LOOH), if not cleared by the cellular antioxidant systems, can propagate LPO to other PUFA-containing PL **(C)**. LPO can lead to ferroptotic cell death (highlighted in red) through several mechanisms **(D)**. First, LOOH can alter membrane properties, which could allow the formation of hydrophilic pores and induce membrane permeabilization (i). Second, lipophilic electrophiles formed during the lipid peroxidation event could affect membrane-bound proteins and their signaling cascade (ii). LOOH can also generate second, more stable and highly reactive LPO products, as malondialdehyde (MDA), and 4-hydroxy-2-nonenal (4-HNE) (iii). Finally, LPO can alter lipidomic signature and affect cancer cell metabolism (iv). Cellular antioxidant systems and phospholipid remodeling can counteract and terminate LPO **(E)**.

finally 4) suppressing KRAS-associated phenotypes *in vitro* and *in vivo* (Fuentes et al., 2018).

On the contrary, MUFA do not have bis-allylic positions, hence are not readily oxidized. Rather, they can act as potent suppressors of ferroptosis in cancer cells. For instance, Magtanong *et al.* found that exogenous OA and palmitoleic acid (POA; C16:1), upon ACSL3-mediated activation, protected HT-1080 and A549 (NSCL, $KRAS^{G12S}$) cancer cells from ferroptosis induced by Erastin or its more potent analog, Erastin2 (Magtanong et al., 2019; Tesfay et al., 2019).

Interestingly, in regard to the potential impact of dietary FA on cancer, SFA and MUFA, but not PUFA, were associated with increased risk of CRC with specific KRAS mutations at codon 12 (Slattery et al., 2000; Weijenberg et al., 2007). On the contrary, dietary consumption of n-3 PUFA, such as EPA and DHA, results in their incorporation into cell membrane PL (Chapkin et al., 1991) and has been associated with reduced CRC risk (Hall et al., 2008).

The central requirement for PUFA oxidation in ferroptosis is also supported by genetic evidence linking specific lipid metabolic genes to the execution of ferroptosis. In particular, a CRISPR-based genetic screen identified ACSL4 and Lysophosphatidylcholine acyltransferase 3 (LPCAT3) as promoters of RSL3-and DPI7-induced ferroptosis (Dixon et al., 2015; Moerke et al., 2019).

ACSL4 is essential for both lipid metabolism and ferroptosis (Müller et al., 2017). Of all 6 ACSL isoforms, only ACSL4 has been positively correlated with ferroptosis likely because of its marked preference for PUFA (AA and EA, in particular) (Doll et al., 2017). Indeed, it was recently proven that increased levels of long n-6 PUFA are dependent on enhanced expression of *ACSL4*. Hence, ACSL4 has been proposed as both a biomarker and a regulator of ferroptosis. On the contrary, ACSL3 is known to preferentially activate MUFA, OA in particular, thus protecting plasma membrane PL from oxidation, supporting KRAS LC and metastasizing melanoma cells (Padanad et al., 2016; Magtanong et al., 2019; Ubellacker et al., 2020).

LPCAT3 preferentially mediates the insertion of AA into membrane PL by re-acylating LysoPL, mostly lysophosphatidylcholines (LysoPC) and lysophosphatidylethanolamines (LysoPE) (Eto et al., 2012; Wang and Tontonoz, 2019; Bartolacci et al., 2021). However, LPCAT3 can insert both PUFA- and MUFA-CoA esters (Hu et al., 2017; Bartolacci et al., 2021). Thus, our current understanding is that the requirement for LPCAT3 in ferroptosis might depend on the pool of available FA, the cell-type and the ferroptotic stimulus. For instance, LPCAT3 was reported as necessary to mediate RSL3-induced ferroptosis in HT-1080 and Calu-1 cells (Dixon et al., 2014), while we recently reported that *LPCAT3* knockdown drives mutant KRAS NSCLC human cell lines to ferroptosis Bartolacci et al., 2021).

ENZYMATIC AND NON-ENZYMATIC LIPID PEROXIDATION: TWO WAYS TO OXIDIZE PUFA

Enzymatic peroxidation is mostly mediated by LOX that catalyze the stereospecific insertion of oxygen into PUFA, such as AA and LA (Kuhn et al., 2005, 2015) (**Figure 3**). Although most LOX

prefer free FA as a substrate, some isoforms, including 15-LOX, can directly oxygenate PUFA-PL without prior release of esterified PUFA by phospholipase A2 (PLA2) (Kuhn et al., 1990). Shintoku *et al.* assessed the contribution LOX activity to ferroptosis in oncogenic RAS-expressing cancer cells (Shintoku et al., 2017). They showed that 12/15-LOX inhibitors -such as baicalein and PD146176-as well as siRNA-mediated silencing of *ALOX15* are able to prevent Erastin- and RSL3-induced ferroptosis in HT-1080, Panc-1 (PDA, $KRAS^{G12D}$) and Calu-1 (NSLC, $KRAS^{G12C}$) human cancer cells (Xie et al., 2016). On the contrary, treatment with ALOX15-activating compounds, as (E)-1-(7-benzylidene-3-phenyl-3,3a,4,5,6,7-hexahydroindazol2-yl)-2-(4-methylpiperazin-1-yl) ethenone, accelerated cell death at low doses of Erastin and RSL3 (Shintoku et al., 2017). Besides LOX enzymes, oxidized lipids can also be synthesized in a controlled manner by CYP450 mono-oxygenases and COX (Wang et al., 2019b). Interestingly enough, *PTGS2*, the gene encoding COX2, was the most upregulated gene in BJ-derived cell lines expressing $HRAS^{G12V}$- upon treatment with either Erastin or RSL3 (Yang et al., 2014). Knockdown of *GPX4* also increases *PTGS2* mRNA abundance in this system. However, ferroptotic cell death by Erastin or RSL3 is not affected by using indomethacin, a PTGS-1/PTGS-2 (COX-1/COX-2) inhibitor, suggesting that PTGS2 does not regulate ferroptosis and *PTGS2* upregulation could be rather considered a downstream marker of ferroptosis (Yang et al., 2014). This is consistent with the notion that not all inhibitors of LOX can rescue ferroptosis: rather, the compounds that can inhibit ferroptosis are radical-trapping antioxidants (RTA) that can protect against non-enzymatic peroxidation (Shah et al., 2018). Thus, we can hypothesize that autoxidation rather than the LOX-controlled lipid peroxidation is the final process of ferroptosis.

Non-enzymatic LPO can be schematically described in three stages: initiation (I), propagation (II) and termination (III) (**Figure 4**). Step (I) involves a free radical (i.e., •OH), which abstracts hydrogen from a polyunsaturated acyl chain of a PL. This process can be initiated by any reaction that generates radical compounds from non-radical molecules, often through redox reaction catalyzed by iron. In cells, iron is tightly regulated: it is found mostly ligated by heme, bound in FeS clusters, or to the iron storage protein ferritin (Lane et al., 2015). However, there are small pools of metabolically available, "labile" iron which is loosely ligated, thus able to react with endogenously produced H_2O_2 or $O_2^{-\bullet}$ to form oxygen centered radicals, through a process known as "Fenton chemistry" (Breuer et al., 2008). Interestingly, long-treatment with iron (as ferric ammonium citrate, FAC) strikingly reduced the growth of ovarian carcinoma cells, upon overexpression of HRAS or KRAS (Bauckman et al., 2013). Once formed, oxygen centered radicals readily react with molecular oxygen to form a PL peroxyl radical (PL-OO•) (II) (Maillard et al., 1983), which in turn can propagate the reaction in multiple ways. PL-OO• abstracts hydrogen from another PL molecule (**Figure 4**, **IIa**) and forms PL-OOH and a PL• radical which propagates the chain reaction. In the presence of Fe^{2+}, PL-OOH can be converted to PL alkoxyl radicals (PL-O•) which also contributes to chain propagation (Buettner, 1993). Alternatively, PL-OO• reacts via addition to the polyunsaturated acyl chain of another PL (**Figure 4**, **IIb**), which effectively forms PL dimers that are linked via a peroxide bond (Morita and Fujimaki, 1973). These dimers along with other intermediates (PL-OO• and PL-OOH) are instable molecules that suffer decomposition reactions, producing the electrophilic end products of PL autoxidation (reactive aldehydes and oxygenated PL). The free radical chain reaction propagates until two free radicals conjugate to each other to form stable molecules or in the presence of a chain-breaking anti-oxidant (Pratt et al., 2011) (**Figure 4**, **III**).

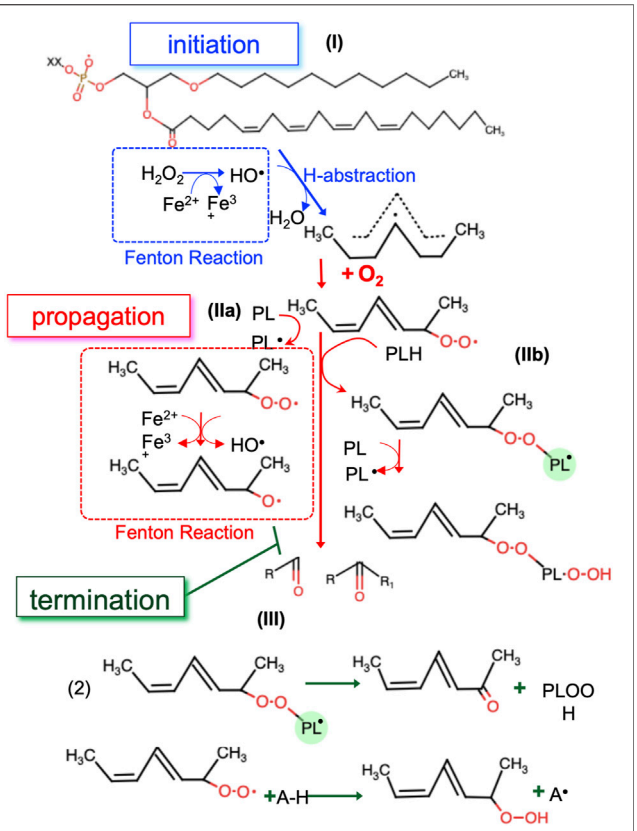

FIGURE 4 | The three steps of non-enzymatic LPO. In the initiation step the first radicals are generated by redox active labile iron **(I)**. In the propagation step radicals are able to react with new substrates, creating new radicals **(II)**. The propagation step repeats until the termination step, where radicals are 'quenched' by antioxidants or reacting with another radical **(III)**. •OH, hydroxyl radical; PL, phospholipid; PL-OO•, PL peroxyl radical; PL•, phospholipid radical, Fe^{2+}, ferrous ion, Fe^{3+}, ferric ion, PL-O•, PL alkoxyl radicals; A-H, antioxidant.

TOXICITY OF LIPID PEROXIDES IN FERROPTOSIS-SENSITIVE CANCER CELLS

Once generated, PLOOH, and more in general LOOH, can navigate cells to ferroptosis in several and still not fully elucidated processes (**Figure 4D**).

Effects on Membrane

Within the plasma membrane the polar chains in oxidized lipids are energetically unfavorable to stay in the bilayer's interior. As a result,

LPO causes the reversal of the polar lipid chain to the bilayer interface and major changes in membrane properties -*e.g.* increase of area per lipid, bilayer thinning, decreased lipid tail order and increased water permeability (Wong-Ekkabut et al., 2007; Beranova et al., 2010; Cwiklik and Jungwirth, 2010; Boonnoy et al., 2017) (**Figure 4D**). Moreover, according to atomistic molecular dynamics (MD) simulations, LOOH increase local membrane curvature, hence the accessibility of oxidants into membrane internal leaflet, which if not counterbalanced by GPX4, results in a vicious cycle that will ultimately destabilize the membrane, leading to pores and micellization (Agmon et al., 2018). Consistently, another MD simulation of oxidized lipid bilayers, containing 1-palmitoyl-2-lauroyl-sn-glycero-3-phosphocholine (PLPC) and its aldehyde derivatives, showed that oxidized lipids self-assemble into aggregates with a water pore rapidly developing across the bilayer (Siani et al., 2016). Vitamin E can prevent pore formation by trapping the polar groups of the oxidized lipids at the membrane–water interface resulting in a decreased probability of the oxidized lipids making contact with the two leaflets and initiating pore formation (Wong-Ekkabut et al., 2007). Interestingly, cholesterol and Vitamin E share similar molecular structures (i.e. a hydrophobic tail and a ring structure with a hydroxyl group) that might explain why cholesterol is a less preferred substrate for oxidation, but rather it is associated with increased bilayer thickness, lipid tail order, organized membrane architecture that help circumvent ferroptosis (Saito and Shinoda, 2011; Gilmore et al., 2013). In accordance with these *in silico* findings, when observed by confocal microscopy, Erastin-treated HT-1080 cells stained with LOOH-sensitive probe BODIPY-C11 581/591, show a distinct "ring" of LPO around the plasma membrane and a blister-like deformation with positive curvature (Tarangelo et al., 2018; Magtanong et al., 2019). Importantly, these data reconcile with RAS nanoclustering in cholesterol-poor domains (Zhou et al., 2017) and further indicate the importance of cell membrane composition in dictating ferroptosis sensitivity.

Effects on Membrane-Bound Proteins

LOOH affect RAS nanoclusters, which are the sites of RAS effector recruitment and activation: as shown by single fluorophore video tracking (SFVT) and electron microscopy (EM) studies, the localization of RAS-GTP to nanoclusters is required for the recruitment and activation of its downstream effector c-Raf (Tian et al., 2007; Zhou and Hancock, 2015) (**Figure 4D**).

Generation of Secondary LPO Products and Changes in the Lipidome

LOOH might further break down into many electrophilic species such as aldehydes which are more stable than primary LOOH and can therefore diffuse across membranes and crosslink primary amines on proteins, DNA and other nucleophilic molecules (Esterbauer et al., 1991; Marnett, 1999; Gaschler and Stockwell, 2017; Zhang et al., 2019). Among lipid aldehydes, malondialdehyde (MDA), and 4-hydroxy-2-nonenal (4-hydroxy-2,3-trans-nonenal, HNE) are the most investigated secondary products of LPO (Esterbauer et al., 1991; Kaur et al., 1997) (**Figure 4D**).

In KRAS human prostate cancer cells, 4-HNE significantly potentiates the antitumor effects of the HDAC inhibitor panobinostat (LBH589) (Pettazzoni et al., 2011). Both single agents and, to a greater extent, their combined treatment induced a G2/M cell cycle arrest in treated cells (Pettazzoni et al., 2011). In KRAS human colon adenocarcinoma cells, 4-HNE was found to inhibit cell proliferation through regulation of the MAP kinase (MAPK) pathway and interacting with transforming growth factor beta (TGF-β) (Vizio et al., 2005). Moreover, KRAS human CRC cells treated with isothiocyanates become resistant to benzo [α]pyrene or H_2O_2-induced cell death upregulating AKR1C1, the enzyme responsible for the reduction of 4-HNE (Bonnesen et al., 2001).

Changes in the lipidome of ferroptotic cancer cells have been widely studied in a variety of cancer models, using different ferroptosis inducers and by different analytic methods. However, it remains to be determined whether such changes are consequential to ferroptosis, or rather have a causative role. For instance, in HT-1080 cells, Erastin induced a depletion of PUFA, *e.g.* LA, EPA and DHA, both as free FA and PUFA-PC cells (Skouta et al., 2014), while increasing the level of LysoPC, which in physiologic conditions represent a minor percentage of cellular membrane lipids (ROBERTSON and LANDS, 1964; Yang et al., 2014). However, when ferroptosis was induced in the same *in vitro* system (i.e. HT-1080 cells), via GPX4-inhibition by $FINO_2$, it resulted in the accumulation of a wide array of oxidized PL, i.e. phosphatidylethanolamine (PE), PS, phosphatidylinositol (PI), and cardiolipin (CL) (Gaschler et al., 2018).

Moreover, it should be noted that also wild type (wt) RAS cancer cells undergoing ferroptosis show alterations in their lipidomic profile. As an example, in diffuse large B cell lymphoma (DLBCL) cell lines, IKE decreased levels of LysoPC, PC, PE, and TAG mainly containing PUFA (Zhang et al., 2019). The decrease in TAG upon IKE treatment indicates that in this specific context TAG may be the major oxidation target during ferroptosis, suggesting a possible protective role of this lipid class as a buffer against oxidation stress. However, untargeted lipidomics performed on tumor xenografts of mice treated with a single dose of IKE revealed increases in free FA, PL, and DAG, especially enriched in LA and AA (Listenberger et al., 2003).

These diverse and apparently contradictory results suggest that context specific characteristics (cell membrane composition, tissue of origin, nature of the ferroptosis inducing stimuli) may critically influence the lipids involved in the execution of ferroptosis. Thus, this field remains a very active subject of investigation that will undoubtedly benefit from analytical advances in detecting and quantifying the labile lipid species that are involved in ferroptosis.

DEGRADATION OF LIPID PEROXIDES TO ESCAPE FERROPTOSIS

To ensure membrane integrity and minimize damages associated with primary or secondary LPO products, cells employ several antioxidant enzymes as described earlier in this review. These

defense mechanisms might either detoxify LOOH and/or repair damaged lipids (Girotti, 1998) (**Figures 2F**, **3E**, **5**).

Vitamin E acts as a chain breaker to suppress LPO propagation reactions. This might explain why supplementing the diet with the antioxidants vitamin E markedly increases tumor progression and reduces survival in mouse models of KRAS–induced LC (Sayin et al., 2014).

The selenoprotein glutathione peroxidase 4 (GPX4) has been recognized as the master regulator of the enzymatic defense against membrane LPO as it is the only enzyme capable of reducing esterified oxidized FA and cholesterol hydroperoxides (Ursini et al., 1985; Seiler et al., 2008) (Brigelius-Flohé and Maiorino, 2013). Consistently, GPX4 inhibition leads to the rapid accumulation of LOOH, while its overexpression blocks RSL3-induced cell death (Yang et al., 2014; Conrad and Friedmann Angeli, 2015). However, the relation between RAS status and GPX4 is still controversial. For instance, Erastin and RSL3 caused ferroptosis in human tumor cells engineered to express $HRAS^{G12V}$ at lower concentrations than wild-type isogenic cells (Yagoda et al., 2007; Yang et al., 2014; Sui et al., 2018), and inhibiting GPX4 re-sensitized KRAS-expressing NSCLC cell lines (A549 and H460) made radioresistant (Pan et al., 2019). Nevertheless, cancer cells with no oncogenic RAS, as HT29 colon cancer cells, are sensitive to GPX4 inhibition, too (Sui et al., 2018), and ectopic expression of $NRAS^{12V}$, $KRAS^{12V}$, or $HRAS^{12V}$ protects RMS13 rhabdomyosarcoma cells from Erastin-induced apoptosis (Schott et al., 2015).

De novo Lipogenesis

We recently described that mutant KRAS LC deploys *de novo* lipogenesis to limit the amount of PUFA incorporated into membrane PL, deflecting LPO and ferroptosis (Bartolacci et al., 2021) (**Figures 3E**, **5**). These data suggest that mutant KRAS LC leverages lipid synthesis to withstand oxidative stress in the lung environment, which is rich in PUFA and oxygen (Bartolacci et al., 2021). This evidence is consistent with early studies reporting that in hypoxic conditions and in presence of oncogenic RAS, cancer cells scavenge serum lysolipids to meet their needs for SFA and MUFA (Kamphorst et al., 2013), and it provides further mechanistic insights into this dependency.

FERROPTOSIS AND ONCOGENIC RAS: A COMPLICATED RELATIONSHIP

On account of the highly intricate interplay with LPO and oxidative stress, the relationship between oncogenic RAS and ferroptosis is still controversial. On the one hand, pioneer studies in this field reported that expression of oncogenic RAS and/or activation of the RAS/MAPK pathway sensitize cells to ferroptosis inducers (Yagoda et al., 2007; Yang and Stockwell, 2008; Poursaitidis et al., 2017). Additionally, silencing of oncogenic *KRAS* in KRAS-mutant Calu-1 cells significantly reduces the lethality of Erastin. However, the potential link between RAS oncogenes and ferroptosis was later questioned by several observations. Firstly, DLBCL and renal cell carcinoma cell lines, which do not typically contain RAS pathway mutations, outstood as the most sensitive to Erastin sensitivity across a panel of 117 cancer cell lines (Yang et al., 2014). Secondly, RMS13 rhabdomyosarcoma cells ectopically overexpressing oncogenic *HRAS*, *KRAS* or *NRAS* are resistant to Erastin and RSL3 (Schott et al., 2015). However, these findings are in contrast with the observation that EGFR, KRAS, BRAF, and PIK3CA mutations sensitized LC to cystine deprivation–induced death (Poursaitidis et al., 2017). In addition, another study performed on rhabdomyosarcoma and myoblast cell lines showed that cells with high RAS/ERK activation are instead highly proliferative and more susceptible to Erastin and RSL3 (Codenotti et al., 2018).

Reasonable explanations for this apparently confusing picture include the diversity in cell lineage, mutant RAS protein level, proliferative and metabolic status, tumor stage, the existence of niche specific factors and epigenetic changes acquired during tumorigenesis/tumor progression which might contribute to ferroptosis execution/escape.

Many small molecule drugs have been developed to trigger ferroptosis and to inhibit the main enzymes able to metabolize LPO products and/or repair LOOH. Moreover, several FDA-approved drugs that are already in clinical use or have a strong potential for clinical translation were found to promote ferroptosis. Here, we will discuss several therapeutics that are FDA approved or that are being tested in RAS-driven cancers (**Figure 5**).

Immunotherapy

Immune checkpoint inhibitors (ICIs) have revolutionized the clinical management of patients with cancer. ICIs act blocking Cytotoxic T-Lymphocyte Antigen 4 (CTLA4), Programmed cell death protein 1 (PD-1) and its ligand PD-L1, thereby activating an effective cytotoxic anti-tumor immune response. Interferon gamma (IFNγ) released from cytotoxic T cells activates the JAK–STAT1 pathway, which in turn downregulates the expression of *SLC7A11* and *SLC3A2* inducing ferroptosis in cancer cells (Wang et al., 2019c) (**Figure 5**). Moreover, other cytokines released during immunotherapy, such as TGF-ß, can facilitate ferroptosis (Kim et al., 2020). Even though inhibition of PD-L1 failed in KRAS-mutant CRC (Infante et al., 2016), KRAS mutations in NSCLC were predictive of superior response to ICI compared to wild-type patients (Torralvo et al., 2019). Several co-occurring mutations have been described to mediate efficacy of immunotherapy in RAS-mutant LC. Indeed, while TP53 co-mutations are associated with clinical benefit, STK11 (alias LKB1) loss showed ineffectiveness of immunotherapy (Koyama et al., 2016; Dong et al., 2017). It is worth to note that both TP53 and STK11 are involved in ferroptosis regulation. TP53 has been shown to directly or indireclty promote ferroptosis by suppressing SLC7A11 or other metabolic genes (Jiang et al., 2015; Ou et al., 2016; Zhang et al., 2017). On the other hand, LKB1 suppresses ferroptosis via the LBK1-AMPK-ACC-FASN axis (Li et al., 2020a). Therefore, it is tempting to speculate that presence of mutant KRAS and concomitant mutations in TP53 and/or STK11 might influence ICI therapy efficacy by modulating ferroptosis susceptibility.

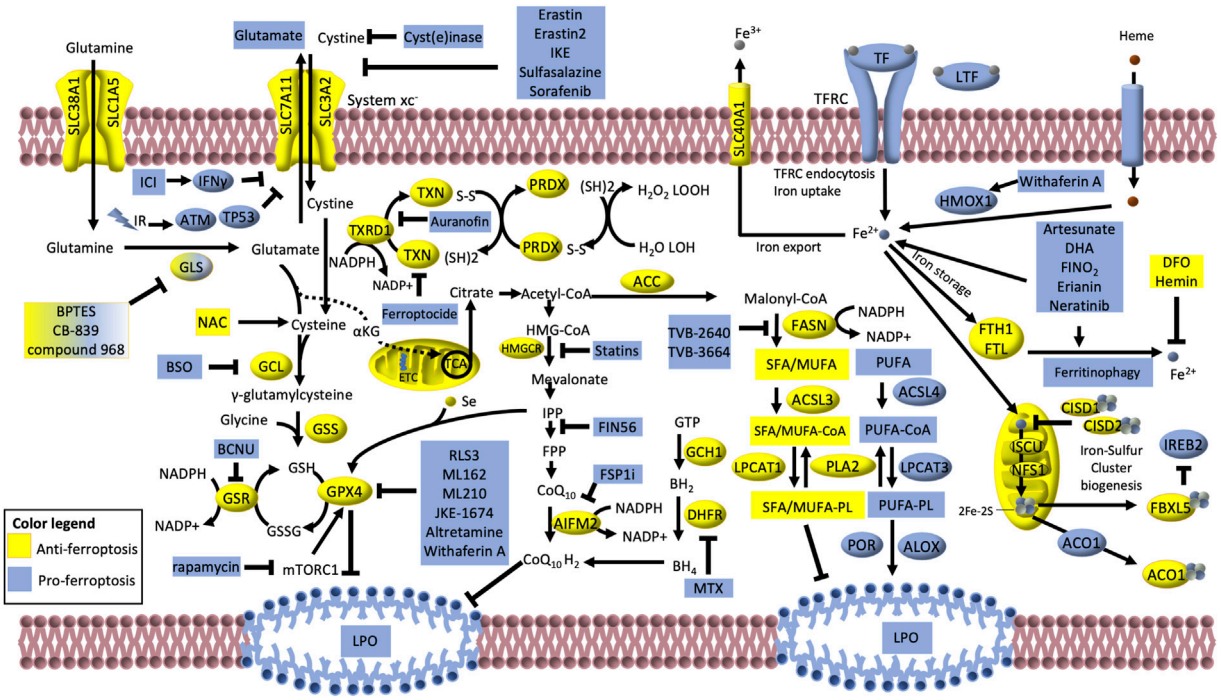

FIGURE 5 | Iron-dependent lipid peroxidation is the hallmark of ferroptosis. The cystine/glutamate transporter, consisting of the SLC3A2 and SLC7A11 (alias xCT) subunits, (collectively known as system xc–) imports cystine in exchange for glutamate. Glutamate is produced via glutaminase (GLS) -dependent glutaminolysis of glutamine. If not exported, glutamate can either be converted into α-ketoglutarate and enter the TCA cycle or participate to glutathione (GSH) synthesis via two sequential reactions catalyzed by glutamate–cysteine ligase (GCL) and glutathione synthetase (GSS). Glutathione peroxidase GPX4 uses GSH to buffer lipid peroxidation (LPO) and protect cells from ferroptosis. The oxidized glutathione (GSSG) is then reduced to GSH via glutathione–disulfide reductase (GSR) using NADPH as electron donor. GSH is a tripeptide antioxidant derived from glutamate, glycine and cysteine, which is turn produced by the reduction of cystine catalyzed by the thioredoxin reductase 1 (TXRD1). Along with the GPX4/GSH system, the TXRD/TXN and the peroxiredoxin (PRDX) systems can convert the phospholipid hydroperoxides (H_2O_2 LOOH) to alcohols and water (H_2O LOH). The AIFM2 (FSP1)–CoQ10 can also counteract LPO and ferroptosis. Moreover, the mevalonate pathway, can indirectly inhibit ferroptosis giving rise to CoQ10 and producing the isopentenyl diphosphate (IPP) that is the precursor for the selenium (Se)-containing GPX4. Also, the GCH1–dihydrofolate reductase (DHFR) system protects lipid membranes from autoxidation catalyzing the biosynthesis of the tetrahydrobiopterin (BH4). Many proteins involved in iron transport, storage and metabolism are key determinants of ferroptosis execution: these include transferrin (TF), lactotranferrin (LTF), transferrin receptor (TFRC), solute carrier family 40 member 1 (SLC40A1), heme oxygenase (HMOX1) and ferritin components (FTH1 and FTL). Also, the mitochondrial proteins cysteine desulfurase (NFS1) and iron–sulfur cluster assembly (ISCU) can reduce the availability of iron by sequestering Fe^{2+} for the biosynthesis of iron–sulfur clusters (2Fe–2S). The iron-regulatory proteins CISD1, CISD2, ACO1 and FBXL5/IREB2 usually negatively regulate ferroptosis. However, under low 2Fe–2S, ACO1 and IREB2 can translationally regulate iron metabolism-related proteins (such as TFRC, SLC11A2, SLC40A1, FTH1 and FTL), thus facilitating ferroptosis. Lipid synthesis and metabolism also play a central role in ferroptosis, by regulating the availability of substrates for LPO. Acetyl- CoA carboxylase (ACC)/FASN axis mediates the synthesis of fatty acids (FA), mainly saturated (SFA) and monounsaturated (MUFA), which have low susceptibility to LPO. SFA/MUFA are conjugated to CoA by the long-chain fatty acid–CoA ligase 3 (ACSL3) prior to be incorporated into membrane phospholipids (PL) via the lysophosphatidylcholine acyltransferase 1 (LPCAT1). On the other hand, Long-chain fatty acid–CoA ligase 4 (ACSL4) and lysophosphatidylcholine acyltransferase 3 (LPCAT3) promote the incorporation of exogenous or lipophagy-derived polyunsaturated FA (PUFA) into PL forming PUFA-PL, which are susceptible to free radical oxidation mediated by lipoxygenases (ALOX) and cytochrome P450 oxidoreductases (POR). Phosholipase A2 (PLA2) can partially counteract this process by cutting out the oxidized FA chains of PUFA-PL. Compounds, proteins, treatments that induce and inhibit ferroptosis are depicted in blue and yellow, respectively, and are discussed in the main text of this review. BSO, buthionine sulfoximine; BCNU, 1,3-bis(2-chloroethyl)-1-nitrosourea; ETC, electron transport chain; GCH1, GTP cyclohydrolase 1; MTX, methotrexate; DFO, deferoxamine; IR, ionizing radiation; ICI, immune checkpoint inhibitor; NAC, N-acetyl cysteine.

Radiotherapy

Radiotherapy is used alone or in combination with other therapies for several solid tumors, including RAS-driven cancers. Radiotherapy has been described to induce ferroptosis in preclinical cancer models and it synergizes with immunotherapy in the suppression of SLC7A11 (Lang et al., 2019) (**Figure 5**). Ionizing radiation (IR) also activates *ACSL4* expression, thus promoting the formation of PUFA–PL and subsequent LPO (Lei et al., 2020). One more way by which radiation causes ferroptosis is through the release of irradiated tumor cell-released microparticles (RT-MPs) which seem to be at the base of the so-called "radiation-induced bystander effect (RIBE) (Mothersill and Seymour, 2004; Wan et al., 2020). Finally, radiotherapy can promote autophagy-dependent ferroptosis, via activation of cyclic GMP–AMP synthase (cGAS) (Li et al., 2020b). The fact that RAS oncogene has been implicated in establishing radioresistance (Sklar, 1988; McKenna et al., 2003; Wang et al., 2018; Dong et al., 2021) provides the rationale for searching common ground with RAS-induced resistance to ferroptosis in certain cancers (Schott et al., 2015).

Sorafenib

Sorafenib is an inhibitor of RAF kinases which has being evaluated in clinical trials for several malignancies (NCT03247088, NCT02559778, and NCT00064350). RAF kinases are integral part of the RAS/RAF/MEK/ERK pathway. Therefore cancers driven by RAS have been shown as good candidates for sorafenib treatment (Samalin et al., 2016; Lim et al., 2018; Khoury et al., 2020). Even though sorafenib was reported to induce apoptosis and autophagy in cancer cells trough suppression of RAS/RAF signaling pathway (Ullén et al., 2010; Garten et al., 2019), many other studies suggested that sorafenib induces ferroptosis by inhibiting the system xCT independently of the inhibition of RAF pathways (Dixon et al., 2014; Lachaier et al., 2014; Sun et al., 2016) (**Figure 5**). Therefore, it is likely that the sensitivity of RAS-driven cancers to sorafenib is due to the susceptibility to ferroptosis induction rather than solely to inhibition of RAS/RAF/MEK/ERK pathway. Future studies and combination trials with other ferroptosis inducers might be useful to understand to which extend ferroptosis contributes to the anticancer effect of sorafenib.

Sulfasalazine

Sulfasalazine is an anti-inflammatory drug that can suppress the cancer growth by inhibiting the system xCT, inducing ferroptosis in preclinical models (Gout et al., 2001; Dixon et al., 2012) (**Figure 5**). Sulfasalazine has been evaluated in phase I clinical trials for glioblastoma and breast cancer (NCT04205357, NCT01577966, and NCT03847311). As it regards LC, sulfasalazine has been recently reported to selectively kill KRAS-mutant LC, indicating that it might be a good drug candidate in this tumor type (Hu et al., 2020).

Cyst(e)inase

Cyst(e)inase is an engineered human enzyme that can degrade cysteine and cystine (cyst(e)ine), causing cell death in cancer cells (Cramer et al., 2017). In particular, cyst(e)inase-mediated depletion of cyst(e)ine is well tolerated and can induce ferroptosis in preclinical models of mutant Kras/Tp53 PDAC (Badgley et al., 2020). These data suggest that strategies regulating extracellular cyst(e)ine levels using cyst(e)inase or cyst(e)ine-deprived diet could offer new therapeutic opportunities in combination with other ferroptosis inducing drugs.

The Glutamine Metabolism Dilemma

The need of cancer cells for glutamine, the so called "glutamine addiction", represents a vulnerability that can be exploited therapeutically, especially in KRAS-driven cancers (Son et al., 2013; Toda et al., 2017; Bernfeld and Foster, 2019; Galan-Cobo et al., 2019). Moreover, glutamine, like cysteine, is intimately connected to ferroptosis. If on the one hand, generation of glutamate via GLS1/2-mediated glutaminolysis of glutamine promotes the activity of the xCT system and the synthesis of GSH, on the other hand glutamine is essential to execute ferroptosis under cysteine deprivation (Gao et al., 2015).

Moreover, glutamine contributes to maintenance of the redox balance via the production of aspartate through the transamination pathway. This leads to the formation of malate and pyruvate, concomitantly producing NAD+ and NADPH.

In addition, Muir *et al.* showed that cystine levels dictate glutamine dependence via xCT and concurrent high expression of GLS and xCT may predict response to glutaminase inhibition (Muir et al., 2017). It is unclear whether glutaminase inhibitors like BPTES, CB-839 and compound 968, exert their anticancer effects by modulating ferroptosis sensitivity in KRAS tumor cells and how glutamine dependency might be a predictive marker of ferroptosis susceptibility.

Neratinib

The tyrosine kinase inhibitor neratinib induces ferroptosis in RAS-, EGFR-, and HER2-driven cancer cells (Booth et al., 2019; Dent et al., 2019, 2020; Nagpal et al., 2019). Neratinib is being tested in trial combination therapy with valproate for advanced RAS-mutated solid tumors (NCT03919292). A further connection between RAS and neratinib is given by recent data showing that RAS-dependent reactivation of mTORC1 accounts for the resistance to neratinib (Sudhan et al., 2020). Therefore, it would be of interest to further investigate whether concomitant RAS/mTORC1 inhibition might synergize with neratinib at inducing ferroptosis.

GPX4 Inhibitors

RSL3 was first identified in a high-throughput screening as a compound that can selectively induce ferroptosis in transformed cells harboring activated HRAS (Yang and Stockwell, 2008). Affinity purification experiments identified GPX4 as a direct target of RSL3 (Yang et al., 2014) (**Figure 5**). Similar to RSL3, ML162, another GPX4 inhibitor, was identified in a drug screening for compounds targeting HRAS (Weïwer et al., 2012). However, poor pharmacokinetic properties and promiscuous binding to targets other than GPX4, have limited the use of RSL3 and ML162 in *in vivo* studies and clinical trials (Eaton et al., 2020). On the other end, the pro-drug GPX4 inhibitor ML210 and its derivative, JKE-1674, have shown higher specificity and favorable bioavailability that maybe exploited for cancer therapy (Eaton et al., 2020). Altretamine, an FDA-approved alkylating agent, has been shown to induce ferroptosis (Woo et al., 2015) and was tested in HIV-related lymphoma and sarcoma (NCT00002936). Also the natural compound Withaferin A, has shown a multifaceted pro-ferroptotic activity via inhibition of GPX4, activation of XMOX1, induction of ROS and inhibition of the MAPK/RAS/RAF pathway (Hassannia et al., 2018, 2020; Yin et al., 2020). This pleiotropic effect, targeting multiple dependencies and vulnerabilities of RAS-driven cancers, along with its development into nanocarriers (Hassannia et al., 2018) warrant future investigation to establish whether Withaferin A might be an effective ferroptosis inducer.

Statins and FASN Inhibitors

Statins are widely prescribed cholesterol-lowering drugs that inhibit HMG-CoA reductase (HMGCR), the rate-limiting enzyme of the mevalonate metabolic pathway, which gives rise to cholesterol (**Figure 5**). Also, statins block the formation of

isopentenyl pyrophosphate (IPP), the precursor of GPX4 and coenzyme Q10, facilitating ferroptosis. Since the mevalonate pathway influences several aspects of the signaling pathways in cancer (Mullen et al., 2016), their potential application in cancer therapy (reviewed in (Longo et al., 2020) has been tested in several tumors, including in RAS-driven cancers. The initial observation that RAS activation may enhance sensitivity to statins (Yu et al., 2018), was then challenged by the failure of several clinical trials (Hong et al., 2014; Lee et al., 2014; Baas et al., 2015). A possible explanation of these outcomes might be that statins induce a feedback activation of the Sterol Regulatory Element-binding transcription Factor 1/2 (SREBP1/SREBP2) pathways which activate the genes of the mevalonate and lipid synthesis. Indeed, suppression of SREBP2 has been reported to sensitize cancer cells to statin-induced death (Longo et al., 2019). Interestingly, mutant KRAS activates the SREBP1/FASN pathway in LC (Gouw et al., 2017) and FASN inhibition is a selective vulnerability of mutant KRAS LC (Bartolacci et al., 2017, 2021). Indeed, the FASN inhibitor TVB-3664 has been reported to induce ferroptosis specifically in KRAS-mutant LC models and its human specific isomer, TVB-2640 is being tested in phase 2 clinical trial KRAS-mutant LC patients (NCT03808558, (Bartolacci et al., 2021). Therefore, we can speculate that combination of statins and SREBP/FASN inhibition might be an efficient strategy to induce ferroptosis in this cancer type.

Auranofin and Ferroptocide

A combination of the anti-rheumatoid arthritis drug Auranofin and rapamycin is now in phase I, II clinical trial for RAS-mutant small and squamous LC (NCT01737502). Both compounds are being reported to induce ferroptosis and to synergize. Indeed, auranofin induces ferroptosis through inhibition of thioredoxin reductase (TXNRD) activity (Yang et al., 2020) (**Figure 5**) and has been shown as a successful strategy to induce ferroptosis in small cell lung cancer (SCLC) in combination with BSO-dependent GPX4 inhibition (Bebber et al., 2021). On the other hand, rapamycin, the most used and characterized mTOR inhibitor and inducer of autophagy, has been recently described to induce degradation of GPX4 (**Figure 5**), thereby activating autophagy-dependent ferroptosis in PDA cell lines (Liu et al., 2021).

Ferroptocide is another molecule targeting the TXN/TXRD system, which induces ferroptosis covalently binding to TXN (Llabani et al., 2019). Of note, TXN is dysregulated in pancreatic cancer where it regulates KRAS signaling pathway (Schultz et al., 2017), indicating that it may represent a good strategy to induce ferroptosis in RAS-driven cancers.

Methotrexate

Methotrexate is an inhibitor of the dihydrofolate reductase (DHFR), which catalyzes the biosynthesis of the tetrahydrobiopterin (BH4) (**Figure 5**). BH4 is not only the precursor of nucleotides, but it is also a potent antioxidant that protects lipid membranes from autoxidation. Blocking BH4 synthesis, genetically or via methotrexate treatment, synergizes with GPX4 inhibition at inducing ferroptosis (Soula et al., 2020). Methotrexate is now being tested in combination with regorafenib in phase II clinical trial for recurrent or metastatic KRAS-mutant NSCLC (NCT03520842). Interestingly, methotrexate was initially reported to target RAS by inhibiting the isoprenylcysteine carboxyl methyltransferase. This enzyme is responsible for the carboxyl methylation of RAS protein and its inhibition causes RAS mis localization from the membrane impairing downstream signaling and cell proliferation (Winter-Vann et al., 2003). Ongoing clinical trials and future investigations will determine whether the two mechanisms of action contribute to the anticancer activity of methotrexate in RAS-driven cancers.

Natural Compounds Inducing Ferroptosis

Several naturally occurring compounds are emerging as potential ferroptosis inducers in RAS cancers. Initially discovered as naturally occurring anti-malarial compounds extracted from *Artemisia annua*, artemisinins have shown potential as anti-cancer therapies (Kiani et al., 2020). In particular, artesunate, one of the most popular artemisinins, can trigger ferroptosis in KRAS-mutant PDA cancer cells by increasing the intracellular levels of free iron (Eling et al., 2015; Wang et al., 2019d). Another natural product, Erianin, isolated from *Dendrobium chrysotoxum Lindl*, has been shown to induce ferroptosis in preclinical models of KRAS-mutant LC by causing high levels of intracellular iron and calcium (Chen et al., 2020). Also, bromelain, a mixture of proteolytic enzymes derived from pineapple stem (*Ananas comosus* L., family Bromeliaceae), has been shown to mediate ferroptosis in KRAS-mutant CRC via upregulation of *ACSL4* (Park et al., 2018).

CONCLUSIONS: THE PATH FORWARD

Recent years have witnessed dramatic advancements in our understanding of how cancers driven by oncogenic RAS have altered metabolic needs, leading to the recognition that lipids have roles that go far beyond being simple substrates for energy storage and production. Instead, lipids regulate critical cellular processes. For instance, LPO is involved in the regulation of ferroptosis, a special type of cell death, with potential applications in cancer therapy. In our review of the literature, we explored ferroptosis in the context of oncogenic RAS-driven cancers.

The basic knowledge that has accumulated so far provides an opportunity to reconsider the importance of lipid metabolism and oxidative stress in RAS-driven cancers. However, there is still much work to be done to fully understand RAS metabolic dependencies and their implications in terms of ferroptosis susceptibility. Firstly, it is likely that *RAS* mutations have tissue-specific effects on metabolism. This is due to the intrinsic metabolic wiring in the tissue of origin of a particular tumor and its interaction with oncogenic RAS. In addition, cancer cells undergo a profound lipid metabolism reprogramming during metastasis which in turn may influence their susceptibility to ferroptosis. (Rozeveld et al., 2020; Ubellacker et al., 2020; Ferraro et al., 2021). Also, some evidences have suggested that high proliferative cancer cells are more prone to ferroptosis induction (Codenotti et al., 2018). However, whether the tumor stage and the proliferation rate of *RAS*-driven cancers might affect their susceptibility to oxidative stress and ferroptosis, remains to be elucidated. These and other cancer specific features

may create distinct metabolic dependencies for *RAS* mutations in different tumor types that should be explored in a systematic fashion. In a similar manner, *RAS* mutations act in the context of co-occurring mutations—namely other oncogenic events as well as deletion/mutation of a constellation of tumor suppressor genes. For instance, the tumor suppressor p53 has been shown to have an impact on multiple facets of lipid metabolism and ferroptosis (reviewed by (Liu et al., 2020)). Therefore, it will be important to consider the tumor suppressor background when studying the interplay among mutant RAS/lipid metabolism/ferroptosis. Another aspect that requires additional study will be how these RAS-dependent metabolic changes are altered *in vivo* in the TME. This includes areas of hypoxia, limited nutrients, as well as potential metabolic crosstalk between tumor and stromal cells. To understand these complex relationships will require the use of sophisticated autochthonous tumor models as well as the ability to perform metabolic tracing studies *in vivo*. Additionally, in regard to therapeutic targeting of altered lipid metabolism and/or ferroptosis inducers, it will be of significance to identify adaptive responses of *RAS*-driven cancers which could promote therapeutic resistance. As new approaches in lipidomics are applied to the study of ferroptosis in RAS-driven cancers, we anticipate that new biomarkers will be identified, the mechanisms behind ferroptosis-susceptibility will unfold and inform how to integrate ferroptosis inducers with existing chemotherapeutic agents.

AUTHOR CONTRIBUTIONS

CB and CA equally contributed to the review (shared co-first authorship). They performed literature search, organized and critically reviewed available information, conceived how to structure the review, and addressed several aspects of the topic. They wrote the manuscript and made the figures. YE-G helped search for literature and articles relevant to the field. PS contributed to conceive the review, revised the manuscript and provided important comments.

REFERENCES

Agmon, E., Solon, J., Bassereau, P., and Stockwell, B. R. (2018). Modeling the Effects of Lipid Peroxidation during Ferroptosis on Membrane Properties. *Sci. Rep.* 8, 5155. doi:10.1038/s41598-018-23408-0

Al Saati, T., Clerc, P., Hanoun, N., Peuget, S., Lulka, H., Gigoux, V., et al. (2013). Oxidative Stress Induced by Inactivation of TP53INP1 Cooperates with KrasG12D to Initiate and Promote Pancreatic Carcinogenesis in the Murine Pancreas. *Am. J. Pathol.* 182, 1996–2004. doi:10.1016/j.ajpath.2013.02.034

Asturias, F. J., Chadick, J. Z., Cheung, I. K., Stark, H., Witkowski, A., Joshi, A. K., et al. (2005). Structure and Molecular Organization of Mammalian Fatty Acid Synthase. *Nat. Struct. Mol. Biol.* 12, 225–232. doi:10.1038/nsmb899

Baas, J. M., Krens, L. L., Ten Tije, A. J., Erdkamp, F., Van Wezel, T., Morreau, H., et al. (2015). Safety and Efficacy of the Addition of Simvastatin to Cetuximab in Previously Treated KRAS Mutant Metastatic Colorectal Cancer Patients. *Invest. New Drugs* 33, 1242–1247. doi:10.1007/s10637-015-0285-8

Babior, B. M. (1999). NADPH Oxidase: An Update. *Blood* 93, 1464–1476. doi:10.1182/blood.v93.5.1464

Badgley, M. A., Kremer, D. M., Maurer, H. C., DelGiorno, K. E., Lee, H.-J., Purohit, V., et al. (2020). Cysteine Depletion Induces Pancreatic Tumor Ferroptosis in Mice. *Science* 368, 85–89. doi:10.1126/science.aaw9872

Bartolacci, C., Padanad, M., Andreani, C., Melegari, M., Rindhe, S., George, K., et al. (2017). Fatty Acid Synthase Is a Therapeutic Target in Mutant KRAS Lung Cancer. *J. Thorac. Oncol.* 12, S1538. doi:10.1016/j.jtho.2017.06.030

Bartolacci, C., Andreani, C., Dias do Vale, G., Berto, S., Melegari, M., Crouch, A. C., et al. (2021). Targeting de novo lipogenesis and the Lands cycle induces ferroptosis in KRAS-mutant lung cancer. *bioRxiv*. doi:10.1101/2021.03.18.434804

Basuroy, S., Bhattacharya, S., Leffler, C. W., and Parfenova, H. (2009). Nox4 NADPH Oxidase Mediates Oxidative Stress and Apoptosis Caused by TNF-α in Cerebral Vascular Endothelial Cells. *Am. J. Physiol.-Cell Physiol.* 296, C422–C432. doi:10.1152/ajpcell.00381.2008

Bauckman, K. A., Haller, E., Flores, I., and Nanjundan, M. (2013). Iron Modulates Cell Survival in a Ras- and MAPK-dependent Manner in Ovarian Cells. *Cell Death Dis* 4, e592. doi:10.1038/cddis.2013.87

Bebber, C. M., Thomas, E. S., Stroh, J., Chen, Z., Androulidaki, A., Schmitt, A., et al. (2021). Ferroptosis Response Segregates Small Cell Lung Cancer (SCLC) Neuroendocrine Subtypes. *Nat. Commun.* 12, 2048. doi:10.1038/s41467-021-22336-4

Beranova, L., Cwiklik, L., Jurkiewicz, P., Hof, M., and Jungwirth, P. (2010). Oxidation Changes Physical Properties of Phospholipid Bilayers: Fluorescence Spectroscopy and Molecular Simulations. *Langmuir* 26, 6140–6144. doi:10.1021/la100657a

Bernfeld, E., and Foster, D. A. (2019). Glutamine as an Essential Amino Acid for KRas-Driven Cancer Cells. *Trends Endocrinol. Metab.* 30, 357–368. doi:10.1016/j.tem.2019.03.003

Bonnesen, C., Hayes, J. D., and Eggleston, I. M. (2001). Dietary Indoles and Isothiocyanates that Are Generated from Cruciferous Vegetables Can Both Stimulate Apoptosis and Confer protection against DNA Damage in Human colon Cell Lines. *Cancer Res.* 61, 6120–6130.

Boonnoy, P., Karttunen, M., and Wong-Ekkabut, J. (2017). Alpha-tocopherol Inhibits Pore Formation in Oxidized Bilayers. *Phys. Chem. Chem. Phys.* 19, 5699–5704. doi:10.1039/c6cp08051k

Booth, L., Roberts, J. L., Sander, C., Lalani, A. S., Kirkwood, J. M., Hancock, J. F., et al. (2019). Neratinib and Entinostat Combine to Rapidly Reduce the Expression of K-RAS, N-RAS, Gαq and Gα11 and Kill Uveal Melanoma Cells. *Cancer Biol. Ther.* 20, 700–710. doi:10.1080/15384047.2018.1551747

Breuer, W., Shvartsman, M., and Cabantchik, Z. I. (2008). Intracellular Labile Iron. *Int. J. Biochem. Cel Biol.* 40, 350–354. doi:10.1016/j.biocel.2007.03.010

Brigelius-Flohé, R., and Maiorino, M. (2013). Glutathione Peroxidases. *Biochim. Biophys. Acta (Bba) - Gen. Subjects* 1830, 3289–3303. doi:10.1016/j.bbagen.2012.11.020

Buettner, G. R. (1993). The Pecking Order of Free Radicals and Antioxidants: Lipid Peroxidation, α-Tocopherol, and Ascorbate. *Arch. Biochem. Biophys.* 300, 535–543. doi:10.1006/abbi.1993.1074

Canuto, R. A., Muzio, G., Maggiora, M., Biocca, M. E., and Dianzani, M. U. (1993). Glutathione-S-transferase, Alcohol Dehydrogenase and Aldehyde Reductase Activities during Diethylnitrosamine-Carcinogenesis in Rat Liver. *Cancer Lett.* 68, 177–83. doi:10.1016/0304-3835(93)90144-X

Carracedo, A., Cantley, L. C., and Pandolfi, P. P. (2013). Cancer Metabolism: Fatty Acid Oxidation in the Limelight. *Nat. Rev. Cancer* 13, 227–232. doi:10.1038/nrc3483

Chapkin, R. S., Akoh, C. C., and Miller, C. C. (1991). Influence of Dietary N-3 Fatty Acids on Macrophage Glycerophospholipid Molecular Species and Peptidoleukotriene Synthesis. *J. Lipid Res.* 32, 1205–13. doi:10.1016/s0022-2275(20)41983-2

Chen, P., Wu, Q., Feng, J., Yan, L., Sun, Y., Liu, S., et al. (2020). Erianin, a Novel Dibenzyl Compound in Dendrobium Extract, Inhibits Lung Cancer Cell Growth and Migration via Calcium/calmodulin-dependent Ferroptosis. *Sig Transduct Target. Ther.* 5, 51. doi:10.1038/s41392-020-0149-3

Chirala, S. S., and Wakil, S. J. (2004). Structure and Function of Animal Fatty Acid Synthase. *Lipids* 39, 1045–1053. doi:10.1007/s11745-004-1329-9

Chun, S. Y., Johnson, C., Washburn, J. G., Cruz-Correa, M. R., Dang, D. T., and Dang, L. H. (2010). Oncogenic KRAS Modulates Mitochondrial Metabolism in Human colon Cancer Cells by Inducing HIF-1a and HIF-2a Target Genes. *Mol. Cancer* 9, 293. doi:10.1186/1476-4598-9-293

Codenotti, S., Poli, M., Asperti, M., Zizioli, D., Marampon, F., and Fanzani, A. (2018). Cell Growth Potential Drives Ferroptosis Susceptibility in Rhabdomyosarcoma and Myoblast Cell Lines. *J. Cancer Res. Clin. Oncol.* 144, 1717–1730. doi:10.1007/s00432-018-2699-0

Conrad, M., and Friedmann Angeli, J. P. (2015). Glutathione Peroxidase 4 (Gpx4) and Ferroptosis: What's So Special about it?. *Mol. Cell Oncol.* 2, e995047. doi:10.4161/23723556.2014.995047

Conrad, M., Kagan, V. E., Bayir, H., Pagnussat, G. C., Head, B., Traber, M. G., et al. (2018). Regulation of Lipid Peroxidation and Ferroptosis in Diverse Species. *Genes Dev.* 32, 602–619. doi:10.1101/gad.314674.118

Cramer, S. L., Saha, A., Liu, J., Tadi, S., Tiziani, S., Yan, W., et al. (2017). Systemic depletion of L-cyst(e)ine with cyst(e)inase increases reactive oxygen species and suppresses tumor growth. *Nat. Med.* 23, 120–127. doi:10.1038/nm.4232

Cwiklik, L., and Jungwirth, P. (2010). Massive Oxidation of Phospholipid Membranes Leads to Pore Creation and Bilayer Disintegration. *Chem. Phys. Lett.* 486, 99–103. doi:10.1016/j.cplett.2010.01.010

Davies, S. S., and Guo, L. (2014). Lipid Peroxidation Generates Biologically Active Phospholipids Including Oxidatively N-Modified Phospholipids. *Chem. Phys. Lipids* 181, 1–33. doi:10.1016/j.chemphyslip.2014.03.002

Denicola, G. M., Karreth, F. A., Humpton, T. J., Gopinathan, A., Wei, C., Frese, K., et al. (2011). Oncogene-induced Nrf2 Transcription Promotes ROS Detoxification and Tumorigenesis. *Nature* 475, 106–109. doi:10.1038/nature10189

Dent, P., Booth, L., Roberts, J. L., Liu, J., Poklepovic, A., Lalani, A. S., et al. (2019). Neratinib Inhibits Hippo/YAP Signaling, Reduces Mutant K-RAS Expression, and Kills Pancreatic and Blood Cancer Cells. *Oncogene* 38, 5890–5904. doi:10.1038/s41388-019-0849-8

Dent, P., Booth, L., Poklepovic, A., Hoff, D. V., and Hancock, J. F. (2020). Enhanced Signaling via ERBB3/PI3K Plays a Compensatory Survival Role in Pancreatic Tumor Cells Exposed to [neratinib + Valproate]. *Cell Signal.* 68, 109525. doi:10.1016/j.cellsig.2020.109525

Dianzani, M. U., and Barrera, G. (2008). "Pathology and Physiology of Lipid Peroxidation and Its Carbonyl Products," in *Free Radical Pathophysiology*. Editors A. Alvarez, S. Evelson, and P. Boveris (Trivandrum: Transworld Research Network), 19–38.

Dixon, S. J., and Stockwell, B. R. (2019). The Hallmarks of Ferroptosis. *Annu. Rev. Cancer Biol.* 3, 35–54. doi:10.1146/annurev-cancerbio-030518-055844

Dixon, S. J., Lemberg, K. M., Lamprecht, M. R., Skouta, R., Zaitsev, E. M., Gleason, C. E., et al. (2012). Ferroptosis: an Iron-dependent Form of Nonapoptotic Cell Death. *Cell* 149, 1060–1072. doi:10.1016/j.cell.2012.03.042

Dixon, S. J., Patel, D. N., Welsch, M., Skouta, R., Lee, E. D., Hayano, M., et al. (2014). Pharmacological Inhibition of Cystine-Glutamate Exchange Induces Endoplasmic Reticulum Stress and Ferroptosis. *Elife* 3, e02523. doi:10.7554/eLife.02523

Dixon, S. J., Winter, G. E., Musavi, L. S., Lee, E. D., Snijder, B., Rebsamen, M., et al. (2015). Human Haploid Cell Genetics Reveals Roles for Lipid Metabolism Genes in Nonapoptotic Cell Death. *ACS Chem. Biol.* 10, 1604–1609. doi:10.1021/acschembio.5b00245

Doll, S., Proneth, B., Tyurina, Y. Y., Panzilius, E., Kobayashi, S., Ingold, I., et al. (2017). ACSL4 Dictates Ferroptosis Sensitivity by Shaping Cellular Lipid Composition. *Nat. Chem. Biol.* 13, 91–98. doi:10.1038/nchembio.2239

Dolma, S., Lessnick, S. L., Hahn, W. C., and Stockwell, B. R. (2003). Identification of Genotype-Selective Antitumor Agents Using Synthetic Lethal Chemical Screening in Engineered Human Tumor Cells. *Cancer Cell* 3, 285–296. doi:10.1016/S1535-6108(03)00050-3

Dong, Z. Y., Zhong, W. Z., Zhang, X. C., Su, J., Xie, Z., Liu, S. Y., et al. (2017). Potential Predictive Value of TP53 and KRAS Mutation Status for Response to PD-1 Blockade Immunotherapy in Lung Adenocarcinoma. *Clin. Cancer Res.* 23, 3012–3024. doi:10.1158/1078-0432.CCR-16-2554

Dong, Y.-L., Vadla, G. P., Lu, J.-Y., Jim)Ahmad, V., Klein, T. J., et al. (2021). Cooperation between Oncogenic Ras and Wild-type P53 Stimulates STAT Non-cell Autonomously to Promote Tumor Radioresistance. *Commun. Biol.* 4, 374. doi:10.1038/s42003-021-01898-5

Eaton, J. K., Furst, L., Ruberto, R. A., Moosmayer, D., Hilpmann, A., Ryan, M. J., et al. (2020). Selective Covalent Targeting of GPX4 Using Masked Nitrile-Oxide Electrophiles. *Nat. Chem. Biol.* 16, 497–506. doi:10.1038/s41589-020-0501-5

Edderkaoui, M., Nitsche, C., Zheng, L., Pandol, S. J., Gukovsky, I., and Gukovskaya, A. S. (2011). NADPH Oxidase Activation in Pancreatic Cancer Cells Is Mediated through Akt-dependent Up-Regulation of P22. *J. Biol. Chem.* 286, 7779–7787. doi:10.1074/jbc.M110.200063

Eling, N., Reuter, L., Hazin, J., Hamacher-Brady, A., and Brady, N. R. (2015). Identification of Artesunate as a Specific Activator of Ferroptosis in Pancreatic Cancer Cells. *Oncoscience* 2, 517–532. doi:10.18632/oncoscience.160

Ellis, J. M., Frahm, J. L., Li, L. O., and Coleman, R. A. (2010). Acyl-coenzyme A Synthetases in Metabolic Control. *Curr. Opin. Lipidol.* 21, 212–217. doi:10.1097/MOL.0b013e32833884bb

Eser, S., Schnieke, A., Schneider, G., and Saur, D. (2014). Oncogenic KRAS Signalling in Pancreatic Cancer. *Br. J. Cancer* 111, 817–822. doi:10.1038/bjc.2014.215

Esterbauer, H., Schaur, R. J., and Zollner, H. (1991). Chemistry and Biochemistry of 4-hydroxynonenal, Malonaldehyde and Related Aldehydes. *Free Radic. Biol. Med.* doi:10.1016/0891-5849(91)90192-6

Eto, M., Shindou, H., Koeberle, A., Harayama, T., Yanagida, K., and Shimizu, T. (2012). Lysophosphatidylcholine Acyltransferase 3 Is the Key Enzyme for Incorporating Arachidonic Acid into Glycerophospholipids during Adipocyte Differentiation. *Ijms* 13, 16267–16280. doi:10.3390/ijms131216267

Ferraro, D., Corso, S., Fasano, E., Panieri, E., Santangelo, R., Borrello, S., et al. (2006). Pro-metastatic Signaling by C-Met through RAC-1 and Reactive Oxygen Species (ROS). *Oncogene* 25, 3689–3698. doi:10.1038/sj.onc.1209409

Ferraro, G. B., Ali, A., Luengo, A., Kodack, D. P., Deik, A., Abbott, K. L., et al. (2021). Fatty Acid Synthesis Is Required for Breast Cancer Brain Metastasis. *Nat. Cancer* 2, 414–428. doi:10.1038/s43018-021-00183-y

Fuentes, N. R., Mlih, M., Barhoumi, R., Fan, Y.-Y., Hardin, P., Steele, T. J., et al. (2018). Long-chain N-3 Fatty Acids Attenuate Oncogenic Kras-Driven Proliferation by Altering Plasma Membrane Nanoscale Proteolipid Composition. *Cancer Res.* 78, 3899–3912. doi:10.1158/0008-5472.CAN-18-0324

Galan-Cobo, A., Sitthideatphaiboon, P., Qu, X., Poteete, A., Pisegna, M. A., Tong, P., et al. (2019). LKB1 and KEAP1/NRF2 Pathways Cooperatively Promote Metabolic Reprogramming with Enhanced Glutamine Dependence in KRAS-Mutant Lung Adenocarcinoma. *Cancer Res.* 79, 3251–3267. doi:10.1158/0008-5472.CAN-18-3527

Gao, M., Monian, P., Quadri, N., Ramasamy, R., and Jiang, X. (2015). Glutaminolysis and Transferrin Regulate Ferroptosis. *Mol. Cel* 59, 298–308. doi:10.1016/j.molcel.2015.06.011

Garten, A., Grohmann, T., Kluckova, K., Lavery, G. G., Kiess, W., and Penke, M. (2019). Sorafenib-induced Apoptosis in Hepatocellular Carcinoma Is Reversed by SIRT1. *Ijms* 20, 4048. doi:10.3390/ijms20164048

Gaschler, M. M., and Stockwell, B. R. (2017). Lipid Peroxidation in Cell Death. *Biochem. Biophys. Res. Commun.* 482, 419–425. doi:10.1016/j.bbrc.2016.10.086

Gaschler, M. M., Andia, A. A., Liu, H., Csuka, J. M., Hurlocker, B., Vaiana, C. A., et al. (2018). FINO2 Initiates Ferroptosis through GPX4 Inactivation and Iron Oxidation. *Nat. Chem. Biol.* 14, 507–515. doi:10.1038/s41589-018-0031-6

Gilmore, S. F., Yao, A. I., Tietel, Z., Kind, T., Facciotti, M. T., and Parikh, A. N. (2013). Role of Squalene in the Organization of Monolayers Derived from Lipid Extracts of Halobacterium Salinarum. *Langmuir* 29, 7922–7930. doi:10.1021/la401412t

Girotti, A. W. (1998). Lipid Hydroperoxide Generation, Turnover, and Effector Action in Biological Systems. *J. Lipid Res.*, 39, 1529, 42. doi:10.1016/s0022-2275(20)32182-9

Gout, P., Buckley, A., Simms, C., and Bruchovsky, N. (2001). Sulfasalazine, a Potent Suppressor of Lymphoma Growth by Inhibition of the Xc − Cystine Transporter: a New Action for an Old Drug. *Leukemia* 15, 1633–1640. doi:10.1038/sj.leu.2402238

Gouw, A. M., Eberlin, L. S., Margulis, K., Sullivan, D. K., Toal, G. G., Tong, L., et al. (2017). Oncogene KRAS Activates Fatty Acid Synthase, Resulting in Specific ERK and Lipid Signatures Associated with Lung Adenocarcinoma. *Proc. Natl. Acad. Sci. USA* 114, 4300–4305. doi:10.1073/pnas.1617709114

Hall, M. N., Chavarro, J. E., Lee, I.-M., Willett, W. C., and Ma, J. (2008). A 22-year Prospective Study of Fish, N-3 Fatty Acid Intake, and Colorectal Cancer Risk in Men. *Cancer Epidemiol. Biomarkers Prev.* 17, 1136–1143. doi:10.1158/1055-9965.EPI-07-2803

Hammer, A., Ferro, M., Tillian, H. M., Tatzber, F., Zollner, H., Schauenstein, E., et al. (1997). Effect of Oxidative Stress by Iron on 4-hydroxynonenal Formation and Proliferative Activity in Hepatomas of Different Degrees of Differentiation. *Free Radic. Biol. Med.* 23, 26–33. doi:10.1016/S0891-5849(96)00630-2

Hassannia, B., Wiernicki, B., Ingold, I., Qu, F., Van Herck, S., Tyurina, Y. Y., et al. (2018). Nano-targeted Induction of Dual Ferroptotic Mechanisms Eradicates High-Risk Neuroblastoma. *J. Clin. Invest.* 128, 3341–3355. doi:10.1172/JCI99032

Hassannia, B., Vandenabeele, P., and Vanden Berghe, T. (2019). Targeting Ferroptosis to Iron Out Cancer. *Cancer Cell* 35, 830–849. doi:10.1016/j.ccell.2019.04.002

Hassannia, B., Logie, E., Vandenabeele, P., Vanden Berghe, T., and Vanden Berghe, W. (2020). Withaferin A: From Ayurvedic Folk Medicine to Preclinical Anti-cancer Drug. *Biochem. Pharmacol.* 173, 113602. doi:10.1016/j.bcp.2019.08.004

Havas, K. M., Milchevskaya, V., Radic, K., Alladin, A., Kafkia, E., Garcia, M., et al. (2017). Metabolic Shifts in Residual Breast Cancer Drive Tumor Recurrence. *J. Clin. Invest.* 127, 2091–2105. doi:10.1172/JCI89914

Holmström, K. M., and Finkel, T. (2014). Cellular Mechanisms and Physiological Consequences of Redox-dependent Signalling. *Nat. Rev. Mol. Cel Biol.* 15, 411–421. doi:10.1038/nrm3801

Hong, J. Y., Nam, E. M., Lee, J., Park, J. O., Lee, S.-C., Song, S.-Y., et al. (2014). Randomized Double-Blinded, Placebo-Controlled Phase II Trial of Simvastatin and Gemcitabine in Advanced Pancreatic Cancer Patients. *Cancer Chemother. Pharmacol.* 73, 125–130. doi:10.1007/s00280-013-2328-1

Hu, Y., Lu, W., Chen, G., Wang, P., Chen, Z., Zhou, Y., et al. (2012). K-rasG12V Transformation Leads to Mitochondrial Dysfunction and a Metabolic Switch from Oxidative Phosphorylation to Glycolysis. *Cell Res* 22, 399–412. doi:10.1038/cr.2011.145

Hu, Y., Tanaka, T., Zhu, J., Guan, W., Wu, J. H. Y., Psaty, B. M., et al. (2017). Discovery and fine-mapping of Loci Associated with MUFAs through Trans-ethnic Meta-Analysis in Chinese and European Populations. *J. Lipid Res.* 58, 974–981. doi:10.1194/jlr.P071860

Hu, K., Li, K., Lv, J., Feng, J., Chen, J., Wu, H., et al. (2020). Suppression of the SLC7A11/glutathione axis Causes Synthetic Lethality in KRAS-Mutant Lung Adenocarcinoma. *J. Clin. Invest.* 130, 1752–1766. doi:10.1172/JCI124049

Inder, K., Harding, A., Plowman, S. J., Philips, M. R., Parton, R. G., and Hancock, J. F. (2008). Activation of the MAPK Module from Different Spatial Locations Generates Distinct System Outputs. *MBoC* 19, 4776–4784. doi:10.1091/mbc.E08-04-0407

Infante, J. R., Hansen, A. R., Pishvaian, M. J., Chow, L. Q. M., McArthur, G. A., Bauer, T. M., et al. (2016). A Phase Ib Dose Escalation Study of the OX40 Agonist MOXR0916 and the PD-L1 Inhibitor Atezolizumab in Patients with Advanced Solid Tumors. *Jco* 34, 101. doi:10.1200/jco.2016.34.15_suppl.101

Irani, K., Xia, Y., Zweier, J. L., Sollott, S. J., Der, C. J., Fearon, E. R., et al. (1997). Mitogenic Signaling Mediated by Oxidants in Ras-Transformed Fibroblasts. *Science* 275, 1649–1652. doi:10.1126/science.275.5306.1649

Jeong, S. M., Hwang, S., and Seong, R. H. (2016). Transferrin Receptor Regulates Pancreatic Cancer Growth by Modulating Mitochondrial Respiration and ROS Generation. *Biochem. Biophys. Res. Commun.* 471, 373–379. doi:10.1016/j.bbrc.2016.02.023

Jiang, L., Kon, N., Li, T., Wang, S.-J., Su, T., Hibshoosh, H., et al. (2015). Ferroptosis as a P53-Mediated Activity during Tumour Suppression. *Nature* 520, 57–62. doi:10.1038/nature14344

Kamphorst, J. J., Cross, J. R., Fan, J., de Stanchina, E., Mathew, R., White, E. P., et al. (2013). Hypoxic and Ras-Transformed Cells Support Growth by Scavenging Unsaturated Fatty Acids from Lysophospholipids. *Proc. Natl. Acad. Sci.* 110, 8882–8887. doi:10.1073/pnas.1307237110

Kanda, M., Matthaei, H., Wu, J., Hong, S. M., Yu, J., Borges, M., et al. (2012). Presence of Somatic Mutations in Most Early-Stage Pancreatic Intraepithelial Neoplasia. *Gastroenterology* 142, 730–733. doi:10.1053/j.gastro.2011.12.042

Kaur, K., Salomon, R. G., O'Neil, J., and Hoff, H. F. (1997). (Carboxyalkyl)pyrroles in Human Plasma and Oxidized Low-Density Lipoproteins. *Chem. Res. Toxicol.* 10, 1387–1396. doi:10.1021/tx970112c

Kerr, E. M., Gaude, E., Turrell, F. K., Frezza, C., and Martins, C. P. (2016). Mutant Kras Copy Number Defines Metabolic Reprogramming and Therapeutic Susceptibilities. *Nature* 531, 110–113. doi:10.1038/nature16967

Khoury, J. D., Tashakori, M., Yang, H., Loghavi, S., Wang, Y., Wang, J., et al. (2020). Pan-raf Inhibition Shows Anti-leukemic Activity in Ras-Mutant Acute Myeloid Leukemia Cells and Potentiates the Effect of Sorafenib in Cells with Flt3 Mutation. *Cancers* 12, 3511. doi:10.3390/cancers12123511

Kiani, B. H., Kayani, W. K., Khayam, A. U., Dilshad, E., Ismail, H., and Mirza, B. (2020). Artemisinin and its Derivatives: a Promising Cancer Therapy. *Mol. Biol. Rep.* 47, 6321–6336. doi:10.1007/s11033-020-05669-z

Kim, M.-J., Woo, S.-J., Yoon, C.-H., Lee, J.-S., An, S., Choi, Y.-H., et al. (2011). Involvement of Autophagy in Oncogenic K-Ras-Induced Malignant Cell Transformation. *J. Biol. Chem.* 286, 12924–12932. doi:10.1074/jbc.M110.138958

Kim, D. H., Kim, W. D., Kim, S. K., Moon, D. H., and Lee, S. J. (2020). TGF-β1-mediated Repression of SLC7A11 Drives Vulnerability to GPX4 Inhibition in Hepatocellular Carcinoma Cells. *Cel Death Dis* 11, 406. doi:10.1038/s41419-020-2618-6

Kong, B., Qia, C., Erkan, M., Kleeff, J., and Michalski, C. W. (2013). Overview on How Oncogenic Kras Promotes Pancreatic Carcinogenesis by Inducing Low Intracellular ROS Levels. *Front. Physiol.*, 4, 246. doi:10.3389/fphys.2013.00246

Kopnin, P. B., Agapova, L. S., Kopnin, B. P., and Chumakov, P. M. (2007). Repression of Sestrin Family Genes Contributes to Oncogenic Ras-Induced Reactive Oxygen Species Up-Regulation and Genetic Instability. *Cancer Res.* 67, 4671–4678. doi:10.1158/0008-5472.CAN-06-2466

Koyama, S., Akbay, E. A., Li, Y. Y., Aref, A. R., Skoulidis, F., Herter-Sprie, G. S., et al. (2016). STK11/LKB1 Deficiency Promotes Neutrophil Recruitment and Proinflammatory Cytokine Production to Suppress T-Cell Activity in the Lung Tumor Microenvironment. *Cancer Res.* 76, 999–1008. doi:10.1158/0008-5472.CAN-15-1439

Kuhn, H., Belkner, J., Wiesner, R., and Brash, A. R. (1990). Oxygenation of Biological Membranes by the Pure Reticulocyte Lipoxygenase. *J. Biol. Chem.* doi:10.1016/s0021-9258(17)44759-4

Kuhn, H., Saam, J., Eibach, S., Holzhütter, H.-G., Ivanov, I., and Walther, M. (2005). Structural Biology of Mammalian Lipoxygenases: Enzymatic Consequences of Targeted Alterations of the Protein Structure. *Biochem. Biophys. Res. Commun.* 338, 93–101. doi:10.1016/j.bbrc.2005.08.238

Kuhn, H., Banthiya, S., and Van Leyen, K. (2015). Mammalian Lipoxygenases and Their Biological Relevance. *Biochim. Biophys. Acta (Bba) - Mol. Cel Biol. Lipids* 1851, 308–330. doi:10.1016/j.bbalip.2014.10.002

Lachaier, E., Louandre, C., Godin, C., Saidak, Z., Baert, M., Diouf, M., et al. (2014). Sorafenib Induces Ferroptosis in Human Cancer Cell Lines Originating from Different Solid Tumors. *Anticancer Res.* 34, 6417–22.

Lane, D. J. R., Merlot, A. M., Huang, M. L.-H., Bae, D.-H., Jansson, P. J., Sahni, S., et al. (2015). Cellular Iron Uptake, Trafficking and Metabolism: Key Molecules and Mechanisms and Their Roles in Disease. *Biochim. Biophys. Acta (Bba) - Mol. Cel Res.* 1853, 1130–1144. doi:10.1016/j.bbamcr.2015.01.021

Lang, X., Green, M. D., Wang, W., Yu, J., Choi, J. E., Jiang, L., et al. (2019). Radiotherapy and Immunotherapy Promote Tumoral Lipid Oxidation and Ferroptosis via Synergistic Repression of SLC7A11. *Cancer Discov.* 9, 1673–1685. doi:10.1158/2159-8290.CD-19-0338

Lee, A. C., Fenster, B. E., Ito, H., Takeda, K., Bae, N. S., Hirai, T., et al. (1999). Ras Proteins Induce Senescence by Altering the Intracellular Levels of Reactive Oxygen Species. *J. Biol. Chem.* 274, 7936–7940. doi:10.1074/jbc.274.12.7936

Lee, J., Hong, Y. S., Hong, J. Y., Han, S. W., Kim, T. W., Kang, H. J., et al. (2014). Effect of Simvastatin Plus Cetuximab/irinotecan for KRAS Mutant Colorectal Cancer and Predictive Value of the RAS Signature for Treatment Response to Cetuximab. *Invest. New Drugs* 32, 535–541. doi:10.1007/s10637-014-0065-x

Lei, G., Zhang, Y., Koppula, P., Liu, X., Zhang, J., Lin, S. H., et al. (2020). The Role of Ferroptosis in Ionizing Radiation-Induced Cell Death and Tumor Suppression. *Cel Res* 30, 146–162. doi:10.1038/s41422-019-0263-3

Li, C., Dong, X., Du, W., Shi, X., Chen, K., Zhang, W., et al. (2020a). LKB1-AMPK axis Negatively Regulates Ferroptosis by Inhibiting Fatty Acid Synthesis. *Sig Transduct Target. Ther.*, 5, 187. doi:10.1038/s41392-020-00297-2

Li, C., Zhang, Y., Liu, J., Kang, R., Klionsky, D. J., and Tang, D. (2020b). Mitochondrial DNA Stress Triggers Autophagy-dependent Ferroptotic Death. *Autophagy* 17, 948–960. doi:10.1080/15548627.2020.1739447

Lim, H. Y., Merle, P., Weiss, K. H., Yau, T., Ross, P., Mazzaferro, V., et al. (2018). Phase II Studies with Refametinib or Refametinib Plus Sorafenib in Patients with RAS-Mutated Hepatocellular Carcinoma. *Clin. Cancer Res.* 24, 4650–4661. doi:10.1158/1078-0432.CCR-17-3588

Lim, J. K. M., Delaidelli, A., Minaker, S. W., Zhang, H.-F., Colovic, M., Yang, H., et al. (2019). Cystine/glutamate Antiporter xCT (SLC7A11) Facilitates Oncogenic RAS Transformation by Preserving Intracellular Redox Balance. *Proc. Natl. Acad. Sci. USA* 116, 9433–9442. doi:10.1073/pnas.1821323116

Liou, G.-Y., Döppler, H., DelGiorno, K. E., Zhang, L., Leitges, M., Crawford, H. C., et al. (2016). Mutant KRas-Induced Mitochondrial Oxidative Stress in Acinar Cells Upregulates EGFR Signaling to Drive Formation of Pancreatic Precancerous Lesions. *Cel Rep.* 14, 2325–2336. doi:10.1016/j.celrep.2016.02.029

Listenberger, L. L., Han, X., Lewis, S. E., Cases, S., Farese, R. V., Ory, D. S., et al. (2003). Triglyceride Accumulation Protects against Fatty Acid-Induced Lipotoxicity. *Proc. Natl. Acad. Sci.* 100, 3077–3082. doi:10.1073/pnas.0630588100

Liu, J., Zhang, C., Wang, J., Hu, W., and Feng, Z. (2020). The Regulation of Ferroptosis by Tumor Suppressor P53 and its Pathway. *Ijms* 21, 8387. doi:10.3390/ijms21218387

Liu, Y., Wang, Y., Liu, J., Kang, R., and Tang, D. (2021). Interplay between MTOR and GPX4 Signaling Modulates Autophagy-dependent Ferroptotic Cancer Cell Death. *Cancer Gene Ther.* 28, 55–63. doi:10.1038/s41417-020-0182-y

Llabani, E., Hicklin, R. W., Lee, H. Y., Motika, S. E., Crawford, L. A., Weerapana, E., et al. (2019). Diverse Compounds from Pleuromutilin lead to a Thioredoxin Inhibitor and Inducer of Ferroptosis. *Nat. Chem.* 11, 521–532. doi:10.1038/s41557-019-0261-6

Longo, J., Mullen, P. J., Yu, R., van Leeuwen, J. E., Masoomian, M., Woon, D. T. S., et al. (2019). An Actionable Sterol-Regulated Feedback Loop Modulates Statin Sensitivity in Prostate Cancer. *Mol. Metab.* 25, 119–130. doi:10.1016/j.molmet.2019.04.003

Longo, J., van Leeuwen, J. E., Elbaz, M., Branchard, E., and Penn, L. Z. (2020). Statins as Anticancer Agents in the Era of Precision Medicine. *Clin. Cancer Res.* 26, 5791–5800. doi:10.1158/1078-0432.CCR-20-1967

Maciag, A., Sithanandam, G., and Anderson, L. M. (2004). Mutant K-rasV12 Increases COX-2, Peroxides and DNA Damage in Lung Cells. *Carcinogenesis* 25, 2231–2237. doi:10.1093/carcin/bgh245

Maellaro, E., Casini, A. F., Del Bello, B., and Comporti, M. (1990). Lipid Peroxidation and Antioxidant Systems in the Liver Injury Produced by Glutathione Depleting Agents. *Biochem. Pharmacol.* 39, 1513–1521. doi:10.1016/0006-2952(90)90515-M

Magtanong, L., Ko, P.-J., To, M., Cao, J. Y., Forcina, G. C., Tarangelo, A., et al. (2019). Exogenous Monounsaturated Fatty Acids Promote a Ferroptosis-Resistant Cell State. *Cel Chem. Biol.* 26, 420–432. doi:10.1016/j.chembiol.2018.11.016

Maier, T., Jenni, S., and Ban, N. (2006). Architecture of Mammalian Fatty Acid Synthase at 4.5 A Resolution. *Science* 311, 1258–1262. doi:10.1126/science.1123248

Maillard, B., Ingold, K. U., and Scaiano, J. C. (1983). Rate Constants for the Reactions of Free Radicals with Oxygen in Solution. *J. Am. Chem. Soc.* 105, 5095–5099. doi:10.1021/ja00353a039

Marnett, L. J. (1999). Lipid Peroxidation - DNA Damage by Malondialdehyde. *Mutat. Res. - Fundam. Mol. Mech. Mutagen.*, 424, 83, 95. doi:10.1016/S0027-5107(99)00010-X

Marumo, T., Schini-Kerth, V. B., Fisslthaler, B., and Busse, R. (1997). Platelet-Derived Growth Factor-Stimulated Superoxide Anion Production Modulates Activation of Transcription Factor NF-κB and Expression of Monocyte Chemoattractant Protein 1 in Human Aortic Smooth Muscle Cells. *Circulation* 96, 2361–2367. doi:10.1161/01.CIR.96.7.2361

Gillies McKenna, W., Muschel, R. J., Gupta, A. K., Hahn, S. M., and Bernhard, E. J. (2003). The RAS Signal Transduction Pathway and its Role in Radiation Sensitivity. *Oncogene* 22, 5866–5875. doi:10.1038/sj.onc.1206699

Medes, G., Thomas, A., and Weinhouse, S. (1953). Metabolism of Neoplastic Tissue. IV. A Study of Lipid Synthesis in Neoplastic Tissue Slices *In Vitro*. *Cancer Res.* 13, 27–29.

Menendez, J. A., and Lupu, R. (2007). Fatty Acid Synthase and the Lipogenic Phenotype in Cancer Pathogenesis. *Nat. Rev. Cancer* 7, 763–777. doi:10.1038/nrc2222

Mitsushita, J., Lambeth, J. D., and Kamata, T. (2004). The Superoxide-Generating Oxidase Nox1 Is Functionally Required for Ras Oncogene Transformation. *Cancer Res.* 64, 3580–3585. doi:10.1158/0008-5472.CAN-03-3909

Miyazaki, M., and Ntambi, J. M. (2008). "Fatty Acid Desaturation and Chain Elongation in Mammals," in *Biochemistry of Lipids, Lipoproteins and Membranes*. Editors D. E. Vance and J. E. Vance (San Diego: Elsevier), 191–211. doi:10.1016/B978-044453219-0.50009-X

Moerke, C., Theilig, F., Kunzendorf, U., and Krautwald, S. (2019). "ACSL4 as the First Reliable Biomarker of Ferroptosis under Pathophysiological Conditions," in *Ferroptosis in Health and Disease*. Editor D. Tang (Cham: Springer), 111–123. doi:10.1007/978-3-030-26780-3_7

Moon, D.-O., Kim, B. Y., Jang, J. H., Kim, M.-O., Jayasooriya, R. G. P. T., Kang, C.-H., et al. (2012). K-RAS Transformation in Prostate Epithelial Cell Overcomes H2O2-Induced Apoptosis via Upregulation of Gamma-Glutamyltransferase-2. *Toxicol. Vitro* 26, 429–434. doi:10.1016/j.tiv.2012.01.013

Morita, M., and Fwjimaki, M. (1973). Non-hydroperoxy-type Peroxides as Autocatalysts of Lipid Autoxidation. *Agric. Biol. Chem.* 37, 1213–1214. doi:10.1271/bbb1961.37.1213

Mothersill, C., and Seymour, C. B. (2004). Radiation-induced Bystander Effects - Implications for Cancer. *Nat. Rev. Cancer* 4, 158–164. doi:10.1038/nrc1277

Müller, T., Dewitz, C., Schmitz, J., Schröder, A. S., Bräsen, J. H., Stockwell, B. R., et al. (2017). Necroptosis and Ferroptosis Are Alternative Cell Death Pathways that Operate in Acute Kidney Failure. *Cell. Mol. Life Sci.* 74, 3631–3645. doi:10.1007/s00018-017-2547-4

Muir, A., Danai, L. V., Gui, D. Y., Waingarten, C. Y., Lewis, C. A., and Vander Heiden, M. G. (2017). Environmental Cystine Drives Glutamine Anaplerosis and Sensitizes Cancer Cells to Glutaminase Inhibition. *Elife* 6, e27713. doi:10.7554/eLife.27713

Mullen, P. J., Yu, R., Longo, J., Archer, M. C., and Penn, L. Z. (2016). The Interplay between Cell Signalling and the Mevalonate Pathway in Cancer. *Nat. Rev. Cancer* 16, 718–731. doi:10.1038/nrc.2016.76

Nagpal, A., Redvers, R. P., Ling, X., Ayton, S., Fuentes, M., Tavancheh, E., et al. (2019). Neoadjuvant Neratinib Promotes Ferroptosis and Inhibits Brain Metastasis in a Novel Syngeneic Model of Spontaneous HER2+ve Breast Cancer Metastasis. *Breast Cancer Res.* 21, 94. doi:10.1186/s13058-019-1177-1

Nguyen, T., Nioi, P., and Pickett, C. B. (2009). The Nrf2-Antioxidant Response Element Signaling Pathway and its Activation by Oxidative Stress. *J. Biol. Chem.* 284, 13291–13295. doi:10.1074/jbc.R900010200

Ogrunc, M., Di Micco, R., Liontos, M., Bombardelli, L., Mione, M., Fumagalli, M., et al. (2014). Oncogene-induced Reactive Oxygen Species Fuel Hyperproliferation and DNA Damage Response Activation. *Cell Death Differ* 21, 998–1012. doi:10.1038/cdd.2014.16

Ou, Y., Wang, S.-J., Li, D., Chu, B., and Gu, W. (2016). Activation of SAT1 Engages Polyamine Metabolism with P53-Mediated Ferroptotic Responses. *Proc. Natl. Acad. Sci. USA* 113, E6806–E6812. doi:10.1073/pnas.1607152113

Padanad, M. S., Konstantinidou, G., Venkateswaran, N., Melegari, M., Rindhe, S., Mitsche, M., et al. (2016). Fatty Acid Oxidation Mediated by Acyl-CoA Synthetase Long Chain 3 Is Required for Mutant KRAS Lung Tumorigenesis. *Cel Rep.* 16, 1614–1628. doi:10.1016/j.celrep.2016.07.009

Pan, X., Lin, Z., Jiang, D., Yu, Y., Yang, D., Zhou, H., et al. (2019). Erastin Decreases Radioresistance of NSCLC Cells Partially by Inducing GPX4-mediated Ferroptosis. *Oncol. Lett.* 17, 3001–3008. doi:10.3892/ol.2019.9888

Park, S., Oh, J., Kim, M., and Jin, E.-J. (2018). Bromelain Effectively Suppresses Kras-Mutant Colorectal Cancer by Stimulating Ferroptosis. *Anim. Cell Syst.* 22, 334–340. doi:10.1080/19768354.2018.1512521

Pettazzoni, P., Pizzimenti, S., Toaldo, C., Sotomayor, P., Tagliavacca, L., Liu, S., et al. (2011). Induction of Cell Cycle Arrest and DNA Damage by the HDAC Inhibitor Panobinostat (LBH589) and the Lipid Peroxidation End Product 4-hydroxynonenal in Prostate Cancer Cells. *Free Radic. Biol. Med.* 50, 313–322. doi:10.1016/j.freeradbiomed.2010.11.011

Poursaitidis, I., Wang, X., Crighton, T., Labuschagne, C., Mason, D., Cramer, S. L., et al. (2017). Oncogene-Selective Sensitivity to Synchronous Cell Death following Modulation of the Amino Acid Nutrient Cystine. *Cell Rep.* 18 (11), 2547–2556. doi:10.1016/j.celrep.2017.02.054

Pratt, D. A., Tallman, K. A., and Porter, N. A. (2011). Free Radical Oxidation of Polyunsaturated Lipids: New Mechanistic Insights and the Development of Peroxyl Radical Clocks. *Acc. Chem. Res.* 44, 458–467. doi:10.1021/ar200024c

Prior, I. A., Harding, A., Yan, J., Sluimer, J., Parton, R. G., and Hancock, J. F. (2001). GTP-dependent Segregation of H-Ras from Lipid Rafts Is Required for Biological Activity. *Nat. Cel Biol.* 3, 368–375. doi:10.1038/35070050

Prior, I. A., Muncke, C., Parton, R. G., and Hancock, J. F. (2003). Direct Visualization of Ras Proteins in Spatially Distinct Cell Surface Microdomains. *J. Cel Biol.* 160, 165–170. doi:10.1083/jcb.200209091

Recktenwald, C. V., Kellner, R., Lichtenfels, R., and Seliger, B. (2008). Altered Detoxification Status and Increased Resistance to Oxidative Stress by K-Ras Transformation. *Cancer Res.* 68, 10086–10093. doi:10.1158/0008-5472.CAN-08-0360

Robertson, A. F., and Lands, W. E. (1964). Metabolism of Phospholipids in Normal and Spherocytic Human. *J. Lipid Res.* 5, 88–93.

Rozeveld, C. N., Johnson, K. M., Zhang, L., and Razidlo, G. L. (2020). KRAS Controls Pancreatic Cancer Cell Lipid Metabolism and Invasive Potential through the Lipase HSL. *Cancer Res.* 80, 4932–4945. doi:10.1158/0008-5472.CAN-20-1255

Saito, H., and Shinoda, W. (2011). Cholesterol Effect on Water Permeability Through DPPC and PSM Lipid Bilayers: A Molecular Dynamics Study. *J. Phys. Chem. B* 115, 15241–15250. doi:10.1021/jp201611p

Samalin, E., De La Fouchardiere, C., Thezenas, S., Boige, V., Senellart, H., Guimbaud, R., et al. (2016). Sorafenib and Irinotecan Combination for Pre-treated RAS-Mutated Metastatic Colorectal Cancer Patients: A Multicentre Randomized Phase II Trial (NEXIRI 2). *Jco* 34, 635. doi:10.1200/jco.2016.34.4_suppl.635

Santillo, M., Mondola, P., Serù, R., Annella, T., Cassano, S., Ciullo, I., et al. (2001). Opposing Functions of Ki- and Ha-Ras Genes in the Regulation of Redox Signals. *Curr. Biol.* 11, 614–619. doi:10.1016/S0960-9822(01)00159-2

Sato, H., Tamba, M., Ishii, T., and Bannai, S. (1999). Cloning and Expression of a Plasma Membrane Cystine/glutamate Exchange Transporter Composed of Two Distinct Proteins. *J. Biol. Chem.* 274, 11455–11458. doi:10.1074/jbc.274.17.11455

Sayin, V. I., Ibrahim, M. X., Larsson, E., Nilsson, J. A., Lindahl, P., and Bergo, M. O. (2014). Antioxidants Accelerate Lung Cancer Progression in Mice. *Sci. Translational Med.* 6, 221ra15. doi:10.1126/scitranslmed.3007653

Schott, C., Graab, U., Cuvelier, N., Hahn, H., and Fulda, S. (2015). Oncogenic RAS Mutants Confer Resistance of RMS13 Rhabdomyosarcoma Cells to Oxidative Stress-Induced Ferroptotic Cell Death. *Front. Oncol.*, 5, 131. doi:10.3389/fonc.2015.00131

Schultz, M. A., Diaz, A. M., Smite, S., Lay, A. R., DeCant, B., McKinney, R., et al. (2017). Thioredoxin System-Mediated Regulation of Mutant Kras Associated Pancreatic Neoplasia and Cancer. *Oncotarget* 8, 92667–92681. doi:10.18632/oncotarget.21539

Seiler, A., Schneider, M., Förster, H., Roth, S., Wirth, E. K., Culmsee, C., et al. (2008). Glutathione Peroxidase 4 Senses and Translates Oxidative Stress into 12/15-Lipoxygenase Dependent- and AIF-Mediated Cell Death. *Cel Metab.* 8, 237–248. doi:10.1016/j.cmet.2008.07.005

Shah, R., Shchepinov, M. S., and Pratt, D. A. (2018). Resolving the Role of Lipoxygenases in the Initiation and Execution of Ferroptosis. *ACS Cent. Sci.* 4, 387–396. doi:10.1021/acscentsci.7b00589

Shen, Z., Song, J., Yung, B. C., Zhou, Z., Wu, A., and Chen, X. (2018). Emerging Strategies of Cancer Therapy Based on Ferroptosis. *Adv. Mater.* 30, 1704007. doi:10.1002/adma.201704007

Shin, E. A., Kim, K. H., Han, S. I., Ha, K. S., Kim, J. H., Kang, K. Il., et al. (1999). Arachidonic Acid Induces the Activation of the Stress-Activated Protein Kinase, Membrane Ruffling and H2O2 Production via a Small GTPase Rac1. *FEBS Lett.* 452, 355–359. doi:10.1016/S0014-5793(99)00657-2

Shintoku, R., Takigawa, Y., Yamada, K., Kubota, C., Yoshimoto, Y., Takeuchi, T., et al. (2017). Lipoxygenase-mediated Generation of Lipid Peroxides Enhances Ferroptosis Induced by Erastin and RSL3. *Cancer Sci.* 108, 2187–2194. doi:10.1111/cas.13380

Siani, P., de Souza, R. M., Dias, L. G., Itri, R., and Khandelia, H. (2016). An Overview of Molecular Dynamics Simulations of Oxidized Lipid Systems, with a Comparison of ELBA and MARTINI Force fields for Coarse Grained Lipid Simulations. *Biochim. Biophys. Acta (Bba) - Biomembr.* 1858, 2498–2511. doi:10.1016/j.bbamem.2016.03.031

Singh, A., Ruiz, C., Bhalla, K., Haley, J. A., Li, Q. K., Acquaah-Mensah, G., et al. (2018). De Novo lipogenesis Represents a Therapeutic Target in Mutant Kras Non-small Cell Lung Cancer. *FASEB j.* 32, 7018–7027. doi:10.1096/fj.201800204

Sklar, M. (1988). The Ras Oncogenes Increase the Intrinsic Resistance of NIH 3T3 Cells to Ionizing Radiation. *Science* 239, 645–647. doi:10.1126/science.3277276

Skouta, R., Dixon, S. J., Wang, J., Dunn, D. E., Orman, M., Shimada, K., et al. (2014). Ferrostatins Inhibit Oxidative Lipid Damage and Cell Death in Diverse Disease Models. *J. Am. Chem. Soc.* 136, 4551–4556. doi:10.1021/ja411006a

Slattery, M. L., Curtin, K., Anderson, K., Ma, K. N., Edwards, S., Leppert, M., et al. (2000). Associations between Dietary Intake and Ki-Ras Mutations in colon Tumors: A Population-Based Study. *Cancer Res.* 60, 6935–6941.

Smith, L. L. (1987). Cholesterol Autoxidation 1981-1986. *Chem. Phys. Lipids* 44, 87–125. doi:10.1016/0009-3084(87)90046-6

Son, J., Lyssiotis, C. A., Ying, H., Wang, X., Hua, S., Ligorio, M., et al. (2013). Glutamine Supports Pancreatic Cancer Growth through a KRAS-Regulated Metabolic Pathway. *Nature* 496, 101–105. doi:10.1038/nature12040

Soula, M., Weber, R. A., Zilka, O., Alwaseem, H., La, K., Yen, F., et al. (2020). Metabolic Determinants of Cancer Cell Sensitivity to Canonical Ferroptosis Inducers. *Nat. Chem. Biol.* 16, 1351–1360. doi:10.1038/s41589-020-0613-y

Sprecher, H., Luthria, D. L., Mohammed, B. S., and Baykousheva, S. P. (1995). Reevaluation of the Pathways for the Biosynthesis of Polyunsaturated Fatty Acids. *J. Lipid Res.* 36, 2471–7. doi:10.1016/s0022-2275(20)41084-3

Stephen, A. G., Esposito, D., Bagni, R. K., and Mccormick, F. (2014). Dragging Ras Back in the Ring. *Canc. Cell* 25, 272–281. doi:10.1016/j.ccr.2014.02.017

Storz, P. (2005). Reactive Oxygen Species in Tumor Progression. *Front. Biosci.* 10, 1881. doi:10.2741/1667

Sudhan, D. R., Guerrero-Zotano, A., Won, H., González Ericsson, P., Servetto, A., Huerta-Rosario, M., et al. (2020). Hyperactivation of TORC1 Drives Resistance to the Pan-HER Tyrosine Kinase Inhibitor Neratinib in HER2-Mutant Cancers. *Cancer Cell* 37, 183–199. doi:10.1016/j.ccell.2019.12.013

Sui, X., Zhang, R., Liu, S., Duan, T., Zhai, L., Zhang, M., et al. (2018). RSL3 Drives Ferroptosis through GPX4 Inactivation and Ros Production in Colorectal Cancer. *Front. Pharmacol.*, 9, 1371. doi:10.3389/fphar.2018.01371

Sun, X., Ou, Z., Chen, R., Niu, X., Chen, D., Kang, R., et al. (2016). Activation of the P62-Keap1-NRF2 Pathway Protects against Ferroptosis in Hepatocellular Carcinoma Cells. *Hepatology* 63, 173–184. doi:10.1002/hep.28251

Szatrowski, T. P., and Nathan, C. F. (1991). Production of Large Amounts of Hydrogen Peroxide by Human Tumor Cells. *Cancer Res.* 51, 794–798.

Tabuso, M., Christian, M., Kimani, P. K., Gopalakrishnan, K., and Arasaradnam, R. P. (2020). KRAS Status Is Associated with Metabolic Parameters in Metastatic Colorectal Cancer According to Primary Tumour Location. *Pathol. Oncol. Res.* 26, 2537–2548. doi:10.1007/s12253-020-00850-y

Taguchi, K., Motohashi, H., and Yamamoto, M. (2011). Molecular Mechanisms of the Keap1-Nrf2 Pathway in Stress Response and Cancer Evolution. *Genes to Cells* 16, 123–140. doi:10.1111/j.1365-2443.2010.01473.x

Tarangelo, A., Magtanong, L., Bieging-Rolett, K. T., Li, Y., Ye, J., Attardi, L. D., et al. (2018). p53 Suppresses Metabolic Stress-Induced Ferroptosis in Cancer Cells. *Cel Rep.* 22, 569–575. doi:10.1016/j.celrep.2017.12.077

Tesfay, L., Paul, B. T., Konstorum, A., Deng, Z., Cox, A. O., Lee, J., et al. (2019). Stearoyl-CoA Desaturase 1 Protects Ovarian Cancer Cells from Ferroptotic Cell Death. *Cancer Res.* 79, 5355–5366. doi:10.1158/0008-5472.CAN-19-0369

Tian, T., Harding, A., Inder, K., Plowman, S., Parton, R. G., and Hancock, J. F. (2007). Plasma Membrane Nanoswitches Generate High-Fidelity Ras Signal Transduction. *Nat. Cel Biol.* 9, 905–914. doi:10.1038/ncb1615

Toda, K., Nishikawa, G., Iwamoto, M., Itatani, Y., Takahashi, R., Sakai, Y., et al. (2017). Clinical Role of ASCT2 (SLC1A5) in KRAS-Mutated Colorectal Cancer. *Ijms* 18, 1632. doi:10.3390/ijms18081632

Torralvo, J., Friedlaender, A., Achard, V., and Addeo, A. (2019). The Activity of Immune Checkpoint Inhibition in Kras Mutated Non-small Cell Lung Cancer: A Single centre Experience. *Cancer Genomics Proteomics* 16, 577–582. doi:10.21873/cgp.20160

Ubellacker, J. M., Tasdogan, A., Ramesh, V., Shen, B., Mitchell, E. C., Martin-Sandoval, M. S., et al. (2020). Lymph Protects Metastasizing Melanoma Cells from Ferroptosis. *Nature* 585, 113–118. doi:10.1038/s41586-020-2623-z

Ullén, A., Farnebo, M., Thyrell, L., Mahmoudi, S., Kharaziha, P., Lennartsson, L., et al. (2010). Sorafenib Induces Apoptosis and Autophagy in Prostate Cancer Cells *In Vitro*. *Int. J. Oncol.*, 37, 15–20. doi:10.3892/ijo_00000648

Ursini, F., Maiorino, M., and Gregolin, C. (1985). The Selenoenzyme Phospholipid Hydroperoxide Glutathione Peroxidase. *BBA - Gen. Subj.*, 839, 62, 70. doi:10.1016/0304-4165(85)90182-5

Vizio, B., Poli, G., Chiarpotto, E., and Biasi, F. (2005). 4-Hydroxynonenal and TGF-B1 Concur in Inducing Antiproliferative Effects on the Caco-2 Human colon Adenocarcinoma Cell Line. *BioFactors* 24, 237–246. doi:10.1002/biof.5520240128

Voss, A., Reinhart, M., Sankarappa, S., and Sprecher, H. (1991). The Metabolism of 7,10,13,16,19-docosapentaenoic Acid to 4,7,10,13,16,19-docosahexaenoic Acid in Rat Liver Is Independent of a 4-desaturase. *J. Biol. Chem.* 266, 19995, 20000. doi:10.1016/s0021-9258(18)54882-1

Wagle, S., Bui, A., Ballard, P. L., Shuman, H., Gonzales, J., and Gonzales, L. W. (1999). Hormonal Regulation and Cellular Localization of Fatty Acid Synthase in Human Fetal Lung. *Am. J. Physiol.-Lung Cell Mol. Physiol.* 277, L381–L390. doi:10.1152/ajplung.1999.277.2.l381

Wan, C., Sun, Y., Tian, Y., Lu, L., Dai, X., Meng, J., et al. (2020). Irradiated Tumor Cell-Derived Microparticles Mediate Tumor Eradication via Cell Killing and Immune Reprogramming. *Sci. Adv.* 6, eaay9789. doi:10.1126/sciadv.aay9789

Wang, B., and Tontonoz, P. (2019). Phospholipid Remodeling in Physiology and Disease. *Annu. Rev. Physiol.* 81, 165–188. doi:10.1146/annurev-physiol-020518-114444

Wang, P., Zhu, C.-f., Ma, M.-z., Chen, G., Song, M., Zeng, Z.-l., et al. (2015). Micro-RNA-155 Is Induced by K-Ras Oncogenic Signal and Promotes ROS Stress in Pancreatic Cancer. *Oncotarget* 6, 21148–21158. doi:10.18632/oncotarget.4125

Wang, L., Zhao, Y., Xiong, Y., Wang, W., Fei, Y., Tan, C., et al. (2018). K-ras Mutation Promotes Ionizing Radiation-Induced Invasion and Migration of Lung Cancer in Part via the Cathepsin L/CUX1 Pathway. *Exp. Cel Res.* 362, 424–435. doi:10.1016/j.yexcr.2017.12.006

Wang, K., Jiang, J., Lei, Y., Zhou, S., Wei, Y., and Huang, C. (2019a). Targeting Metabolic-Redox Circuits for Cancer Therapy. *Trends Biochem. Sci.* 44, 401–414. doi:10.1016/j.tibs.2019.01.001

Wang, K., Zhang, Z., Wang, M., Cao, X., Qi, J., Wang, D., et al. (2019b). Role of GRP78 Inhibiting Artesunate-Induced Ferroptosis in KRAS Mutant Pancreatic Cancer Cells. *Ddt* 13, 2135–2144. doi:10.2147/DDDT.S199459

Wang, W., Green, M., Choi, J. E., Gijón, M., Kennedy, P. D., Johnson, J. K., et al. (2019c). CD8+ T Cells Regulate Tumour Ferroptosis during Cancer Immunotherapy. *Nature* 569, 270–274. doi:10.1038/s41586-019-1170-y

Wang, W., Zhang, J., and Zhang, G. (2019d). Cytochrome P450 Monooxygenase-Mediated Eicosanoid Pathway: A Potential Mechanistic Linkage between Dietary Fatty Acid Consumption and colon Cancer Risk. *Food Sci. Hum. Wellness* 8, 337–343. doi:10.1016/j.fshw.2019.11.002

Weïwer, M., Bittker, J. A., Lewis, T. A., Shimada, K., Yang, W. S., MacPherson, L., et al. (2012). Development of Small-Molecule Probes that Selectively Kill Cells Induced to Express Mutant RAS. *Bioorg. Med. Chem. Lett.* 22, 1822–1826. doi:10.1016/j.bmcl.2011.09.047

Weijenberg, M. P., Lüchtenborg, M., De Goeij, A. F. P. M., Brink, M., Van Muijen, G. N. P., de Bruïne, A. P., et al. (2007). Dietary Fat and Risk of colon and Rectal Cancer with Aberrant MLH1 Expression, APC or KRAS Genes. *Cancer Causes Control* 18, 865–879. doi:10.1007/s10552-007-9032-6

Weinberg, F., Hamanaka, R., Wheaton, W. W., Weinberg, S., Joseph, J., Lopez, M., et al. (2010). Mitochondrial Metabolism and ROS Generation Are Essential for Kras-Mediated Tumorigenicity. *Proc. Natl. Acad. Sci.* 107, 8788–8793. doi:10.1073/pnas.1003428107

Winter-Vann, A. M., Kamen, B. A., Bergo, M. O., Young, S. G., Melnyk, S., James, S. J., et al. (2003). Targeting Ras Signaling through Inhibition of Carboxyl Methylation: An Unexpected Property of Methotrexate. *Proc. Natl. Acad. Sci.* 100, 6529–6534. doi:10.1073/pnas.1135239100

Wong-Ekkabut, J., Xu, Z., Triampo, W., Tang, I.-M., Peter Tieleman, D., and Monticelli, L. (2007). Effect of Lipid Peroxidation on the Properties of Lipid Bilayers: A Molecular Dynamics Study. *Biophys. J.* 93, 4225–4236. doi:10.1529/biophysj.107.112565

Woo, J. H., Shimoni, Y., Yang, W. S., Subramaniam, P., Iyer, A., Nicoletti, P., et al. (2015). Elucidating Compound Mechanism of Action by Network Perturbation Analysis. *Cell* 162, 441–451. doi:10.1016/j.cell.2015.05.056

Xie, Y., Song, X., Sun, X., Huang, J., Zhong, M., Lotze, M. T., et al. (2016). Identification of Baicalein as a Ferroptosis Inhibitor by Natural Product Library Screening. *Biochem. Biophys. Res. Commun.* 473, 775–780. doi:10.1016/j.bbrc.2016.03.052

Yagoda, N., Von Rechenberg, M., Zaganjor, E., Bauer, A. J., Yang, W. S., Fridman, D. J., et al. (2007). RAS-RAF-MEK-Dependent Oxidative Cell Death Involving Voltage-Dependent Anion Channels. *Nature* 447, 865–869. doi:10.1038/nature05859

Yang, W. S., and Stockwell, B. R. (2008). Synthetic Lethal Screening Identifies Compounds Activating Iron-Dependent, Nonapoptotic Cell Death in Oncogenic-RAS-Harboring Cancer Cells. *Chem. Biol.* 15, 234–245. doi:10.1016/j.chembiol.2008.02.010

Yang, J. Q., Li, S., Domann, F. E., Buettner, G. R., and Oberley, L. W. (1999). Superoxide Generation in V-Ha-Ras-Transduced Human Keratinocyte HaCaT Cells. *Mol. Carcinog* 26, 180–188. doi:10.1002/(sici)1098-2744(199911)26:3<180::aid-mc7>3.0.co;2-4

Yang, W. S., Sriramaratnam, R., Welsch, M. E., Shimada, K., Skouta, R., Viswanathan, V. S., et al. (2014). Regulation of Ferroptotic Cancer Cell Death by GPX4. *Cell* 156, 317–331. doi:10.1016/j.cell.2013.12.010

Yang, W. S., Kim, K. J., Gaschler, M. M., Patel, M., Shchepinov, M. S., and Stockwell, B. R. (2016). Peroxidation of Polyunsaturated Fatty Acids by Lipoxygenases Drives Ferroptosis. *Proc. Natl. Acad. Sci. USA* 113, E4966–E4975. doi:10.1073/pnas.1603244113

Yang, L., Wang, H., Yang, X., Wu, Q., An, P., Jin, X., et al. (2020). Auranofin Mitigates Systemic Iron Overload and Induces Ferroptosis via Distinct Mechanisms. *Sig Transduct Target. Ther.* 5, 138. doi:10.1038/s41392-020-00253-0

Yin, X., Yang, G., Ma, D., and Su, Z. (2020). Inhibition of Cancer Cell Growth in Cisplatin-Resistant Human Oral Cancer Cells by Withaferin-A Is Mediated via Both Apoptosis and Autophagic Cell Death, Endogenous ROS Production, G2/M Phase Cell Cycle Arrest and by Targeting MAPK/RAS/RAF Signalling Pathway. *J. BUON* 25 (1), 332–337.

Young, T. W., Mei, F. C., Yang, G., Thompson-Lanza, J. A., Liu, J., and Cheng, X. (2004). Activation of Antioxidant Pathways in Ras-Mediated Oncogenic Transformation of Human Surface Ovarian Epithelial Cells Revealed by Functional Proteomics and Mass Spectrometry. *Cancer Res.* 64, 4577–4584. doi:10.1158/0008-5472.CAN-04-0222

Yu, R., Longo, J., Van Leeuwen, J. E., Mullen, P. J., Ba-Alawi, W., Haibe-Kains, B., et al. (2018). Statin-induced Cancer Cell Death Can Be Mechanistically Uncoupled from Prenylation of RAS Family Proteins. *Cancer Res.* 78, 1347–1357. doi:10.1158/0008-5472.CAN-17-1231

Yun, S.-H., Shin, S.-W., and Park, J.-I. (2017). Expression of Fatty Acid Synthase Is Regulated by PGC-1α and C-ontributes to I-ncreased C-ell P-roliferation. *Oncol. Rep.* doi:10.3892/or.2017.6044

Zamkova, M., Khromova, N., Kopnin, B. P., and Kopnin, P. (2013). Ras-induced ROS Upregulation Affecting Cell Proliferation Is Connected with Cell Type-specific Alterations of HSF1/SESN3/p21Cip1/WAF1pathways. *Cell Cycle* 12, 826–836. doi:10.4161/cc.23723

Zhang, Y., Qian, Y., Zhang, J., Yan, W., Jung, Y.-S., Chen, M., et al. (2017). Ferredoxin Reductase Is Critical for P53-dependent Tumor Suppression via Iron Regulatory Protein 2. *Genes Dev.* 31, 1243–1256. doi:10.1101/gad.299388.117

Zhang, Y., Tan, H., Daniels, J. D., Zandkarimi, F., Liu, H., Brown, L. M., et al. (2019). Imidazole Ketone Erastin Induces Ferroptosis and Slows Tumor Growth in a Mouse Lymphoma Model. *Cel Chem. Biol.* 26, 623–633. doi:10.1016/j.chembiol.2019.01.008

Zheng, J., and Conrad, M. (2020). The Metabolic Underpinnings of Ferroptosis. *Cel Metab.* 32, 920–937. doi:10.1016/j.cmet.2020.10.011

Zhou, Y., and Hancock, J. F. (2015). Ras Nanoclusters: Versatile Lipid-Based Signaling Platforms. *Biochim. Biophys. Acta (Bba) - Mol. Cel Res.* 1853, 841–849. doi:10.1016/j.bbamcr.2014.09.008

Zhou, Y., Prakash, P., Liang, H., Cho, K.-J., Gorfe, A. A., and Hancock, J. F. (2017). Lipid-Sorting Specificity Encoded in K-Ras Membrane Anchor Regulates Signal Output. *Cell* 168, 239–251. doi:10.1016/j.cell.2016.11.059

Conflict of Interest: The authors declare that the research was conducted in the absence of any commercial or financial relationships that could be construed as a potential conflict of interest.

Publisher's Note: All claims expressed in this article are solely those of the authors and do not necessarily represent those of their affiliated organizations, or those of the publisher, the editors and the reviewers. Any product that may be evaluated in this article, or claim that may be made by its manufacturer, is not guaranteed or endorsed by the publisher.

frontiers in Molecular Biosciences

MINI REVIEW
published: 15 September 2021
doi: 10.3389/fmolb.2021.729830

K-RAS4A: Lead or Supporting Role in Cancer Biology?

Veronica Aran *

Laboratorio de Biomedicina Do Cérebro, Instituto Estadual Do Cérebro Paulo Niemeyer, Rio de Janeiro, Brazil

The RAS oncogene is one of the most frequently mutated genes in human cancer, with K-RAS having a leading role in tumorigenesis. K-RAS undergoes alternative splicing, and as a result its transcript generates two gene products K-RAS4A and K-RAS4B, which are affected by the same oncogenic mutations, are highly homologous, and are expressed in a variety of human tissues at different levels. In addition, both isoforms localise to the plasma membrane by distinct targeting motifs. While some evidence suggests nonredundant functions for both splice variants, most work to date has focused on K-RAS4B, or even just K-RAS (i.e., without differentiating between the splice variants). This review aims to address the most relevant evidence published regarding K-RAS4A and to discuss if this "minor" isoform could also play a leading role in cancer, concluding that a significant body of evidence supports a leading role rather than a supporting (or secondary) role for K-RAS4A in cancer biology.

Keywords: K-ras, K-Ras4A, K-Ras4B, alternative splicing, cancer

OPEN ACCESS

Edited by:
Mahendra Pratap Kashyap, University of Alabama at Birmingham, United States

Reviewed by:
Sangwoo Kim, Yonsei University, South Korea
Avaniyapuram Kannan Murugan, King Faisal Specialist Hospital and Research Centre, Saudi Arabia

***Correspondence:**
Veronica Aran
varanponte@gmail.com

Specialty section:
This article was submitted to Molecular Diagnostics and Therapeutics, a section of the journal Frontiers in Molecular Biosciences

Received: *23 June 2021*
Accepted: *01 September 2021*
Published: *15 September 2021*

Citation:
Aran V (2021) K-RAS4A: Lead or Supporting Role in Cancer Biology?. Front. Mol. Biosci. 8:729830. doi: 10.3389/fmolb.2021.729830

INTRODUCTION

The importance of gene alternative splicing has been well documented. This conserved biological process occurs when a single gene produces different mRNA transcripts, thus helping to contribute to the formation of a vast transcriptome and proteome (Kelemen et al., 2013). This process generates protein diversity, as a single gene can result in the production of different variants of a protein, which may exhibit differential tissue expression (Sorek and Amitai 2001). In summary, alternative splicing results in different: 1) protein function; 2) tissue expression; 3) localisation; enzymatic activities; and 4) protein-protein interactions (Kelemen et al., 2013). The differences between splice variants are of pharmaceutical importance since they may contribute to variable treatment responses.

There are three RAS genes encoding four isoforms, which are ubiquitously expressed in human cells and share 82–90% sequence homology. These four isoforms are H-RAS, N-RAS, K-RAS4A and K-RAS4B (Cox and Der 2010). *RAS* mutations are frequently found in cancer (~24% of all cancers) (Stalnecker and Der 2020), where the K-RAS gene is mutated in approximately 17% of all cancer types (46,213 mutant samples/272047 samples tested), N-RAS gene is mutated in ~5.1% (7,926 mutant samples/154172 samples tested), and H-RAS in ~2.3% (2,404 mutant samples/106318 samples tested) (as reported in the Catalog of Somatic Mutated in Cancer, COSMIC database, v94, in August 2021). RAS mutations are crucial for personalised medicine since they can direct targeted therapies and serve as diagnostic and prognostic markers for different cancers (Murugan et al., 2019). In fact, K-RAS mutations were considered adverse prognostic factors and indicators of EGFR-targeted therapy resistance in certain cancer types such as lung and colorectal (Pao et al., 2005; Marks et al., 2008; Normanno et al., 2009). **Figure 1** summarizes some of the most frequently K-RAS mutated tissues based on the COSMIC database (searched in COSMIC database, v94, in May 2021).

The discovery over 35 years ago (McGrath et al., 1983; Shimizu et al., 1983) of the fourth exons 4A and 4B resulted in the identification of the existence of two protein isoforms, K-RAS4A and K-RAS4B [189 and

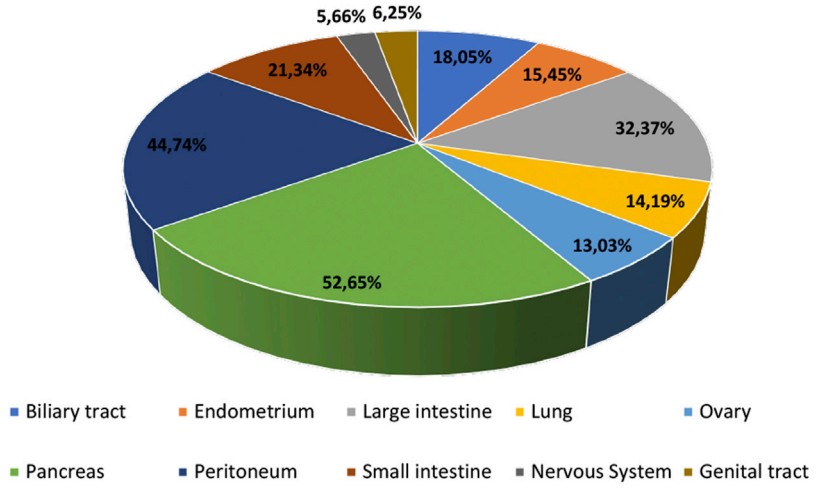

FIGURE 1 | Most frequent human tissues affected by K-RAS mutations based on the COSMIC database, v94 (data obtained in May 2021).

188 amino acids (aa), respectively]. The 21-kDa RAS gene products shares 100% sequence homology in the first 86 aa residues among different RAS isoforms (K-, N- and H-RAS) (Messina et al., 2019). The RAS G domain comprises the first 165 aa, representing the catalytic and switching region where the exchange between GDP/GTP occurs. It is also the domain to which different effectors, exchange factors, and GTPase-activating proteins (GAPs) bind. K-RAS plays an essential role in mouse embryonic development (Koera et al., 1997; Hobbs, Der, and Rossman 2016), whereas K-RAS4A, H-RAS and N-RAS expression is dispensable for mouse development (Esteban et al., 2001; Plowman et al., 2003). Unlike K-RAS4A, K-RAS4B has been heavily researched.

Mutations that activate K-RAS usually affect codons 12, 13, and 61 (the majority being missense substitutions), which are common to both genes, thus rendering both oncogenic (Capon et al., 1983). The biological relevance of the alternative splicing of K-RAS has never been fully elucidated. Most studies have concentrated their attention on K-RAS4B rather than K-RAS4A. For example, while a *Pubmed* search on "K-RAS" or "KRAS" yields 21,408 results, a search on "K-RAS4A" or "KRAS4A"or "K-Ras4A" or "KRas4A" or "K-Ras4a" or "KRas4a" yields 54 results and a search on "K-RAS4B" or "KRAS4B″or "K-Ras4B" or "KRas4B" or "K-Ras4B" or "K-Ras4b" or "KRas4b" yields 213 results (all searched on May 20, 2021). This finding suggests that most studies have not discriminated by K-RAS isoform. Nevertheless, the two splice variants exhibit differential tissue expression (Newlaczyl et al., 2017). Therefore, the present review aims to improve the general understanding of each isoform by describing previous work an discussing potential roles of K-RAS4A in cancer.

K-RAS4A VERSUS K-RAS4B: STRUCTURE AND SIGNALLING

It is well stablished that RAS isoforms exhibit distinct biological activities and subcellular localisations that depend mainly on the interaction between the C-terminal hypervariable region (HVR) and host membranes (Hancock 2003; Laude and Prior 2008). The HVR region is composed of a linker domain comprising aa 166–178/179, and a targeting domain comprising aa 179/180–189/188, which undergoes posttranslational modifications that mediate membrane binding. The HVR contains a C-terminal CAAX (CAAX motif) sequence, which is modified posttranslationally (Wright and Philips 2006). The C-terminal cysteine is farnesylated for weak membrane interaction; further membrane binding stabilisation requires a second signal within the HVR region (Hancock et al., 1991). For K-RAS4B, this signal is electrostatic (i.e., six contiguous lysines), whereas for the other RAS isoforms (K-RAS4A, H-RAS and N-RAS), this stabilisation is mediated by palmitoylation (Hancock et al., 1990). The isoform H-RAS contains two palmitoylation sites within the HVR region, whereas N-RAS and K-RAS4A are monopalmitoylated (Zhou et al., 2018). Additionally, K-RAS4B displays a unique feature, a phosphorylation site (aa S181) that behaves as an electrostatic farnesyl switch, inducing K-RAS4B translocation from the plasma membrane to other endomembrane compartments (Barcelo et al., 2014). The different posttranslational modifications that occur in the RAS C-terminal region were, and still are, considered potential targets for anti-cancer therapies despite the failure of farnesyltransferase inhibitors in the past (James, Goldstein, and Brown 1996; Konstantinopoulos et al., 2007; Ahearn et al., 2018).

RAS interaction with the plasma membrane is required for its function. K-RAS4A and K-RAS4B differ mainly in their C-terminal regions (Laude and Prior 2008; Tsai et al., 2015), which in the case of K-RAS4A, contains a site of palmitoylation and a bipartite polybasic region able to independently deliver K-RAS4A to the plasma membrane (Laude and Prior 2008; Tsai et al., 2015; Zhao et al., 2015). This indicates that, compared to other RAS proteins, K-RAS4A is the only one harbouring a dual membrane-targeting motif and that K-RAS4B is more positively charged and less hydrophobic than K-RAS4A. It has been proposed that the bipartite polybasic region alongside the monopalmitoylation and farnesylation of K-RAS4A may affect its function and expression, in addition to place this variant

between K-RAS4B and N-RAS in terms of protein similarities (Laude and Prior 2008; Nussinov et al., 2016).

Structural analysis using atom molecular dynamics simulations investigated K-RAS4A placement at membranes that contain anionic lipids (POPS or PIP2) (Li and Buck 2017). This study demonstrated that K-RAS4A prefers different orientations at the membrane, where both its topology and the electrostatic interaction between its charged residues and the anionic lipids influence its orientation (Li and Buck 2017). Hancock and others reported that inhibition of acid sphingomyelinase mislocalises K-RAS4A and K-RAS4B from the plasma membrane to the endomembrane and blocks their nanoclustering, thus suggesting that an indirect inhibitor of sphingomyelinase could serve as a potential anti-K-RAS agent (Cho et al., 2016).

The protein conformations of K-RAS4A and K-RAS4B have also been compared by all-atom molecular dynamics simulations to identify isoform-specific differences. The results suggested that the catalytic domain of GDP-bound K-RAS4A differs from that of K-RAS4B by presenting a more exposed nucleotide binding pocket, also showing distinct dynamic fluctuations in switch I and II regions, which could affect the interaction between the catalytic domain and downstream effectors (Chakrabarti et al., 2016).

All four RAS isoforms have been shown to possess different biological activities and effector signalling. At least 11 different RAS effector families have been described, which drive distinct signalling cascades (Hobbs et al., 2016). Although all RAS proteins can differentially activate the Raf-MEK-ERK signalling pathway and affect cell phenotype *in vitro*, K-RAS4A and K-RAS4B have been shown to differentially affect Raf-1 (Voice et al., 1999). Furthermore, application of stable isotope labelling with amino acids in cell culture (SILAC) and affinity-purification mass spectrometry (AP-MS) to characterize the nucleotide-dependent protein interactomes of K-RAS4A and K-RAS4B revealed novel interactomes for each variant, with comparable numbers of interacting proteins for both wildtype and mutant versions of each splice variant (Zhang et al., 2018). Zhang and others described that K-RAS4A interacts with Raf-1 with higher affinity than K-RAS4B, leading to increased RAF1-1MEK-ERK signalling cascade, and that K-RAS4A showed increased anchorage-independent growth in assays that compared K-RAS4A- and K-RAS4B-transformed NIH 3T3 cells (Zhang et al., 2018). Interestingly, Bigenzahn and others performed proteomic analysis using K-562 chronic myeloid leukaemia cell lines. They reported that, while the two RAS isoforms share 28 interactors, they also each have distinct interactomes, with K-RAS4A specifically binding to fewer proteins than K-RAS4B (15 proteins versus 29, respectively) (Bigenzahn et al., 2018). Cumulatively, these findings suggest a certain degree of functional overlap and also raise the possibility that the splice variants cooperate with each another or compensate for each other's function, depending on the cell type and intracellular pathway involved.

K-RAS4A protein was identified as a defattyacylation substrate of SIRT2, a member of the sirtuin family of protein lysine deacylases (Jing et al., 2017). Through biochemical and cell biology approaches, Jing and others found that K-RAS4A is fatty acylated on lysine residues at its C-terminal HVR, and that SIRT2 removes lysine fatty acylation from K-RAS4A, resulting in increased endomembrane localisation, interaction with A-Raf, and in turn enhanced K-RAS4A transforming activity (Jing et al., 2017). Thus, the study of small molecules that could inhibit the defatty-acylation activity of sirtuins may have therapeutic potential. Spiegelman and others developed a SIRT2 inhibitor, named JH-T4, which was the first such inhibitor to enhance K-RAS4A lysine fatty acylation *in vitro* (Spiegelman et al., 2019). Although JH-T4 showed anti-cancer effects in cancer cells, it was also toxic to normal cells, suggesting a lack of cancer cell selectivity (Spiegelman et al., 2019). Thus, JH-T4, while potentially promising, awaits further improvements that may enhance its cancer cell selectivity.

Collectively, the studies suggest that RAS effector pathways may be differentially impacted by RAS structural conformation, localisation to membranes, and isoform-specific binding affinities, which may lead to variable signalling outputs. **Figure 2** compares the K-RAS4A and K-RAS4B protein sequences, highlighting the important residues for membrane binding, and also the simplified schematic representation of the RAS pathway indicates that each isoform has its own binding affinities for different effectors, which may result in a variety of cell responses.

COMPARISON OF K-RAS4A AND K-RAS4B TISSUE EXPRESSION PROFILES

Profiling of K-RAS splice variant expression have shown that K-RAS4A and K-RAS4B expression levels differ across tissues. The K-RAS4A/4B expression ratio varies according to normal versus tumour tissues, as well as by tumour type analysed (e.g. lung, pancreas and colorectal cancer) (Plowman et al., 2003; Abubaker et al., 2009; Aran et al., 2018). For example, in patients with non-small cell lung cancer (NSCLC), K-RAS4B mRNA showed higher expression than K-RAS4A (Aran et al., 2018). In contrast, similar splice variant levels were reported in the colon (Pells et al., 1997). When the gene expression profiles of each RAS isoform were characterized in a full developmental time course mouse tissue panel, K-RAS4B expression was frequently higher than K-RAS4A (Newlaczyl et al., 2017). The findings suggested that K-RAS4A is the most dynamically regulated RAS isoform (upregulated in pre-term in stomach, intestine, kidney and heart) (Newlaczyl et al., 2017).

A quantitative RT-PCR assay has been developed to detect the splice junction region and thus measure variant expression in human cancer cell lines (Tsai et al., 2015). Of the 30 cell lines tested, the isoform K-RAS4A was expressed in all of them; with similar levels to that of K-RAS4B detected in 17 human colorectal tumours. Analysis with splice variant-specific antibodies supported this finding (Tsai et al., 2015). K-RAS4A showed higher expression in colon cancer and melanoma cell lines than in other cell lines tested (Tsai et al., 2015). Furthermore, there were no significant differences in the relative abundance of the two K-RAS mRNAs among cells that harboured wildtype versus mutant K-RAS. Another study showed that K-RAS4A was found to be expressed in both human renal cell carcinomas and human renal cell carcinoma cells lines, with its upregulation sensitive to aldosterone (King et al., 2014).

As previously mentioned, the K-RAS4A HVR sequence shares similarities with those of K-RAS4B and N-RAS. Nussinov and

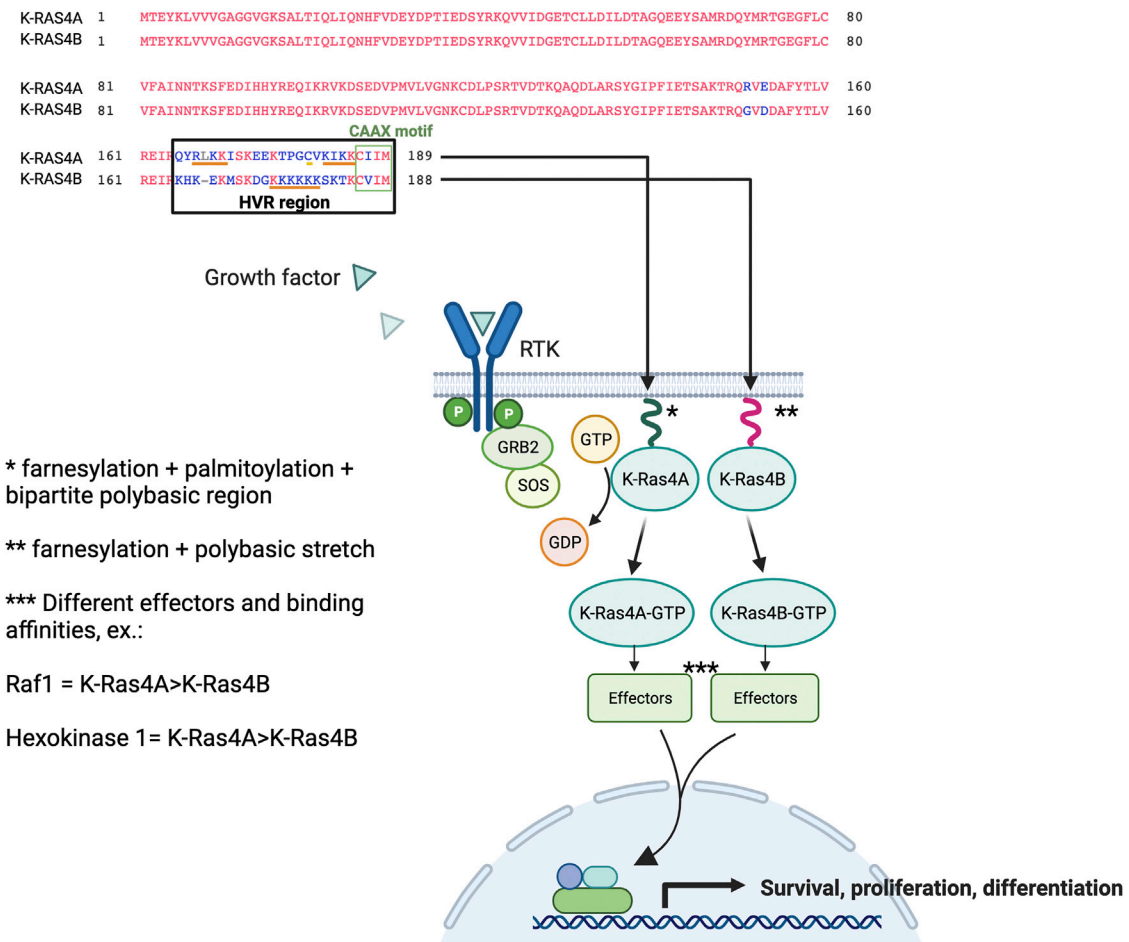

FIGURE 2 | K-RAS4A versus K-RAS4B protein sequence and signalling. RAS proteins contain a G domain (residues 1–165) responsible for the catalytic and switching portion of the protein that interacts with GDP/GTP, exchange factors, and GTPase-activating proteins (GAPs). The less homologous part corresponds to the hypervariable region (HVR) domains (final 23/24 residues). RAS are farnesylated on their C-terminal cysteine residue (CAAX motif), undergo AAX proteolysis and receive carboxyl methylation at the C-terminal prenylcysteine to allow the first step in membrane binding. A second motif improves this weak binding, which is a hexa-lysine polybasic stretch (residues 175–180) that interacts electrostatically with membranes in the case of K-RAS4B. Whereas, K-RAS4A membrane binding is stabilised by a monopalmitoylation site (residue 180), whereas this site is absent in the isoform K-RAS4B (Hancock et al., 1991). The KIKK motif (residues 182–185) was shown to be an additional membrane-targeting motif for K-RAS4A (Zhao et al., 2015), in addition to other basic motif corresponding to RLKK (residues 167–170) (Tsai et al., 2015). The binding of growth factors to the extracellular regions of receptor tyrosine kinases (RTKs) initiates the signal that will lead to the activation of RAS proteins downstream of the receptor. The isoforms can bind to a variety of effectors with variable affinities where, for example, hexokinase 1 was shown to bind to K-RAS4A with higher affinity than to K-RAS4B; the same was observed for Raf1 (Zhang et al., 2018; Amendola et al., 2019). Part of the figure was built and adapted from the "Ras Pathway" template, by BioRender.com.

colleagues proposed that the N-RAS-like state of K-RAS4A (i.e., palmitoylated and farnesylated) could influence its high expression in melanoma, and that the K-RAS4B-like state of K-RAS4A (i.e., farnesylated) could contribute to the high expression levels seen in colon cancer (Nussinov et al., 2016).

Regarding benign tumour tissues, Shahrabi-Farahani and colleagues reported that during the proliferative phase of the menstrual cycle, K-RAS4A mRNA was upregulated (2.7-fold higher) in eutopic endometrium in patients with endometriosis compared to controls (Shahrabi-Farahani et al., 2015), whereas no significant correlation was observed between K-RAS4B and the different menstrual cycle phases (Farahani et al., 2015). Shahrabi-Farahani and colleagues proposed that increasing the K-RAS4A\4B ratio could affect the equilibrium between proliferation and apoptosis, two processes that are responsible for maintaining a normal eutopic endometrium, thus leading to the proliferative phase defect seen in patients with endometriosis. Furthermore, expression of both splice variants was also detected in patients with leiomyoma (i.e., uterine tumours originating from smooth muscle cells) (Zolfaghari et al., 2017).

POSSIBLE ROLES FOR K-RAS4A IN TUMORIGENESIS

Different roles have been attributed to K-RAS4A. Studies of embryonic stem cells have suggested that K-RAS4A promotes

apoptosis while K-RAS4B inhibits it, and that the K-RAS4A/4B isoform ratio regulates tumorigenesis by influencing stem cell differentiation and survival (Plowman et al., 2006). In addition, K-RAS4A was recently shown to be enriched in cancer stem-like cells under hypoxia conditions, whereas K-RAS4B was mainly induced by ER stress (Chen et al., 2021). Chen and colleagues also suggested that K-RAS4A splicing could be controlled by the DCAF15/RBM39 pathway (Chen et al., 2021). Another study used a matrix metalloproteinase 2 (MMP-2) promoter-luciferase reporter assay to demonstrate that the transcription of MMP-2 in K-RAS knockout fibroblasts was partially restored by transient expression of K-RAS4B but not K-RAS4A (Liao et al., 2003). This finding suggests that K-RAS4B has a greater metastatic potential than K-RAS4A, because tumour cells that express oncogenic RAS have a higher metastatic potential partially due to up-regulation of MMP-2 (Liao et al., 2003). Overall, both reports support a more tumorigenic role for K-RAS4B than K-RAS4A.

Interestingly, K-RAS4A shares similarities with H-RAS; both have been shown to induce lung tumours in wildtype and H-RAS knock-in mice (To et al., 2008). Since K-RAS presents mutations at the same regions in both splice variants, the vast majority affecting codon G12, some cancers may harbour mutations in one or even both isoforms simultaneously. Thus, blocking one isoform might not be enough to fully reduce the cell's oncogenic potential. Oncogenic K-RAS4A has also been shown to induce lung carcinogenesis in mice (To et al., 2008), and a recent publication by the Barbacid group demonstrated that expression of K-RAS4A^{G12V} in mice that lack K-RAS4B is sufficient to promote metastatic lung adenocarcinomas (Salmon et al., 2021). These reports highlight K-RAS4A's oncogenic potential, suggesting it could serve as a future therapeutic target.

Studies performed on patient samples have also supported different roles for each isoform. Abubaker and colleagues found an association between K-RAS4A overexpression and improved overall survival in patients with colorectal cancer, whereas overexpression of K-RAS4B was significantly associated with larger tumour size (Abubaker et al., 2009). The RAS oncogene is also involved in cell metabolism, and it was suggested that distinct RAS mutations might lead to variable metabolic dependencies (Kimmelman 2015). Recently, hexokinase 1 (HK1) was shown to be a K-RAS4A effector, which could impact on the tumours' cells metabolism (Amendola et al., 2019).

In human K-RAS-mutant leukaemia cell lines and in acute myeloid leukaemia (AML) cells, K-RAS4A is also expressed, and Zhao and colleagues showed that cells harbouring mutations at the palmitoylation site of oncogenic K-RAS4A (i.e., palmitoylation-defective mutant K-RAS4A$^{G12D/C180S}$) present a reduction in leukemogenicity potential. Unlike the results seen with mutations at the palmitoylation site of N-RAS (i.e., palmitoylation-defective mutant N-RAS$^{G12D/C181S}$), palmitoylation-defective K-RAS4A could still induce leukaemia in mice (Zhao et al., 2015). The KIKK motif of K-RAS4A appears to impact on its transforming activity since mutations affecting both the palmitoylation site and the KIKK motif blocked oncogenic K-RAS4A from inducing leukaemia in mice (Zhao et al., 2015). These findings support a role for the different posttranslational modifications in RAS function and oncogenic potential.

The fact that both splice variants are identical in the region where most K-RAS oncogenic mutations occur suggests that previous reports of mutations in K-RAS may actually have uncovered mutations in both transcripts, not just in K-RAS4B. In addition, cancers harbouring K-RAS mutations may behave differently depending on which splice variant is predominantly affected, which could impact on therapy response. As K-RAS4A and K-RAS4B possess slightly different structures when in the GDP-bound state, with GDP-bound K-RAS4A presenting a more exposed nucleotide binding pocket than GDP-bound K-RAS4B (Chakrabarti et al., 2016), compounds developed to target this catalytic domain could also be considered as a means to differentiate between the oncogenic mutant variants. The recent FDA approval of Sotorasib or Lumakras (previously known as AMG 510, Amgen), a K-RAS^{G12C} inhibitor able to reduce K-RAS^{G12C} tumours (Canon et al., 2019; Hong et al., 2020), is a major breakthrough in RAS biology, since for many years RAS was considered an undruggable target. How efficient this drug is when comparing K-RAS4A^{G12C} versus K-RAS4B^{G12C} in different cancer types remains to be determined. It would be interesting to see the development of novel mutation- and splice variant-specific inhibitors in those cancers where both isoforms are simultaneously affected. Nevertheless, more analysis should be performed to better clarify if there are any significant differences between mutant K-RAS4A and mutant K-RAS4B in response to distinct therapies.

CONCLUSION

K-RAS4B research has historically overshadowed that of K-RAS4A, suggesting that K-RAS4A is a minor variant. Nevertheless, the fact that K-RAS4A is evolutionarily conserved and binds distinct effectors at different affinities compared to K-RAS4B, in addition to the fact that K-RAS4A expression varies across tissue types, argue for a more important role than previously thought. Additional work is needed to unravel the different roles that each splice variant plays in normal versus tumours tissues. Such knowledge may help inform understanding of therapy resistance and improve disease management of cancer types with differential splice variant expression. Personalised medicine has exploited K-RAS-mutation-specific tumour differences for the development of mutation-selective anti-RAS strategies; thus, it could be beneficial to place K-RAS4A in the spotlight and perhaps achieve more selective cancer treatment strategies.

AUTHOR CONTRIBUTIONS

VA contributed to conception, writting and design of the study.

ACKNOWLEDGMENTS

I would like to thank Dr Lindsay Carpp and Dr Marion S Gilbert for proofreading the final version of this manuscript.

REFERENCES

Abubaker, J., Bavi, P., Al-Haqawi, W., Sultana, M., Al-Harbi, S., Al-Sanea, N., et al. (2009). Prognostic Significance of Alterations in KRAS Isoforms KRAS-4A/4B andKRASmutations in Colorectal Carcinoma. *J. Pathol.* 219, 435–445. doi:10.1002/path.2625

Ahearn, I., Zhou, M., and Philips, M. R. (2018). Posttranslational Modifications of RAS Proteins. *Cold Spring Harb Perspect. Med.* 8. doi:10.1101/cshperspect.a031484

Amendola, C. R., Mahaffey, J. P., Parker, S. J., Ahearn, I. M., Chen, W.-C., Zhou, M., et al. (2019). KRAS4A Directly Regulates Hexokinase 1. *Nature* 576, 482–486. doi:10.1038/s41586-019-1832-9

Aran, V., Masson Domingues, P., Carvalho de Macedo, F., Moreira de Sousa, C. A., Caldas Montella, T., de Souza Accioly, M. T., et al. (2018). A Cross-Sectional Study Examining the Expression of Splice Variants K-Ras4a and K-Ras4b in Advanced Non-small-cell Lung Cancer Patients. *Lung Cancer* 116, 7–14. doi:10.1016/j.lungcan.2017.12.005

Barceló, C., Paco, N., Morell, M., Alvarez-Moya, B., Bota-Rabassedas, N., Jaumot, M., et al. (2014). Phosphorylation at Ser-181 of Oncogenic KRAS Is Required for Tumor Growth. *Cancer Res.* 74, 1190–1199. doi:10.1158/0008-5472.can-13-1750

Bigenzahn, J. W., Collu, G. M., Kartnig, F., Pieraks, M., Vladimer, G. I., Heinz, L. X., et al. (2018). LZTR1 Is a Regulator of RAS Ubiquitination and Signaling. *Science* 362, 1171–1177. doi:10.1126/science.aap8210

Canon, J., Rex, K., Saiki, A. Y., Mohr, C., Cooke, K., Bagal, D., et al. (2019). The Clinical KRAS(G12C) Inhibitor AMG 510 Drives Anti-tumour Immunity. *Nature* 575, 217–223. doi:10.1038/s41586-019-1694-1

Capon, D. J., Seeburg, P. H., McGrath, J. P., Hayflick, J. S., Edman, U., Levinson, A. D., et al. (1983). Activation of Ki-Ras2 Gene in Human colon and Lung Carcinomas by Two Different point Mutations. *Nature* 304, 507–513. doi:10.1038/304507a0

Chakrabarti, M., Jang, H., and Nussinov, R. (2016). Comparison of the Conformations of KRAS Isoforms, K-Ras4A and K-Ras4B, Points to Similarities and Significant Differences. *J. Phys. Chem. B* 120, 667–679. doi:10.1021/acs.jpcb.5b11110

Chen, W.-C., To, M. D., Westcott, P. M. K., Delrosario, R., Kim, I.-J., Philips, M., et al. (2021). Targeting KRAS4A Splicing through the RBM39/DCAF15 Pathway Inhibits Cancer Stem Cells. *Nat. Commun.* 12, 4288. doi:10.1038/s41467-021-24498-7

Cho, K.-j., van der Hoeven, D., Zhou, Y., Maekawa, M., Ma, X., Chen, W., et al. (2016). Inhibition of Acid Sphingomyelinase Depletes Cellular Phosphatidylserine and Mislocalizes K-Ras from the Plasma Membrane. *Mol. Cel Biol* 36, 363–374. doi:10.1128/mcb.00719-15

Cox, A. D., and Der, C. J. (2010). Ras History. *Small GTPases* 1, 2–27. doi:10.4161/sgtp.1.1.12178

Esteban, L. M., Vicario-Abejo´n, C., Ferna´ndez-Salguero, P., Ferna´ndez-Medarde, A., Swaminathan, N., Yienger, K., et al. (2001). Targeted Genomic Disruption of H- Ras and N- Ras , Individually or in Combination, Reveals the Dispensability of Both Loci for Mouse Growth and Development. *Mol. Cel Biol* 21, 1444–1452. doi:10.1128/mcb.21.5.1444-1452.2001

Farahani, M. S., Shahbazi, S., Moghaddam, S. A., and Mahdian, R. (2015). Evaluation of KRAS Gene Expression and LCS6 Variant in Genomic and Cell-free DNA of Iranian Women with Endometriosis. *Reprod. Sci.* 22, 679–684. doi:10.1177/1933719114556478

Hancock, J. F., Cadwallader, K., Paterson, H., and Marshall, C. J. (1991). A CAAX or a CAAL Motif and a Second Signal Are Sufficient for Plasma Membrane Targeting of Ras Proteins. *EMBO J.* 10, 4033–4039. doi:10.1002/j.1460-2075.1991.tb04979.x

Hancock, J. F., Paterson, H., and Marshall, C. J. (1990). A Polybasic Domain or Palmitoylation Is Required in Addition to the CAAX Motif to Localize P21ras to the Plasma Membrane. *Cell* 63, 133–139. doi:10.1016/0092-8674(90)90294-o

Hancock, J. F. (2003). Ras Proteins: Different Signals from Different Locations. *Nat. Rev. Mol. Cel Biol* 4, 373–385. doi:10.1038/nrm1105

Hobbs, G. A., Der, C. J., and Rossman, K. L. (2016). RAS Isoforms and Mutations in Cancer at a Glance. *J. Cel Sci* 129, 1287–1292. doi:10.1242/jcs.182873

Hong, D. S., Fakih, M. G., Strickler, J. H., Desai, J., Durm, G. A., Shapiro, G. I., et al. (2020). KRASG12C Inhibition with Sotorasib in Advanced Solid Tumors. *N. Engl. J. Med.* 383, 1207–1217. doi:10.1056/nejmoa1917239

James, G., Goldstein, J. L., and Brown, M. S. (1996). Resistance of K-RasBV12 Proteins to Farnesyltransferase Inhibitors in Rat1 Cells. *Proc. Natl. Acad. Sci.* 93, 4454–4458. doi:10.1073/pnas.93.9.4454

Jing, H., Zhang, X., Wisner, S. A., Chen, X., Spiegelman, N. A., Linder, M. E., et al. (2017). 'SIRT2 and Lysine Fatty Acylation Regulate the Transforming Activity of K-Ras4a, *Elife* 6. doi:10.7554/elife.32436

Kelemen, O., Convertini, P., Zhang, Z., Wen, Y., Shen, M., Falaleeva, M., et al. (2013). Function of Alternative Splicing. *Gene* 514, 1–30. doi:10.1016/j.gene.2012.07.083

Kimmelman, A. C. (2015). Metabolic Dependencies in RAS-Driven Cancers. *Clin. Cancer Res.* 21, 1828–1834. doi:10.1158/1078-0432.ccr-14-2425

King, S., Bray, S., Galbraith, S., Christie, L., and Fleming, S. (2014). Evidence for Aldosterone-dependent Growth of Renal Cell Carcinoma. *Int. J. Exp. Path.* 95, 244–250. doi:10.1111/iep.12074

Koera, K., Nakamura, K., Nakao, K., Miyoshi, J., Toyoshima, K., Hatta, T., et al. (1997). K-ras Is Essential for the Development of the Mouse Embryo. *Oncogene* 15, 1151–1159. doi:10.1038/sj.onc.1201284

Konstantinopoulos, P. A., Karamouzis, M. V., and Papavassiliou, A. G. (2007). Post-translational Modifications and Regulation of the RAS Superfamily of GTPases as Anticancer Targets. *Nat. Rev. Drug Discov.* 6, 541–555. doi:10.1038/nrd2221

Laude, A. J., and Prior, I. A. (2008). Palmitoylation and Localisation of RAS Isoforms Are Modulated by the Hypervariable Linker Domain. *J. Cel Sci* 121, 421–427. doi:10.1242/jcs.020107

Li, Z.-L., and Buck, M. (2017). Computational Modeling Reveals that Signaling Lipids Modulate the Orientation of K-Ras4A at the Membrane Reflecting Protein Topology. *Structure* 25, 679–689. doi:10.1016/j.str.2017.02.007

Liao, J., Wolfman, J. C., and Wolfman, A. (2003). K-ras Regulates the Steady-State Expression of Matrix Metalloproteinase 2 in Fibroblasts. *J. Biol. Chem.* 278, 31871–31878. doi:10.1074/jbc.m301931200

Marks, J. L., Broderick, S., Zhou, Q., Chitale, D., Li, A. R., Zakowski, M. F., et al. (2008). Prognostic and Therapeutic Implications of EGFR and KRAS Mutations in Resected Lung Adenocarcinoma. *J. Thorac. Oncol.* 3, 111–116. doi:10.1097/jto.0b013e318160c607

McGrath, J. P., Capon, D. J., Smith, D. H., Chen, E. Y., Seeburg, P. H., Goeddel, D. V., et al. (1983). Structure and Organization of the Human Ki-Ras Proto-Oncogene and a Related Processed Pseudogene. *Nature* 304, 501–506. doi:10.1038/304501a0

Messina, S., De Simone, G., and Ascenzi, P. (2019). Cysteine-based Regulation of Redox-Sensitive Ras Small GTPases. *Redox Biol.* 26, 101282. doi:10.1016/j.redox.2019.101282

Murugan, A. K., Grieco, M., and Tsuchida, N. (2019). RAS Mutations in Human Cancers: Roles in Precision Medicine. *Semin. Cancer Biol.* 59, 23–35. doi:10.1016/j.semcancer.2019.06.007

Newlaczyl, A. U., Coulson, J. M., and Prior, I. A. (2017). Quantification of Spatiotemporal Patterns of Ras Isoform Expression during Development. *Sci. Rep.* 7, 41297. doi:10.1038/srep41297

Normanno, N., Tejpar, S., Morgillo, F., De Luca, A., Van Cutsem, E., and Ciardiello, F. (2009). Implications for KRAS Status and EGFR-Targeted Therapies in Metastatic CRC. *Nat. Rev. Clin. Oncol.* 6, 519–527. doi:10.1038/nrclinonc.2009.111

Nussinov, R., Tsai, C.-J., Chakrabarti, M., and Jang, H. (2016). A New View of Ras Isoforms in Cancers. *Cancer Res.* 76, 18–23. doi:10.1158/0008-5472.can-15-1536

Pao, W., Wang, T. Y., Riely, G. J., Miller, V. A., Pan, Q., Ladanyi, M., et al. (2005). KRAS Mutations and Primary Resistance of Lung Adenocarcinomas to Gefitinib or Erlotinib. *Plos Med.* 2, e17. doi:10.1371/journal.pmed.0020017

Pells, S., Divjak, M., Romanowski, P., Impey, H., Hawkins, N. J., Clarke, A. R., et al. (1997). Developmentally-regulated Expression of Murine K-Ras Isoforms. *Oncogene* 15, 1781–1786. doi:10.1038/sj.onc.1201354

Plowman, S., Arends, M., Brownstein, D., Luo, F., Devenney, P., Rose, L., et al. (2006). The K-Ras 4A Isoform Promotes Apoptosis but Does Not Affect Either Lifespan or Spontaneous Tumor Incidence in Aging Mice. *Exp. Cel Res.* 312, 16–26. doi:10.1016/j.yexcr.2005.10.004

Plowman, S. J., Williamson, D. J., O'Sullivan, M. J., Doig, J., Ritchie, A.-M., Harrison, D. J., et al. (2003). While K- Ras Is Essential for MouseDevelopment, Expression of the K- Ras 4A Splice VariantIsDispensable. *Mol. Cel Biol* 23, 9245–9250. doi:10.1128/mcb.23.24.9245-9250.2003

Salmón, M., Paniagua, G., Lechuga, C. G., Fernández-García, F., Zarzuela, E., Álvarez-Díaz, R., et al. (2021). KRAS4A Induces Metastatic Lung Adenocarcinomas *In Vivo* in the Absence of the KRAS4B Isoform. *Proc. Natl. Acad. Sci. U S A.*, 118. doi:10.1073/pnas.2023112118

Shahrabi-Farahani, M., Shahbazi, S., Mahdian, R., and Amini-Moghaddam, S. (2015). K-ras 4A Transcript Variant Is Up-Regulated in Eutopic Endometrium of Endometriosis Patients during Proliferative Phase of Menstrual Cycle. *Arch. Gynecol. Obstet.* 292, 225–229. doi:10.1007/s00404-014-3596-7

Shimizu, K., Birnbaum, D., Ruley, M. A., Fasano, O., Suard, Y., Edlund, L., et al. (1983). Structure of the Ki-Ras Gene of the Human Lung Carcinoma Cell Line Calu-1. *Nature* 304, 497–500. doi:10.1038/304497a0

Sorek, R., and Amitai, M. (2001). Piecing Together the Significance of Splicing. *Nat. Biotechnol.* 19, 196. doi:10.1038/85613

Spiegelman, N. A., Hong, J. Y., Hu, J., Jing, H., Wang, M., Price, I. R., et al. (2019). A Small-Molecule SIRT2 Inhibitor that Promotes K-Ras4a Lysine Fatty-Acylation. *ChemMedChem* 14, 744–748. doi:10.1002/cmdc.201800715

Stalnecker, C. A., and Der, C. J. (2020). RAS, Wanted Dead or Alive: Advances in Targeting RAS Mutant Cancers. *Sci. Signal.* 13. doi:10.1126/scisignal.aay6013

To, M. D., Wong, C. E., Karnezis, A. N., Del Rosario, R., Di Lauro, R., and Balmain, A. (2008). Kras Regulatory Elements and Exon 4A Determine Mutation Specificity in Lung Cancer. *Nat. Genet.* 40, 1240–1244. doi:10.1038/ng.211

Tsai, F. D., Lopes, M. S., Zhou, M., Court, H., Ponce, O., Fiordalisi, J. J., et al. (2015). K-Ras4A Splice Variant Is Widely Expressed in Cancer and Uses a Hybrid Membrane-Targeting Motif. *Proc. Natl. Acad. Sci. USA* 112, 779–784. doi:10.1073/pnas.1412811112

Voice, J. K., Klemke, R. L., Le, A., and Jackson, J. H. (1999). Four Human Ras Homologs Differ in Their Abilities to Activate Raf-1, Induce Transformation, and Stimulate Cell Motility. *J. Biol. Chem.* 274, 17164–17170. doi:10.1074/jbc.274.24.17164

Wright, L. P., and Philips, M. R. (2006). Thematic Review Series: Lipid Posttranslational Modifications CAAX Modification and Membrane Targeting of Ras. *J. Lipid Res.* 47, 883–891. doi:10.1194/jlr.r600004-jlr200

Zhang, X., Cao, J., Miller, S. P., Jing, H., and Lin, H. (2018). Comparative Nucleotide-dependent Interactome Analysis Reveals Shared and Differential Properties of KRas4a and KRas4b. *ACS Cent. Sci.* 4, 71–80. doi:10.1021/acscentsci.7b00440

Zhao, H., Liu, P., Zhang, R., Wu, M., Li, D., Zhao, X., et al. (2015). Roles of Palmitoylation and the KIKK Membrane-Targeting Motif in Leukemogenesis by Oncogenic KRAS4A. *J. Hematol. Oncol.* 8, 132. doi:10.1186/s13045-015-0226-1

Zhou, Y., Prakash, P., Gorfe, A. A., and Hancock, J. F. (2018). Ras and the Plasma Membrane: A Complicated Relationship. *Cold Spring Harb Perspect. Med.* 8. doi:10.1101/cshperspect.a031831

Zolfaghari, N., Shahbazi, S., Torfeh, M., Khorasani, M., Hashemi, M., and Mahdian, R. (2017). Identification of Differentially Expressed K-Ras Transcript Variants in Patients with Leiomyoma. *Reprod. Sci.* 24, 1438–1443. doi:10.1177/1933719116689596

Conflict of Interest: The author declares that the research was conducted in the absence of any commercial or financial relationships that could be construed as a potential conflict of interest.

Publisher's Note: All claims expressed in this article are solely those of the authors and do not necessarily represent those of their affiliated organizations, or those of the publisher, the editors and the reviewers. Any product that may be evaluated in this article, or claim that may be made by its manufacturer, is not guaranteed or endorsed by the publisher.

Advantages of publishing in Frontiers

OPEN ACCESS
Articles are free to read for greatest visibility and readership

FAST PUBLICATION
Around 90 days from submission to decision

HIGH QUALITY PEER-REVIEW
Rigorous, collaborative, and constructive peer-review

TRANSPARENT PEER-REVIEW
Editors and reviewers acknowledged by name on published articles

Frontiers
Avenue du Tribunal-Fédéral 34
1005 Lausanne | Switzerland

Visit us: www.frontiersin.org
Contact us: frontiersin.org/about/contact

REPRODUCIBILITY OF RESEARCH
Support open data and methods to enhance research reproducibility

DIGITAL PUBLISHING
Articles designed for optimal readership across devices

FOLLOW US
@frontiersin

IMPACT METRICS
Advanced article metrics track visibility across digital media

EXTENSIVE PROMOTION
Marketing and promotion of impactful research

LOOP RESEARCH NETWORK
Our network increases your article's readership